New polysiloxane based encapsulation materials for high energy LEDs

Dissertation

submitted towards the degree

Doctor of Natural Sciences (*Dr. rer. nat.*)

of the Faculties of Natural Sciences and Technology

of Saarland University

Submitted by

M. Sc. Dennis Meier

Saarbrücken

2020

Day of the Colloquium: 08.04.2021

Dean: Prof. Dr. Jörn Walter

Rapporteur: Prof. Dr. Guido Kickelbick

Prof. Dr.-Ing. Markus Gallei

Chair: Prof. Dr. Gregor Jung

Academic Staff: Dr.-Ing. Steffen Hau

The present dissertation was prepared in the time between January 2015 and October 2018 in the Institute of Inorganic Solid State Chemistry of the Faculty of Natural Science and Technology at Saarland University under the supervision of Prof. Dr. Guido Kickelbick.

Acknowledgement

Abstract

In the development of new high-energy LEDs, there is a great need for encapsulation materials that increase luminous efficacy while being thermally stable at high operating temperatures. Polysiloxanes are widely used as encapsulation materials due to their optical transparency, chemical inertness, thermal stability and resistance to radiation degradation. One of the main drawbacks of them is their low refractive index. The aim of this work was to develop novel polysiloxanes and nanocomposites with increased refractive index while retaining the other positive properties of polysiloxane resins. New nanocomposites embedding hafnia or zirconia nanoparticles in polysiloxane matrices were synthesised. In a second approach, electron-rich atoms (Zr, Sn, Hf, and Ta) were copolymerised with siloxane monomers and thus incorporated into the polymer backbone. Both approaches only have a small increase in refractive index and had a significant effect on other parameters, such as viscosity. The third method investigated was based on the use of highly refractive, self-synthesised siloxane monomers containing oxygen or sulphur atoms in combination with phenyl or phenanthrenyl groups in the organic residues on the silicon atom. To increase the mechanical flexibility, the obtained systems were copolymerised with low refractive index siloxane monomers. These copolymers were cured using a platinum-catalysed reaction and tested in real LED castings.

Zusammenfassung

Bei der Entwicklung neuer Hochenergie-LEDs besteht ein großer Bedarf an Verkapselungsmaterialien, die die Lichtausbeute erhöhen und gleichzeitig bei den hohen Betriebstemperaturen thermisch stabil sind. Polysiloxane werden aufgrund ihrer optischen Transparenz, chemischen Inertheit, thermischen Stabilität und Strahlungsstabilität häufig hierfür eingesetzt. Einer ihrer Hauptnachteile ist ihr niedriger Brechungsindex. Ziel dieser Arbeit war es, neuartige Polysiloxane und Nanokomposite mit erhöhtem Brechungsindex unter Beibehaltung der anderen positiven Eigenschaften von Polysiloxanharzen zu entwickeln. Es wurden neue Nanokomposite synthetisiert, die Hafnia- oder Zirkonia-Nanopartikel in Polysiloxan-Matrizen einbetten. In einem zweiten Ansatz wurden elektronenreiche Atome (Zr, Sn, Hf und Ta) mit Siloxanmonomeren copolymerisiert und so in das Polymerrückgrat eingebaut. Beide Ansätze führten zur geringen Erhöhung des Brechungsindexes und hatten signifikante Einflüsse auf andere Parameter, wie die Viskosität. Die dritte untersuchte Methode verwendete hochbrechende, selbstsynthetisierte Siloxanmonomere, die Sauerstoff- oder Schwefelatome in Kombination mit Phenyl- oder Phenanthrenylgruppen in den organischen Resten am Siliziumatom enthalten. Um die mechanische Flexibilität zu erhöhen, wurden die erhaltenen Systeme mit Siloxanmonomeren mit niedrigem Brechungsindex copolymerisiert. Diese Copolymere wurden mit einer platinkatalysierten Reaktion ausgehärtet und in realen LEDs getestet.

Symbols and abbreviations

2θ	Diffraction angle
aq.	Aqueous
$Ba(OH)_2$	Barium hydroxide
BPO	Benzoyl peroxide
cat.	Catalyst
$CDCl_3$	Deuterated chloroform
CHN	Elemental analysis
conc.	Concentrated
CP	Cross polarization (NMR)
d	Doublet (NMR)
δ	Chemical shift (NMR)
δ	Deformation vibration (FT-IR)
DLS	Dynamic light scattering
DMSO	Dimethyl sulfoxide
DSC	Differential scanning calorimetry
EA	Ethyl acetate
E_m	Integrated Energy of the melting signal (DSC)
EtOH	Ethanol
EP	Epoxide
FT-IR	Fourier-transform infrared spectroscopy
SEC	Size exclusion chromatography
H	Hydride
H_{450}	Haze value at 450 nm
HBMC	Heteronuclear multiple bond correlation (NMR)
$HCl_{(aq)}$	Hydrochloric acid
HRI	High refractive index
Hz	Hertz
^{i}Pr	*iso*-propyl

IUPAC	International Union of Pure and Applied Chemistry
J	Coupling constant (NMR)
kHz	kilohertz
λ	Wavelength
lm	Lumen
LRI	Low refractive index
m	Multiplet (NMR)
M	methyl
mA	Milliampere
MA	methacryl
MAS	Magic Angle Spinning (NMR)
mbar	Millibar
MeOH	Methanol
Met	Metal
MHz	Megahertz
MM	-Si(Me$_2$)-O-
mW	Milliwatt
ν	Stretching vibration (FT-IR)
n	Refractive index
NEt$_3$	Triethylamine
N^{t}Bu$_4$OH	Tetrabutylammonium hydroxide
^{n}Pr	*n*-propyl
P	phenyl
PDI	Polydisperisty index
PDMS	Polydimethylsiloxane
PDPS	Polydiphenylsiloxane
PH	9-phenantrenyl
PHM	Phenanthren-9-ylmethylsiloxane/ Phenanthren-9-ylmethyldimethoxysilane
PHP	Phenanthren-9-ylphenylsiloxane/ Phenanthren-9-ylphenyldimethoxysilane
PM	Phenylmethylsiloxane/Phenylmethyldimethoxysilane

PMPS	Polymethylphenylsiloxane
POP	Phenoxyphenyl
POPP	Phenoxyphenylphenylsiloxane/4-(phenoxy)phenylphenyldimethoxysilane
PP	Diphenylsiloxane/Diphenylsilanediol
PTFE	Polytetrafluoroethylene (Teflon)
PSM	Phenylthiomethyl
PSMP	Phenylthiomethylphenylsiloxane/4-(methylthio)phenylphenyldimethoxysilane
R	Organic rest
RI	Refractive index
rpm	Revolutions per minute
s	Singlet (NMR)
t	Triplet (NMR)
T450	Transmission at 450 nm
T_b	Boiling temperature
TEM	Transmission electron microscopy
T_g	Glass transition temperature (DSC)
TGA	Thermogravimetric analysis
THF	Tetrahydrofuran
T_m	Melting temperature (DSC)
TP	Triphenylsiloxane/Triphenylsilanol
V	Vinyl
WI	Whiteness index
wt%	Weight percent
XRD	X-ray powder diffraction
YI	Yellowness index

Table of contents

1 Introduction and motivation

The first LEDs were developed in the 1980s using an AlGaInP chip which produces red, orange or yellow light.[1] Ten years later GaInP chips were used for violet, blue or green light emittance.[1] By combining these chips white light LEDs could be developed.[1] The bare chips have to be protected from the surrounding, which resulted in the encapsulation with resins like epoxides.[2-10] The aim to increase the light output lead to the development of a new LED generation containing chips with higher energy consumption. The so far used encapsulation materials were not suitable anymore because of the resulting increase of the operating temperature above 100 °C which leads to yellowing.[11-12] Polysiloxanes as encapsulation material were much more suitable for these temperatures.[12] The downside of these materials is the low refractive index of the industrially used polydimethylsiloxane (1.41)[13] or polymethylphenylsiloxane (1.53 – 1.56)[14,1,15-24] The low refractive index of the encapsulant in combination with the high refractive index of the LED chip leads to a low light extraction efficiency. Encapsulants with higher values increase the efficiency of the LED. Therefore, there was a strong need for new polysiloxanes with higher refractive indices. The search and synthesis for these new materials is the motivation for the thesis.

2   Theoretical background

2.1   Light emitting diode

2.1.1   Solid-state LEDs

In 1907, Henry J. Round was the first person to emit yellow light from a crystal in a laboratory by directly applying $10 – 110$ V.[24] Eugene G. Acheson produced the first emitting material for solid-state LEDs in 1981 in a commercial process made from silicon dioxide and carbon.[24-25] He named the resulting silicon carbide (SiC) "carborundum".[24-25] Modern white LEDs are more complex in their design (Figure 1). The LED is built on a metal coated or metallic baseplate for heat dissipation (Al or Cu, heatsink). The anode of the chip is electrically conducted over the bottom of the chip using a silver coating on the electrically isolated heatsink. The cathode side is connected via a gold wire to another area of silver coated and electrically isolated heatsink. A polymer, exemplarily polyphthalamide (PPA) filled with titanium oxide nanoparticles, serves as housing and reflector cup for increasing the light extraction efficiency. The main part of the LED is the chip which is often located in the middle of the reflector cup. It consists of a n- and a p-doped semiconductor material like the commonly used blue emitting diode $In_{1-x}Ga_xN$. The doping can be performed by adding Si^{4+} for the n-semiconductor side and Mg^{2+} for the p-side.[24, 26] The upper side of the chip (anode) is conducted with a high conductive noble metal bond wire like platinum or gold through the housing to the base plate.[1, 23-24, 26]
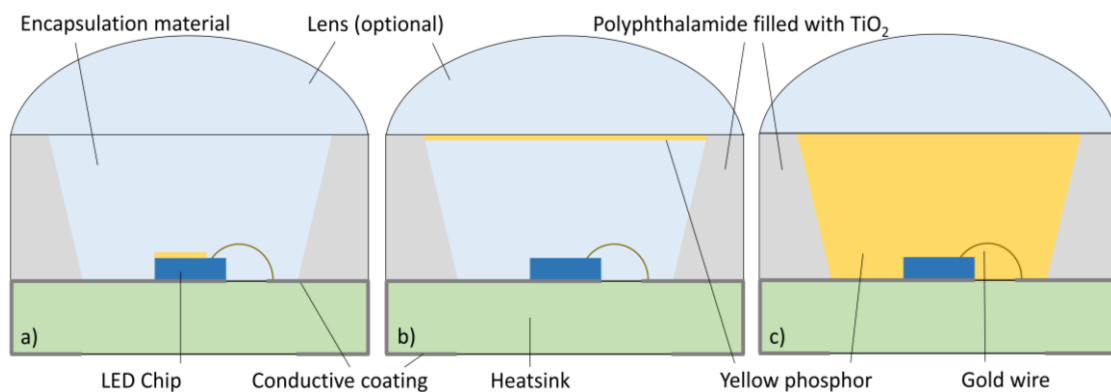
Figure 1: Common designs of a cold white light emitting diode, a) phosphor located directly over the chip, b) phosphor located above the encapsulation material (remote-phosphor) and c) phosphor mixed inside the whole encapsulation material.

The emitted blue photons are generated by applying a DC voltage in p-n junction. In the p-semiconductor area electrons are transported to the recombination zone which is located in between the p- and n-semiconductor. Positive charge carriers (holes) are transported in the n-semiconductor also to the recombination zone. During recombination, photons with the energy of the band gap of the semiconductor material are emitted. The energy of the band gap directly coheres

with the wavelength and therefore the colour of the chip which can be adjusted by the material and composition of the semiconductor.[1, 23-24, 26] The external quantum efficiency (EQE, formula (1)) of LEDs describes the ratio of the number of photons emitted from the LED to the number of electrons acquired by the chip.[27-29]

$$EQE = Injection\ efficiency * Internal\ quantum\ efficiency$$
$$* Extraction\ efficiency$$

(1)

The injection efficiency describes the proportion of electrons which are recombined with the holes in the active region of the semiconductor between the p- and n-layer to the amount of electrons absorbed by the device.[27-29] The internal quantum efficiency (IQE or radiative efficiency) is the proportion of electron hole recombination that produce radiation (photons) to the amount of recombination's that overall occur.[27-29] The extraction efficiency (optical efficiency) is the proportion of photons emitted by the device to the photons created at the recombination zone.[27-29] The highest EQE of the commonly used materials has the $In_{1-x}Ga_xN$ at 450 nm, which is therefore used for white light emitting diodes. The chip is covered with an encapsulation material that is filled with a yellow phosphor consisting of inorganic metal oxide microparticles. The phosphor filled encapsulation material can be located directly onto the chip in a thin layer, mixed inside the encapsulation material or above the colourless encapsulation material in a remote-phosphor design. The blue light (Figure 2) emitted by the chip is partially absorbed by the inorganic phosphor which converts it to yellow light. $Y_3Al_5O_{12}:Ce^{3+}$ is commonly used because of the high fluorescence efficiency of the Ce^{3+}: 5d $\rightarrow$ 4f transition which emits light in a broad range between 500 nm to 750 nm.[30]
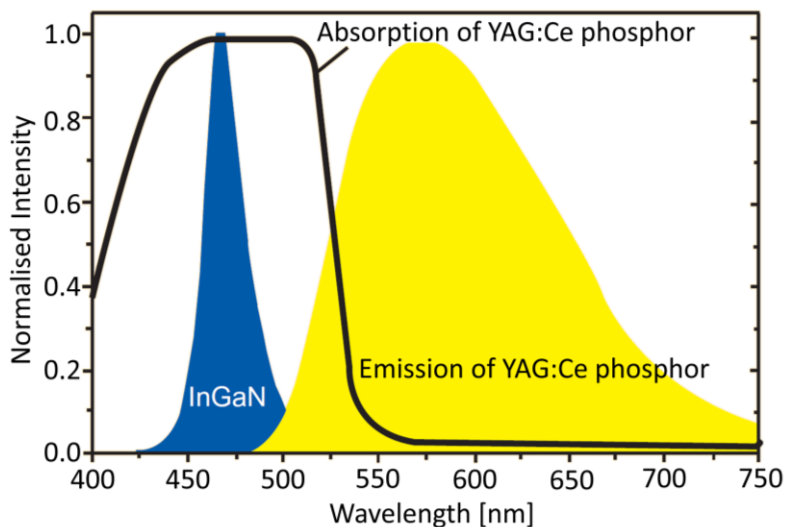
Figure 2: The emission spectrum of the blue $In_{1-x}Ga_xN$ chip covered with YAG:Ce^{3+} phosphor. Adapted from Born and Jüstel.[26]

The cold white light impression is generated by the blue light emitted by the chip and the yellow light emitted by the phosphor. Commonly used phosphors like $CaAlSiN_3:Eu^{2+}$, $(Ba, Sr, Ca)_2Si_5N_8:Eu^{2+}$, $Lu_3Al_5O_{12}:Ce^{3+}$, $Y_3Al_5O_{12}:Ce^{3+}$ or β-$Si_{6-z}Al_zO_z N_{8-z}:Eu^{2+}$ contain rare earth metals.[26, 31-39] In order to achieve a warm white light three different methods are used (Figure 3).[1, 24, 26, 40] A full conversion approach starting with UV light from Hg-vapor ($\lambda = 254$ nm) or violet one from a GaN chip converts all primary radiation using a blue, a green and a red phosphor to secondary radiation. This conversion is inefficient and therefore rarely used.[1, 41-42] The cold white LED uses the partial conversion approach with the already mentioned blue chip and yellow phosphor which are more efficient because of the lower wavelength-conversion losses due to lower Stokes-Shift losses.[1] The name refers to the low emission in the range of 480 – 520 nm relating to green light and in the range of 650 – 700 nm relating to the red light (Figure 2). To achieve warm white light, an additional red phosphor has to be used with the yellow one or a red and green one can be used.[38, 43-44] Another approach for generating a warm white light impression is the use of a blue (GaInN), a red (AlGaInP or GaAs) and a green (GaInN or GaP:N) chip and no secondary conversion.[1, 38, 43-44]
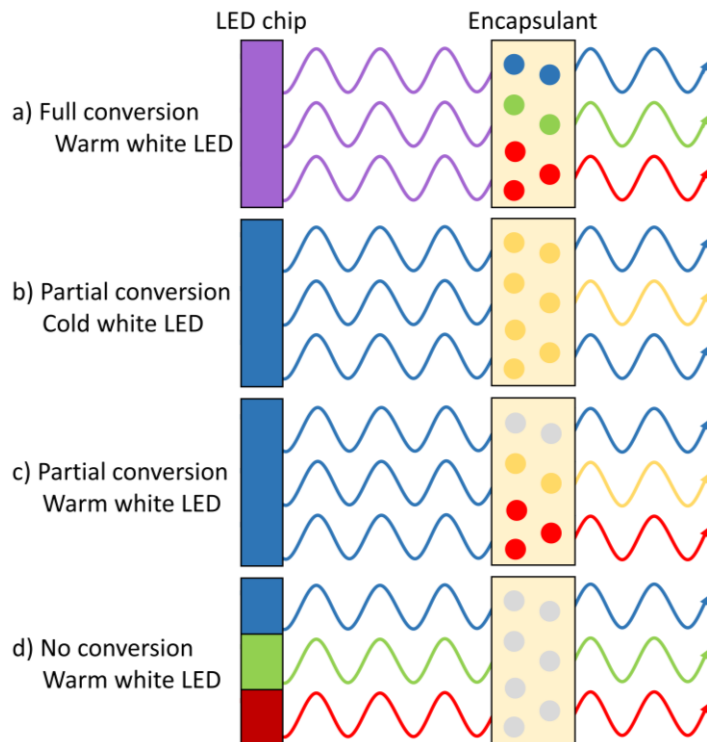
Figure 3: Four different methods to receive a white LED: a) full conversion from an UV chip using a blue, red and green phosphor, b) cold white LED from a blue chip using a yellow phosphor, c) warm white LED from a blue chip using a yellow and a red phosphor and d) warm light LED from a blue, a red and a green chip.[1, 24, 26, 40]

2.1.2 Organic hybrid and quantum dot LEDs

Organic light emitting diodes (OLED) as well as quantum-dot light emitting diodes (QLED) use a different type of converter of phosphor compared to solid-state LEDs.[45-48] They are now commonly used in display applications. The photons of the OLEDs are generated directly by applying an electrical current to an emissive electroluminescent organic layer, which is located between two electrodes where at least one is transparent.[46-48] Small organic molecules like tris(8-hydroxyquinolinato)aluminium[49], polymers like poly(*p*-phenylene vinylene)[50] or phosphorescent materials like tris[2-(*p*-tolyl)pyridine]iridium(III)[51] are used. The OLEDs allow the productions of slimmer screens with darker black colours, stronger contrasts and higher screen refresh rates compared to LED displays.[45-48] The downside of the OLED displays is their lower external quantum efficiency and lower lifetime because of the organic phosphor.[45-48] Hybrid organic LEDs use organic molecules like perylene partially or completely substituting the inorganic phosphor particles.[52] Because they are less stable towards the heat and radiation generated by the chip, normally a so-called remote-design is used (Figure 1 b)).[45-48]

QLEDs use photo-emissive or electro-emissive quantum dots, which emit pure monochromatic light either by the conversion of a backlight or directly from the electrical current.[45, 53-54] Photo-emissive quantum dots can consist of organic-inorganic perovskites $CH_3NH_3PbX_3$, where the colour can be adjusted by substituting the halogen anion X from chlorine over bromine to iodine which results in a successive redshift ranging from 380 nm to 740 nm.[55] Electro-emissive quantum dots can consist of a CdSe core with a ZnS shell.[54] Hybrid applications are also known using CdZnS/ZnS and CdZnSeS/ZnS core-shell particles with tris(1-phenylisoquinoline)iridium(III).[56] The emission of monochromatic light results in a higher brightness and a full colour coverage compared to LEDs or OLEDs. The black colour and the contrast are equivalent to OLEDs. The downside of QLEDs is the use of toxic chemicals like cadmium, lead or selenium.[45]

2.1.3 Reliability

The lifetime of LEDs depends on their design, application, and environment. Ultra-high-brightness LEDs operate at more than 3 W of power consuming over 1000 mA.[29] Despite having a high efficiency temperatures around 200 °C can be reached inside the chip.[29] The whole LED package including the reflectors cup, the light emitting diode, the phosphor as well as the encapsulant has to withstand the mechanical, thermal, electrical and photophysical stress.[29] The LEDs lifetime is determined by measuring the lumen maintenance thus the light output and the colour, which slightly reduces over the time. Because LEDs rarely fail completely, the lifetime

is determined based on 50 % light output degradation by the display industry (L50) and 70 % light out degradation by the lightning industry (L70), respectively.[29] These definitions result in a lifetime of 50000 h to 70000 h.[29] These number are extrapolated operating times using the lifetime determined with accelerated conditions, for example using 2000 mA and environmental conditions of 150 °C and 85 % humidity. The colour change is determined by calculating the colour rendering index (CRI) and the efficiency is calculated in lumen/watt by measuring the lumen output and the consumed power.[29] External factors reducing the lifetime are high temperatures, high humidity or pollutants, which contain R_2NH or RSH groups like ammonia or hydrogen sulfide.[57-59] Internal failures can be divided into three groups: the package, the interconnects and the semiconductors. The proportion of all internal failures across 212 million operating hours are displayed in Figure 4.[60] The main failure category is the driver power supply with 73 % and the second most failures relate from the housing integrity with 17 %. The electrical constant, the driver controls and the LED package add up the remaining 10 %.
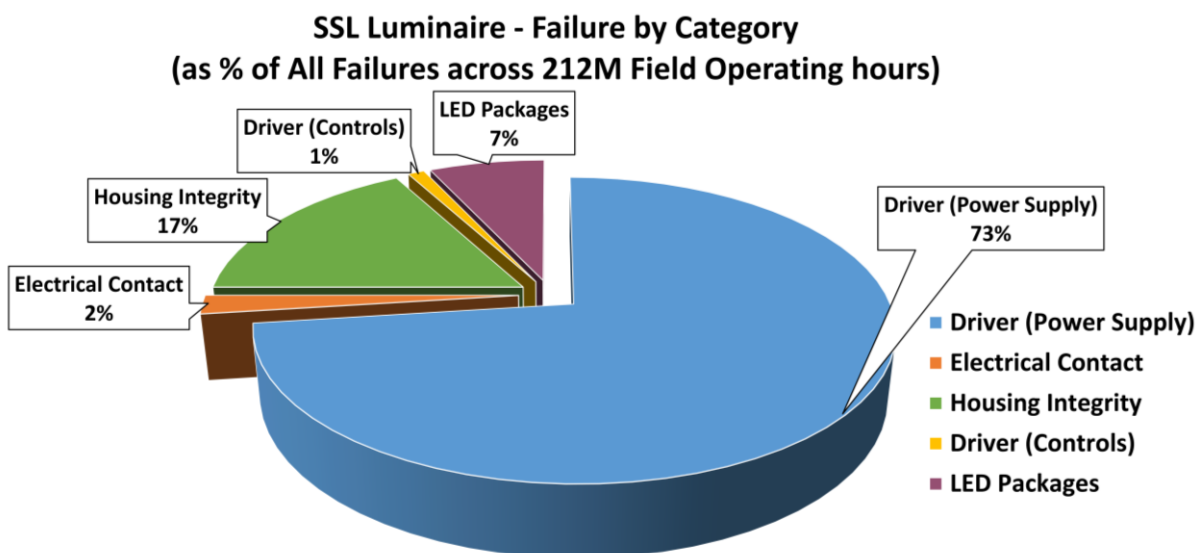
Figure 4: SSL Luminaire - Failure by category, as % of all failures across 212 M field operating hours. Redrawn from Next Generation Lighting Industry Alliance, LED Systems Reliability Consortium.[60]

The package related failure mechanisms can be separated into:

- Carbonisation of the plastic encapsulant which results in a conductive path across the LED causing a short circuit and the loss of protecting ability of the encapsulant from the surroundings because of high ambient temperatures or electrical overstress leading to Joule heating.[61-62]

- Delamination resulting from cyclic stress causing the loss of mechanical adhesion between the silicone encapsulant and the diode,[63] between the LED chip and the diode holder[64-65] or the packaging lead frame and the encapsulant[66].

- Encapsulant yellowing and aging caused by the high energy radiation and the high temperatures generated by the diode leading to hardening of the epoxide or polysiloxane resin which causes cracking, chain scission by radical formation and yellowing.[67-69] The latter parameter also results in a reduced amount of light emitted and a change of the colour.[70-72]

- Lens cracking caused by poor board assembly processing, hygro-mechanical or thermo-mechanical stress resulting in a decreased amount of light output due to internal reflections.[24, 73-74]

- Phosphor thermal quenching describing the efficiency reduction of the phosphor with increasing temperature resulting from the increase of the nonradiative transition due to thermally driven phosphorescence decay.[75-78]

- Solder joint fatigue and describes the degradation of electrical connections and the LED with time caused by the different thermal expansion coefficients resulting in shear because of the temperature changes.[79-82] The interconnect related failures can result from electrical overstress-induced bond wire fracture or wire ball bond fatigue caused by high forward current.[63, 83]

Also electrical contact metallurgical interdiffusion causes failures because of thermally activated semiconductor-metal and metal-metal interdiffusion resulting from the alloying and intermixing of the contact metals by in- and out-diffusion of the electrical contact.[84-85] The electrostatic discharge (ESD) failure mechanism only occurs in LEDs with sapphire substrates caused by rapid open circuit failure in LEDs because of the reversed biased pulse.[86-87] The semiconductor can failure by a crystal defect resulting in a reduction in the lifetime of non-equilibrium electron hole pairs.[88] This also increases the multi-phonon emissions under high currents, which then result in strong vibrations of the defect atoms leading in a reduction of the energy barrier for defect motions like migration, creation or clustering.[89-94] Extreme thermal shocks as well as high electrical stress can result in diode cracking, first resulting from the difference in the thermal expansion coefficient.[63, 86, 92] Another semiconductor failure is caused by the electromigration of atoms from the electrical contact to the chip surface which leads to a short circuit or of metal diffusion in the inner region from the p-contact across the junction creating current spikes.[94-96] Because of all these possible failures, LED manufacturer are evaluating their devices in various tests at different temperatures maintaining or cycling in the range of −40 °C to 200 °C, different humidity's of up to 85 % and different currents up to several amperes.[29, 97] The data obtained by these tests

allow a lumen maintenance forecast accurately to 60000 hours using the Arrhenius model (Equation (2))[29] or the Weilland distribution (Equation (3))[97].

$$Acceleration\ Factor_{Temp} = e^{\frac{E_a}{k}\left(\frac{1}{T_u}-\frac{1}{T_a}\right)} \tag{2}$$

$$f(x;k;\lambda) = \frac{k}{\lambda}\left(\frac{x}{\lambda}\right)^{k-1} e^{-\left(\frac{x}{\lambda}\right)^k} \tag{3}$$

2.2 Overview of LED encapsulation materials

Encapsulants for LEDs have to meet different requirements including high refractive index, high-temperature stability, high transparency, chemical stability and hermeticity.[24] Usmani *et al.* specified these requirements for their polymer investigations.[98-99] The refractive index at 25 °C has to exceed 1.50 while a value of 1.60 is desirable. The resin should withstand 85 °C and 85 % relative humidity for over 1000 hours. A good temperature performance including some degree of flexibility because of the different thermal expansion coefficients has to be available to withstand thermocycling. Other requirements are a hydrolytic stability, low moisture sensitivity, good clarity, a straightforward curing process where nongaseous products are evolved and the shrinkage has to be below 8.0 %.[98-100] The cured resin has to be tough, preferably infusible and has to have a good adhesion to the housing, good wetting of the metallic components but no interference with the electronic parts. In addition, a resistance to polymerisation or depolymerisation under ambient conditions and to corrosion has to be given. Considering these requirements, four material classes are suitable (Table 1).[98-100]

Table 1: Advantages and disadvantages of commonly used materials, rewritten from Usmani *et al.*[98-99]

| Material	Advantages	Disadvantages
Epoxides	Wide range of formulation	Moisture sensitivity
	Low shrinkage	Reversion on prolonged exposure to high temperature and humidity
	Excellent adhesion	Loss of mechanical properties in elevated temperature/high humidity environments
Polyesters	Wide range of formulation	High shrinkage
	Low cost	High exotherm
	Short cure cycle	Poor thermal shock
Silicones	Low exotherm	High cost
	Wide range of temperature usage (-75 °C to 260 °C)	Poor adhesion to most materials
		Poor mechanical properties
	Flexible	Small range of formulation
Urethanes	Abrasion resistance	Toxicity
	Toughness	Limited temperature range (95 °C max.)
	Flexibility	Sensitive to moisture

Polyesters have a wide range of formulations, are very cheap and can be cured very fast, but the downsides are the high shrinkage and the highly exothermic reaction.[98-99] The usable temperature range is small and they have to be heated up and cooled down slowly, respectively.[98-99] Urethanes have a good abrasion resistance, toughness and flexibility, but they are toxic, sensitive to moisture and can only be used at lower temperatures.[98-99] Recently polyurethanes also are used in car headlights or LED stripes as protective layer and as encapsulant because the toxicity and moisture sensitivity is here reduced.[101]

The advantages of epoxides are their wide range of formulation, low shrinkage, and excellent adhesion in addition to their low cost. The downsides are mostly irrelevant for low energy LEDs with an amperage of around 20 mA because they operate at low temperatures and ambient humidity environments.[29] Therefore, epoxy resins were already used in the 1970s because they meet these characteristics for the commercial available LEDs at that time.[100] The system often is a two component system with an epoxide resin and a hardener which are mixed in a 10:1 ratio and cured at 120 °C to 200 °C for several minutes.[24] The synthesis of the resin is performed by an acidic hydroxyl-group and epichlorohydrin, where the alcohol often is bisphenol A (Figure 5).[102-107] Novalac, aliphatic or halogenated epoxy resins are also commonly used.[102-107]

DGEBA (Diglycidyl ether of bisphenol A)
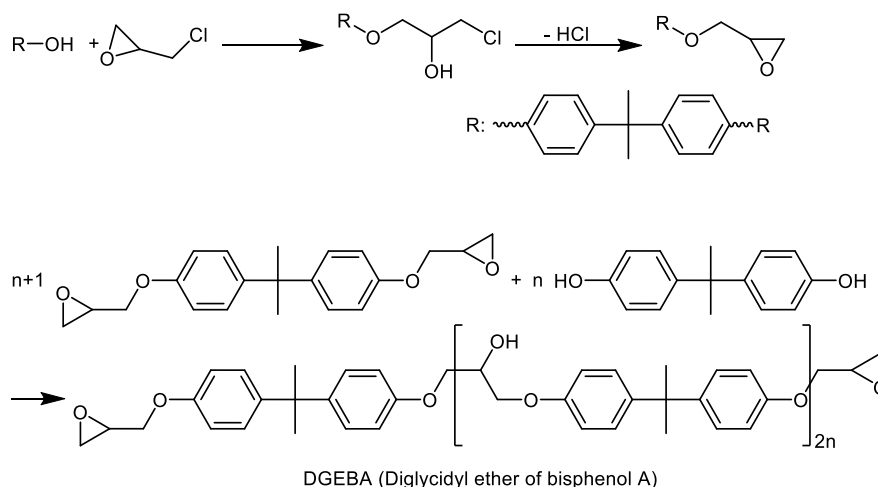
Figure 5: Synthesis of the liquid epoxide component exemplarily shown for DEGBA.

The hardener often contains primary or secondary amines like triethylenetetramine, which reacts with DEGBA in an addition reaction (Figure 6).[98, 102, 105, 107] Epoxides also can be cured with various substances ranging from an anionic or cationic catalyst which then results in a copolymerisation towards anhydrides, phenols or thiols.[102, 105] Besides the thermally catalysed curing reaction it also can be photocatalysed by UV light using onium salts like triphenylsulfonium hexafluorophosphate.[104, 108]
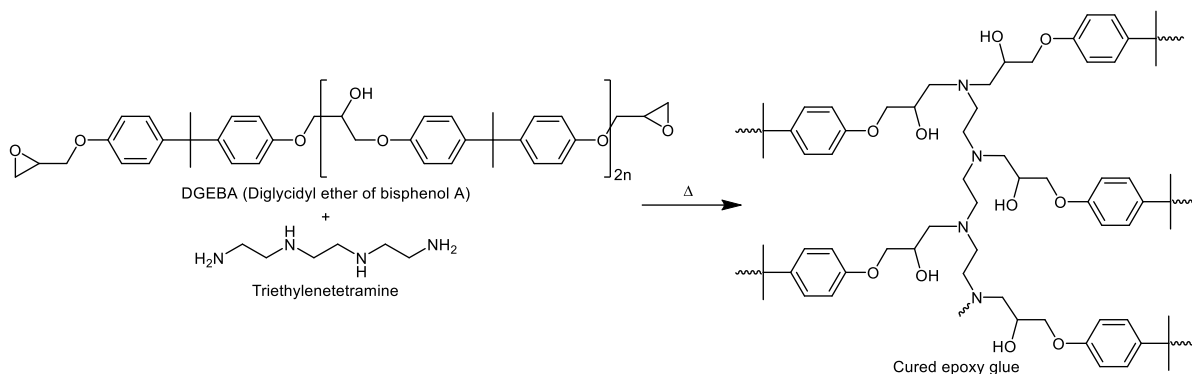
Figure 6: Synthesis of epoxide resin from DGEBA and triethylenetetramine.

An additional disadvantage of epoxides is the loss of transparency in LEDs using short wavelengths dies in the ultraviolet, violet or blue range because the encapsulant cracks and isolates part of the junction reducing the light output in addition to yellowing.[109] Modern high energy LEDs with an amperage of over 1000 mA produce up to 200 °C which exceeds the thermal stability of epoxides which are chemically long-term stable up to 120 °C.[24, 29] The ideal encapsulant for these high temperatures are the silicones. They are commercially used since the early 2000s, because of their thermal stability even at over 200 °C.[24] Their flexibility which remains forever compared to plastics with softeners because it relates from the atom structure of both silicon and oxygen and therefore also the resulting Si-O bond.[110] Because the curing reaction is low exothermal, they can be mixed and cured in large sample sizes making them suitable for high throughput manufacturing and industrial scale. The downsides are the relatively high cost for these materials compared to the other three and the poor adhesion to most materials and poor mechanical properties but these downsides have been solved in the last decade.[24, 111-115] Another important disadvantage is the relatively low refractive index because of the limited formulations available to the industry. Mainly methyl and phenyl side-groups are used and established, respectively. This leads to a RI between 1.40 and 1.55 which cannot easily be increased compared to epoxides.[13-14] The heat generated by the chip cannot be conducted away by both the epoxides and silicones because they have a low thermal conductivity of 0.5 W/(m·K)[116] and 0.9 W/(m·K)[17], respectively. This leads to a more complex construction of the high energy LEDs including the heat sinks. Other possibilities for increasing the thermal conductivity is the incorporation of nanoparticles like titanium oxide, which increased it from 0.9 W/m·k to 1.4 W/m·k using 2 wt% nanoparticles in OE-6550[17, 117] or graphene with OE-6630 from 1.5 W/cm·k to 4.7 W/cm·k[118].

2.3 Polysiloxanes

2.3.1 Structural characteristics of polysiloxanes

The polymer chain of polysiloxanes consist of Si-O bonds, which are different compared to the C-C bond because they are partially ionic and thus reveal a partial double bond character.[119] This results from the large difference of the electronegativities of silicon with 1.8 and oxygen with 3.5 according to Pauling, which results in an estimated 37 % to 51 % ionic character.[119-121] This partial double bond character leads to higher bond energy of 460.5 kJ/mol compared to 358.0 kJ/mol for the C-O bond or 304.0 kJ/mol for the C-C bond.[122] The Si-C bond has an energy of 318.0 kJ/mol and is therefore comparable to those of C-O and C-C bonds.[123] The high bond energy is the reason for the unusual high thermal stability compared to epoxides or poly(methyl methacrylates).[121, 124] The bond length in linear polysiloxanes is with 164 pm slightly larger than the 154 pm of the C-C or 142 pm of the C-O bond.[119, 121-122] The Si-C bond length to organic substituents is very long with 188 pm[121] and thus allows an easy rotation even for sterically demanding side-groups. The Si-O bond has a rotation barrier of < 0.8 kJ/mol and the Si-C one of 6.7 kJ/mol compared to 11.3 kJ/mol for C-O and 15.1 kJ/mol for C-C bonds.[121, 125] Another reason for the flexibility despite the longer bonds are the alternation of the different bond angles between Si-O-Si and O-Si-O in the backbone which can vary between 110° and 143°.[119, 121] Both result in a very low glass transition temperature compared to other organic materials used in the optical field.[126] The Si-O backbone is strongly polarized but is not having strong intermolecular interactions, because the nonpolar side-groups shield the backbone. This reason results in a very low critical surface tension comparable to Teflon and leads to a high chemical inertness, also because of the high Si-O bond energy.[127-129] Silicones have a very high transparency, because their band gap is energetically too high to be reached by photons of the visible light.[129] The vibrational overtone and combination bands of the methyl-groups cause the main absorption loss.[130] Silicones have a very high gas permeability compared to most of other polymers. The permeability can be reduced slightly by increasing the amount of cross-linking and by adding fillers.[121] The flexibility of the Si-O backbone creates "openings" which are free volume. Gases diffuse into these free volumes and migrate from one to another free volume. [131] PDMS has a very high permeability towards water vapour (Figure 7). The moisture permeability ranges from 68 $g \cdot m^{-2} \cdot 24 \cdot h^{-1}$ to 122 $g \cdot m^{-2} \cdot 24 \cdot h^{-1}$ compared to the 28 $g \cdot m^{-2} \cdot 24 \cdot h^{-1}$ to 37 $g \cdot m^{-2} \cdot 24 \cdot h^{-1}$ for epoxides.[132]
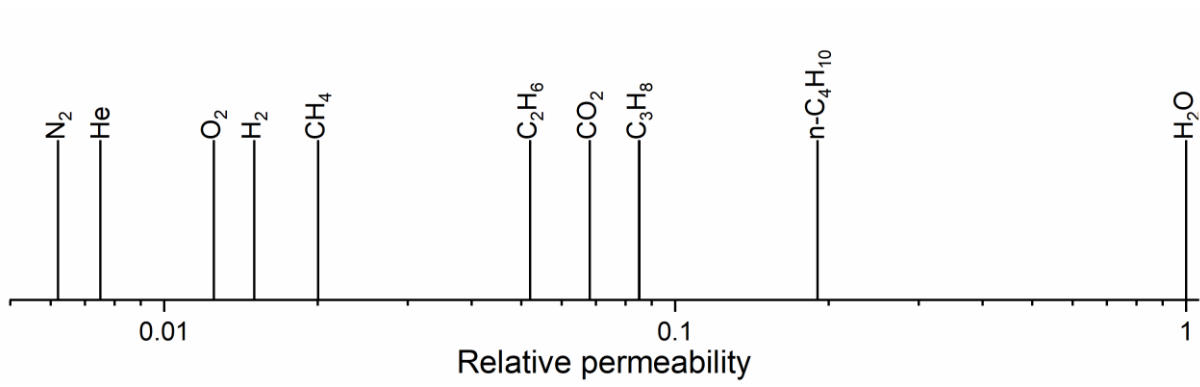
Figure 7: Relative gas permeability compared to water for PDMS. Redrawn from S. J. Metz.[133]

2.3.2 Synthesis of silicon monomers and polysiloxanes

Polysiloxanes (Figure 8) consists of linear or cross-linked Si-O bonds with Si-C and Si-H bonds, respectively. They are named M (monovalent), D (divalent), T (trivalent) and Q (quadrivalent) depending on the substitution pattern around the Si atom.[134] The terms silicone is often referred to polymers while siloxane is referred to oligomers which are linear molecules with up to nine repeating units (L$_9$), although no exact naming is defined.[135] Besides linear oligomers (L$_2$ to L$_9$), small cyclic units called cyclosiloxanes with three to six Si-O building blocks (D$_3$ to D$_6$) also belong to the group of siloxane molecules.[134]
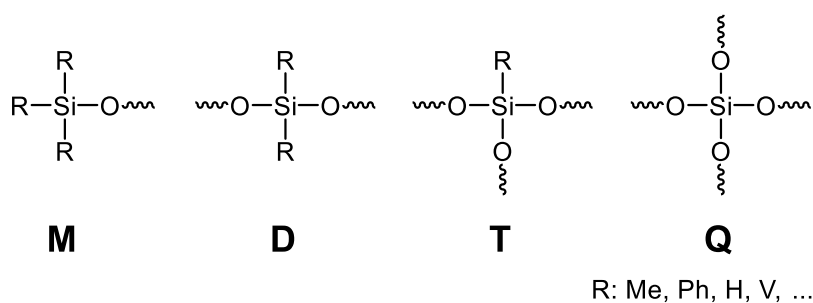
Figure 8: Structure elements of polysiloxanes.

The monomers with at least two alkoxide or hydroxide-groups can be polymerised using either a basic catalyst like *n*-tetrabutylammonium hydroxide or acidic catalyst like hydrochloric acid.[136-138] Under acidic conditions (Figure 9) the first step in the hydrolysis involves the fast proton addition.[139-141] A water molecule then reacts in a slow S$_N$2 reaction and releases an alcohol and a proton resulting in a λ^1-silanol. In the condensation step this new group is first protonated in a fast reaction and then another λ^1-silanol molecule reacts with the protonated species to form a new Si-O-Si bond under hydronium secession.
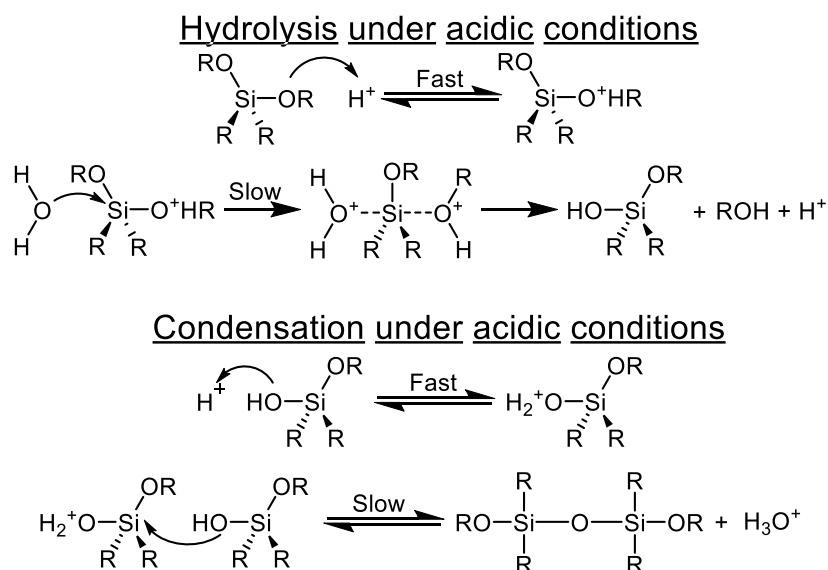
Figure 9: Mechanism of acid catalysed hydrolysis and condensation in a polycondensation.[139, 142-143]

For the acid catalysed reaction the rate-controlling step is the formation of the Si-O-Si bond which leads to more linear-like networks which are minimally branched with a low amount of siloxane bond and a high amount of silanol bonds.[139-142]

Under basic conditions (Figure 10) the first hydrolysis step involves a S_N2 reaction of the hydroxide to the silicon atom which results in an alkoxide leaving group.[139-142] In the condensation step another hydroxide deprotonates the λ^1-silanol in a fast reaction under water release. The resulting siloxide ion reacts nucleophilic with another λ^1-silanol in a slow reaction leading to a new Si-O-Si bond and a hydroxide. The base catalysed reaction has a high rate of condensation which leads to a dense and highly cross-linked network with fewer silanol-groups compared to the amount in the acid catalysed reaction.[139-142, 144]
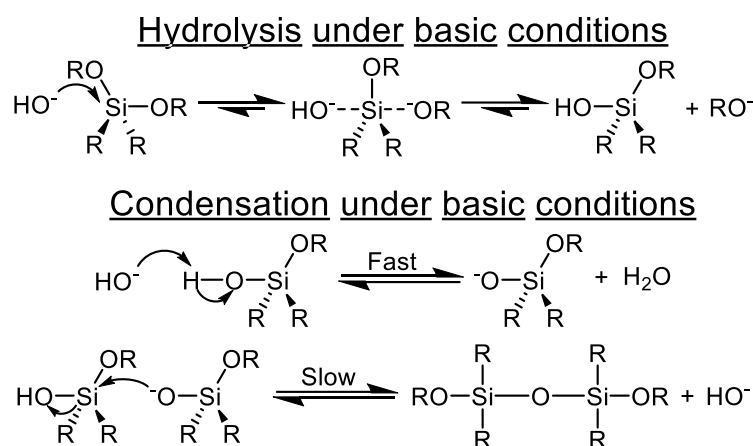

Figure 10: Mechanism of base catalysed hydrolysis and condensation in a polycondensation.[139, 142-143]

In Figure 11 the relative reaction speeds are shown for the hydrolysis and the condensation reaction under different pH values.[139, 142, 144]
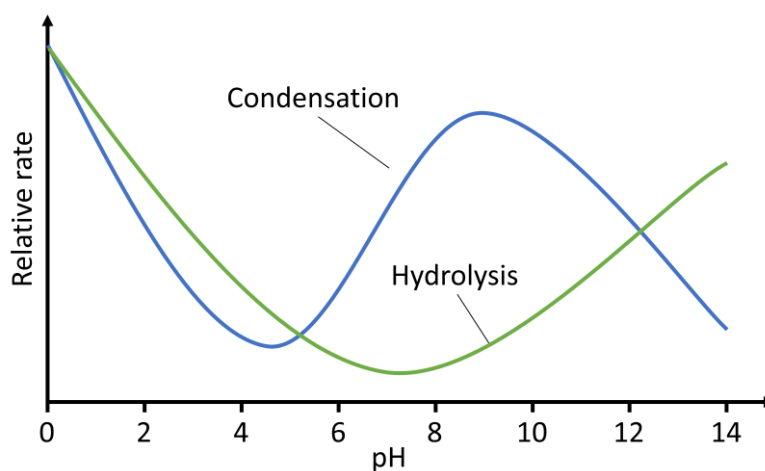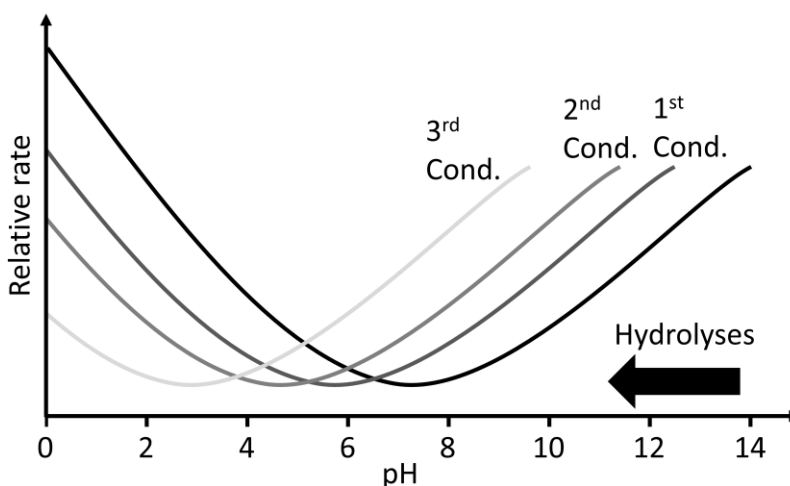

Figure 11: Relative reaction rate for condensation and hydrolysis depending on the pH value. Redrawn from Schubert *et al.*[145]

At low pH values between zero and five both reaction speeds are similar and decrease with increasing pH value starting from a high reaction rate.[142, 145] The reaction rate of the hydrolysis further slows down and reaches a minimum at pH seven.[142, 145] Afterwards the speed increases again to a medium fast reaction rate at pH = 14.[142, 145] Between the pH value of five to 14 the condensation rate increases up to a value of nine and then decreases again showing that the optimal pH value is around nine.[142, 145] Factors that also control the reaction speed are the type of alkoxide R. Because of sterical effects the speed of the hydrolysis is reduced in the order: $Si(OMe)_4 > Si(OEt)_4 > Si(O^nPr)_4 > Si(O^iPr)_4$.[145-146] The hydrolysis is affected by the amount of condensation reactions (Figure 12) which have occurred at the same silicon atom. The minimal turning point shifts with each reaction to lower pH values by about 1.2 pH values because the silanol acidity increases.[145, 147]


Figure 12: Hydrolysis relative reaction rate depending on the pH value and increase amount of occurred condensation reactions at the same silicon atom. Redrawn from Loy *et al*.[147]

The substitution pattern in polycondensation reactions is also relevant. An increased number of organic substituents from $Q < T < D < M$ silicon atom increases the hydrolysis reaction speed because of the higher electron density at the silicon atom.[145-146] The type of organic side-group only slightly changes the hydrolysation speed. The minimal turning point shifts towards lower pH values and overall is located slightly higher resulting in a decreased speed from phenyl > methyl > ethyl > propyl > butyl.[147-149] The hydrolysis and therefore also the condensation reaction according to Delattre *et al*. cannot be 100 % completed using sterical demanding monomers with a high amount of possible cross-linking reactions like methacryloxypropyl trimethoxysilane and water in stoichiometric amounts.[150] 5 % of unreacted methoxy-groups are still present after 14 days.[150]
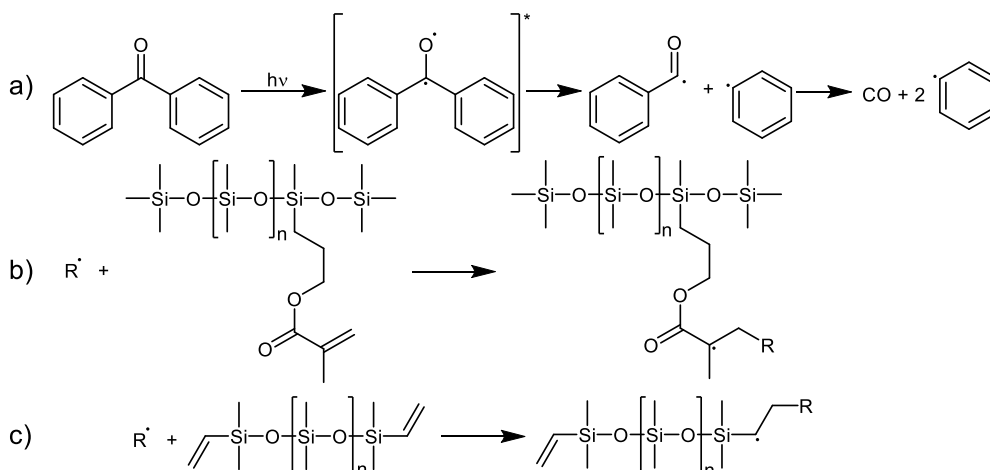
2.3.3 Cross-linking reactions

Sol-gel reactions can result in solid polysiloxanes with the downside that during the polymerisation, the alkoxide and hydroxyl-groups react to alcohol and water, respectively. This leads to release of partially poisonous gases in the case of methanol and to shrinkage of the material leading to mechanical stress. Another type of these one-component reaction is the curing through moisture at room temperatures (RTV rubber = room temperature vulcanising rubber).[151-153] The moisture curing mechanism for the organotin carboxylate-catalysed hydrolytic condensation is similar to the sol-gel process. The main difference is that in a sol-gel process T and Q silicon atoms are present which form colloidal particles and in a RTV rubber long and already cross-linked polysiloxanes with mainly D silicon atoms are present and only a few alkoxide-groups are left for further cross-linking with an organotin catalyst like dibutyltindiacetate (Figure 13).[151]
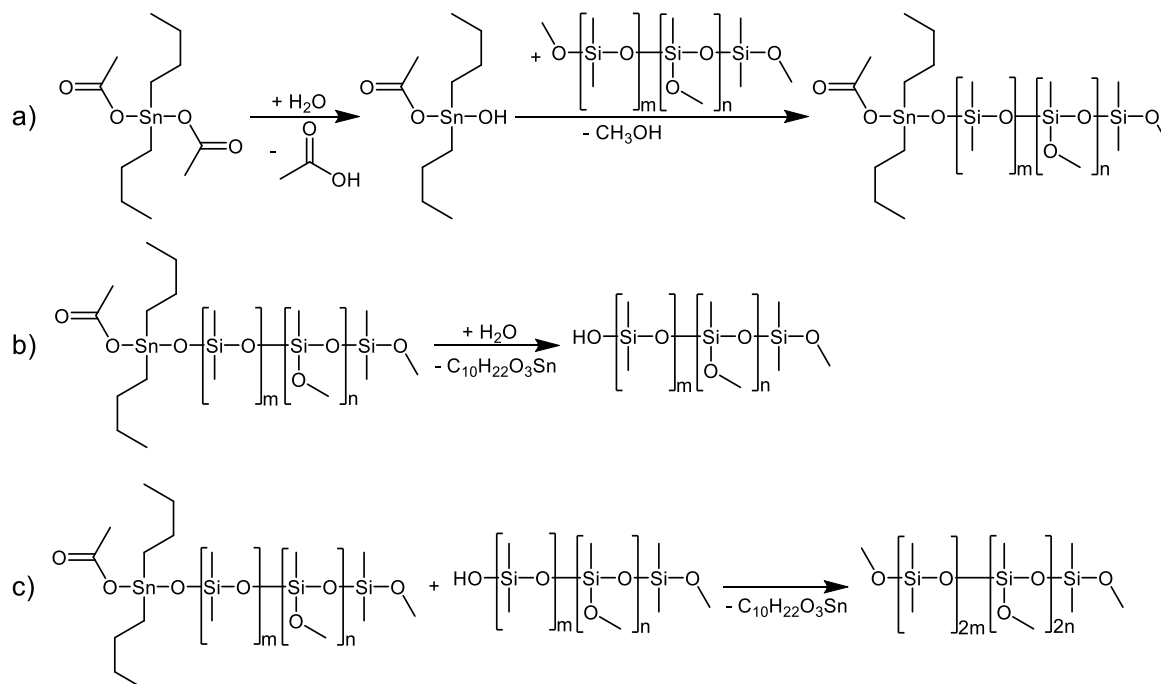
Figure 13: Reaction mechanism of the organotin carboxylate catalysed hydrolytic condensation. A) Formation of the reactive polysiloxane-tin-species, b) hydrolysis of this species and formation of a silanol-group terminated polymer and c) reaction of a) and b) resulting in a cured polysiloxane with the release of the active tin species R$_3$SnOH.[151]

The catalyst hydrolyses under acetic acid release and this unstable species reacts then with an alkoxide-group of the polysiloxane (Figure 13, a)).[151] The organotin-silicone terminated macromolecule hydrolyses to the silanol-group terminated polysiloxane (Figure 13, b)).[151] The active tin species a) and the silanol-group containing polymer b) then react under release of the active organo-tin catalyst towards a new polysiloxane (Figure 13, c)).[151] If reaction b) and c) occur at least three-times inside the cain, the result will be a cross-linked polymer.

To solve the problems of toxicity and shrinkage, the curing of one or two component systems is performed using addition reactions which show a shrinkage of below 1 %.[13-14, 154-155] The required special silicon homo- or copolymers were polymerised in a polycondensation process or ring-opening reaction. One possible class of compounds are methacrylate or vinyl side-group containing polysiloxanes which can be cross-linked in a photoinduced radical reaction.[156-160] This reaction is often used in one component systems and can be started at room temperature. The radical mechanism for the photoinduced reaction starts with the formation of an excited photoinitiator like benzophenone turning into an instable biradical (Figure 14, a)).[157-158] This decomposes into a benzoyl and a phenyl radical. The benzoyl radical further decomposes into CO and a phenyl radical. The chain propagation reactions can then be performed using methacrylate (Figure 14, b)) or vinyl-groups (Figure 14, c)).[157-158]


Figure 14: Photoinduced radical mechanism of silicone polymers for cross-linking using benzophenone as starter. A) photoactivation of the initiator, b) continuous chain propagation with methacrylate side-groups and c) a similar reaction applying vinyl-group induced cross-linking.[157-158]

Another possibility is the use of the thiol-ene reaction using vinyl (Si-V) and thiol (S-H) groups (Figure 15),[161-162] which can be cross-linked thermally, applying a direct photoinitiation without the use of a photoinitiator, or by using a thermally activated radical initiator like azobisisobutyronitrile (AIBN). In optical application the probably mostly used cross-linking reaction is the hydrosilylation between hydride (Si-H) and vinyl (Si-V) groups.[163-164]
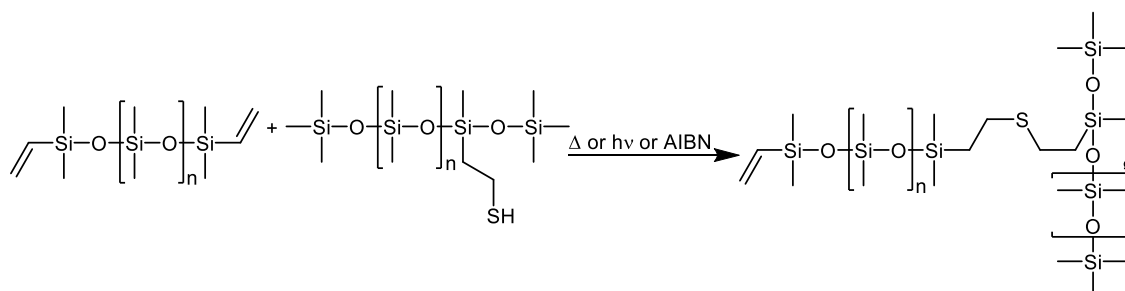
Figure 15: Thiol-ene reaction of polysiloxanes.[161-162]

Various catalysts can be used including iron, cobalt, nickel or even organic catalysts like tetrabutyl phosphonium chloride.[165] The most common commercially used catalyst types are platinum based.[163, 166-207] Five widely used catalysts are shown in Figure 16.[165, 172, 182, 208-209] The *Speier*'s catalyst was the first one used for hydrosilylation reactions, it is highly active but often requires a co-catalyst because it easily poisons.[182, 189, 209] The *Lamoreaux*'s catalyst has a low reactivity, increases the flammability resistance of silicones, and requires high temperatures around 170 °C to operate.[209-210] The *Karstedt*'s catalyst is the most known one since it is used in industrially available silicone mixtures because it already starts at room temperature and is already very fast at lower temperatures of around 100 °C.[209-212] The *Ashby-Karstedt*'s or just *Ashby*'s catalyst is used for cross-linking at moderately elevated temperatures around 60 °C.[209-210, 213] The *Osskos*'s catalyst is used when the curing is supposed to start at elevated temperatures around 100 °C.[209-210] One advantage of a catalyst which starts at higher temperatures is that solvent evaporates before the curing process starts, which avoids the formation of bubbles in the cross-linked material.
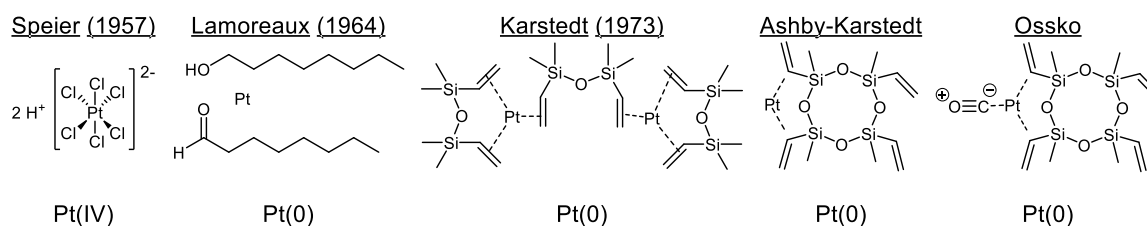
Figure 16: Commonly used platinum catalysts for the hydrosilylation reaction.[165, 172, 182, 208-209]

The Chalk-Harrod mechanism describes the platinum catalysed hydrosilylation reaction (Figure 17).[165, 172] The catalytic cycle starts with the activation of the catalyst by a ligand release. The oxidative addition with the silane results in a Pt(II) centre. The vinyl-group containing siloxane then coordinates to the metal centre. The vinyl-group insertion reaction can then occur according the Chalk-Harrod mechanism by transferring the hydrogen atom to the opened double bond while the silicon atom remains at the metal core. In a reductive elimination reaction this silicon atom is transferred to the opened double bond and the platinum is reduced to valence zero. The modified Chalk-Harrod mechanism describes the vinyl insertion reaction differently, the silicone atom is transferred to the double bond while the hydrogen atom remains coordinated at the platinum centre. The reductive elimination reaction then transfers this hydrogen atom to the carbon atom. The valence of the platinum is reduced to zero and the molecule or polymer is released, respectively. The addition for polymers occurs according to the anti-Markovnikov's rule because of the sterical hindrance of the silicone atoms neighbouring groups.[165, 214] For small molecules the hydrosilylation reaction can also happen according to Markovnikov's rule.[215-216]
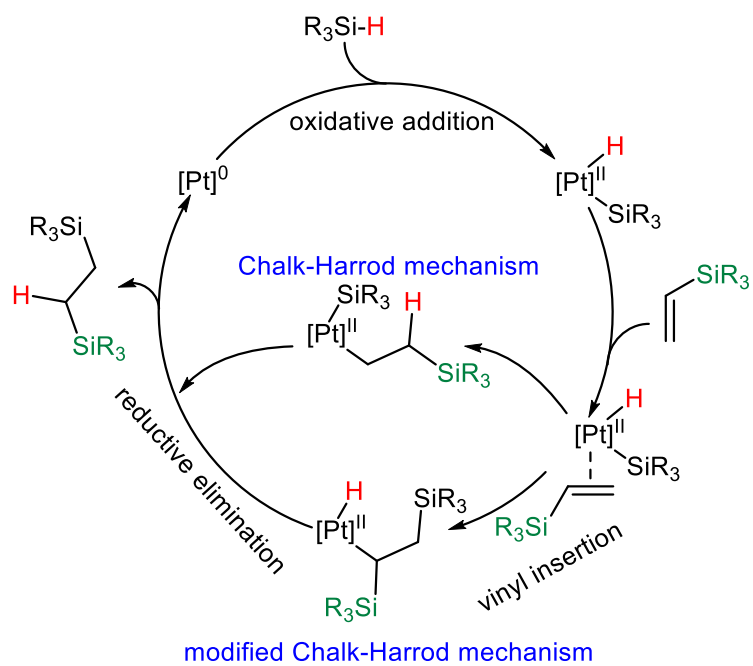
**Figure 17: Chalk-Harrod and modified Chalk-Harrod mechanism.[165]**

2.3.4 Thermal decomposition mechanisms

The special bonds present in polysiloxanes result in a different decomposition mechanism compared to the thermal degradation processes occurring in plastics. Linear siloxanes are known to decompose thermally in an intramolecular backbiting mechanism (IBBM) resulting in the elimination of small cyclosiloxanes like D_3 or D_4 (Figure 18 a).[119] This type of decomposition is facilitated if the polymer chains are long and flexible where at least four silicon D groups being present next to each other.[119] The activation energy is between 159 kJ/mol to 178 kJ/mol according to Dvornic and around 167 kJ/mol according to Grassie *et al.*[217-218] A similar decomposition mechanism is the intermolecular depolymerisation which occurs when two parallel linear polysiloxanes form a cyclosiloxane under chain rearrangements (Figure 18 b).[119] The other decomposition mechanism is called preliminary hydrolysis occurring at the end of the polymer chain in the presence of a silanol terminated linear silicon D chain with at least three silicon atoms and water which also results in the release of small cyclic molecules like D_3 or D_4 (Figure 18 c).[119] The activation energy here is lower with around 35 kJ/mol.[217-218]
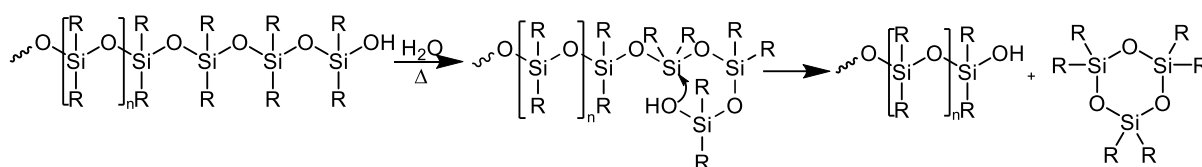
a) Intramolecular backbiting
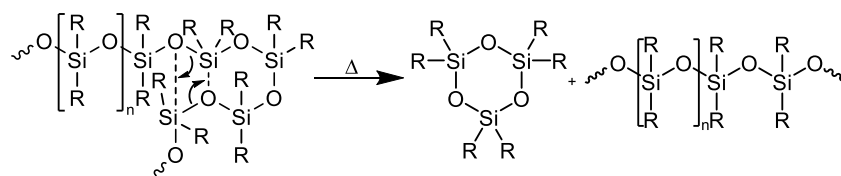
b) Intermolecular depolymerisation
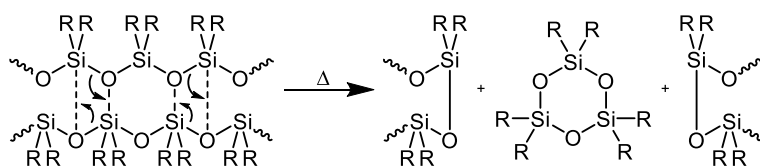
c) Preliminary hydrolysis

Figure 18: Thermal degradation mechanisms, a) intramolecular backbiting, b) intermolecular depolymerisation and c) preliminary hydrolysis.

Linear silanol-group terminated polysiloxanes have a similar decomposition temperature, here referred to 5 % mass loss, of 380 °C compared to the trimethylsilyl terminated ones with around 420 °C according to Grassie and Macfarlane.[217] The silanol-group can be removed in a target manner by adding chlorotrimethylsilane with a weak Lewis base like triethylamine (Figure 19).[219-221]
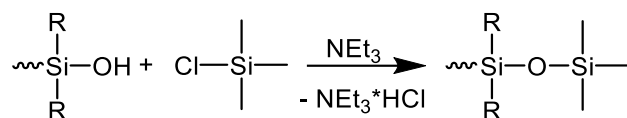
Figure 19: End group capping of silanol terminated polysiloxanes using trimethylamine and chlorotrimethylsilane.

If phenyl side-groups are also present besides methyl side-groups an additional decomposition reaction can occur.[222] Silanol end groups slightly reduce the thermal stability because of the preliminary hydrolysis but at the same time when a phenyl-group containing silicon D group is nearby the M + D group can react at around 300 °C to form a cross-linked T group under benzene release which then blocks the IBBM and increases the thermal stability.[218, 222]
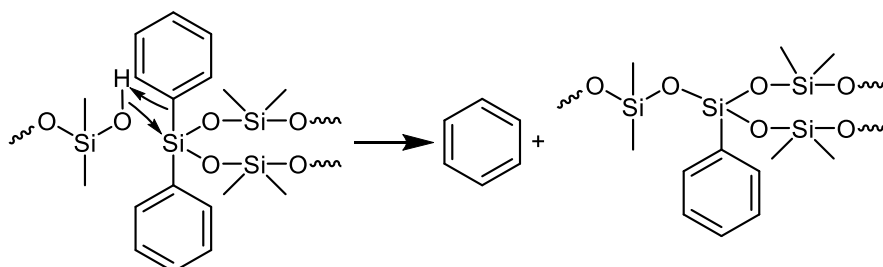
Figure 20: Benzene formation when a silanol M silicon atom and a phenyl-group containing silicon D atom react towards a silicon T atom.

After the polycondensation it is important to remove the remaining catalyst acid or base because they drastically reduce the activation energy for the thermal decomposition by a hydrolytical degradation reaction initiated by H^+ or HO^- down to around 130 °C which was shown by adding 5 % KOH to the earlier mentioned silanol terminated polysiloxanes according to Grassie and Macfarlane.[217] The reason for all of these degradation mechanisms is the presence of several silicon D atoms next to each other and therefore additional T or Q silicon atoms or D atoms with already cross-linked side-groups from the hydrosilylation reaction (2.3.3) need to be present. If exemplarily an IBBM occurs the volatile cyclosiloxane is not released from the polymer (Figure 21). A higher amount of cross-linking inside the material can be achieved by adding small highly hydride or vinyl functionalised molecules like Q-resins, $D_3^{H, Me}$ or $D_4^{V, Me}$ cyclosiloxanes.[223-225]
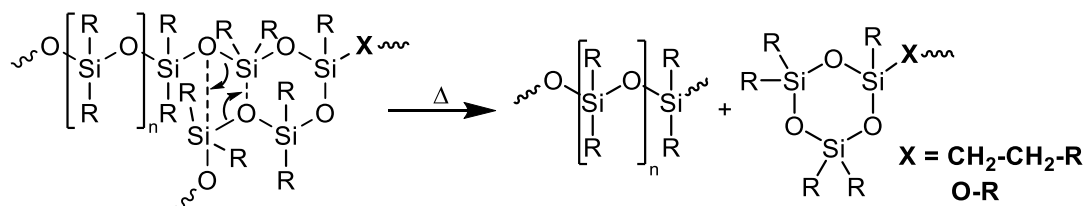
Figure 21: Intramolecular backbiting in the presence of a functional D atom or T group.

All described reaction mechanisms are present under oxygen or inert atmosphere. A different mechanism is the thermo-oxidative degradation which occurs at temperatures above 350 °C only in the presence of oxygen. The biradical O_2 starts the decomposition by the insertion in a C-H bond from a methyl side-group to form a peroxide. In the case of PDMS the decomposition products are ~25 % CO, ~17 % H_2O, ~4 % CH_2O, ~2 % CO_2, methanol, and formic acid.[119] The remaining solid at around 600 °C is pure silica.[119] The stability of the organic side-groups decreases from phenyl over vinyl over methyl to ethyl.[226]

2.3.5 Refractive indices of polysiloxanes

The refractive index of the encapsulant is important for the light extraction efficiency P_{out} of the LED. Because the diodes in high energy LEDs have a high RI of over 2.5, the RI of the encapsulant has to be high, ideally in the middle between the values of the chip and the lens. This results in the maximum amount of light extraction efficiency and therefore brightness of the LED. The difference of the RI's results in a change of the angle of the incident ray to the angle of the refracted ray (Figure 22) according to Snell's law (Equation (4) and (5)).[227]

$$n_1 \sin \theta_1 = n_2 \sin \theta_2 \tag{4}$$

$$P_{out} = \frac{P_{escape}}{P_{source}} = 1 - \cos\left(\arcsin \frac{n_2}{n_1}\right) \tag{5}$$

If the incident ray has an angle larger than the critical angle Θ_C total internal reflection occurs (Equation (6)). The critical angle therefore has to be as large as possible to reduce the amount of efficiency loss of the LED.

$$\theta_C = \arcsin\left(\frac{n_2}{n_1} sin\, \theta_2\right) \tag{6}$$

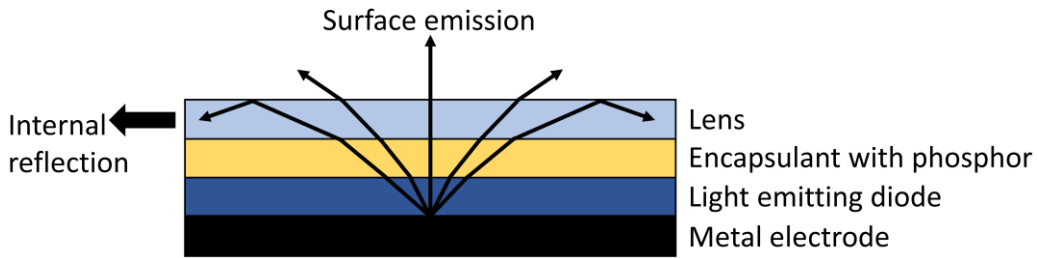**Figure 22: Light extraction paths inside a LED.[47]**

The efficiency for a GaN chip based LED with a RI of 2.5 depends on the RI of the encapsulant (Figure 23) as shown in equation (5).[137] The curve shape shows that the encapsulant has to have a RI of over 2.2 to achieve 50 % light output. The effect of a lens is here not considered.
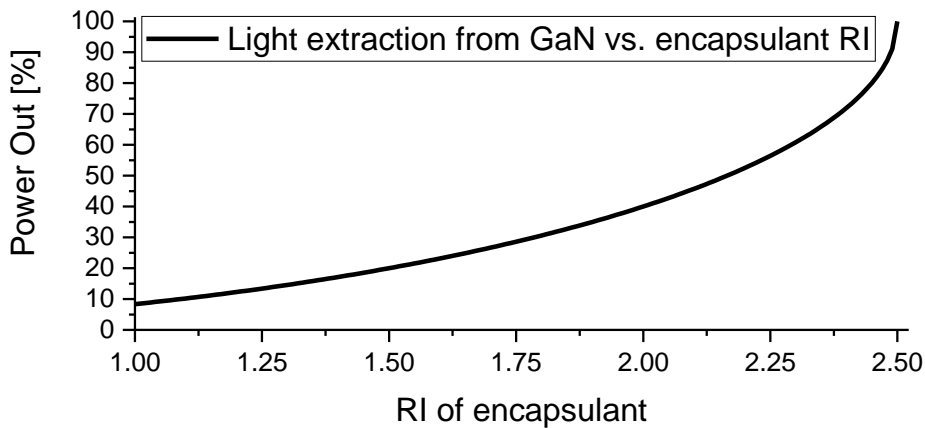

Figure 23: Light extraction from GaN depending on the encapsulant RI.[137]

The RI also has to be as high as possible because during the LED operation the generated heat decreases the RI of the polysiloxanes.[121] Commonly used encapsulation materials are divided into low refractive index (LRI) polymers and high refractive index (HRI) polymers. LRI polysiloxanes have a RI around 1.41 and consist of polydimethylsiloxanes like Shin-Etsu KJR 9022E-1.[13] HRI polysiloxanes have a RI of over 1.53 and consist of polymethylphenylsiloxanes and polydiphenylsiloxanes like Dow Corning OE-6630, respectively.[14] The RI of the HRI systems is still too low to archive a high light output when using high energy LED chips with a RI of over 2.5. For estimating the refractive index of polymers the Lorentz-Lorenz formula (Equation (7) and (8))[136] can be used.

$$\frac{n^2 - 1}{n^2 + 2} = \frac{\sum_i R_i}{\sum_i V_i} \tag{7}$$

$$n = \sqrt{\frac{1 + 2\sum_i R_i / \sum_i V_i}{1 - \sum_i R_i / \sum_i V_i}} \tag{8}$$

The empirical constants (Table 2) for the molar refraction (R_M) and molar volume (V_M) slightly vary depending on the source.[20, 136, 228-230] The RI can be increased by using atoms or groups with a high R_M/V_M value like phenyl or sulfur. When comparing the halogens, the RI impact increases with increasing atom size and electron amount, respectively.

Table 2: Empirical constants for the Lorentz-Lorenz equation.[20, 136, 228-230]

	Si	**O**	**S**	**Me**	**Ph**	**V**	**H**	**OH**	**F**	**Cl**	**Br**	**I**
R_M [cm³/mol]	9.00	1.62	8.3	5.90	25.8	10	1.40	2.44	0.95	5.97	8.86	13.9
V_M [cm³/mol]	31.2	9.05	16.6	25.8	74.1	39	10.3	12.2	18	24	30	31.5
R_M/V_M	0.29	0.18	0.50	0.23	0.35	0.26	0.14	0.20	0.05	0.25	0.30	0.44

2.3.6 Overview of recent literature

In the recent years, many different approaches were made to improve commercially available polysiloxanes or compare them with their own systems by using either nanocomposites, different organic side-groups or by incorporating metal atoms inside the polymer backbone. The OE-6630 system is used in various patents,[231-233] as well as in literature for comparing with self-synthesised systems, for example with a polydiphenylsiloxane (Figure 24) by Kim *et al.*[138, 234-235]
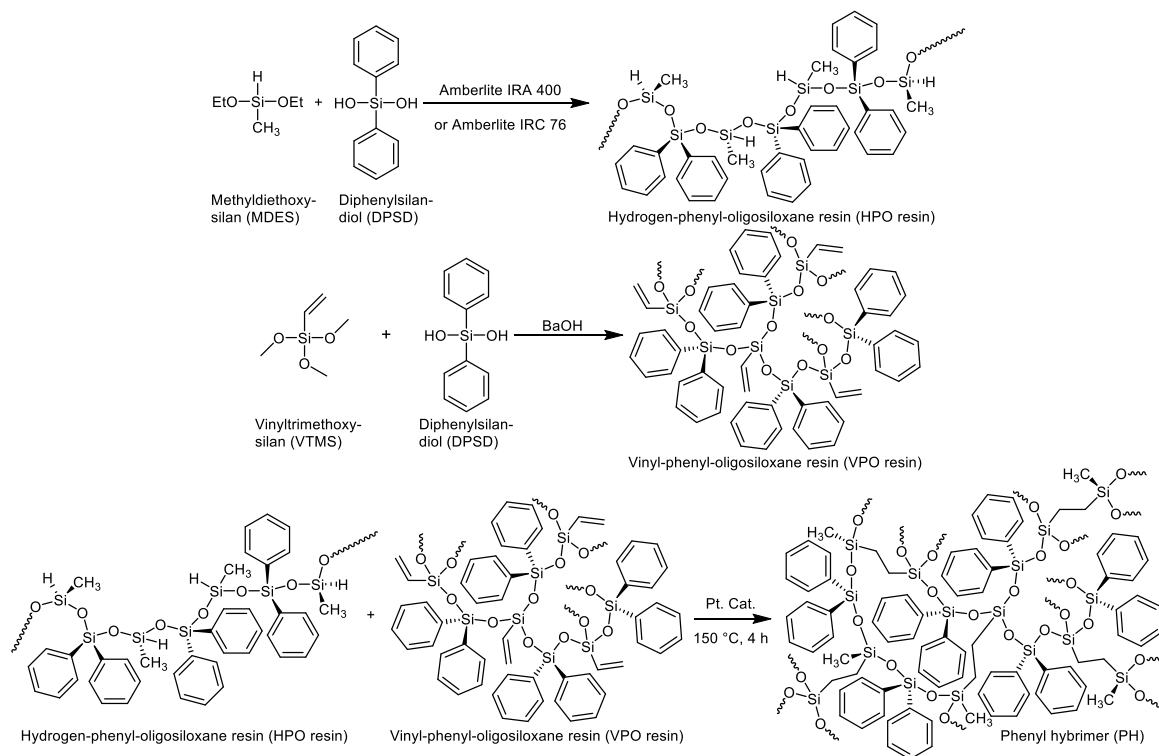
Figure 24: Synthesis procedure for the polydiphenylsiloxane by Bae *et al.* (Redrawn).[235]

They compared the refractive index, as well as the transmission and the photoluminescence of two fabricated LEDs during an aging test at 85 % relative humidity and 85 °C for 1008 hours with their own highly phenylic two component system to show the advantages.[234] They achieved a RI of up to 1.57 compared to the 1.53 of the OE-6630 and a transmittance of 90 % and a thermal stability with 5 % mass loss of 431 °C. [234]

In a later study, they also compared the OE-6630 system with their advanced highly phenylic polymer, which consists of up to 5 wt% zirconium.[138] Kim *et al.* could increase the refractive index up to 1.58 and a transmittance of 88 %.[138] They also compared the thermomechanical property, the luminous flux as well as the light extraction efficiency and changes in the CIE colour coordinates during an aging test at 85 % relative humidity and 85 °C for 1008 hours onto a fabricated LED chip.[138]

Yang *et al*. compared the OE-6630 system with their UV-curable polysiloxane with epoxide side-groups to be able to cure them with antioxidants and an oxetane cross-linker.[108] The anti-oxidants were used to drastically reduce the yellowing during the thermal aging at 120 °C for 1008 h.[108] The OE-6630 as well as the self-prepared system did not change the transmittance after the initial 90 %.[108] The refractive index is with 1.54 slightly higher than the one of the OE-6630.[108]

Chung *et al.* also compared their own zirconia rich polysiloxane with the commercial OE-6630 system to show the superiority of their system.[236] They synthesised methacrylate-group surface modified zirconia nanoparticles with a diameter of 6.6 nm.[236] Their one-component polysilox-ane consists of methyl, phenyl and methacrylate-groups which enables the cross-linking with BPO to receive a solid material.[236] They compared the viscosity, hardness, refractive index and luminescence intensity, which are all outstanding.[236] A transparency of 97 % with a refractive index of 1.62 could be achieved, but with a $T_{95\%}$ of 260 °C.[236] The relative output power under a "Temperature-Humidity Bias Life Test" showed that their system cannot endure these testing conditions.[236]

The OE-6630 polysiloxane was used in a study of Jang *et al.*, where they embedded up to 0.15 wt% graphene sheets into the polymer to reduce the high gas permeability, which was tested with hydrogen sulfide gas.[118] They also observed that these layers reduce the ratio of generated cracks form 65 % to 15 % in their test setup and increased the thermal conductivity by 260 %.[118] The thermal conductivity increased by 263 % und the thermal expansion coeffi-cient decreased by 92 %.[118] The transmittance dropped to 83 %.[118]

2.4   Methods for increasing the refractive index

The refractive index (RI) of the materials is mainly affected by the electrons and therefore by the elemental composition of the encapsulant. Thus, it appears that generally the incorporation of heavier elements in the material will have a positive effect on the RI. The used materials are siloxane-based, meaning that they consist of silicon, oxygen, carbon, and hydrogen, which are all relatively light elements with low refractive indices. Three main possibilities can be used for the incorporation of heavier elements in the materials. First is mixing the siloxane matrix with inorganic nanoparticles (e.g. TiO_2 or ZrO_2). The particles have to be colourless in order to receive a colourless encapsulant. Also, the size of the particles and their compatibility with the matrix which can be influenced by capping agents are important to obtain transparent materials. The difference in the refractive indices of the particles and the matrix is important. The nanoparticles can either be simply mixed into the matrix or covalently connected with it. Second is the modification of the siloxane matrix with heavier elements directly connected to the backbone formally carried out by replacing oxygen with sulfur or silicon with zirconium. This is possible by changing the precursor molecules in the synthesis of the silicone or by co-condensation in a non-hydrolytic polycondensation process. Third and last is the modification of the siloxane matrix by introducing larger aromatic moieties than phenyl-groups for example naphthyl or phenanthrenyl ones or by adding more organic-groups as well as high RI atoms using an ether or thioether bridge.

2.4.1 Synthesis of metal oxide nanoparticles

One method to increase the refractive index as well as the thermal conductivity is the incorporation nanoparticles into the matrix material.[17] These particles need special properties in order to receive a highly transparent polymer with an increased RI.[17] The RI of these particles has to be higher than the one of the matrix to overall be able to increase it. The particles need to be colourless, because otherwise the encapsulant would be coloured, which would decrease the transmission in the visible region. The particles have to be temperature-[237-238] and chemically stable[20, 239-241] as well as stable towards radiation in the area of 450 nm to 700 nm[20, 239-241], which is the case for most of the oxide nanoparticles.[20, 239-241] Because of the above mentioned reasons, ZrO_2 and HfO_2 were chosen as suitable nanoparticles for this thesis. The particles have to be smaller than the critical size that causes Rayleigh scattering to reduce the transmission loss.[17, 242-244] The amount of transmittance ($T = I / I_0$) can be estimated by the proposed formulas (9) from Novak *et al.*[245] and (10) from Nussbaumer[246], where λ is the wavelength of the light, χ the optical path length, Φ_p the amount of nanoparticles inside the matrix, r and n_p the radius and refractive index of the nanoparticles and n_m the refractive index of the matrix.[244]

$$\frac{I}{I_0} = e^{-\left[\frac{3\Phi_p \chi r^3}{4\lambda^4}\left(\frac{n_p}{n_m}-1\right)\right]} \tag{9}$$

$$\frac{I}{I_0} = e^{-\left[\frac{32\Phi_p \pi^4 \chi r^3 n_m^4}{\lambda^4}\left(\frac{\left(\frac{n_p}{n_m}\right)^2 - 1}{\left(\frac{n_p}{n_m}\right)^2 + 2}\right)^2\right]} \tag{10}$$

The estimated transmittance using formula (10) depending on the nanoparticle size is shown for 10.0 wt%, 20.0 wt% and 30.0 wt% of cubic ZrO_2 inside the OE-6630 polysiloxane in a 100 µm thick film at 450 nm wavelength (Figure 25). The transmittance is reduced by the number of nanoparticles as well as the particle diameter. To archive a high transmittance of over 90 % the particles have to be smaller than 10 nm when using 20.0 wt% or more.
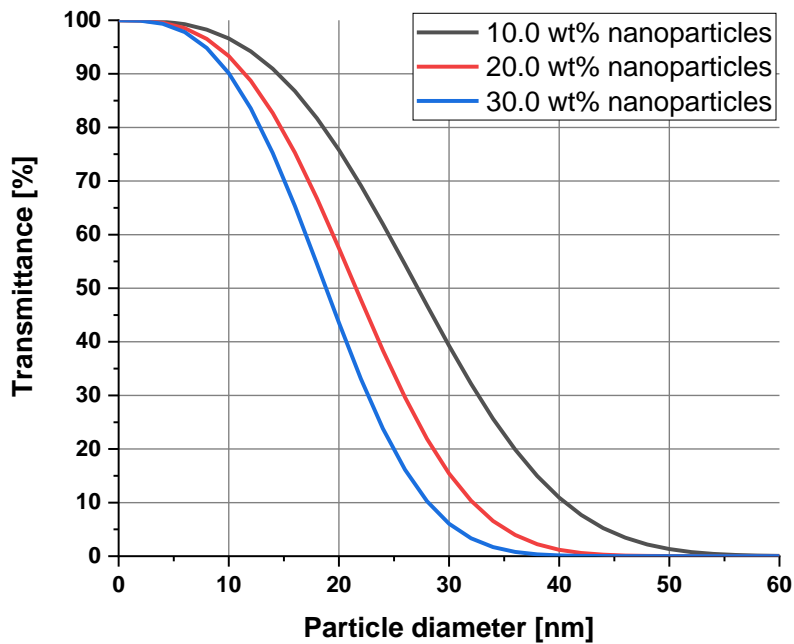
Figure 25: Estimated transmittance depending on the particle size of cubic ZrO₂ (RI = 2.1966 at 450 nm, stabilized with 12.0 mol% yttria)[247] inside OE-6630 (RI = 1.552 at 450 nm)[14] at 450 nm wavelength in a 100 μm thick film. (For HfO₂: RI = 2.142 at 450 nm with 9.6 mol% yttria for stabilisation).[248]

Four different synthesis routes (Figure 26) for the chosen metal oxide nanoparticles were performed during this thesis. Two high pressure solvothermal autoclave reactions were carried out,[238, 241, 249-250] where the chlorine route is not performed for the ZrO₂ synthesis and two ambient pressure solvothermal reactions were performed,[16, 251] where one solvothermal route can only be applied for the ZrO₂ synthesis. The reported size of the product particles is in the range of 2 nm to 10 nm.[16, 238, 241, 249-251]
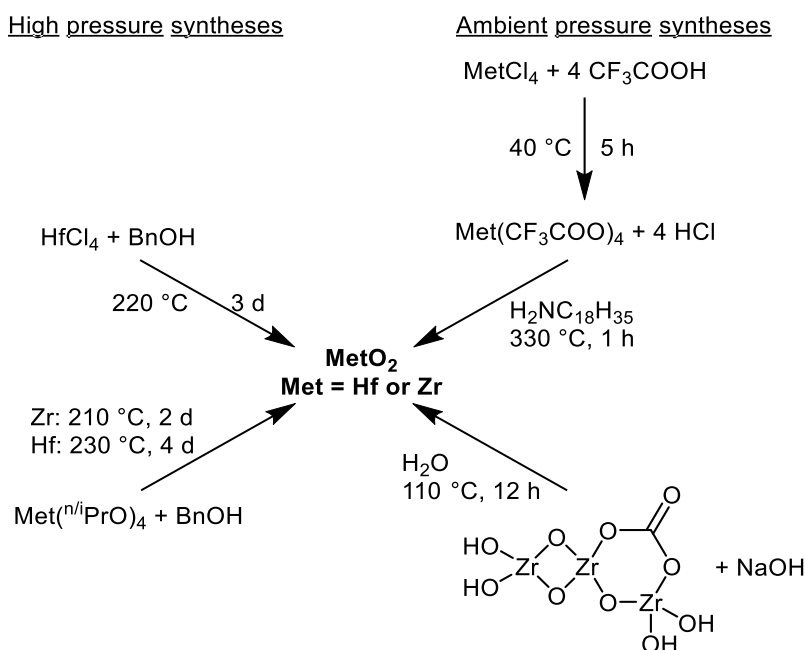

**Figure 26: Overview for possible syntheses of metal oxide (MetO₂ with Met = Hf or Zr) nanoparticles.**

The small nanoparticles can be incorporated into a polysiloxane matrix either by mixing them with the polymer[110, 239, 249, 252-255] or covalently bind them to the matrix.[242, 256-258] In both ways the particles have to be surface modified to receive a highly transparent and homogeneous nanocomposite.[110, 239, 242, 249, 252-258] Suitable anchor-groups for oxide nanoparticles are carboxylate-,[242, 256-257, 259-263] phosphonate-[242, 256-257, 263-266], or phosphate-[259, 266] groups. The carboxylates form weaker bonds to the surface than the phosphonates or phosphates because only two relatively weak bonds can be formed while the phosphorous compounds form three stronger ones.[242, 259, 263, 266]

2.4.1.1 Metal oxides starting from metal alkoxides applying an autoclave synthesis

The ZrO_2 synthesis route (Figure 27) from Garnweitner et al. uses a metal alkoxide precursor (Metal = Met) and benzyl alcohol (BnOH), which serves as reactant and solvent.[238, 249-250] The reaction was performed in a stirred stainless steel autoclave with a Teflon inlet. The received turbid suspension was centrifuged and washed with THF. After a postmodification with a carboxylic acid, the particles were dispersed in chloroform to receive a transparent suspension. While the authors used hexadecanoic, stearic, octadecanoic or oleic acid,[249] ^{n}Bu-PDMS-$C_{10}H_{20}$-COOH was used in this work for the incorporation in the commercial polysiloxanes. The synthesis was performed analogously with the hafnium alkoxide precursor where the temperature and reaction time have to be increased to form nanoparticles.
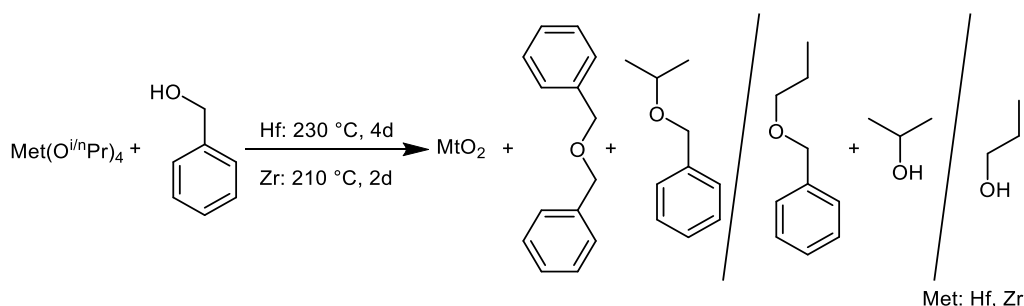
Figure 27: Synthesis overview for the nanoparticles from the alkoxide autoclave route.

The proposed reaction mechanism (Figure 28) by Stolzenburg et al.[238] starts with the substitution of an alkoxide with the benzyl alcohol. In the next step two alkoxide-groups bound to zirconium react to form a Zr-O-Zr bond as well as a benzyl ether derivate. This reaction continues and forms nanoparticles, some benzyl-groups remain at the surface and increase the stability of the suspension.
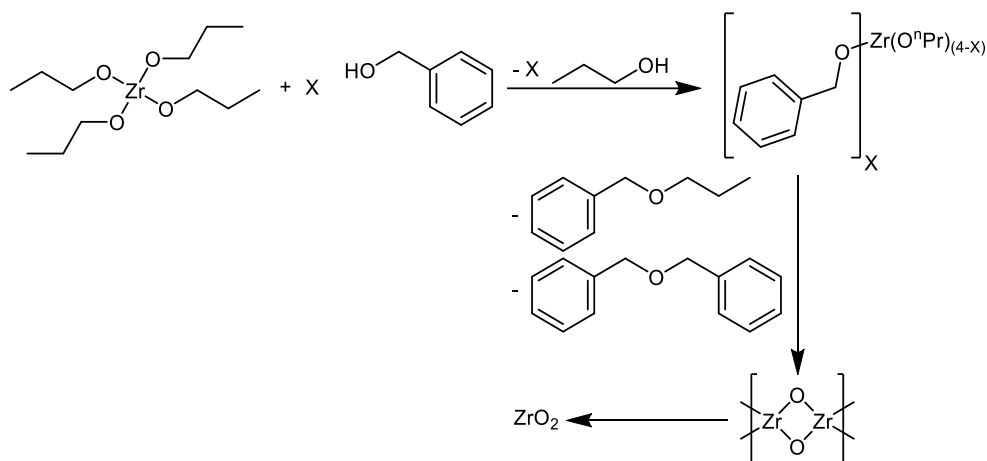
Figure 28: Proposed reaction mechanism by Stolzenburg *et al.* exemplarily shown for Zr(OⁿPr)₄.[238]

2.4.1.2 HfO₂ from chloride precursor obtained by the autoclave synthesis

The synthesis of HfO_2 nanoparticles (Figure 29) was carried by De Roo *et al.*,[267] which was adapted by Buha *et al.*'s patented reaction scheme.[268] The synthesis is described in two routes, a microwave synthesis and a solvothermal synthesis. The particles have a diameter of 8 nm to 16 nm in both cases. The $HfCl_4$ in benzyl alcohol was heated in an autoclave at 220 °C for three days. The postmodification was carried out with dodecanoic acid and oleylamine to receive a clear and stable particle suspension.[267]
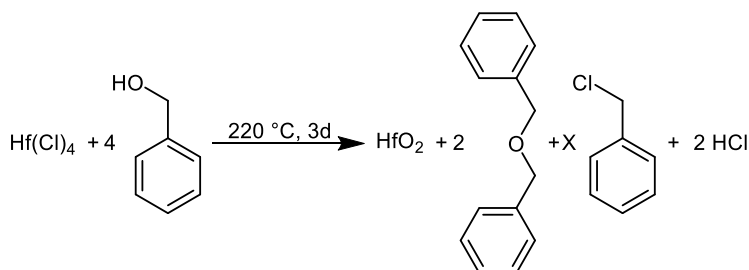

Figure 29: Synthesis of HfO₂ from the chloride precursor with benzyl alcohol in an autoclave reaction.

The reaction mechanism is analogue to the one shown in Figure 28, although the presence of HCl leads to about 1.5 % of different side products (Figure 30) as observed by De Roo *et al.*[267]
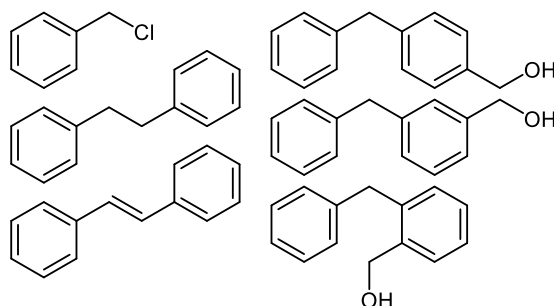

Figure 30: Side products of the HfO₂ synthesis from the chloride precursor observed by De Roo *et al.*[267]

2.4.1.3 Metal oxides starting from metal trifluoroacetates

In early 2015, Liu *et al.*[251] described a new method for the preparation of hafnium oxide nano-particles and in 2016 they expanded their synthesis route for ZrO_2 and TiO_2 to cover all group 4 metals.[16] The advantages of these synthesis routes are the short reaction time of one and a half hour and the abandonment of an autoclave. However, the temperature must be increased from around 220 °C to 330 °C. The received nanoparticles have a size of 5.0 nm to 5.5 nm for HfO_2 and 5.5 nm to 6.0 nm for ZrO_2 determined by XRD and TEM.[16, 251] The synthesis proceeds in two steps, the first involves the preparation of a stable, water and oxygen inert organometallic precursor (Figure 31) from a chlorine metal source.[16, 251] This synthesis was adapted by them from Sartori and Weidenbruch which reported the formation of $Zr(CF_3COO)_4$ in 1964.[269]

$$MetCl_4 + 4\ CF_3COOH \xrightarrow{\ 40\ °C,\ 5\ h\ } Met(CF_3COO)_4 + 4\ HCl$$

Met: Hf, Zr
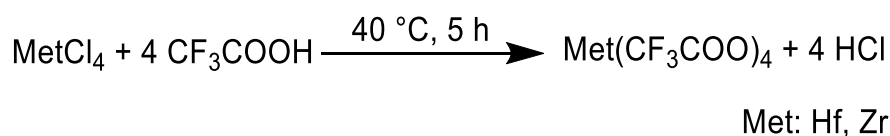
Figure 31: Metal (Met) trifluoroacetate precursor synthesis for hafnium and zirconium.

The received white powder is then heated with oleylamine to 110 °C under high vacuum for around 30 minutes until the suspension turns transparent and then to 330 °C under argon atmosphere for one hour to form nanoparticles (Figure 32). The oleylamine serves at the same time as solvent, reactant and surface modifier for the nanoparticles and hinders their aggregation because of the relatively strong Met-N bond.[270-271]

$$Met(CF_3COO)_4 + Oleylamine \xrightarrow[330\ °C,\ 1\ h,\ Ar]{110\ °C,\ 30\ min,\ vaccum} MetO_2$$

Met: HF, Zr
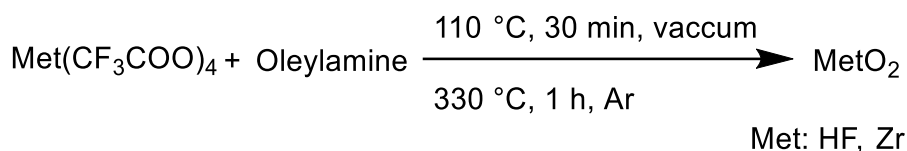
Figure 32: Nanoparticle synthesis with the trifluoroacetate precursor route.

The proposed reaction mechanism by Liu *et al.* is shown in Figure 33.[16, 251] The trifluoroester reacts with the oleylamine to form an amide and a free hydroxide-group at the metal centre. The further condensation then leads to the particle formation.
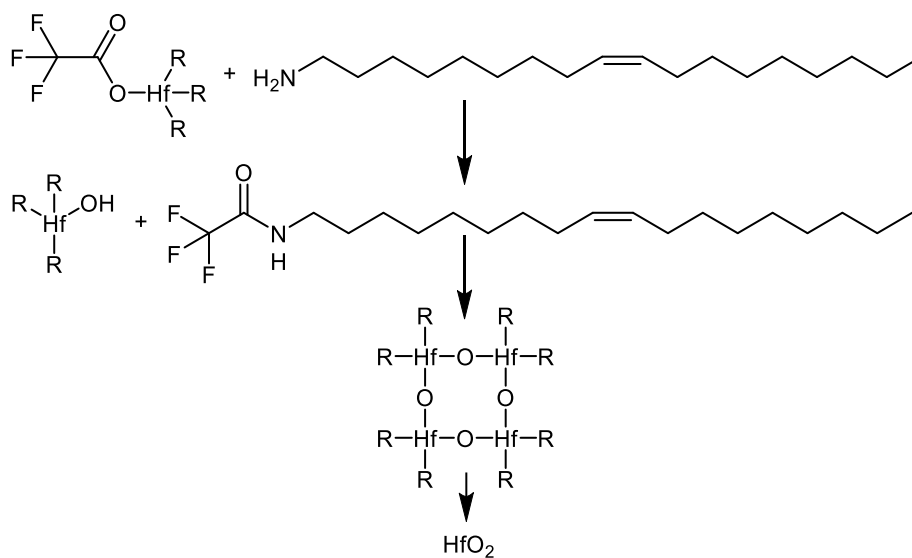
Figure 33: Proposed reaction mechanism by Liu *et al.* exemplarily shown for the hafnium route.[16, 251]

2.4.2 Synthesis of metal oxide nanoparticles for the covalent binding to self-pre-pared polysiloxanes

2.4.2.1 Synthesis of methacrylate-group containing polysiloxane for cross-linking with methacrylate-surface modified ZrO_2 nanoparticles

The previously mentioned syntheses include a surface modification of the particles with mon-ofunctionalised anchor groups to improve the miscibility of the particles with a polysiloxane. A different approach for the synthesis of nanocomposites is the covalent binding of the particles to the polysiloxane. Chung *et al.*[236] reported a triphenylsiloxane terminated poly[(3-methacry-loxypropyl)-*co*-dimethyl-*co*-diphenyl]siloxane (Figure 34) which does not contain any hydride or vinyl-groups for the cross-linking or curing, respectively. Instead, the cross-linking is per-formed by methacrylate-groups which are also present on the surface of the zirconium nano-particles. The curing reaction is therefore platinum free by using benzoyl peroxide (BPO) as radical starter. The advantage of the methacrylate-groups being covalently bound onto the na-noparticle surface is a denser and more stable network towards agglomeration or sedimentation. The colourless and transparent polymer with 3-methacryloxypropylsiloxane and butyric acid surface modified zirconium dioxide nanoparticles was then cured at 150 °C for four hours with benzoyl peroxide as radical starter. The nanocomposite reported by Chung *et al.* shows a major disadvantage during a heat treatment, because the methacrylate-group in this system leads to a yellow colouration of the film which is reported by the authors.[236]
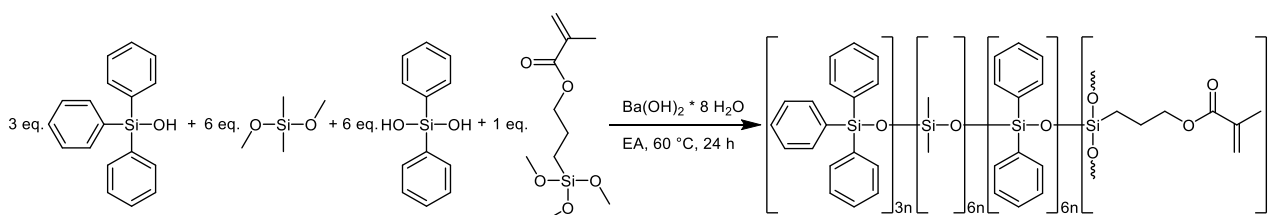
Figure 34: Reaction scheme for the synthesis of triphenylsiloxane terminated poly[(3-methacryloxypro-pyl)-*co*-dimethyl-*co*-diphenyl]siloxane.[236]

2.4.2.2 ZrO_2 from basic carbonate precursor

Chung *et al.* described a different synthesis without the use of an autoclave for ZrO_2 nanopar-ticles[236] adapted from the patent of Chiang *et al.*[272] Zirconium basic carbonate ($3ZrO_2 \cdot CO_2 \cdot yH_2O$) reacts with sodium hydroxide at 110 °C for twelve hours (Figure 35) to form cubic nanoparticles which should have a size of around 6.6 nm determined by TEM and XRD.[236] The postmodification was performed with butyric acid to increase the solubility and afterwards with 3-methacryloxypropyl trimethoxysilane to be able to covalently cross-link it with a polysiloxane matrix.[236]
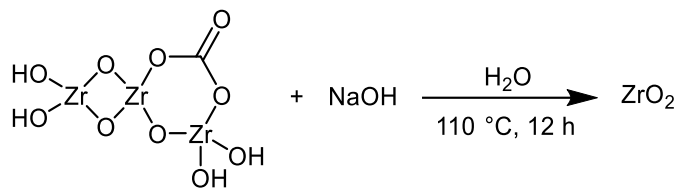
Figure 35: Synthesis of ZrO₂ nanoparticles from the zirconium basic carbonate route (structure of the zirconium precursor was redrawn from https://www.chemicalbook.com/CAS_12671-00-0.htm).

A reaction mechanism was not proposed by Chung *et al.*,[236] although because the zirconia network is already partially present, the further condensation should result in the formation of water and carbon dioxide.

2.4.2.3 Synthesis of the triphenylsiloxane terminated poly[(3-methacryloxypropyl)-co-dimethyl-co-diphenyl]siloxane

Chung *et al.* synthesised a methacrylate-group containing siloxane polymer to be able to covalently cross-link it with the surface modified nanoparticles.[236] Besides the methacryl-group only methyl and phenyl ones are present in the triphenylsiloxane terminated poly[(3-methacryloxypropyl)-*co*-dimethyl-*co*-diphenyl]siloxane. The composition of the polymer consists mainly of diphenylsilanediol (PP) and dimethoxydimethylsilane (MM) to form linear chains with each contributing 37.5 % of the total silicon content. The high methyl content ensures a low hardness, brittleness and viscosity of the polymer while the phenyl-groups increase the RI.[10, 121, 236, 273] 18.7 % of the silicon content result from triphenylsilanol (TP) which is used to terminate the chains and to keep the molecular weight low to achieve a low viscosity.[121, 273] For the remaining 6.3 % of the silicon content, a methacrylate cross-linker (MA) with three methoxy-groups was used, which serves as internal cross-linker for the polysiloxane and later as linker between the particles and the polymer. MA6.3_MM37.5_PP37.5_TP18.7 was polymerised in a basic sol-gel reaction at 60 °C for 24 h (Figure 34).[236]

2.4.3   Synthesis of HRI polysiloxanes by modification of the backbone

A different approach to increase the refractive index is the implementation of metal atoms inside the siloxane chain.[138, 274-275] Usually, electron rich metals with an oxidation number of +4 are used like zirconium or titanium.[138, 274-275] Kim *et al*. already prepared metal-containing polysiloxanes.[138] These contained up to 5 % zirconium, but the ones with 5 % have a low transmittance of 80 %. For these reasons, the topic will be analysed to find out whether the refractive index can be increased as described in the literature by the metal atom incorporation into the backbone of the siloxane network.[10] In addition, other metal atoms were incorporated and the properties of the hydride, vinyl and cured polysiloxanes were investigated, respectively. Also, the metal content was increased to evaluate their potential. With their four possible bonds (Figure 36), these metal atoms can increase the cross-linking inside to polymer compared to the D silicon atom when comparing them to the cross-linkable hydride or vinyl-group containing silicon atoms.
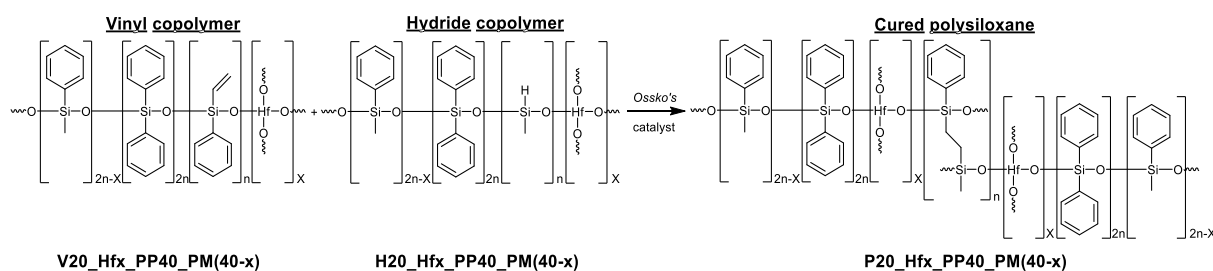
Figure 36: General synthesis scheme of the hydrosilylation reaction of a hydride- and vinyl- as well as hafnium-containing copolymer to the cured polysiloxane.

Because of the increased cross-linking, Kim *et al.* could not produce crack-free films with a zirconium content over 5 %.[138] Also, the use of tetravalent atoms can increase the cross-linking so much that not all four bonds can be established, hydroxide or alkoxide-groups remain. Other metal atoms besides zirconium from the titanium-group 4 like titanium or hafnium can also be used. Also, the more electron-rich tin is comparable to silicone and therefore very suitable as substituent because of the chemical similarity towards reactions since both belong to the carbon-group.[276-277] Using tin leads to some problems, on one hand tin also favours the oxidation state +2 beneath the desired +4 which can result in side reactions because of the redox activity or in the formation of complexes.[278-281] Tin(II) is more toxic compared to Tin(IV).[282] On the other hand tin can interfere with the platinum, which is used to catalyse the hydrosilylation reaction, in unintentional side reaction for example with the Si-H group.[164, 283-291] Tin can be used as a catalyst instead of an acid or a base for the sol-gel or polycondensation reaction, later one used in so-called room temperature vulcanised (RTV) silicone rubbers.[292] These systems use tin in a moisture catalysed condensation reaction and therefore leads to shrinking during

the curing process. This unwanted curing process is neglected when using only M or D silicon monomers and additional hydride respectively vinyl-groups for a second addition reaction catalysed by platinum. In contrast though, this leads to the advantage that the amount of not condensated or hydrolysed monomers respectively end groups is reduced. Adding early-transition metals like zirconium and titanium support the platinum catalysed hydrosilylation reaction.[138, 293-296] The hydrolysis reaction rate of metal oxides is up to 10^5 times faster than the silicon alkoxide one because of the increased Lewis acidity in the order $Si(OR)_4 <<< Sn(OR)_4$, $Ti(OR)_4 < Zr(OR)_4$.[145-146] Because this faster reaction time often leads to the formation of metal oxide particles, bidentate ligands like acetylacetonate can be used to slow down the hydrolysis because of their sterical hindrance.[145-146]

Kim *et al.* used 25 % vinyltrimethoxysilane, 20 % methyldiethoxysilane and 55 % diphenylsilanediol for their metal-free polysiloxane (Figure 37) and added 1.0 mol%, 3.0 mol% and 5.0 mol% of zirconium *n*-propoxide relative to the silicon atom content.[138] These polysiloxanes have therefore a high density of cross-linking because of the high amount of hydride and vinyl-groups and the additional cross-linking introduced by the silicon T group from the vinyltrimethoxysilane. Also, since more vinyltrimethoxysilane than methyldiethoxysilane was used, 5% of unreacted vinyl-groups should remain inside the polysiloxane.
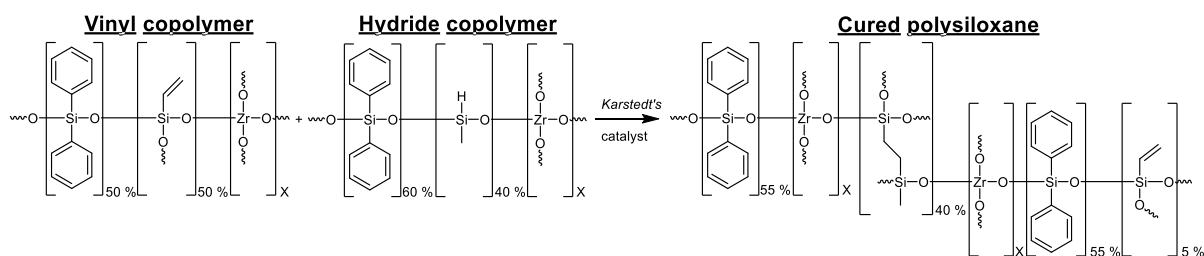

Figure 37: Reaction scheme for the zirconium-containing polysiloxanes by Kim *et al.*[138]

2.4.4 Synthesis of HRI polysiloxanes by modification of side-groups

The third possibility to increase the refractive index is the use of larger aromatic side-groups. The higher aromatic content is realised by either applying ether or thioether bridges for the introduction of an additional phenyl-group as described by Mosley *et al.*[136] or by the use of condensed aromatics. The high transmission and the high thermal stability have to be remained also under the operating conditions of high energy LEDs like long term thermal treatment and radiation stability in the range of the operating LEDs chip. Mosley *et al.* already synthesised phenoxyphenyl and phenylthiophenyl-group containing polysiloxanes.[136] These polymers are highly temperature stable and show a high transmission of over 90 % during a thermal heat treatment at 200 °C. Refractive indices of 1.60 at 633 nm for the phenoxyphenyl polymer and 1.62 at 633 nm for the phenylthiophenyl one were achieved.[136]

2.4.4.1 Synthesis and characterisation of phenoxyphenyl-group containing polysiloxanes

Mosley *et al.* described a Grignard reaction for the synthesis of 4-(phenoxy)phenylphenyl-dimethoxysilane (POPP) starting from 4-bromodiphenylether and phenyltrimethoxysilane (Figure 38).[136]
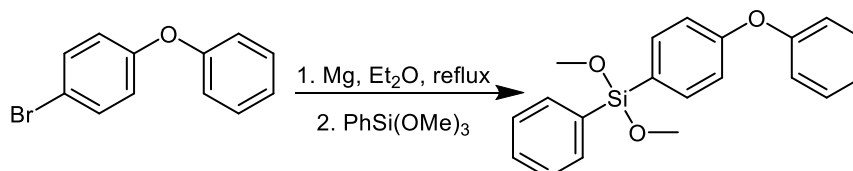

Figure 38: Grignard synthesis of POPP performed by Mosley *et al.*[136]

With this monomer and methyl, phenyl, hydride and vinyl-group containing silicon monomers, they synthesised two copolymers for the hydrosilylation reaction (Figure 149).[136] For the vinyl copolymer they used 34.5 % POPP, 52.4 % diphenyldimethoxysilane and 13.1 % phenyltri-methoxysilane and achieved a refractive index of 1.60 and a T_g of 2.5 °C. For the hydride co-polymer they used 60.0 % methylhydrocyclosiloxanes and 40.0 % diphenyldimethoxysilane and determined a refractive index of 1.56 and a Tg of –60.0 °C. Both copolymers were cross-linked using *Ossko*'s catalyst and a T_g of 23 °C was measured.
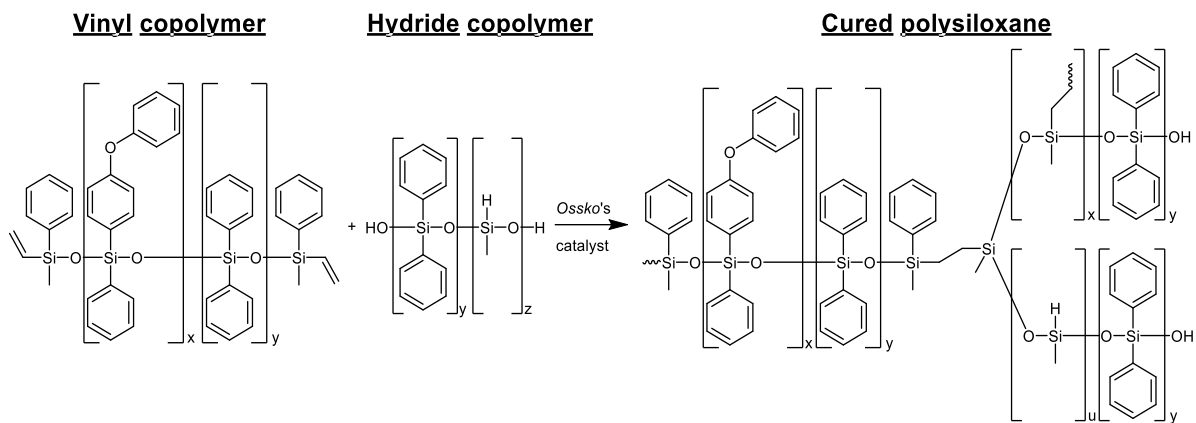
Figure 39: Chemical structure of vinyl and hydride copolymers as well as the cured polysiloxanes.[136]

2.4.4.2 Synthesis and characterisation of phenylthiophenyl-group containing polysiloxanes

The second system invented by Mosley et al.,[136] involves a phenylthiophenyl side-group, which is also interesting, because of the even higher refractive index of the cured polymer with 1.62 at 633 nm. The only reason for this increase is the substitution of the oxygen atom with sulfur in the ether bridge because the rest of the synthesis procedure was maintained. Instead of the classical Grignard reaction they performed a Barbier-based procedure staring with magnesium, iodine, MeMgBr and trimethoxyphenyl silane. They then added the 4-bromodiphenyl sulfide in tetrahydrofuran (Figure 40).[136]
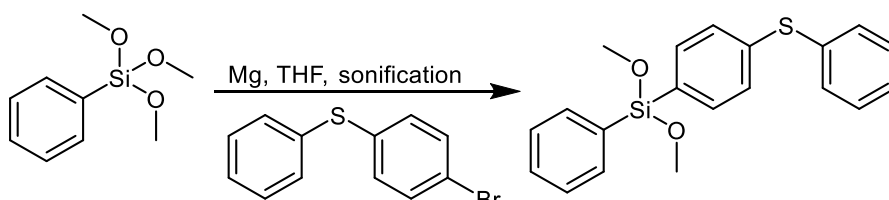

Figure 40: Synthesis of PSP described by Mosley et al.[136]

For the vinyl copolymer they used 79 % POPP, 8 % tetramethyldiethoxydisilane and 13 % phenylmethylvinylmethoxysilane and achieved a refractive index of 1.62 and did not report a T_g.[136] For the hydride copolymer they used the same as in the phenoxyphenyl-group containing hydrosilylation reaction. They reported a high viscosity of the hydride and vinyl polymer and therefore had to heat them up between 60 °C to 80 °C in order to be able to mix them properly.[136] Because of the high temperature during the mixing they used *Ossko*'s catalyst to increase the shelf-life as well as the inhibitor 3,5-dimethyl-1-hexyn-3-ol.[136] Both copolymers were cross-linked using *Ossko*'s catalyst (Figure 41).[136]
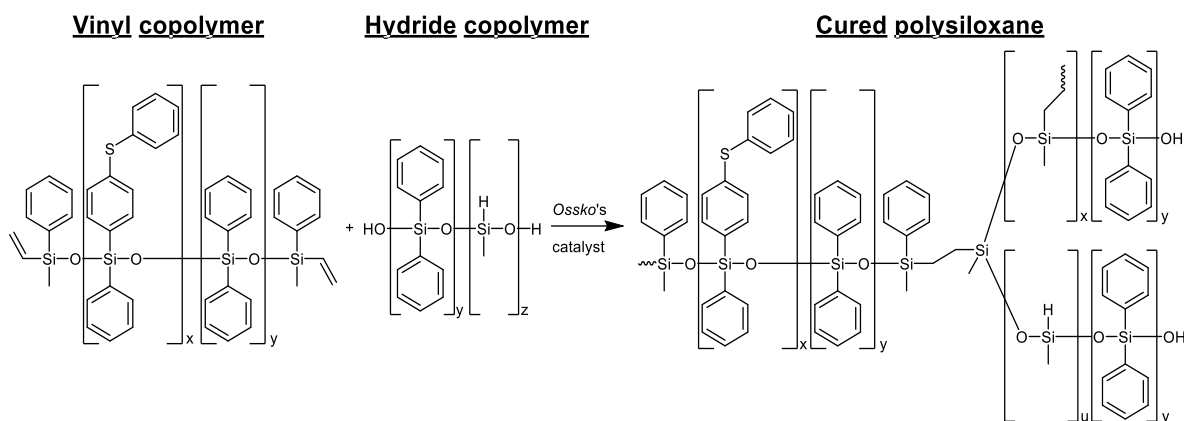
Figure 41: Chemical structure of vinyl and hydride copolymers as well as the cured polysiloxane.[136]

2.4.4.3 Synthesis of highly aromatic side-group containing polysiloxanes

Another approach to introduce more "phenyl-groups" and raise the RI is the use of conjugated aryl-groups like the naphthyl,[297-298] anthracenyl[299] or pyrenyl[300] ones, although their use in literature is not the high RI. The naphthyl-group containing polymers (Figure 42, a)) were used for stationary phases for capillary column gas chromatography by Lee *et al*. in 1984.[297] The anthracenyl-group containing polysiloxane (Figure 42, b)) was used for fluorescence spectroscopy investigations regarding the thermal relaxation processes by Dominguez *et al*. in 2010.[299] The pyrene-group containing polymer was used as solubilising agent for single-walled nanotubes (Figure 42, c)) by Lu *et al*. in 2013.[300] Larger conjugated aryl-groups like perylene are not suitable because they absorb the light emitted by the blue chip and therefore are coloured.[52, 301-302]
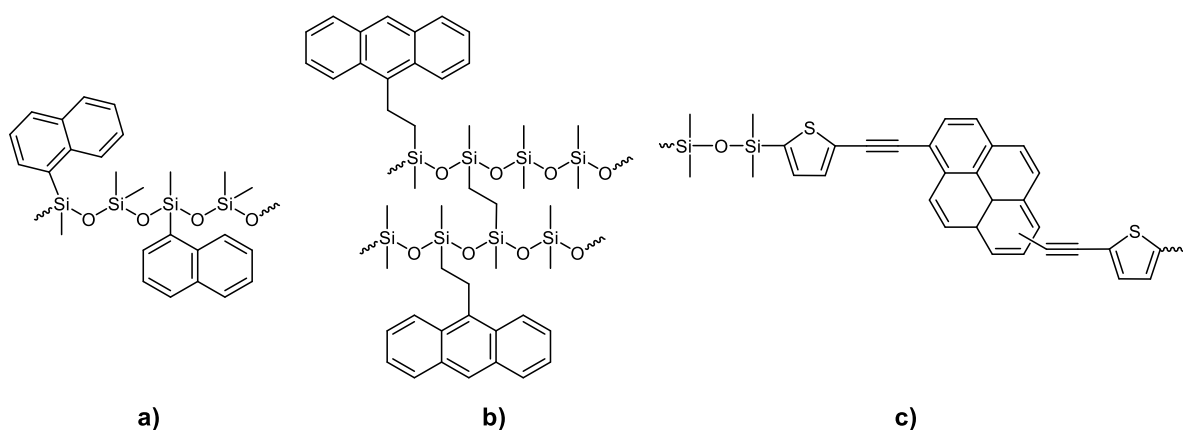

a)   b)   c)

Figure 42: Polysiloxanes containing a) naphthyl-, b) anthracenyl- and c) pyrenyl-groups.[297, 299-300]

3   Goals of the thesis

In this thesis possibilities for increasing the refractive index using three different approaches were investigated. The thermal stability as well as the high transparency of these new LED encapsulation materials must be close to the commercial used ones in order to make them attractive for industry. An ideal LED encapsulant should have the following properties: a high stability concerning aging by irradiation and thermal stress, a high thermal conductivity, a high refractive index, good adhesion characteristics, a low permeability for water and oxygen, a good mechanical strength and a good processability.[15-20] Polysiloxane based polymers show a very high potential to fulfil most of these properties. In addition, they allow a chemical tailoring comparable to epoxy resins, to fulfil specific properties.

The optimisation of the materials was based on approaches of previous research projects between *OSRAM Opto Semiconductors* and *Saarland University*.[223-224, 303] These assisted in the development of suitable improvement concepts both for commercial available silicones and for a novel polysiloxane (KAIST system).[138]

Within this work several subprojects should be investigated, which are described in the following chapters:

3.1   Investigation of the structure and the properties of the commercial polysiloxanes

Full characterisation of the composition of commercial two component encapsulants provided by *OSRAM Opto Semiconductors,* which were fabricated by Shin-Etsu and Dow Corning: in detail the polydimethylsiloxane Shin-Etsu KJR-9022E-1[13] and the polymethylphenylsiloxane Dow Corning OE-6630[14], were characterised for reason of comparison to self-synthesised materials. The copolymers and the cured films will be investigated using FT-IR, NMR and UV/Vis spectroscopy, TG, TG-FT-IR, DSC and SEC measurements and RI and viscosity determinations as well as studying the colouration using thermal aging.

3.2   Zirconium and hafnium oxide nanoparticles

Beyond the already successful approaches for a better cross-linking in commercial silicones via the use of molecular additives,[223, 303] the present project aims at the investigations for increasing the refractive index using ZrO_2 and HfO_2 nanoparticles as additives in encapsulation materials for blue LEDs,[5, 10, 267-268, 304-307] which may help to fulfil both targets. For this reason, both types of nanoparticles have to be synthesised and characterised. The nanoparticles have to be tailored to be miscible with the used encapsulation materials. Additionally, the final nanocomposites

have to show a high transparency with low yellowing index. Hence, modified surface-modifications of the particles with tailored molecules are necessary to fulfil these basic requirements.[308-309] Furthermore, the nanoparticles should be cross-linked with tailored one component polysiloxanes to achieve novel nanocomposites.

Zirconium and hafnium oxide are chosen because of their high refractive index of above 2.0. The refractive index must be higher than the one of the used polysiloxane matrices (Shin-Etsu KJR-9022E-1: 1.410 and Dow Corning OE-6630: 1.552). Additionally, the particles must be colourless (at most slightly yellow), to receive a transparent, colourless film for LED encapsulation. The incorporation of zirconium and titanium oxide nanoparticles is literature known for epoxide and silicone encapsulation materials,[17, 310-311] indicating that hafnium oxide nanoparticles may also work because of their chemical similarity (group 4 elements). Oxide particles are used because of their low toxicity and high thermal stability under oxygen atmosphere.[312-314] Furthermore, the literature shows that a covalently binding of the particles to the polysiloxane network is suitable for LED applications; therefore this topic is also studied.[17, 19, 117, 236, 310-311, 315] Different bottom-up preparation methods for the synthesis of the particles should be compared. The particle formation is investigated using TEM images, DLS measurements and XRD analyses. The surface modification will be studied using FT-IR and NMR spectroscopy and TG measurements. The incorporation into polysiloxanes will be investigated using FT-IR and UV/Vis spectra, TG and DSC measurements and the RI determination.

3.3 Integration of electron rich metal atoms inside the polysiloxane backbone

In a third step, the tailor-made encapsulation material should be modified to obtain a reduced amount of organic-groups due to potential higher thermal stability in combination with increased refractive index. One goal was the substitution of silicon atoms in the polymer chain against group 4 metals (Hf, Zr), which was partially already discussed in literature,[138, 277, 316] as well as silicon similar elements like tin and an electron rich element (Ta). In addition, studies on the impact of the resulting composition on the final mechanical properties as well as the process ability. The copolymers and the cured film will be investigated using FT-IR, NMR and UV/Vis spectroscopy, TG and DSC measurements and RI and viscosity determinations as well as studying the colouration using thermal aging.

3.4 Kinetic study of the polycondensation reaction

The fourth part of the thesis includes a kinetic investigation of the acid and basic catalysed polycondensation reaction. Kinetic studies and characterisation of the obtained polymers applying FT-IR, SEC and NMR are necessary to reach important information on the development of the polymeric systems.

3.5 High refractive index side-groups

An additional goal was the development of novel systems based on a hybrid material developed by the Korea Advanced Institute of Science and Technology (KAIST)[138] as well as by *Mosley et al*. and Chung *et al*.[136, 236] Based on these published concepts, further optimisations via compositional and structural changes will be carried out by synthesising new promising monomers with phenoxyphenyl, methylthiophenyl and phenanthrenyl side-groups using Grignard reactions which are studied using FT-IR and NMR spectroscopy and single crystal analyses. The copolymers will be synthesised using polycondensation reactions with liquid catalysts. The cured films will be investigated using FT-IR, NMR and UV/Vis spectroscopy, TG, DSC and SEC measurements and RI determinations as well as studying the colouration under thermal aging. A further increase of the refractive index seems to be accessible if highly polarising elements such as oxygen or sulfur are incorporated into the side-groups.[136-137, 235, 317-319]

3.6 Testing performed by OSRAM Opto Semiconductors

In the last part of the studies *OSRAM Opto Semiconductors* will test selected polysiloxane systems on operating LED chips to evaluate the thermal and radiation stability of the encapsulant at operating LEDs.

4   Results and discussion

4.1   Characterisation of the commercial polysiloxanes and catalysts

The overall aim of the thesis is the development of new polysiloxanes with refractive indices that exceed those of commercial applied systems. Two different systems were investigated in order to compare the properties of the newly synthesised polymers with commonly used systems. Therefore, a complete analysis applying NMR and FT-IR spectroscopy, TG and DSC measurements was necessary. In addition, the viscosity and refractive index has to be determined, as well as the transparency, haze value and thermal stability with a thermal treating test. The first investigated commercially available encapsulation system was the KJR-9022E-1 from Shin-Etsu Chemical (Chiyoda, Japan), which is a low refractive index (LRI) polydimethylsiloxane-based polymer.[13] The second system is the OE-6630 from Dow Corning Inc. (DowDuPont Inc. after the fusion in 2017, Wilmington, United States of America), which is a high refractive index (HRI) polymethylphenylsiloxane.[14]

4.1.1 Characterisation of Shin-Etsu KJR-9022E-1

The Shin-Etsu KJR-9022E-1 is a two-component system, which is mixed in a ratio of 10:1 of the components KJR-9022E and C-9022E.

4.1.1.1 NMR spectroscopy of KJR-9022E-1

In the ^{1}H NMR spectrum of KJR-9022E (Component A, Figure 43) only vinyl- (5.8 ppm to 6.2 ppm) and methyl- (0.2 ppm) groups can be identified.[320] The integration results in a ratio of around 124:1 methyl-groups to vinyl-groups. In ^{13}C (experimental section, Figure 216) and ^{29}Si NMR (Figure 44), terminal methyl- (M^{Me3}) groups are also visible at 12 ppm,[321] which are directly located beneath the Q groups around −110 ppm.[321]
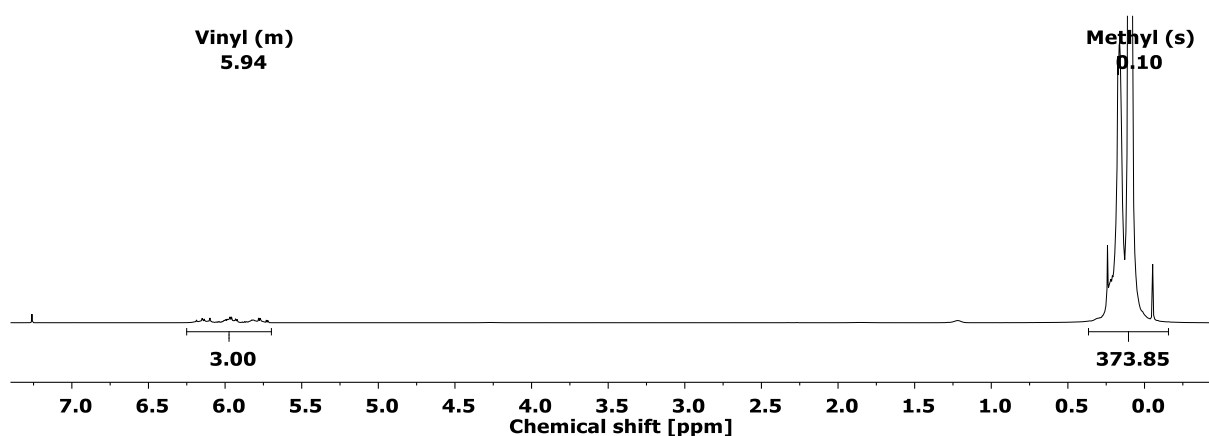

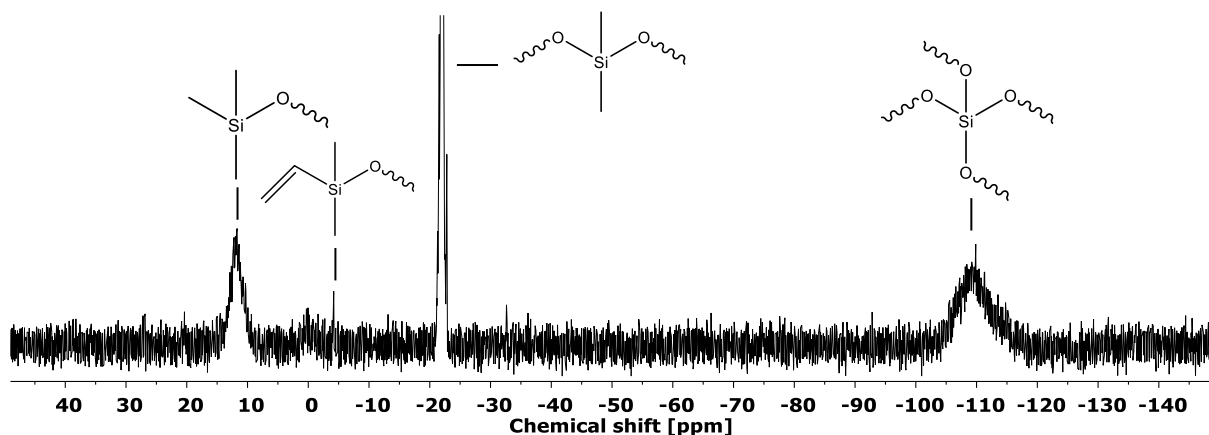**Figure 43: ^{1}H NMR spectra (400 MHz, CDCl₃) of KJR-9022E.**

Figure 44: ^{29}Si NMR spectra (79 MHz, CDCl₃) of KJR-9022E measured in a Teflon NMR tube.

Besides the M^{Me3} groups, D^{Me2} groups can be assigned in the region of −21 ppm to −23 ppm,[321-324] as well as the vinyldimethyl ($M^{Vi,Me2}$) end-groups at −4 ppm,[325] as shown in Figure 44. Component A is a polydimethylsiloxane, which is already cross-linked with some Q groups and terminated with trimethyl- respectively vinyldimethylsiloxane-groups for additional cross-linking via hydrosilylation. The ^{1}H NMR spectrum of C-9022E (Figure 45) shows a relatively broad signal at 4.7 ppm,[326] indicating the hydride-group which, according to ^{29}Si NMR (Figure 46),

is located at the end of the chain as $M^{H,Me2}$ group, because of a signal from -5 ppm to -7 ppm[327-330] and also as $D^{H,Me}$ group from -33 ppm to -38 ppm[323-324, 331] in the middle of the polysiloxane. In the range of 0.2 ppm to 0.0 ppm in ^{1}H NMR the methyl-groups are present.[136] From -17 ppm to -22 ppm in the ^{29}Si NMR are the D^{Me2} methyl-groups located.[321-324] There are around 5.5 methyl-groups per hydride-group. The ^{13}C NMR shows all expected signals (experimental section, Figure 217).
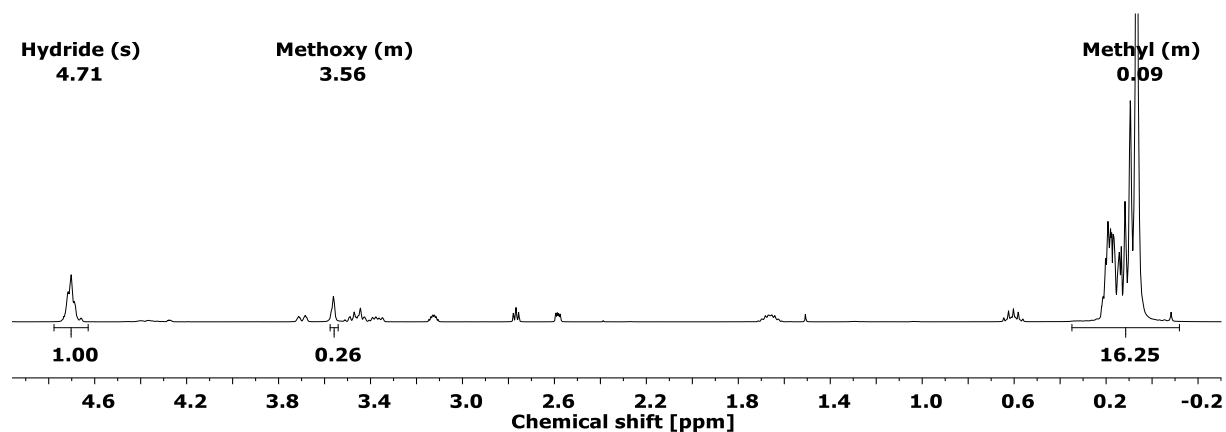

Figure 45: ^{1}H NMR spectra (400 MHz, CDCl$_3$) of C9022E.

The small signal in the ^{29}Si NMR spectrum at -65 ppm belongs to a methylsiloxane T^{Me} group.[321, 324, 331] The relatively sharp signal in the ^{1}H NMR at 3.6 ppm belongs to methoxy-groups which, with the aid of ^{1}H ^{29}Si HMBC NMR spectra, can be assigned to the siloxane Q^{OMe} group. Fully reacted Q groups at -110 ppm are also present, which can be detected in the ^{29}Si NMR (experimental section, Figure 218) using the PTFE NMR tube (Figure 213). The signals are overall very weak and broad, hence for assigning the silicon-groups, the NMR from the glass tube measurement is presented here.
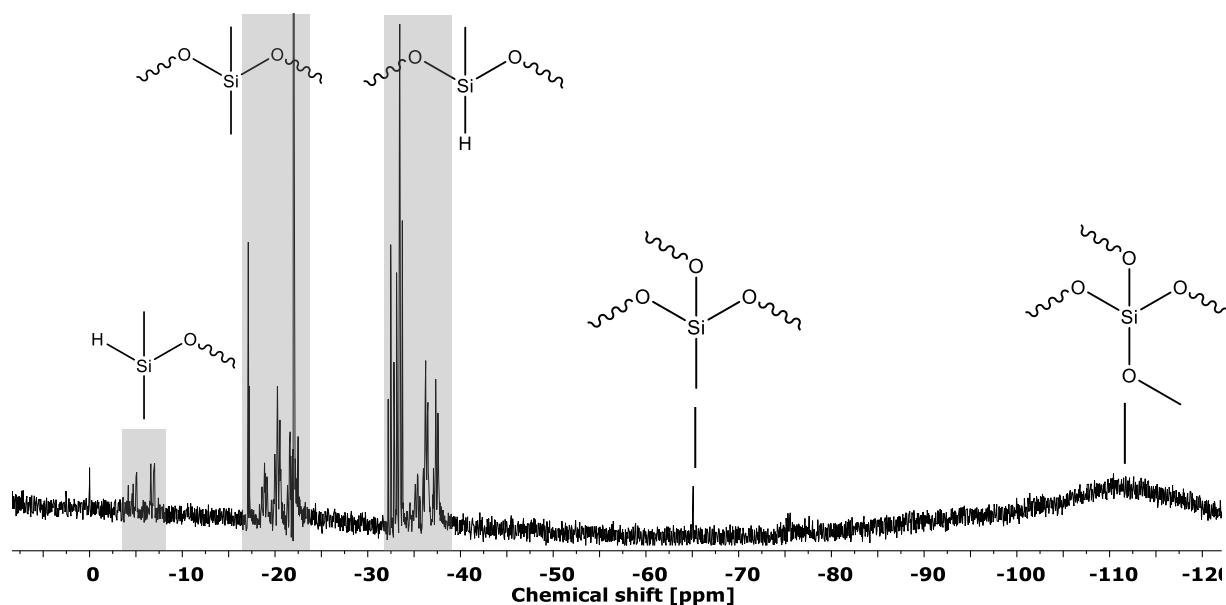

Figure 46: ^{29}Si NMR spectra (79 MHz, CDCl$_3$) of C-9022E measured in a glass tube.

The analysis showed, that the polyhydromethylsiloxane is already cross-linked because some T and Q units are present with additional hydride-groups for a platinum catalysed hydrosilylation. Noteworthy, many low intensity signals in the range from 0.5 ppm to 3.8 ppm are visible in the ^{1}H NMR, which probably refer to additional cross-linkers or additives, which cannot be identified without further information. Industry often uses dimethyl fumarate or dimethyl maleate serving as catalyst inhibitors,[208] which cannot be assigned here. The manufacturer reported a list of possible additives, but it covers every substance which contains nitrogen, sulfur, phosphorus or tin atoms.[13] The polymer consists of two components: A being a vinyl and methyl terminated polydimethylsiloxane with Q groups and B being a cross-linked hydride terminated poly[dimethyl-*co*-hydromethyl]siloxane with T and Q groups.

Recording a solid-state NMR of the cured elastomer is difficult because it cannot be grounded or milled to a homogenous powder. Therefore, a Teflon mould was invented which allows to receive solid rods which exactly fit inside the zirconia rotor (experimental section, Figure 214). The CP MAS NMRs of the polysiloxane rod, which was obtained after the hydride and vinyl mixture was cured inside the mould shows all expected groups, both in the ^{13}C and in the [29]Si spectrum (Figures 7 and 8). In the ^{13}C CP MAS NMR the signals of the methyl-groups are visible at 0.6 ppm to 1.1 ppm.[322, 332] The peak of the ethyl bridge is located at 8.6 ppm[333] and the methyl signals at the silicon atom near the bridge show a signal at -1.2 ppm.[333] The ^{29}Si CP MAS NMR has a low signal to noise ratio because the high flexibility of the polymer limits the cross polarisation.[260, 321, 325, 334-342] All silicon atoms present in the liquid ^{29}Si NMRs also have to be present in the solid-state NMR, therefore even very small signals are assigned. The signal of the dimethyl-group containing silicon atoms at the ethyl bridge located at 11 ppm show the successful hydrosilylation reaction.[321-322, 324, 343-344] A small signal around -4 ppm shows both unreacted hydride and vinyl end groups,[325, 327-328, 330] a clear differentiation cannot be made because of the low signal intensity. From -17 ppm to -25 ppm there are the dimethylsilyl signals[321-324] as well as the signal from the methylethyl-containing silicon atom.[331, 333] A small signal around -37 ppm shows the unreacted hydridomethyl-containing silicon atom.[323-324, 331] The methyl T^{Me} signal is located at -68 ppm[321, 324, 331] and the Q signal at -111 ppm.[321, 324, 327] The solid-state NMR shows a small amount unreacted hydride and probably also vinyl-groups, although they cannot clearly be seen in the ^{13}C NMR, but should be located at 130 ppm.[332] The reason for this is the Teflon mould where the polysiloxane was cured. The shrinkage processes as well as the air free environment hinders the cross-linking reaction which was also observed in larger moulds where the siloxane at the bottom did not harden. The methoxy-groups are not visible anymore, they should generate a signal at 47 ppm to 51 ppm in the ^{13}C NMR.[345]
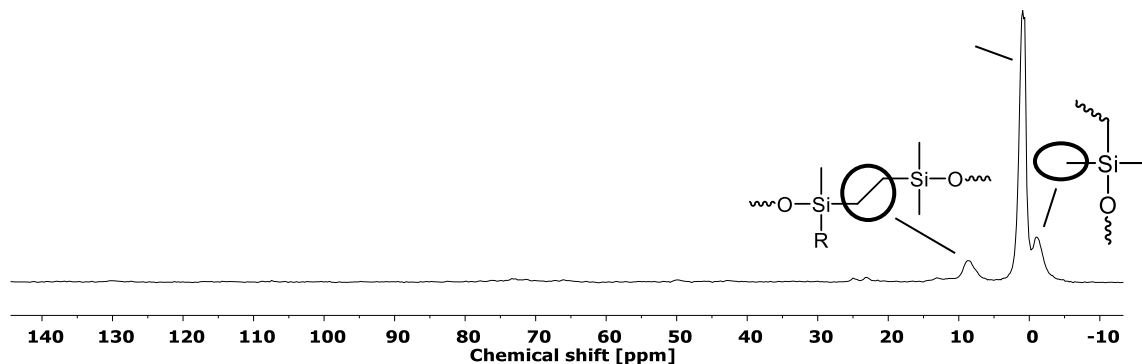
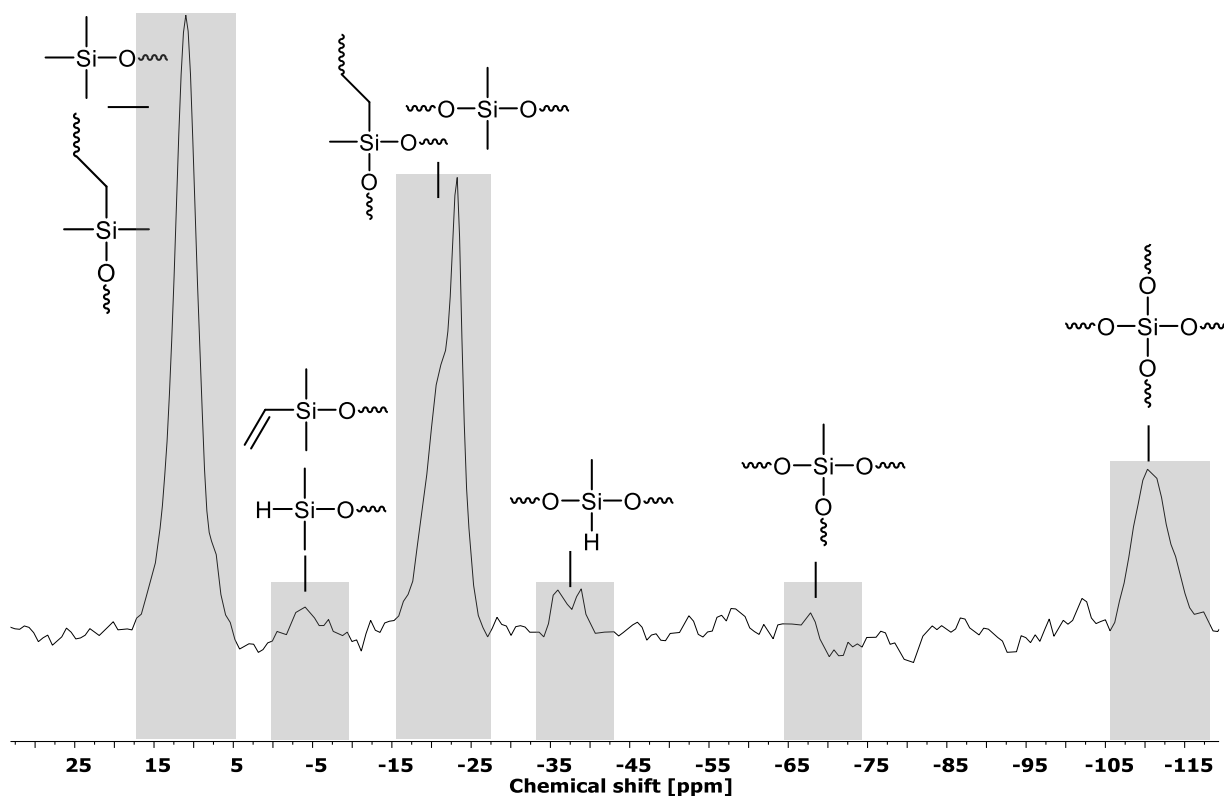**Figure 47:** ^{13}C CP MAS NMR (101 MHz, 13 kHz) spectrum of the cured KJR-9022E-1.

Figure 48: ^{29}Si CP MAS NMR (80 MHz, 13 kHz) spectrum of the cured KJR-9022E-1.

4.1.1.2 FT-IR spectroscopy of KJR-9022E-1

The FT-IR spectra of the KJR components confirm the groups observed in the NMR spectra. In both components, the specific C-H[346-347] at 2960 cm^{-1} and 2902 cm^{-1}, Si-CH$_3$[346-347] at 1257 cm^{-1} and 784 cm^{-1} and Si-O[346-347] at 1065 cm^{-1} and 1008 cm^{-1} vibrations (Figure 49) are visible. Component A shows a very weak vinyl stretching vibration[319, 348-350] at 1599 cm^{-1} and 1453 cm^{-1}, the other characteristic vinyl vibrations at 1010 cm^{-1} and 960 cm^{-1} cannot be observed because they overlap with various CH vibrations. Component B shows the strong Si-H bands at 2159 cm^{-1} and 906 cm^{-1}.[346-347] The cured polysiloxane shows all signals of the components expect the Si-H and Si-V vibrations indicating a fully cross-linked polysiloxane.
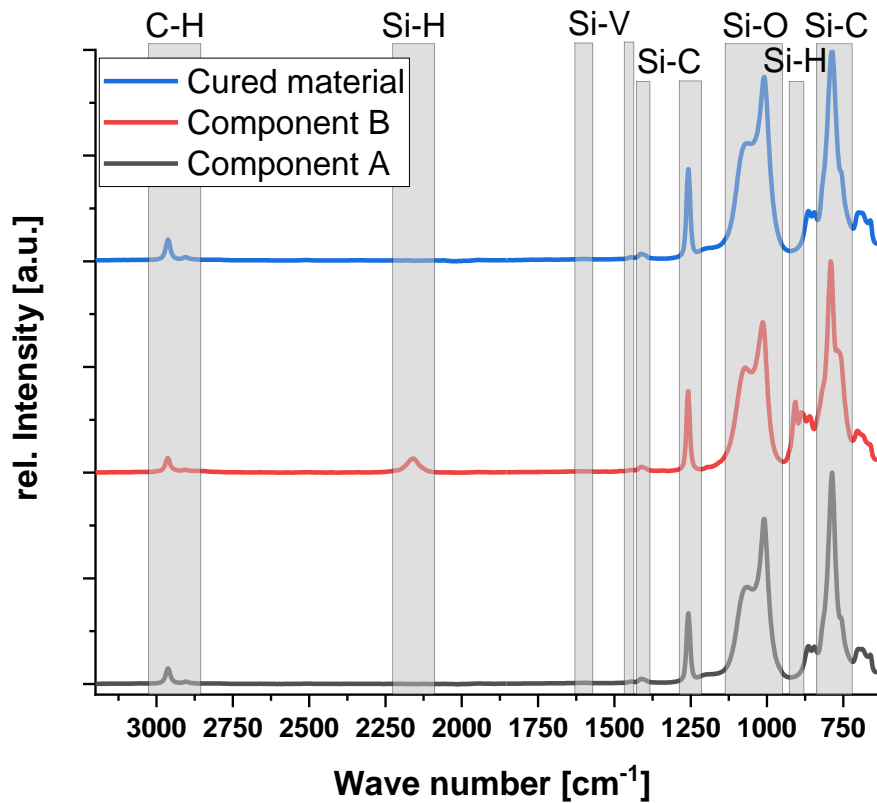
Figure 49: FT-IR spectrum of KJR-9022E-1 component A, B and the cured polysiloxane.

4.1.1.3 Thermogravimetric analyses of KJR-9022E-1

TG measurements were performed for both of the components as well as the cured polysiloxane from room temperature up to 900 °C under oxygen or nitrogen, respectively (Figure 50). The decomposition temperatures and residual masses are shown below (Table 3).
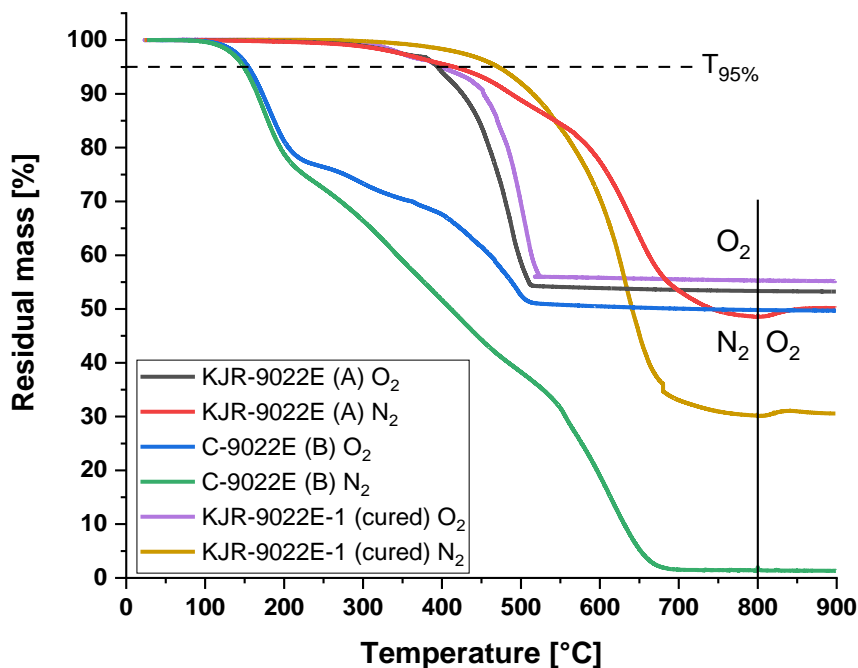

Figure 50: TGA of KJR-9022E-1 components A and B and the cured polysiloxane under oxygen and nitrogen atmosphere.

The decomposition temperatures (Table 3), defined here as the temperature at 5 % mass loss like in literature[7, 222, 316, 351-352] of component A respectively B show only small differences between oxygen and nitrogen atmosphere. Component A (vinyl terminated polydimethylsiloxane) has a $T_{95\%}$ temperature of around 400 °C, which is high for polysiloxanes and most likely results from the cross-linking due to the Q groups.[222, 351]

The cross-linking component B (hydride terminated polyhydromethylsiloxane), which has high amounts of hydride-groups as well as some additives, shows a much smaller value of around 150 °C under both atmospheres, because of the small amount of T and Q groups, which are responsible for the cross-linking. Interestingly, under nitrogen atmosphere, a residual mass of only 1.3 % remains, which implies that compound B easily decomposes mostly into cyclic and small siloxanes as stated by the literature, either through intramolecular or intermolecular reactions.[119, 353] Under oxygen, as described by Camino *et al.*, another decomposition mechanism occurs.[354] The methyl side-groups can be oxidised to form carboxylic acid side-groups, which after the removal of CO_2, form Si-H groups. Two hydride-groups from this decomposition mechanism as well as the Si-H groups already present in the polymer react with additional oxygen under the removal of water to form $R_3Si\text{-}O\text{-}SiR_3$ bonds. Therefore, after around 25 % mass loss, the increased cross-linking prevents the polysiloxane to further decompose via intramolecular or intermolecular degradation, resulting in a high residual mass.[354] The cured system is stable up to 399 °C under oxygen atmosphere and 471 °C under nitrogen atmosphere and the residual mass at 900 °C is 55 % and 31 %, respectively. Although the thermal stability of the cured system is not significantly higher, at least under oxygen atmosphere, the curing process is needed to receive a solid, but very flexible material out of the liquid monomers. The $T_{95\%}$ value for a linear methyl terminated poly[dimethyl-*co*-vinylmethyl]siloxane under nitrogen atmosphere is around 405 °C,[354] while a pure polydimethylsiloxane under nitrogen atmosphere with a heating rate of 6.25 °C shows a $T_{95\%}$ value of around 400 °C.[355] Gädda *et al.* reported a TGA measurement of linear methyl terminated PDMS with a $T_{95\%}$ value of around 360 °C.[344] These values are minimally lower than the $T_{95\%}$ value for component A under inert atmosphere, because here the polysiloxane has some cross-linking. The cured polysiloxane with a high amount of cross-linking therefore exceeds the value for linear polymers by 60 °C to 110 °C. The high thermal stability is as expected because the further increased cross-linking hinders the described decomposition mechanism, which results in a material suitable for high temperature LED applications.

Table 3: T$_{95\%}$ values and residual masses for the TG analyses of the KJR-9022E-1 system.

	T$_{95\%}$ O$_2$ [°C]	Residual mass O$_2$ [%]	T$_{95\%}$ N$_2$ [°C]	Residual mass N$_2$ [%]
KJR-9022E (A)	395	53.2	416	50.2
C-9022E (B)	155	49.7	149	1.3
KJR-9022E-1 (cured)	399	55.2	471	30.6

4.1.1.4 Thermogravimetric analysis coupled with FT-IR spectroscopy of the cured KJR-9022E-1

The TGA-FT-IR spectrum of cured KJR-9022E-1 (Figure 51) was measured under nitrogen atmosphere up to 1000 °C. Three infrared spectra from the TG-FT-IR measurement (Figure 52) of the three observable decomposition stages are shown. The H$_2$O bands do not change in their intensity because they are related to residual gas inside the IR detector chamber. In the first stage at about 460 °C, C-H, Si-O and Si-C vibrations are visible in the FT-IR spectrum, which indicate the formation of hexamethylcyclotrisiloxane due to the unzipping and intramolecular decomposition.[110, 356-357] Polydimethylsiloxane decomposes into hexamethylcyclotrisiloxane even at room temperature.[358] Despite the fact that the dissociation energy of the Si-O bond is higher than the one of the Si-C bond,[122] the Si-O bond breaks at lower temperatures. The bond energy of Si-O is lowered below the energy of the Si-C bond because of the chain mobility.
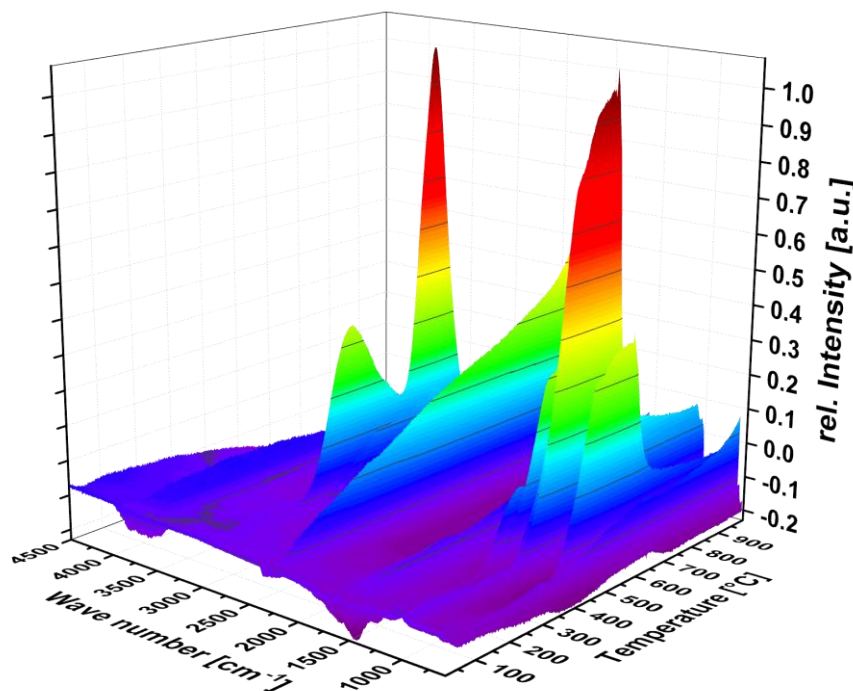
Figure 51: TGA-FT-IR spectrum of KJR-9022E-1 under nitrogen atmosphere.

Camino *et al.* explained this effect that the chain flexibility allows the silicon *d*-orbitals the involvement in the cyclic transition state and therefore lowers the energy of the bond.[354, 359] In the second step at about 600 °C, the intensity of the C-H signals decreases, those of Si-O backbone and Si-C increase, because of the increased cross-linking, the IBBM cannot further continue.[354, 359] Therefore, the decomposition of T and Q silicon atoms as well as the Si-CH$_2$-CH$_2$-Si bridge mainly occurs as well as the release of Si$^+$(CH$_3$)$_2$-O-Si$^+$(CH$_3$)$_2$ dimers[351] reducing the amount of cross-linking.

In the last step at 715 °C, the intensity at around 3000 cm^{-1} increases again, referring to C-H groups, which again can be referred to hexamethylcyclotrisiloxane as well as the terminal CH$_3$-Si$^+$ groups.[351] Also, the intensity of the Si-O and Si-C groups decreases, because the decomposition is nearly finished. At 900 °C only 30 % residual mass is left (Figure 50).
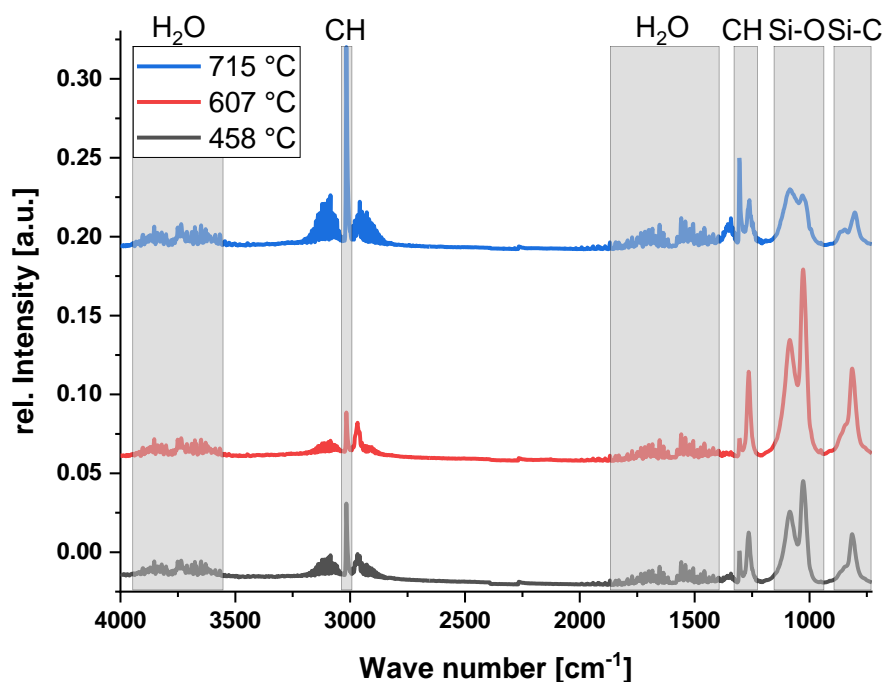

Figure 52: FT-IR spectrum of cured KJR-9022E-1 at 458 °C (black), 607 °C (red) and 715 °C (blue).

4.1.1.5 DSC measurements of KJR-9022E-1

Differential scanning calorimetry (DSC) was also measured for the components A and B as well as the cured polysiloxane under nitrogen atmosphere with 10 K/min from −150 °C up to 150 °C in two cycles. Component A, as a vinyl terminated polydimethylsiloxane with a small amount of Q groups, shows a glass transition temperature T_g of −125 °C, which is close to the value of −123 °C for pure polydimethylsiloxane.[119] At −99 °C a crystallisation occurs, which is reported in literature and ranges from −97 °C for small up to −84 °C for larger hydride terminated polydimethylsiloxanes.[344] At −41 °C a small melting peak (T_m) is visible, which occurs from −48 °C up to −45 °C for hydride terminated polydimethylsiloxanes.
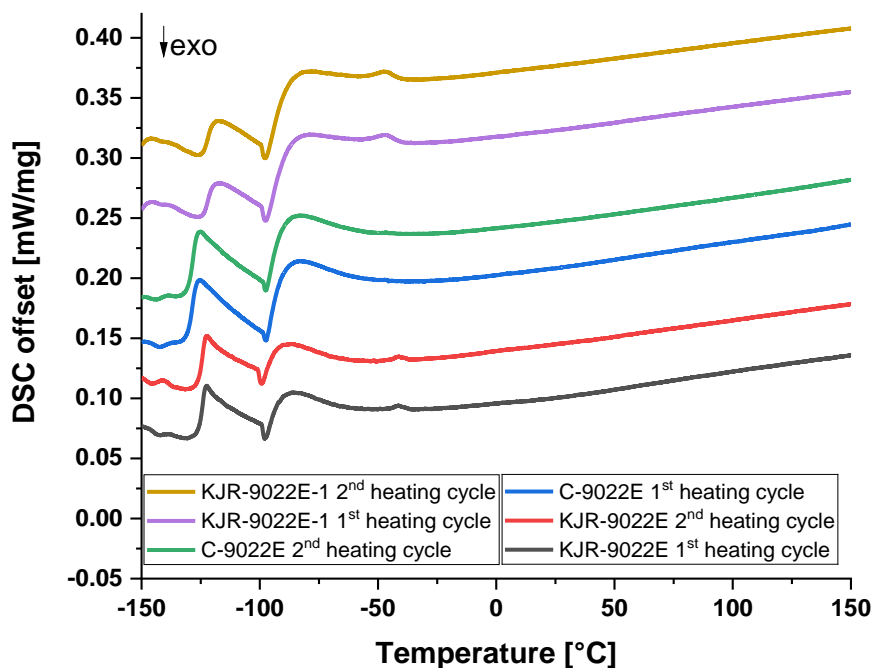
Figure 53: First and second heating cycle of DSC curves of KJR-9022E-1 component A, B and the cured polysiloxane.

The vinyl and the Q groups increase this value because of the reduced mobility, also the higher molecular weight increases the T_m value.[344] The component B (hydride terminated polyhydromethylsiloxane) shows a similar T_g value of -128 °C. The temperature for this component is lower than for component A or a pure polydimethylsiloxane, because of the smaller amount of cross-linking occurring from some T and Q groups and the high amount of hydride-groups. These increase the mobility of the side-groups compared to CH_3 and therefore lower the T_g value. The T_g is in the typical range for low molecular hydride terminated polydimethylsiloxanes.[344] For comparison, the value of a pure polyhydromethylsiloxane is $T_g = -135$ °C.[344] The measured value is therefore in agreement to theory, because a higher mobility due to the smaller groups decrease the T_g value.[119] The crystallisation occurs at a slightly higher temperature ($T_g = -97$ °C) and a melting point cannot be observed. The cured polysiloxane shows a T_g of -122 °C. The increased value, compared to the components A and B, results from the increased cross-linking because of the hydrosilylation and therefore the reduced mobility of the polymer and its side-groups. The crystallisation temperature of -98 °C remains close to the one of component A and B, indicating that the structure only slightly changed. The amount of energy is in between A and B showing that less crystals could be formed, because of the reduced flexibility from the cross-linking. The melting temperature slightly decreases to -47 °C, compared to the one of compound A, although the amount of energy is increased because A also had a very low crystallisation energy.

Table 4: Melting temperatures and melting energy as well as observed glass transition temperatures of compound A, B and the cured polysiloxane.

	T_g [°C]	T_c [°C]	E_c [J/g]	T_m [°C]	E_m [J/g]
A	−124.6	−99.1	−0.358	−41.3	0.073
B	−128.5	−97.5	−3.107	−	−
Cured	−122.1	−97.7	−1.615	−47.4	0.241

4.1.1.6 Refractive index and viscosity of KJR-9022E-1

The refractive index of polydimethylsiloxane is stated with 1.4 in literature at 620 nm.[360-361] The RI of compound A (KJR-9022E) is determined with 1.409, which is slightly higher than the one for compound B (C-9022E) with 1.406. The refractive index is in agreement with the 1.418 of the cross-linked polymethylsiloxanes synthesised from methyltrialkoxysilane.[362] During the curing process, the value of KJR-9022E-1 changes and was determined with 1.410. The RI of the cured, hydride and vinyl-group free film is in good agreement with pure trimethylsiloxane terminated polydimethylsiloxane, which is reported with 1.403 at 20 °C.[363] The viscosity at 25 °C of compound A is determined with 2791 ± 4 mPa·s and 108 ± 3 mPa·s for compound B. Mixing the polymers in a 10:1 ratio for A and B, the final viscosity is around 400 mPa·s, as stated by the manufacturer.[13]

4.1.1.7 UV/Vis spectroscopy of KJR-9022E-1

For UV/Vis measurements with an integration sphere (Figure 54), the mixed and degassed KJR-9022E-1 system was doctor bladed with 120 µm onto a cleaned microscope glass slide. The cured sample is around 85 µm. At 450 nm a high transmission of 101 % can be measured. Here the glass slide has a RI of 1.517 and the polymer a RI of 1.410, because the measurement is corrected with the one of the pure glass slide, a transmission over 100 % can be measured when the RI of the polymer is lower than the one of the glass. A small part of the light, which is backscattered from the sphere to the glass slide will, according to Snell's law, be totally reflected because of the lower RI of the polymer. Additionally, the haze value was calculated with 6 % at 450 nm.
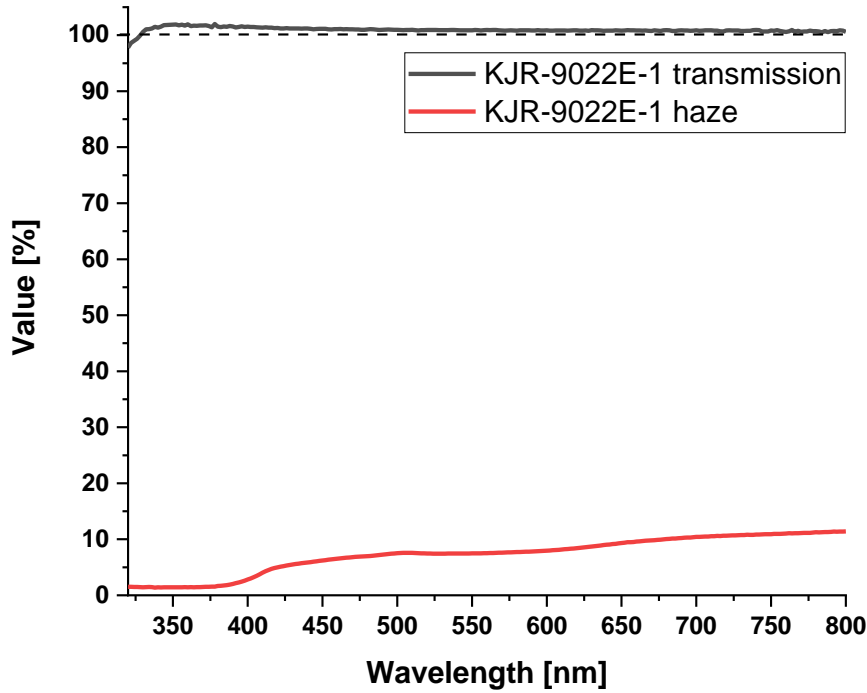
Figure 54: Transmission spectrum and haze curve of cured Shin-Etsu KJR-9022E-1 onto a glass slide.

4.1.1.8 Thermal aging test of KJR-9022E-1

A thermal aging test was performed to evaluate the performance reliability. UV/Vis measurements of the sample were carried out to validate the change of transmittance and colouration during the heat treatment. Additional calculations of the yellowness and whiteness indices were performed before and after the study. The sample was doctor bladed with 120 µm onto a microscope glass slide and cured following the general procedure. 180 °C was appointed as simulated operating LED chip temperature, on one hand because Kim *et al.*[138] uses the same temperature, on the other hand Watzke and Altieri-Weimar from *OSRAM Opto Semiconductors* simulated the temperature distribution of a 1000 mA white light LED on a cold plate at 85 °C and found temperatures from 110 °C at the corners to 230 °C at the centre.[364] The thermal treatment (Figure 55) was performed for 69 days (1656 h). The high transmission of around 100 % is maintained for the whole period from 370 nm to 800 nm which proves the thermal resistance over time.

The colouration was evaluated with the yellowness and whiteness index calculations (Table 5). The YI before the treatment was slightly above zero, indicating a slightly yellow colour, while after the post-curing the value dropped slightly below zero, indicating a blueish colour. The WI before and after the treatment is slightly above 100 and marginally increasing after the aging test, indicating a slightly blueish colour. Overall, these values are close to the ideal values for colourless materials and the change over 69 days is so small that no significant colouration can be observed.
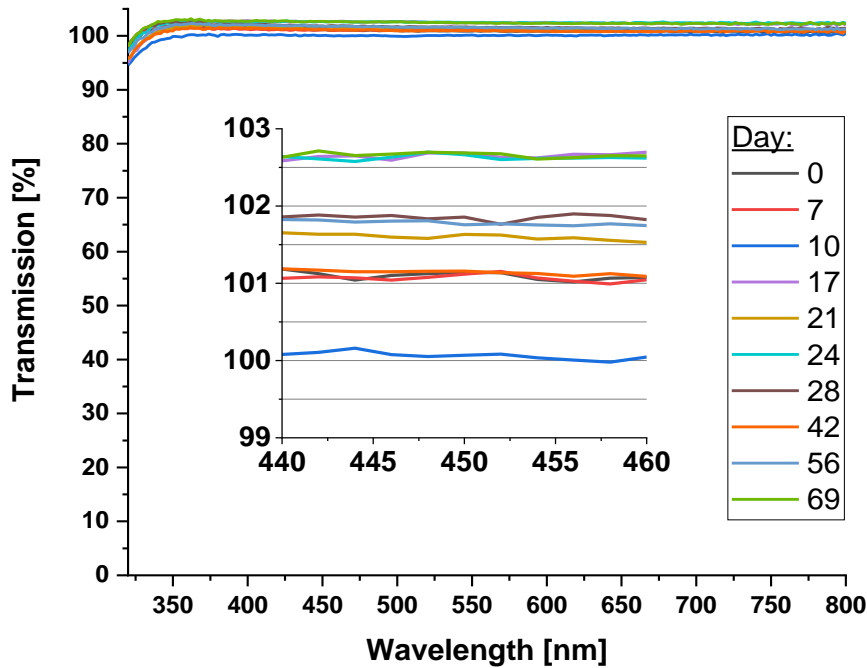
Figure 55: Transmission spectra of Shin-Etsu KJR-9022E-1 onto a glass slide at 180 °C during a period of 69 days (1656 h).

Table 5: Yellowness and whiteness indices of Shin-Etsu KJR-9022E-1 before and after thermal aging.

	YI	WI
After synthesis	0.2	101.6
After 69 days	−0.2	102.7

4.1.1.9 Summary of KJR-9022E-1

The KJR-9022E-1 system from Shin-Etsu is a LRI (RI = 1.410) polydimethylsiloxane (Figure 56). The polymer consists of two components: A being a vinyl respectively methyl terminated polydimethylsiloxane with Q groups and B being a cross-linked hydride terminated poly[dimethyl-*co*-hydromethyl]siloxane with T and Q groups. T and Q groups are often present in polysiloxanes and can be added with Q resins.[365-367] The copolymers as well as the cured polysiloxane shows T_g values between −130 °C and −120 °C. The cured polysiloxane shows a high thermal stability of 399 °C under O_2 and 471 °C under N_2. With its high transmission of around 100 % even after 69 days at 180 °C it is very suitable for LED applications.
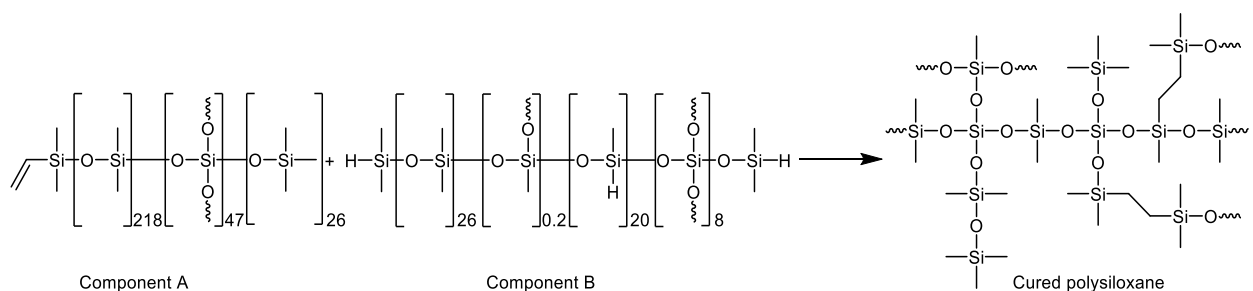

Figure 56: General structures of the KJR-9022E-1 system.

4.1.2 Characterisation of Dow Corning OE-6630

The Dow Corning OE-6630 system consists of two components A and B, which are mixed in a ratio of 1:4 and this system is called HRI polymer. The two components were investigated by liquid ^{1}H, ^{13}C and ^{29}Si NMR spectroscopy, SEC, and rheological measurements. The components and the cured polymer were investigated by TG, TG-FT-IR, DSC, IR spectroscopy, and the RI measurements. The cured polysiloxane was also analysed by ^{13}C and ^{29}Si solid-state NMR and UV/Vis spectroscopy, as well as an aging test for simulating the colouration during the exposure of heat.

4.1.2.1 NMR spectroscopy of Dow Corning OE-6630

Integration of the ^{1}H NMR spectrum of OE-6630 component A revealed ten phenyl-groups and twelve methyl-groups per vinyl-group (Figure 57). Some broad signals are in the region of 1.5 ppm to 4.0 ppm, which are probably additives or residues from the synthesis. Because their content is so low, they cannot be assigned properly.
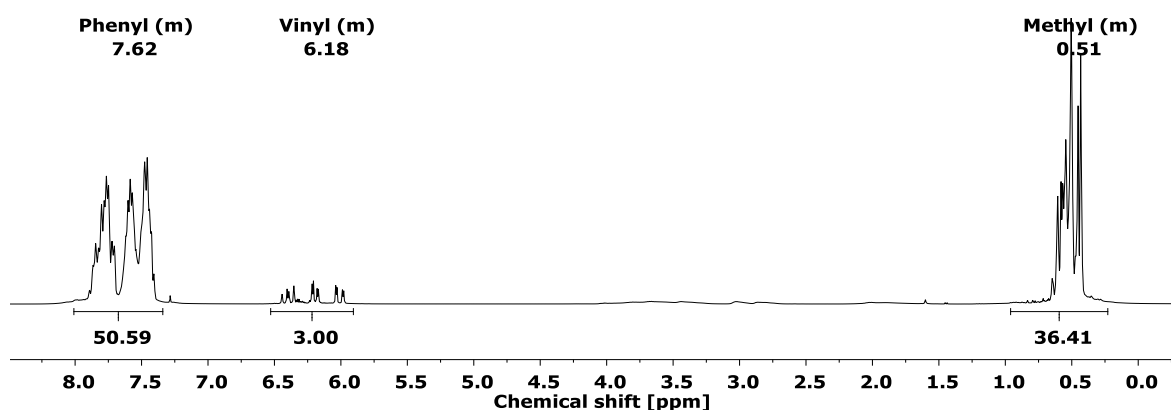

Figure 57: ^{1}H NMR spectrum (400 MHz, CDCl₃) of OE-6630 component A.

The ^{29}Si NMR (Figure 58) of the component shows two signals, one at −2 ppm which can be referred to vinyldimethylsilyl $M^{Vi,Me2}$ group[325] and the second one at −33 ppm which can be referred to methylphenylsilyl D^{MePh} group.[368]

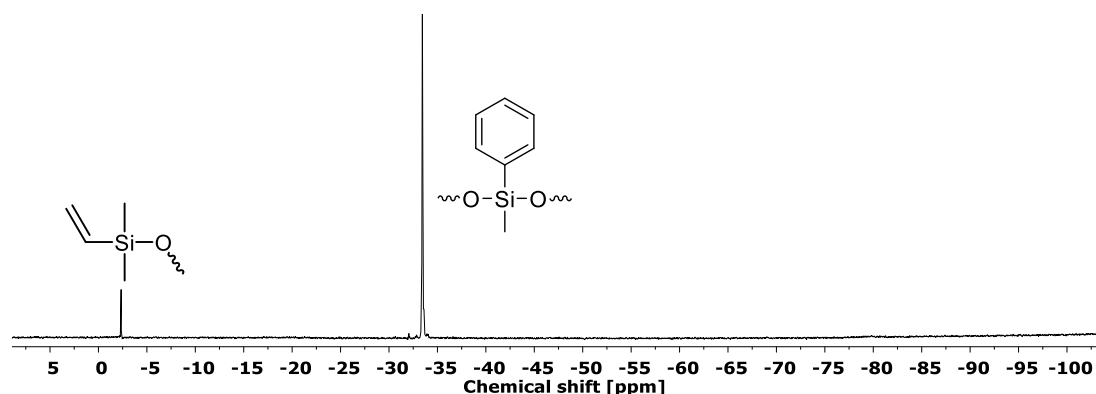**Figure 58: ^{29}Si NMR sprectrum (79 MHz, CDCl₃) of O-E6630 component A.**

The ^{13}C NMR (experimental section, Figure 219) confirms the interpretation by ^{1}H and ^{29}Si NMR. The analysed spectra show that OE-66630 component A is a linear vinyl terminated polymethylphenylsiloxane, because it is linear, an average molecular weight of 3000 g/mol can be calculated. Between the two vinyldimethylsilyl end groups around 20 methylphenylsilyl-groups are present.

Component B (Figure 59) has about 4.5 phenyl and 4.5 methyl-groups as well as around one vinyl-group per hydride-group (Figure 60). In the ^{29}Si NMR five groups of signals are visible. The signals around −1 ppm belong to a vinyldimethylsilyl $M^{Vi,Me2}$ group[325] and the signal at −4 ppm to a hydrodimethylsilyl $M^{H,Me2}$ group.[327-328, 330] A very small peak at −21 ppm is visible which belongs to a dimethylsilyl D^{Me2} group.[321-324] At −45 ppm the diphenylsilyl D^{Ph2} group can be seen[234-235, 319, 324, 331, 368] and around −80 ppm the phenylsilyl T^{Ph} group is present.[321, 324] The ^{13}C NMR confirms the observed groups (experimental section, Figure 220). The analysis showed that component B is an already by T^{Ph} groups cross-linked poly[dimethyl-*co*-diphenyl]siloxane with terminal hydride and vinyl-groups.
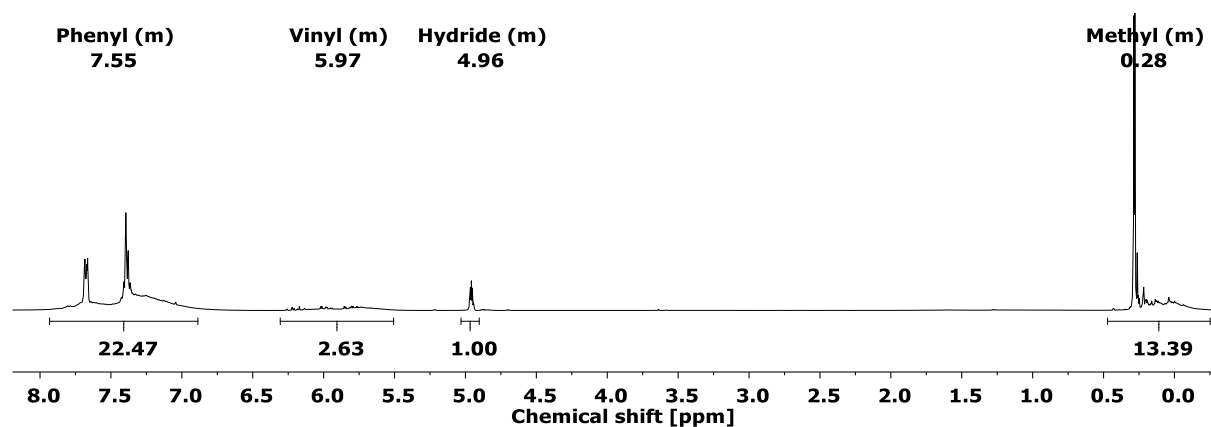

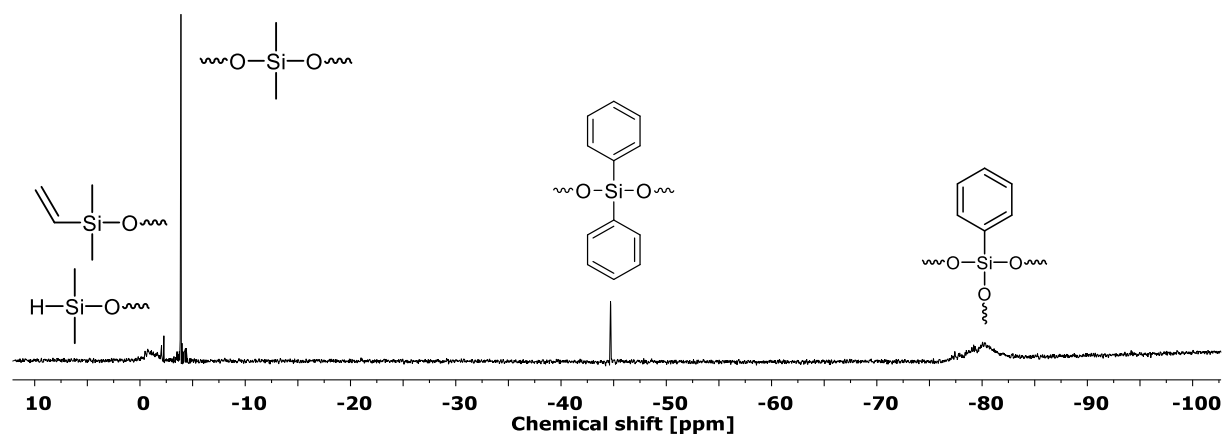Figure 59: ^{1}H NMR spectra (400 MHz, CDCl$_3$) of OE-6630 component B.

Figure 60: ^{29}Si NMR spectrum (79 MHz, CDCl$_3$) of OE-6630 component B.

The CP MAS NMRs after the curing shows all expected groups both in the ^{13}C and in the ^{29}Si NMR spectra (Figure 61, Figure 62). The ^{13}C CP MAS NMR shows three signals. In the range of 140 ppm to 120 ppm are the phenyl carbon atoms,[332, 369] at 9 ppm are the -CH$_2$-CH$_2$- carbon atoms[333] resulting from the hydrosilylation reaction, and at −1 ppm the methyl carbon atoms[322, 332]. In the ^{29}Si CP MAS NMR a small signal of unreacted hydride can be observed at −4 ppm[327-330] even after 16 h of curing, while no remaining vinyl is present. A reason for this is the curing process, a special self-developed Teflon mould was used to cure the siloxane in a cylindrical form which exactly fits the solid-state zirconia rotor (experimental section, Figure 214). This step was necessary because the elastomer cannot be grounded or milled. This sealed and firm mould hinders the polysiloxane to fully condense because the vinyl and hydride-groups cannot reach each other at a certain point because of the shrinking process during the curing. The FT-IR spectrum (4.1.2.2) of the cured polysiloxane was recorded with a thin film onto a glass slide which proved that the polymer can react completely. At −11 ppm are the silicon atoms from the ethyl bridge formed by the cross-linking visible.[45-47, 59-60] The D^{Me2} signal is located at −19 ppm,[321-324] the D^{MePh} signal at −33 ppm,[368] the D^{Ph2} signal at −46 ppm[35-36, 42, 47, 55, 78] and the T^{Ph} signal at −79 ppm[321, 324].

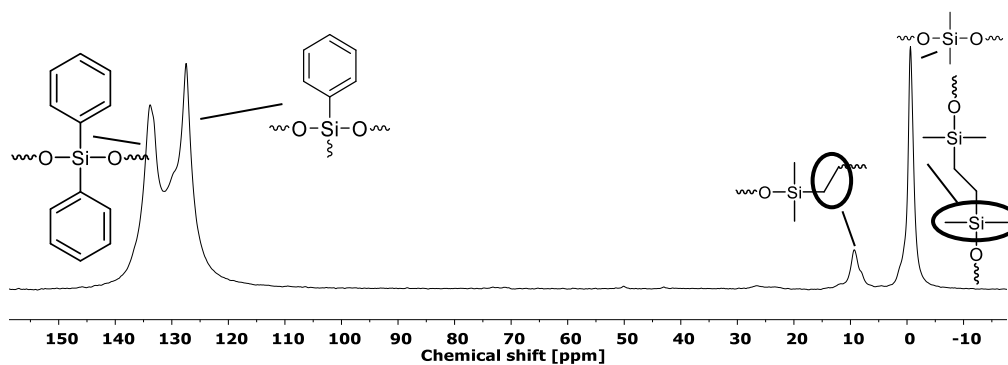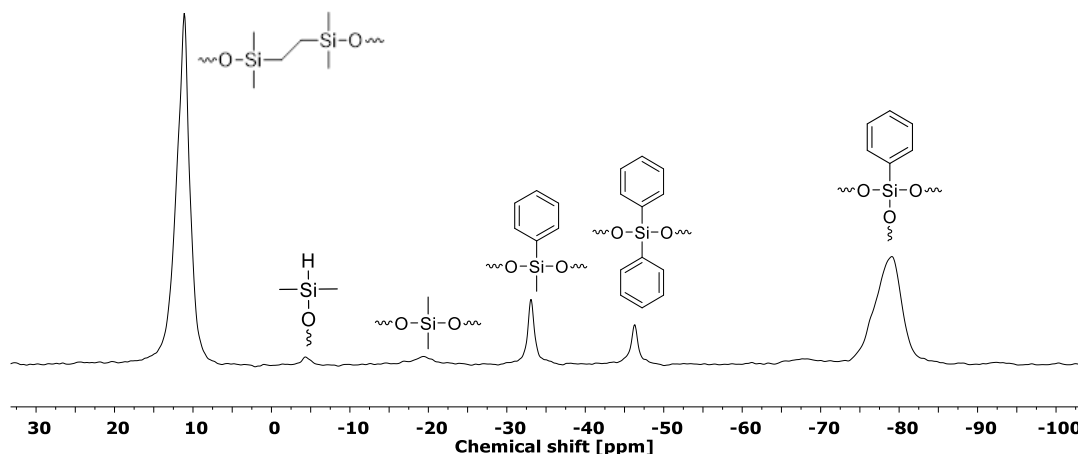**Figure 61: ^{13}C CP MAS NMR (101 MHz, 13 kHz) of the cured OE-6630 system.**

Figure 62: ^{29}Si CP MAS NMR (80 MHz, 13 kHz) of the cured OE-6630 system.

4.1.2.2 *FT-IR spectroscopy of Dow Corning OE-6630*

The characterisation of the two compounds as well as the cured system with FT-IR spectroscopy showed the expected signals for aromatic and aliphatic C-H (dark grey) bonds at 3072 cm^{-1}, 3049 cm^{-1}, 2953 cm^{-1} and 2909 cm^{-1}, C-C bonds at 1590 cm^{-1} and 1430 cm^{-1}, Si-C bonds at 1413 cm^{-1}, 1257 cm^{-1} and 784 cm^{-1} and the dominating signal of the Si-O-Si vibration at 1115 cm^{-1} and 1024 cm^{-1} (Figure 63).[234-235, 319, 346-347, 349-350, 370] The vinyl-group of component A and B is only barely visible in component A at 1655 cm^{-1}.[234-235, 319, 370] The hydride-group of component B reveals strong signals at 2129 cm^{-1} and 896 cm^{-1}.[234-235, 319, 346-347] No hydride or vinyl-groups can be seen in the spectrum of the cured polysiloxane indicating a fully condensed network.
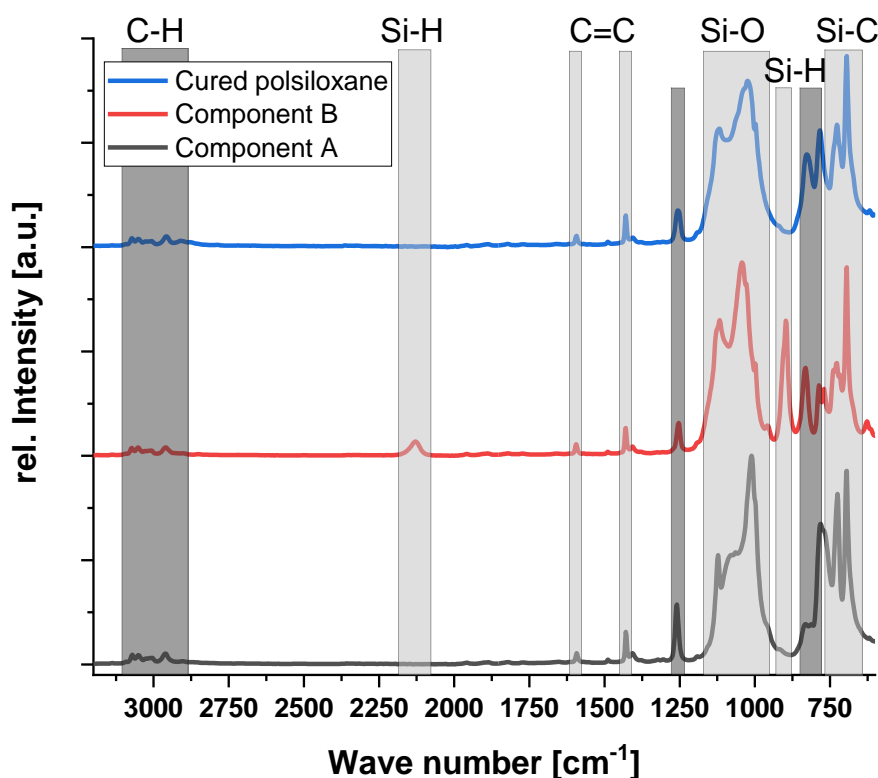

Figure 63: FT-IR spectra of OE-6630 component A, B and of the cured material.

4.1.2.3 *Thermogravimetric analysis of Dow Corning OE-6630*

Thermogravimetric analyses (Figure 64) of the polymers A and B as well as of the cured polysiloxane were performed. The decomposition temperature, here defined at 5 % mass loss, (Table 6) of each component as well as the cured polysiloxane shows little to no difference when heated in oxygen or nitrogen atmosphere. The residual masses in both measurements equal each other, although for the cured system the end of the decomposition is not reached by the end of the measurement at 900 °C. The linear component A shows a very high decomposition temperature of around 400 °C under both atmospheres, while the cross-linked component B shows a

low $T_{95\%}$ value of 180 °C. Component A is a relatively small polymer with a molecular weight of 3000 g/mol and therefore the percentage of the end groups compared to the chain atoms is large. These end groups reduce the possibility of the intramolecular back biting mechanism.[119]
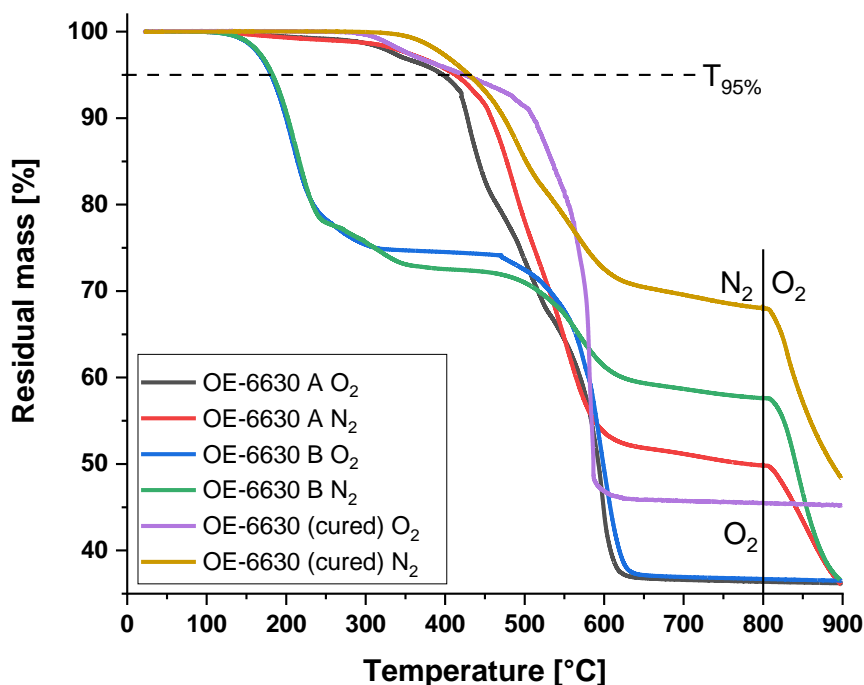

Figure 64: TGA of OE-6630 components A and B and the cured polysiloxane under oxygen or nitrogen.

The high residual mass under nitrogen atmosphere proves the literature observation, the previously described decomposition mechanisms occur. The cured polysiloxane shows an even higher thermal stability compared to the two polymers of around 425 °C under both atmospheres resulting from the increased cross-linking because of the hydrosilylation process.

Table 6: $T_{95\%}$ values and residual masses for the TG analyses of the OE-6630 system.

	$T_{95\%}$ O_2 [°C]	Residual mass O_2 [%]	$T_{95\%}$ N_2 [°C]	Residual mass N_2 [%]
A	397	36.2	413	36.0
B	181	36.5	183	36.6
Cured	425	45.2	430	48.4

4.1.2.4 Thermogravimetric analysis coupled with FT-IR spectroscopy of Dow Corning OE-6630

To analyse the different decomposition steps, TG-FT-IR spectra were recorded under N_2 up to 800 °C followed by an oxidation step from 800 °C to 900 °C for the components. The three FT-IR spectra at the selected temperatures are shown in Figure 65, the detailed assignment is in the previous chapter. In the first decomposition step of component A around 530 °C the

C-H$_{Ar}$, C=C-C$_{Ar}$, C-H$_{Ar}$ and Si-O bands are visible. In the second step at around 710 °C, the bands of Si-O and Si-V are present and also a sharp signal at 3017 cm^{-1}.[347] The last step at 840 °C shows the decomposition into water and carbon dioxide under O$_2$ atmosphere.[351, 371]
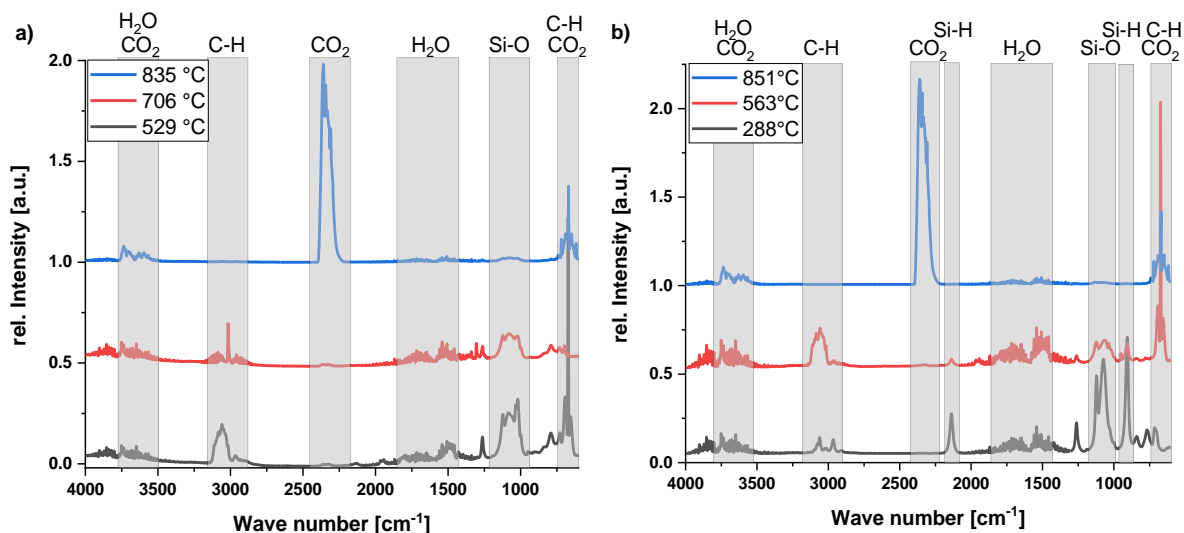
Figure 65: FT-IR spectra at selected temperatures of evolved gas during TG measurement of OE-6630 component a) A and b) B under N$_2$ until 800 °C, from 800 °C to 900 °C under O$_2$.

Component B, despite having a large amount of cross-linking, decomposes at lower temperatures. Kim *et al.* and Schiavon *et al.* showed that a very high amount of cross-linking reduces the T$_{95\%}$ compared to more flexible polysiloxanes.[234, 353] These observations show that by increasing the amount of cross-linking, the thermal stability first rises up to a maximum and afterwards it decreases. The FT-IR spectra of compound B at three selected temperatures are shown in Figure 65. In the FT-IR spectra of the first step at around 290 °C shows the Si-H, Si-O and CH$_3$ bands. In the second step at 560 °C mainly the phenyl-groups are evolving, because of the C-H$_{Ar}$ and C=C-C$_{Ar}$ bands. The vinyl signals cannot be observed in both spectra, because of the overlap with C-H and water bands. In the last step under oxygen atmosphere at 851 °C the remaining organic is decomposed into H$_2$O and CO$_2$.[351]

The TGA-FT-IR measurement (Figure 66) of the cured material was performed up to 1000 °C under N$_2$. The material shows a T$_{95\%}$ of 430 °C. In the subsequent region, a large mass loss of 29.6 % occurs (Figure 64) up to 600 °C. From 600 °C to 1000 °C the mass loss is not so significant. The FT-IR spectra reveal no change in the gas composition, only the intensity changes. The spectra at 553 °C (Figure 67) reveals signals of the Si-O backbone at 1115 cm^{-1} and 1024 cm^{-1}, the C-H groups at around 3000 cm^{-1} and the C=C groups at 1590 cm^{-1}, 1430 cm^{-1} and 990 cm^{-1}.
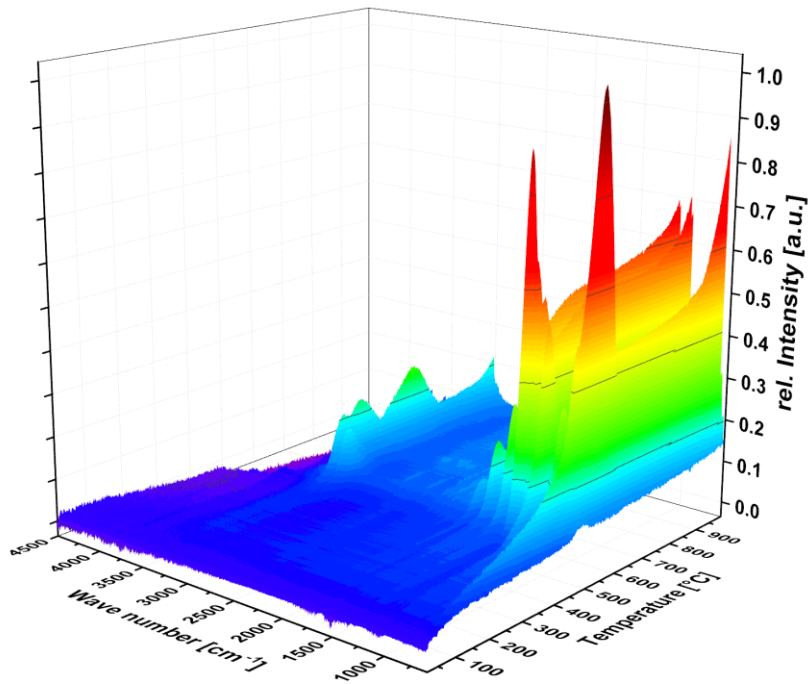
Figure 66: Temperature depending FT-IR plot of evolved gas from the cured OE-6630 up to 1000°C under nitrogen atmosphere.

The signal intensity increases strongly with increasing temperature up to 485 °C, where the Si-O signal shows the maximum absorbance followed by the C-H signal with a highest absorption at 553 °C. The FT-IR intensity of the evolved gas decreases till 600 °C. Further increasing the temperature to 900 °C leads to a constant signal.
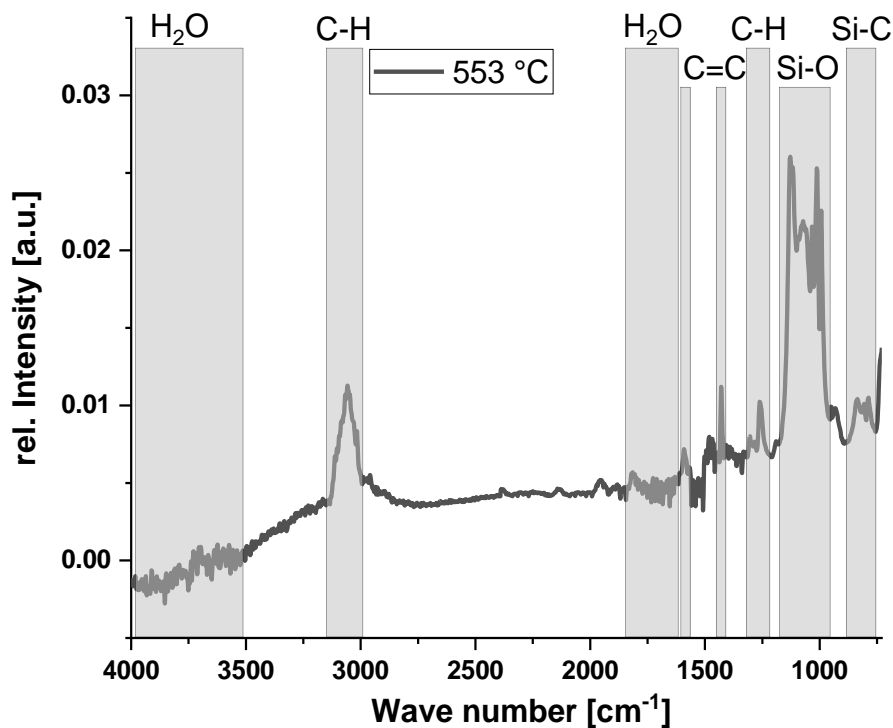
Figure 67: FT-IR spectrum of cured OE-6630 at 553 °C under nitrogen atmosphere.

A last increase of the FT-IR signal between 900 °C and 1000 °C can be observed although no significant mass loss occurs. The evolving species are probably residues in the upper part of the furnace or the transfer cannula, which now, due to the high temperatures, were desorbed and directed to the detector.

4.1.2.5 DSC analyses of Dow Corning OE-6630

Differential scanning calorimetry (DSC) was measured for the components A and B as well as the cured polysiloxane under N_2 with 10 K/min from −90 °C up to 150 °C in two cycles for the copolymers and from −50 °C up to 150 °C in two cycles for the cured polysiloxane (Figure 68). Component A (Table 7), being a linear methyl and phenyl-group containing polysiloxane, shows a strong T_g at −44.7 °C, indicating more than 50 % methyl side-groups, because the reference T_g for a polymethylphenylsiloxane is −28 °C and the T_g for a poly[diphenyl-*co*-dimethyl]siloxane 50:50 mol% is −30 °C.[119] Lower values indicate a higher methyl content like in poly[diphenyl-*co*-dimethyl]siloxane 3:7 mol% which has a T_g of −64 °C.[119] Component B has a lower T_g (Figure 68, Table 7) of −55.4 °C, despite having the higher phenyl content compared to component A, because of the presence of Si-H groups which lower the value.[119]
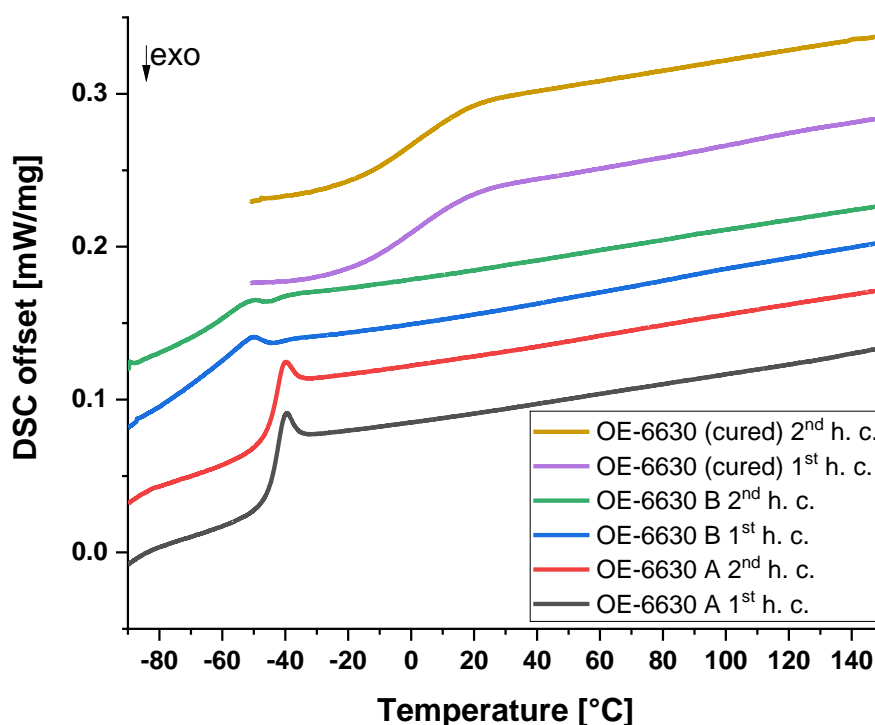

Figure 68: First and second heating cycle from the DSC measurement of OE-6630 component A, B and the cured polysiloxane.

The intensity is lower because of the already existing cross-linking of the T groups which limit the degrees of freedom of the polymer.[119] The curing increases the cross-linking respectively

reduces the mobility of the polymer chains and side-groups. This results in a higher glass transition temperature. Therefore, the DSC curves were only measured from −50 °C to 150 °C. The cured polysiloxane shows a drastically increased T_g of 5.5 °C. No melting temperatures could be observed in the measured temperature range.

Table 7: Melting temperatures and melting energy as well as observed glass transition temperatures of OE-6630 compound A, B and the cured polysiloxane.

	T_m [°C]	E_m [J/g]	T_g [°C]
A	−	−	−44.7
B	−	−	−55.4
Cured	−	−	5.5

4.1.2.6 Refractive index, viscosity, and SEC analyses of Dow Corning OE-6630

The refractive indices of the two components A ($n = 1.542$) and B ($n = 1.534$) are lower than 1.552, which is the value of the cured polysiloxane (589 nm, 20 °C). This is congruent with a pure polymethylphenylsiloxane that has a refractive index of 1.554.[363] The cross-linking process leads to a denser polymer, the polymer shrinks, which results in a higher refractive index. Also, in the components A and B solvent residues of the synthesis process are present, which are removed by the high-temperature curing process at 150 °C. The degassing process, which mainly aims at removing the air which was introduced by rigorously stirring the components before the curing process, removes some of them, but due to the relatively high viscosity of 2962 ± 55 mPa·s for component A (manufacturer: 2975 mPa·s) and 2531 ± 31 mPa·s for component B (manufacturer: 2775 mPa·s) not all can be removed.[14] The molecular weight was determined using a SEC analyses in THF. A molecular weight of 4680 g/mol for the RI detector and 4730 g/mol for the UV detector could be determined with a PDI of 1.83 respectively 1.62 for the OE-6630 component A which is larger than the 3000 g/mol calculated by ^{1}H NMR spectroscopy. For component B a bimodal deviation was observed with a molecular weight of 1670 g/mol using the RI detector and 1640 g/mol using the UV detector with a PDI of 1.21 respectively 1.17. The second area represents a much smaller molecular weight of 370 g/mol independent of the detector with a PDI of 1.03 respectively 1.02.

4.1.2.7 UV/Vis spectroscopy of Dow Corning OE-6630

For UV/Vis measurements (Figure 69), the mixed and degassed OE-6630 system was doctor bladed with 120 µm onto a cleaned microscope glass slide and cured. At 450 nm a high transmission of 99 % can be measured. Additionally, the haze value was calculated using the scattering and the corrected transmission spectra. A haze value at 450 nm of 7 % is obtained.
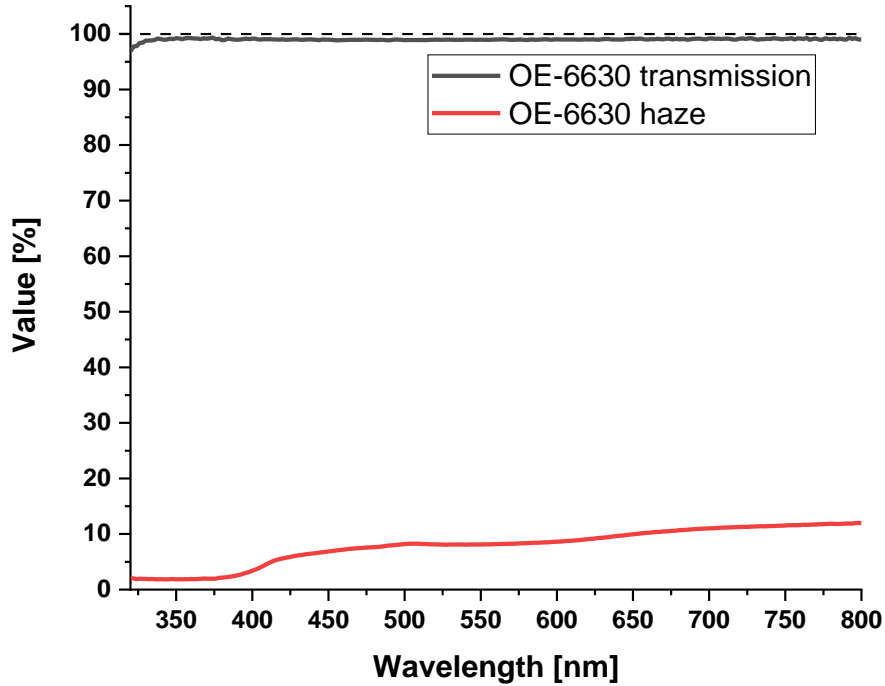
Figure 69: Transmission and haze spectra of the cured Dow Corning OE-6630 onto a glass slide.

4.1.2.8 Thermal aging test of Dow Corning OE-6630

The performance reliability was evaluated using a thermal aging test at 180 °C. UV/Vis measurements of the sample were performed to validate the amount of colouration and transmittance during the heating process. The yellowness and whiteness indices were calculated before and after the study. The heat treatment (Figure 70) was performed for 69 days (1656 h).
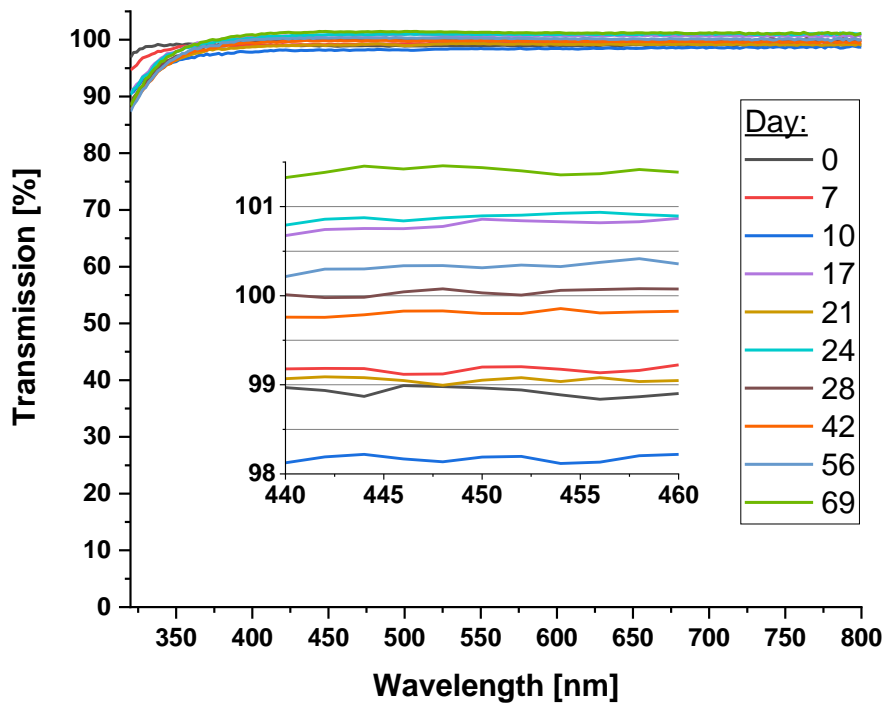

Figure 70: Transmission spectra of Dow Corning OE-6630 onto a glass slide over 69 days (1656 h).

The high transmission of around 100 % can be maintained for the whole period from 370 nm to 800 nm showing the thermal resistance over time. The colouration was calculated using the yellowness (YI) and whiteness (WI) indices (Table 8). The YI after the synthesis is slightly over zero indicating a slightly yellow colour, after the treatment the value is zero which implies an optimal neither yellow nor blue colour. The WI increases after the heating, from a slightly yellowish colour to a slightly bluish one. In summary, the material maintains its high transmission and remains its uncoloured appearance even after 1600 hours at 180 °C.

Table 8: Yellowness and Whiteness Index of Dow Corning OE-6630 before and after thermal aging.

	YI	WI
After synthesis	0.5	99.0
After 69 days	0.1	100.8

4.1.2.9 Summary of Dow Corning OE-6630

The OE-6630 system from Dow Corning is a high refractive index ($n = 1.552$) polymethylphenylsiloxane (Figure 71). The polymer consists of two components: A being a linear vinyl terminated polymethylphenylsiloxane and B being a cross-linked hydride and vinyl terminated poly[dimethyl-*co*-diphenyl]siloxane. The thermal stability ($T_{95\%}$ values) of the cured polysiloxane is 425 °C under oxygen and 430 °C under nitrogen. The glass transition temperatures increase from −45 °C for component A respectively −55 °C for B to 5 °C for the cured polymer. With its high transmission of around 100 % even under high temperatures for over 1600 h it is very suitable for LED applications.
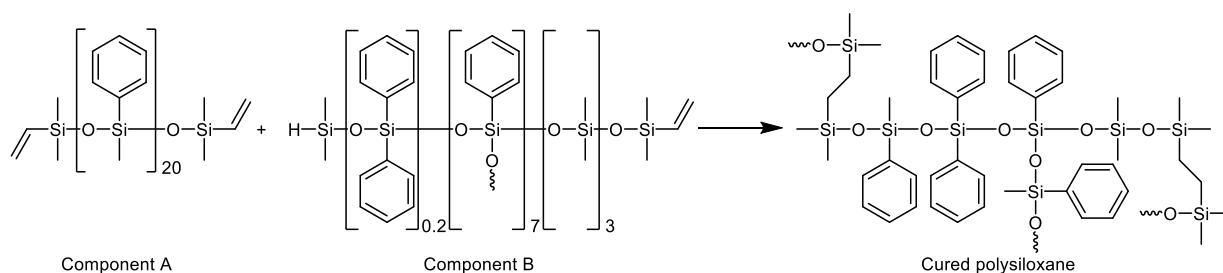
Figure 71: General structures of the OE-6630 system.

4.1.3 Conclusion for the commercial polysiloxanes

The commercial systems show very good properties. The SEC and NMR analyses showed that they have relatively low molecular weights and thus low viscosities around 3000 mPa·s. The thermal stability $T_{95\%}$ is very high with around 400 °C. The T_g of the polymethylphenylsiloxane OE-6630 is around –50 °C for the polymers and 5 °C for the cured system. The transparencies are around 100 % and the haze values are around 10 %. The self-prepared systems have to reach those properties with the difference that they have to excel the refractive index of 1.53.

4.2 Enhancement of the refractive index with metal oxide nanoparticles

Hafnium and zirconium dioxide were chosen because of the already mentioned reasons: they are colourless, nontoxic, have an inertness under oxygen atmosphere and have a high thermal stability and a RI over 2.0. Three high pressure synthesis were performed and three ambient pressure ones (Figure 72) to receive small nanoparticles under 10 nm. The nanoparticles can then be mixed in polysiloxanes or covalently bound to them. These new polysiloxanes also have to be synthesised first.
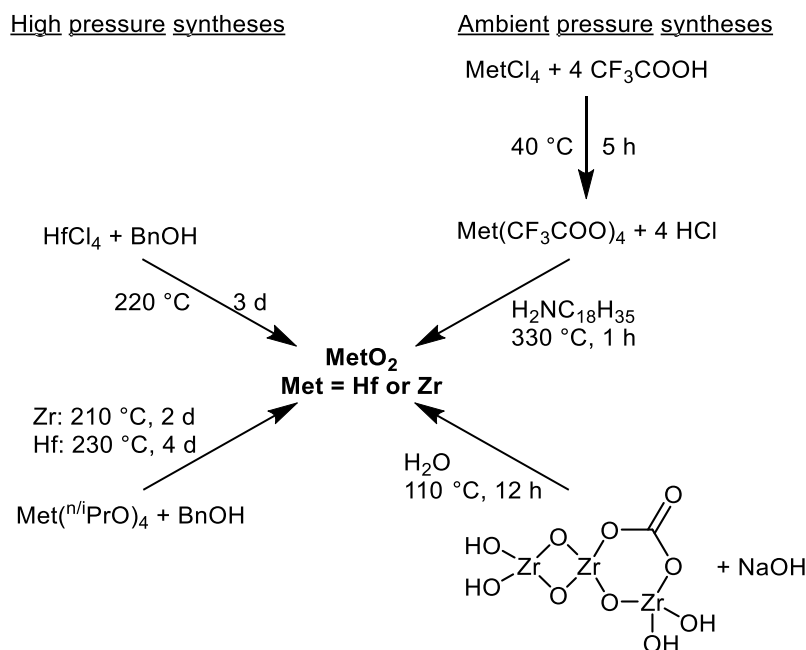

Figure 72: Overview for possible syntheses of metal oxide (MetO$_2$ with Met = Hf or Zr) nanoparticles.

4.2.1 Synthesis of metal oxide nanoparticles

4.2.1.1 Metal oxides from iso- or n-propoxide precursors obtained by autoclave synthesis

4.2.1.1.1 ZrO$_2$ with PDMS-OH for the incorporation into polysiloxanes

The synthesis was performed after Garnweitner *et al.*[249] The metal precursor (Zr(O^{i}Pr)$_4$ or Zr(O^{n}Pr)$_4$) were mixed with benzyl alcohol (BnOH) in a stainless steel autoclave and heated for 210 °C for two days for the ZrO$_2$ nanoparticles under nitrogen atmosphere. The resulting suspension was centrifuged, and the powder was washed with THF twice. The obtained particles were briefly dried before the XRD measurement (Figure 73). A Rietveld refinement was performed and showed the formation of cubic ZrO$_2$ with a crystallite size of 3.3 ± 0.1 nm, while the literature reported a slightly smaller one with around 2.8 nm.[249]
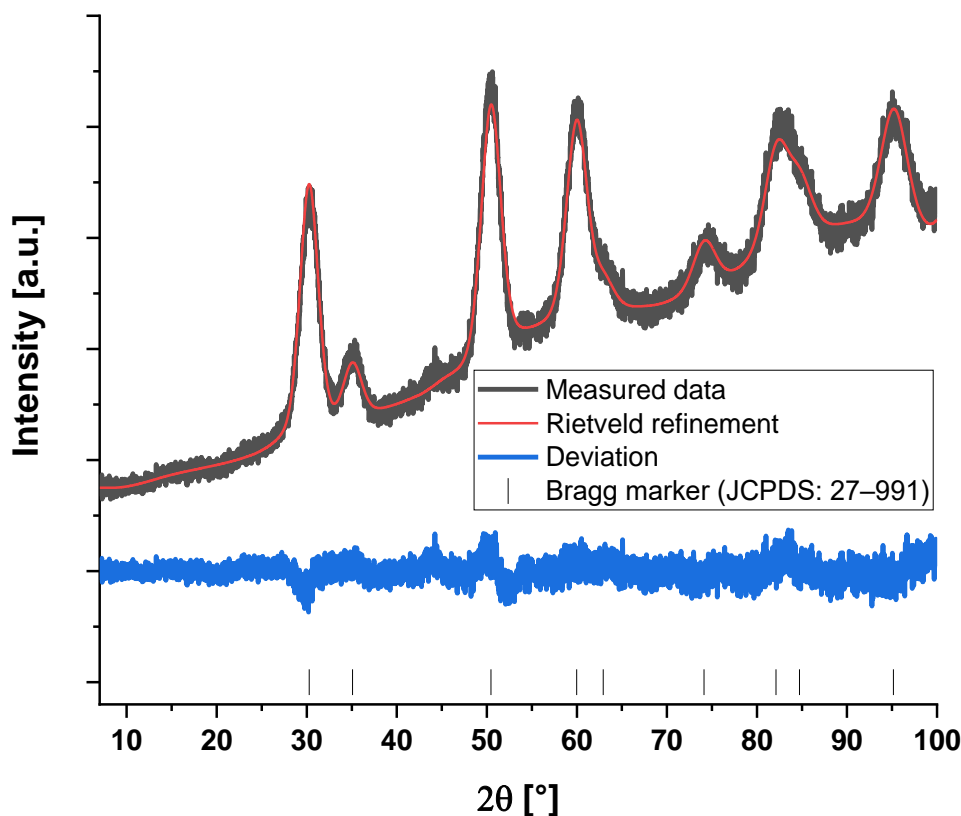
Figure 73: Diffractogram of cubic ZrO$_2$ nanoparticles (JCPDS: 27–991).[249]

The prepared ZrO$_2$ nanoparticles were surface modified with 1500 g/mol α-C$_{10}$H$_{20}$-COOH, ω-^{n}Bu PDMS (PDMS-COOH) until a transparent and stable solution (Figure 74) was formed which was adapted from Li *et al.*[257]
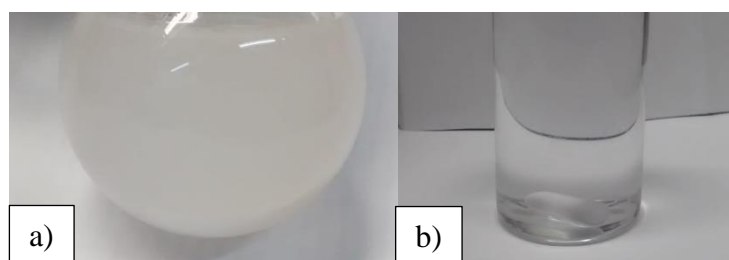

Figure 74: Zirconia suspension modified with benzyl alcohol in THF, a) before the addition of PDMS-COOH and b) after the addition.

TEM images (Figure 75) of the ZrO$_2$ particles show a uniform size distribution of 4.6 ± 0.9 nm after the synthesis and 4.1 ± 0.8 nm after the modification with PDMS-COOH (Figure 76). Measurement of the particles by TEM from the unmodified particles after the synthesis was more difficult due to the agglomerations which results in the small size difference. The particles showed a size between 3 nm to 4 nm in literature, but they were surface modified with smaller carboxylic acids like palmitic or stearic acid. The particles are spherical and highly dispersed as described in literature.[238, 241, 249-250]
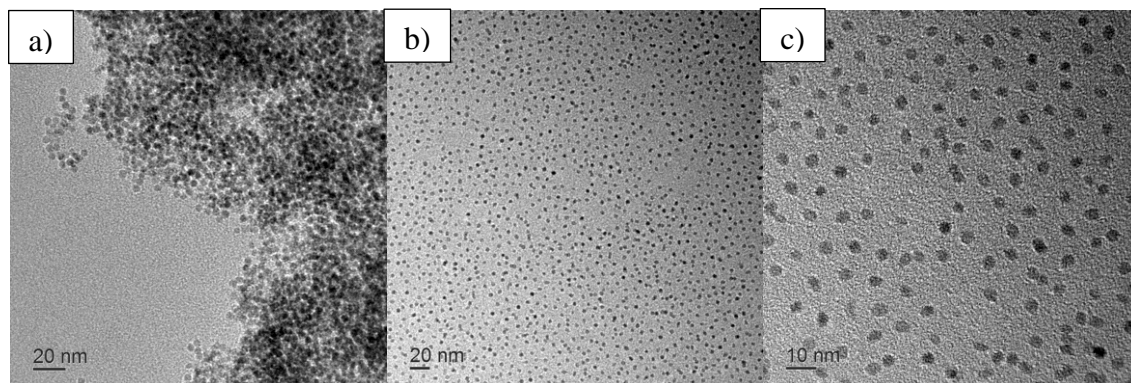
Figure 75: TEM image of ZrO₂ nanoparticles a) after synthesis, scale: 20 nm, b) modified with 1500 g/mol PDMS-COOH, scale: 20 nm and c) scale: 10 nm.
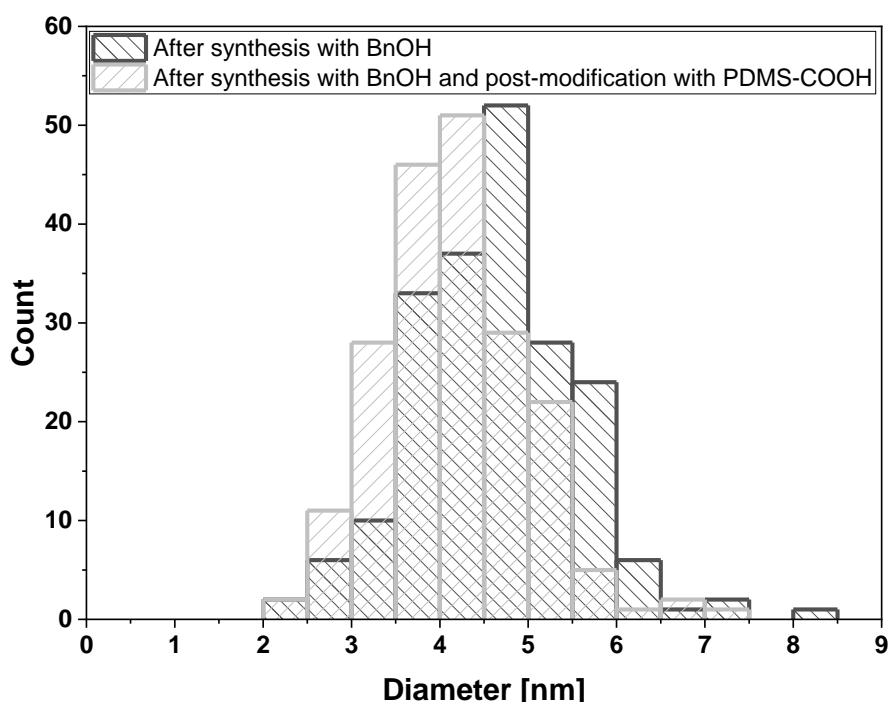
Figure 76: 200 counted ZrO₂ particles with their respected size before and after the postmodification.

DLS measurements (experimental section, Figure 221) were recorded directly after the synthesis in benzyl alcohol which results in agglomerates with a hydrodynamic diameter of 342.6 ± 0.6 nm. After the washing process with THF the particles were transferred into fresh THF and surface modifies with PDMS-COOH. They showed a size of 58.8 ± 0.2 nm and after 30 min of sonification with ultrasound, the particle size dropped to 14.4 ± 0.4 nm which supports the TEM images because in DLS measurements the hydrodynamic size is determined.

The FT-IR measurements (experimental section, Figure 222) show the desired bands from α-$C_{10}H_{20}$-COOH, ω-^{n}Bu PDMS after the postmodification as well as some remaining bands from benzyl alcohol indicating that it is still bound to the surface. In the FT-IR spectrum of ZrO₂ after the synthesis and after modification are the characteristic bands of PDMS visible at 2965 cm^{-1}, 1258 cm^{-1}, 1073 cm^{-1}, 1014 cm^{-1} and 790 cm^{-1}.[226, 346, 372-373] The vibration bands of

the CH_2 and C-C=C groups from the benzyl alcohol overlap with those of PDMS. In the unmodified sample spectrum, the signals of benzyl alcohol are visible at 716 cm^{-1} and in the range of 1323 cm^{-1} to 1613 cm^{-1}.[374-375] After the modification, the signals are still present, indicating that benzyl alcohol is still covalently bound onto the particle surface.

The TG measurements (experimental section, Figure 223) were carried out under nitrogen atmosphere. The TGA of the ZrO_2 nanoparticles directly after the synthesis reveals a two-step degradation. Starting at 170 °C the remaining liquid benzyl alcohol with a boiling point of 205 °C begins to evaporate, the sample loses 4.2 % mass. From 450 °C to about 600 °C there is a further mass loss of 13.7 %, in which the covalently bound benzyl alcohol is cleaved from the surface.[249] The dried PDMS-COOH modified particles show one decomposition step starting at 270 °C and ending at 710 °C resulting in the complete degradation of the PDMS and residual benzyl alcohol.[249, 353, 356, 376]

4.2.1.1.2 ZrO₂ with epoxides for the cross-linking with polysiloxanes by the ring opening reaction of epoxides

The ZrO_2 nanoparticles prepared by the autoclave reaction (4.2.1.1.1) were also used for a different nanocomposite system in which the particles are covalently bound to the polysiloxane. This reaction is performed using the ring opening reaction of epoxides. Therefore, the ZrO_2 nanoparticles received after the autoclave synthesis with benzyl alcohol onto the surface were surface modified using 3-glycidyloxypropyl trimethoxysilane.

The successful surface modification was verified using proton NMR after the washing process. All expected protons (Figure 77) could be assigned and the data also showed that no epoxide opening occurred during the surface modification.
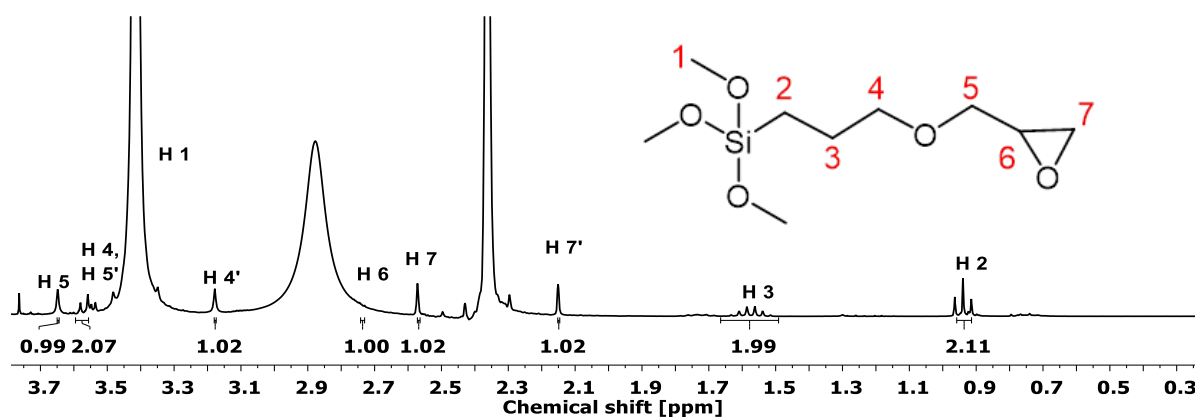

Figure 77: ¹H NMR (300 MHz, CDCl₃) of 3-glycidyloxypropylsiloxane surface modified nanoparticles with toluene, benzyl alcohol and methanol.

The signal of the methoxy-groups (H1) is very large because of remaining methanol from the precipitation and washing process, the same applies for benzyl alcohol and toluene. ^{13}C and ^{29}Si

NMRs could not be recorded because the particles were not stable in solution for the longer measurement time.

The TEM images (Figure 78) show very small round particles with a diameter of 2.5 ± 0.5 nm (Figure 79). Showing that this batch produced smaller particles than the one in 4.2.1.1.1 with 4.6 ± 0.9 nm. The particles are agglomerated because of the surface modification with 3-glycidyloxypropylsiloxane.
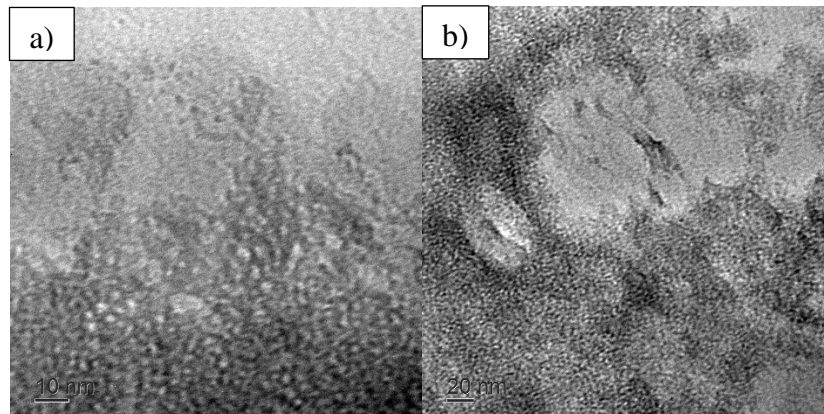
Figure 78: TEM images of ZrO₂ nanoparticles surface modified with 3-glycidyloxypropylsiloxane in different enlargements a) scale: 10 nm and b) scale: 20 nm.

The DLS curves (experimental section, Figure 224) show a hydrodynamic diameter of 2.6 ± 0.1 nm after the autoclave synthesis in benzyl alcohol which is identical with the size determined by the TEM images.
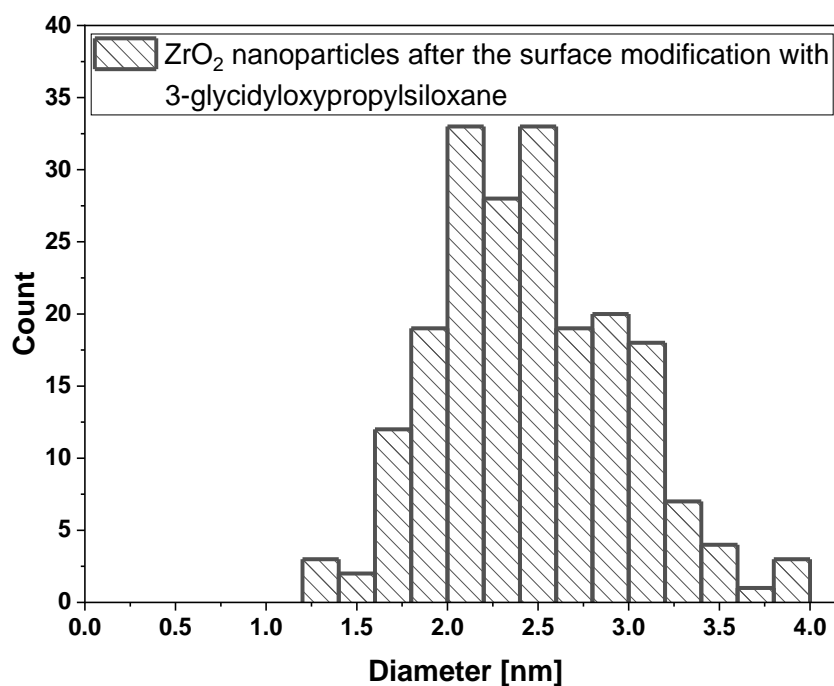
Figure 79: 200 counted ZrO₂ particles with their respected size after the surface modification with 3-glycidyloxypropylsiloxane.

After the surface modification with epoxides, the particles show a hydrodynamic diameter of 60.1 ± 0.8 nm, the aggregation of the modified particles is also visible in the TEM images. The TGA analysis (experimental section, Figure 225) under oxygen atmosphere shows two decomposition steps, the first from 40 °C to 180 °C with 3.7 % mass loss resulting from residual solvent methanol and toluene. The second step from 180 °C to 500 °C results from the release of the surface bound benzyl alcohol and the decomposition of 3-glycidyloxypropylsiloxane.

4.2.1.1.3   HfO$_2$ with PDMS-COOH for the incorporation into polysiloxanes

The synthesis of the hafnium oxide nanoparticles was performed analogously to the zirconium oxide nanoparticles, but the temperature was increased to 230 °C and the time was increased to four days according to Garnweitner *et al*. and Niederberger *et al*.[241, 250] The surface modification was performed with PDMS-COOH in THF after the washing process with THF.

The XRD measurement (Figure 80) showed the formation of monoclinic HfO$_2$ nanoparticles with a crystalline size of 2.0 ± 0.1 nm which is over one nanometre smaller than the ZrO$_2$ particles. The narrow reflex at 10.9° belongs to the organic from the precursor.[377-378]
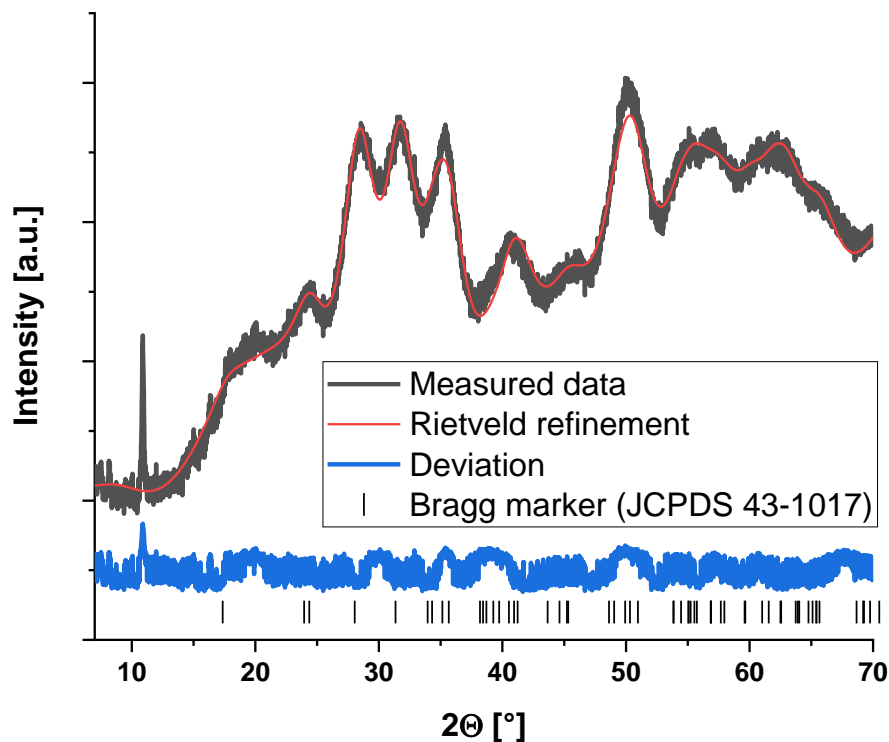

Figure 80: Diffractogram of monoclinic HfO$_2$ nanoparticles synthesised from the alkoxide precursor (JCPDS 43-1017).

The TEM images (Figure 81) show uniform oval particles with a diameter of 5.1 ± 1.5 nm (Figure 82). Due to the high loading of the copper net, an agglomeration of the particles occurs. The

DLS measurement (experimental section, Figure 226) after the synthesis reveals particles with a diameter of 38.8 ± 0.2 nm.
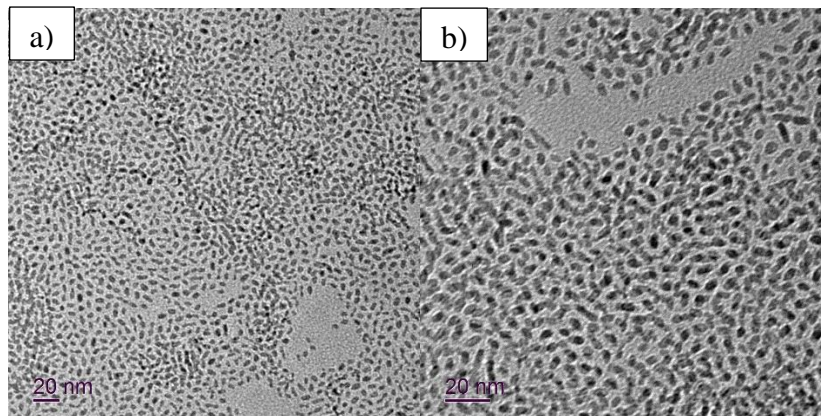
Figure 81: TEM images of HfO₂ nanoparticles from the Hf(OⁱPr)₄ in different enlargements a) and b) with a scale of 20 nm.
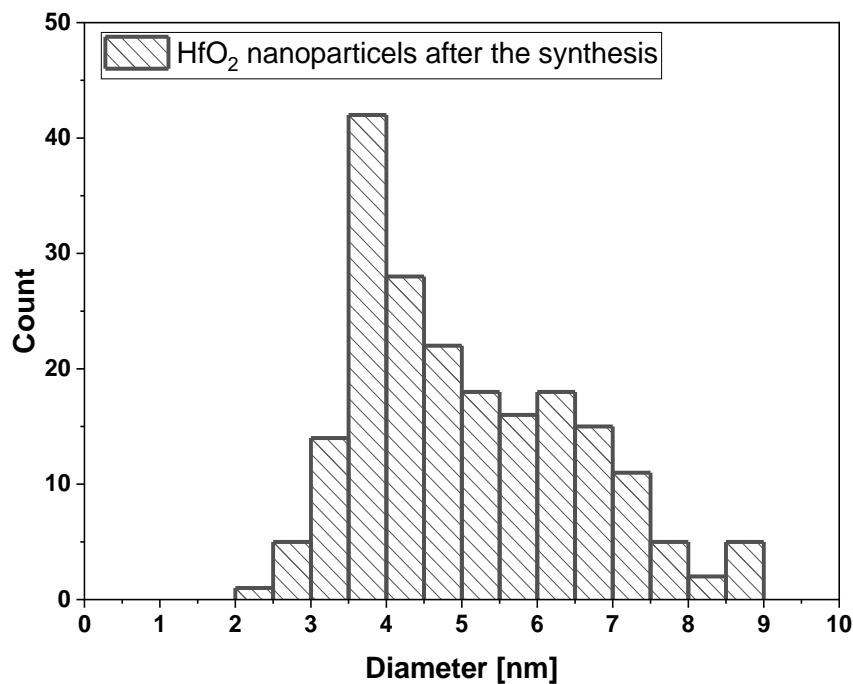
Figure 82: 200 counted HfO₂ particles with their respected size before the postmodification with PDMS-COOH.

The hydrodynamic diameter increased to 45.2 ± 0.2 nm after the surface modification with PDMS-COOH which is reduced again to 27.0 ± 0.2 nm after the sample was washed and filtered. The larger sizes determined by DLS relate to the strong agglomeration which is visible in the TEM images.

The vibrations in the FT-IR spectra (experimental section. Figure 227) were assigned analogously to the one in the FT-IR spectra recorded for the ZrO₂ sample surface modified with PDMS-COOH.

The TG measurements (experimental section, Figure 228) under nitrogen of the particles after the synthesis show a 1.5 % mass loss from 165 °C to 250 °C for the residual benzyl alcohol.[249] The second step with 26.7 % starting at 260 °C relates to the evaporation of the surface bound benzyl alcohol. The PDMS-COOH modified particles show a first step with 7.3 % mass loss from 160 °C to 290 °C because of the same reason. The second step starts at 290 °C and ends at 700 °C resulting in an 81.1 % mass loss because of the remaining surface bound benzyl alcohol and the degradation of PDMS-COOH.[249, 353, 356, 376]

4.2.1.2 HfO_2 from chloride precursor obtained by the autoclave synthesis

The synthesis was performed accordingly to De Roo *et al.*[267] which adapted the route from Buha *et al.*[268] and Niederberger *et al.*[241] The hafnium chloride was mixed with benzyl alcohol in an autoclave and heated to 220 °C for three days. After washing with ethanol and diethyl ether, the post modification was performed in chloroform with dodecanoic acid and oleylamine accordingly to De Roo *et al.*[267]

XRD analysis (Figure 83) confirms that the prepared compound is HfO_2 in the monoclinic phase with a crystallite size of 5.0 ± 0.1 nm, which is slightly smaller than the crystallite size in the literature of 6.3 nm to 8.0 nm.[267]
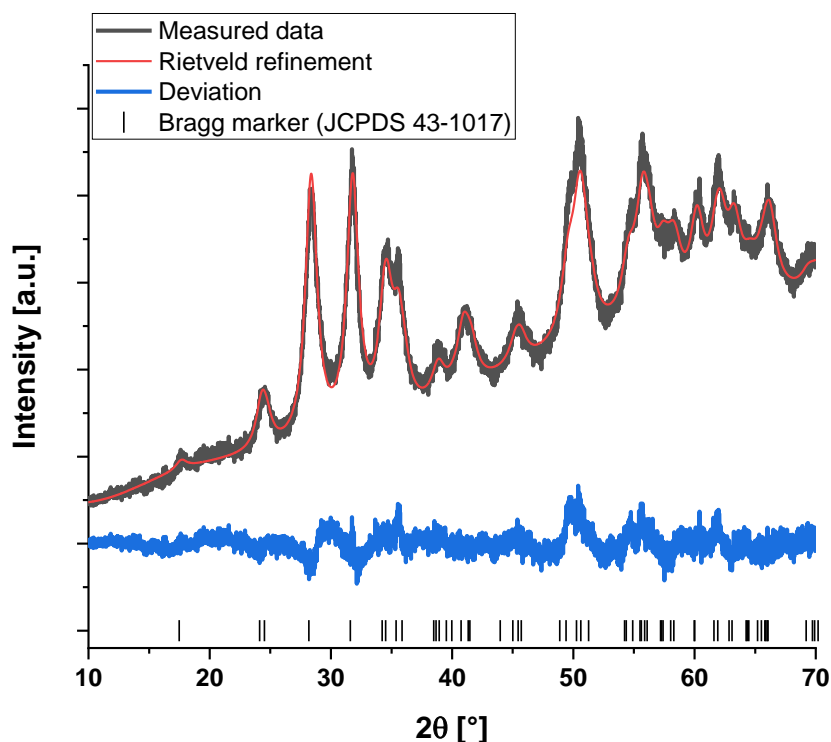

Figure 83: Diffractogram of monoclinic HfO_2 nanoparticles (JCPDS 43-1017).

The TEM images (Figure 84) are in agreement with the XRD data, particles with a diameter of 5.6 ± 1.6 nm (Figure 85) can be seen. They are not uniform; besides round particles some elongated ones are present which results in a broader size distribution. The literature size determined by TEM is 5.2 ± 1.5 nm.[267]
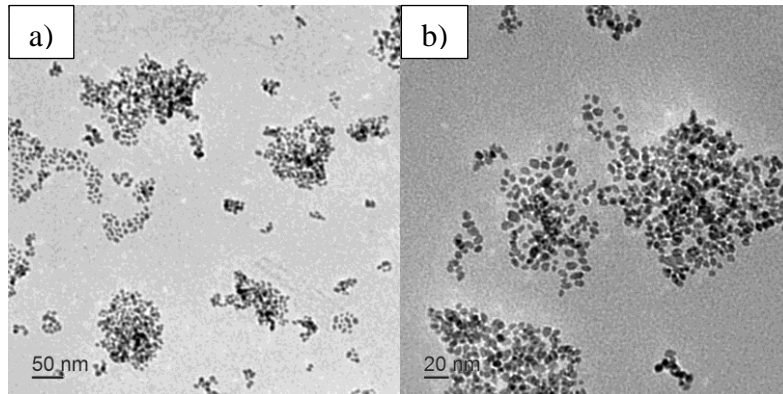
Figure 84: TEM images of HfO₂ nanoparticles from the HfCl₄ precursor in different resolutions a) scale: 50 nm and b) scale: 20 nm.
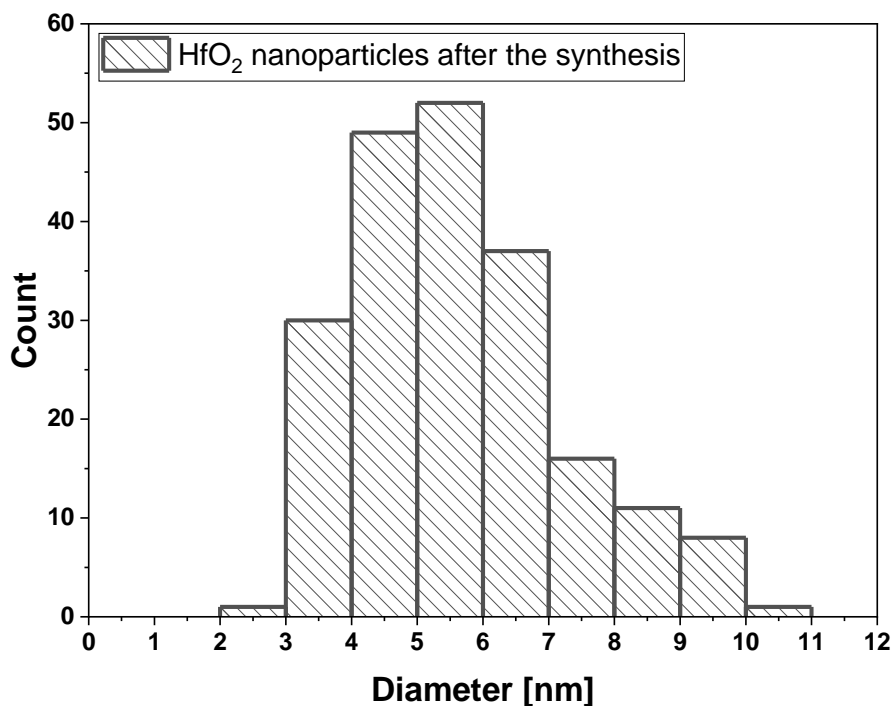
Figure 85: 200 counted HfO₂ particles with their respected size before the postmodification with dodecanoic acid and oleylamine.

The DLS measurement (experimental section, Figure 229) after the synthesis shows particles with a larger hydrodynamic diameter than the TEM images of 16.0 ± 0.6 nm, which confirms the literature data.[267] The particles showed a hydrodynamic diameter of 25.8 ± 0.2 nm after postmodification.

In the FT-IR spectrum (experimental section, Figure 230) of the HfO_2 particles after the synthesis the signals of the OH groups located on the particle surface are in the range from 2400 cm^{-1} to 3600 cm^{-1}.[261, 347, 379-380] The O-H valence vibration of benzyl alcohol is in the range of 1620 cm^{-1} and the C-H deformation oscillations of the aromatic in the range of 600 cm^{-1} to 800 cm^{-1}.[261, 347, 379-380] After the particles were modified with dodecanoic acid and oleylamine, the typical bands of the C-H vibrations as well as the carboxylic acid at 1470 cm^{-1}. Other bands overlap with C-C and C-H vibrations.[251, 380] The N-H vibrations[16] are visible at 3309 cm^{-1} and 1537 cm^{-1}.[261, 347, 379-380]

TG analyses of the nanoparticles (experimental section, Figure 231) show only a small mass loss of 7.4 % for the unmodified particles, where the initial mass loss of 1.3 % occurs in the range of 50 °C to 160 °C relating to solvent residues of ethanol and chloroform. The subsequent mass loss is referred to benzyl alcohol, which is partially bound to the surface.[249, 353, 356, 376] The mass loss of the postmodified particles is much higher with 56.9 % and shows the parallel decomposition of dodecanoic acid and oleylamine despite of their different boiling temperatures of 298 °C and 364 °C, respectively.[381] The additional effect of the stronger surface bonding of the dodecanoic acid compared to the oleylamine has also to be taken into account.[270-271] Oleylamine alone mainly decomposes in two steps from 200 °C to 500 °C and further slowly decomposes up to 900 °C.[16]

4.2.1.3 *Metal oxide from trifluoroacetate precursor*

4.2.1.3.1 $\underline{ZrO_2\text{ with oleylamine}}$

The particles were synthesised accordingly to Liu *et al*.[16] First an organic metal precursor was synthesised from zirconium tetrachloride and trifluoroacetic acid which was stirred for five hours at 40 °C. After drying the $Zr(CF_3COOH)_4$ precursor was obtained which then was mixed with oleylamine, which serves as solvent and surface modifier, and stirred under vacuum at 110 °C for 30 min. The transparent solution was then heated to 330 °C for one hour. After adding acetone, the nanoparticles flocculated and could be collected. They were washed with toluene and ethanol and dispersed in toluene. Further surface modifications were not applied.

A XRD measurement (Figure 86) was performed and the Rietveld refinement showed the formation of monoclinic ZrO_2 with a crystalline size of 3.7 ± 0.2 nm.[382-383] The literature reported the formation of the cubic phase with a larger crystalline size of 5.9 ± 0.1 nm,[251] but also reported that they expected the monoclinic one due to other literature.[382-383]
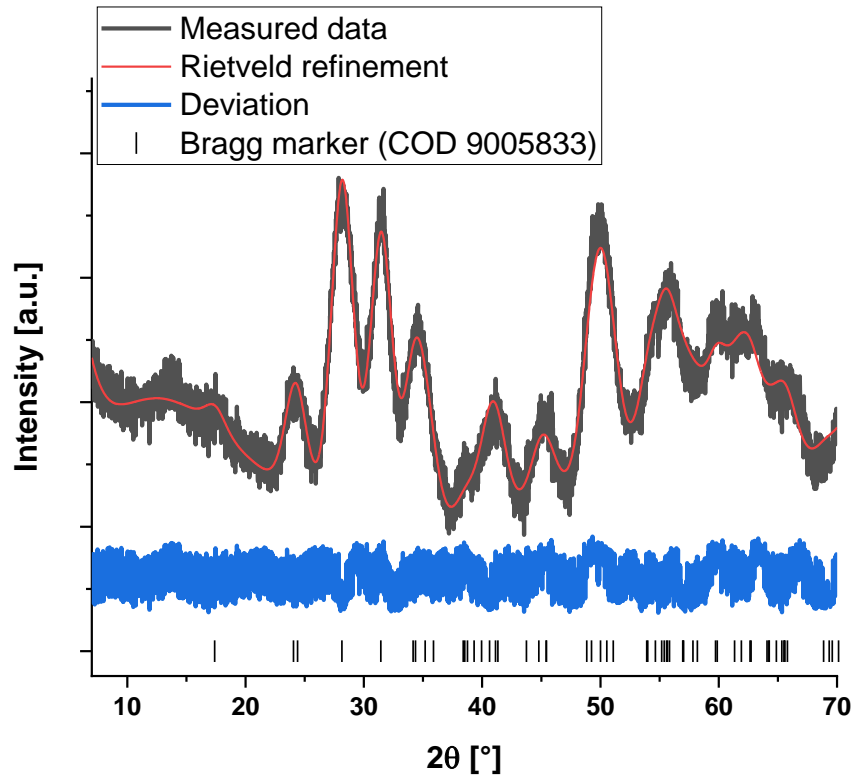
Figure 86: Diffractogram of monoclinic ZrO$_2$ nanoparticles (COD 9005833).[251, 382-383]

The TEM images (Figure 87) show mostly elongated particles and some spherical ones with a size of 8.1 ± 4.0 nm (Figure 88) which is double the amount determined by XRD showing that large areas of the particles are amorphous. The large size and standard deviation results from a few larger particles up to 23 nm. The literature size is reported with 5.5 ± 0.8 nm.[16]

Figure 87: TEM images of ZrO$_2$ nanoparticles from the Zr(CF$_3$COO)$_4$ precursor in different resolutions a) scale: 50 nm and b) scale: 20 nm.

Figure 88: 200 counted ZrO₂ particles with their respected size after the synthesis.

The DLS measurement (experimental section, Figure 232) shows a hydrodynamic diameter of 10.4 ± 0.4 nm, which is in agreement with the size determined by TEM.

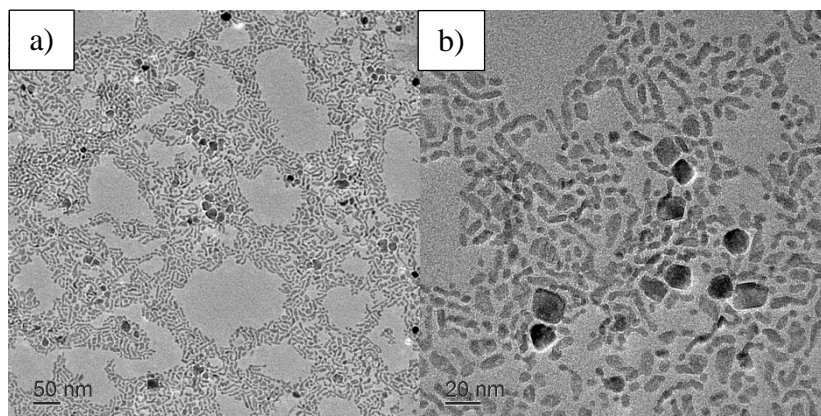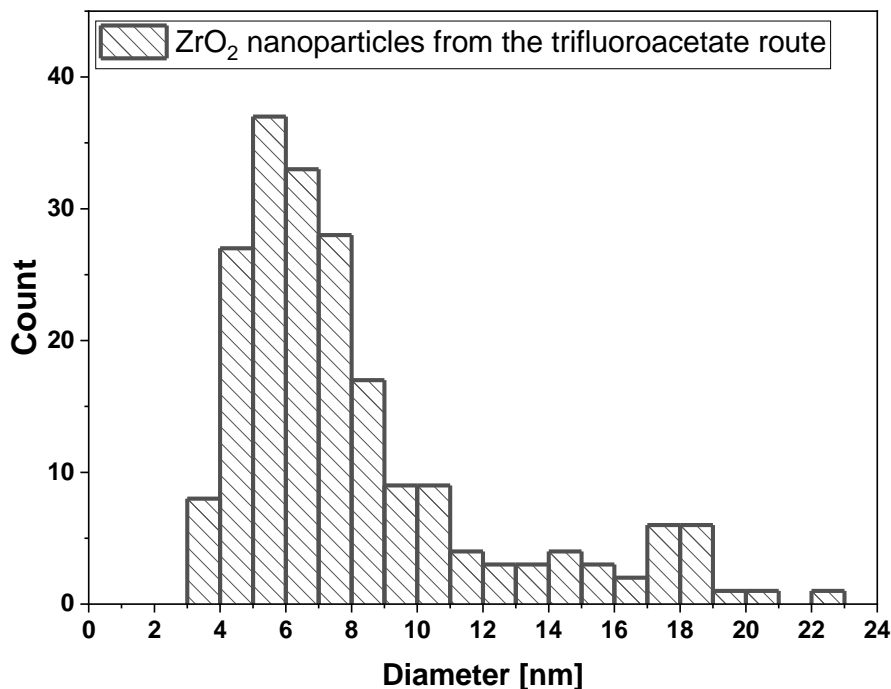In the FT-IR spectrum (experimental section, Figure 233) are only the oleylamine bands visible. The C-H vibrations are in the range of 2800 cm^{-1} to 3000 cm^{-1}, [131, 154] at 1470 cm^{-1} [131, 154] and at 700 cm^{-1} to 800 cm^{-1} [261, 347, 379-380].[251, 380] The N-H vibrations are located at 3000 cm^{-1} to 3300 cm^{-1} [16] and 1537 cm^{-1}.[261, 347, 379-380]

TGA measurements (experimental section, Figure 234) up to 900 °C were carried out under N₂. The curve is in agreement with the literature for oleylamine surface modified ZrO₂ nanoparticles.[16] The first 1.5 % mass loss are due to remaining ethanol from the washing process.[16] The decomposition of oleylamine occurs in two steps, a first fast step from 150 °C to 480 °C with 21.6 % mass loss and a second slower one up to 700 °C with 4.0 % mass loss.

4.2.1.3.2 HfO₂ with oleylamine

The synthesis was performed accordingly to Liu *et al.*, which is an identical synthesis as the one for the ZrO₂ nanoparticles with oleylamine.[251]

The XRD measurement (Figure 89) confirmed the formation of the monoclinic phase with a crystallite size of 3.2 ± 0.1 nm, while the size reported in literature is 5.7 ± 0.3 nm.[251] One possibility is that the temperature was slightly lower than 330 °C because this strongly affects the crystallite size. Liu *et al.* investigated this correlation on ZrO₂ in a later publication and showed

that a temperature of 315 °C would match a particle size of 4.1 nm for ZrO_2.[16] Taken into account that the ZrO_2 nanoparticles are around 0.5 nm larger than the HfO_2 ones synthesised by the same group in the same synthesis route, the reaction occurred at around 315 °C.[16, 251] The problem was that the old heater equipped with a thermocouple inside the flask could not reach the temperature of 330 °C starting from room temperature in exactly one hour, but oscillated.
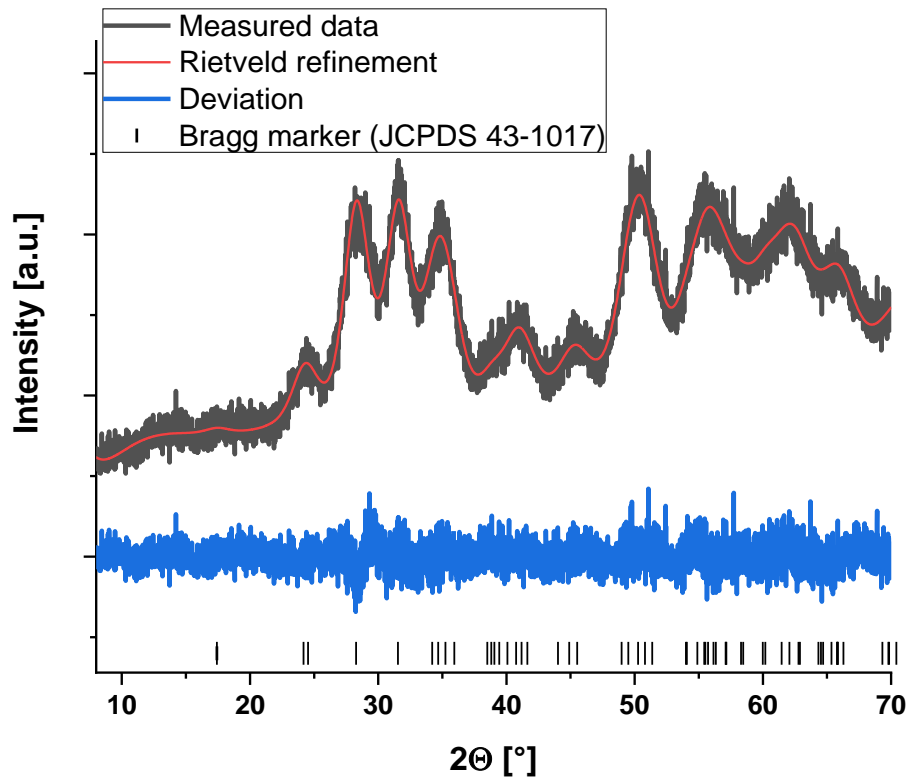
Figure 89: Diffractogram of monoclinic HfO₂ nanoparticles (JCPDS 43-1017).

TEM recordings (Figure 90) were performed to verify the XRD measurements. An average particle size of 4.8 ± 1.2 nm (Figure 91) could be determined, the literature size is reported with around 5 nm.[251] The particles are mostly spherical but some are elongated with a size of up to 9 nm.
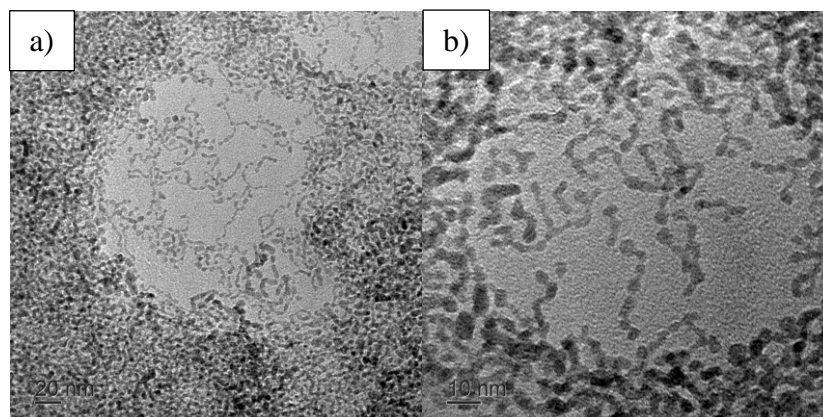
Figure 90: TEM images of HfO₂ nanoparticles from the Hf(CF₃COO)₄ precursor in different resolutions a) scale: 20 nm and b) scale: 10 nm.
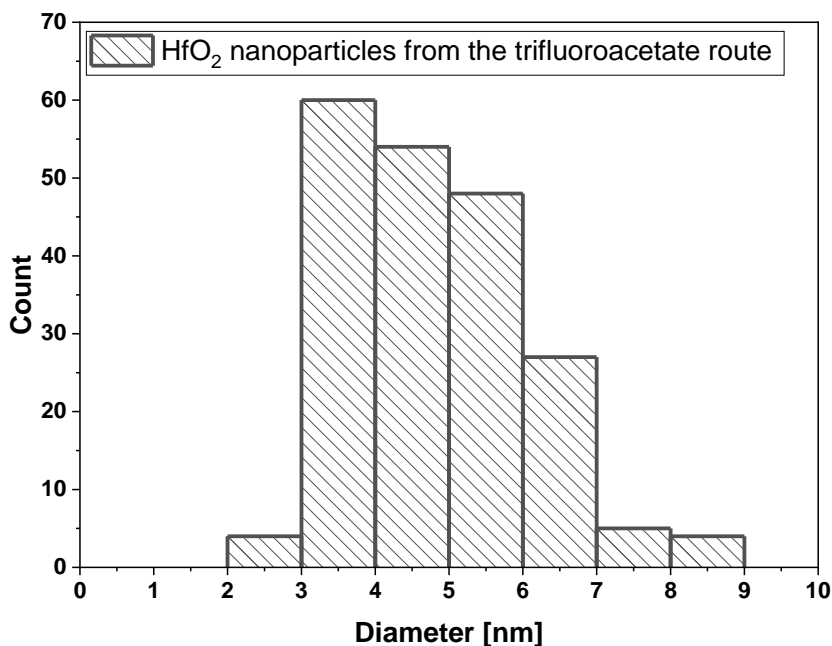
Figure 91: 200 counted HfO₂ particles with their respected size after the synthesis.

The DLS measurement (experimental section, Figure 235) showed a bimodal distribution, one region with a hydrodynamic diameter of 7.0 ± 0.1 nm and one region with 23.2 ± 0.6 nm. The smaller size agrees with the XRD and TEM measurements. The larger size probably results from an agglomeration in solution because in the TEM image of the dried particles such large ones cannot be observed.

In the FT-IR spectrum (experimental section, Figure 236) are only the oleylamine bands visible like in the ZrO_2 spectrum.[16, 251, 261, 347, 379-380]

TGA measurements (experimental section, Figure 237) under nitrogen atmosphere were carried out up to 900 °C, the degradation curve is in accordance with the $ZrO_2$ curve and the literature for oleylamine surface modified ZrO_2 nanoparticles.[16] The first 2.2 % mass loss is due to remaining ethanol from the washing process. The decomposition of the oleylamine occurs in two steps,[16] a first fast step from 200 °C to 450 °C with 17.6 % mass loss and a second slower one up to 700 °C with 4.3 % mass loss.

4.2.1.4 *ZrO₂ with 3-methacryloxypropyl trimethoxysilane from basic carbonate precursor*

The synthesis was performed accordingly to Chung *et al.*[236] Zirconium basic carbonate was mixed with distilled water and sodium hydroxide and heated up to 110 °C for twelve hours. After the supernatant was discarded, the particles were washed with ammonium bicarbonate and water. The particles were then mixed with water and butyric acid and heated up to 70 °C for four hours. The sediment was centrifuged and washed with water and the particles were

dried under reduced pressure and dispersed in ethyl acetate. 3-Methacryloxypropyl trimethoxysilane was added and they were heated up to 70 °C for one hour. The particles were precipitated with water, centrifuged, dried, and dispersed in toluene.

An XRD measurement (Figure 92) before the postmodification of the nanoparticles was carried out to determine the crystallinity and phase of the sample. The cubic phase of ZrO_2 with a crystalline size of 4.6 ± 0.1 nm was obtained which is slightly smaller than the 6.6 nm described in literature.[236]
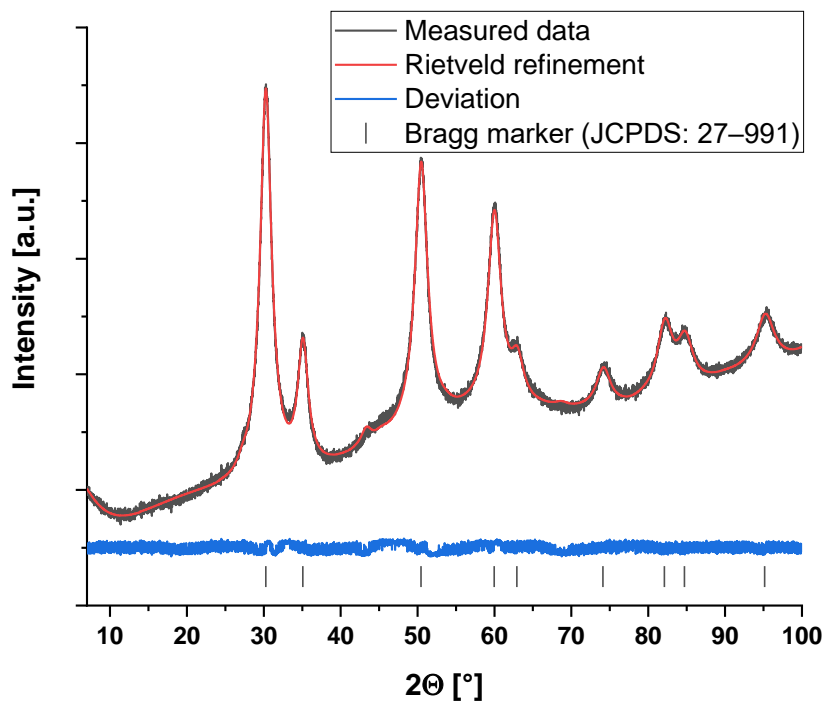
Figure 92: Diffractogram of cubic ZrO₂ nanoparticles (JCPDS: 27–991).[249]

TEM images (Figure 93) after the post-modification revealed that the obtained particles are not uniform, they have a diameters of 4.3 ± 0.7 nm (Figure 94) which is in agreement with the XRD data. The large deviation results from the agglomerates (darker areas).
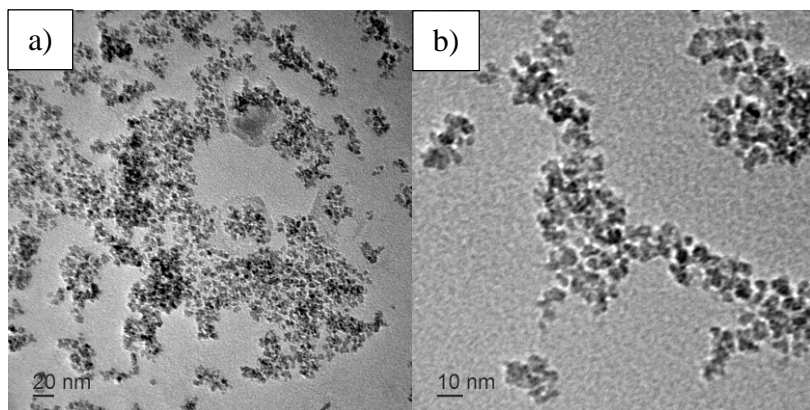
Figure 93: TEM image of the ZrO₂ nanoparticles from the basic carbonate precursor after the postmodification with butyric acid and 3-methacryloxypropyl trimethoxysilane a) scale: 20 nm and b) scale: 10 nm.
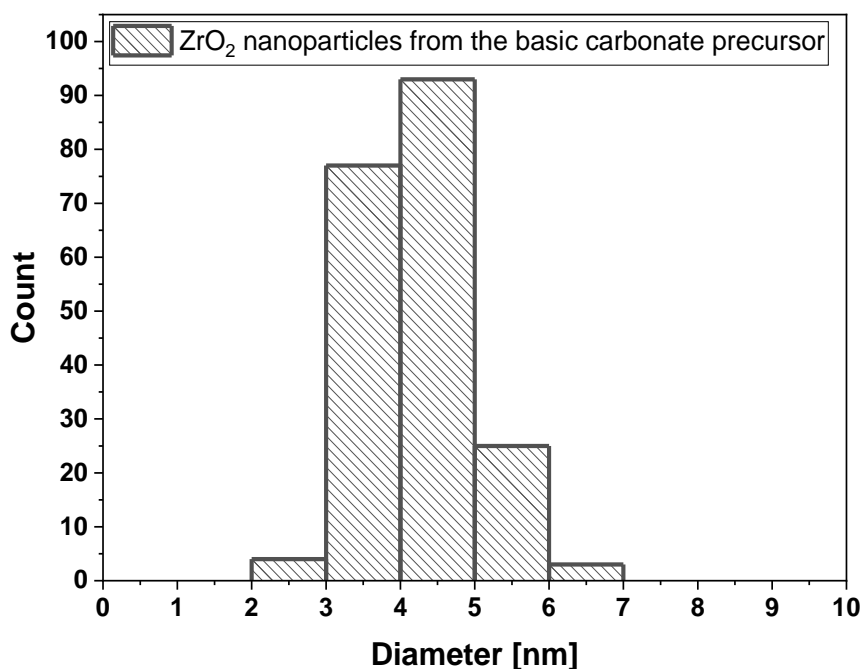
Figure 94: 200 counted ZrO₂ particles with their respected size from the basic carbonate precursor after the post-modification with butyric acid and 3-methacryloxypropyl trimethoxysilane.

The DLS measurements after the post-modification showed a hydrodynamic diameter of 15.8 ± 0.6 nm because of the agglomerations seen in the TEM image (experimental section, Figure 238).

The FT-IR measurements (experimental section, Figure 239) show the bands from butyric acid and 3-methacryloxypropyl trimethoxysilane. The vibrations of the Si-O bond are located at $1164\ cm^{-1}$ and $983\ cm^{-1}$ and the ones from the Si-C are visible at $1321\ cm^{-1}$, $1296\ cm^{-1}$, $816\ cm^{-1}$ and $773\ cm^{-1}$.[226, 346, 372-373] The vibration bands of the C-H and C-C groups from butyric acid overlap with those of the siloxane in the region of $2807\ cm^{-1}$ to $3040\ cm^{-1}$ and $1384\ cm^{-1}$ to $1720\ cm^{-1}$.[226, 372-375] The $C=C_V$ vibration from the methacrylate-group is visible at $937\ cm^{-1}$.[380, 384]

The TGA under oxygen atmosphere (experimental section, Figure 240) shows one decomposition step starting at 176 °C and ending at 580 °C resulting in a 39.0 % mass loss because of the surfactants.

^{1}H, ^{13}C and ^{29}Si NMR spectra (experimental section, Figures 95, 241 and 242) of the surface modified particles were recorded, in the ^{1}H NMR all signals of the 3-methacryloxypropyl trimethoxysilane surface modifier are visible. An integration of 5.7 for the methoxy protons shows that the silicon atom mainly forms one bond to the particle surface, in the mean 1.1 of the 3.0 methoxy-groups anchored. Therefore, in the ^{29}Si NMR (Figure 242) are two signals visible, one larger at -42 ppm for the T^1 silicon atom and at -51 ppm for the T^2 silicon atom.[236, 321, 331] The

signals of the butyric acid are barely visible at 0.9 ppm for the CH_3, 1.7 ppm for the C-CH_2-CH_3 and at 2.3 ppm for the C-CH_2-CH_2 group, which are around 3 % in correlation to the 3-methacryloxypropyl di/trimethoxysilane. A nearly complete exchange of the surfactant occurred.
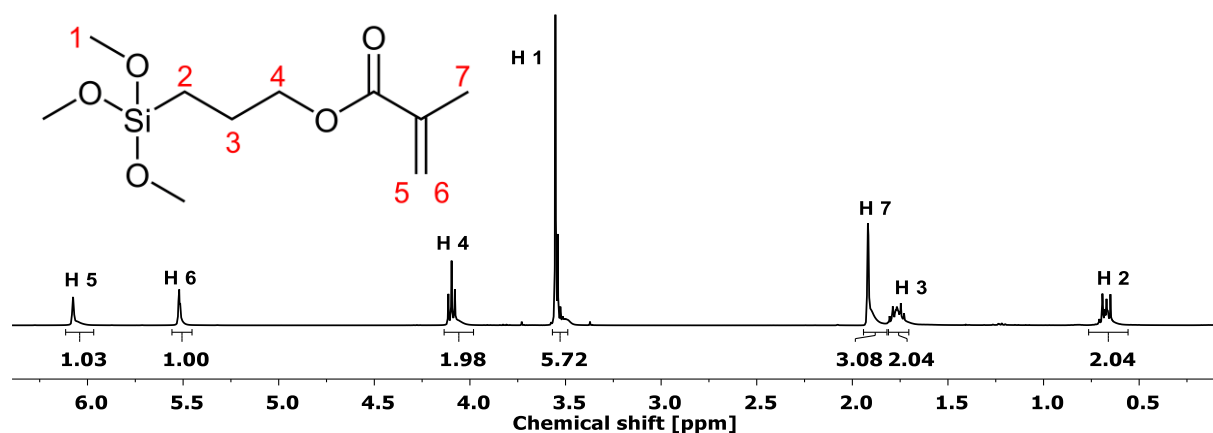
Figure 95: ^{1}H NMR (400 MHz, CDCl$_3$) of ZrO$_2$ nanoparticles after the postmodification with butyric acid and 3-methacryloxypropyl trimethoxysilane.

4.2.1.5 Conclusion

An overview of all synthesised ZrO$_2$ and HfO$_2$ routes are shown in Table 9. The zirconium routes allow good batch sizes in the gram scale, the high temperature cubic phase was received twice and the low temperature monoclinic phase once.[385] The trifluoroacetate route is not recommend, although it is very fast, because of larger elongated particles and agglomerates which can be seen in the TEM images. The basic carbonate and the *n*-propoxide route show identical diameters determined by TEM images but the autoclave reaction of the *n*-propoxide shows a smaller crystallite size. The basic carbonate route is four times faster with only half of the temperature needed compared to the *n*-propoxide one. The hafnium routes with the *iso*-propoxide and the trifluoroacetate precursor allow batch sizes in the gram scale, while the chloride route only reaches the milligram range. All synthesised HfO$_2$ particles are in the low temperature monoclinic phase.[385] The crystallite size increases from *iso*-propoxide over trifluoroacetate to the chloride precursor reaction. The diameter as well as the deviations measured by TEM images are comparable. Therefore, the trifluoroacetate synthesis is the most suitable one because of the over 50 times faster synthesis compared to the *iso*-propoxide route. The higher temperature of 330 °C has only be applied for one hour, while for the *iso*-propoxide synthesis needs 230 °C for 96 hours.

Table 9: Overview of the synthesised ZrO_2 and HfO_2 nanoparticles with their size determined by XRD, TEM and DLS, their received phase (c: cubic, m: monoclinic) and the synthesis process.

Particle	Precursor	XRD crystallite size [nm]	TEM diameter [nm]	DLS hydrodynamic diameter [nm]	Reaction time, temperature
ZrO_2 (c)	*n*-propoxide	3.3 ± 0.1	4.1 ± 0.8	14.4 ± 0.4	48 h, 210 °C
ZrO_2 (m)	trifluoroacetate	3.7 ± 0.2	8.1 ± 4.0	10.4 ± 0.4	0.5 h, 110 °C
					1 h, 330 °C
ZrO_2 (c)	basic carbonate	4.6 ± 0.1	4.3 ± 0.7	15.8 ± 0.6	12 h, 110 °C
HfO_2 (m)	*iso*-propoxide	2.0 ± 0.1	5.1 ± 1.5	27.0 ± 0.2	96 h, 230 °C
HfO_2 (m)	chloride	5.0 ± 0.1	5.6 ± 1.6	25.8 ± 0.2	72 h, 220 °C
HfO_2 (m)	trifluoroacetate	3.2 ± 0.1	4.8 ± 1.2	7.0 ± 0.1	0.5 h, 110 °C
				23.2 ± 0.6	1 h, 330 °C

4.2.2 Incorporation of metal oxide nanoparticles into polysiloxanes

The surface modified nanoparticles in solution were mixed into the commercial polysiloxanes KJR-9022-E1 from Shin-Etsu as a polydimethylsiloxane and OE-6630 from Dow Corning as a polymethylphenylsiloxane. Additionally, a self-prepared polydiphenylsiloxane over a route patented in a previously OSRAM project was also used.[223-224] This HRI polymer has a RI of 1.576 which is slightly higher than the 1.552 of the OE-6630 system. It consists out of two components which were synthesised in polycondensation reactions and has a very high amount of phenyl-groups as well as a higher degree of cross-linking. Component A being a hydride-group containing copolymer was synthesised using diphenylsilanediol and methyldiethoxysilane with gaseous hydrogen chloride as catalyst. Component B being a vinyl-group containing copolymer was synthesised using diphenylsilanediol and vinyltrimethoxysilane with gaseous ammonia as catalyst. After mixing the polymer with the particle suspension, the solvent was removed under reduced pressure at 2 mbar and continuous stirring. The polymer mixture was casted onto cleaned microscope glass slides with about 3 mm thickness or doctor bladed with 120 µm which results in a 60 µm film, cured at 150 °C for four hours and the refractive index at 20.0 °C and 589 nm was determined. For later samples, the transmission at 450 nm and the $T_{95\%}$ values are reported. The particles prepared from the *n*-propoxide reaction always have benzyl alcohol and the ones from trifluoroacetic acid always oleylamine on their surface after the synthesis because these molecules serve as solvent and stabilising agent during the reaction. However, surfactants, which form stronger or more bonds, like carboxylic, phosphinic or phosphonic acids respectively phosphate esters can replace the amine or alcohol-group containing surfactants.[259-260, 262-263, 266] This was performed with the PDMS-OH, lauric acid, butyric acid as well as trimethoxysilanes.

4.2.2.1 3.0 wt% ZrO$_2$ mixed in polydimethylsiloxane

Sample 01 (Table 10) shows the pure KJR-9022-E1 casted by hand onto the glass slide and cured, the 1 mm thick film is transparent and colourless. In sample 02 3.0 wt% of ZrO$_2$ nanoparticles from the alkoxide route, surface modified with benzyl alcohol and oleylamine, were mixed into the polydimethylsiloxane, the film is white and opaque, and no RI could be determined. The missing chemically similar surface modifier leads to light scattering.[242-244, 256-257]

Table 10: 3.0 wt% of ZrO₂ nanoparticles mixed into the commercial polysiloxane KJR-9022-E1.

Sample	01	02
Polysiloxane	KJR-9022-E1	KJR-9022-E1
Precursor	–	$Zr(O^nPr)_4$
Particles	–	3.0 wt% ZrO_2
Surfactant	–	Benzyl alcohol + Oleylamine
RI	1.4100	–
Image		

4.2.2.2   3.0 wt% ZrO₂ mixed in polymethylphenylsiloxane

All samples were casted by hand which results in a film thickness of around 1 mm. The sample 03 (Table 11) shows the pure polymethylphenylsiloxane OE-6630, the film is colourless and highly transparent. In sample 04, 3.0 wt% of ZrO_2 from the autoclave synthesis with the $Zr(O^nPr)_4$ precursor and oleylamine as surfactant were mixed inside the polysiloxane and cured. The film is slightly yellow and opaque indicating that oleylamine is not suitable as surfactant. The amine-group also hinders the hydrosilylation reaction because it is a platinum catalyst poison, it is possible, that some free oleylamine was in the particle suspension or a duple layer of oleylamine could be present on the particle surface with the free amine-group on the outside because the aliphatic rest stacks.[386] The RI of the ZrO_2 containing sample is around 0.0025 higher than that of the pure silicone. In sample 05, the surface modifier was changed into ^nBu-PDMS-$C_{10}H_{20}$-COOH (PDMS-COOH) and a transparent and colourless polysiloxane was received, but the RI was slightly lower because of the introduction of PDMS chains which has a RI of 1.410.[360-362] For sample 06, other ZrO_2 nanoparticles from the $Zr(CF_3COO)_4$ precursor route were surface modified with ^nBu-PDMS-$C_{10}H_{20}$-COOH and mixed into OE-6630. The film here is thinner with around 1 mm, colourless and transparent. The RI increase is negligible, the positive effect of the particles and the negative one from the PDMS negate each other.
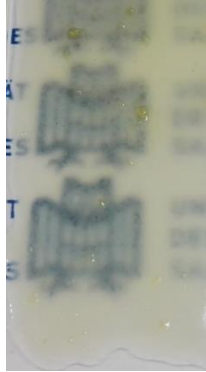
Table 11: 3.0 wt% of ZrO$_2$ nanoparticles mixed into the commercial polysiloxane OE-6630.

Sample	03	04	05	06
Polysiloxane	OE-6630	OE-6630	OE-6630	OE-6630
Precursor	–	Zr(O^{n}Pr)$_4$	Zr(O^{n}Pr)$_4$	Zr(CF$_3$COO)$_4$
Particles	–	3.0 wt% ZrO$_2$	3.0 wt% ZrO$_2$	3.0 wt% ZrO$_2$
Surfactant	–	Benzyl alcohol + Oleylamine	Benzyl alcohol + PDMS-COOH	Oleylamine + PDMS-COOH
RI	1.5515	1.5540 (+0.16 %)	1.5529 (+0.09 %)	1.5520 (+0.03 %)
Image				

4.2.2.3   10.0 wt% ZrO$_2$ mixed in polymethylphenylsiloxane

All samples were casted by hand which results in a film thickness of around 1 mm. For sample 07 (Table 12), the particle amount was increased to 10.0 wt% and no additional surface modifier was introduced. The sample is yellow and opaque. The effect is much stronger than in sample 04 because of the oleylamine, a RI could not be determined because the sample is turbid. Sample 08 was surface modified with 850 g/mol α-(1-propyl-3-phosphonate), ω-(*n*-butyl) PDMS (PDMS-PO(OH)$_2$), the yellowing is slightly reduced, and the transparency is higher but still opaque. Sample 09 was modified with a longer PDMS of 4750 g/mol and the yellowing is further reduced but the transparency is lower than in sample 08, close to sample 07. The effect of the oleylamine which cannot be fully removed even with stronger surfactants like phosphonates results in a particle synthesis change, the trifluoroacetate route therefore is not further recommend.
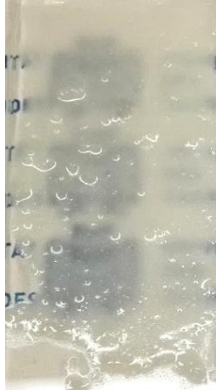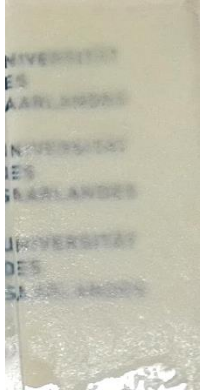
Table 12: 10.0 wt% of ZrO$_2$ nanoparticles mixed into the commercial polysiloxane OE-6630.

Sample	03	07	08	09
Polysiloxane	OE-6630	OE-6630	OE-6630	OE-6630
Precursor	–	Zr(CF$_3$COO)$_4$	Zr(CF$_3$COO)$_4$	Zr(CF$_3$COO)$_4$
Particles	–	10.0 wt% ZrO$_2$	10.0 wt% ZrO$_2$	10.0 wt% ZrO$_2$
Surfactant	–	Oleylamine	Oleylamine + PDMS-PO(OH)$_2$ 850 g/mol	Oleylamine + PDMS-PO(OH)$_2$ 4750 g/mol
RI	1.5515	–	–	–
Image				

4.2.2.4 10.0 wt% HfO$_2$ mixed in polymethylphenylsiloxane

All samples were casted by hand which results in a film thickness of around 1 mm. Sample 10 (Table 13) shows the pure polysiloxane with 10.0 wt% HfO$_2$ nanoparticles synthesised from the trifluoroacetate precursor and therefore oleylamine is on the particle surface. The film is slightly opaque and transparent, but a RI could not be determined. In sample 11 the particles were surface modified with 5000 g/mol α-(1-propoxyethyl-6-phosphate), ω-(n-butyl) PDMS (PDMS-OPO(OH)$_2$), the film is opaque, colourless and the surface is uneven. For sample 12 the nanoparticles were surface modified with 10000 g/mol α-(1-propoxyethyl-6-phosphate), ω-(n-butyl) PDMS, the film is slightly transparent, colourless and the surface is uneven, but less rough. The sample 13 was bimodal surface modified, first with the 10000 g/mol phosphate and then with the 5000 g/mol PDMS-OPO(OH)$_2$ analogously to Li *et al.*[242, 256-257] The expected effect of the bimodal surface modification is not observable. The film is opaque, colourless, and comparable to sample 11. The surface is uneven but finer than in sample 11. Here again the missing chemically similar surfactant leads to a transparency loss.[242-244, 256-257] No RI for the samples 10 to13 could be determined.

Table 13: 10.0 wt% of HfO$_2$ nanoparticles mixed into the commercial polysiloxane OE-6630.

Sample	10	11	12	13
Polysiloxane	OE-6630	OE-6630	OE-6630	OE-6630
Precursor	Hf(CF$_3$COO)$_4$	Hf(CF$_3$COO)$_4$	Hf(CF$_3$COO)$_4$	Hf(CF$_3$COO)$_4$
Particles	10.0 wt% HfO$_2$	10.0 wt% HfO$_2$	10.0 wt% HfO$_2$	10.0 wt% HfO$_2$
Surfactant	Oleylamine	Oleylamine + PDMS-OPO (OH)$_2$ 5k g/mol	Oleylamine + PDMS-OPO (OH)$_2$ 10k g/mol	Oleylamine + PDMS-OPO(OH)$_2$ 5k + 10k g/mol
RI	–	–	–	–
Image				

4.2.2.5 10.0 wt% to 30.0 wt% HfO$_2$ mixed in polymethylphenylsiloxane and polydiphenylsiloxane

All samples were doctor-bladed with 120 µm which results in a film thickness of around 80 µm. The surface modification with PDMS phosphate or phosphonate is not suitable because it does not result in a highly transparent film when using an HRI polymer, which is shown in previous chapters. Therefore, no PDMS containing surfactants were used for the HfO$_2$ particles synthesised from the trifluoroacetate precursor. The particles were used in 10.0 wt%, 20.0 wt% and 30.0 wt% inside the polymethylphenylsiloxane OE-6630 and a polydiphenylsiloxane (PDPS) which was prepared and patented in a previous project with *OSRAM Opto Semiconductors* (Figure 96).[223-224] The synthesis route was adapted from Kim *et al.*[235, 319] and Bae *et al.*[234] but gaseous catalysts (ammonia respectively hydrogen chloride) were used to facilitate the catalyst removal after the synthesis. Additionally, some of the nanoparticles were surface modified with diphenylphosphinic acid to introduce some phenyl-groups onto the surface.
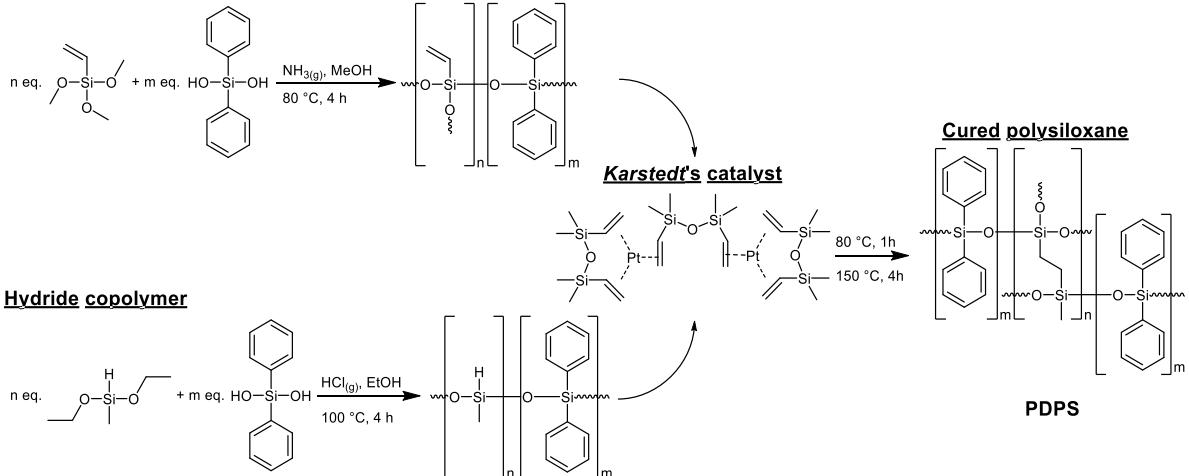
Figure 96: Synthesis of polydiphenylsiloxane (PDPS) with gaseous sol-gel catalysts.[223-224]

The prepared samples with 10.0 wt%, 20.0 wt% and 30.0 wt% HfO_2 without further surface modification and 10.0 wt% HfO_2 surface modified with Ph_2POOH incorporated into OE-6630 are shown in Table 14.

Table 14: 10.0 wt%, 20.0 wt% and 30.0 wt% HfO_2 incorporated into OE-6630.

Sample	14	15	16	17
Polysiloxane	OE-6630	OE-6630	OE-6630	OE-6630
Precursor	$Hf(CF_3COO)_4$	$Hf(CF_3COO)_4$	$Hf(CF_3COO)_4$	$Hf(CF_3COO)_4$
Particles	10.0 wt% HfO_2	20.0 wt% HfO_2	30.0 wt% HfO_2	10.0 wt% HfO_2
Surfactant	Oleylamine	Oleylamine	Oleylamine	Oleylamine + Ph_2POOH
RI	1.5525 (+0.06 %)	1.5515 (+0.00 %)	1.5520 (+0.03 %)	1.5585 (+0.45 %)
Transmission [%, 450 nm]	93	94	93	85
$T_{95\%}$ [°C, O_2]	344	389	416	450
Image				
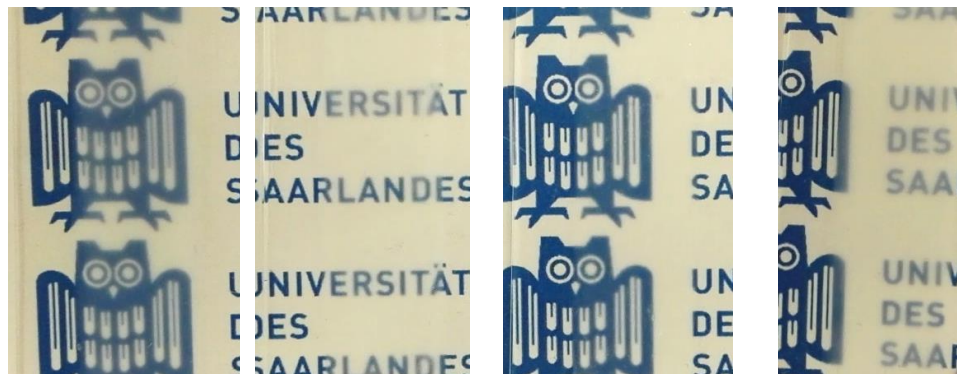
Sample 14 is identical with the composition of sample 10 with 10.0 wt% of HfO_2 nanoparticles prepared by the trifluoroacetate route, but the polymer was doctor bladed which allowed the determination of the RI and the transmission. FT-IR spectra were recorded and a TGA under oxygen was measured (experimental section, Figures 243 - 245). The RI slightly increased by 0.06 % compared to the 1.552 of the pure OE-6630. The transmission decreased from 99 % to 93 %, the thermal stability under oxygen decreased from 425 °C to 344 °C. With an increase of the particle content over 20.0 wt% to 30.0 wt% in sample 15 and 16, the transmission is maintained at around 94 %. This shows that the increase of the particle amount is not the reason for the transmission reduction because the particle free film shows the same value. More likely the oleylamine is the reason for the slightly opaque resin. The refractive indices are not increased with a higher particle loading, but the thermal stability increased to 389 °C with 20.0 wt% and to 416 °C with 30.0 wt% which is in the range of the particle free film. The increase of the particle content leads to an increase of the thermal stability, the RI does not change significantly compared to the pure polysiloxane, but the transmission decreases to around 93 % because of the oleylamine.

In sample 17, the 10.0 wt% of HfO_2 particles were surface modified with diphenylphosphinic acid which results in an RI increase of 0.45 % to 1.559 because the low RI surfactant oleylamine is replaced with the high RI surfactant diphenylphosphinic acid. The transmission is reduced to 85 % probably because of the chemical difference between the highly phenylic surfactant and the methyl and phenyl-group containing matrix. The thermal stability increases to 450 °C because of the particle loading which is 25 °C higher than for the particle free film.[5, 10, 387-389]

The FT-IR spectra (experimental section, Figure 243) mainly show the vibrations of the polysiloxane. In the range of 2800 cm^{-1} to 3000 cm^{-1},[251, 380] at 1470 cm^{-1}, at 1250 cm^{-1} [226, 372-375] and at 700 cm^{-1} to 800 cm^{-1} [261, 347, 379-380] are the C-H vibrations visible. The C_{Ar} bands are present at 1593 cm^{-1} and 1491 cm^{-1}.[226, 372-375] The vibrations of the Si-O bands are visible between 1170 cm^{-1} and 950 cm^{-1} and the Si-C ones are present around 1428 cm^{-1}, 1257 cm^{-1} and from 680 cm^{-1} to 840 cm^{-1}.[226, 346, 372-373] Some unreacted Si-H bands at 2130 cm^{-1} and at 902 cm^{-1} are also visible. [234-235, 319, 346-347] Some of the bands overlap with the N-H vibrations at around 3300 cm^{-1} and 1540 cm^{-1} and therefore are hardly visible.[16, 261, 347, 379-380] Some free O-H vibrations from the HfO_2 particle surface can be present in the range of 2400 cm^{-1} to 3500 cm^{-1}, but cannot be assigned because the C-H bands overlap.[261, 347, 379-380] The FT-IR bands of diphenylphosphinic acid are located at 1589 cm^{-1}, at 1485 cm^{-1}, at 729 cm^{-1} and at 695 cm^{-1} for the

phenyl-groups, at 1438 cm^{-1} for the P-Ph vibration, at 964 cm^{-1} for the P-O one, at 1129 cm^{-1} for the P=O one and at 2615 cm^{-1} for the O-H one.[390]

For the samples 18 to 21 (Table 15) the polymethylphenylsiloxane OE-6630 was substituted with the polydiphenylsiloxane (PDPS) prepared by the patented route (Figure 96).[223-224] The FT-IR bands assignment is identical with the one for the polymethylphenylsiloxane matrix because only the ratio of the different side-groups changed.

Table 15: 10.0 wt%, 20.0 wt% and 30.0 wt% HfO$_2$ incorporated into polydiphenylsiloxane (PDPS).

Sample	18	19	20	21
Polysiloxane	PDPS	PDPS	PDPS	PDPS
Precursor	Hf(CF$_3$COO)$_4$	Hf(CF$_3$COO)$_4$	Hf(CF$_3$COO)$_4$	Hf(CF$_3$COO)$_4$
Particles	10.0 wt% HfO$_2$	20.0 wt% HfO$_2$	30.0 wt% HfO$_2$	10.0 wt% HfO$_2$
Surfactant	Oleylamine	Oleylamine	Oleylamine	Oleylamine + Ph$_2$POOH
RI 20.0 °C	1.5765 (+0.00 %)	1.5725 (−0.25 %)	−	1.5755 (−0.06 %)
Transmission [%, 450 nm]	91	92	91	85
T$_{95\%}$ [°C, O$_2$]	339	341	171	431
Image				

The PDPS has a RI of 1.576, a transmission of 100 % at 450 nm and a T$_{95\%}$ of 345 °C under oxygen atmosphere. Sample 18 with 10.0 wt% HfO$_2$ shows a comparable RI and T$_{95\%}$ value and the transmission decreases to 91 %. The 20.0 wt% sample 19 shows a lower RI probably because of the higher amount of oleylamine which reduces the RI when mixed with the high RI polysiloxane. The transmission and the T$_{95\%}$ values are equal to the one of sample 18. Sample 20 with 30.0 wt% HfO$_2$ shows the same transmission of around 91 % like the 10.0 wt% and 20.0 wt% sample. The result is identical with the one observed by the OE-6630 matrix, the

increase of these small nanoparticles does not lower the transmission, more likely the RI and chemical difference of the oleylamine is the cause for the transmission loss. The RI difference between the oleylamine and the PDPS is larger and therefore the transmission is lower. The $T_{95\%}$ for the 30.0 wt% sample is very low because of an initial mass loss caused by residual solvent. A RI could not be determined because of the uneven surface which can be seen in the image. Sample 21 with 10.0 wt% HfO_2 and Ph_2POOH as additional surfactant shows a negligible RI increase. The transmission is determined with 85 % at 450 nm and equal to sample 17. Despite the surfactant and the matrix being highly phenylic, the transmission decreases probably still due to the chemical difference of the small surfactant. The thermal resistance drastically increases from 345 °C for the particle free polysiloxane to 431 °C for the particle loaded one. In both the OE-6630 and the PDPS the HfO_2 particles with Ph_2POOH surfactant show higher $T_{95\%}$ values than the pure polymer but the transmission decreases down to 85 %.

4.2.3 Synthesis of methacrylate-group containing polysiloxane for cross-linking with 10.0 wt%, 20.0 wt% and 30.0 wt% methacrylate-surface modified ZrO2 nanoparticles

4.2.3.1 Synthesis and curing of the triphenylsiloxane terminated poly[(3-methacry-loxypropyl)-co-dimethyl-co-diphenyl]siloxane.

The synthesis was performed accordingly to Chung *et al.*[236] The one component polysiloxane was synthesised in a polycondensation reaction. 3-methacryloxypropyl trimethoxysilane, di-phenylsilanediol, dimethoxydimethylsilane, triphenylsilanol and barium hydroxide octahydrate were mixed with ethyl acetate and heated up to 60 °C for 24 h. The catalyst was filtered off and the solvents were removed under reduced pressure. The ^{1}H, ^{13}C and ^{29}Si NMRs (experimental section, Figures 97, 250 and 251) show the expected signals. The proton signal from the methyl-groups is slightly lower than estimated because some of the dimethyldimethoxysilane evaporated before it could react which is known from the literature.[345, 391] This problem could be solved by reducing the temperature for the first few hours. Chung *et al.* did not report any ^{1}H NMR data of the polymer where this problem could be confirmed.[236] In the ^{29}Si NMR (Figure 97) at −8 ppm to −11 ppm are the D^1 signals[236, 325, 327-328] of SiMe$_2$ and at −19 ppm to −22 ppm are the D^2 signals[236, 321-324] visible. The Ph$_3$Si peak is located at −15 ppm.[236, 368] The D^1 signals[236, 321] of SiPh$_2$ are visible between −37 ppm to −39 ppm and the D^2 signals[236, 324, 368] are located around −42 ppm to −48 ppm. The silicon atom with the methacrylate-group only shows T^3 signals at −64 ppm to −66 ppm.[236, 321, 324, 331] In comparison with the literature, in the present synthesis a T^2 signal of the methacrylate-containing silicon atom at −58 ppm to −60 ppm cannot be observed.[236, 321, 331]
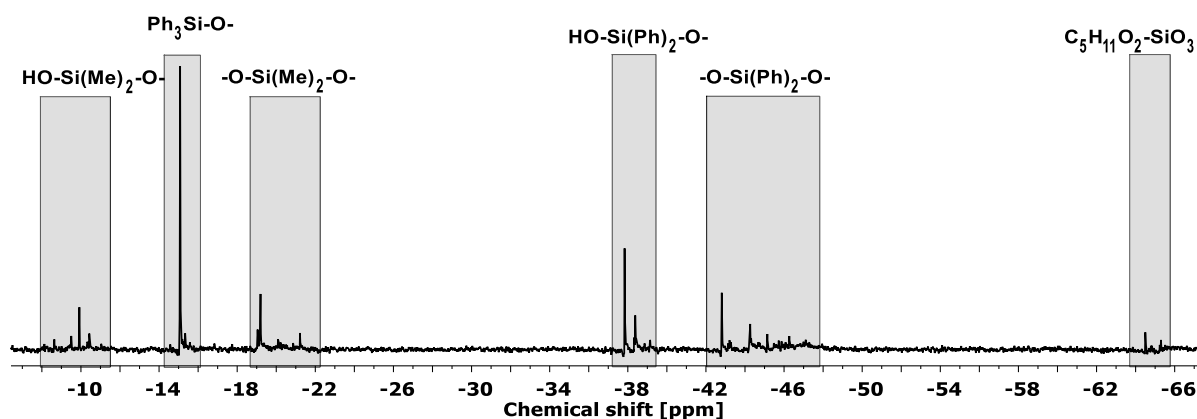

Figure 97: ^{29}Si NMR (79 MHz, CDCl$_3$) of triphenylsiloxane terminated poly[(3-methacryloxypropyl)-*co*-dimethyl-*co*-diphenyl]siloxane.

The FT-IR measurements of MA6.3_MM37.5_PP37.5_TP18.7 after the synthesis and after curing are shown in Figure 252 and show the same bands of the polymethylphenylsiloxane

OE-6630 and the 3-methacryloxypropyl trimethoxysilane modified nanoparticles described in the nanoparticle synthesis. The vibrations of the Si-O bands are visible at 950 cm^{-1} to 1140 cm^{-1} and of the Si-C ones can be seen at 1429 cm^{-1}, at 1261 cm^{-1} and from 650 cm^{-1} to 850 cm^{-1}.[226, 346, 372-373] The vibration bands of the C-H and C-C groups from 3-methacryloxypropyl silane overlap with those of the siloxane in the region of 2866 cm^{-1} to 3099 cm^{-1}, at 1591 cm^{-1}, at 1487 cm^{-1}, at 1261 cm^{-1} and in the region of 650 cm^{-1} to 850 cm^{-1}.[226, 372-375] The C-O-C ether bands can range from 1030 cm^{-1} to 1150 cm^{-1} [392-393] and they are not visible in the prepared samples because they overlap with the strong bands from the Si-O group. The C=O vibrations from the ester-group cannot be assigned clearly because no signal between 1710 cm^{-1} and 1740 cm^{-1} is visible.[350, 393-395] The vinyl vibrations from the methacrylate-group are visible at 920 cm^{-1}.[380, 384]

Because of the methacrylate-groups, the polymer can be cured by adding benzoyl peroxide and heating the polymer up to 150 °C for four hours. The cured polysiloxane shows a much smaller vinyl band from the methacrylate-group indicating the successful, but not complete reaction. The uncomplete cross-linking results from the reduced mobility of the polymer chains during the reaction.[396] The addition of a second methacrylate-containing species is therefore necessary, for example small nanoparticles.

The refractive index can be determined with 1.584 for the polymer after synthesis and 1.604 after curing without nanoparticles. The RI reported in literature is much lower with 1.541, both were measured at 589 nm but Chung *et al.* measured their sample at 30.0 °C while the measurement here was conducted at 20.0 °C.[236] However, this temperature difference should only relate of around 0.001.[228, 397] Although not stated by the authors, the RI was measured before the curing, because they reported the RI of OE-6630 with 1.533 which is the value from the manufacturer for the uncured polymer.[14] The RI of the cured polymer was determined with 1.552, which is in agreement with other literature.[363] The difference between the uncured polymers strongly depends on residual solvent like ethyl acetate or larger amounts of methoxygroups. The NMR data showed a slightly higher degree of conversion in the self-prepared samples, but this should not result in such a high RI difference.

TGA (Figure 98) curves before and after the curing were recorded under oxygen atmosphere like in literature. The uncured polymer shows a $T_{95\%}$ value of 231 °C which is slightly lower than the 248 °C reported by Chung *et al.*,[236] which can be caused by several reasons like the time difference between the synthesis and the measurement or residual solvent. The thermal stability of the cured sample is 337 °C, which is lower than the $T_{95\%}$ value of the commercial

OE-6630 with 425 °C, the difference results from the overall looser network. Both curves show an equal shape which is identical with the literature one.[236] Chung *et al.* did not report a TG curve of the cured and particle free material.[236]
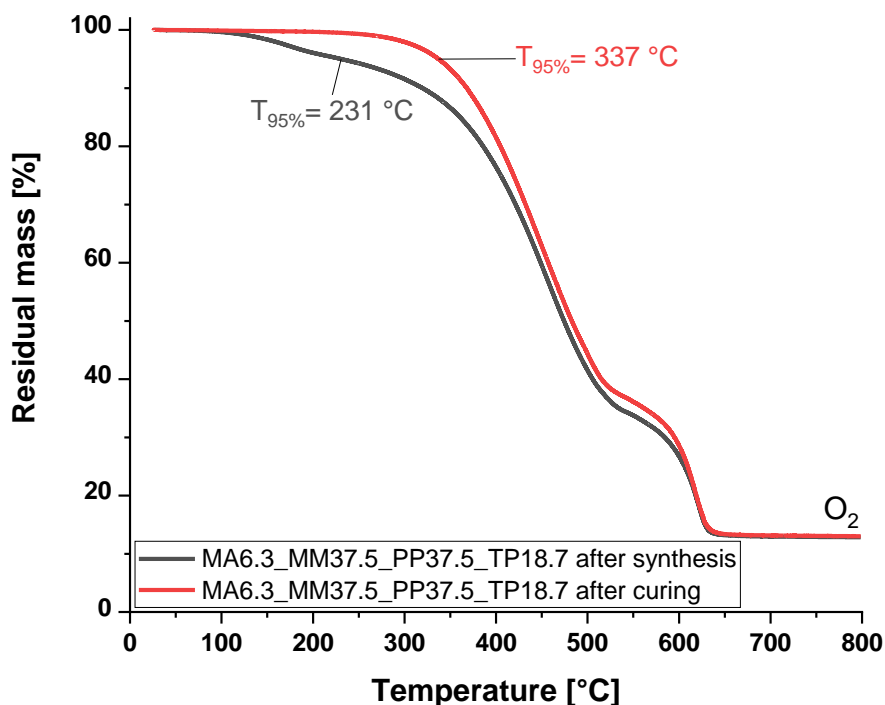
Figure 98: TGA of MA6.3_MM37.5_PP37.5_TP18.7 after synthesis and after curing with BPO under oxygen atmosphere.

DSC curves (experimental section, Figure 253) of the cured MA6.3_MM37.5_PP37.5_TP18.7 were recorded, a melting signal at 59.8 °C with 1.614 J/g was determined in the first heating curve. The second one showed a T_g of 14.6 °C for the nanoparticle free polysiloxane. Chung *et al.* did not report any DSC data.[236]

An UV/Vis spectrum (Figure 99) of the cured polysiloxane was recorded and the haze curve was calculated. The literature reported a transmission of 90 % at 450 nm.[236] The polysiloxane is slightly less transparent with 87 % transmission. The haze value at 450 nm is 8 %.
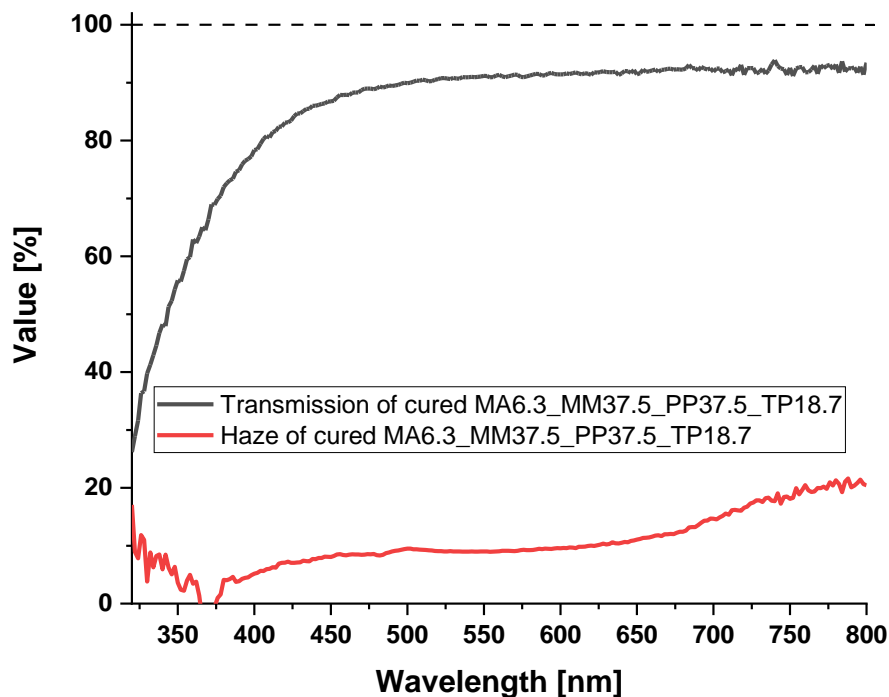
Figure 99: Transmission und haze curves of MA6.3_MM37.5_PP37.5_TP18.7 after curing with BPO onto a glass slide.

4.2.3.2 Synthesis and curing of a ZrO$_2$/polysiloxane nanocomposite cross-linked by methacrylate-groups

Nanocomposites (Figure 100, Table 16) consisting of 10.0 wt%, 20.0 wt% and 30.0 wt% ZrO$_2$ nanoparticles from the zirconium basic carbonate route and a methyl and phenyl-group containing polysiloxane were synthesised using the 3-methacryloxypropyl dimethylsiloxane and butyric acid surface modified particles and MA6.3_MM37.5_PP37.5_TP18.7, which also contains methacrylate-groups.
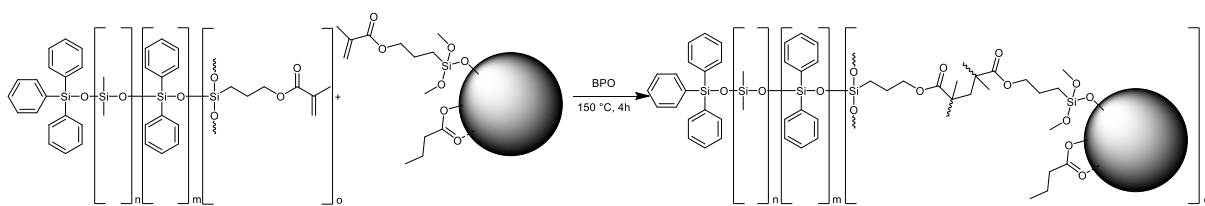
Figure 100: Cross-linking reaction between the polysiloxane and the nanoparticles using benzoyl peroxide (BPO).[398]

The cross-linking was started using benzoyl peroxide dissolved in ethyl acetate and the mixture was cured at 150 °C for four hours.[236, 398] Sample 22 represents the particle free system and is listed here for comparison. Slightly yellow films were obtained in all cases. Sample 24 with 20.0 wt% ZrO$_2$ and sample 25 with 30.0 wt% ZrO$_2$ show an uneven surface which was also observed in earlier studies carried out in cooperation with *OSRAM Opto Semiconductors*. This results from a dense and hard network which was caused by a high particle and methacrylate content, respectively.

Table 16: Overview of nanocomposites with 10.0 wt% to 30.0 wt% surface modified ZrO$_2$ nanoparticles cured in a methacrylate-group containing polysiloxane MA6.3_MM37.5_PP37.5_TP18.7.

Sample	22	23	24	25
Polysiloxane		MA6.3_MM37.5_PP37.5_TP18.7		
Particles	−	10.0 wt% ZrO$_2$	20.0 wt% ZrO$_2$	30.0 wt% ZrO$_2$
Surfactant	−	Butyric acid, 3-methacryloxypropyl trimethoxysilane		
Catalyst	BPO in EE	BPO in EE	BPO in EE	BPO in EE
Appearance	yellow, transparent	light yellow, transparent	yellow, transparent, uneven surface	yellow, transparent, uneven surface
RI	1.6041	1.6157 (+0.72 %)	1.6167 (+0.79 %)	−
Transmission [%, 450 nm]	87	87	81	81
T$_{95\%}$ [O$_2$, °C]	337	302	271	261
T$_g$ [°C]	14.6	25.2	66.1	76.7
Images				

The FT-IR spectra (experimental section, Figure 254) of the cured metal oxide containing nano-composite shows the same vibrations as the particle free polymer. The vinyl band of the meth-acrylate-group shows an increasing strength with rising particle content at 943 cm^{-1},[380, 384] which shows that some methacrylate-groups cannot react properly because of the immobility of these groups on the particle surface during the cross-linking reaction.[396] Nevertheless, solid and non-sticky films were obtained.

RI determinations were performed under standard conditions. Adding 10.0 wt% of ZrO_2 nanoparticles increase the RI by 0.72 % to 1.616, the addition of 20.0 wt% ZrO_2 increases the RI only slightly further by a total of 0.79 % to 1.617. The RI of the 30.0 wt% sample could not be determined because the surface is too uneven. The non-linear increase was also observed by Chung *et al.*[236] because the vol% of the filler correlates linear with the RI but not the wt%. Because their particle-free polymer shows a much lower RI than ours, their increase is around 0.6 % for the 10.0 wt% ZrO_2 film and 1.3 % for the 20.0 wt% one.[236]

The TG analyses (Figure 101) of the cured films show a decrease of the $T_{95\%}$ temperature with increasing particle content in MA6.3_MM37.5_PP37.5_TP18.7 under oxygen atmosphere.[236] The curves are identical with theirs.[236] The self-prepared particle free film has a decomposition temperature of 337 °C while Chung *et al.* did not report any.[236] Adding 10.0 wt%, 20.0 wt% and 30.0 wt% ZrO_2 and curing results in a lower temperature of 302 °C, 271 °C respectively 261 °C. Chung *et al.* reported 228 °C for their 39.5 wt% film at 5 % mass loss.[236] The self-prepared system shows higher overall thermal stability, but it is also stronger affected by higher particle loadings in comparison to theirs.
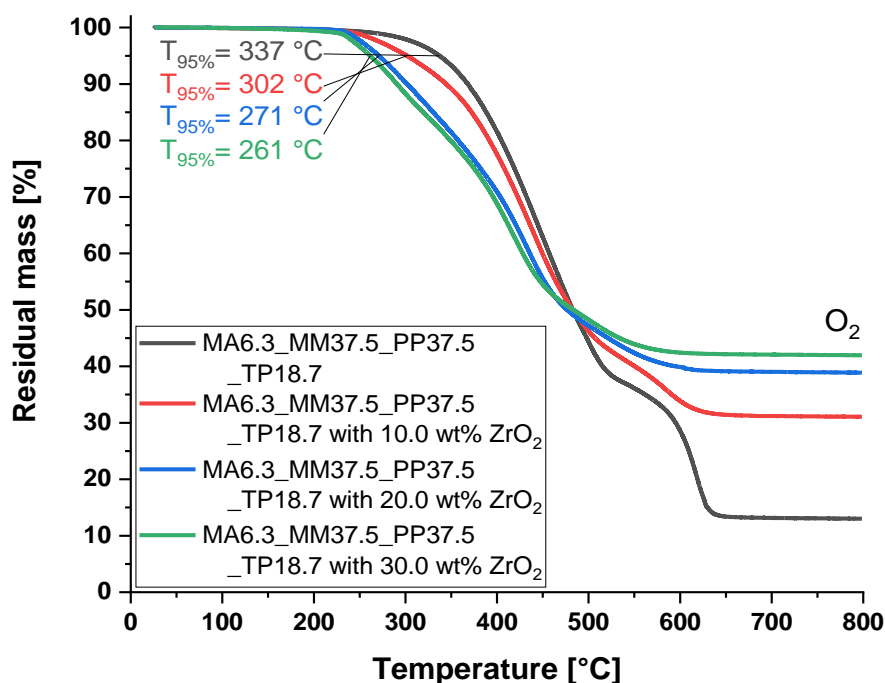
Figure 101: TGA of cured MA6.3_MM37.5_PP37.5_TP18.7 without and with 10.0 wt%, 20.0 wt% and 30.0 wt% ZrO₂ with surface modification of butyric acid and 3-methacryloxypropyl dimethoxysiloxane under oxygen atmosphere.

DSC curves (experimental section, Figures 255 and 256) were also recorded and the melting temperature, the integrated energy, and the T_g's are displayed in Table 17. The melting temperature decreased from the particle free film to the 10.0 wt% ZrO_2 one from 60 °C to 49 °C, while

the integrated energy triples. T_m could not be observed in sample 24 and 25. The T_g increases with particle loading because of the increased amount of methacrylate-group increases the cross-linking and lowers the degrees of freedom.[121, 275, 399-400] The T_g increases from 14.6 °C to 25.2 °C when incorporating and covalently cross-link 10.0 wt% ZrO$_2$. An overall content of 20.0 % rises the T_g to 66.1 °C and a content of 30.0 wt% ZrO$_2$ further increases the value to 76.7 °C.

Table 17: Melting temperatures, the integrated energy and the glass transition temperature of MA6.3_MM37.5_PP37.5_TP18.7 without and with 10.0 wt%, 20.0 wt% and 30.0 wt% ZrO$_2$ with surface modification of butyric acid and 3-methacryloxypropyl dimethoxysiloxane.

Sample	Wt% ZrO$_2$	T_m [°C]	E_m [J/g]	T_g [°C]
22	0.0	59.8	1.614	14.6
23	10.0	48.6	4.418	25.2
24	20.0	–	–	66.1
25	30.0	–	–	76.7

UV/Vis measurements (experimental section, Figure 257) and the calculation of the haze values, the yellowness, and whiteness index at 450 nm were also performed (Table 18). The transmission drops from 87 % for the particle free and 10.0 wt% particle loaded film to 81 % for the 20.0 wt% respectively 30.0 wt% ZrO$_2$ containing film at 450 nm. Chung *et al.* only reported a value of 90 % transmission for the particle free film and 73 % transmission for the film with 51.7 wt% ZrO$_2$,[236] showing that the particle increase lowers the transmission. The haze value increases with increasing particle content because of scattering effects from 8 % for the particle free respectively 10.0 wt% ZrO$_2$ film over 11 % for the 20.0 wt% film to 28 % for sample 25 with 30.0 wt%. The yellowness index ranges from three to five for all samples, showing that the yellow colouration results from the curing reaction of the transparent particle-free polymer with benzoyl peroxide. The filler content does not increase the yellowing. Although the whiteness index slightly decreases with increasing particle content from 88 to 82 for the 20.0 wt% ZrO$_2$ film. Sample 25 shows a slightly higher value of 84, which also has the lowest YI of 3.2. The yellow colour results from the curing process when free methacrylate-groups remain, which are present in all samples as indicated by FT-IR and which was observed by Chung *et al*[236] and is reported in literature for free radical polymerisations of methacrylates.[401] An additional UV curing (Figure 102) of these free groups by exposing the samples for three days at 450 nm with ~450 mW/cm^2 significantly reduced the yellow colour of the sample.

Table 18: Transmission, haze, yellowness and whiteness indices at 450 nm for MA6.3_MM37.5_PP37.5_TP18.7 without and with 10.0 wt%, 20.0 wt% and 30.0 wt% ZrO$_2$ with surface modification of butyric acid and 3-methacryloxypropyl dimethoxysiloxane.

Sample	Wt% ZrO$_2$	T$_{450}$ [%]	H$_{450}$ [%]	YI	WI
22	0.0	87	8	4.4	87.9
23	10.0	87	8	4.7	86.8
24	20.0	81	11	4.2	81.5
25	30.0	81	28	3.2	83.9

Bae *et al.* used a photoinitiator (2,2-dimethoxy-2-phenyl-acetophenone) for the UV curing for three minutes and afterwards heating the sample to 150 °C for two hours.[275] Because no photoinitiator was inside the sample, the high energy UV light was used for a longer time after the thermal curing. The yellow colour can be reduced but is still present.

Figure 102: Images of the cured 10.0 wt% ZrO$_2$ containing MA6.3_MM37.5_PP37.5_TP18.7, a) after curing and b) after exposure to 450 nm light for three days.

4.2.3.3 Conclusion

A methacryl-group containing polysiloxane, triphenylsiloxane terminated poly[(3-methacryloxypropyl-*co*-dimethy-*co*-diphenyl)]siloxane, was successfully prepared in a basic sol-gel reaction. Zirconium dioxide nanoparticles with a diameter of around 4.5 nm were synthesised using a basic solvothermal reaction. They were surface modified first with butyric acid and second with 3-methacryloxypropyl trimethoxysilane which nearly completely exchanges with the butyric acid. The methacrylate-groups on the particle surface and the ones from the polysiloxane can be cross-linked using benzoyl peroxide as radical starter (Figure 103).[236, 398]
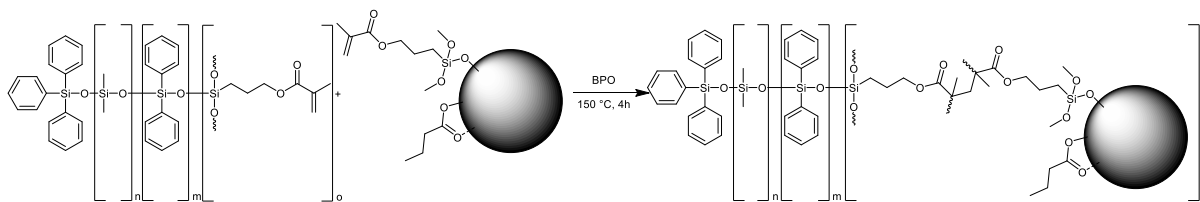
Figure 103: Cross-linking reaction between the polysiloxane and the nanoparticles using methacrylate-groups and benzoyl peroxide (BPO).[398]

The particle content was changed from 10.0 wt% to 30.0 wt%. The refractive index only slightly increased by around 1 % compared to the particle free film with 1.604, which is around 3 % higher than the RI of the commercial polysiloxane OE-6630 with 1.552, probably because of the higher phenyl content and the methacryloxypropylsiloxane. The thermal stability decreases from 337 °C down to 261 °C when incorporating up to 30.0 wt% nanoparticles. The commercial reference shows a much higher decomposition temperature with 425 °C under oxygen atmosphere. The particle free film shows a lower decomposition temperature because of the lower degree of cross-linking. The introduction of nanoparticles further reduces the thermal stability despite raising the degree of cross-linking which is reported by Chung *et al.*[236] This specific nanocomposite shows the opposite trend when incorporating nanoparticles compared to other publications in literature. The glass transition temperature increases from 14.6 °C to 76.7 °C with rising particle content, while OE-6630 shows a much lower value of 5.5 °C. Here the particle free film contains around 74 % phenyl-groups while the OE-6630 contains only 44 % which reduces the mobility of the polymer chains and increases the T_g.[402-404] The transmission for the particle free film is 87 % and decreases to 81 % with 30.0 wt% particle loading, while the commercial polysiloxane shows a higher value of 99 %. The transmission loss results from the yellow colour of the sample after the curing which was determined by a YI of 4.5 compared to the 0.5 of the OE-6630 and a WI of 87.9 compared to the 99.0. Overall, a suitable nanocomposite with ZrO_2 particles was successfully synthesised which shows a high RI of over 1.6, but the disadvantages are the lower thermal stability and transmission compared to the commercial methyl and phenyl-group containing polysiloxane. Because the pure methacrylate polymer is colourless and all other methacrylate free polysiloxane systems remain colourless after the thermal treatment, this methacrylate-group is the reason for the colouration, which was also observed by Chung *et al.*[236] Therefore, a different cross-linking group has to be used.

4.2.4 Synthesis of epoxide-group containing polysiloxane for cross-linking with 10.0 wt% epoxide-surface modified ZrO₂ nanoparticles

4.2.4.1 *Synthesis of the triphenylsiloxane terminated poly[(3-glycidyloxypropyl)-co-dimethyl-co-diphenyl]siloxane with 10.0 wt% 3-glycidyloxypropylsiloxane surface modified ZrO₂*

Because the methacrylate-group containing nanocomposite shows a yellow colour after the curing, a different cross-linking group is used. The methacrylate-groups were exchanged with epoxides. Therefore, the 3-methacryloxypropyl trimethoxysilane (MA) in the previous polymer synthesis (MA6.3_MM37.5_PP37.5_TP18.7) and the particle surface modification was changed to 3-glycidyloxypropyl trimethoxysilane (EP) to perform the cross-linking using epoxide-groups. The reaction procedure and the quantitative ratio of the monomers (Figure 104) remains unchanged.
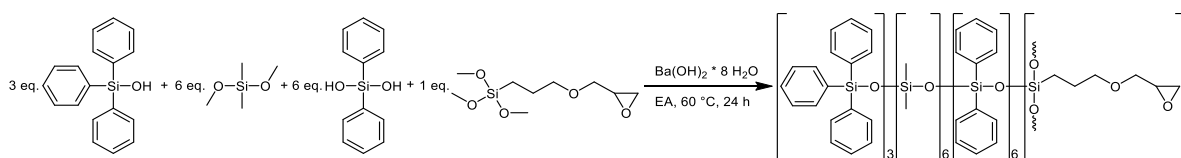
Figure 104: Reaction scheme for the synthesis of triphenylsiloxane terminated poly[(3-glycidyloxypropyl)-co-dimethyl-co-diphenyl]siloxane.

The other difference is that this cross-linking reaction is catalysed by heat and therefore does not need an additional catalyst.[3, 405-408] The pure polymer remains sticky and elastic even after curing for 48 h at 150 °C, indicating that the number of epoxide-groups inside the polymer is too low to create a rigid film. Therefore, all analyses for the cured material are performed with the 10.0 wt% epoxide surface modified nanoparticle containing polysiloxane.

Besides the cross-linker change, the zirconium oxide nanoparticles were synthesised using the zirconium tetra-*n*-propoxide autoclave reaction because the purification is faster than in the zirconium basic carbonate reaction. The nanoparticles were surface modified without butyric acid, because as seen from the methacrylate modified particles, the butyric acid is nearly completely exchanged with the siloxane. Nevertheless, the surface modification with benzyl alcohol is performed during the particle synthesis because it also used as solvent. The epoxide-groups also lead to another advantage compared to the methacrylate-groups, because they serve as adhesion promoters between the polysiloxane and the metallic surface of the LED lead frame or the chip surface.[3] The ring opening reaction of the epoxide does not need any additional catalysts or starters because it is thermally driven (Figure 105) and starts when remaining hydroxide-groups from the polymer or residual water reacts with the epoxide.[3, 405-408] This effect

also leads to a disadvantage because the shelf-life is much shorter than for the methacrylate or the hydrosilylation systems.
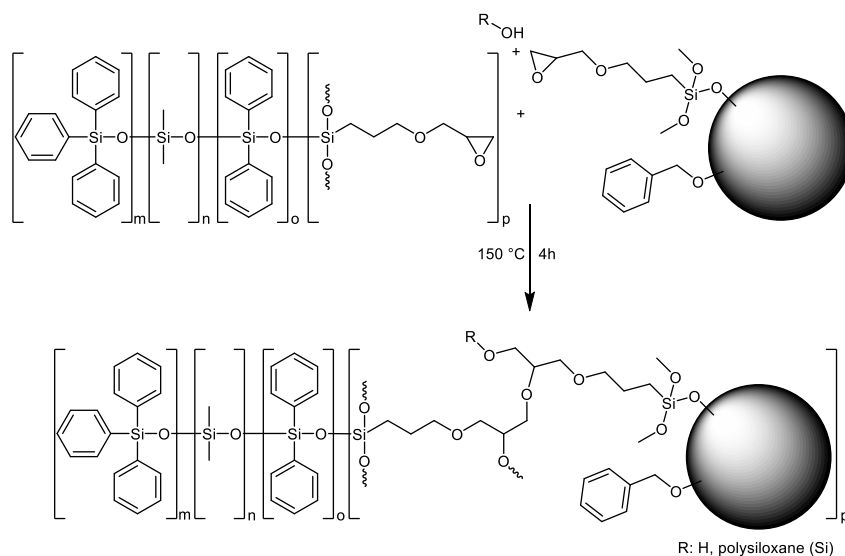
Figure 105: Cross-linking reaction between the polysiloxane and the nanoparticles using epoxide-groups and hydroxyl terminated polysiloxanes respectively water.[405-408]

^{1}H, ^{13}C and ^{29}Si NMRs (experimental section, Figures 106, 259 and 260) in chloroform were recorded and all expected signals are present.[3, 236] The polycondensation reaction of the epoxide-group containing polysiloxane does not lead to an epoxide opening because the reaction temperature and time is with 70 °C for 24 hours much lower than the curing temperatures which are between 100 °C and 150°C for two to four hours.[3] The ^{1}H NMR shows some overlapping signals because of the broadening resulting from the polymerisation.[236] Some methoxy-groups are still present indicating a not complete reaction, but because the epoxide-groups are not thermally stable, the reaction time was not increased. Even less methyl signals than in MA6.3_MM37.5_PP37.5_TP18.7 are visible despite using the same reaction conditions and equipment.[345, 391] Some ethyl acetate is still visible in the ^{1}H and ^{13}C NMR from the synthesis even after drying under high vacuum ($5 \cdot 10^{-3}$ mbar).

The ^{29}Si NMR (Figure 106) of the polymer EP6.3_MM37.5_PP37.5_TP18.7shows expected signals in the NMR, because the change from the methacrylate to the epoxide-group does not modify the chemical environment of the silicon atoms because of the $-CH_2-CH_2-CH_2-O-$ spacer in between them. Additional signals show that the condensation reaction is not completed, some Si-OMe groups are present, which is evidenced by the signal at -5 ppm representing MeO-Si(Me)$_2$-O-[409] and at -55 ppm for the T^2 epoxide-group containing silicon atom $C_6H_{11}O_2$-Si(OH)O$_2$-[321, 331]. The signals around -34 ppm most likely result from the MeO-Si(Ph)$_2$-O- group, although diphenylsilanediol and hexaphenylcyclotrisiloxane also show signals in this region.[324]

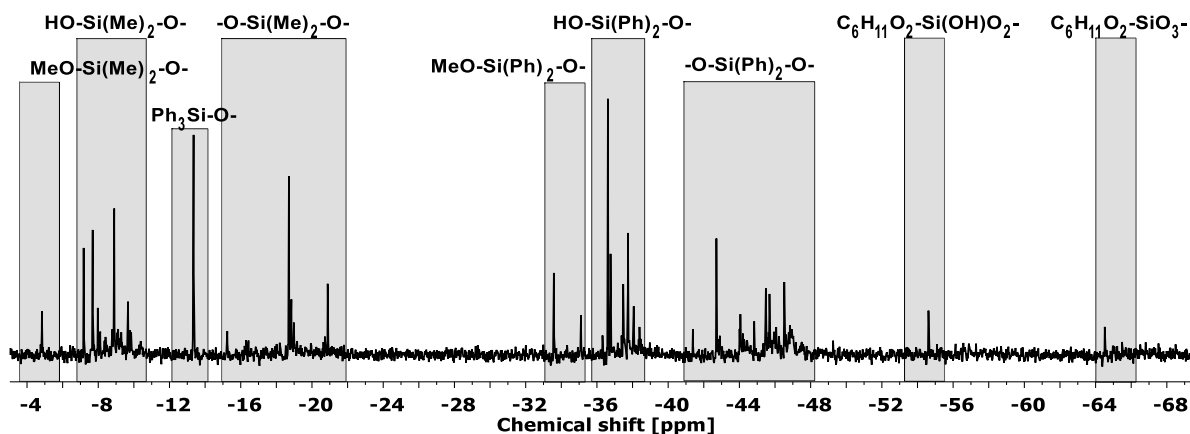**Figure 106: ^{29}Si NMR (79 MHz, CDCl₃) of triphenylsiloxane terminated poly[(3-glycidyloxypropyl)-*co*-dimethyl-*co*-diphenyl]siloxane.**

The FT-IR spectra (experimental section, Figure 261) were recorded after the mixing and after the curing of 10.0 wt% of the 3-glycidyloxypropylsiloxane surface modified ZrO_2 nanoparticles with EP6.3_MM37.5_PP37.5_TP18.7.[3, 236] Because only the methacrylate-group was exchanged with an epoxide one, the difference between the spectra is limited to the disappearing of the vinyl and carbonyl-group and the existence of the epoxide-group mainly visible at 901 cm^{-1}.[3] The C-H stretching vibration of the oxirane ring around 3060 cm^{-1} overlaps with other C-H vibrations.[392] The stretching vibration of C-O-C from the oxirane-group at 830 cm^{-1} also overlaps with other bands from Si-C and C-H.[392] The FT-IR spectra after the curing no longer shows the epoxide vibrations at 900 cm^{-1} which indicates a successful cross-linking reaction.

The refractive index of the polymer was determined after the synthesis with 1.582, which is slightly lower than the 1.584 for the MA6.3_MM37.5_PP37.5_TP18.7 polymer. The 10.0 wt% ZrO_2 containing EP6.3_MM37.5_PP37.5_TP18.7 shows a RI of 1.608 after the curing, which is slightly higher than the 1.604 of the methacrylate system with 10.0 wt% particles.

The viscosity of EP6.3_MM37.5_PP37.5_TP18.7 before the curing and without nanoparticles was determined with 168 ± 9 mPa·s which is very low compared to the 2960 mPa·s for OE-6630 component A and 2530 mPa·s for the component B, respectively.

The thermal analysis (experimental section, Figure 262) was carried out under oxygen atmosphere and showed a thermal decomposition temperature of 254 °C for the particle-free polymer which was thermally cross-linked but is still sticky. The addition of 10.0 wt% ZrO_2 nanoparticles increases the $T_{95\%}$ value to 269 °C for the solid film because of the increased cross-linking. Both temperatures are much lower than the 337 °C for the particle free methacrylate system and the 302 °C for the 10.0 wt% ZrO_2 nanocomposite, respectively. The OE-6630 polysiloxane

shows a very high $T_{95\%}$ temperature of 425 °C. These low decomposition temperatures show that the amount of present respectively cross-linked epoxide-groups is still too low even with 10 wt% nanoparticles.

A DSC measurement (experimental section, Figure 263) for the cured EP6.3_MM37.5_PP37.5_TP18.7 with 10.0 wt% ZrO_2 nanoparticles was performed. A glass transition temperature of −32.2 °C could be determined which is very low compared to the 14.6 °C for the cured MA6.3_MM37.5_PP37.5_TP18.7 with 10.0 wt% ZrO_2 nanoparticles. This shows that less epoxide-groups are present on the particle surface respectively more unreacted groups after the thermal treatment which results in a more flexible system. The melting temperature although is 77.9 °C with a measured enthalpy of 0.526 J/g of the epoxide system is higher than the T_m of 48.6 °C with an enthalpy of 4.418 J/g of the methacrylate-group containing polymer. The OE-6630 system shows a T_g of 5.5 °C which is in between the T_g of the methacrylate respectively epoxide-containing nanocomposites.

The cured film is colourless, highly transparent, and bubble-free (Figure 107).

Figure 107: Image of the cured EP6.3_MM37.5_PP37.5_TP18.7 with 10.0 wt% ZrO_2 nanoparticles doctor bladed onto a microscope glass slide.

UV/Vis spectra were recorded and the haze curve was calculated for the cured EP6.3_MM37.5_PP37.5_TP18.7 with 10.0 wt% ZrO_2 nanoparticles (experimental section, Figure 264). At 450 nm the film shows a transmission of 100 % and a haze value of 8 %. The methacrylate system with 10.0 wt% ZrO_2 shows the identical haze value but only 87 % transmission. The OE-6630 system shows a slightly lower transmission of 99 % and a haze value of 7 %. The yellowness and whiteness indices were calculated with 0.4 for the YI and 99.1 for the WI confirming that the film does not show a yellow colour which shows that the epoxide-groups do not lead to a colouration. The methacrylate system shows a YI of 4.7 and a WI of 86.8 while the OE-6630 system has a slightly higher YI of 0.5, and a slightly lower WI of 99.0 showing a marginally more yellow colour.

4.2.4.2 Conclusion

An epoxide-group containing polysiloxane, triphenylsiloxane terminated poly[(3-glycidyloxy-propyl-*co*-dimethy-*co*-diphenyl)]siloxane, was successfully prepared with the identical synthesis route of the methacrylate system but changing the 3-methacryloxypropyl trimethoxysilane with 3-glycidyloxypropyl trimethoxysilane. Benzyl alcohol surface modified zirconium dioxide nanoparticles with a size of 3 nm to 4 nm after the synthesis were surface modified with 3-glycidyloxypropyl trimethoxysilane after the autoclave synthesis. 10.0 wt% nanoparticles were mixed into the polysiloxane and thermally cured for four hours at 150 °C to receive a new nanocomposite (Figure 108).[405-408]
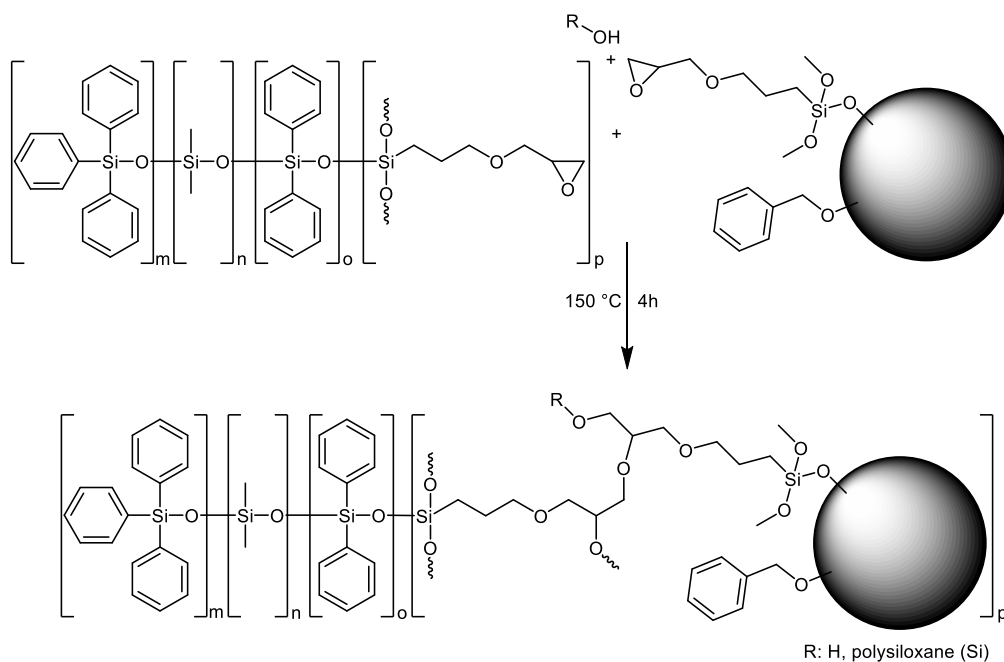
Figure 108: Cross-linking reaction between the polysiloxane and the nanoparticles using epoxide-groups and hydroxyl terminated polysiloxanes respectively water.[405-408]

The main aim was to achieve a colourless nanocomposite which was successfully received. It shows a RI of 1.608 which is slightly higher than the one of the methacrylate system. The thermal stability ($T_{95\%}$) although is reduced by 33 °C to 269 °C. The glass transition temperature (T_g) is determined with -32.2 °C which is 46.8 °C lower. Both indicating that a lower amount of epoxides is present compared to the methacrylate amount and therefore leads to a more flexible polymer with a lower degree of cross-linking than the methacrylate system. The transmission is with 100 % around 14 % higher while the haze values are identical with 8 %. The YI and the WI show values close to zero and 100 indicating that no yellow colouration occurred during the cross-linking reaction, respectively. Because of these results, this nanocomposite was selected for *OSRAM*'s steady state lifetime test (4.6.2).

4.3 Synthesis of HRI polysiloxanes by modification of the backbone

Four different metal atoms were chosen, zirconium and hafnium from the titanium-group and tin because it is chemically comparable with silicone. Additionally, the electron-rich tantalum was used. The metal atoms Zr and Hf were used as *n*-propyl alkoxides.[138] Tin was used as tin(IV)chloride and tantalum as tantalum(V) ethoxide. Five different metal (Met) concentrations X were chosen, namely 1.0 mol%, 3.0 mol%, 5.0 mol%, 10.0 mol%, and 15.0 mol% for both the hydride and vinyl copolymers (Table 19). Additionally, two reference metal-free co-polymers, which can be cross-linked with the metal-containing copolymers were synthesised. The metal-free hydride was chosen over the metal-free vinyl polymer because the metal atoms can react with the Si-H group.[410-412] This results in a lower amount of free hydride-groups in the metal-containing polymer, which can lead to a reduced tendency to harden. Therefore, a larger amount of the metal-free hydride copolymer was synthesised to cross-link it with the metal-containing vinyl copolymers to receive more cured samples with other metal contents of 1.5 mol%, 2.5 mol%, 5.0H mol% and 7.5 mol%. In these samples the metal atoms were introduced only by the vinyl polymer, because the hydride polymer is metal-free.

The composition of these copolymers consists out of three monomer groups (Figure 109). 20 mol% of the combined silicon and metal atom content of the copolymers consists of the cross-linking group *A* monomers, containing vinylphenyldiethoxysilane (V) and methyldiethoxysilane (H). The inorganic high refractive index monomer group *B* contains the metal monomers with X mol%. From the organic high refractive index group *C*, 40 mol% of diphenylsilanediol (PP) and (40-X) mol% of phenylmethyldimethoxysilane (PM) were used where X relates to the percent of metal atoms (Met). The 20 mol% of cross-linking group *A* monomers were chosen because the experience showed, that the initial 40 mol% which was used by Kim *et al.* is not required to receive a solid resin,[138, 234, 317, 319] especially with higher metal contents. Instead, lower amounts are more suitable because they result in softer films, which have better thermal properties due to the slight flexibility of the polymer chains compared to the one from Mosley *et al.*[136-137] Also, higher RI side-groups, which are sterically more demanding and reduce the flexibility, can then be incorporated. The composition was optimised to have the highest amount of phenyl side-groups without creating a polymer that is already solid at room temperature, which creates problems in the manufacturing process. Therefore, a relatively high amount of methylphenyldimethoxysilane of up to 40 mol% is used. When adding metal atoms, the methylphenylsiloxane content is reduced instead of the diphenylsiloxane one to better evaluate their positive impact in the increase of the refractive index and the temperature stability

compared to the methylphenyl-group. This allows a comparison to the cured polymethylphen-ylsiloxane OE-6630. Otherwise, reducing the amount of the diphenyl-groups would maybe lower or maintain the RI and no clear statement could be made.
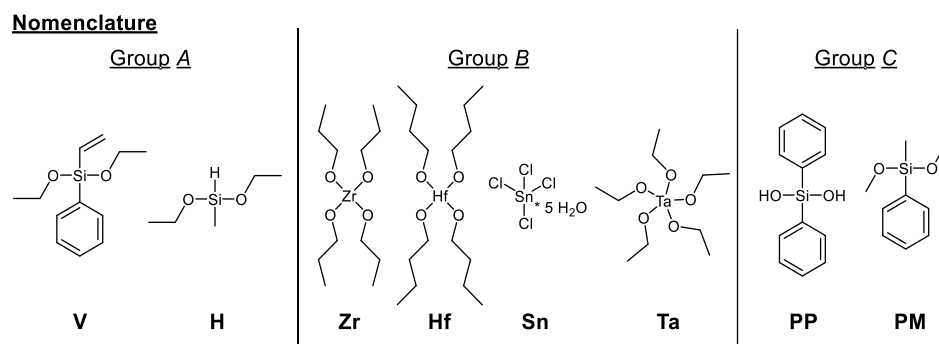

Figure 109: Overview of used monomers and their abbreviation for the synthesis of metal-containing co-polymers.

With the selected monomers, various vinyl- and hydride-containing copolymers were synthe-sised based on modified syntheses routes reported by Mosley *et al.*[136] and Kim *et al.*[138, 317] Using the metal atoms in the hydride or vinyl copolymer synthesis already leads to a cross-linked polymer because four (Zr, Hf and Sn) respectively five (Ta) possible bonds can be formed. Therefore, the general synthesis has to be adapted to compensate the increased viscosity with an additional high boiling solvent (xylene), an additional or different catalyst and longer reac-tion times compared to previous syntheses.[223-225] The nomenclature gives the relative mol% of the silicon and metal atoms as well as the chosen metal itself inside the name (4.3.1, Table 19).

4.3.1 Synthesis and characterisation of the hydride- or vinyl-group and metal atom containing copolymers

The synthesis (Figure 110) was performed in two steps. First an unfunctionalised but already cross-linked copolymer was synthesised using the metal precursor, diphenylsilanediol and methylphenyldimethoxysilane and the solid basic catalyst barium hydroxide monohydrate in-stead of a liquid one like tetra-*n*-butylammonium hydroxide. For the metal-free copolymers, no group *B* monomer was used. Kim *et al.* also used solid catalysts in their one-step zirco-nium-containing polysiloxane synthesis. The authors applied barium hydroxide for the vinyl polymerisation and the weakly acidic cation exchange resin Amberlite IRC76 which contains carboxylic acid-groups for the hydride polymerisation.[138] Liquid catalysts were applied in a first approach, but they seem to react too fast with the metal monomer and therefore these mon-omers mainly reacted with themselves, while the siloxanes reacted afterwards where the metal oxide cluster was already formed which is also described by Kim *et al.*[138] This leads to precip-itates inside the silicone. Kim *et al.* avoided this problem by first reacting the siloxanes for one

hour and then adding the metal monomers as well as by choosing solid catalysts.[138] Heterogenic reactions often are slower than homogeneous reactions because of the possible inhibition of mass transfer at the catalyst.[413-418]
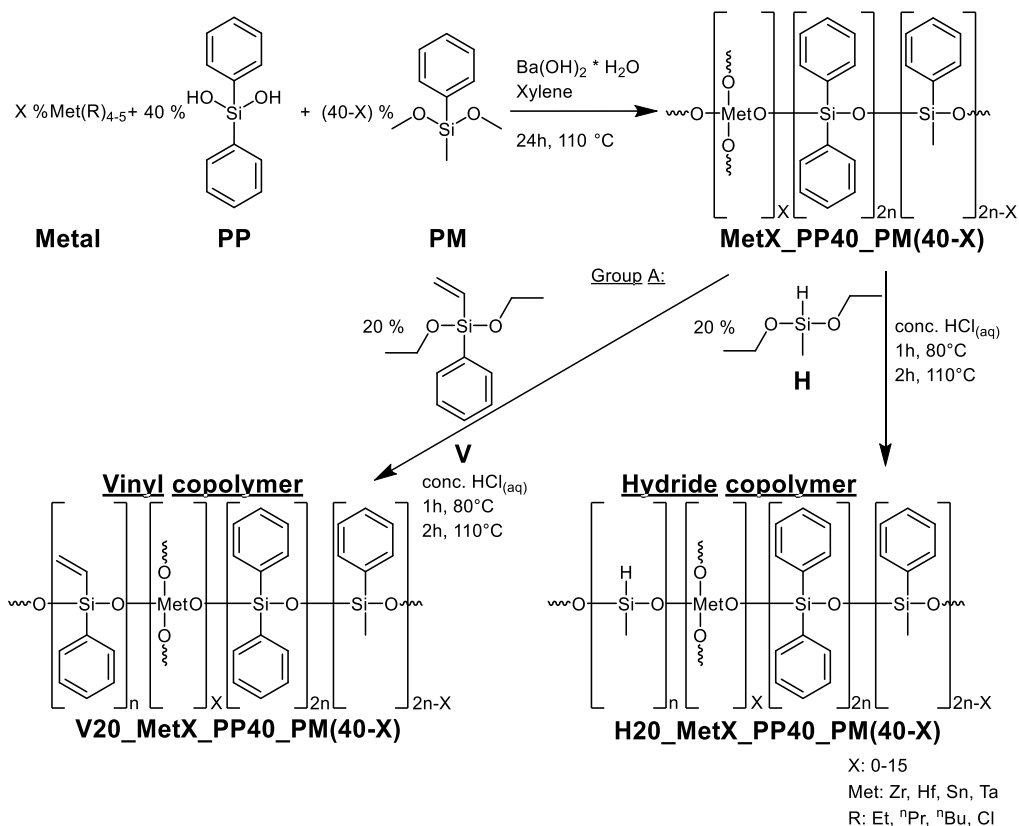
Figure 110: Reaction scheme for the hydride or vinyl and metal atom containing copolymer syntheses.

A different possibility to reduce the reaction speed is by lowering the temperature. However, using a temperature below 100 °C is not suitable because the alcohols, like *n*-propanol with a $T_b = 97$ °C or *n*-butanol with a $T_b = 118$ °C have to be removed from the reaction in order to achieve high yields.[419] An ion exchange resin was not used because of the complicated separation of the silicone polymer and the ion exchange resin after the reaction. Therefore, solid barium hydroxide monohydrate was used for the first reaction step to produce the MetX_PP40_PM(40-X) polysiloxanes which were reacted at 110 °C with additional xylene for 24 hours because of the dilution and the slower solid-liquid reaction. The catalyst was removed with a syringe filter after the reaction.

In the second step, concentrated hydrochloric acid was added to the already cross-linked polymer to switch the pH_0 value from basic to acidic, because the sol-gel reaction with the functional monomer (H or V) can both be performed under these conditions. Also, the purification is slightly faster than for the basic sol-gel reaction. After stirring the solution for around ten minutes at room temperature, vinylphenyldiethoxysilane to receive V20_MetX_PP40_PM(40-X) or methyldiethoxysilane to receive H20_MetX_PP40_PM(40-X) were added. After one

hour at 80 °C and two hours at 110 °C the polymer was purified by washing, filtering, and drying under high vacuum.

Noteworthy, the polymer mixture received in the first step would turn acidic when adding $Sn(Cl)_4 \cdot 5H_2O$ because of the released HCl. Also, the solid tin precursor is barely soluble in the monomer and xylene mixture. Therefore, the tin monomer was solved in absolute methanol to receive a clear solution, which was then added to the siloxanes. Afterwards, additional barium hydroxide or sodium hydroxide equal to the calculated released HCl was added to shift the pH_0 value back to basic. Various tin alkoxides were also used, but they reacted too fast and formed clusters or particles which could not be dissolved during the rest of the reaction.

All synthesised hydride- respectively vinyl-group and metal atom containing copolymers are listed in Table 19. Besides FT-IR, liquid NMR, TGA and DSC measurements, the RI and the viscosity were determined. Because of the pour solubility of some polymers and the risk of nanoparticle formations, no SEC measurements were performed.

Table 19: Overview of all synthesised metal atom containing copolymers, from zirconium over hafnium and tin to tantalum.

Group *A*	Group *B*	Group *C*		Copolymer
20 % H	0 % Met	40 % PP	40 % PM	H20_Met0_PP40_PM40
20 % V	0 % Met	40 % PP	40 % PM	V20_Met0_PP40_PM40
20 % H	1 % Zr	40 % PP	39 % PM	H20_Zr1_PP40_PM39
20 % V	1 % Zr	40 % PP	39 % PM	V20_Zr1_PP40_PM39
20 % H	3 % Zr	40 % PP	37 % PM	H20_Zr3_PP40_PM37
20 % V	3 % Zr	40 % PP	37 % PM	V20_Zr3_PP40_PM37
20 % H	5 % Zr	40 % PP	35 % PM	H20_Zr5_PP40_PM35
20 % V	5 % Zr	40 % PP	35 % PM	V20_Zr5_PP40_PM35
20 % H	10 % Zr	40 % PP	30 % PM	H20_Zr10_PP40_PM30
20 % V	10 % Zr	40 % PP	30 % PM	V20_Zr10_PP40_PM30
20 % H	15 % Zr	40 % PP	25 % PM	H20_Zr15_PP40_PM25
20 % V	15 % Zr	40 % PP	25 % PM	V20_Zr15_PP40_PM25
20 % H	1 % Hf	40 % PP	39 % PM	H20_Hf1_PP40_PM39
20 % V	1 % Hf	40 % PP	39 % PM	V20_Hf1_PP40_PM39
20 % H	3 % Hf	40 % PP	37 % PM	H20_Hf3_PP40_PM37

Group A	Group B	Group C		Copolymer
20 % V	3 % Hf	40 % PP	37 % PM	V20_Hf3_PP40_PM37
20 % H	5 % Hf	40 % PP	35 % PM	H20_Hf5_PP40_PM35
20 % V	5 % Hf	40 % PP	35 % PM	V20_Hf5_PP40_PM35
20 % H	10 % Hf	40 % PP	30 % PM	H20_Hf10_PP40_PM30
20 % V	10 % Hf	40 % PP	30 % PM	V20_Hf10_PP40_PM30
20 % H	15 % Hf	40 % PP	25 % PM	H20_Hf15_PP40_PM25
20 % V	15 % Hf	40 % PP	25 % PM	V20_Hf15_PP40_PM25
20 % H	1 % Sn	40 % PP	39 % PM	H20_Sn1_PP40_PM39
20 % V	1 % Sn	40 % PP	39 % PM	V20_Sn1_PP40_PM39
20 % H	3 % Sn	40 % PP	37 % PM	H20_Sn3_PP40_PM37
20 % V	3 % Sn	40 % PP	37 % PM	V20_Sn3_PP40_PM37
20 % H	5 % Sn	40 % PP	35 % PM	H20_Sn5_PP40_PM35
20 % V	5 % Sn	40 % PP	35 % PM	V20_Sn5_PP40_PM35
20 % H	10 % Sn	40 % PP	30 % PM	H20_Sn10_PP40_PM30
20 % V	10 % Sn	40 % PP	30 % PM	V20_Sn10_PP40_PM30
20 % H	15 % Sn	40 % PP	25 % PM	H20_Sn15_PP40_PM25
20 % V	15 % Sn	40 % PP	25 % PM	V20_Sn15_PP40_PM25
20 % H	1 % Ta	40 % PP	39 % PM	H20_Ta1_PP40_PM39
20 % V	1 % Ta	40 % PP	39 % PM	V20_Ta1_PP40_PM39
20 % H	3 % Ta	40 % PP	37 % PM	H20_Ta3_PP40_PM37
20 % V	3 % Ta	40 % PP	37 % PM	V20_Ta3_PP40_PM37
20 % H	5 % Ta	40 % PP	35 % PM	H20_Ta5_PP40_PM35
20 % V	5 % Ta	40 % PP	35 % PM	V20_Ta5_PP40_PM35
20 % H	10 % Ta	40 % PP	30 % PM	H20_Ta10_PP40_PM30
20 % V	10 % Ta	40 % PP	30 % PM	V20_Ta10_PP40_PM30
20 % H	15 % Ta	40 % PP	25 % PM	H20_Ta15_PP40_PM25
20 % V	15 % Ta	40 % PP	25 % PM	V20_Ta15_PP40_PM25

4.3.1.1 FT-IR spectroscopy of the hydride- or vinyl-group and metal atom containing copolymers

FT-IR spectra of all vinyl- and hydride-containing copolymers were recorded (experimental section, Figures 265 – 268). Exemplarily, in Figure 111 six spectra are shown, the two reference copolymers, as well as a vinyl and zirconium or hafnium and a hydride and tin or tantalum one,

all with 15 % metal and 85 % silicone content. The signals generated by the poly[diphenyl-*co*-methylphenyl]siloxane were already described earlier. The Si-H bands[234-235, 319, 346-347] are located at 2164 cm^{-1} and 899 cm^{-1} and the intensities are reduced at higher metal contents because of the Si–H and Met side reactions.[410-412] The vinyl copolymers show weak signals at 1408 cm^{-1} and 968 cm^{-1},[234-235, 319, 370] which are close to the Si-O-Si respectively Si-C or C-H signals. The alkoxy signals at 1000 cm^{-1} to 1200 cm^{-1} are barely visible because of the overlap with the broad Si-O region[347] and therefore, no clear statement on the degree of conversion can be made. The Si-O-Met bonds are visible beneath the Si-O bands at 900 cm^{-1} to 1000 cm^{-1} in the dark grey region.[138, 275, 420-423] More precisely, the hafnium band is located at 940 cm^{-1},[347, 373, 424] the zirconium one between 940 cm^{-1} and 950 cm^{-1},[138, 277, 373] the tin one at 960 cm^{-1} to 1000 cm^{-1}, [276, 425] and the tantalum one at 918 cm^{-1} and 976 cm^{-1}.[423]
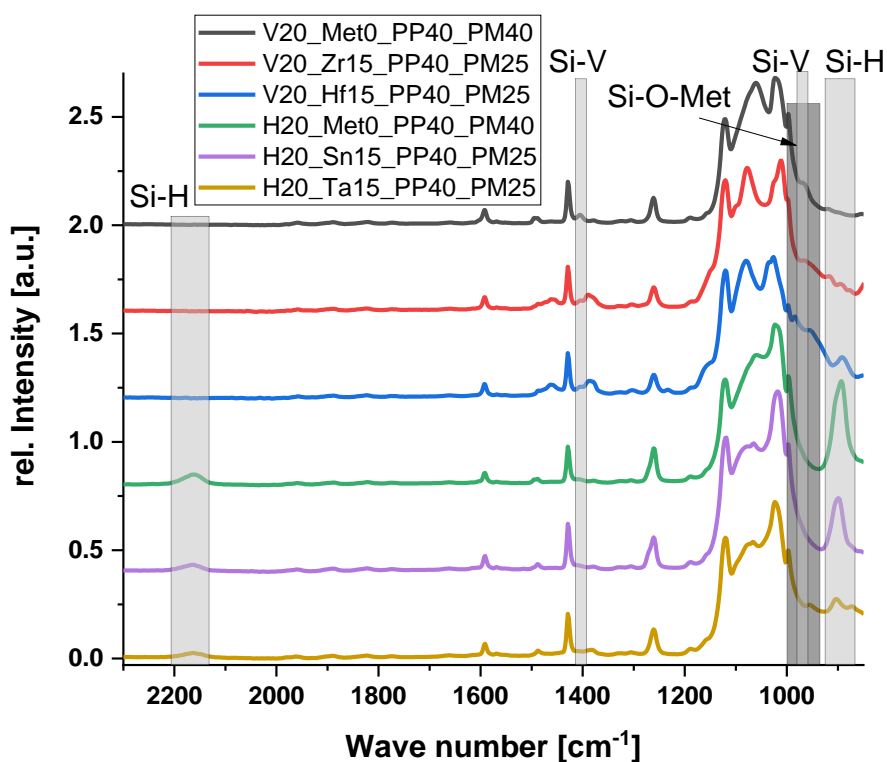

Figure 111: FT-IR spectra of the two metal-free reference copolymers as well as four metal containing copolymers with 15 mol% metal content.

4.3.1.2 NMR spectroscopy of the hydride- or vinyl-group and metal atom containing copolymers

^{1}H, ^{13}C and ^{29}Si NMR spectra were recorded from all samples (Figures 269 – 310). Additionally, ^{119}Sn NMR of the tin containing samples were recorded, but no clear signal could be detected despite using 500 mg to 1000 mg of sample with 2 mL of deuterated chloroform, because of the low amount of tin atoms in the polymers. Although zirconium and hafnium are also NMR active nuclei, it is not possible to measure a [91]Zr, [177]Hf or [179]Hf NMR with the present systems

because they are not equipped with a low frequency probe head. [181]Ta NMR is maybe possible, but in literature it is even less common than zirconium or hafnium. No references for the zirconium, hafnium, or tantalum NMR related to the self-prepared polymer system could be found.

The ^{1}H and ^{29}Si NMR spectra of V20_Ta1_PP40_PM39 and H20_Sn5_PP40_PM35 are exemplarily shown (Figure 112). The phenyl signals are located at 6.8 ppm to 7.9 ppm, the methyl ones are visible at 0.7 ppm to −0.3 ppm, and the hydride ones are located at 5.4 ppm to 4.3 ppm and the vinyl ones at 6.4 ppm to 5.6 ppm, respectively.[334, 338, 396] In the spectra, residual toluene and xylene signals are visible.[426-428] Additionally, the alkoxy signals for some copolymers are visible, methoxy in the tin samples, ethoxy in the tantalum samples, propoxy in the zirconium samples and butoxy in the hafnium samples.[426-428] Generally, the amount of residual alkoxides increases with their increasing molecular weight because of the higher resulting boiling temperature.[381] The amount also rises with increasing metal content, which adds more alkoxides as well as increase the viscosity due to the raised degree of cross-linking because of the four respectively five possible bonds which reduce the potential to remove volatile solvents. The ^{13}C NMR shows all the aromatic and aliphatic bands of the side-groups as well as the alkoxy-groups and the residual solvents.

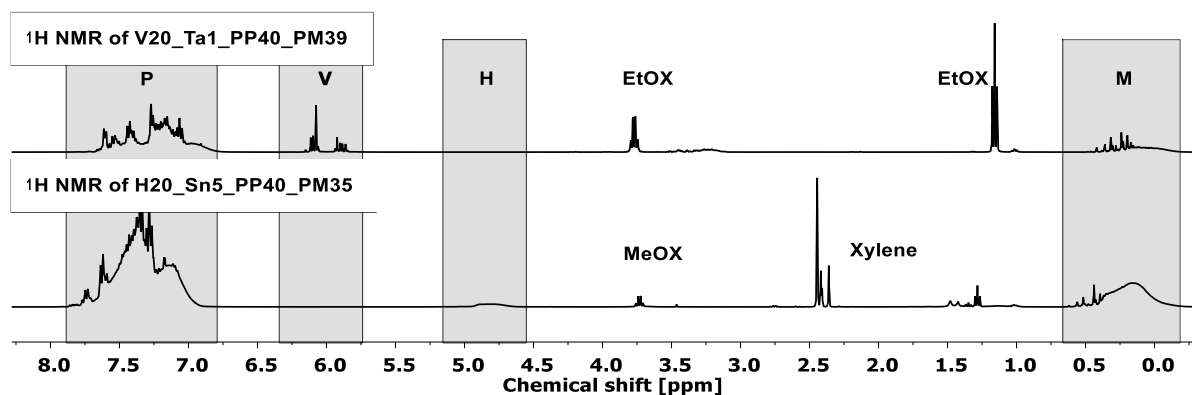**Figure 112: ^{1}H NMR (400 MHz, CDCl₃) of V20_Ta1_PP40_PM39 and H20_Sn5_PP40_PM35.**

The ^{29}Si NMRs of these two copolymers are also displayed (Figure 113). The typical region for the methylphenyl (PM) silicon atoms is at −27 ppm to −33 ppm,[331, 368] for the hydridomethyl (H) signals at −34 ppm to −38 ppm,[323-324, 331] for the vinylphenyl (V) ones at −41 ppm to −46 ppm,[331, 368] and for the diphenyl-group (PP) containing silicon atoms are located at −42 ppm to −48 ppm.[324, 331, 368] Also, for some copolymers, signals in the region from −17 ppm to −24 ppm can be observed which can be assigned to Si-O-H or Si-O-C$_x$H$_y$ groups with methylphenyl side-groups. When comparing D silicon atoms inside the chain against the one at the end of the chain with a free OH group, the chemical shift is around 10 ppm higher, while for methoxylated silicon atoms at the end of a polymer chain the chemical shift is around 7 ppm

to 8 ppm higher.[321-325, 327-331, 333-335, 338-342, 368, 403, 409, 429-447] Therefore, other silanol or alkoxysilane end groups than PM are present which can also be observed in the ^{1}H NMRs and their signals overlap with the other signals from silicon atoms inside the polymer chain. Signals at lower chemical shifts cannot be observed and therefore no additional cross-linking or side reactions occur, which results in the formation of T or Q groups.
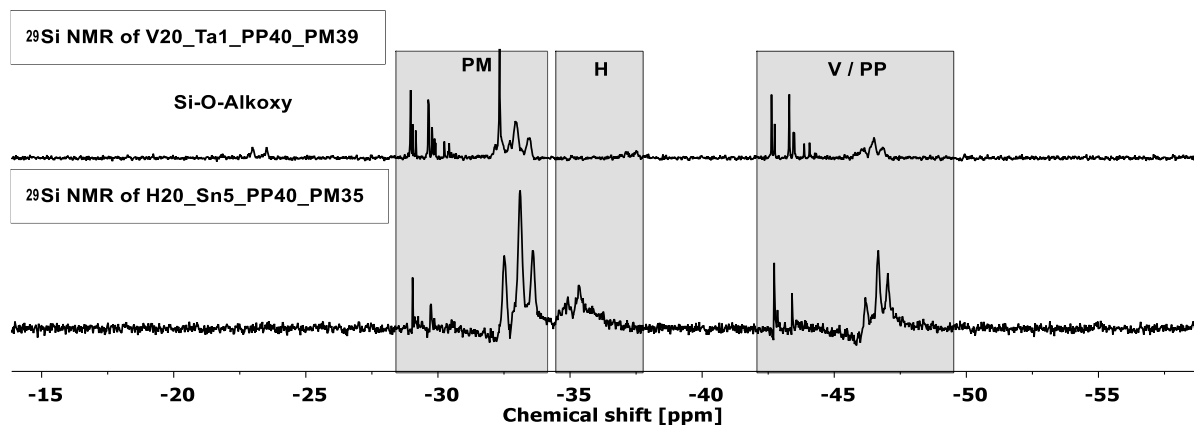

Figure 113: ^{29}Si NMR (79 MHz, CDCl₃) of V20_Ta1_PP40_PM39 and H20_Sn5_PP40_PM35.

4.3.1.3 Refractive index of the hydride- or vinyl-group and metal atom containing co-polymers

The refractive index of the metal atom and vinyl- or hydride-group containing copolymers were determined and are displayed in Figure 114, the exact values are listed in the experimental section. The RI should increase with the incorporation of metal atoms inside polymer chain.[138, 274-275] The problems here are the drastically increased viscosity because of the cross-linking provided by the metals and the incomplete reaction and removal of alkoxides.[138, 274-275] The metal-free vinyl copolymer has a RI of 1.573, which is higher than most of the metal containing vinyl copolymers. In the zirconium-group the RI systematically drops with increasing metal content from 1.564 to 1.547, which is due to the increasing number of present unreacted propox-ide-groups. Because the viscosity increases during the reaction, the removal of solvent and the establishment of new bonds slows down, which is visible in the FT-IR and NMR spectra.[379, 448-449] The hafnium-group shows the same trend in case of the butoxide-groups, the RI decreases from 1.559 to 1.534 with increasing metal content because of the increase of remaining alkoxy-groups. Both the propoxide and the butoxide-groups have a lower reactivity in the sol-gel reac-tion[379, 448-449] and their relatively high boiling point makes it difficult to remove them at 150 °C during the reaction. For hafnium and zirconium, the chlorine salts were also tested, but the hydrolysis and condensation reactions are too fast under the selected reaction conditions and lead to the formation of solid HfO₂ respectively ZrO₂. The tin samples show a slightly different result. The 1.0 mol% tin containing sample has the same value as the metal-free copolymers

and the 3.0 mol% one shows the highest RI of all copolymers with 1.581. The 5.0 mol% and 15.0 mol% samples have lower values than the metal-free copolymer because of the incomplete polycondensation reaction. The 10.0 mol% tin copolymer has a slightly higher RI of 1.576. The tantalum probes show lower values for the 1.0 mol% and 3.0 mol% samples with 1.562, which slightly increases for the 5.0 mol% and 15.0 mol% ones, but it still remains under the RI of the metal-free copolymer. Despite using the lower boiling ethanol, the presence of five alkoxide-groups sterically hinders the reaction. The 10.0 mol% tantalum sample has an increased RI of 1.577 compared to the metal-free polymer.
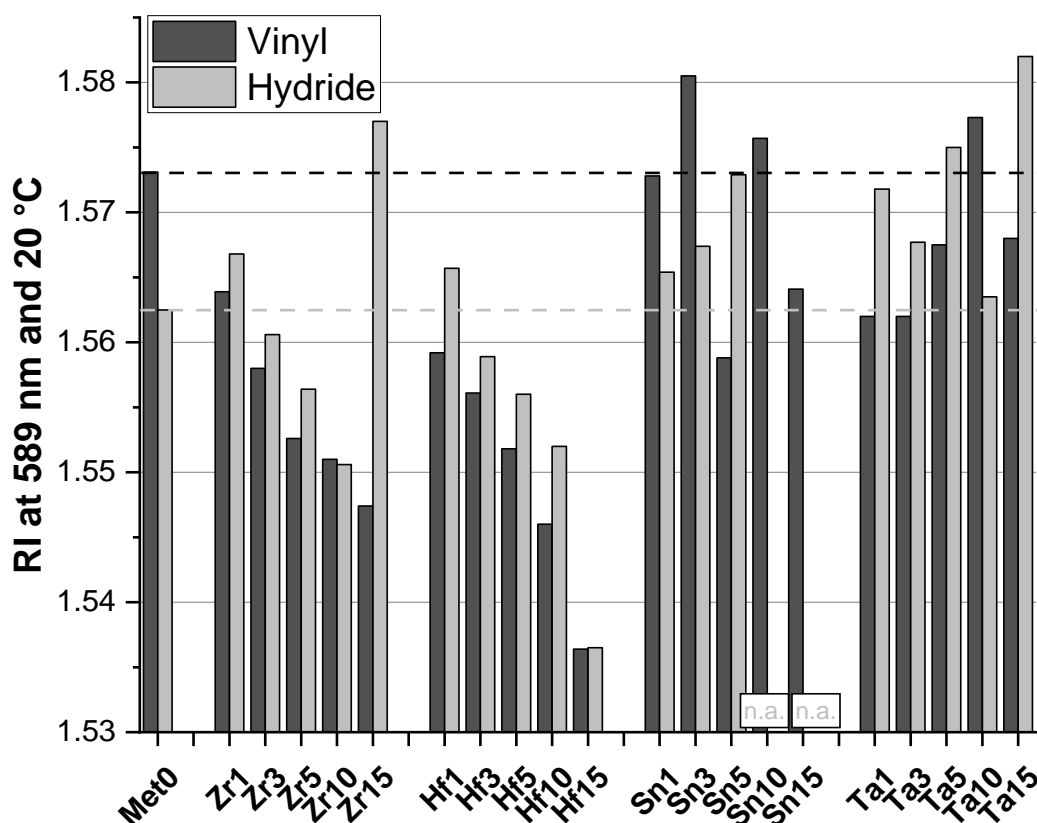

Figure 114: Refractive indices of the metal and vinyl- or hydride-group containing copolymers.

The hydride metal-free copolymer shows a RI of 1.563, which is lower than the one of the vinyl copolymer because of the here used methyldiethoxysilane instead of the vinylphenyldiethox-ysilane. Overall, the zirconium- and the hafnium-groups show the same effect, the metal increase leads to a more incomplete reaction and lowers the RI. Also, the hydride and metal side reactions have to be taken into account, which increase the cross-linking but generate problems for the later hydrosilylation reaction.[410-412] The 1.0 mol% samples of Zr and Sn have an increased RI of 1.567 and 1.566 compared to the metal-free copolymers. The other samples show a reduced and further decreasing value when increasing the metal content, besides the 15.0 mol% tin sample, which has a high RI of 1.577. The tin samples with 1.0 mol%, 3.0 mol%

and 5.0 mol% show the desired RI increase from 1.565 over 1.567 to 1.573. For the 10.0 mol% and 15.0 mol% sample no RI could be measured because they are opaque or white. The tantalum polymers also show an overall increase of the RI with raising metal content. The 1.0 mol%, 5.0 mol% and 15.0 mol% samples show increasing values from 1.572 over 1.575 to 1.582 which is the overall highest achieved RI for the metal containing copolymers. The 3.0 mol% and 10.0 mol% samples show a lower value of 1.568 and 1.564 which is still higher than the RI of the metal-free copolymer.

Overall, the vinyl metal copolymers barely reach or exceed the RI of the metal-free polymer, while the hydride copolymers show higher values for all 1.0 mol% metal samples. The residual zirconium and hafnium samples have lower values. All tin and tantalum polymerss reveal higher values than the metal-free polymers. Noteworthy, the 10.0 mol% and 15.0 mol% hydride tin samples could not be measured. The prepared copolymers reveal higher RIs compared to the OE-6630 system, expect the zirconium and hafnium samples with higher metal content.

4.3.1.4 *Viscosity of the hydride- or vinyl-group and metal atom containing copolymers*

Rheological measurements (Table 20) were also performed to determine the viscosity at room temperature, the standard deviations are reported in the experimental section (6.2.6). The viscosity is an indicator for the polymer length, the amount of branching and the length of the side arms or side-groups.[450-454] Here, it also relates to the remaining alkoxy-groups, which did not condensate and the amount of hydride-groups, which do not side react with the metal atoms. Therefore, a relation to the refractive index can sometimes be made. The viscosity of the hydride metal-free copolymer is determined with 2800 mPa·s and therefore comparable to the 3000 mPa·s respectively 2500 mPa·s of compound A and B from the OE-6630 system. The vinyl polymer shows a very high viscosity of 508000 mPa·s. The viscosity of the hydride and metal containing copolymers range from about 2000 mPa·s to eleven million mPa·s. For the zirconium ones, the viscosity increases with rising metal content up to 680000 mPa·s for H20_Zr15_PP40_PM25. The hafnium- and hydride-containing samples show no trend and remain rather low in the ten thousand except H20_Hf5_PP40_PM35 with 3120000 mPa·s. The tin sample with 3.0 mol% shows a high viscosity of 276000 mPa·s and the 1.0 mol% and 5.0 mol% ones one around 28000 mPa·s. The viscosity of the tantalum samples roughly relates with the metal content, H20_Ta3_PP40_PM37 has the lowest viscosity of 2160 mPa·s. The polymer with 15.0 mol% Ta shows the highest viscosity of 10.6 million mPa·s.

Table 20: The viscosity of all metal and hydride- or vinyl-group containing copolymers at 25 °C.

Hydride copolymer	Viscosity at 25 °C [mPa·s]	Vinyl copolymer	Viscosity at 25 °C [mPa·s]
H20_Met0_PP40_PM40	2800	V20_Met0_PP40_PM40	508000
H20_Zr1_PP40_PM39	25200	V20_Zr1_PP40_PM39	332
H20_Zr3_PP40_PM37	7220	V20_Zr3_PP40_PM37	323
H20_Zr5_PP40_PM35	7090	V20_Zr5_PP40_PM35	500
H20_Zr10_PP40_PM30	30200	V20_Zr10_PP40_PM30	831
H20_Zr15_PP40_PM25	680000	V20_Zr15_PP40_PM25	258
H20_Hf1_PP40_PM39	20000	V20_Hf1_PP40_PM39	1430
H20_Hf3_PP40_PM37	26600	V20_Hf3_PP40_PM37	299
H20_Hf5_PP40_PM35	3120000	V20_Hf5_PP40_PM35	294
H20_Hf10_PP40_PM30	54000	V20_Hf10_PP40_PM30	136
H20_Hf15_PP40_PM25	6640	V20_Hf15_PP40_PM25	61600
H20_Sn1_PP40_PM39	30600	V20_Sn1_PP40_PM39	5260
H20_Sn3_PP40_PM37	276000	V20_Sn3_PP40_PM37	1170000
H20_Sn5_PP40_PM35	26800	V20_Sn5_PP40_PM35	330
H20_Sn10_PP40_PM30	n. a.	V20_Sn10_PP40_PM30	541000
H20_Sn15_PP40_PM25	n. a.	V20_Sn15_PP40_PM25	84
H20_Ta1_PP40_PM39	16700	V20_Ta1_PP40_PM39	4490
H20_Ta3_PP40_PM37	2160	V20_Ta3_PP40_PM37	340
H20_Ta5_PP40_PM35	20300	V20_Ta5_PP40_PM35	887
H20_Ta10_PP40_PM30	25200	V20_Ta10_PP40_PM30	159000
H20_Ta15_PP40_PM25	10600000	V20_Ta15_PP40_PM25	2310

The vinyl and metal-free copolymer already is highly viscous with 508000 mPa·s. The zirconium vinyl polymers show a very low viscosity of 260 mPa·s to 830 mPa·s, which indicates low M_W polymers and a high amount of alkoxy-groups which is in agreement with the FT-IR and NMR data. The Hf samples with a lower metal content ranging from 1.0 mol% to 10.0 mol% reveal low viscosities decreasing from 1430 mPa·s to 136 mPa·s with increasing metal content, relating to the increased amount of remaining alkoxides. The 15.0 mol% Hf samples although show a higher viscosity of 62000 mPa·s because of the high metal content.

The tin samples with 3.0 mol% and 10.0 mol% metal content show the highest values, while the 5.0 mol% and 15.0 mol% polymers show the lowest ones with 330 mPa·s and 84 mPa·s. The tantalum vinyl copolymers range from 350 mPa·s to 4500 mPa·s despite the 10.0 mol% one, which is with 159000 mPa·s very high.

Overall, the high amount of phenyl-groups are a problem for the vinyl copolymer syntheses, resulting from the vinylphenyl-group compared to the hydridomethyl-group used in the hydride copolymer syntheses. During the reaction, the steric hindrance is very high and therefore many alkoxide-groups remain unreacted and smaller polymers result. Therefore, most of the viscosities do not exceed 1000 mPa·s which is 510 times lower than the metal-free polymer. This observation can also be seen in the RI graph (Figure 114). Polymers with a very low viscosity also show a lower RI than V20_Met0_PP40_PM40, resulting from the remaining alkoxide-groups. The hydride samples show all higher or equal viscosities compared to the metal-free hydride-group containing polymer, which results from the metal incorporation and the unwanted Met-OR + Si-H side reaction, which also increases the cross-linking.[410-412]

4.3.1.5 *Thermogravimetric analyses of the hydride- or vinyl-group and metal atom containing copolymers*

TGA curves from all metal-free and metal containing copolymers were recorded under oxygen respectively nitrogen atmosphere up to 900°C to determine the $T_{95\%}$ value and the decomposition progress (experimental section, Figures 311 – 314).

The $T_{95\%}$ values are reported in Table 21. The incorporation of these metal atoms with four or five connectable bonds into the linear metal-free copolymers allow a cross-linking of the polymers which increases the thermal stability.[218] The presence of unreacted alkoxy-groups as well as residual solvent drastically decreases the $T_{95\%}$ value because of the low boiling point of C1 to C4 alcohols and toluene or xylene, respectively. The amount of the residual groups and molecules increases with increasing metal content because of the increased viscosity and sterical hindrance caused by these metal atoms during the sol-gel reaction. The difference between the decomposition temperatures under oxygen or inert atmosphere is often negligible. Larger differences relate to different measurement times of the same sample because some polymers had to be measured again which then resulted in different amounts of volatile components. The metal-free hydride polymer shows $T_{95\%}$ values of 320 °C. The decomposition temperature of the 1.0 mol% Met samples is always higher because of the increased amount of cross-linking. The zirconium-group shows decreasing temperatures from 360 °C for the 1.0 mol% Zr sample down to around 180 °C for the 15.0 mol% one because of the earlier described problems.

Table 21: T$_{95\%}$ values for the metal-free and containing copolymers under O$_2$ or N$_2$ atmosphere.

Hydride copolymer	T$_{95\%}$ O$_2$ [°C]	T$_{95\%}$ N$_2$ [°C]	Vinyl copolymer	T$_{95\%}$ O$_2$ [°C]	T$_{95\%}$ N$_2$ [°C]
H20_Met0_PP40_PM40	321	320	V20_Met0_PP40_PM40	310	316
H20_Zr1_PP40_PM39	360	361	V20_Zr1_PP40_PM39	218	180
H20_Zr3_PP40_PM37	235	242	V20_Zr3_PP40_PM37	175	144
H20_Zr5_PP40_PM35	271	209	V20_Zr5_PP40_PM35	178	149
H20_Zr10_PP40_PM30	250	225	V20_Zr10_PP40_PM30	191	159
H20_Zr15_PP40_PM25	201	158	V20_Zr15_PP40_PM25	191	165
H20_Hf1_PP40_PM39	356	354	V20_Hf1_PP40_PM39	162	138
H20_Hf3_PP40_PM37	232	193	V20_Hf3_PP40_PM37	207	153
H20_Hf5_PP40_PM35	220	197	V20_Hf5_PP40_PM35	251	246
H20_Hf10_PP40_PM30	191	196	V20_Hf10_PP40_PM30	184	167
H20_Hf15_PP40_PM25	172	179	V20_Hf15_PP40_PM25	169	165
H20_Sn1_PP40_PM39	364	317	V20_Sn1_PP40_PM39	187	131
H20_Sn3_PP40_PM37	307	295	V20_Sn3_PP40_PM37	192	188
H20_Sn5_PP40_PM35	378	328	V20_Sn5_PP40_PM35	196	130
H20_Sn10_PP40_PM30	359	286	V20_Sn10_PP40_PM30	178	166
H20_Sn15_PP40_PM25	339	326	V20_Sn15_PP40_PM25	276	274
H20_Ta1_PP40_PM39	374	360	V20_Ta1_PP40_PM39	261	155
H20_Ta3_PP40_PM37	367	344	V20_Ta3_PP40_PM37	161	157
H20_Ta5_PP40_PM35	309	333	V20_Ta5_PP40_PM35	300	205
H20_Ta10_PP40_PM30	281	271	V20_Ta10_PP40_PM30	173	177
H20_Ta15_PP40_PM25	257	275	V20_Ta15_PP40_PM25	297	256

The hafnium samples show the same trend, the 1.0 mol% sample has a slightly lower T$_{95\%}$ value of 355 °C which decreases down to 170 °C for the 15.0 mol% one. The hydride-groups and tin atom containing samples show values over 300 °C, because the released methanol can be removed more easily than the C3 or C4 alcohol ones from Zr or Hf because of the lower molecular weight, nevertheless some methoxy-groups are present. Additionally the Si-H reaction with the Met-OX increases the cross-linking even further.[410-412]

The 3.0 mol% Sn sample shows the lowest value of 300 °C, the other ones range from 340 °C to 380°C under oxygen and from 290 °C to 330 °C under nitrogen atmosphere but no clear trend can be seen. The tantalum samples show again the same trend as the Zr and Hf samples, the 1.0 mol% Ta has an even higher $T_{95\%}$ value of 368 °C because of the five cross-linking bonds. The increasing metal content reduces the decomposition temperature down to 265 °C for the 15.0 mol % Ta sample. The metal-free vinyl copolymer reveals a $T_{95\%}$ value of 310 °C, which is slightly higher than the one of the hydride polymer. All vinyl-group and metal atom containing copolymers show very low $T_{95\%}$ temperatures from 130 °C to 300 °C. In the TG curves a first decomposition step starting at around 100 °C is visible because of the evaporation of residual solvent. All the metal copolymer groups show no clear trend, the decomposition temperature of the zirconium ones is around 200 °C under oxygen and around 160 °C under nitrogen. Most of the hafnium and the tin containing copolymers show the same results. Only the V20_Hf5_PP40_PM35 and the V20_Sn15_PP40_PM25 polymers show higher values with 250 °C respectively 275 °C. In the tantalum-group the $T_{95\%}$ temperatures range from 150 °C to 300 °C and the difference between the oxygen and inert decomposition temperature is up to 100 °C.

Overall, the 1.0 mol% hydride samples show a higher thermal stability than the metal-free samples, also most of the tin samples and the 3.0 mol% and 5.0 mol% tantalum samples show comparable decomposition temperatures. No vinyl-group and metal atom containing copolymer can reach the $T_{95\%}$ of the metal-free copolymer with 310 °C. The highest achievable temperature is 300 °C with the 5.0 mol% tantalum sample under oxygen atmosphere. The main problem are the unreacted alkoxy-groups and the residual solvents, which could not be removed even under high vacuum and 40 °C. The linear component A of OE-6630 shows a very high $T_{95\%}$ of around 400 °C, which is higher than the 370 °C of H20_Ta1_PP40_PM39 independent from the atmosphere. The cross-linked component B has a decomposition temperature of 180 °C, which all but one hydride and metal containing copolymers reached and is in the range of the vinyl and metal containing ones.

4.3.1.6 *Differential scanning calorimetry of the hydride- or vinyl-group and metal atom containing copolymers*

DSC curves of all hydride and vinyl copolymers were recorded from −100 °C or −60 °C to 150 °C under nitrogen atmosphere (experimental section, Figures 315 – 322). The glass transition and the melting temperatures with their integrated energy are reported in Table 22. The glass transition temperatures should increase with increasing metal content due to the provided

raised amount of possible cross-linking[275, 400] and with the polymer length,[121, 455] but also slightly decrease because of the reduced amount of present phenyl-groups from the reduced amount of PM monomer.[402-404] The T_g also decreases when the metal atoms are not fully condensed and alkoxy-groups remain, which additionally results in a wider network respectively shorter polymer chains.[399, 455] The here named melting temperature T_m can more precisely be called crystal-liquid crystal transition temperature T_{lc}.[456]

The hydride and metal-free copolymer H20_Met0_PP40_PM40 has a T_g of -14 °C, which is in between the -7 °C of poly[di-*p*-propylphenyl]siloxane and the -28 °C of polymethylphenyl-siloxane.[119, 457-458] The zirconium containing copolymers range from -32 °C to -12 °C, the 1.0 mol% and 10.0 mol% polymers show lower values than the metal-free one while the other three show equal T_g's. The T_g of the hafnium samples ranges from -26 °C to -16 °C. Here the theoretical T_g increase because of the cross-linking is not observable. The unreacted alkoxy-groups and the therefore lower M_W decreases the T_g under the -14 °C of the metal-free copolymer. The tin samples range from -26 °C to -6 °C. The 3.0 mol%, 10.0 mol% and 15.0 mol% show higher T_g's than the H20_Met0_PP40_PM40 with increasing metal content. The 1.0 mol% and 5.0 mol% samples have a lower value of -26 °C and -21 °C. The hafnium samples range from -27 °C to -8 °C, the 5.0 mol% copolymer has a slightly lower value of -15 °C than the metal-free sample and the 15.0 mol% Ta copolymer shows a higher value of -8 °C.

The metal-free vinyl copolymer has a T_g of -7 °C, which is slightly higher than the one of the hydride sample because the vinyl- and phenyl-group containing silicon atom reduces the polymer flexibility compared to the hydride- and methyl-group one used in H20_Met0_PP40_PM40. The Zr samples range from -52 °C to -32 °C, which is very low compared to the poly[vinylphenyl-*co*-diphenyl-*co*-phenylmethyl]siloxane (V20_Met0_PP40_PM40). The not fully condensed metals drastically reduce the degree of polymerisation and additionally the introduction of flexible propoxide-groups lowers the T_g below the -30 °C of poly[diphenyl-*co*-dimethyl]siloxane (1:1) and nearly ranges down to the -64 °C of poly[diphenyl-*co*-dimethyl]siloxane (3:7).[119, 458] The overall tendency shows a T_g increase with a metal content increase up to -32 °C for the 15.0 mol% tin sample. The T_g of the hafnium copolymers range from -55 °C to -31 °C and show the same problems except that instead of propoxide-groups butoxide ones are present, but a clear tendency cannot be observed. The T_g of the tin samples range from -57 °C to -12 °C, where the 1.0 mol%, 3.0 mol% and 10.0 mol% samples are the closest to the metal-free copolymer. The T_g of the tantalum copolymers range from -55 °C to -14 °C.

Table 22: Glass transition temperatures (T$_g$) and melting temperatures (T$_m$) with the integrated energy (E$_m$) from the metal atom containing copolymers.

Hydride polymer H20_	T$_g$ [°C]	T$_m$ [°C]	E$_m$ [J/g]	Vinyl polymer V20_	T$_g$ [°C]	T$_m$ [°C]	E$_m$ [J/g]
Met0_PP40_PM40	−14.2	−10.6	0.164	Met0_PP40_PM40	−6.6	61.6	8.801
Zr1_PP40_PM39	−23.3	119.5	1.426	Zr1_PP40_PM39	−48.8	71.2	0.787
Zr3_PP40_PM37	−14.4	106.4	14.93	Zr3_PP40_PM37	−43.1	64.7	0.180
Zr5_PP40_PM35	−11.9	99.2	15.49	Zr5_PP40_PM35	−51.7	65.5	0.352
Zr10_PP40_PM30	−31.9	109.0	0.063	Zr10_PP40_PM30	−44.8	89.5	1.202
Zr15_PP40_PM25	−12.6	109.3	20.46	Zr15_PP40_PM25	−31.9	99.4	6.719
Hf1_PP40_PM39	−23.4	109.0	0.425	Hf1_PP40_PM39	−31.4	67.6	0.555
Hf3_PP40_PM37	−17.7	90.0	9.473	Hf3_PP40_PM37	−51.6	66.7	1.063
Hf5_PP40_PM35	−19.9	119.9	19.02	Hf5_PP40_PM35	−55.0	68.5	0.833
Hf10_PP40_PM30	−16.3	112.7	26.52	Hf10_PP40_PM30	−43.4	101.9	7.720
Hf15_PP40_PM25	−25.6	119.6	7.351	Hf15_PP40_PM25	−36.9	89.2	12.34
Sn1_PP40_PM39	−25.7	115.6	2.981	Sn1_PP40_PM39	−16.7	−23.6	2.357
Sn3_PP40_PM37	−11.3	110.4	2.486	Sn3_PP40_PM37	−12.3	64.6	0.006
Sn5_PP40_PM35	−21.5	117.0	0.940	Sn5_PP40_PM35	−57.4	64.4	0.118
Sn10_PP40_PM30	−9.1	117.7	1.533	Sn10_PP40_PM30	−18.4	81.0	11.39
Sn15_PP40_PM25	−5.8	124.0	1.543	Sn15_PP40_PM25	−47.3	148.2	6.767
Ta1_PP40_PM39	−21.7	114.1	1.402	Ta1_PP40_PM39	−50.4	60.8	0.836
Ta3_PP40_PM37	−27.2	126.4	5.780	Ta3_PP40_PM37	−54.6	60.6	0.822
Ta5_PP40_PM35	−15.2	132.2	3.646	Ta5_PP40_PM35	−38.0	93.9	1.743
Ta10_PP40_PM30	−27.2	84.7	0.736	Ta10_PP40_PM30	−13.7	107.9	12.29
Ta15_PP40_PM25	−7.7	109.8	11.54	Ta15_PP40_PM25	−15.2	96.5	8.254

The T$_g$ increases with increasing metal content. The 10.0 mol% and 15.0 mol% Ta copolymers show T$_g$'s of −14 °C and −15 °C, respectively. A melting temperature of around −10 °C to 260 °C results from the crystal to liquid crystal transition,[119] while lower temperatures relate to a crystal-crystal transition.[459-462] Higher temperatures over 400 °C usually show the transition from the liquid crystal to the isotropic melt, but these phenyl-group containing polysiloxanes often decompose already at these temperatures.[119] The T$_m$ of the hydride-group and metal-free

copolymer is −11 °C, while all T_m's of the metal containing polymers are in between 85 °C to 132 °C and no clear tendency can be observed. The integrated energy ranges from low amounts of 0.06 J/g to large amounts of 26.53 J/g. The vinyl-group and metal-free copolymer shows a T_m of 62 °C, while the metal containing polymers range from −24 °C to 148 °C. Here a small tendency is observable, the T_m increases roughly with increasing metal content. The integrated energy varies from 0.01 J/g to 12.34 J/g.

Overall, most of the hydride polymers show glass transition temperatures which are lower or equal than the one of H20_Met0_PP40_PM40. Only the 5.0 mol% and 15.0 mol% Zr, 3.0 mol%, 10.0 mol% and 15.0 mol% Sn and the 15.0 mol% Ta samples have higher values up to −6 °C. The higher metal content of up to 15.0 mol% can therefore increase the T_g value when a high degree of condensation can be achieved. All of the vinyl-group and metal atom containing copolymers show a lower T_g of −58 °C to −12 °C than the metal-free V20_Met0_PP40_PM40 with −7 °C. The metal atoms here have no positive impact in increasing the T_g value resulting from possible additional cross-linking because of residual alkoxide-groups. The resulting rather wider network leads to a drastically lower glass transition temperature compared to the metal-free copolymers. The linear component A of OE-6630 shows a low T_g of −45 °C and most of the self-prepared polymers show equal to higher values. The already cross-linked component B of OE-6630 has an even lower T_g of −55 °C.

4.3.2 Synthesis and characterisation of the cured metal atom containing copolymers

The syntheses of novel polysiloxanes by curing the vinyl- and hydride-group copolymers was performed in a 1:1 ratio with the *Ossko*'s platinum catalyst in a thermally driven hydrosilylation reaction (Figure 115). The temperature was gradually raised to 150 °C in three steps. Besides curing the samples in a disposable glass, the polysiloxanes were also cured onto a microscope glass slide for the RI determinations and the UV/Vis analyses. Additionally, FT-IR measurements and TG and DSC analyses were performed.
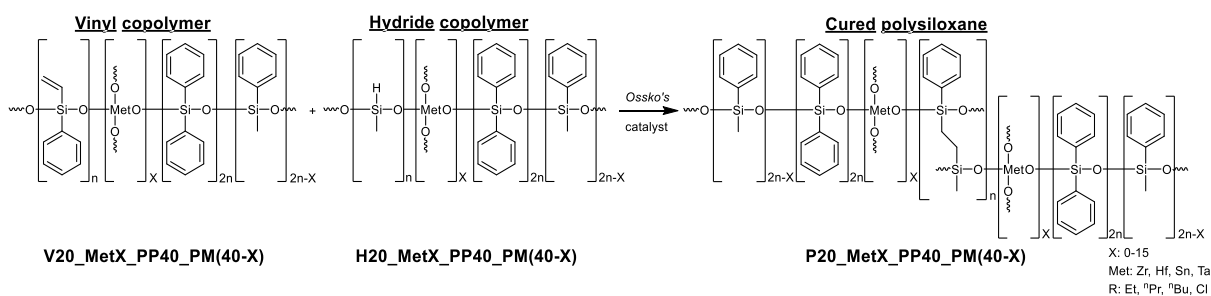
Figure 115: Synthesis of the cured and metal containing polysiloxanes.

The associate vinyl and hydride copolymers are mixed with the equal amount of metal content, for example H20_Zr3_PP40_PM37 and V20_Zr3_PP40_PM37 are cured to receive P20_Zr3_PP40_PM37. Also, the vinyl samples were mixed with the metal-free hydride sample to reduce the metal content by 50 % in the cured polymer, for example H20_Met0_PP40_PM40 and V20_Zr15_PP40_PM25 are cured to receive P20_Zr7.5_PP40_PM32.5. Overall, samples with metal concentrations were produced namely with 1.0 mol%, 1.5 mol%, 2.5 mol%, 3.0 mol%, 5.0 mol%, 7.5 mol%, 10.0 mol% and 15.0 mol% metal content. Additionally for the 5.0 mol% metal content polysiloxanes, two variants were synthesised using either the V20_Met5_PP40_PM40 with H20_Met5_PP40_PM40 or V20_Met10_PP40_PM40 with H20_Met0_PP40_PM40, the latter system is named with an "H" after the metal percentage (P20_Met5H_PP40_PM40). All compositions are reported in Table 23. The nomenclature slightly changes, the "H" respectively "V" was substituted with a "P" because of the reaction of these groups. The amount of each monomer is still reported after each monomer abbreviation in mol%. Images of the cured films are displayed in Figure 119 in 4.3.2.6.

Table 23: Polysiloxane mixtures for the metal-free and metal atom containing cured polymers.

Hydride copolymer	Vinyl copolymer	Cured polysiloxane
H20_Met0_PP40_PM40	V20_Met0_PP40_PM40	P20_Met0_PP40_PM40
H20_Zr1_PP40_PM39	V20_Zr1_PP40_PM39	P20_Zr1_PP40_PM39

Hydride copolymer	Vinyl copolymer	Cured polysiloxane
H20_Met0_PP40_PM40	V20_Zr3_PP40_PM37	P20_Zr1.5_PP40_PM38.5
H20_Met0_PP40_PM40	V20_Zr5_PP40_PM35	P20_Zr2.5_PP40_PM37.5
H20_Zr1_PP40_PM39	V20_Zr1_PP40_PM39	P20_Zr1_PP40_PM39
H20_Met0_PP40_PM40	V20_Zr3_PP40_PM37	P20_Zr1.5_PP40_PM38.5
H20_Met0_PP40_PM40	V20_Zr5_PP40_PM35	P20_Zr2.5_PP40_PM37.5
H20_Zr3_PP40_PM37	V20_Zr3_PP40_PM37	P20_Zr3_PP40_PM37
H20_Zr5_PP40_PM35	V20_Zr5_PP40_PM35	P20_Zr5_PP40_PM35
H20_Met0_PP40_PM40	V20_Zr10_PP40_PM30	P20_Zr5H_PP40_PM35
H20_Met0_PP40_PM40	V20_Zr15_PP40_PM25	P20_Zr7.5_PP40_PM32.5
H20_Zr10_PP40_PM30	V20_Zr10_PP40_PM30	P20_Zr10_PP40_PM30
H20_Zr15_PP40_PM25	V20_Zr15_PP40_PM25	P20_Zr15_PP40_PM25
H20_Hf1_PP40_PM39	V20_Hf1_PP40_PM39	P20_Hf1_PP40_PM39
H20_Met0_PP40_PM40	V20_Hf3_PP40_PM37	P20_Hf1.5_PP40_PM38.5
H20_Met0_PP40_PM40	V20_Hf5_PP40_PM35	P20_Hf2.5_PP40_PM37.5
H20_Hf3_PP40_PM37	V20_Hf3_PP40_PM37	P20_Hf3_PP40_PM37
H20_Hf5_PP40_PM35	V20_Hf5_PP40_PM35	P20_Hf5_PP40_PM35
H20_Met0_PP40_PM40	V20_Hf10_PP40_PM30	P20_Hf5H_PP40_PM35
H20_Met0_PP40_PM40	V20_Hf15_PP40_PM25	P20_Hf7.5_PP40_PM32.5
H20_Hf10_PP40_PM30	V20_Hf10_PP40_PM30	P20_Hf10_PP40_PM30
H20_Hf15_PP40_PM25	V20_Hf15_PP40_PM25	P20_Hf15_PP40_PM25
H20_Sn1_PP40_PM39	V20_Sn1_PP40_PM39	P20_Sn1_PP40_PM39
H20_Met0_PP40_PM40	V20_Sn3_PP40_PM37	P20_Sn1.5_PP40_PM38.5
H20_Met0_PP40_PM40	V20_Sn5_PP40_PM35	P20_Sn2.5_PP40_PM37.5
H20_Sn3_PP40_PM37	V20_Sn3_PP40_PM37	P20_Sn3_PP40_PM37
H20_Sn5_PP40_PM35	V20_Sn5_PP40_PM35	P20_Sn5_PP40_PM35
H20_Met0_PP40_PM40	V20_Sn10_PP40_PM30	P20_Sn5H_PP40_PM35
H20_Met0_PP40_PM40	V20_Sn15_PP40_PM25	P20_Sn7.5_PP40_PM32.5
H20_Sn10_PP40_PM30	V20_Sn10_PP40_PM30	P20_Sn10_PP40_PM30
H20_Sn15_PP40_PM25	V20_Sn15_PP40_PM25	P20_Sn15_PP40_PM25
H20_Ta1_PP40_PM39	V20_Ta1_PP40_PM39	P20_Ta1_PP40_PM39
H20_Met0_PP40_PM40	V20_Ta3_PP40_PM37	P20_Ta1.5_PP40_PM38.5
H20_Met0_PP40_PM40	V20_Ta5_PP40_PM35	P20_Ta2.5_PP40_PM37.5

Hydride copolymer	Vinyl copolymer	Cured polysiloxane
H20_Ta3_PP40_PM37	V20_Ta3_PP40_PM37	P20_Ta3_PP40_PM37
H20_Ta5_PP40_PM35	V20_Ta5_PP40_PM35	P20_Ta5_PP40_PM35
H20_Met0_PP40_PM40	V20_Ta10_PP40_PM30	P20_Ta5H_PP40_PM35
H20_Met0_PP40_PM40	V20_Ta15_PP40_PM25	P20_Ta7.5_PP40_PM32.5
H20_Ta10_PP40_PM30	V20_Ta10_PP40_PM30	P20_Ta10_PP40_PM30
H20_Ta15_PP40_PM25	V20_Ta15_PP40_PM25	P20_Ta15_PP40_PM25

4.3.2.1 *FT-IR analyses of the cured metal atom containing copolymers*

FT-IR spectra from all synthesised cured metal containing polysiloxanes were recorded (Figures 323 – 326). The spectra only slightly differ from the ones of the copolymers, the hydride and vinyl vibrations show no or a smaller intensity because of the hydrosilylation process and also the alkoxides have a reduced intensity because the high temperature during the curing process pushes incomplete polymerisations further along. Here, only the metal-free and the 5.0 mol% metal atom containing polysiloxanes are shown in Figure 116.
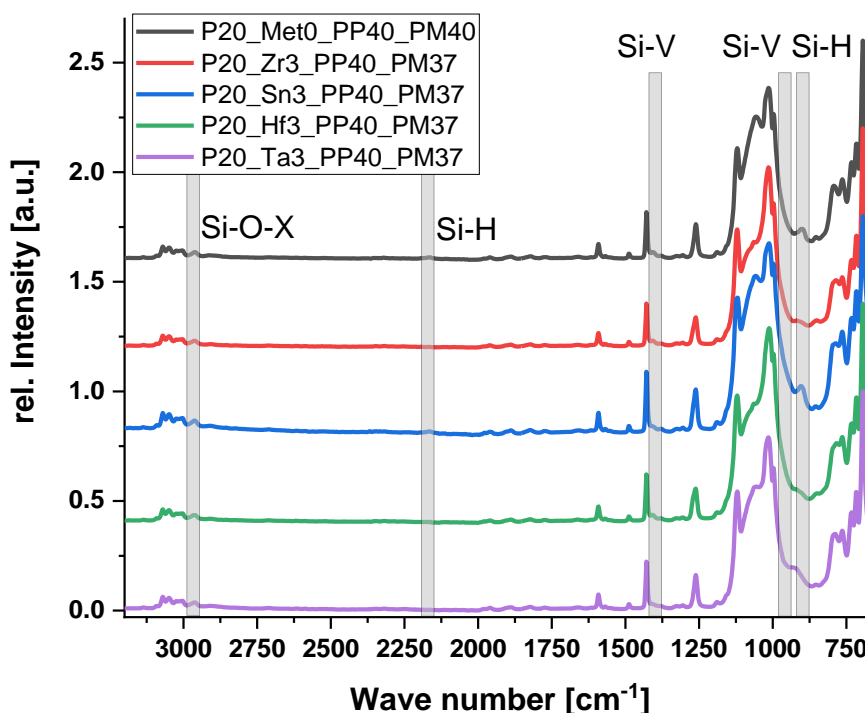
Figure 116: FT-IR spectra of the metal-free and the 5.0 mol% metal atom containing cured polysiloxanes.

The signals at 1405 cm^{-1} are generated by the vinyl-group[26,27,48,85] as well as the region around 965 cm^{-1},[26,27,48,85] which overlap with the Si-O signals. The Si-H group is located at 2160 cm^{-1} and 895 cm^{-1}.[234-235, 319, 346-347] Remaining methoxy-groups show a signal at 2840 cm^{-1} while the ethoxy-groups reveal a signal at 2880 cm^{-1}.[138] In the 5.0 mol% from P20_Met5H_PP40_PM35 and the 7.5 mol% zirconium, the 1.0 mol%, 1.5 mol%, 7.5 mol% and 10.0 mol% tin as well as

the 7.5 mol% tantalum samples are small residual Si-H signals visible. Overall, nearly all samples show a completed hydrosilylation reaction. The high viscosity of some samples hinders the 100 % conversion during the curing process.[136, 318, 395]

4.3.2.2 Refractive indices of the cured metal atom containing copolymers

The refractive indices of the cured metal containing polysiloxanes onto microscope slides were determined using 1-bromonaphthalene as contact fluid. Some polysiloxanes could not be measured due to being opaque or having an uneven surface. Therefore, only the measurable RI's are shown in Figure 117, the exact values are reported in the experimental section 6.2.6.4. The metal-free polymer shows a RI of 1.583. The cured OE-6630 has a lower RI of 1.552 because of the lower phenyl content. A comparable polysiloxane by Kim *et al.* showed a RI of 1.578 when using slightly different monomers.[138] They used vinyltrimethoxysilane instead of vinylphenyldiethoxysilane and no methylphenyldimethoxysilane. This results in a value of 1.15 phenyl-groups per silicon and zirconium atom, while we have a value of 2.00. They reached 1.580 with 1.0 mol% Zr, 1.581 with 3.0 mol% Zr and 1.583 with 5.0 mol% Zr.
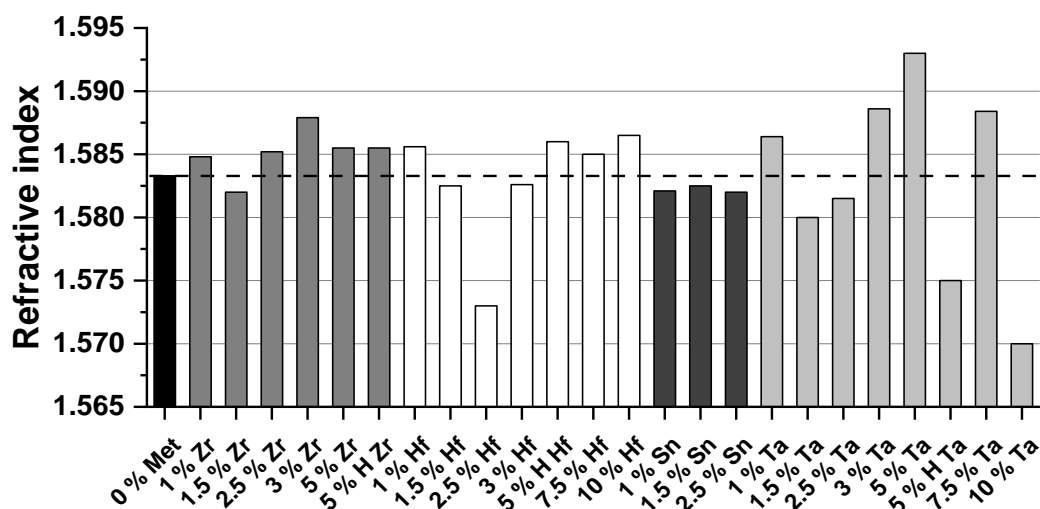
Figure 117: Refractive indices of the metal-free respectively metal containing and cured polysiloxanes.

The zirconium samples besides the 1.5 mol% one show an increased value compared to the metal-free sample, while the 5.0 mol% Zr sample shows the highest one. The higher zirconium content samples show an equally high RI than the 3.0 mol% one. These high metal-containing polysiloxanes still show some unreacted groups after the thermal treatment. The high amount of these tetra- or pentavalent atoms lead to a very hard polymer, which shows cracks or shatters when the glass slide is transported. This hardness results in a reduced mobility of the polymer and a higher degree of condensation. The samples, resulting from the metal- and vinyl-group containing sample cured with the metal-free hydride copolymer, namely 1.0 mol%, 5.0 mol% H, 7.5 mol% and 10.0 mol% hafnium samples have an equal RI which are higher than the one

of the metal-free polymer. No tendency can be seen because the 1.0 mol% Hf sample shows an equally high RI than the metal richer ones. The 2.5 mol% polysiloxane shows a very low value of 1.573. Only three tin containing samples with 1.0 mol%, 1.5 mol% and 2.5 mol% metal could be measured but all show low RI values around 1.582. The remaining samples show cracks or peel off from the glass. The tantalum samples with 1.0 mol%, 3.0 mol%, 5.0 mol% and 7.5 mol% show higher values than the metal-free containing ones. The 5.0 mol% one shows the highest value with 1.593. The other measurable samples show a decreasing RI with increasing metal content, which is most likely based on showing the lower degree of cross-linking and more remaining alkoxide-groups.

Overall, only half of the measurable polysiloxanes show an increase of the RI and it does not correlate with the metal content because of an incomplete polycondensation or cross-linking reaction. Although all measurable RI's are higher than the one of the OE-6630 with 1.552.

4.3.2.3 *Thermogravimetric analyses of the cured metal atom containing copolymers*

Thermogravimetric analyses from all synthesised cured polysiloxanes were record under oxygen up to 900 °C or nitrogen up to 800 °C with a switching step to oxygen and the measurement continued up to 900 °C (experimental section, Figures 327 – 334). The $T_{95\%}$ values (Table 24) of the metal-free polysiloxane are 338 °C under nitrogen atmosphere and 326 °C under oxygen atmosphere, which are lower than the reported 355 °C under air reported by Kim *et al.* because the self-prepared systems contain more methyl-groups instead of additional cross-linking ones provided by the usage of more hydride- and vinyl-groups.[138] The amount of phenyl-groups is slightly higher in the self-synthesised polymer. Most of the decomposition temperatures are comparable under nitrogen and oxygen atmosphere and therefore often the median is compared. The 1.0 mol% zirconium sample shows a higher decomposition temperature with 360 °C, the further increase of Zr content decreases the $T_{95\%}$ value down to 250 °C. Kim *et al.* reported a $T_{95\%}$ value increase by 5 °C for the 1.0 mol% Zr sample, further 7 °C for the 3.0 mol% one and another 5 °C for the 5.0 mol% one. The 1.0 mol% hafnium samples show a decomposition temperature of around 350 °C, a metal content from 1.5 mol% to 5.0 mol% reduces the temperature between 320 °C to 300 °C while a further hafnium increase lowers the $T_{95\%}$ to 260 °C. The 1.0 mol% tin sample shows a decomposition temperature of 329 °C under N_2 and 353 °C under O_2. The increase of tin to 2.5 mol% raises the temperature to around 365 °C under both atmospheres, where a further metal increase slightly lowers the value to 330 °C to 350 °C. The higher contents of 10.0 mol% or 15.0 mol% show lower values of around 320 °C. The P20_Sn7.5_PP40_PM32.5 sample shows a high decomposition temperature of 390 °C under

oxygen atmosphere. The 1.0 mol% tantalum sample has a $T_{95\%}$ value of 335 °C under nitrogen and 317 °C under oxygen atmosphere. The increase of Ta up to 5.0 mol% shows no change in these values. The 5.0 mol% Ta H and 10.0 mol% Ta sample have higher values with 365 °C under N_2 and 340 °C under O_2. The 7.5 mol% and 15.0 mol% sample show lower values of around 300 °C. Overall, the $T_{95\%}$ values decrease with increasing metal content because of the reduced degree of cross-linking relates to some unreacted groups which cannot react because the polymer hardens.[396, 463] The thermal resistance under both atmospheres often equals each other.

Table 24: $T_{95\%}$ values for the metal atom containing cured polysiloxanes under oxygen respectively nitrogen atmosphere.

Cured polymer P20_	$T_{95\%}$ N_2 [°C]	$T_{95\%}$ O_2 [°C]	Cured polymer P20_	$T_{95\%}$ N_2 [°C]	$T_{95\%}$ O_2 [°C]
Met0_PP40_PM40	338	326			
Zr1_PP40_PM39	359	358	Sn1_PP40_PM39	328	353
Zr1.5_PP40_PM38.5	323	318	Sn1.5_PP40_PM38.5	344	338
Zr2.5_PP40_PM37.5	303	302	Sn2.5_PP40_PM37.5	363	367
Zr3_PP40_PM37	325	312	Sn3_PP40_PM37	333	336
Zr5_PP40_PM35	291	279	Sn5_PP40_PM35	354	334
Zr5H_PP40_PM35	303	299	Sn5H_PP40_PM35	342	358
Zr7.5_PP40_PM32.5	297	282	Sn7.5_PP40_PM32.5	343	390
Zr10_PP40_PM30	265	268	Sn10_PP40_PM30	323	330
Zr15_PP40_PM25	249	247	Sn15_PP40_PM25	340	325
Hf1_PP40_PM39	353	343	Ta1_PP40_PM39	335	317
Hf1.5_PP40_PM38.5	316	307	Ta1.5_PP40_PM38.5	324	319
Hf2.5_PP40_PM37.5	310	320	Ta2.5_PP40_PM37.5	320	317
Hf3_PP40_PM37	314	312	Ta3_PP40_PM37	331	315
Hf5_PP40_PM35	308	301	Ta5_PP40_PM35	334	325
Hf5H_PP40_PM35	299	287	Ta5H_PP40_PM35	361	340
Hf7.5_PP40_PM32.5	283	280	Ta7.5_PP40_PM32.5	302	293
Hf10_PP40_PM30	267	259	Ta10_PP40_PM30	372	336
Hf15_PP40_PM25	266	271	Ta15_PP40_PM25	304	297

In some cases, like the 7.5 mol% tin sample, the stability is with 390 °C around 45 °C higher under oxygen than under nitrogen atmosphere. Other examples like in the 10.0 mol% tantalum sample the nitrogen value is with 372 °C around 35 °C higher. Especially the 1.0 mol% metal atom content polysiloxanes show higher $T_{95\%}$ values than the metal-free ones, which shows the huge impact of small amounts of metal. Some of the higher metal content polymers show higher values than P20_Met0_PP40_PM40 when a high amount of cross-linking was reached. The cured OE-6630 shows thermal degradation temperatures of around 425 °C which no self-synthesised polymer reached.

4.3.2.4 *Differential scanning calorimetry of the cured metal atom containing copolymers*

DSC curves from all cured and metal containing polysiloxanes were recorded (Figures 335 – 342). The T_g and T_m as well as the integrated energy are listed in Table 25. The metal-free polysiloxane shows a T_g of 11 °C and it should increase when adding metal atoms because of the provided cross-linking. The zirconium samples show a lower glass transition temperature between −23 °C and 1 °C but they barely relate to the Zr content. The 3.0 mol%, 5.0 mol% and 10.0 mol% samples show very low values around −20 °C while the others show a T_g around 0 °C. Here again the not completed sol-gel and hydrosilylation reactions lead to a wider network resulting in a lower T_g. The highly cross-linked ZPH3 (3.0 mol% Zr added to 100.0 mol% of silicon content) from Kim *et al.* shows a T_g of 26 °C because they used vinyltrimethoxysilane instead of vinylphenyldiethoxysilane.[138] The hafnium samples range from −13 °C to 3 °C and no clear tendency can be seen, although the spreading is smaller than for the Zr samples. The tin containing polysiloxanes range from −7 °C to 8 °C with the same result. The tantalum samples range from −8 °C to 38 °C where the P20_Ta5H_PP40_PM35 sample shows the highest T_g of 38 °C. The 10.0 mol% Ta and the 15.0 mol% Ta also show higher glass transition temperatures of 20 °C and 12 °C than the metal-free one, respectively. The OE-6630 shows a T_g of 5.5 °C, which is lower than the metal-free system because it contains more phenyl-groups and is in between the metal atom containing polymers. Overall, most of the metal atom containing samples show lower T_g values because of unreacted groups in the form of alkoxide, hydride or vinyl ones. The melting temperature of the metal-free polysiloxanes is 71 °C, the Zr samples range from 47 °C to 93 °C but P20_Zr1_PP40_PM39, which shows no melting temperature but a crystallisation temperature at −44 °C. The hafnium samples range from 48 °C to 100 °C, the tin ones from 42 °C to 76 °C and the tantalum ones from 74 °C to 108 °C. Overall, most of the T_m values are in the range from 60 °C to 90 °C but no clear tendency can be observed. The integrated energy ranges from around zero to 27 J/g.

Table 25: Glass transition (T$_g$) and melting temperatures (T$_m$) with the integrated energy (E$_m$) of the cured metal containing polysiloxanes.

Cured polysiloxane P20_	T$_g$ [°C]	T$_m$ [°C]	E$_m$ [J/g]	Cured polysiloxane P20_	T$_g$ [°C]	T$_m$ [°C]	E$_m$ [J/g]
Met0_PP40_PM40	11.3	70.8	1.59				
Zr1_PP40_PM39	−8.6	−43.8	−1.23	Sn1_PP40_PM39	4.7	−	−
Zr1.5_PP40_PM38.5	−1.0	46.9	0.05	Sn1.5_PP40_PM38.5	7.7	76.2	2.21
Zr2.5_PP40_PM37.5	−2.1	−	−	Sn2.5_PP40_PM37.5	−7.2	73.7	0.42
Zr3_PP40_PM37	−17.7	93.1	7.30	Sn3_PP40_PM37	7.2	60.4	1.08
Zr5_PP40_PM35	−22.6	87.3	7.25	Sn5_PP40_PM35	−7.1	70.3	0.11
Zr5H_PP40_PM35	−0.4	65.2	2.18	Sn5H_PP40_PM35	0.4	68.5	0.78
Zr7.5_PP40_PM32.5	1.2	71.1	6.26	Sn7.5_PP40_PM32.5	2.7	63.7	0.48
Zr10_PP40_PM30	−18.1	91.4	9.02	Sn10_PP40_PM30	4.8	43.4	3.49
Zr15_PP40_PM25	−2.9	74.1	7.17	Sn15_PP40_PM25	5.7	42.0	4.93
Hf1_PP40_PM39	0.6	80.9	2.40	Ta1_PP40_PM39	−7.9	74.1	0.36
Hf1.5_PP40_PM38.5	0.3	48.3	1.46	Ta1.5_PP40_PM38.5	−6.5	92.9	0.58
Hf2.5_PP40_PM37.5	2.6	77.5	5.02	Ta2.5_PP40_PM37.5	3.1	73.7	1.13
Hf3_PP40_PM37	−7.6	88.1	6.21	Ta3_PP40_PM37	−6.3	79.1	1.24
Hf5_PP40_PM35	−12.5	99.9	4.53	Ta5_PP40_PM35	1.0	73.9	2.18
Hf5H_PP40_PM35	−0.7	70.6	6.08	Ta5H_PP40_PM35	38.2	105.5	1.21
Hf7.5_PP40_PM32.5	1.3	76.1	9.09	Ta7.5_PP40_PM32.5	5.7	74.1	3.62
Hf10_PP40_PM30	−7.9	91.6	13.7	Ta10_PP40_PM30	20.2	107.7	10.2
Hf15_PP40_PM25	−4.6	85.7	26.6	Ta15_PP40_PM25	10.6	74.3	11.9

4.3.2.5 UV/Vis measurements of the cured metal atom containing copolymers

UV/Vis measurements from all the cured polysiloxane films were performed (Figures 343 – 350). Images of the cured polymers onto the microscope glass slides are visible in Figure 119 in the next chapter. The pictures show clear transparent colourless samples in most cases, the 15.0 mol% Hf sample shows a strong white colour which could relate to the formation of haf-nium oxide. Some tin samples are slightly yellow and the 10.0 mol% tantalum one shows cracks after the curing. The transmission at 450 nm as well as the yellowness and whiteness indices are reported in Table 26, the haze values at 450 nm are not reported but the calculated curves are shown in the experimental section. The transmission of the metal-free polysiloxane is

around 99 %, the zirconium samples show equal to values around 97 % to 99 % independently of the metal content. The hafnium polysiloxanes show the same transmission except the 15.0 mol% Hf sample, where only 54 % can be measured. The tin samples show lower values around 87 % to 98 % where the 3.0 mol% tin containing sample has the lowest value of 87 %.

Table 26: Transmission values at 450 nm (T$_{450}$), yellowness (YI) and whiteness indices (WI) of the cured metal containing polysiloxanes onto glass slides.

Cured polysiloxane P20_	T$_{450}$ [%]	YI	WI	Cured polysiloxane P20_	T$_{450}$ [%]	YI	WI
Met0_PP40_PM40	99	0.2	99.8				
Zr1_PP40_PM39	98	0.6	98.3	Sn1_PP40_PM39	95	2.1	92.2
Zr1.5_PP40_PM38.5	98	0.7	97.4	Sn1.5_PP40_PM38.5	89	7.0	78.0
Zr2.5_PP40_PM37.5	99	0.3	99.4	Sn2.5_PP40_PM37.5	98	0.8	97.4
Zr3_PP40_PM37	98	0.7	97.4	Sn3_PP40_PM37	87	7.8	73.9
Zr5_PP40_PM35	99	0.5	98.9	Sn5_PP40_PM35	98	0.7	97.7
Zr5H_PP40_PM35	98	0.7	98.3	Sn5H_PP40_PM35	90	6.2	80.3
Zr7.5_PP40_PM32.5	98	0.6	97.8	Sn7.5_PP40_PM32.5	93	4.2	86.9
Zr10_PP40_PM30	97	0.7	96.7	Sn10_PP40_PM30	95	1.6	93.9
Zr15_PP40_PM25	99	−0.3	99.9	Sn15_PP40_PM25	97	1.0	96.2
Hf1_PP40_PM39	97	0.7	97.6	Ta1_PP40_PM39	98	0.6	98.4
Hf1.5_PP40_PM38.5	98	0.6	98.0	Ta1.5_PP40_PM38.5	99	0.5	99.4
Hf2.5_PP40_PM37.5	98	1.2	96.6	Ta2.5_PP40_PM37.5	100	0.2	100
Hf3_PP40_PM37	99	0.6	98.9	Ta3_PP40_PM37	98	0.5	98.9
Hf5_PP40_PM35	98	−0.1	99.3	Ta5_PP40_PM35	98	0.5	98.5
Hf5H_PP40_PM35	99	0.5	99.3	Ta5H_PP40_PM35	99	0.5	99.5
Hf7.5_PP40_PM32.5	98	0.7	98.2	Ta7.5_PP40_PM32.5	98	0.6	98.3
Hf10_PP40_PM30	97	0.3	97.0	Ta10_PP40_PM30	91	1.1	90.5
Hf15_PP40_PM25	54	2.6	49.5	Ta15_PP40_PM25	98	−0.1	98.9

The tantalum ones range from 97 % to 100 % except the 10.0 mol% Ta containing sample which has 91 % transmission. Kim *et al.* reported 90 % transmission for their 1.0 mol% Zr polysiloxane and 80 % transmission at 5.0 mol% Zr for their 2 mm thick sample.[138] Interestingly their measurement of the OE-6630 material only shows an 85 % transmittance. Besides the

15.0 mol% Hf sample all other show a good to very good transmittance in the range of 87 % to 100 %.

The yellowness and whiteness indices also were calculated, the YI of the metal-free polysiloxane is 0.2 and the WI is close to 99.8, which shows that the polysiloxane is colourless. The zirconium samples show slightly higher YI values and slightly lower WI values up to 0.7 respectively down to 96.7 which represents a minimally yellow colour. The 15.0 mol% Zr containing polysiloxane shows a negative YI value of −0.3 and a WI of around 100, which indicates a minimally bluish colour. Most of the hafnium samples range from −0.1 to 0.7 Yi and 96.5 to 99.3 WI and show a minimally yellow colour. The 2.5 mol% Hf containing sample has a higher YI of 1.2 indicating a slightly yellow colour. The 15.0 mol% Hf containing sample shows a stronger yellow colour with a YI of 2.5 and a WI of 49.5. Most of the tin containing polysiloxanes show a stronger yellow colour, yellowness indices of up to 7.8 and whiteness indices down to 73.9. The colourless to minimally yellow tantalum samples range from −0.1 to 0.6 YI and 98.3 to 100 WI except the 10.0 mol% Ta sample with a YI of 1.1 and a WI of 90.5, which indicates a slightly yellow colour.

Overall, except for four samples all others reached respectively surpassed 95 % transmission at 450 nm. Most of the samples show no to a marginally yellow colouration after the curing, which is shown by YI of zero to two respectively WI close to 100. Only four tin containing samples with 1.5 mol%, 3.0 mol%, 5.0 mol% H and the 7.5 mol% one have larger values indicating a slight yellow colour. The commercial OE-6630 system shows a transmission of 100 % with a YI of 0.1 and a WI of 100.8, which indicates that no yellow colouration occurred.

4.3.2.6 Thermal aging of the cured metal atom containing copolymers

A thermal aging at 180 °C for 70 days (1680 h) of the polysiloxanes onto glass slides was performed to simulate the heat exposure during the LED operation. Pictures from all samples were recorded before and after the thermal treatment (Figures 118 – 122). The metal-free polysiloxane shows no difference before and after the treatment like most of the metal containing ones. The 7.5 mol% and 15.0 mol% zirconium samples show cracks and shatters after the treatment, all other Zr samples do not show a difference. The hafnium containing polysiloxanes Hf5H and Hf7.5 also shatters and cracks.
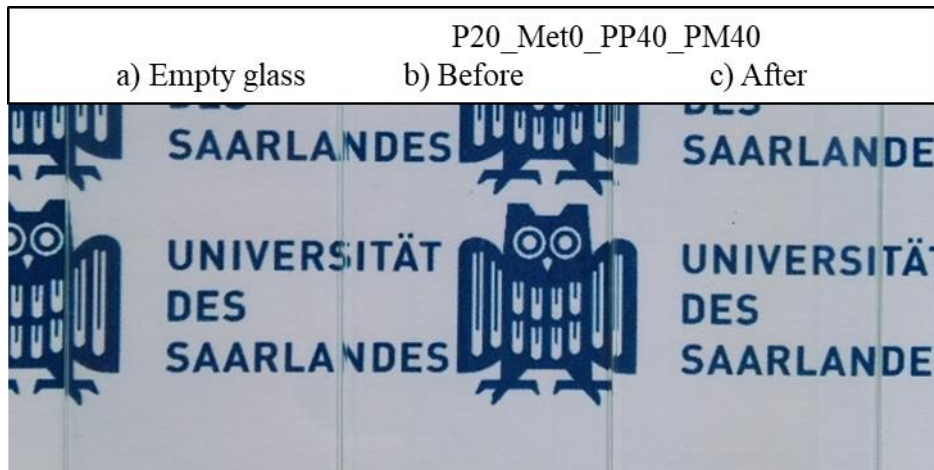
Figure 118: a) empty glass slide, P20_Met0_PP40_PM40 b) before and c) after the thermal treatment.
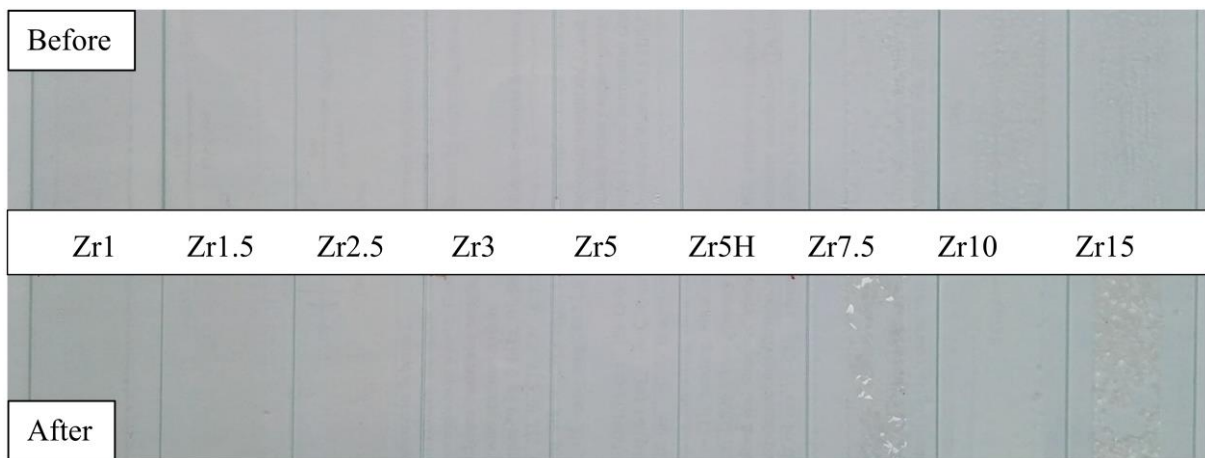
Figure 119: Pictures of the zirconium containing polysiloxane films (P20_ZrX_PP40_PM(40-X)) onto glass slides, before and after the thermal treatment.
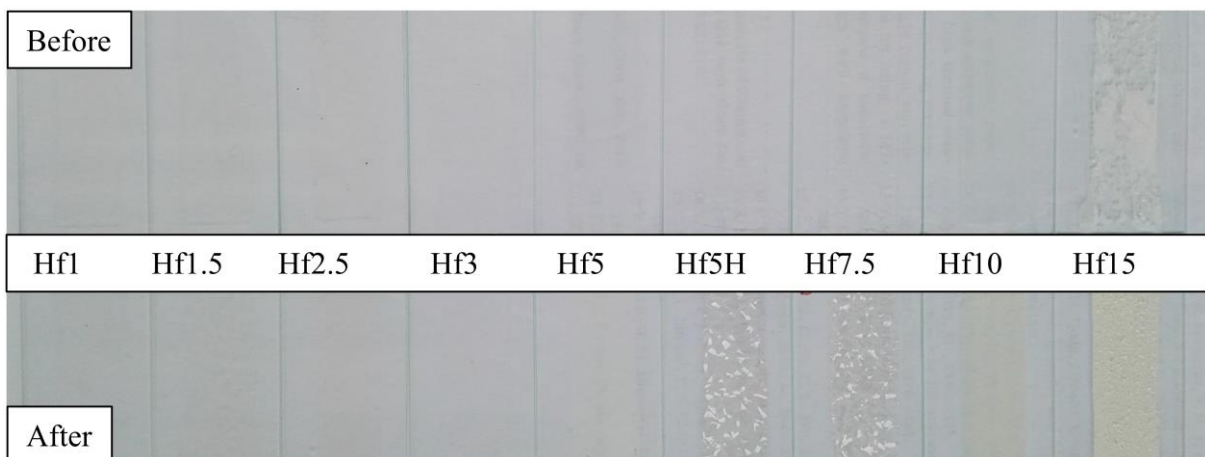
Figure 120: Pictures of the hafnium containing polysiloxane films (P20_HfX_PP40_PM(40-X)) onto glass slides, before and after the thermal treatment.
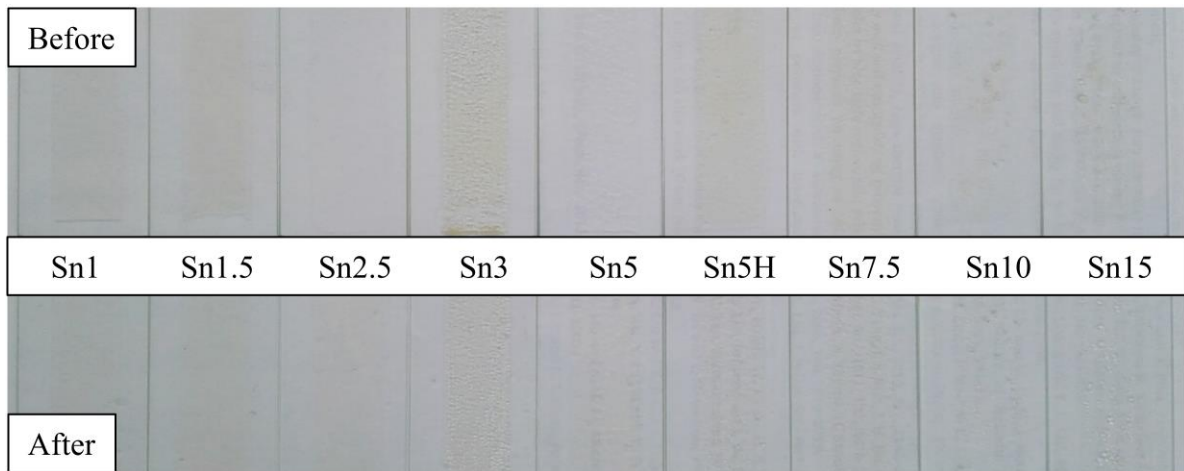
Figure 121: Pictures of the tin containing polysiloxane films (P20_SnX_PP40_PM(40-X)) onto glass slides, before and after the thermal treatment.
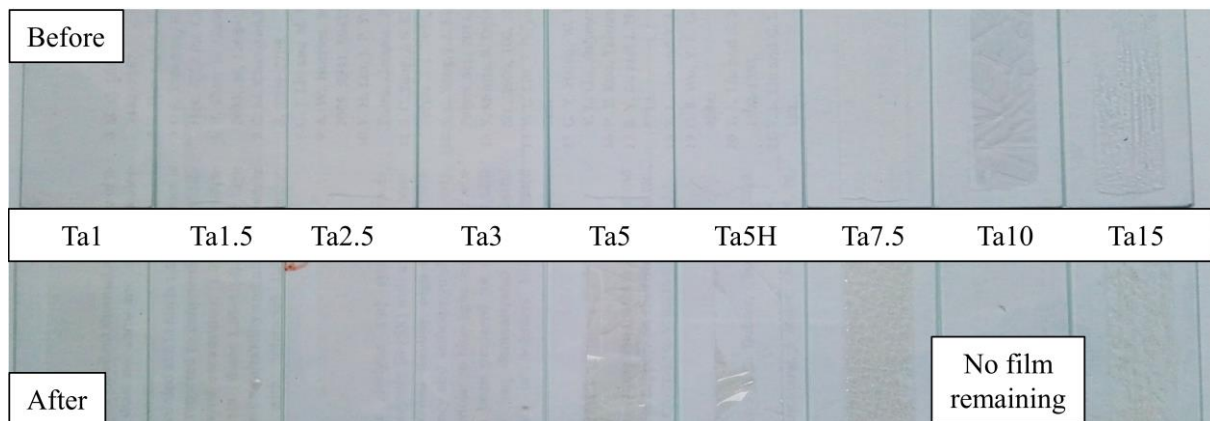
Figure 122: Pictures of the tantalum containing polysiloxane films (P20_TaX_PP40_PM(40-X)) onto glass slides, before and after the thermal treatment.

The 10.0 mol% and 15.0 mol% Hf samples show a strong white to yellow colouration. Some tin samples still show the yellow colouration which was slightly reduced during the treatment. The Ta5 and Ta5H shattered and peeled off during the treatment, the Ta10 sample peeled off completely before the measurement for the third day. The Ta7.5 and Ta15 probe showed a yellow colouration. To evaluate the change in transmission and haze, UV/Vis measurements were performed during the thermal treatment and the transmissions at 450 nm are shown in Figure 123, the haze curves in Figures 351 – 354. The curve of the metal-free polysiloxane (black) is visible in all graphs for better comparability.

The exact values are reported in Table 27. The transmission of the metal-free polysiloxane does not change during the thermal treatment. The transmission of the zirconium samples slightly increases but is in the error range of the measurement. The thermal treatment leads to shattering of the polysiloxanes because the sol-gel reaction continues, the polymers harden and shrink resulting them peeling off the glass. The Zr7.5 and Zr15 ones show lower values of 95 %. The

transmission of the polysiloxanes with 1.0 mol% to 3.0 mol% hafnium content does not change, but the 5.0 mol% to 10.0 mol% Hf ones show a lower transmission with increasing metal content down from 95 % for the 5.0 mol% Hf one to 68 % for the 10.0 mol% Hf one. The 15.0 mol% Hf sample showed an initial transmission of 54 % which is reduced to 32 % after the 70 days. Most of the tin containing polysiloxanes show a small increase in transmission up to 5 %, the Sn5H sample shows an increase of 9 %, which is caused by the shattering and removal of the polymer. The tantalum containing polysiloxanes show a slight increase which is in the error range of the measurement, except the 5.0 mol% sample, which shows a 6 % lower transmission. P20_Ta10_PP40_PM30 could not be measured because no polymer was left on the glass.
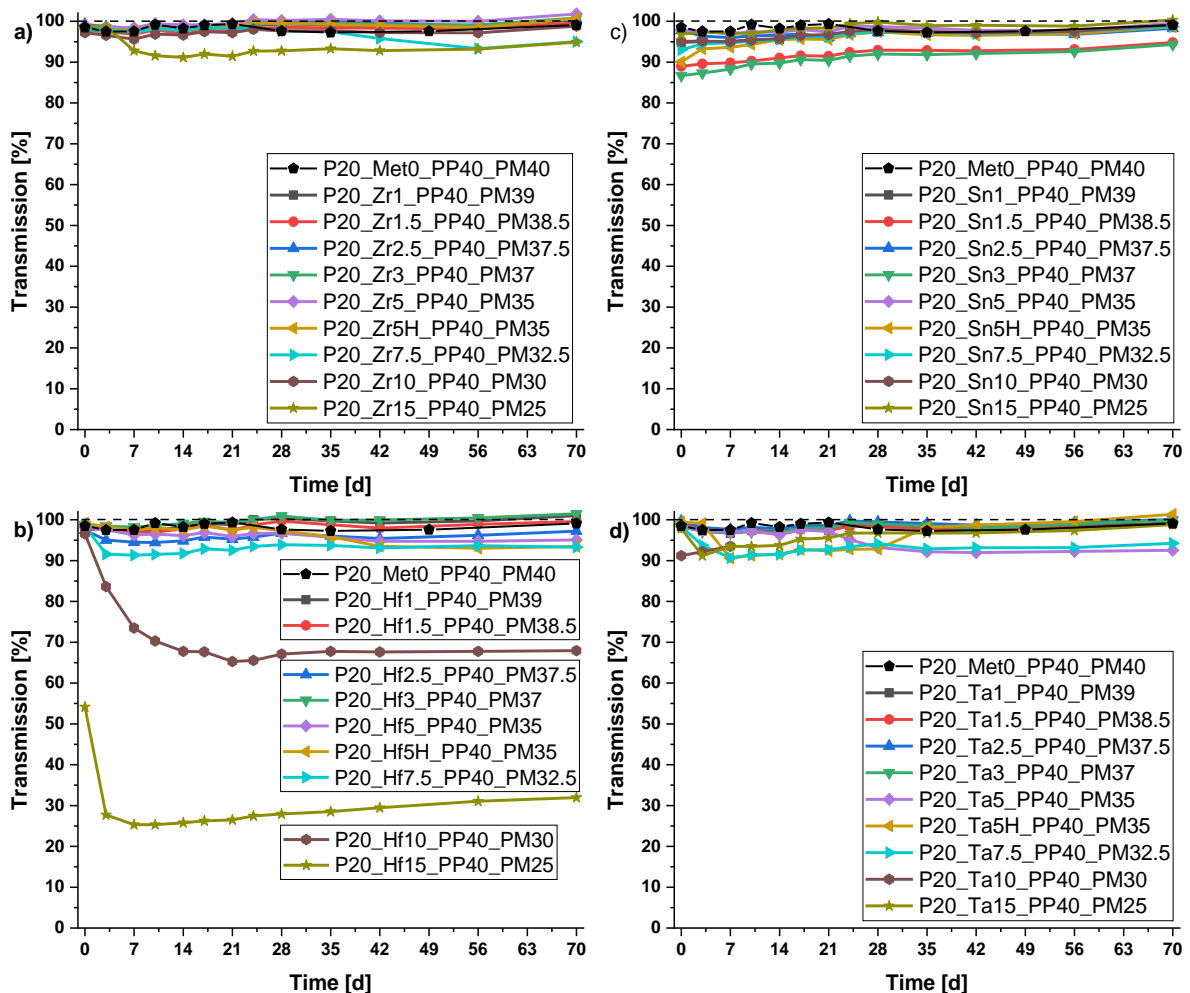
Figure 123: Transmission at 450 nm of the cured metal-free and metal containing polysiloxanes onto glass slides during the 70 days thermal treatment, a) zirconium, b) hafnium, c) tin, and d) tantalum.

The calculated haze curves at 450 nm are shown in the experimental section (6.2.6.5.5). Most of the haze values are under 10 %. Exceptions are the 10.0 mol% zirconium containing sample which shows a haze of 60 % after the thermal treatment started. Also, the 15 .0 mol% one started at 54 % haze, the value increased to 70 % after three days and then is successively reduced to

60 % after the 70 days. The 5.0 mol% hafnium containing polysiloxane shows a 75 % haze and the 10.0 mol% Hf one a 90 % haze after the experiment. The 15.0 mol% Hf one has an initial 95 % haze which is reduced to 80 % after the treatment. The tin samples show overall higher values between 10 % and 30 % haze increasing with higher metal content. The 15.0 mol% tantalum containing polysiloxane shows a 50 % haze at the beginning which is reduced to 20 % during the treatment.

Table 27: Transmission values at 450 nm (T$_{450}$), yellowness (YI) and whiteness indices (WI) of the cured metal containing polysiloxanes onto glass slides after the thermal treatment at 180 °C for 70 days.

Cured polysiloxane P20_	T$_{450}$ [%]	YI	WI	Cured polysiloxane P20_	T$_{450}$ [%]	YI	WI
Met0_PP40_PM40	99	2.1	94.4				
Zr1_PP40_PM39	100	0.7	99.0	Sn1_PP40_PM39	99	1.1	96.5
Zr1.5_PP40_PM38.5	100	1.0	97.8	Sn1.5_PP40_PM38.5	95	4.1	87.4
Zr2.5_PP40_PM37.5	101	1.0	98.7	Sn2.5_PP40_PM37.5	98	2.2	94.0
Zr3_PP40_PM37	101	0.2	100.1	Sn3_PP40_PM37	94	3.8	87.4
Zr5_PP40_PM35	102	0.1	101.1	Sn5_PP40_PM35	100	1.8	95.8
Zr5H_PP40_PM35	101	0.6	98.7	Sn5H_PP40_PM35	99	1.8	95.0
Zr7.5_PP40_PM32.5	95	0.9	92.5	Sn7.5_PP40_PM32.5	99	1.6	95.9
Zr10_PP40_PM30	99	0.3	97.7	Sn10_PP40_PM30	99	0.4	98.2
Zr15_PP40_PM25	95	1.3	91.9	Sn15_PP40_PM25	100	0.2	99.7
Hf1_PP40_PM39	101	0.1	100.6	Ta1_PP40_PM39	99	1.1	97.5
Hf1.5_PP40_PM38.5	100	1.0	97.6	Ta1.5_PP40_PM38.5	99	1.9	95.5
Hf2.5_PP40_PM37.5	97	2.3	93.2	Ta2.5_PP40_PM37.5	100	1.2	97.9
Hf3_PP40_PM37	101	0.2	100.9	Ta3_PP40_PM37	100	0.9	98.0
Hf5_PP40_PM35	95	2.4	91.2	Ta5_PP40_PM35	92.5	1.9	89.4
Hf5H_PP40_PM35	94	1.6	90.6	Ta5H_PP40_PM35	101	−0.1	101.7
Hf7.5_PP40_PM32.5	93	1.5	91.9	Ta7.5_PP40_PM32.5	94.2	1.7	91.1
Hf10_PP40_PM30	68	5.5	57.9	Ta10_PP40_PM30	−	−	−
Hf15_PP40_PM25	32	14.7	−0.3	Ta15_PP40_PM25	98.8	1.1	97.5

The yellowness and whiteness indices were also calculated. The metal-free P20_Met0_PP40_PM40 shows a slight yellow colouration with a YI of 2.1 and a WI of 94.4.

The zirconium samples show a small change in the YI and WI values to a slightly more yellow colour. The Zr15 polysiloxane showed the strongest yellow colour and colour change of Δ1.6 YI and Δ8.0 WI. The hafnium samples show slightly higher YI and lower WI values in most cases showing yellow colourations. The strongest colourations show the Hf10 polysiloxane with an increased YI by 5.2 and a reduced WI by 39.1 and the Hf15 one with an increased YI by 12.1 and a reduced WI by 49.8. The tin samples which showed a slightly yellow colour indicated by a YI over 1.6 show no significant difference in the YI and WI. Samples which were minimally yellow with a YI under one slightly increased the yellow colour. The tantalum containing polysiloxanes change slightly except the Ta5 one which shows an increased YI by 1.4 and a reduced WI by 5.5.

Overall, the transmission of over 90 % can be remained for nearly all samples during the 70 days heat treatment. The yellow colouration is small but observable. Interestingly, some tin samples show a reduced yellow colour after the treatment. Kim *et al.* reported a transmission of 89 % for their 3.0 mol% Zr containing polysiloxane after the synthesis where the self-prepared system showed a 98 % transmission.[138] After their thermal aging test for 1008 h at 85°C and 85 % rel. humidity, their transmission remained at around 89 % and ours at 100 % after the thermal treatment.[138] They reported a ΔYI of 8.1 for their 3.0 mol% Zr containing 2 mm thick sample where the self-prepared system has a ΔYI of −0.5 taken in mind it is only 50 µm to 60 µm thick.[138]

4.3.3   Conclusion of the cured metal atom containing copolymers

Various hydride and vinyl copolymers with 1.0 mol% to 15.0 mol% metal content were syn-
thesised in a basic to acidic sol-gel reaction (Figure 124). Four different metals were used,
zirconium, hafnium, tin, and tantalum.
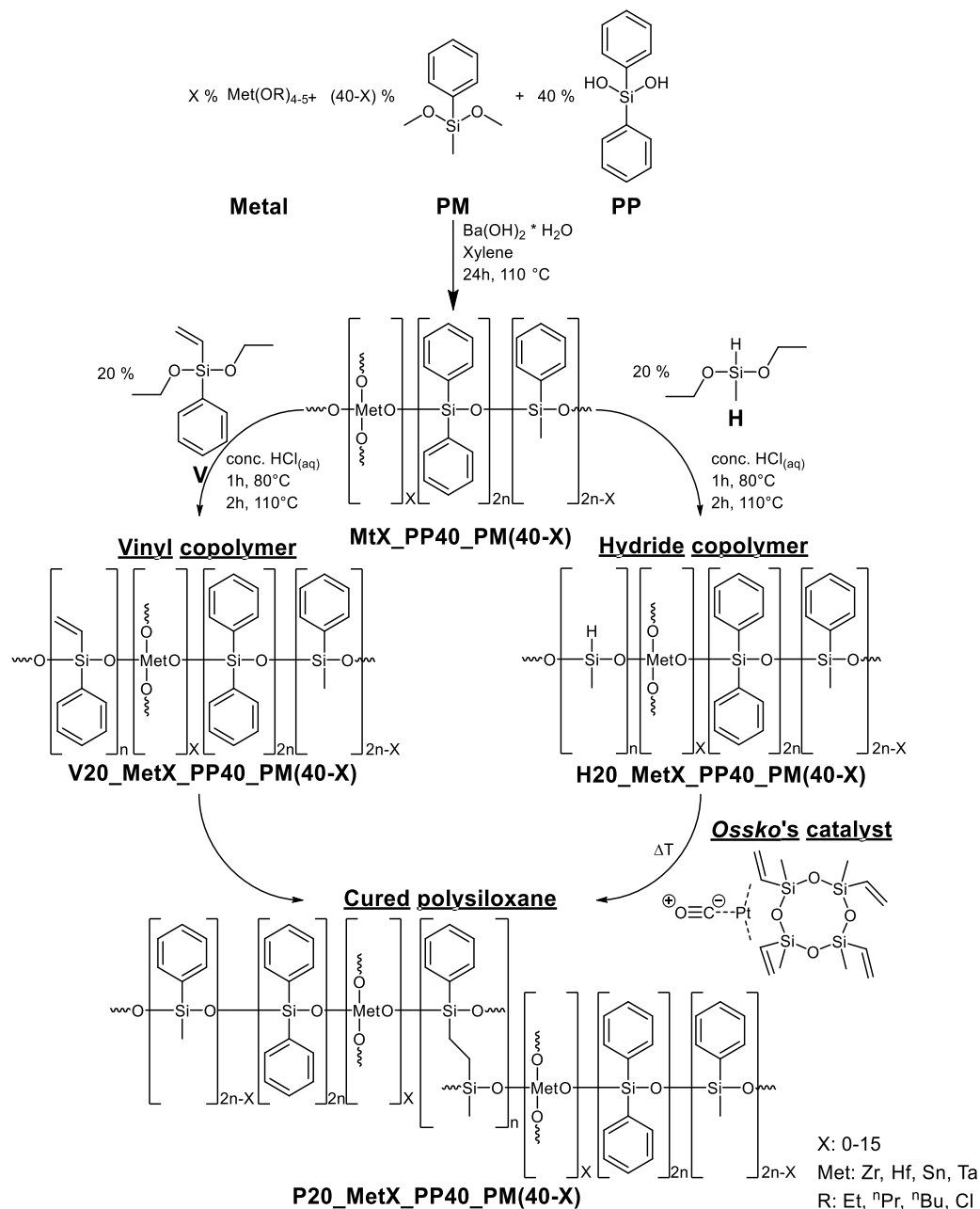
Figure 124: Overview of the synthesis for metal atom containing polysiloxanes.

The increase of the metal content should increase the refractive index, the thermal stability as
well as the glass transition temperature. In comparison with the metal-free copolymers
V20_Met0_PP40_PM40 with a RI of 1.573 and H20_Met0_PP40_PM40 with a RI of 1.563,
most of the vinyl and metal containing copolymers showed a lower RI. Although
V20_Sn3_PP40_PM37 showed the highest RI with 1.581. The hydride and metal containing
polymers showed better results, H20_Ta15_PP40_PM25 has the highest RI with 1.582, but

only a small increase could be determined for around half of the copolymers. The $T_{95\%}$ values under both atmospheres of the hydride copolymers with small metal amounts is higher than the samples of the metal-free copolymer, which shows the effect of additional cross-linking provided by the tetra- or pentavalent atoms. The vinyl and metal atom containing copolymers show lower or equal temperatures than the metal-free ones. The glass transition temperatures of the hydride copolymers with a high amount of metal content are higher than the one of the reference material, but the vinyl and metal atom containing copolymers all show lower values. The reason for the lower thermal stability despite having metal atoms is the incomplete polycondensation reaction. In the NMR and FT-IR spectra some remaining alkoxide-groups as well as solvents are visible.

With these copolymers, nine different solid polysiloxanes for each metal atom were synthesised using *Ossko*'s catalyst. The refractive indices of the 1.0 mol% and from 5.0 mol% to 10.0 mol% metal content are higher than the metal-free P20_Met0_PP40_PM40 with 1.583. All 15.0 mol% samples could not be measured because they are opaque or have an uneven surface. The thermal stability is higher for lower metal content polysiloxanes than the reference with 330 °C, but decreases with increasing metal content for the zirconium, hafnium, and tantalum samples. The tin ones have overall higher $T_{95\%}$ values than the reference but no trend can be observed when the metal content is increased. A transmission of over 97 % for nearly all metal containing polysiloxanes could be achieved after the synthesis. The yellowness and whiteness indices show colourless samples. The very high transmission and the colourlessness could even be maintained over 70 days under 180 °C for most of them. Some samples, especially with higher metal content, show cracks which can even lead to a detaching of the material because the high temperature continues the cross-linking and the sol-gel reaction to form a very solid and brittle material.

Overall, the incomplete condensation reactions lead to the problems with only equal or slightly better properties than the metal-free polysiloxane. The amount of remaining alkoxide-groups increase with the metal content, therefore the 1.0 mol% metal polysiloxanes often show the best values. The polymerisation process has still to be optimised. Also, even the 15.0 mol% samples only show a small increase in the refractive index and the thermal stability which increase was the main goal when introducing metal atoms inside the polymer chain.

4.3.4 Further investigations with 20.0 mol% metal content

The metal content still has to be increased to increase the thermal stability and the RI. Therefore copolymers with 20.0 mol% zirconium or hafnium were synthesised using a different monomer composition (Figure 125). To solve the problem with the incomplete polycondensation reaction, two of the four bonds from the metal atom were blocked for the sol-gel reaction by introducing acetylacetone (acac) as a metal ligand.[377] The bidentate character of the ligand leads to stable complexes[464-467] with a high stability constant $\log(\beta)$ of 11.25 ± 0.10 for $Zr(acac)_4$[464] showing that the chelate complex is very stable. Chananašvili *et al.* reported the synthesis of poly[diphenyl-*co*-titaniumdiacetylacetonate]siloxane in 1984 with the downside of it being very hard and having an orange colour due to the metal complex.[468] A coloured polysiloxane is generally not a problem, as long as the colour coordinates remain unchanged during the LED operation. Therefore, some experiments with acetylacetone were performed. The syntheses were performed similarly to the other metal content copolymer reactions. 50.0 mol% of methyldiethoxysilane respectively vinyltrimethoxysilane were used with 30.0 mol% of diphenylsilanediol. The 20.0 mol% metal content were introduced using zirconium tetra-*n*-propoxid or hafnium tetra-*n*-butoxid which were stirred with two equivalents of acetylacetone at room temperature before adding the silicone containing monomers.
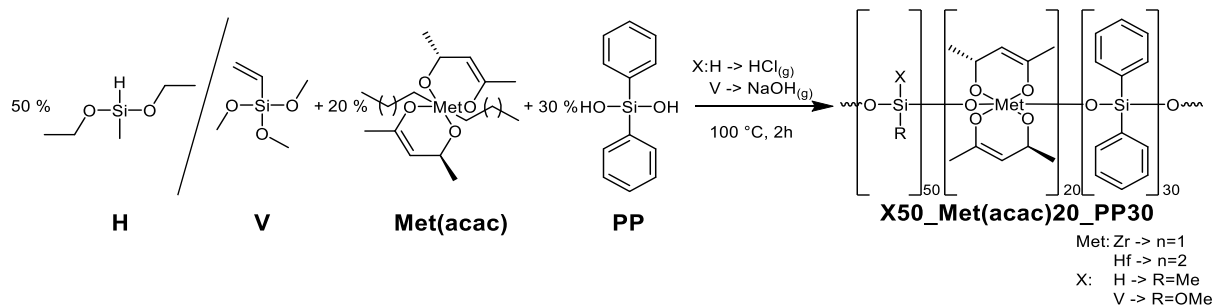
Figure 125: Reaction scheme for the acetylacetone complexed metal atom containing copolymers.

The zirconium and hafnium copolymers show colours from bright yellow over orange to light red because of the complex formation (Figure 126). The viscosity is too high for processing, the copolymers are solid at room temperature and start melting at 50 °C. The NMR analyses are overall very difficult because the baseline is uneven, but the methyl- and phenyl-groups can be assigned in the ^{1}H NMR. Despite using high amounts of copolymer, no clear signal can be observed in the ^{29}Si NMR.
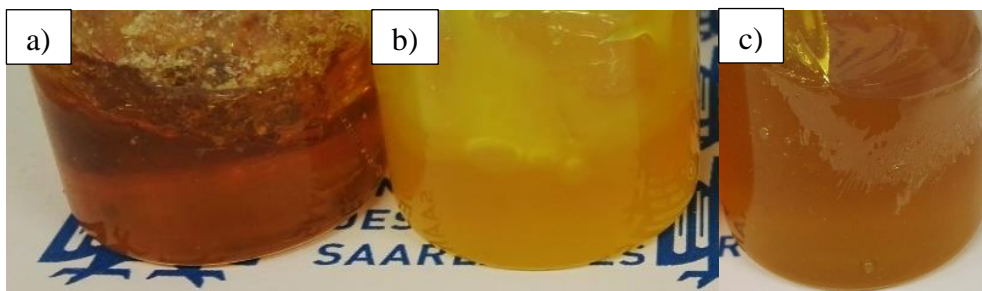
Figure 126: Pictures of a) V50_Zr(acac)20_PP30, b) H50_Zr(acac)20_PP30 and c) H50_Hf(acac)20_PP30.

The two polymers V50_Zr(acac)20_PP30 and H50_Zr(acac)20_PP30 were mixed in a 1:1 ratio, because of their high brittleness and viscosity 1.5 mL of chloroform have to be added. *Osskos*'s catalyst was added under gentle heating. The doctor bladed samples obtained after four hours at 150 °C were very brittle, vesicular, yellow and splintered (Figure 127). The degree of cross-linking is far too high for applications as coatings. The transparency is very low in both thin and thicker films.
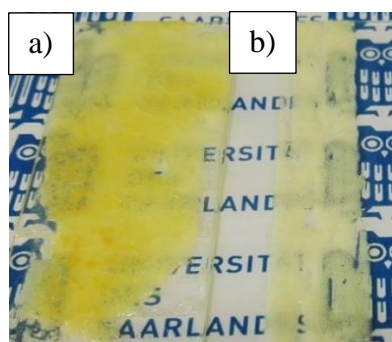
Figure 127: Picture of a) a thick film (2 mm) and b) a thin film (60 μm) of the cured P50_Zr(acac)20_PP30.

Overall, the first experimental results show no satisfying copolymer synthesis, the material is very hard which results in a brittleness and shows a very low transmission because it is opaque. The cured film has the same issues and the surface is uneven. Therefore, no further investigations were made.

4.4 Kinetics study - Polymerisation of hydride- and vinyl-group containing polymethylphenylsiloxanes

A detailed polymerisation study was performed for hydride- or vinyl-group containing poly-methylphenylsiloxanes to investigate the polymer length depending on the polymerisation process. Different temperatures, reaction times and catalysts were previously investigated in our research group[223-225, 303] and in other-groups.[6, 136, 138, 234-235, 317, 319, 469] The knowledge received by these experiments will be used to synthesise new polysiloxanes with modified side-groups. Therefore, a hydride- and a vinyl-group containing polymer were chosen as model systems with both methyl- and phenyl-groups. Like in previous polymerisations 20 mol% of the cross-linking monomers methyldiethoxysilane or vinylphenyldiethoxysilane were used together with 40 mol% of methylphenyldimethoxysilane and diphenylsilanediol. This results in polymers of the composition of H20_PP40_PM40 and V20_PP40_PM40. Although they consist of the same monomers as H20_Met0_PP40_PM40 and V20_Met0_PP40_PM40 they are named differently, because of the different catalysts and reaction conditions. The choice of catalysts was based on Mosley *et al.*[136] Liquid chemicals were used for both polymerisations because of the high miscibility. The hydride polymerisation is performed with hydrochloric acid as catalyst. For the basic vinyl polymerisation tetra-*n*-butylammonium hydroxide was as described in literature.[136] The synthesis was performed in a glass flask with a distillation head on top of it to collect the solvents. The temperature was raised to 85 °C for one hour, afterwards it was increased to 115 °C for four to five hours. Every 30 minutes a sample was taken, purified, and analysed by FT-IR, ^{1}H NMR and SEC. For the hydride polymer (Figure 128), methyldiethoxysilane, methylphenyldimethoxysilane and diphenylsilanediol were used. The vinyl polymer was synthesised using vinylphenyldiethoxysilane, methylphenyldimethoxysilane and diphenylsilanediol.
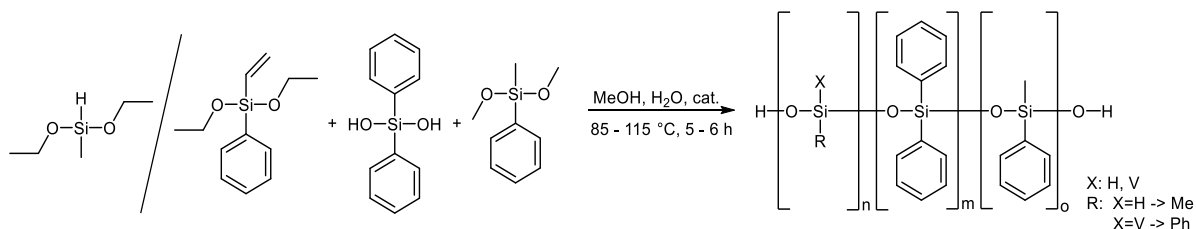
Figure 128: General polymerisation procedure for the hydride respectively vinyl polysiloxane X20_PP40_PM40.

For calculation of the molecular mass by ^{1}H NMR like *tert*-butyldimethylchlorosilane[221, 470] (Figure 129) was used, which was reacted with the silanol end groups after the polycondensation polymerisation.[220] Triethylamine leads to a selective reaction between the Si-OH and Si-Cl

group.[219] The possible side reaction would be a homocondensation of two silanol terminated polysiloxanes under water elimination, which is not observed in this case.[471]
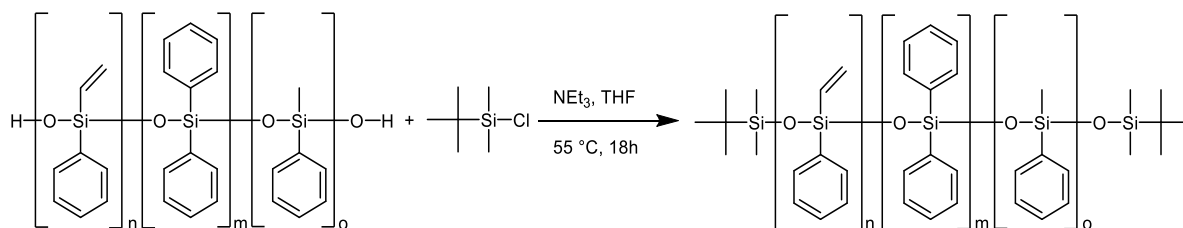
Figure 129: Exemplary reaction for the end group capping of V20_PP40_PM40.

4.4.1 Synthesis and characterisation of hydride-containing polysiloxanes for the kinetics study

The three monomers: methyldiethoxysilane, methylphenyldimethoxysilane and diphenyl-silanediol as well as concentrated hydrochloric acid as catalyst were mixed and heated according to the following temperature profile (Figure 130) to receive H20_PP40_PM40. The isothermal step at 85 °C for one hour was applied for a hydrolysis of the reactants without removing them by distillation because of their low boiling point (methyldiethoxysilane: 94 - 95 °C).[419] However, this temperature is high enough to remove methanol (T_b = 64.7 °C).[419] The isothermal step at 115 °C allows the polymerisation of the precursors. In a first step the polymerisation was carried out with a distillation head for one hour. Afterwards the distillation head was removed to facilitate the removal of methanol, ethanol, and water. A sample was taken and purified every 30 minutes and analysed by FT-IR. For the SEC measurements the sample was dissolved in THF and for the ^{1}H NMR the described reaction was performed, followed by the measurement.
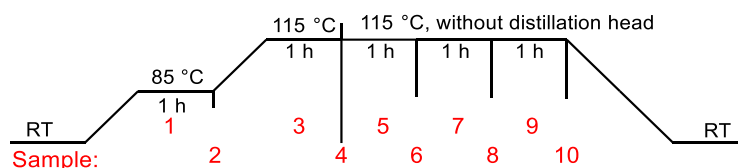
Figure 130: Temperature profile and nomenclature of the samples for the hydride polymerisation.

4.4.1.1 FT-IR-spectra of the kinetics study

The FT-IR spectra of the samples (Figure 131) differ only slightly. The increase in the Si-O band between 950 cm^{-1} and 1150 cm^{-1} is very difficult to differentiate.[472] For this reason, Figure 132 shows both the samples after 30 minutes and five hours and those of the three monomers. In the diphenylsilanediol spectra (PP), the OH vibrations[357] at 2900 – 3400 cm^{-1} as well as the C-H$_{Ar}$[357] ones at 2900 – 3100 cm^{-1} and Si-O vibrations[357] at 960 cm^{-1} and 1130 cm^{-1} can be observed. In the spectra of methylphenyldimethoxysilane (PM), especially the C-H and Si-CH$_3$ vibrations at 3000 cm^{-1} and 1250 cm^{-1} are detected.[217, 357] The Si-O-C vibration at 1190 cm^{-1} indicates the condensation of the polymers when the band decreases respectively vanishes.[347, 424] In the spectrum of methyldiethoxysilane (H)[347] the bands for the Si-H groups (dark grey) at 2158 cm^{-1} and 2119 cm^{-1}, at 950 cm^{-1} and at 880 cm^{-1} [347, 424, 473] are observable in addition to the C-H and Si-CH$_3$ vibrations. The Si-O-CH$_2$-CH$_3$ band at 2974 cm^{-1} is also characteristic for this compound.[347, 424] The polymers only show a little difference in their IR spectra between the 30-minute and the five-hour sample. The heights of the signals in the range of 980 cm^{-1} to 1130 cm^{-1} changed, but they can neither be precisely assigned nor integrated. A measure for the polymerisation progress is the area of the alkoxy band at 1186 cm^{-1} for the methoxy and

1169 cm^{-1} for the ethoxy-groups, but these are already too small for integration even after 30 minutes because they are at the edge of the Si-O bands. A comparison of the relative heights shows a decrease from 0.2716 to 0.2066, which corresponds to a decrease of 24 %.
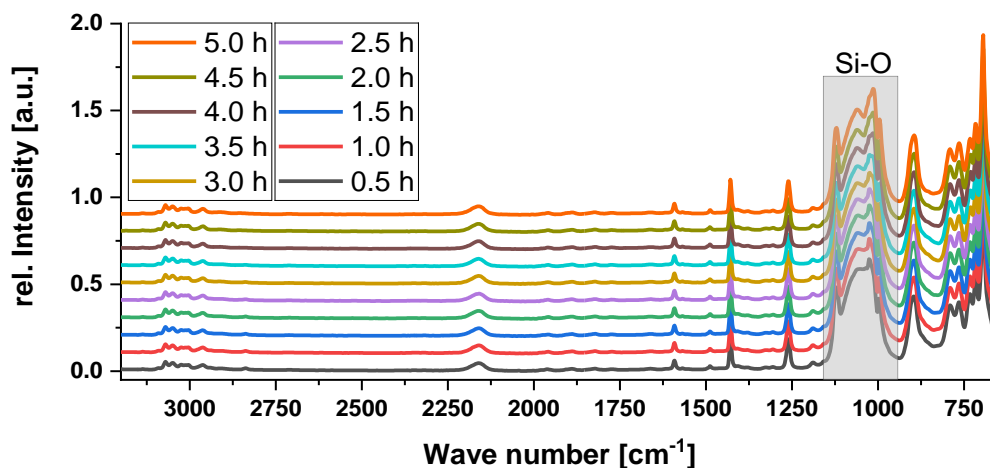
Figure 131: FT-IR spectra of the hydride polymerisation for the ten samples.
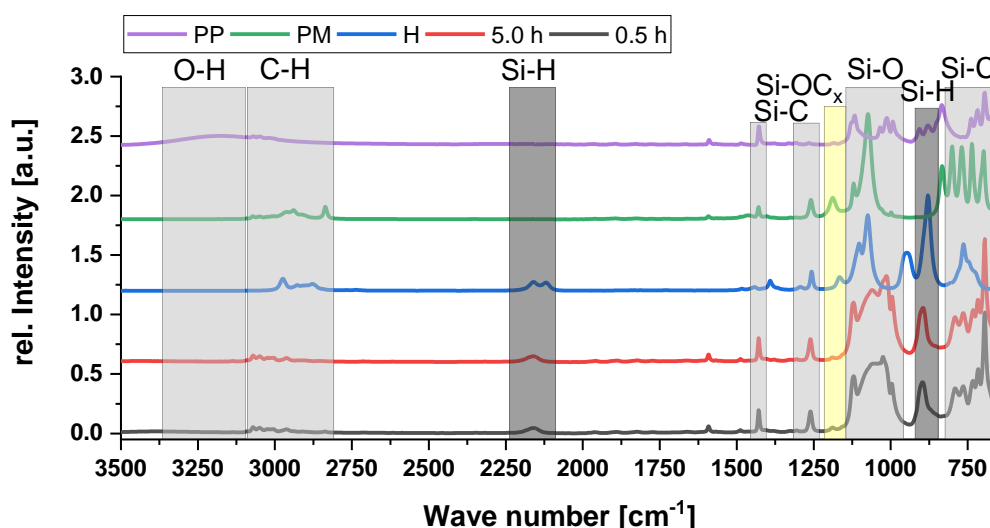
Figure 132: Comparison of the FT-IR spectra of the monomers and polymers after 0.5 h and 5.0 h.

4.4.1.2 NMR spectroscopy of the kinetics study

An overlay of the spectra for the ten samples after the synthesis before the end group reaction with *tert*-butyldimethylchlorosilane[221, 470] reveals the conversion of the monomers to the polymers (Figure 133). As expected the signals for the Si-Ph are between 7.0 ppm to 8.0 ppm,[236, 474-475] the Si-H groups at 5.4 ppm to 5.5 ppm,[236, 474-476] and the methyl-groups at −0.5 ppm to 1.5 ppm[236, 474-476] and they show only small variations from sample to sample. These can be attributed to the increasing chain length, which has an influence on the distinctness of the signals. In the range of alkoxy-groups between 3.0 ppm and 4.0 ppm, a clear decrease can be observed during the reaction. In this range, both the methoxy-groups (methanol: 3.5 ppm) and

ethoxy-groups (ethanol: 3.7 ppm) reveal signals. When integrating this range, an error is generated because a methoxy-group has three protons in this area and an ethoxy-group only two. The ethoxy-group still has a triplet at 1.25 ppm, which is difficult to integrate, but helps to reduce this error.
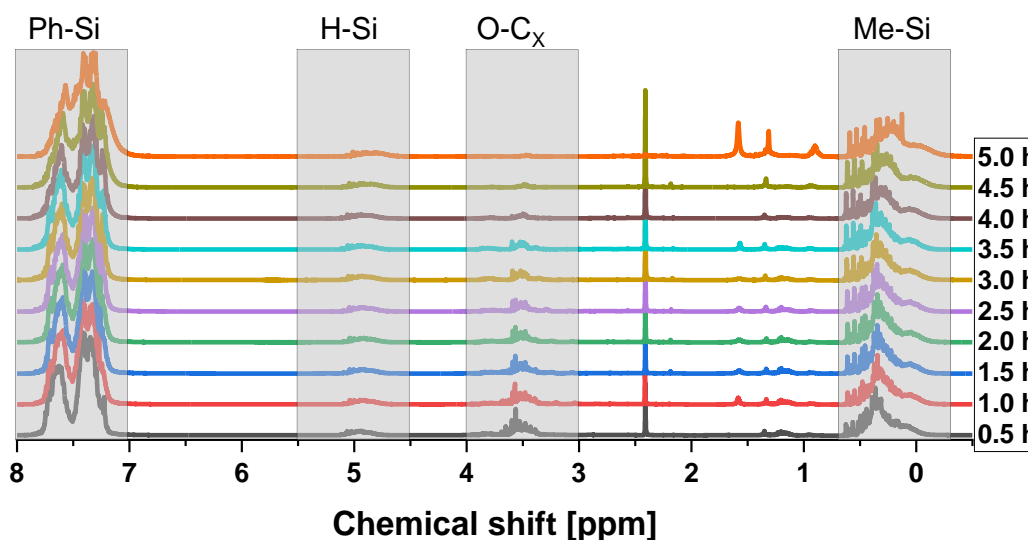
Figure 133: ^{1}H NMR spectra (400 MHz, CDCl₃) from each sample taken every 30 minutes.

The integration of the alkoxy-groups in the range of 3 ppm to 4 ppm can be plotted versus the time, resulting in a straight line (Figure 134) which corresponds to a reaction rate of 0th order.

Equation	y = a + b*x
Intersection	2.62509
Slope	-0.50002
Pearson R	-0.99382
R-Square(COD)	0.98767
Kor. R-Square	0.98613

● O-C$_x$ integration between 3.0 and 4.0 ppm
— linear Fit
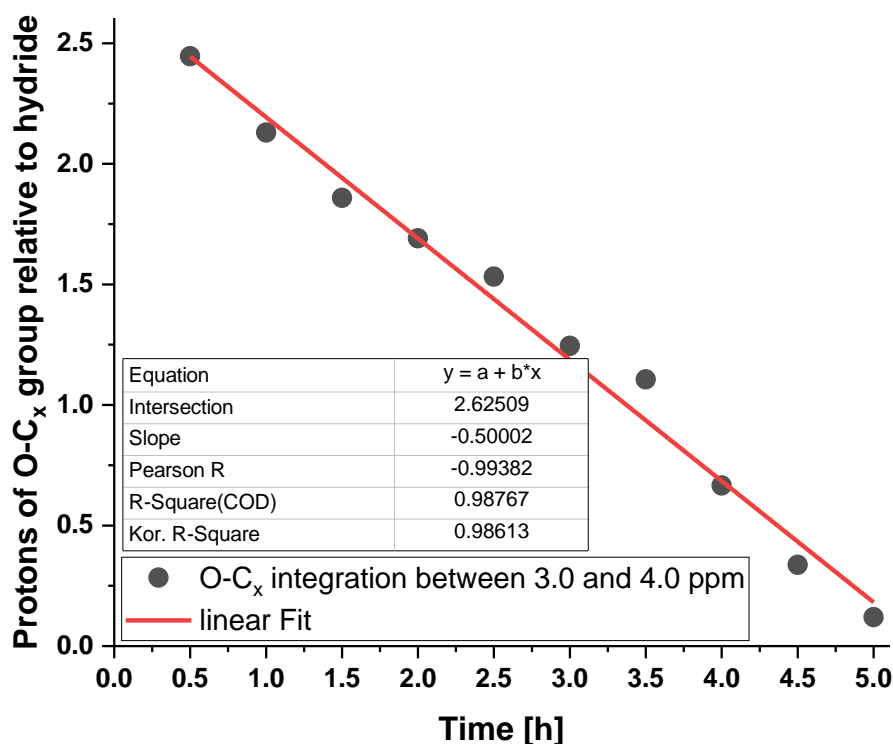
Figure 134: Integration of alkoxy-groups in the range of 3.0 ppm to 4.0 ppm over time which the correction of the ethoxy-groups via the CH₃ signal from the ethoxide at 1.0 ppm to 1.2 ppm.

This is concordant with the literature reported by Matějka *et al.*[477] and Torry *et al.*[478] for acidic polycondensation reactions.[472] By extrapolation, complete conversion can be achieved after around 5.5 hours. The theoretical starting value of the integration for the Si-H group are 16 protons. This cannot be observed because the hydrolysis and condensation within the first 30 minutes are very fast. Also, all monomers and small copolymers were discarded by the washing process when the methanolic aqueous solution is removed. The discarding process is essential to make any statement about the alkoxy-groups, since the methanol signal of the solvent is in the same range. In addition, for a SEC analysis all alcohols must be removed because they may damage the system as stated by the operator.

The range between 1.0 ppm and 1.2 ppm indicates the CH_3 signal of the ethoxy-groups. In Figure 135, these are integrated relative to Si-H. Due to the low number of ethoxy-groups in the synthesis, the signal-to-noise ratio is very poor. The decrease is almost linear after the one-hour treatment at 85 °C. The theoretical initial value is six protons, but after 30 minutes 98 % of the ethoxy-groups are already hydrolysed considering the so far mentioned problems. An extrapolation determines a theoretical reaction time of about 5.5 hours when the first two samples at 85 °C were neglected. The ten withdrawn ^{1}H NMR samples, which were used to determine the alkoxy contents, were dried under high vacuum and used for molecular weight determination by NMR spectroscopy.

Equation	y = a + b*x
Intersection	0.16407
Slope	-0.03027
Pearson R	-0.98176
R-Square(COD)	0.96384
Kor. R-Square	0.95782
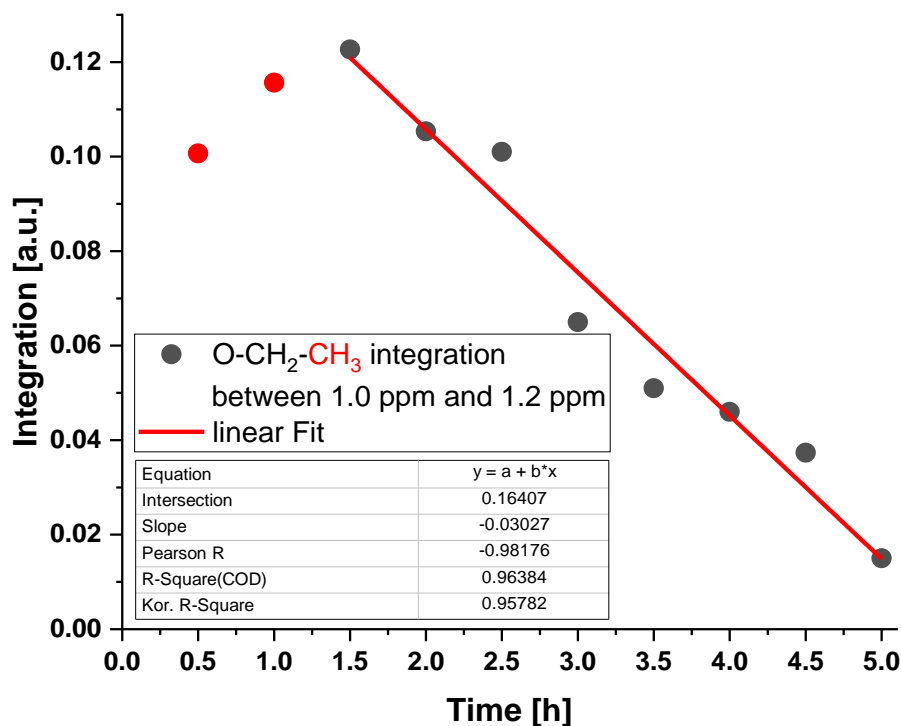
Figure 135: Integration of ethoxy-groups in the range of 1.0 ppm to 1.2 ppm over time. The red marked dots were not included in the fit function.

For linear polymers, an average molecular weight determination can be carried out by integrating the groups in the middle of the chains relative to capping groups at the end of the polymers. For this purpose, it is necessary to introduce end groups that have chemical shifts in an area where no other signals of the methyl- and phenyl-group containing polymer are observed,[136] which is the reason for using *tert*-butyldimethylchlorosilane.[221, 470] The chlorosilane can react in a mild basic solution in THF at 55 °C with the OH groups at the end of the polymers.[471] In this polymerisation, however, since the polycondensation synthesis is not completed, the methoxy-groups must be taken into account. Because these are still present in large numbers after the respective reaction time and only partially react with *tert*-butyldimethylchlorosilane. Ethoxy-groups are also present in the educts, but the largest part already reacted after 30 minutes, therefore these groups can be neglected in the analysis. Thus, both end groups must be included in the chain length calculation. The calculation is based on the Si-H groups, which are used to calculate the number of methyldiethoxysilane in the polymer. With this number and the integration of the methyl-groups, the amount of -SiMePh-O- groups (PM) can be calculated with deduction of the dimethyl-groups on the *tert*-butyldimethylchlorosilane. By integrating the phenyl-groups, taking into account the phenyl-groups of PM, the amount of -SiPh$_2$-O- can be calculated.

Figure 136 shows the molecular weight curve. After only 30 minutes, polymers masses are around 4500 g/mol.
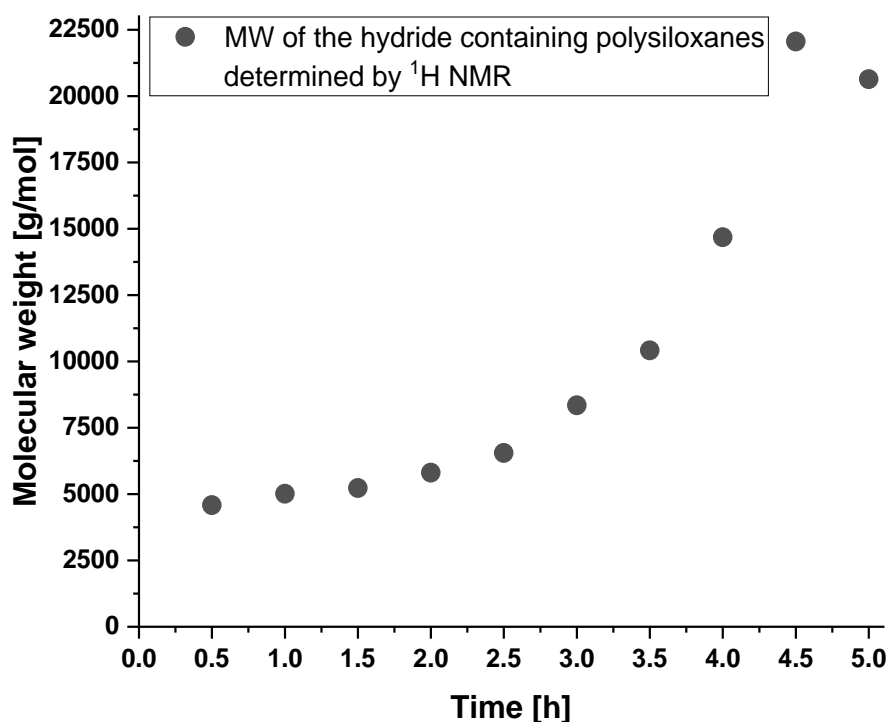
Figure 136: Molar mass of the polymerisation depending on reaction time, monitored by ^{1}H NMR.

In the first two hours the molecular weight slowly increases, but then raises linearly to exponentially after 4.5 hours to 5.0 hours, the molecular weight surpasses 20000 g/mol. The mass after five hours is slightly below the one after 4.5 hours, which can be explained by equilibrium reactions which undergo while the polymers were stored before the measurement.[479]

In addition, ^{1}H ^{29}Si HMBC (Heteronuclear Multiple Bond Correlation) NMR spectra were recorded. In this method, a coherence is generated in the channel of the insensitive core [29]Si, which is then transmitted on the sensitive core (^{1}H) and whose resonances are measured. HMBC experiments are very sensitive and correlations occur over multiple bonds ([2]J, [3]J or [4]J at the used NMR systems). The big drawback is that this method does not provide information about the numbers of the groups respectively atoms. It is not possible to integrate HMBC spectra therefore only a qualitative comparison of the signals can be carried out.

Figures 357 and 358 in the experimental section show ^{1}H ^{29}Si HMBC NMR spectra of samples one and nine. Table 28 shows the observed groups with their chemical shifts. All monomers that have been used are recognisable in the polymer. The ^{29}Si NMR shift from the ^{1}H ^{29}Si HMBC NMR of the M signal of *tert*-butyldimethylsiloxane is observable at 13 ppm,[321-322, 324, 343] the D signal of methylphenylsiloxane is around −33 ppm,[331, 368, 480] the D signal of hydridomethylsiloxane at −36 ppm,[323-324, 331] and the D signal of diphenylsiloxane at −47 ppm.[324, 331, 368]

Table 28: Observed groups and chemical shift in the ^{1}H ^{29}Si HMBC NMR of the hydride-group containing polysiloxanes.

Groups	^{29}Si NMR [ppm]	^{1}H NMR [ppm]
^{t}BuMe$_2$Si-O-MeSiPh-OR	13.3 – 13.4	Me: 0.14 / ^{t}Bu: 1.01
Also: ^{t}BuMe$_2$Si-O-MeSi-OR$_2$		
^{t}BuMe$_2$Si-OMe	10.0	Me: 0.23 / ^{t}Bu: 1.08
RO-PhSiMe-O-SiMe$_2$^{t}Bu	−22.0	Me: 0.71 / Ph: 7.73
RO-PhSiMe-OMe	−23.0	Me: 0.44 / Ph: 7.46 / OMe: 3.27
RO-PhSiMe-OR	−33.2	Me: 0.41 / Ph: 7.63
RO-HSiMe-O-PhSiMe-OMe	−36.6	Me(Si): −0.13 / Ph: 7.77 / H:
Also: RO-HSiMe-OR		5.14 / Me(Si): 0.14 / OMe: 3.33
RO-PhSiPh-OR	−46.7	Ph: 7.71
RO-MeSiOH-OR	−57.0	Me: 0.34
MeSiOR$_3$	−64.2	Me: 0.02

Very small signals at 15 ppm to 20 ppm indicate that a part of the *tert*-butyldimethylchlorosilane dimerizes most likely due to its high excess.[324, 328, 409, 481] The resulting molecules cannot be removed under high vacuum of $5 \cdot 10^{-3}$ mbar at 50 °C. The signal at 10 ppm in the ^{29}Si spectra indicates that a part of *tert*-butyldimethylchlorosilane is methoxylated due to some methanol remaining in the reaction mixture after the washing process and under the basic conditions of the end group capping, respectively. Some further polymerisation can occur, leading to free methanol, which reacts with the excess of *tert*-butyldimethylchlorosilane.

For some silicon atoms, it is possible to identify their neighbouring silicon atoms. Noticeable, this is not possible with the diphenylsiloxane-groups, because no signals of a ^{5}J coupling could be observed in the 2D spectrum. The reaction rate of the hydrolysis of the methoxide-groups under an acidic pH value is higher than the one for the ethoxide-groups which both are higher than for the silanols, because of sterical respectively inductive effects.[149, 482] In the condensation reaction the sterical and inductive difference between the phenyl and methyl side-groups leads to a faster reaction speed of the hydrolysed dimethyldimethoxysilane $Me_2Si(OH)_2$.[149, 482-483]

 An unexpected low intensity of the Si-H groups was observed in the ^{1}H NMR spectra. The ^{1}H ^{29}Si HMBC NMR spectrum reveals an explanation for this observation. New signals in the range of -57 ppm and -64 ppm appear, which can be assigned to T^2 and T^3 groups.[321, 324, 331] These couple exclusively with methyl-groups, which relate to a former Si-H group. These groups can be hydrolysed either under moisture[475] or under the mild basic[484] conditions of NEt_3, which can easily been observed in ^{1}H NMR or FT-IR by the disappearance of the Si-H group.[220] Some of them have reacted to a hydroxyl-group, some have already condensed further and formed Si-O-Si groups. In Figure 137, the ^{29}Si NMRs extracted from the ^{1}H ^{29}Si HMBC NMR of all ten samples are shown, but since the integration and the level of the signals are not comparable it can only be concluded that the Si-OMe groups at -23 ppm and -37 ppm almost disappear.[331, 368]
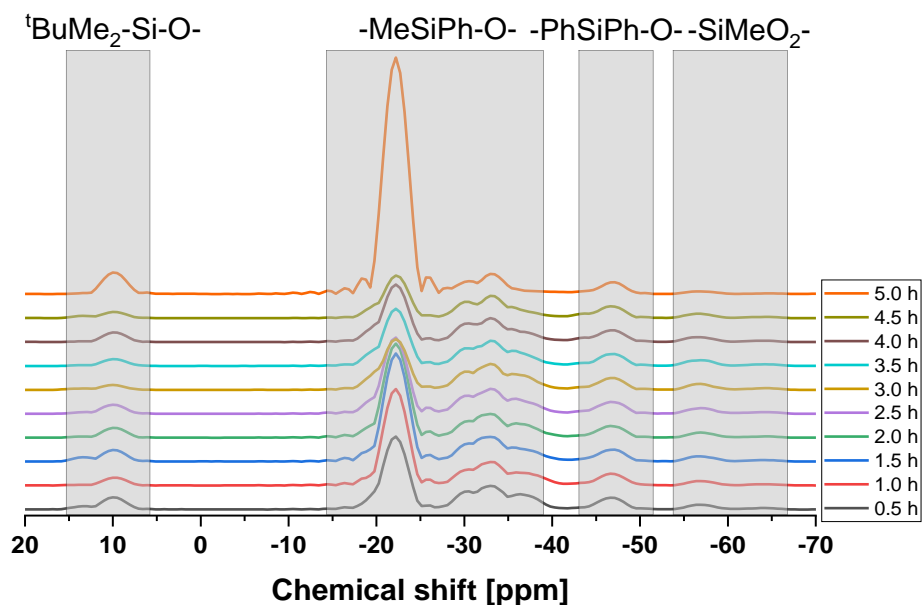
Figure 137: ^{29}Si NMR spectra (79 MHz, CDCl$_3$) from the ^{1}H ^{29}Si HMBC measurement for all ten samples.

4.4.1.3 SEC analysis of the kinetics study

SEC analyses of the ten samples were performed in THF.[485] In the respective detector signals (RI and UV, Figure 138) low molecular weight polymers are initially formed (grey and red curves). They have a relatively narrow M_W distribution, for example from 20.5 mL to 21.5 mL elution volume. A shoulder with higher molecular weight polymer is also recognisable in the range of 19.5 mL to 20.5 mL. Samples taken at the end of the kinetic study after five hours (orange curve) still show intense signals at 20.5 mL to 21.5 mL elution volume, but the distribution becomes bimodal. The shoulder shifts to lower elution volume, which corresponds to a higher molecular weight. Additionally, the shoulder is broadening, ranging now from about 17.5 mL to 20.5 mL elution volume, resulting in a molecular weight of 2600 g/mol determined by the RI detector (PDI: 1.357) and 2670 g/mol determined via UV detection (PDI: 1.374).
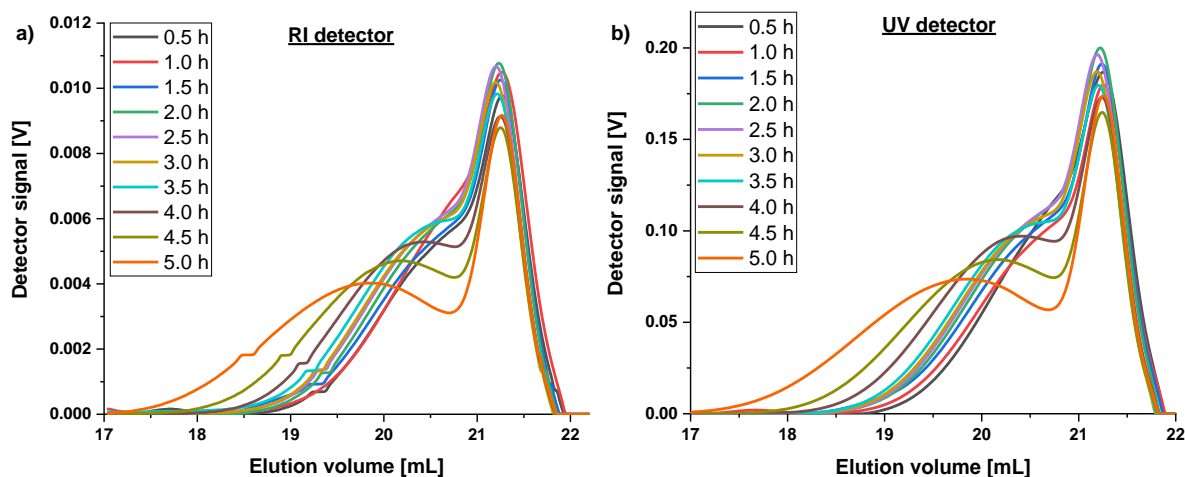
Figure 138: Elugrams of the samples using a) a RI detector and b) a UV detector at 264 nm.

The graphs of molecular weight and polydispersity over time (Figure 139) show the same trend in both detectors. The molecular weight increased in the first hour at 85 °C to 900 g/mol. Then the temperature was raised to 115 °C. In the first 30 minutes, the mass still increased to 967 g/mol and for the next 30 minutes, the molecular weight remained the same. The distiller was then detached to remove the volatiles more easily. The molecular weight increased almost linear to 1066 g/mol (UV) and 1096 g/mol (RI) in 90 minutes from the sample taken after 2.0 h to 3.5 h. Thereafter, the molecular weight increased strongly and, after five hours, the maximum of 1760 g/mol (RI) respectively 1794 (UV) g/mol was reached. The polydispersity curve follows the molecular weight curve. At the beginning of the reaction, the distribution is relatively narrow resulting in a PDI of 1.28 (UV) and 1.34 (RI) when comparing it to literature values of polysiloxane syntheses.[363, 396, 404, 480, 486] With increasing molecular weight, the PDI increases due to the bimodality to 1.95 (RI) and 1.97 (UV). To obtain a higher molecular weight, the reaction time has to be increased significantly. The increase in molecular weight is initially very low.
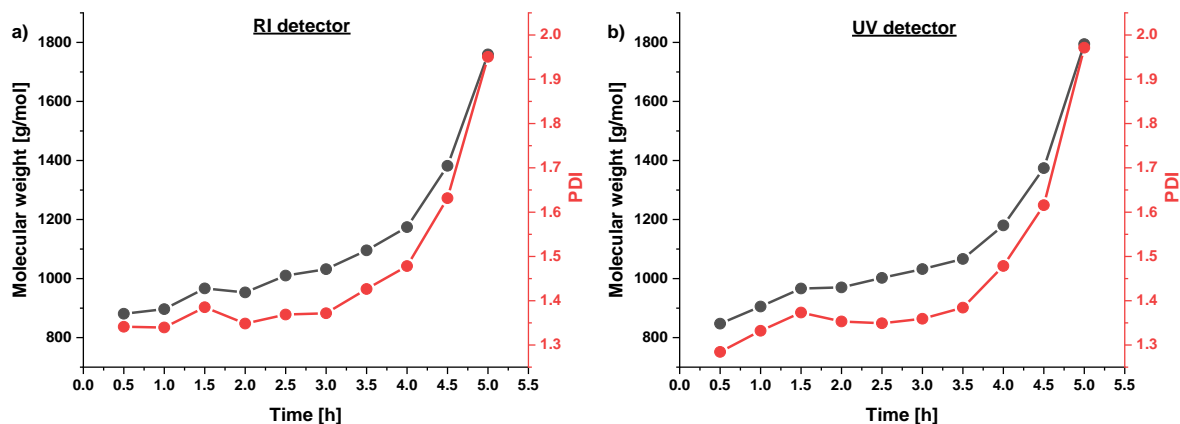
Figure 139: Molar masses and PDI's of the synthesised hydride-group containing polysiloxanes as a function of time, a) determined by the RI detector and b) determined by the UV detector at 264 nm.

After 3.5 hours, when most of the volatile substances were removed, the molecular weight increases significantly, which agrees with the results from the ^{1}H NMR spectra. The pitch at the end of the reaction time is lower in the SEC measurements than in the ^{1}H NMR measurements. Overall, the molecular weights determined by SEC are much lower compared to the NMR results. One possibility is due to the polystyrene calibration of the SEC or the different method of the measurements. In the SEC cyclic systems, which cannot be removed during sample preparation, often elute after the exclusion limit. In the NMR spectrum on the other hand, they are included as "polymer without end group" in the average mass calculation and also the side reactions related to the Si-H group also increase the error.

4.4.2 Synthesis and characterisation of vinyl-containing polysiloxanes

The three monomers vinylphenyldiethoxysilane, methylphenyldimethoxysilane and diphenylsilanediol as well *tetra*-butylammonium hydroxide as catalyst were mixed and, in comparison to the hydride polymerisation, heated one additional hour. Because after five hours, both SEC and ^{1}H NMR showed a drastically increase in molecular weight of H20_PP40_PM40. This indicates that the polymerisation is not even close to the equilibrium state. This additional hour now leads to twelve samples. Therefore, sample eleven was taken after 5.5 h and sample twelve was taken after 6.0 h. The temperature was maintained at 115 °C and the distillation head kept removed. Sample uptake and purification was performed analogous, except for the washing process. The basic probe was washed three times with 1.5 mL of 2 M HCl and two times with 1.5 mL of distilled water. All analyses and sample preparations were carried out corresponding the polymerisation of the hydride polysiloxane.

4.4.2.1 FT-IR spectra of the kinetics study

The FT-IR spectra (Figure 140) only show little difference in the 800 cm^{-1} to 950 cm^{-1} region, where the ethoxy and methoxy-groups are located.[347, 424] Because of the absence of the strong hydride signal, these bands are now recognisable.
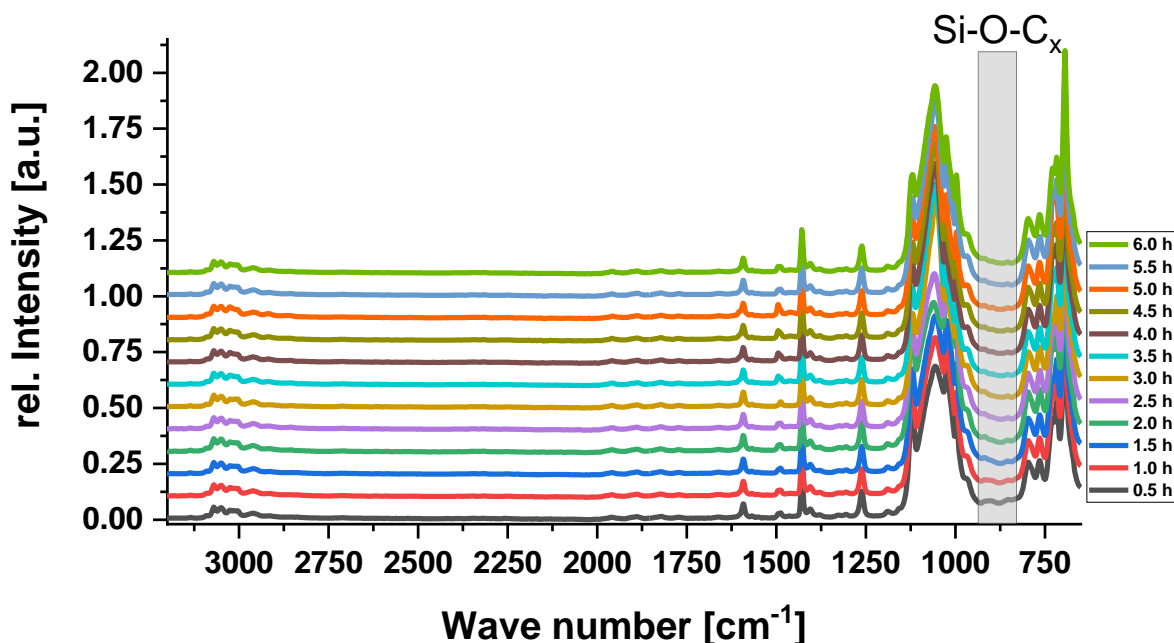
Figure 140: FT-IR spectra of all twelve samples after purification of the vinyl polymerisation.

In the 0.5 hour and 1.0 hour sample a signal can be seen which drastically decreases. In later probes, from 1.5 hours to 6.0 hours, no signal can be seen. Therefore, the spectra of the first and last sample as well as the ones from all three monomers were compared (Figure 141), typical bands are not marked again, as they are reported in Figure 132.
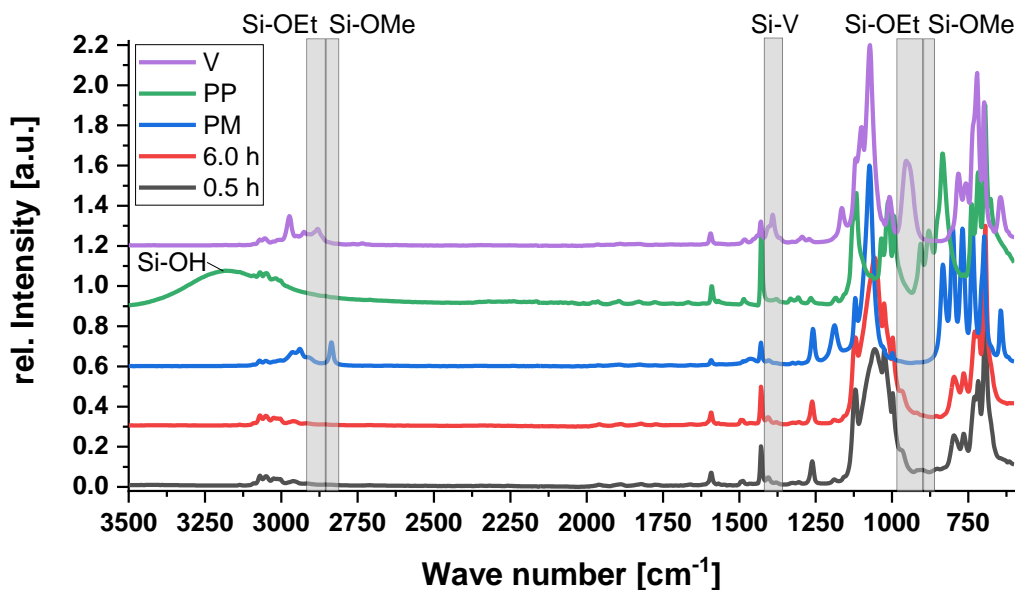
Figure 141: FT-IR spectra of the first and last sample as well as the ones from all monomers.

In the diphenylsilanediol spectra the O-H vibrations at 3000 cm^{-1} to 3300 cm^{-1} are detected,[357] as well as the aromatic and Si-O vibrations are between 400 cm^{-1} and 1200 cm^{-1}.[347, 424] In the spectra of methylphenyldimethoxysilane, especially the C-H and Si-CH$_3$ vibrations at 3000 cm^{-1} and 1250 cm^{-1} are recognisable[217, 487] and also the methoxy signal at 2833 cm^{-1}.[347, 424] In the spectrum of vinylphenyldiethoxysilane the Si-O-CH$_2$-CH$_3$ bands at 2974 cm^{-1} and 955 cm^{-1} are characteristic for this compound,[347, 424] as well as the Si-CH=CH$_2$ band at 1403 cm^{-1}.[487] The polymers only show a little difference between the 30 minute and the six hour sample. The heights of the signals in the range of 980 cm^{-1} to 1130 cm^{-1}, where the bands of the siloxane backbone are located, does not change. This indicates a fast polymerisation process because after 30 minutes most of the resulting Si-O-Si bonds are already formed. The Si-O-C vibration at 1190 cm^{-1} indicates the condensation of the polymers. In comparison to the hydride polymerisation, the small signals of the methoxy-groups at 855 cm^{-1} [346-347, 424] and ethoxy-groups at 905 cm^{-1},[346-347, 424] which are overlapped by the Si-H signal, are now visible. A small decrease of these signal is observable during the polymerisation process, but an integration cannot be made due to the high base line and the strong signals left and right.

4.4.2.2 NMR spectroscopy of the kinetics study

Of the twelve obtained samples before the end group reaction with *tert*-butyldime-thylchlorosilane[221, 470], ^{1}H NMR was recorded in chloroform and referenced to the CH$_3$ signal of toluene and to an integration of three for the Si-V group. The following overview (Figure 142) shows the spectra in ascending order. The region of the Si-Ph groups is located at 7.0 ppm to 8.0 ppm, the Si-V ones at 5.5 ppm to 6.5 ppm and the Si-Me ones at −0.2 ppm to 1.8 ppm.[236, 474-476] The signals change minimally because of the increasing chain length the sharpness of

signals decreases and another, less distinct peak splitting emerges. In the range of alkoxy-groups between 3.0 ppm and 4.0 ppm,[22, 91, 426, 284-285] a clear decrease can be seen during the reaction, likewise in the hydride polymerisation. In this range both the methoxy-groups (methanol: 3.5 ppm) and ethoxy-groups (ethanol: 3.7 ppm) show signals, therefore the same correction with the ethoxides is performed like in the hydride polymerisation.
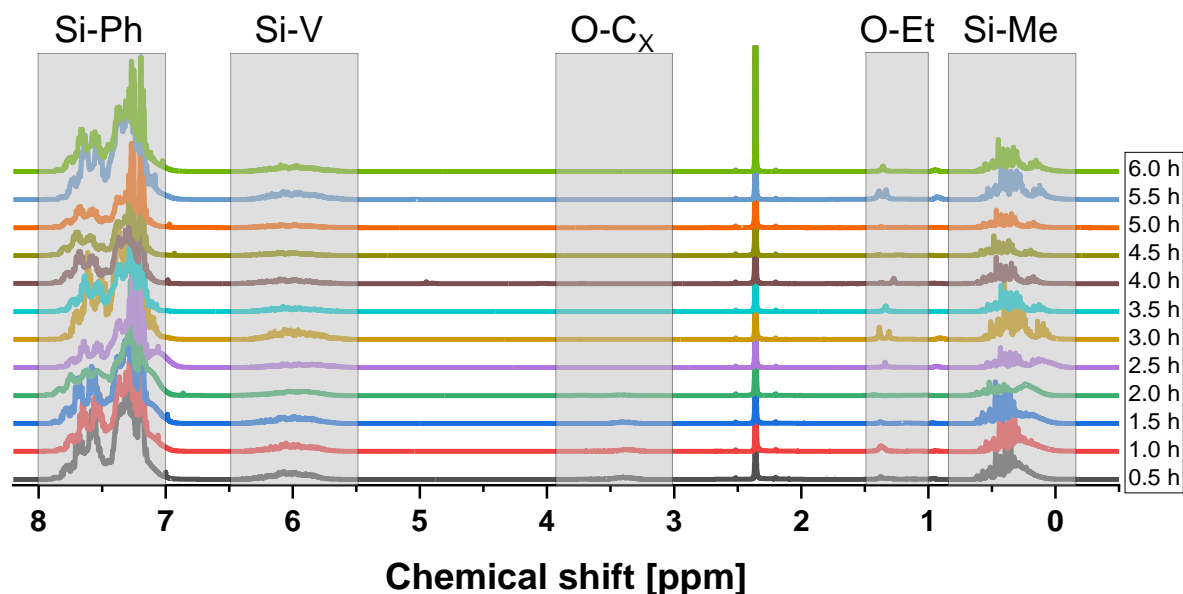
Figure 142: **^{1}H NMR (400 MHz, CDCl$_3$) spectra after every 30 minutes in CDCl$_3$ of the vinyl-group containing polysiloxanes.**

The integration of the alkoxy-groups, which equals the CH$_3$ protons from methoxy-groups and the CH$_2$ protons from ethoxy-groups, in the range of 2.8 ppm to 3.6 pm can be plotted versus the time resulting in an "S"-like curve (Figure 143). Although at the beginning no real plateau can be seen because of the fast reaction, a Boltzmann fit can be applied. This form is reported in literature by Matějka *et al*.[477] and Torry *et al*.[478] for basic polycondensation reactions.[472] After one hour up to 2.5 hours, a straight decrease in the proton integration occurs with a reaction speed of 0.3 proton integration per hour. The theoretical starting value is an integration of 16 protons, but in the first sample only 0.5 are left, indicating that the hydrolysis and condensation within the first 30 minutes was very fast. Also, all monomers and small copolymers were discarded by the washing process when the methanolic-aqueous solution is removed. The discarding process is essential to make any statement about the alkoxy-groups, because of the earlier mentioned reasons. After three hours up to the full six hours of reaction time, no further significant decrease can be observed. The range between 1.0 ppm and 1.2 ppm indicates the CH$_3$ signal of the ethoxy-groups. Plotting the integration of them relative to the vinyl-groups

shows no correlation. Due to the low number of ethoxy-groups in the synthesis, the signal-to-noise ratio is very poor and therefore contains large errors. In the ^{13}C NMR spectra, no signals of methoxy or ethoxy-groups can be detected, despite a large signal-to-noise ratio.

Model	Boltzmann
Equation	y = A2 + (A1-A2)/(1 + exp((x-x0)/dx))
Plot	O-Cx
A1	0.49786
A2	-3.39233E-4
x0	1.79414
dx	0.33636
Reduced Chi-Sqr	4.45857E-5
R-Square (COD)	0.99999
Adj. R-Square	0.99999
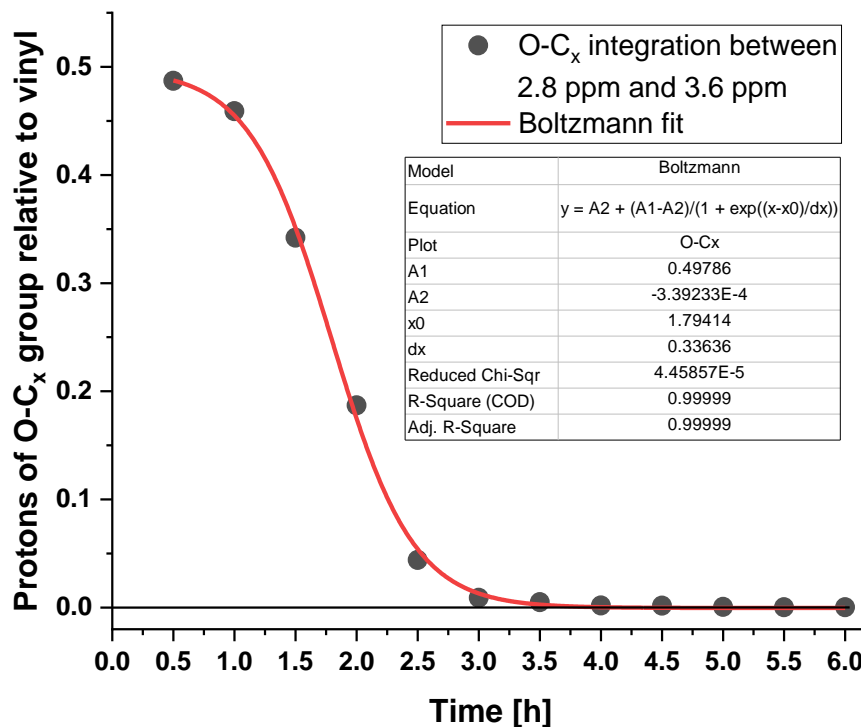
Figure 143: Integration of alkoxy-group protons in the range of 2.8 ppm to 3.6 ppm over time, relative to vinyl protons.

The twelve ^{1}H NMR samples, which were used to determine the alkoxy contents, were dried under high vacuum and used for molecular weight determinations by NMR spectroscopy. For linear polymers, an average M_W determination can be performed by integrating the side-groups relative to the end groups using the earlier reported procedure. In this polymerisation, however, since it is not clear if the synthesis is completed because small residues cannot be seen in ^{1}H NMR or FT-IR but have an impact on the integration, the methoxy-groups must be taken into account. These are still present after the reaction time and only partially react with *tert*-butyl-dimethylchlorosilane. Ethoxy-groups are also present in the educts, but the largest part has already reacted after 30 minutes, so these can be neglected. Thus, both end groups must be included in the chain length calculation. The calculation is based on the vinyl-groups, which are used to calculate the number of vinylphenylsiloxane (V) units in the polymer. With the integration of the methyl-groups, the amount of methylphenyldimethoxysilane (MP) can be calculated with deduction of the dimethyl-groups on the *tert*-butyldimethylchlorosilane. By integrating the phenyl-groups, considering the phenyl-groups of methylphenyldimethoxysilane (MP) and vinylphenyldiethoxysilane (V), the amount of diphenylsilanediol (PP) can be calculated.

Figure 144 shows the molecular weight curve calculated by ^{1}H NMR measurements. After 30 minutes, polymer masses at around 1460 g/mol are already reached.
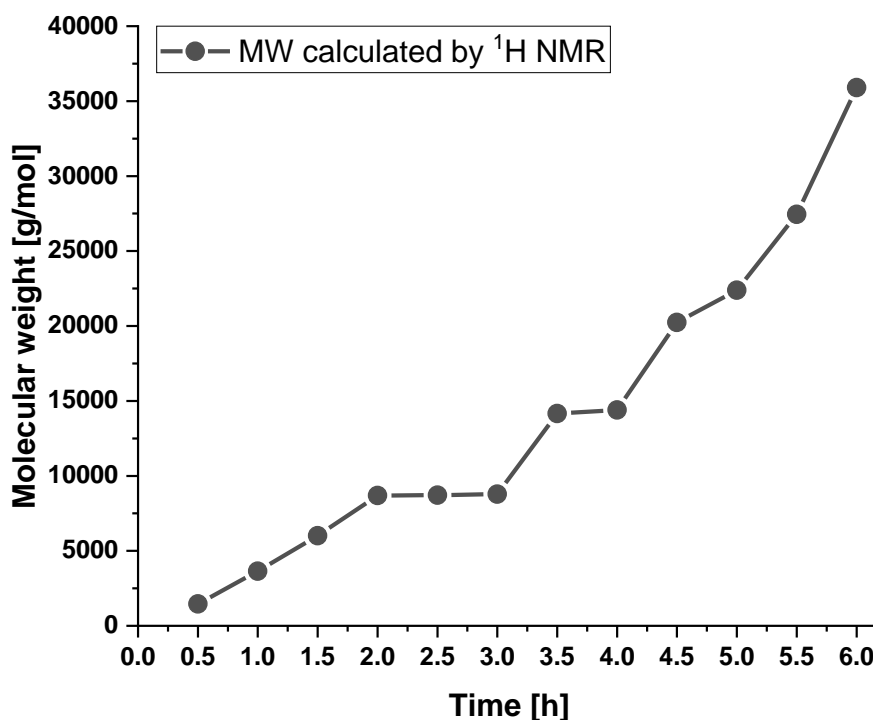
Figure 144: Molecular mass of the basic catalysed polymerisation depending on reaction time, calculated from ^{1}H NMR.

In the first two hours, the molecular weight linearly increases up to 8700 g/mol, followed by a plateau for the next hour when the distillation head is removed. The molecular masse slightly increases to 8800 g/mol. After another increase to 14200 g/mol from 3.0 hours to 3.5 hours, another plateau is reached for 30 minutes. In the last two hours of reaction time, the increase is more rapid with a maximum of 36000 g/mol. Compared to the hydride polymerisation, the molecular weight strongly increases after four hours of reaction time and a weakening of the molecular mass increase is not recognisable. In addition, ^{1}H ^{29}Si HMBC NMR spectra were recorded, Figures 361 and 362 show two spectra of samples one and eleven and Table 29 shows the observed groups with their chemical shifts. The signals indicate that besides the desired reaction, one part of *tert*-butyldimethylchlorosilane is hydrolysed (T_b = 140 °C)[419], one part is dimerised (T_b = 191 – 193 °C)[419] and one part has reacted with methanol to form the *tert*-butyl-methoxydimethylsilane (T_b = 117 – 118 °C)[419] due to high excess, also it cannot be removed under high vacuum at 50 °C. All monomers used are recognisable in the polymer. For some silicon atoms, it is possible to identify their neighbouring silicon atoms. Noticeable, this is hardly possible with the diphenylsiloxane-groups because of the earlier mentioned reasons. In

comparison to the hydride polymerisation, the methoxy-groups of methylphenyldimethoxysilane cannot be detected even in the first spectra after 30 minutes the reaction. Because they were visible in the ^{1}H NMR recorded directly after the washing and drying process, bevor the end group reaction, they must have further polymerised or reacted with the chlorosilane.[89,470-471]

Table 29: Observed ^{1}H and ^{29}Si NMR chemical shifts and the assigned group.

Groups	^{29}Si NMR [ppm]	^{1}H NMR [ppm]
^{t}BuMe$_2$Si-OH	24.3	Me: 0.21 / ^{t}Bu: 0.88
^{t}BuMe$_2$Si-O-SiMe$_2$^{t}Bu	18.9	Me: −0.02 / ^{t}Bu: 0.85
^{t}BuMe$_2$Si-OR	13.5	Me: −0.12 / ^{t}Bu: 0.75
^{t}BuMe$_2$Si-OMe	9.9	Me: −0.02 / ^{t}Bu: 0.82
RO-PhSiMe-O-SiMe$_2$^{t}Bu	−22.2	Me$_2$: 0.04 / Me(Si): 0.45
RO-PhSiMe-OR	−27.0 to −32.8	Me: 0.43 / Ph: 7.55
RO-Ph$_2$SiO-PhSiMe-O-SiPh$_2$-OR	−33.0	Me: 0.42 / Ph: 7.55
RO-PhSiV-OR	−45.9	Vi: 5.92 – 6.28 / Ph: 7.66
RO-PhSiPh-OR	−44.6 to −46.8	Ph: 7.53

When comparing the ^{29}Si spectra from the HMBC measurements (Figure 145) over time, which were normalised to the highest signal at −22 ppm, the spectrum after 30 minutes clearly differs from the rest because only one strong signal at around −22 ppm is visible. This signals can be referred to methylphenylcyclosiloxanes[480] or linear ones with methoxy end groups.[322, 368] Important to note is that in HMBC spectra, comparisons between signal heights or area cannot be carried out. In all later spectra, additional strong signals are visible. In the area of around 20 ppm, where the M groups[321-322, 324, 343] like *tert*-butyldimethylsiloxane are located, a few signals are visible as well as in the D area[331, 368, 480] at −30 ppm of condensed methylphenylsiloxane. The diphenylsiloxane and vinylphenylsiloxane signals are visible at −45 ppm.[324, 331, 368] This shows that the monomers or small polymers were washed off during the cleaning process. The sterical impact of the side-groups in the reaction rate does not change under basic conditions. However, the reaction rate of the hydrolysis of the methoxide-groups under a basic pH value is lower than the one for the ethoxide-groups which both are lower than for the silanols because of inductive effects.[149, 482] In the condensation reaction the inductive difference between the phenyl and methyl side-groups leads to a slower reaction speed of the hydrolysed dimethyldimethoxysilane Me$_2$Si(OH)$_2$.[149, 482-483]
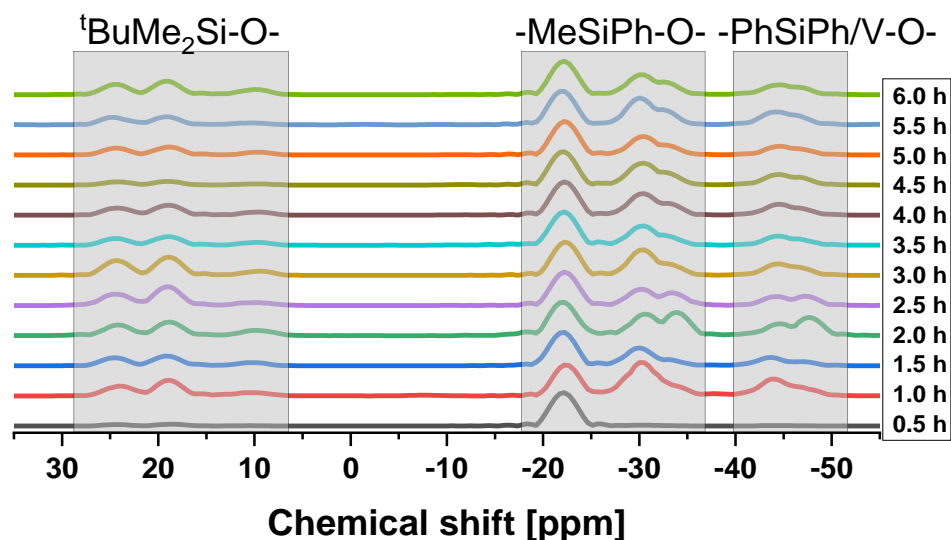
Figure 145: ^{29}Si NMR (79 MHz, CDCl₃) spectra from the ^{1}H ^{29}Si HMBC NMR measurement.

Because the height in HMBC measurements cannot be compared, conventional ^{29}Si NMR spectra of the polymers directly after the synthesis, were recorded (Figure 146). Because only small amounts of sample were used, the signal-to-noise ratio is poor. Nevertheless, all spectra are similar, even the first one after 30 minutes matches the following ones, indicating that all monomer groups have already reacted. A signal below −28 ppm cannot be seen, proofing that the signals in the HMBC measurements have to be related to silicon atoms beneath the *tert*-butyl-dimethylsiloxan-group or from cyclic compounds forming in the post reaction. A small variation in heights can be detected because the spectra were normalised to the highest signal, which changes over time. A normalisation to a specific signal was not performed because there is no signal which is constant over the reaction time.
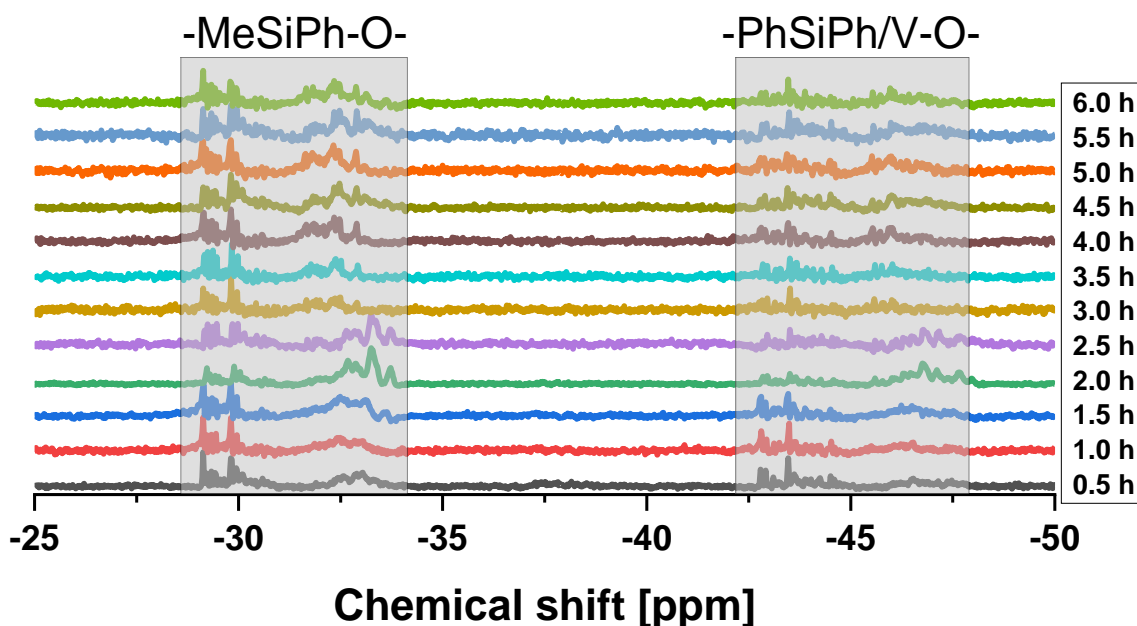
Figure 146: ^{29}Si NMR spectra (79 MHz, CDCl₃) before the end group capping.

4.4.2.3 SEC analysis of the kinetics study

In the respective detector signals (Figure 147) low molecular weight polymers are initially formed after 30 minutes (grey curve) and one hour (red curve). Both have a PDI around 1.35 determined both by the UV and the RI detector (Figure 148) ranging from 19.0 mL to 22.0 mL elution volume. Because the curve has a shoulder towards lower elution volumes and higher molecular weights, respectively. After five hours (orange curve), the initial band at 20.5 mL to 22.0 mL is still very intensive, but the distribution becomes bimodal, the shoulder shifts towards lower elution volume, which corresponds to a higher molecular weight. The shoulder is broadening, ranging from about 17.5 mL to 20.5 mL of elution volume, giving a molecular weight of 1760 g/mol after RI detector (PDI: 1.95) and 1790 g/mol after UV detector (PDI: 1.97). The received molecular weight is lower compared to the hydride polymerisation, which was about 1900 g/mol. This is the opposite compared to literature, because a basic catalysed polymerisation should lead to higher molecular weights than an acid catalysed one.[110, 140, 485, 488] Also, the PDI is higher for the low molecular weight polymers received from the basic synthesis. The two additional samples taken after 5.5 h and 6.0 h show entirely different curves, which is most likely since these samples were measured several days after the first ten. The bimodal curves split even more in both samples and detector signals, the very large low molecular part ranges from 21.0 mL to 22.0 mL, resulting in a molecular mass of around 700 g/mol and a very small high molecular mass part from 20.0 mL to 21.0 mL with around 3700 g/mol. Here, the effect of statistically breaking and tying the bonds occurs and an equilibrium is formed.[479, 489] This results in a small PDI of 1.04 respectively 1.30 for the low and high molecular mass fractions.
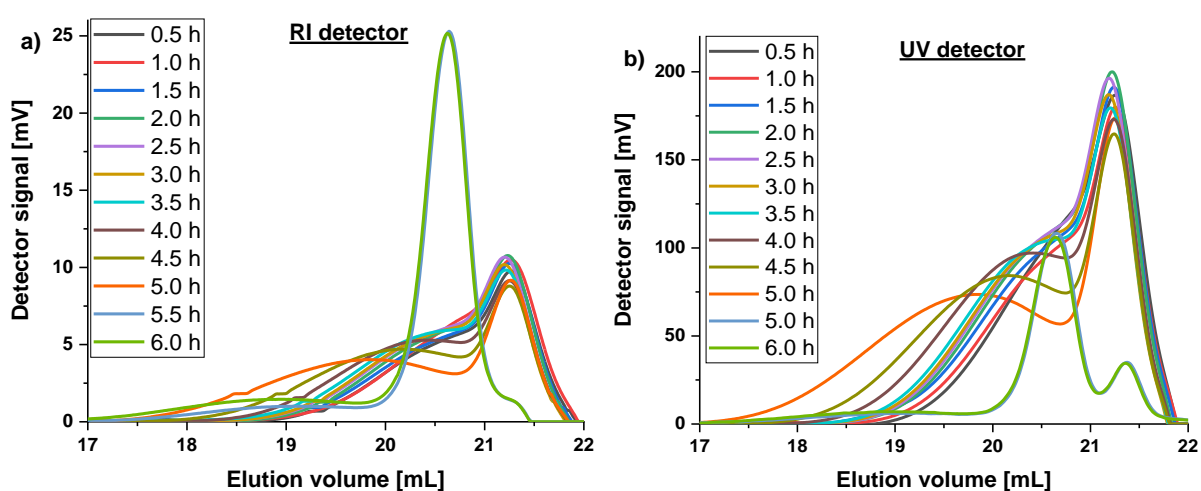
Figure 147: Elugram of the vinyl-groups containing polymer samples with a) a RI detector and b) a UV detector at 264 nm.

The graphs of molecular weight and polydispersity over time (Figure 148) show the same trend in both detectors. The M_W slowly increased in the 3.5 hours hour from 881 g/mol in the RI

detector and 847 g/mol in the UV detector up to 1096 g/mol and 1066 g/mol. The increase of the temperature from 85 °C to 115 °C hardly shows any increase in M_W, as well as the removing of the distillery. In the next 1.5 hours, the M_W increases drastically, a maximum of 1760 g/mol (RI) and 1794 g/mol (UV) was reached after five hours. The last two samples show a bimodal distribution, in the curves the high M_W part is connected to the previous calculated masses with a total maximum of 3772 g/mol (RI) and 3623 g/mol (UV). The low M_W part shows masses around 700 g/mol which is independent from the detector. The polydispersity curve follows the molecular weight curve. At the beginning of the reaction, the distribution with a PDI of 1.28 (UV) and 1.34 (RI) is relatively narrow at least for polysiloxanes.[363, 396, 404, 480, 486] With increasing molecular weight, the PDI increases due to the increasing bimodality. The raised temperature after one hour leads first to an increased PDI of 1.40 then after further 30 minutes, a decrease to the value before of 1.35. After 3.5 hours the value drastically increases up to 1.95 (RI) or 1.97 (UV) after 5.0 hours.
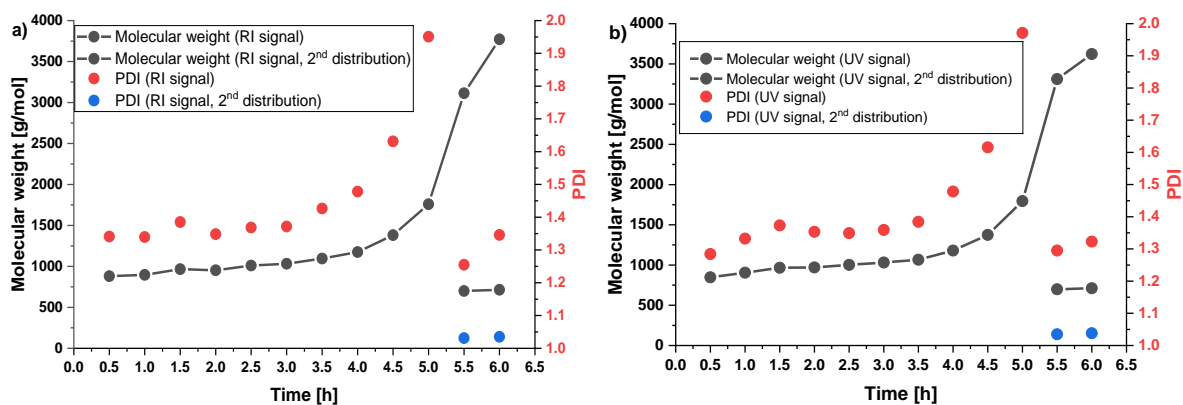
Figure 148: Molecular masses and PDI's of the synthesised vinyl-group containing polysiloxanes as a function of time, a) determined by the RI detector and b) determined by the UV detector at 264 nm.

In the last two samples a bimodality forms, so two values can be calculated, which are very low and around 1.33 for the high mass fraction and 1.04 for the low mass fraction, respectively.

The molecular weight calculation by ^{1}H NMR and the SEC measurements does not match. The slow increase of molecular mass in the beginning of the reaction as seen in the SEC measurements cannot be observed in the ^{1}H NMR calculations, where a nearly linear mass increase occurs. The ^{1}H NMR calculations are more difficult for the vinyl polymer than for the hydride polymer, because more side products of the *tert*-butyldimethylchlorosilane were formed. These drastically reduce the accuracy of the integration of the end groups and therefore the calculated mass. Overall, similar to the hydride polymer synthesis, the M_W are much lower in the SEC measurement. One possibility is due to the polystyrene calibration and another one is because of the different methods of the measurement as well as the earlier mentioned problems.

4.4.3 Conclusion of the kinetics study

Both exemplarily performed polymerisations of a hydride and vinyl polysiloxane were success-ful. After five hours of reaction time, in both the acid as well as the base catalysed polymerisation lead to a molecular weight measured by SEC between 1500 g/mol and 1800 g/mol and a similarly shaped M_W curve. The ^{1}H NMR calculations showed in both cases a maximum M_W of around 23000 g/mol, but a differently shaped M_W curve. For the hydride polymerisation the M_W increased exponentially with increasing reaction time while the vinyl polymerisation increased nearly linearly when excluding the last two samples due to them being bimodal. This leads to the conclusion that with the used type and amount of catalysts identical molecular weights can be achieved using an acidic or basic synthesis route. Both, the M_W calculation by ^{1}H NMR and the measurement by SEC analysis, are afflicted with errors, where the SEC numbers are too low because it is calibrated against polystyrene[363, 404, 486] and the NMR numbers are too high because of cyclic side products as is already described by Fuchise *et al.*[480] Therefore, the calculated M_W is probably in between the NMR and SEC values. For the vinyl polymerisation the reaction time was extended for an additional hour because after five hours the M_W curves in the acidic polymerisation have a strong slope. According to the NMR calculations this additional hour leads to a strong increase of the M_W up to 36000 g/mol for the basic polymerisation. The SEC data show that the M_W also rises but due to the equilibrium reactions these numbers are maybe afflicted with errors. Overall, the reaction time should be as long as possible to enable an equilibrating, but this also leads to a high molecular weight which is not always favourable for the thermal stability as stated by Ručigaj *et al.*[356]

4.5   Synthesis of HRI polysiloxanes by modification of side-groups

4.5.1   Synthesis and characterisation of phenoxyphenyl-group containing polysiloxanes

In comparison with the literature (Figure 149) described method (a)), the self-prepared copolymers were synthesised differently using other monomers (b)).[136] 20 mol% of the methyldiethoxysilane respectively vinyldiphenylsiloxane were used as cross-linking group for the hydrosilylation reaction. The self-synthesised phenoxyphenyl-group containing monomer POPP as well as diphenylsilanediol (PP) were used with 40 mol% each. The received copolymers are therefore called H20_POPP40_PP40 and V20_POPP40_PP40.
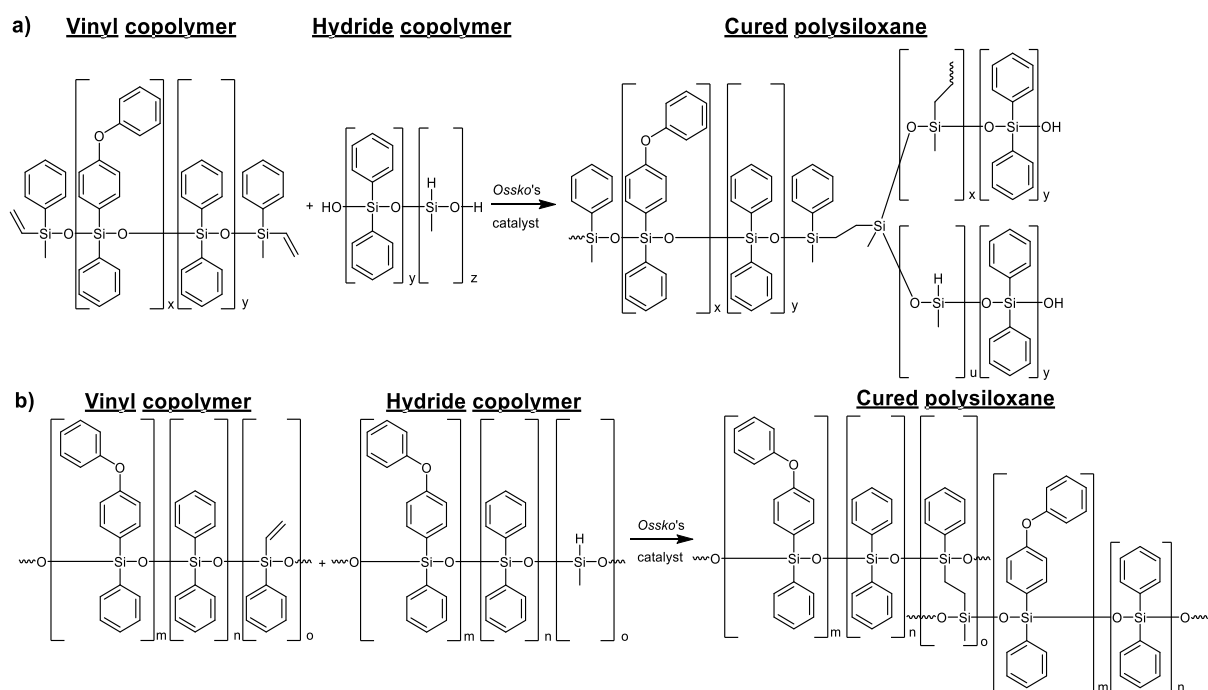
Figure 149: Chemical structure of vinyl and hydride copolymers as well as the cured polysiloxanes, a) the literature method and b) the self-synthesised polymers.[136]

4.5.1.1   Synthesis and characterisation of 4-(phenoxy)phenylphenyldimethoxysilane

The synthesis of the 4-(phenoxy)phenylphenyldimethoxysilane (POPP) monomer was carried out according to Figure 150 using a Grignard reaction with 4-bromodiphenyl ether and phenyltrimethoxysilane in tetrahydrofuran.[136] A colourless oil was received in 72 % yield which crystallised at room temperature after one month. The refractive index of the liquid monomer was determined with 1.570 at 20.0 °C and 589 nm. The FT-IR spectrum and the characterisation are reported and discussed in chapter 4.5.1.2.1.
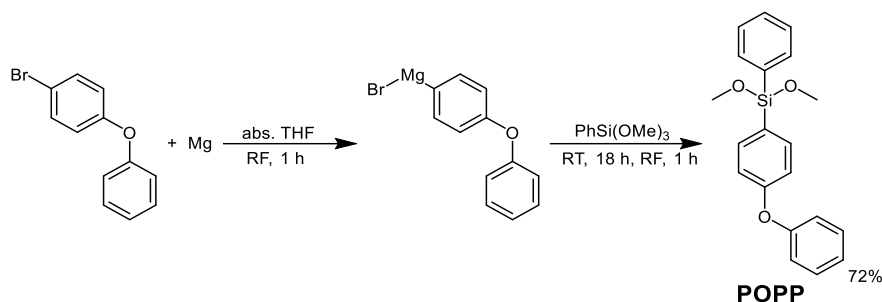
Figure 150: Synthesis scheme for 4-(phenoxy)phenylphenyldimethoxysilane applying a Grignard reaction.

4.5.1.1.1 NMR characterisation of 4-(phenoxy)phenylphenyldimethoxysilane

The ^{1}H NMR (Figure 151) reveals the signals of the phenyl-groups are present from 7.1 ppm to 7.9 ppm and the peak at 3.8 ppm refers to the methoxy-groups.[136] About 1.5 % starting material (phenyltrimethoxysilane) can still be detected in the spectrum because the integration of the methoxy-groups at 3.8 ppm is higher than six and the phenyl integration at 7.5 ppm is also higher than the expected five protons.
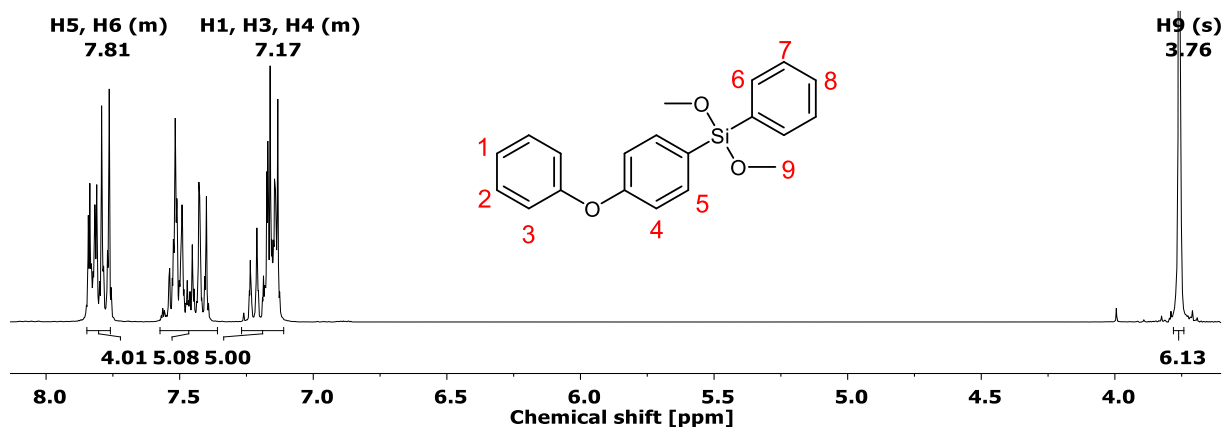
Figure 151: ^{1}H NMR (300 MHz, CDCl₃) of 4-(phenoxy)phenylphenyldimethoxysilane.

The ^{13}C NMR (experimental section, Figure 364) shows all expected carbon signals. In the ^{29}Si NMR (Figure 152), the D^0 product signal is present at −28.8 ppm[441, 490] as well as the small T^0 educt signal of phenyltrimethoxysilane at −54.4 ppm.[433, 441]
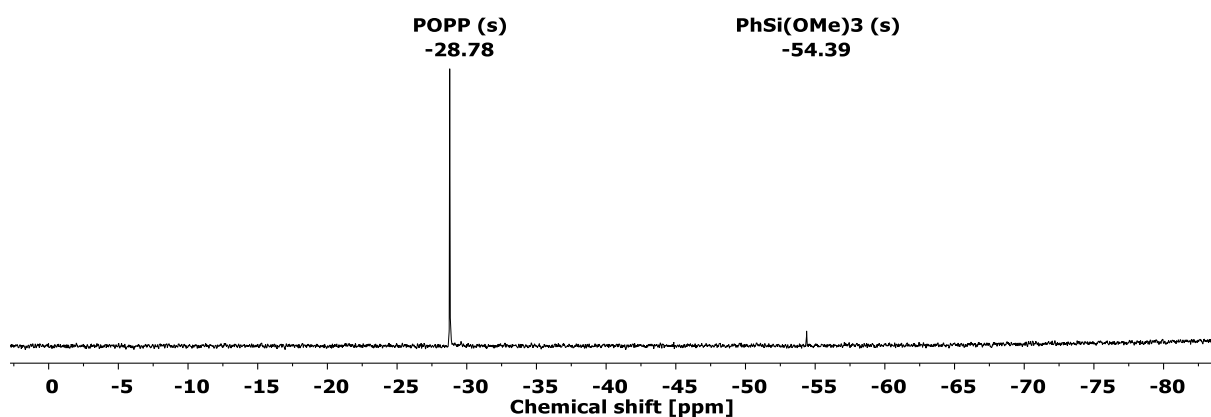
Figure 152: ^{29}Si NMR (60 MHz, CDCl₃) of 4-(phenoxy)phenylphenyldimethoxysilane.

4.5.1.1.2 Crystal structure of 4-(phenoxy)phenylphenyldimethoxysilane

From the clear oil, crystals could be grown and was analysed by single crystal X-ray diffraction (Figures 153 – 154). The obtained molecular structure reveals the targeted 4-(phenoxy)phenylphenyldimethoxysilane.
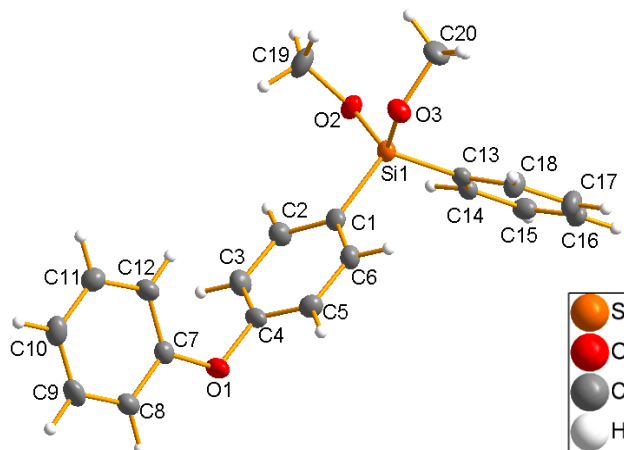
Figure 153: Molecular structure of 4-(phenoxy)phenylphenyldimethoxysilane obtained by single crystal structure determination.
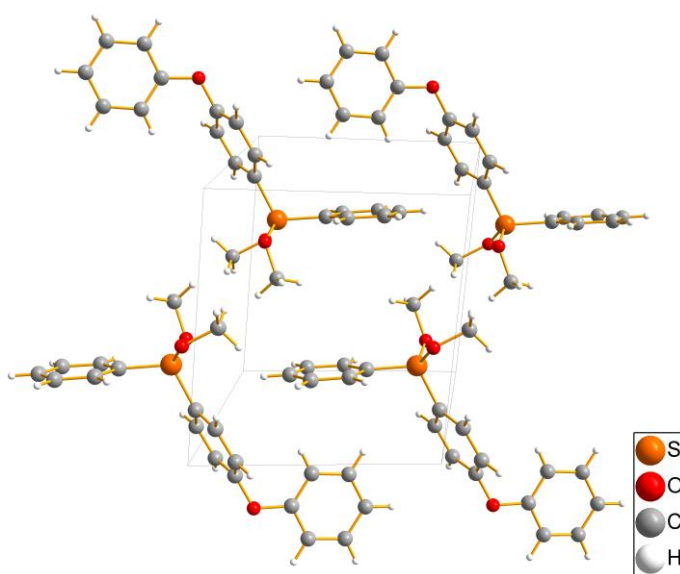
Figure 154: Packing diagram of 4-(phenoxy)phenylphenyldimethoxysilane.

The monomer crystallised in the triclinic space group $P-1$ (Table 30).[491] The length of the two Si-O bonds is minimally larger than the average 163 pm.[123, 491-492] The detected Si-C bond length of phenoxyphenyl (Si-C1) is within the range of comparable structures,[123, 491-492] as well as the Si-C bond length of the phenyl-group (Si-C13). The two C-O lengths of the phenoxyphenyl-group (C4-O1 and C7-O1) are significantly smaller than the average 143 pm. The length between the oxygen and carbon atom of the phenyl ring connected to the silicon atom is 140.0(2) pm. The C-O bond of the phenyl-group is 138.9(2) pm long.[123, 491-492] The reason is the interaction with the two aromatic phenyl-groups, the bond lengths in diphenyl ether for the

two C-O bonds are also shorter than the 140 pm and show a different length. One C-O bond is 138.1(2) pm long while the other one is 139.2(1) pm long, which is comparable.[493] The torsion angle between the two phenyl planes in diphenyl ether is 88.3(0)°, while it is around 10° smaller with 78.9(0)° in 4-(phenoxy)phenylphenyldimethoxysilane, because of the sterical influence of the third phenyl-group (C13 to C18) bound to the silicon atom.[493] All angles around the silicon atom between C1, C13, O2 and O3 differ from the ideal tetragonal angle of 109.5°.[494] The carbon-silicon-carbon angle (C1-Si-C13) is widened by around 4° because of the two sterically demanding phenyl-groups. The C1-Si-O2 and the C13-Si-O3 angles are minimally larger than the tetragonal angle,[494] while the C1-Si-O3 and the C13-Si-O2 angles are 5° and 4° smaller. The oxygen-silicon-oxygen angle (O2-Si-O3) is with 111.9(1)° around 2.5° larger than 109.5°,[494] which is a side effect of the sterically demanding phenyl-groups. The angle between the phenyl-groups of the phenoxyphenyl side-groups is 117.9(2)°, which is identical as in di-phenyl ether.[493]

Table 30: Bond lengths and angles of the synthesised monomer 4-(phenoxy)phenylphenyldimethoxysilane.

	POPP	Bond lengths and angles	POPP
Space	*P -1*	Angle: C1-Si-C13	113.70(8)°
group	triclinic	Angle: C1-Si-O2	110.78(8)°
a	894.74(5) pm	Angle: C1-Si-O3	104.78(8)°
b	973.80(8) pm	Angle: C13-Si-O2	105.81(8)°
c	1039.25(8) pm	Angle: C13-Si-O3	110.37(8)°
α	90.130(3)°	Angle: O2-Si-O3	111.87(8)°
β	106.666(2)°	Angle: C4-O-C7	117.87(15)°
γ	91.016(2)°	Torsion angle between planes: Ph-Si-Ph	65.324(56)°
V	0.86729(11) nm^3	Torsion angle between planes: Ph-O-Ph	78.932(64)°
		Distance: Si-C1	185.97(19) pm
		Distance: Si-C13	185.43(18) pm
		Distance: Si-O2	163.13(14) pm
		Distance: Si-O3	163.35(14) pm
		Distance: C4-O1	140.0(2) pm
		Distance: C7-O1	138.9(2) pm

4.5.1.2 Synthesis and characterisation of phenoxyphenyl-group containing polymers

The synthesised monomer 4-(phenoxy)phenylphenyldimethoxysilane (POPP) was used in the synthesis of a hydride- and a vinyl-group containing copolymer as a precursor for a polymer (Figure 155). The basic catalyst tetra-*n*-butylammonium hydroxide was used for the vinyl polymerisation and the acidic catalyst concentrated hydrochloric acid was used for the hydride copolymer synthesis. 20 Mol% of cross-linker, vinylphenyldiethoxysilane (V) respectively methyldiethoxysilane (H), is used because the amount is high enough to receive a solid cured polysiloxane. Mosley *et al.* mixed the hydride and the vinyl copolymer in a ratio of 2:1 hydride-per vinyl-groups with a low vinyl content of 7.5 mol%.[136] Also 40 mol% of diphenylsilanediol (PP) were added to achieve a high refractive index while remaining a processable polymer, where Mosley *et al.* varied the amount from 22 mol% to 72 mol% using diphenyldimethoxysilane.[136] The remaining 40 mol% were filled with the self-synthesised 4-(phenoxy)phenylphenyldimethoxysilane (POPP), while Mosley *et al.* changed the amount depending on the diphenyl content from 72 mol% to 22 mol%.[136] The received polymers are named H20_POPP40_PP40 for the hydride copolymer and V20_POPP40_PP40 for the vinyl copolymer.
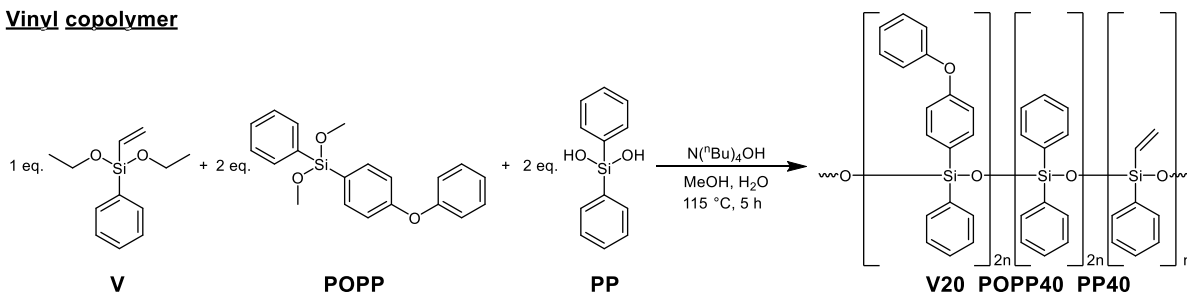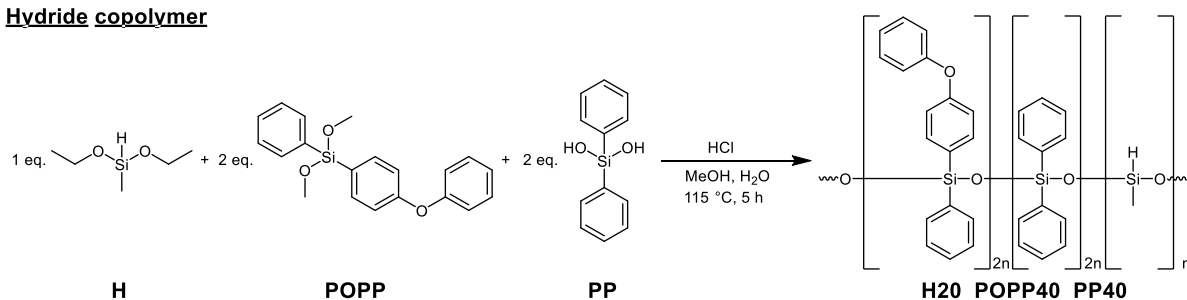
Figure 155: Synthesis route for phenoxyphenyl containing vinyl and hydride copolymers.

The appropriate monomers were mixed with the catalyst, water, and methanol in a round bottom flask with a distillation head. After heating for one hour at 85 °C, the temperature was raised to 115 °C for four hours while after one hour the distillation head was removed to facilitate the removal of water, methanol and ethanol. After washing the polymers by adding toluene and using potassium bicarbonate once for the hydride copolymer or 2 M hydrochloric acid three times for the vinyl copolymer to neutralise the reaction solution. The pure copolymers were

received after washing and drying them under reduced pressure. The hydride and vinyl copolymers were mixed in a 1:1 ratio with *Ossko's* catalyst, degassed and cured for one hour at 80 °C and four additional hours at 150 °C.

4.5.1.2.1 FT-IR spectra of phenoxyphenyl-group containing polymers and POPP

FT-IR spectra of the synthesised monomer as well as the hydride and vinyl copolymer and the cured polysiloxane were recorded (Figure 156). The monomer shows the C-H bands at 2943 cm^{-1}, at 1232 cm^{-1}, at 742 cm^{-1} and at 692 cm^{-1}.[346-347] The aromatic C=C vibrations are located at 1583 cm^{-1} and at 1481 cm^{-1}.[495] The C_{Ar}-O-C_{Ar} bands (dark grey) at 1194 cm^{-1}, at 1059 cm^{-1} and at 866 cm^{-1} partially overlap with other bands,[495] therefore they cannot clearly assigned in the polymers. The Si-C bands are located at 1429 cm^{-1} as well as at 1226 cm^{-1} and in the area of 690 cm^{-1} to 740 cm^{-1} which is in the region of C-H bands.[346-347] The Si-O-C vibration from the methoxy-group is clearly visible at 2839 cm^{-1}.[346] The polymers show the additional Si-O vibrations from 991 cm^{-1} to 1115 cm^{-1}.[346-347] The vinyl copolymer shows no additional bands because the vinyl vibration is too close to the C=C_{Ar} ones.[319, 348-350] The Si-H bands of the hydride copolymer are located at 2171 cm^{-1} and at 900 cm^{-1}.[346-347] The cured polysiloxane (P20_POPP40_PP40) shows no additional bands compared to the copolymers. The polysiloxane is completely cured because there are no remaining Si-H bands visible.
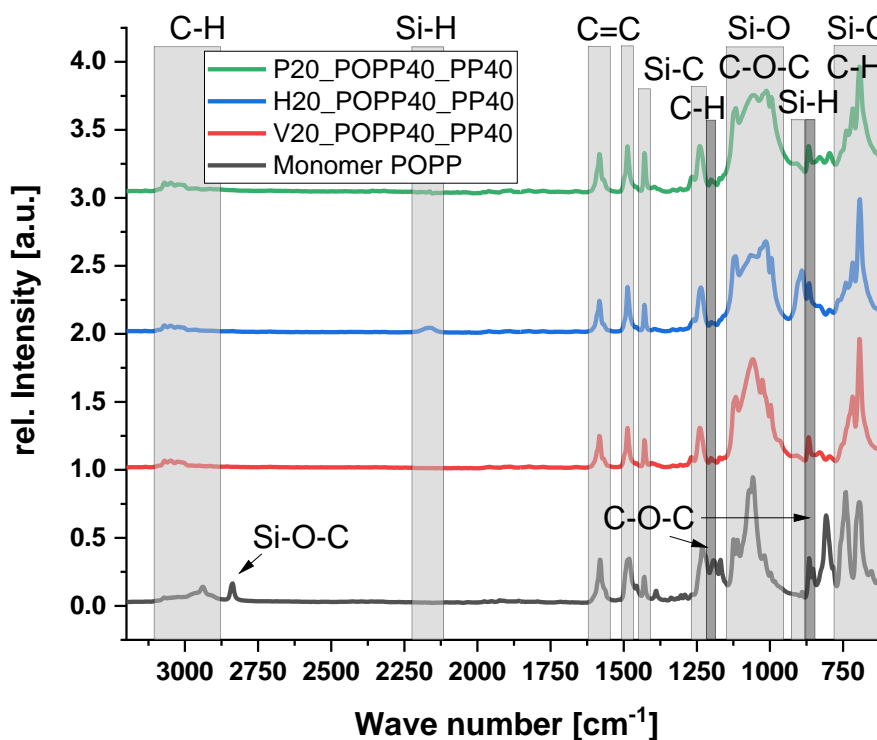
Figure 156: FT-IR spectra of the phenoxyphenyl monomer, the vinyl and hydride copolymer as well as the cured polysiloxane.

4.5.1.2.2 NMR spectra of phenoxyphenyl-group containing copolymers

The ^{1}H and ^{13}C NMRs area displayed in the experimental section (Figures 366 – 367 and 369 – 371). The two copolymers show aromatic bands in the ^{1}H NMR spectrum of the phenyl- and phenoxyphenyl-groups from 6.7 ppm to 7.7 ppm, while the vinyl copolymer has additional bands at 5.6 ppm to 6.2 ppm of the vinyl-group.[136] The hydride copolymer shows the hydride bands at 4.6 ppm to 5.0 ppm and the methyl-groups at −0.5 ppm to 0.3 ppm.[136] In the [29]Si spectrum (Figure 157) of the vinyl copolymer, the signals of the phenylvinylsiloxane (V) and the diphenylsiloxane (PP) are visible in the area of −43 ppm and of −46 ppm, respectively.[331, 368] The 4-(phenoxy)phenylphenylsiloxane signals (POPP) are also in this area.[55, 84] The phenyltrimethoxysilane which remained after the purification generates a small signal at −79 ppm,[321, 324, 368] which can only be observed in ^{1}H ^{29}Si HMBC experiment (Figure 367) because of the glass signal of the NMR tube. In the spectrum of the hydride copolymer, the methylsiloxane (H) signals are located in the area around −33 ppm.[323-324, 331] The signals of PP and POPP are again visible at −46 ppm.[331, 368] In the ^{1}H ^{29}Si HMBC NMR (experimental section, Figure 370) small impurities are also present. Besides the phenylsiloxane T signal at −78 ppm from the remaining PhSi(OMe)$_3$ monomer, [321, 324, 368] some -O-PhSiOH-O- T signals at −71 ppm are also present.
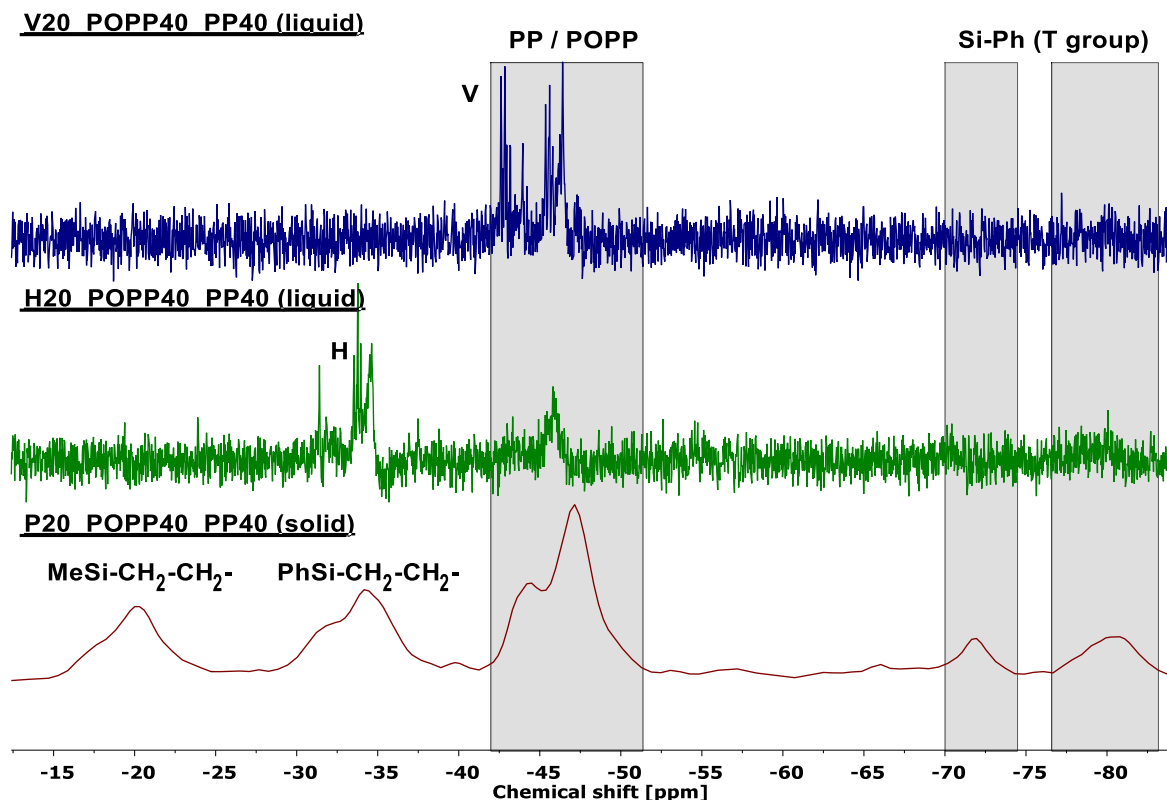
Figure 157: [29]Si liquid (79 MHz, CDCl$_3$) and ^{29}Si CP MAS (80 MHz, 13 kHz) NMR of phenoxyphenyl-group containing polymers.

They also resulted from the PhSi(OMe)$_3$ monomer but did not condensate completely.[321] Additionally some methoxy-groups connected to a silicon atom which generates a signal at −37 ppm related to the hydridomethyl-group is visible. Mosley *et al.* stated out that during the hydride polymerisation some hydride-groups branched, they detected this in the ^{29}Si NMR but did not report any data.[136] The resulting methylsiloxane T group generates signals between −55 ppm to −65 ppm, depending on whether all hydroxyl-groups condensed.[321, 324, 331] These groups could not be observed even in the more sensitive ^{1}H ^{29}Si HMBC NMR spectrum. In the ^{29}Si CP MAS NMR, the signals of the Si-CH$_2$-CH$_2$-Si bridge are present at −20 ppm for the methyl-containing silicon atom from the Si-H group[331, 333] and at −34 ppm for the phenyl-containing silicon atom from the former Si-V group,[331, 368] which indicates a successful hydrosilylation reaction. The PP and POPP bands are unchanged at −47 ppm[331, 368] and at −71 ppm and −80 ppm are the phenylsiloxane T groups[321, 324, 368] visible, respectively.

4.5.1.2.3   Thermogravimetric analyses of phenoxyphenyl-group containing polymers

Thermogravimetric analyses (Figure 158) were performed for both copolymers as well as for the cured polysiloxane under O$_2$ and N$_2$. The hydride and vinyl polymers show low T$_{95\%}$ temperatures because of toluene that was used in the washing process which evaporates between 100 °C and 200 °C.[419] The solvent remains inside the polymer despite applying high vacuum for eight hours. The vinyl polymer shows a decomposition temperature of 391 °C under oxygen and 349 °C under nitrogen atmosphere, while the hydride material decomposes at 274 °C under oxygen and at 177 °C under nitrogen atmosphere. The amount of toluene is different between the measurements under oxygen and nitrogen atmosphere because the sample rested for a different amount of time in the auto sampler.
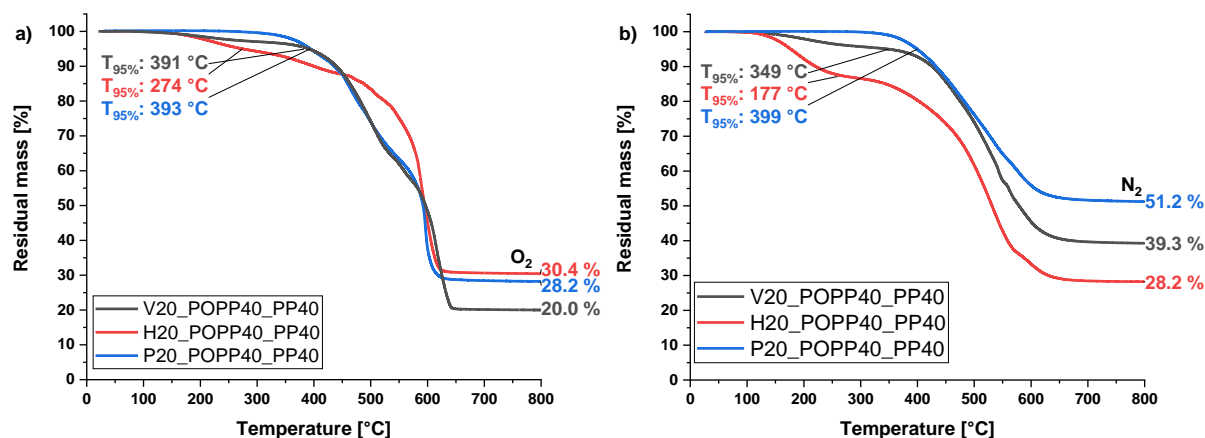
Figure 158: TGA of phenoxyphenyl-group containing polymers, a) under oxygen and b) under nitrogen atmosphere

The residual mass cannot be compared because of the different amount of toluene in the different samples. The cured polysiloxane P20_POPP40_PP40 shows a similar decomposition curve

under both atmospheres, the $T_{95\%}$ value is close to 400 °C. The unzipping mechanism is slower under nitrogen atmosphere than under oxygen,[356] but on the contrary the activation energy is higher under nitrogen,[376] which results in similar values of the $T_{95\%}$ temperature. The residual mass under oxygen is 28 % and the decomposition product should mainly consist of silica while under nitrogen it is over 50 %, which is caused by the different decomposition mechanisms. A side-group oxidation cannot occur under nitrogen and the cross-linking at some point hinders the unzipping and intramolecular backbiting (IBBM) processes.[218]

4.5.1.2.4 <u>Differential scanning calorimetry of phenoxyphenyl-group containing polymers</u>
DSC measurements of the hydride and vinyl polymer as well as of the cured polysiloxane were performed from −40 °C to 150 °C (Figure 159). The glass transition temperature of V20_POPP40_PP40 (Table 31) was measured with 14.3 °C. The group of Mosely et al.[136] reported it with 2.5 °C for their vinyl polymer where the vinyl-group is only at the end of the chain.
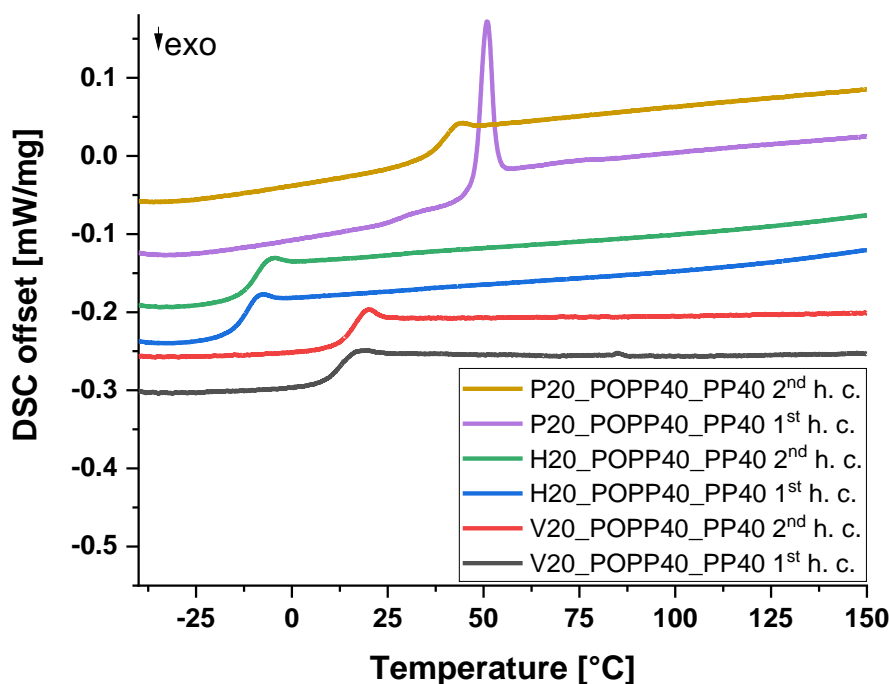
Figure 159: DSC measurements of the phenoxyphenyl- and hydride- or vinyl-group containing copolymers as well as the cured phenoxyphenyl-group containing polysiloxane.

Both polymers consist of three different monomers, where the diphenyl and phenoxy-phenylphenyl repeating units are present in both polymers. The amount of diphenyl component is 40 mol% in the self-prepared polymer and 52 mol% in the literature and the amount of the phenoxyphenylphenyl monomer is 40 mol% in the self-synthesised system and 35 mol% in the one from Mosley et al.[136] On one hand, the higher amount of vinylphenylsiloxane-groups (20 mol%) decreases the T_g value of the self-synthesised polymer because the other monomers

are sterically more demanding[136, 402-403] in comparison to the 13 mol% of the vinylphenylme-thylsiloxane end group from Mosley *et al.*[136] On the other hand, the higher amount of POPP increases the glass transition temperature. The largest difference is the polymer length, the self-prepared polymer is three to four times longer, which increases the T_g value.[121, 455, 496] All these effects lead to an increase of the glass transition temperature by around 12 °C.

Table 31: Glass transition temperature, melting point and melting energy of the phenoxyphenyl-group containing polysiloxanes as well as of the literature systems from Mosley *et al.*[136]

Polymer	T_g [°C]	T_m [°C]	E_m [J/g]
V20_POPP40_PP40	14.3	85.1	0.018
H20_POPP40_PP40	−10.4	−	−
P20_POPP40_PP40	38.1	50.9	4.998
VPM13.1_POPP34.5_PP52.5	2.5	−	−
HM60_PP40	−50.0	−	−

The T_g value of H20_POPP40_PP40 was −10.4 °C, the value is around 25 °C lower than the one from the vinyl polymer because of the substitution of the vinylphenylsiloxane-group with a sterically less demanding hydridomethylsiloxane one.[119, 121, 136, 496] In comparison with the hydride copolymer from Mosley *et al.*, which is a pure poly[hydridomethyl-*co*-diphenyl]silox-ane (HM60_PP40) without any phenoxyphenyl-groups,[136] the self-prepared polysiloxane contains these 4-(phenoxy)phenylphenylsiloxane-groups and therefore is structurally comparable to the self-prepared vinyl polymer. Without these sterically demanding phenoxyphenyl-groups, their T_g value is −50.0 °C with a composition of 60 mol% hydridomethylsiloxane and 40 mol% diphenylsiloxane, which is in accordance with other literature.[119, 403] The glass transition temperature of the cured polysiloxane was determined with 38.1 °C, which is higher than the ones from the polymers because during the hydrosilylation process additional cross-linking occurs which reduces the degrees of freedom of the whole polymer.[121, 319, 400, 496]

For the vinyl polymer and the cured polysiloxane a melting point could also be determined. The vinyl copolymer shows a high melting point at 85.1 °C resulting from the high aromatic content, but only with a very small enthalpy of 0.018 J/g which is almost negligible.[121, 462, 496-497] The cured polysiloxane P20_POPP40_PP40 shows a value of 50.9 °C[121, 462, 496-497] with a stronger enthalpy of around 5 J/g. Mosley *et al.* did not report melting points and therefore they cannot be compared with the literature system.[136]

4.5.1.2.5 Refractive indices and viscosity of phenoxyphenyl-group containing polymers

The refractive indices of the prepared hydride and vinyl-group containing copolymers and of the cured polysiloxane are presented in Table 32. The hydride copolymer contains less phenyl-groups compared to the vinyl one because of the use of methyldiethoxysilane instead of vinylphenyldiethoxysilane. The refractive index of the hydride copolymer is therefore only 1.595 compared to 1.610 of the vinyl copolymer. The copolymers synthesised by Mosley *et al.* were named analogously to the self-chosen nomenclature in the table to compare the used amount of each monomer. Because they used vinylphenylmethylsiloxane which was not used in this research, the new abbreviation VPM was used. The chemically different vinyl copolymer (Figure 149) from Mosley *et al.* shows a RI of 1.615 while the phenoxyphenyl free hydride polymer shows a RI of 1.546.[136] Mixing and curing the polymers increases the refractive index from an averaged 1.60 for the hydride and vinyl copolymer up to 1.613 for the self-prepared cured polysiloxane. Mosley *et al.* reached only 1.600 because of the use of the lower RI hydride polymer.[136] Noteworthy, the RI often decreases with larger wavelengths and can be calculated using the Sellmeier formula,[498] but the difference in this area is neglectable.

Table 32: Refractive indices of phenoxyphenyl-group containing polymers.

Substance self-synthesised	RI at 589 nm	Substance synthesised by Mosley *et al.*[136]	RI at 633 nm
V20_POPP40_PP40	1.610	VPM13.1_POPP34.5_PP52.4	1.615
H20_POPP40_PP40	1.595	HM60_PP40	1.546
P20_POPP40_PP40 (1H:1V)	1.613	Cured polymer (2H:1V)	1.600

The rheological properties of the copolymers at 25 °C were also studied. The vinyl component showed a viscosity of 40200 ± 2500 mPa·s and the hydride component one of 2160 ± 10 mPa·s. The viscosity of the vinyl component is higher because the difference between them are the hydridomethyl-group compared to the sterically more demanding vinylphenyl one. Mosley *et al.* measured a viscosity from 317000 mPa·s to 1756000 mPa·s for the vinyl component at 25 °C, which strongly depends on the remaining toluene inside the polymer.[136] They had not measured the viscosity of the hydride copolymer and gave no further information on how the viscosity was determined.[136] The viscosity of the self-synthesised hydride component is in the range of the commercial ones (see 4.1.1.5 and 4.1.2.5), but the one of the vinyl component is an order of magnitude higher. A small amount of toluene, which remains inside the polymer is therefore suitable for the handling and processing.

4.5.1.2.6 Average molecular weight of phenoxyphenyl-group containing polymers

The average molecular weights determined by SEC measurement as well as ^{1}H NMR calculations are given in Table 33.

Table 33: Average molecular weights determined by SEC and ^{1}H NMR of the phenoxyphenyl-group containing polymers as well as the reference systems.[136]

	Mw [g/mol]	PDI	Mw [g/mol]	PDI
	V20_POPP40_PP40		*H20_POPP40_PP40*	
^{1}H NMR	29100	–	18700	–
SEC analysis [RI detector]	3670	1.27	3290	1.38
SEC analysis [UV detector]	3640	1.26	3260	1.37
SEC analysis [Mosley *et al.*][136]	*VPM13.1_POPP34.5_PP52.5*		*HM60_PP40*	
	900 – 1200	–	3500 – 5000	–

To calculate the molecular mass by ^{1}H NMR spectroscopy, an end group without methyl-, phenyl-, hydride- or vinyl-groups has to be introduced because of the previously mentioned reasons. Therefore, *tert*-butyldimethylchlorosilane is suitable like in the previous M_W calculations.[89,90] The chlorosilane reacts in a basic solution in tetrahydrofuran at 55 °C with the OH end groups of the hydride or vinyl polymer (Figure 160).[136, 471]
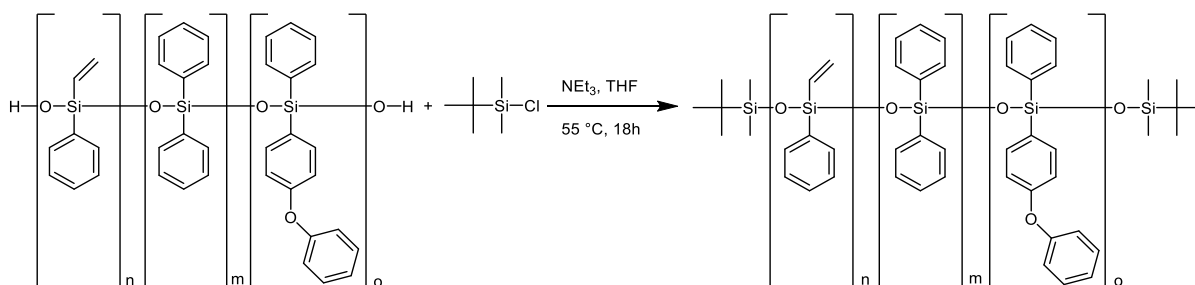
Figure 160: Reaction scheme of V20_POPP40_PP40 with *tert*-butyldimethylchlorosilane for calculating the average molar mass by ^{1}H NMR spectroscopy.

The calculated masses for the vinyl-group containing copolymer are around 30000 g/mol and for the hydride-group containing copolymer are around 20000 g/mol. The SEC measurements show the same tendency but completely different values with 3700 g/mol for the vinyl and 3000 g/mol for the hydride copolymer. Comparing the SEC values of the self-synthesised copolymers with the one from Mosley *et al.*, which were polymerised using the same catalysts but slightly different monomers, the self-synthesised vinyl component shows a M_W three- to four-times larger, while the hydride is in the lower M_W area like in literature.[136] The same flow rate and eluent were used as well as a RI detector. Also a polystyrene calibration was performed

by Mosley *et al*. Noteworthy to mention is that the hydride polymer in the literature does not contain any sterically demanding phenoxyphenyl-groups, which limit the reaction speed.[472]

4.5.1.2.7 <u>UV/Vis measurements and thermal aging test of phenoxyphenyl-group containing polymers</u>

The cured samples of P20_POPP40_PP40 (Figure 161) are colourless and hard even when the sample thickness is around 2 mm.
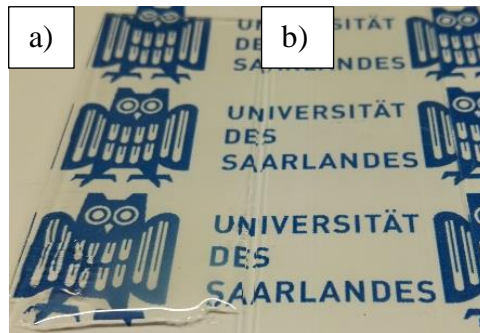
Figure 161: Image of the phenoxyphenyl-group containing polymers, a) 2 mm thick sample and b) 120 μm thick sample.

UV/Vis spectra of the doctor bladed sample onto the glass slide were recorded using an integration sphere. The transmission was corrected against a sample free glass slide and is around 100 % in the visual range of the spectrum (Figures 162, a) and 163, a)). The haze value is around 17 % for the near UV area and decreases down to two in the infrared area.

A thermal treatment for 63 days at 180 °C was also performed to evaluate the transmission decrease during the LED operation (Figures 162 and 163, b)). The humidity in the oven was not changed. The temperature was chosen because of earlier mentioned reasons. When comparing the glass slides, some slightly yellow areas are now visible. A transmission of over 95 % at 450 nm can be maintained throughout the whole experimental time of 1512 h. The haze value decreases from 11 % to 6 % after 24 hours but remains at 6 % to 7 % during the next 62 days. Mosley *et al.* maintained a slightly lower transmittance of over 90 % at 200 °C for seven weeks (1176 h).[136] The high transmission of around 100 % even during heat exposure makes the material very suitable for optoelectronic applications.
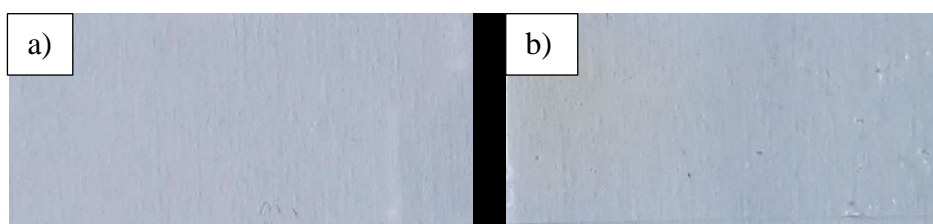
Figure 162: P20_POPP40_PP40 doctor bladed (120 μm) onto a glass slide, a) before and b) after the thermal treatment at 180 °C for 63 days.
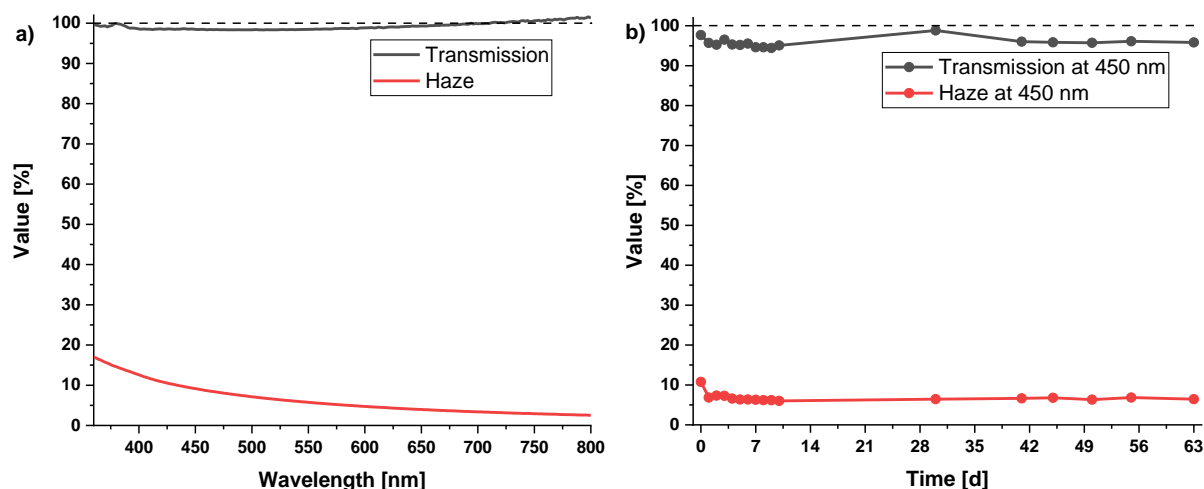
Figure 163: Transmission and haze values of P20_POPP40_PP40 a) after the synthesis and b) during the 63 days thermal treatment at 180 °C.

Yellowness and whiteness indices were calculated before and after the thermal aging using the operating UV/Vis software UV Winlab. The yellowness index changed from 0.3 to 2.5 which implies a colouration from nearly colourless to slightly yellow. The whiteness index shows the same tendency, from a value close to 100 in the beginning down to 92.5 which also shows a slight yellow colouration. The effect of the yellowing due to the temperature is also observed by Mosley *et al.* Additionally, they showed a dependence of the amount of platinum catalyst which increases the yellowing with increasing amount of platinum.[136] They suggested an amount under 2.00 ppm because then the yellowing effect is negligible. A lower amount of 1.63 ppm was therefore used.

Table 34: Yellowness and whiteness indices of P20_POPP40_PP40 after the synthesis and after the 63 days under 180 °C.

P20_POPP40_PP40	YI	WI
after synthesis	0.3	98.4
after 63d	2.5	92.5

4.5.1.3 Conclusion of phenoxyphenyl-group containing polysiloxanes

The 4-(phenoxy)phenylphenyldimethoxysilane monomer published by Mosley *et al.* was successfully synthesised and characterised. In addition to the published literature a single crystal structure analysis of the monomer was obtained. The prepared vinyl respectively hydride co-polymers already showed refractive indices around 1.600, which increased to 1.613 after the curing process. The commercial OE-6630 system only shows a RI of 1.552. A thermally stable material could be received, which is stable up to 400 °C under inert or oxidative atmosphere, which is slightly lower than the 420 °C of the cured OE-6630. The T_g higher than 50 °C is very high compared to the 5 °C of OE-6630 because of the bulky side-groups. The highly transparent polysiloxane P20_POPP40_PP40 (Figure 164) remains its transmission of over 95 % even under 180 °C for 63 days, which is slightly lower than the 100 % of the commercial system. The polymer shows only a slight yellow colouration after the treatment, which was verified by the yellowness and whiteness indices while the OE-6630 system shows no yellow colour at all. Therefore, the synthesised polysiloxane is very suitable for LED applications and achieves or exceeds the properties of the commercial OE-6630.
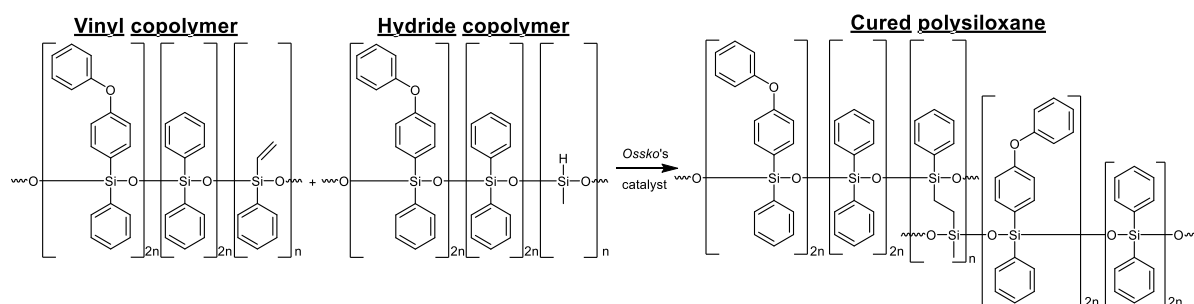
Figure 164: Chemical structure of the cured P20_POPP40_PP40 and of the hydride and vinyl copolymers.

4.5.2 Synthesis and characterisation of phenylthiomethyl-group containing polysiloxanes

To create a new curable polysiloxane which is miscible at room temperature, the thioanisole side-group (PSM) instead of the phenylthiophenyl (PSP) one was used. The formal substitution of the outer phenyl-group which is connected to the sulfur atom with a methyl one should lower the viscosity drastically while remaining the huge RI impact of the sulfur atom. Additionally, the diphenylsiloxane monomer was alternated to a dimethyl- (MM), phenylmethyl- (PM) or diphenylsiloxane (PP) one to investigate the impact of these groups, respectively. The low viscosity of the thioanisylphenyl-group containing monomer (PSMP) allows a doubling of the sulfur content from 40 mol% to 80 mol% content relative to the silicon atoms. The 4-(methylthio)phenylphenyldimethoxysilane was synthesised using the same adjusted Grignard reaction from Mosley *et al.*[136] which was used for the 4-(phenoxy)phenylphenyldimethoxysilane (4.5.1.1) synthesis. The resulting four curable sulfur containing polymer systems (Figure 165) were also intended for OSRAMs study purposes and are therefore produced on a large scale. In comparison with the literature described method, the copolymers were again synthesised differently using other monomers analogously to the P20_POPP40_PP40 system (Figure 149).[136]
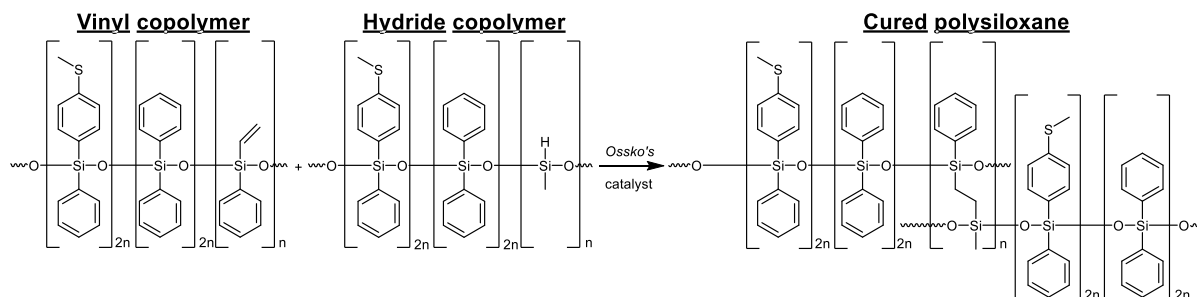
Figure 165: Chemical structure of a vinyl (V20_PSMP40_PP40) and a hydride (H20_PSMP40_PP40) copolymer as well as the resulting cured polysiloxane (P20_PSMP40_PP40).

4.5.2.1 Synthesis and characterisation of 4-(methylthio)phenylphenyldimethoxysilane

The synthesis of the monomer 4-(methylthio)phenylphenyldimethoxysilane (PSMP) was carried out in a Grignard reaction using 4-bromothioanisole and phenyltrimethoxysilane in THF (Figure 166). The slightly yellow crude product was purified by distillation to remove the colour in 67 % yield. After storing the monomer for one year under argon atmosphere, the monomer again showed a yellow colour. Therefore, the monomer has to be freshly distilled every time before continuing with the polymerisation step. The refractive index of the product was 1.578 at 20 °C and 589 nm.
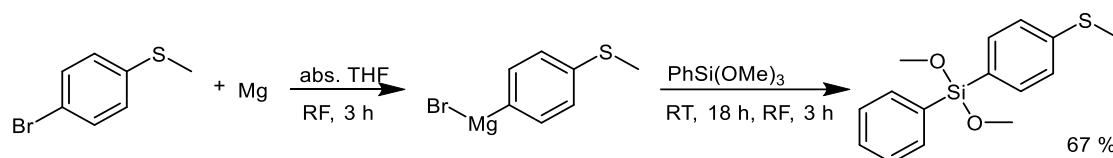
Figure 166: Synthesis of 4-(methylthio)phenylphenyldimethoxysilane.

The FT-IR spectrum is discussed in 4.5.2.2.1 with the spectra of the copolymers. ^{1}H, ^{13}C, and ^{29}Si NMR spectra were recorded, the ^{13}C NMR is shown in the experimental section (Figure 373). In the ^{1}H NMR (Figure 167) all required peaks are present. The phenyl protons are located in the region from 7.3 ppm to 7.8 ppm, the methyl-group at the sulfur atom shows a signal at 2.5 ppm and the methoxy-groups are located at 3.7 ppm.[136] Around 0.8 % additional phenyltrimethoxysilane is also present, which is detected by the integration of the methoxy-groups and the phenyl protons at 7.5 ppm.[433, 441]
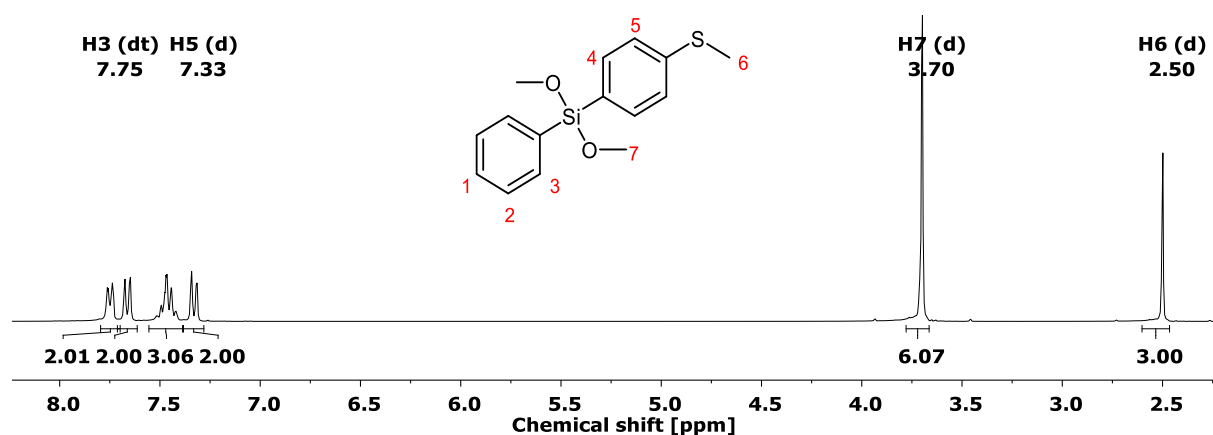
Figure 167: ^{1}H NMR (300 MHz, CDCl₃) of 4-(methylthio)phenylphenyldimethoxysilane.

In the ^{29}Si NMR (Figure 168), a strong signal at −28.8 ppm is visible, which relates to the product and is in the typical range of methoxylated aromatic D[0] type silicon atoms.[490] A small signal at −54.4 ppm is also present and refers to the remaining T[0] type phenyltrimethoxysilane that was not fully removed by the distillation.[433, 441]
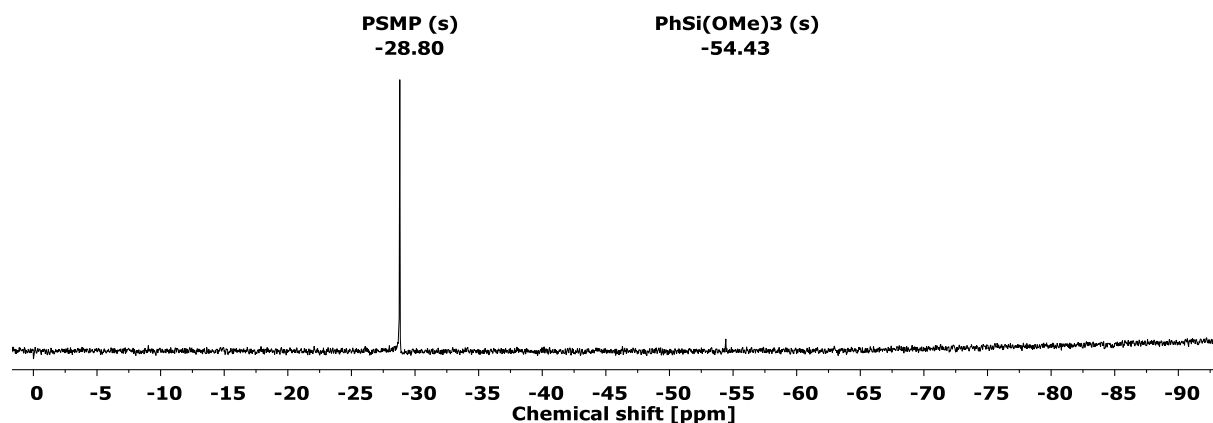
Figure 168: ^{29}Si NMR (60 MHz, CDCl₃) of 4-(methylthio)phenylphenyldimethoxysilane.

4.5.2.2 Synthesis and characterisation of the hydride or vinyl and phenylthiomethyl-group containing copolymers

Analogously to previous polysiloxane syntheses, the prepared 4-(methylthio)phenylphenyl-dimethoxysilane (PSMP) was reacted with diphenyl- (PP), phenylmethyl- (PM) and dimethyl- (MM) group containing D monomers as well as the required hydridomethyl (H) or vinylphenyl (V) monomer (Figure 169). For the hydride polymerisation concentrated hydrochloric acid was used and for the vinyl one tetra-*n*-butylammonium hydroxide solution.[136] In addition, a polymer was prepared without a lower refractive index monomer (MM, PM or PP), therefore the amount of PSMP therefore was doubled. In all cases colourless oils with light to medium viscosity were obtained, which were analysed using NMR and FT-IR spectroscopy and DSC, TGA and SEC measurements. The viscosity and the RI were also determined. The synthesised linear polysiloxanes were assigned according their consisting monomers (Figure 169).
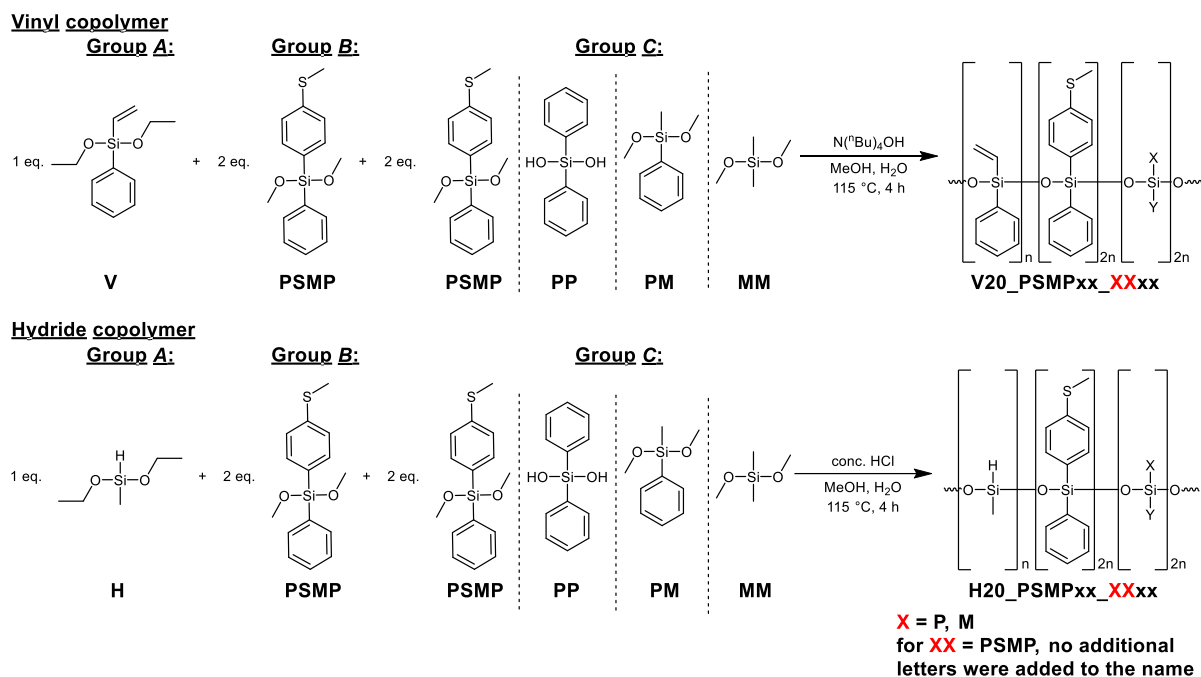
Figure 169: Syntheses and nomenclature of phenylthiomethyl-group containing polysiloxanes.

For the copolymers, the first letter is either V or H to indicate the type of the reactive side-group. To show the condensation of the hydrosilylated, solid polymer, it is named "P" instead of "V" or "H". Following each monomer abbreviation, the amount present inside the copolymer or cured polysiloxane is shown in mol%. After the first letter, four letters (PSMP) follow to indicate the sulfur containing aromatic side-group *B*. The two penultimate letters (XX) show the lower refractive index monomer from group *C* "MM" (dimethyl), "PM" (phenylmethyl) or "PP" (diphenyl). The content for the hydride or vinyl-group containing monomer is remained at 20 mol%. The PSMP content was 40 mol% like the POPP content and the content of the group *C* monomers was therefore also 40 mol%. In case of choosing PSMP as third monomer,

the PSMP content was then 80 mol%, and no additional third monomer letters are used (X20_PSMP80).

4.5.2.2.1 FT-IR spectra of the phenylthiomethyl-group containing copolymers and PSMP

FT-IR spectra of the monomer 4-(methylthio)phenylphenyldimethoxysilane as well as the phenylmethyl- and hydride- or vinyl-group containing copolymers as representatives (X20_PSMP40_PM40) are shown in Figure 170. The remaining ones are display in the experimental section (Figures 375 and 382). The monomer shows the typical vibrations of the Si-O bond at 1000 cm^{-1} to 1100 cm^{-1} and of the Si-C bond at 1383 cm^{-1}, at 1259 cm^{-1} and at 796 cm^{-1}.[234-235, 319, 346-347, 349-350, 370] The vibration of the C-C$_{Ar}$ bands are visible at 1581 cm^{-1}, at 1487 cm^{-1} and at 1429 cm^{-1} and of the C-H bond at 3073 cm^{-1}, at 3052 cm^{-1}, at 2960 cm^{-1}, at 2919 cm^{-1}, at 751 cm^{-1}, at 725 cm^{-1} and at 696 cm^{-1} like for the previously mentioned copolymers.[234-235, 319, 346-347, 349-350, 370] The methoxy signal can be observed at 2837 cm^{-1} and at 1190 cm^{-1}.[346]
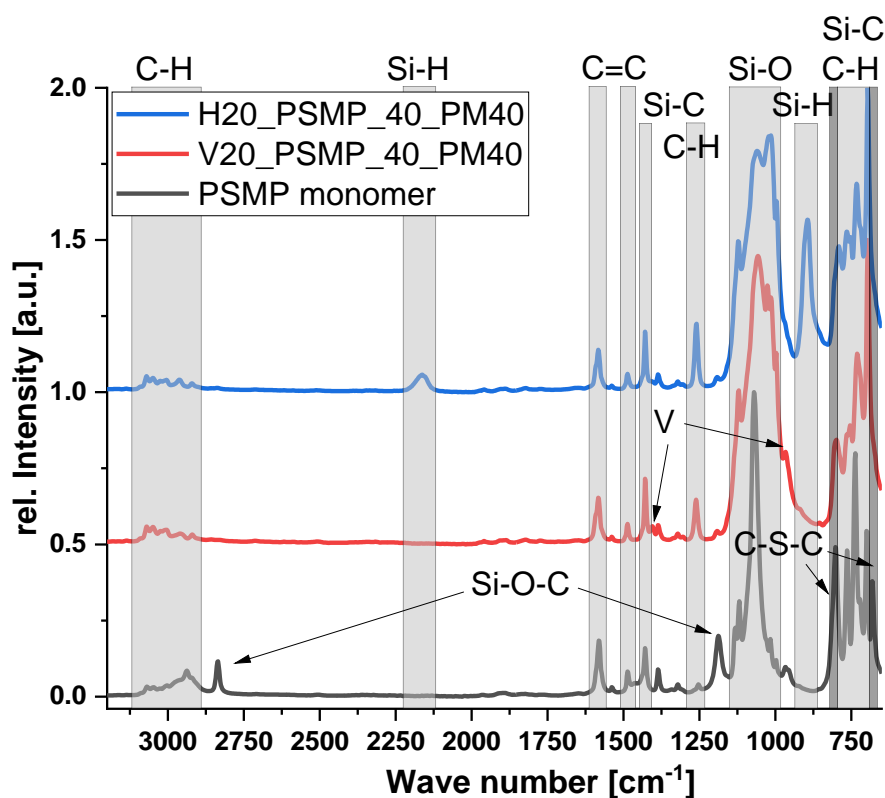
Figure 170: FT-IR spectra of the PSMP monomer and the copolymers of X20_PSMP40_PM40.

The thioether vibration (dark grey) is located at 800 cm^{-1} and at 681 cm^{-1} but both are barely visible due to overlapping with other strong bands.[499] The copolymers show additional bands, the vinyl copolymer has signals at 1406 cm^{-1} and at 963 cm^{-1} representing the vinyl-group in V20_PSMP40_PM40.[26,27,48,85] The hydride component H20_PSMP40_PM40 in contrast, shows additional Si-H signals at 2162 cm^{-1} and at 896 cm^{-1}.[234-235, 319, 346-347]

4.5.2.2.2 NMR spectra of the phenylthiomethyl-group containing copolymers

^{1}H, ^{13}C, and ^{29}Si NMR spectra were recorded from the produced copolymers (Figures 376 – 379 and 383 – 386). The spectra show all the expected signals. The typical chemical shifts in the proton NMR of the side-groups are shown below in Table 35.[136] The ^{29}Si NMRs of these two copolymers are shown and discussed with the ^{29}Si CP MAS NMR in chapter 4.5.2.3.1.

Table 35: Chemical shifts of the side-groups in the proton NMR.

Side-groups	Chem. shift [ppm]	Functional side-groups	Chem. shift [ppm]
Methyl (M)	−0.5 to 0.4	Hydride (H)	4.5 to 5.2
Aryl (P and PSM)	6.8 to 7.8	Vinyl (V)	5.4 to 6.3
Thiomethyl (PSM)	2.2 to 2.5		

4.5.2.2.3 Molecular weight determination of the phenylthiomethyl-group containing co-polymers

To determine the molecular weight, both SEC and ^{1}H NMR were used. The SEC analyses were performed using the as prepared linear polysiloxanes dissolved in THF. For the ^{1}H NMR determination, special end groups were introduced that can be used as reference for the calculation like in the analysis of previous copolymers. Therefore the linear polysiloxanes were dissolved, treated with absolute triethylamine and *tert*-butyldimethylchlorosilane and stirred at 55 °C for 18 hours (Figure 171).[136, 221, 470-471] The calculated as well as the measured average values are displayed in Table 36. The molecular weights determined by ^{1}H NMR are mostly between 4400 g/mol and 13600 g/mol, with the hydride-containing dimethyl component (H20_PSMP40_MM40) having a much higher molecular weight of 43200 g/mol. The molecular masses determined by the SEC measurement vary between 2200 g/mol and 17400 g/mol.
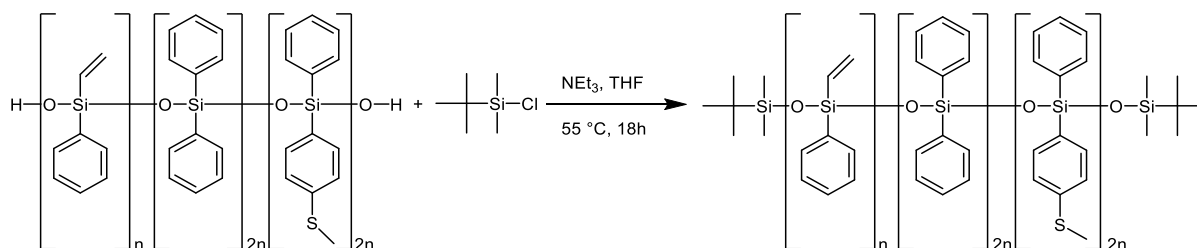
Figure 171: Reaction scheme of V20_PSMP40_PP40 with *tert*-butyldimethylchlorosilane.

Despite the Mw being in the same range for both methods, no correlation can be made. For the dimethyl-containing polysiloxanes both SEC values of around 3000 g/mol are drastically lower than the 11000 g/mol or 13000 g/mol calculated by ^{1}H NMR. A smaller SEC value could be explained because the highly methylic copolymers tend to agglomerate in THF. The phenylmethyl-group containing copolymers (X20_PSMP40_PM40) show the opposite trend, the SEC

measurements show masses 3000 g/mol higher than the NMR calculations. The diphenyl containing polymers (X20_PSMP40_PP40) show no correlation, while for the hydride one the SEC value is with 17400 g/mol around 13000 g/mol higher than the NMR calculation and the vinyl SEC values are with 7100 g/mol around 2200 g/mol lower than the NMR calculation. The highly 4-(methylthio)phenylphenyl-group containing copolymers (X20_PSMP80) show values like the dimethyl containing ones (X20_PSMP40_MM40) where the NMR calculations are significantly higher than the SEC value although the difference is not that large. The PDI values of the SEC measurements correlate with the molecular mass determined by SEC, they increase with increasing M_W indicating a broadening of the mass distribution like seen in the kinetic studies.

Table 36: Molar masses of the copolymers, obtained from ^{1}H NMR and SEC.

Group *A* monomers [20 mol%]	Group *B* monomers [40 mol%]	Group *C* monomers [40 mol%]	M_W [g/mol] by ^{1}H NMR calculations	M_W [g/mol] by SEC analyses	PDI by SEC analyses
H		MM	34200	3300	1.45
V			11100	3200	1.26
H		PM	8900	12300	2.55
V	PSMP		13300	16200	2.72
H		PP	4400	17400	3.37
V			9300	7100	1.75
H		PSMP	13600	8100	2.19
V			9500	2200	1.14

4.5.2.2.4 <u>Viscosity of the phenylthiomethyl-group containing copolymers</u>

The viscosity at 25 °C was determined using a rheometer, the samples were measured for ten minutes and the average was calculated (Table 37), the standard deviation is reported in the experimental section (6.2.9). The viscosity increases with increasing polymer length (M_W) and sterically more demanding side-groups like phenyl compared to methyl ones.[452-453] The viscosity of the hydride copolymers is generally lower than the one of the vinyl polymers because of the sterical difference in the hydridomethyl-group compared to the vinylphenyl one. Also, when comparing each set, the viscosity increases from the X20_PSMP40_MM40 copolymer to the X20_PSMP40_PP40 ones with each methyl to phenyl switch by a factor of 2 to 17. In the hydride-group the viscosity doubles for each switch, while in the vinyl-group the increase is larger and reaches 1.5 million mPa·s for V20_PSMP40_PP40. The samples with 80 mol% PSMP content (X20_PSMP80) show the expected effect, the additional flexible thiomethyl-

group drastically lowers the viscosity compared to X20_PSMP40_PP40 by a factor of 10 from 14000 mPa·s to 1400 mPa·s for the hydride ones and from 1.5 million mPa·s to 150000 mPa·s for the vinyl ones.[450-451, 454] The additional-group also leads to more branching, which when comparing two polymers with the same M_W, reduce the viscosity.[450-451, 454] Overall, the strong effect that larger molecular weights drastically increasing the viscosity[450-454] can hardly be seen here, because the determined M_W is neither constant nor increasing when substituting the methyl-groups with phenyl ones. Additionally, the hydride copolymers often have higher molecular weights than the relating vinyl ones but still have a much lower viscosity.

Table 37: Average viscosity for the hydride or vinyl and phenylthiomethyl-containing copolymers.

Hydride copolymer	Viscosity at 25 °C [mPa·s]	Vinyl copolymer	Viscosity at 25 °C [mPa·s]
H20_PSMP40_MM40	2190	V20_PSMP40_MM40	10000
H20_PSMP40_PM40	5250	V20_PSMP40_PM40	87600
H20_PSMP40_PP40	13800	V20_PSMP40_PP40	1490000
H20_PSMP80	1400	V20_PSMP80	151000

4.5.2.2.5 **<u>Refractive index of the phenylthiomethyl-group containing copolymers</u>**

The refractive index of the hydride and vinyl-group containing copolymers (Table 38) were measured in transmission mode at 20 °C using 589 nm wavelength. High refractive indices between 1.564 and 1.623 were achieved, despite a small amount of toluene being present which reduces the RI because of its smaller value of 1.500.[419] The comparison of the refractive indices shows that the vinyl components have a 0.015 to 0.027 higher value than the relating hydride components with the same amount and type of group *B* and *C* monomers, because the hydridomethyl-group has a drastically lower RI than the vinylphenyl one. When comparing the diethoxy monomers, a difference of 0.105 can be determined (MeHSi(OEt)$_2$: 1.375; PhVSi(OEt)$_2$: 1.480).[419] The successive substitution of the two methyl-groups of the low refractive index monomer starting from V20_PSMP40_MM40 by one phenyl-group (…MM40 → …PM40) shows an increase from 1.580 to 1.599 (+0.020) for the first substitution. The second substitution (…PM40 → …PP40) shows a smaller but still significant increase of +0.017 and exceeds the value of 1.600. If a phenyl-group is replaced by a thioanisole-group (V20_PSMP40_PP40 → V20_PSMP80), the refractive index again slightly increases by 0.007 to 1.623.

The hydride copolymers (H20_PSMP40_MM40) show the same trend when a successive substitution of the dimethyl-groups with phenyl-groups occur. The first substitution (…MM40 →

…PM40) increases the RI from 1.564 to 1.580 by a value of 0.016, where the second one (…PM40 → …PP40) raises the value by 0.019. The addition of the methylthioether-group (H20_PSMP40_*PP*40 → H20_PSMP80) does slightly decreases the RI by 0.003, probably because of more remaining toluene in the H20_PSMP80 copolymer.

Table 38: RIs of the hydride and vinyl 4-(methylthio)phenylphenyl-containing polysiloxanes.

Hydride copolymer	RI at 20°C, 589 nm	Vinyl copolymer	RI at 20°C, 589 nm
H20_PSMP40_MM40	1.564	V20_PSMP40_MM40	1.580
H20_PSMP40_PM40	1.580	V20_PSMP40_PM40	1.599
H20_PSMP40_PP40	1.599	V20_PSMP40_PP40	1.616
H20_PSMP80	1.596	V20_PSMP80	1.623

4.5.2.2.6 <u>Thermogravimetric analyses of the phenylthiomethyl-group containing copolymers</u>

TG analyses were performed from the prepared hydride and vinyl copolymers (experimental section, Figures 388 and 389). The measurements were performed under O_2 and N_2. Table 39 presents the decomposition temperatures for the copolymers. The $T_{95\%}$ value indicates the temperature at 5 % mass loss, where the decomposition starts.[222, 351] The $T_{95\%}$ values under oxygen vary between 230 °C and 370 °C while under nitrogen between 200 °C and 360 °C. The difference between the $T_{95\%}$ values of one copolymer under oxygen and nitrogen varies up to 30 °C. Except for the highly methylic H20_PSMP40_MM40, all decomposition temperatures at 5 % mass loss are higher under oxygen atmosphere than under nitrogen. Li *et al.* reported this phenomenon for poly(*p*-phenylene sulfide) and the reason is the higher activation energy of the decomposition under oxygen atmosphere than under nitrogen.[376] The hydride copolymers always show lower decomposition temperatures than the relating vinyl ones, which is due to the lower phenyl content because of the use of hydridomethylsiloxane instead of vinylphenylsiloxane.[222] While X20_PSMP40_MM40 and X20_PSMP40_PM40 show a difference of the $T_{95\%}$ between the hydride-group containing copolymers of up to 50 °C, X20_PSMP40_PP40 shows a difference of 160 °C. The decomposition of V20_PSMP80 although starts only 10 °C later than H20_PSMP80 under a nitrogen atmosphere, while under oxygen no difference can be measured. Comparing the group *C* monomers (MM, PM, PP, PSMP) under oxygen atmosphere, the $T_{95\%}$ value increases from MM to PM from 280 °C to 310 °C for the hydride ones, because of the higher phenyl content.[222] The PP and PSMP hydride copolymers show lower values around 230 °C. V20_PSMP80 also decomposes at this temperature, because of larger amounts

of remaining toluene, which can be observed in the TGA curves because of the mass loss starting at 100 °C as well as in the ^{1}H and ^{13}C NMRs. The vinyl copolymers under oxygen atmosphere have raising $T_{95\%}$ values with increasing phenyl content from MM over PM to PP from 320 °C to 370 °C.[222] Under nitrogen atmosphere the same trend can be seen, the hydride copolymers show increasing decomposition temperatures with increasing phenyl content,[222] for MM and PM around 290 °C, the PP and PSMP ones have lower values around 210 °C because of the residual toluene. The vinyl copolymers show increasing values from 310 °C for MM over 340 °C for PM to 350 °C for PP under nitrogen atmosphere. The V20_PSMP80 shows a lower temperature of 220 °C because of the remaining toluene.

Table 39: $T_{95\%}$ of the hydride and vinyl phenylthiomethyl-group containing copolymers under oxygen and nitrogen atmosphere.

Group *A* monomer [20 mol%]	Group *B* monomer [40 mol%]	Group *C* monomer [40 mol%]	$T_{95\%}$ O$_2$ [°C]	$T_{95\%}$ N$_2$ [°C]
H		MM	277	297
V		MM	321	311
H		PM	309	291
V		PM	345	338
H	PSMP	PP	228	200
V		PP	369	355
H		PSMP	242	215
V		PSMP	241	225

4.5.2.2.7 <u>Differential scanning calorimetry of the phenylthiomethyl-group containing copolymers</u>

DSC measurements were performed for all synthesised hydride respectively vinyl and phenylthiomethyl-group containing polysiloxanes under nitrogen atmosphere from −50 °C to 150 °C in two cycles (experimental section, Figures 390 – 391), while the first heating cycle was used to determine the melting temperature and the second one for the T_g (Table 40). Comparing the T_g of the hydride copolymers shows that by increasing the phenyl content and reducing the methyl content from MM over PM to PP of the group *C* monomers, the T_g rises from −28.2 °C (MM) over −13.7 °C (PM) to −4.8 °C (PP) due to the reduced flexibility of the polymer chains.[402-404, 462, 496] An increase of the phenylthiomethyl-containing monomer to 80 mol% also increases the T_g value up to 6.6 °C for the same steric reasons.[402-404, 462, 496] Comparing the vinyl copolymers shows the same trend for the exact same reasons. By increasing the phenyl content

and reducing the methyl content from MM over PM to PP of the group C monomers, the Tg rises.[402-404, 462, 496] Additionally, because of the more phenylic-group *A* monomer, all glass transition temperatures are 6 °C to 10 °C higher than the one of their corresponding hydride-group containing copolymer. From −20.0 °C for V20_PSMP40_MM40 it increases to −4.4 °C for the PM one by exchanging one methyl-group of the *C* monomers with a phenyl one. A further substitution raises the value to 1.3 °C. The substitution of the PP monomer with the PSMP one even further increases the value up to 13.1 °C. For some copolymers, like H20_PSMP40_PM40 as well as the highly phenylic ones with PP and PSMP group *C* monomers, a melting temperature of 38 °C to 46 °C can be determined, but the amount of energy is very low. The polysiloxanes with the highest amount of phenyl-groups (V20_PSMP40_PP40) shows an even higher temperature of 76.5 °C as well as the highest amount of melting enthalpy.[402-404, 462, 496] Mosley *et al.* did not report any T_g or T_m values for their sulfur containing polysiloxane.[136]

Table 40: Glass transition and melting temperature as well as the integrated energy of the thioanisole-group containing copolymers.

Group *A* monomer [20 mol%]	Group *B* monomer [40 mol%]	Group *C* monomer [40 mol%]	T_m [°C]	E_m [J/g]	T_g [°C]
H		MM	−	−	−28.2
V		MM	−	−	−20.0
H		PM	45.8	0.176	−13.7
V	PSMP	PM	−	−	−4.4
H		PP	44.3	0.344	−4.8
V		PP	38.4	0.565	1.3
H		PSMP	41.9	0.074	6.6
V		PSMP	76.5	1.183	13.1

4.5.2.3 Synthesis and characterisation of the cured phenylthiomethyl-group containing polysiloxane

The relating hydride and vinyl copolymers, exemplarily H20_PSMP40_PP40 and V20_PSMP40_PP40 (Figure 172), were mixed in a 1:1 ratio and cured analogously to previous polymerisations.
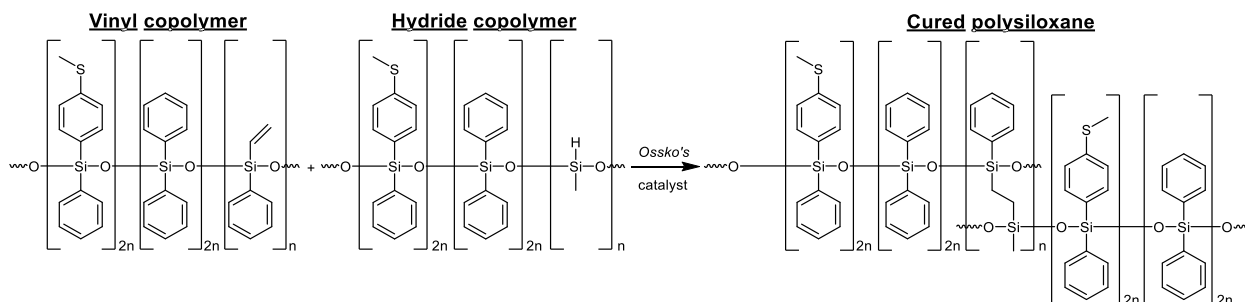
Figure 172: Chemical structure of a vinyl (V20_PSMP40_PP40) and a hydride (H20_PSMP40_PP40) copolymer as well as the resulting cured polysiloxane (P20_PSMP40_PP40).

4.5.2.3.1 <u>FT-IR spectra of the cured phenylthiomethyl-group containing polysiloxanes</u>

FT-IR spectra of the cured polysiloxanes were recorded to investigate if the hydrosilylation reaction is completed after the curing (Figure 173). All other bands were already assigned in the copolymer section. Comparing the remaining signals of the Si-H and Si-V groups indicates a nearly complete reaction for all polymers. P20_PSMP40_MM40 and P20_PSMP40_PM40 show very small signals at 1406 cm^{-1} relating to the vinyl-group.[26,27,48,85]
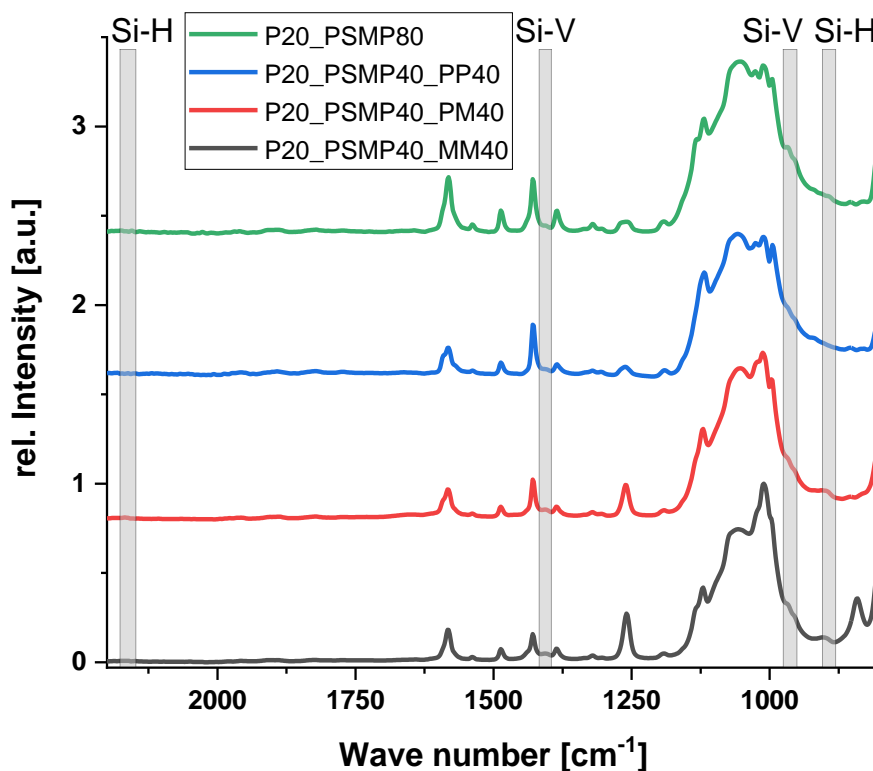
Figure 173: FT-IR spectra of the cured phenylthiomethyl-group containing polysiloxanes.

The second area for detecting vinyl-groups is at 966 cm^{-1},[26,27,48,85] but it overlaps with other signals and does not give clear information if the peak relates to the vinyl-group or the phenyl ones. The small Si-H signal is visible at 2161 cm^{-1} and at 895 cm^{-1}.[234-235, 319, 346-347] A possibility for a not completed addition reaction can be aromatic sulfur-group which is known to reduce the effectiveness up to a complete hindrance of the platinum catalyst.[386] For P20_PSMP40_PP40 and P20_PSMP80 no Si-H and Si-V signals are present. Overall the four polysiloxanes were almost fully condensed,[396] a 100 % conversion cannot be achieved due to the increasing viscosity and reduced immobility of the reactive groups during the curing process.[136, 318, 395]

4.5.2.3.2 NMR spectra of the cured phenylthiomethyl-group containing polysiloxanes

^{13}C and ^{29}Si CP MAS NMRs of the solid sample P20_PSMP80 were recorded exemplarily and the ^{29}Si NMR spectrum is shown here with the linear copolymers H20_PSMP80 and V20_PSMP80 (Figure 174). The ^{13}C CP MAS NMR is reported in the experimental section and shows all expected signals of the phenyl, methyl and thiomethyl carbon atoms (Figure 392).
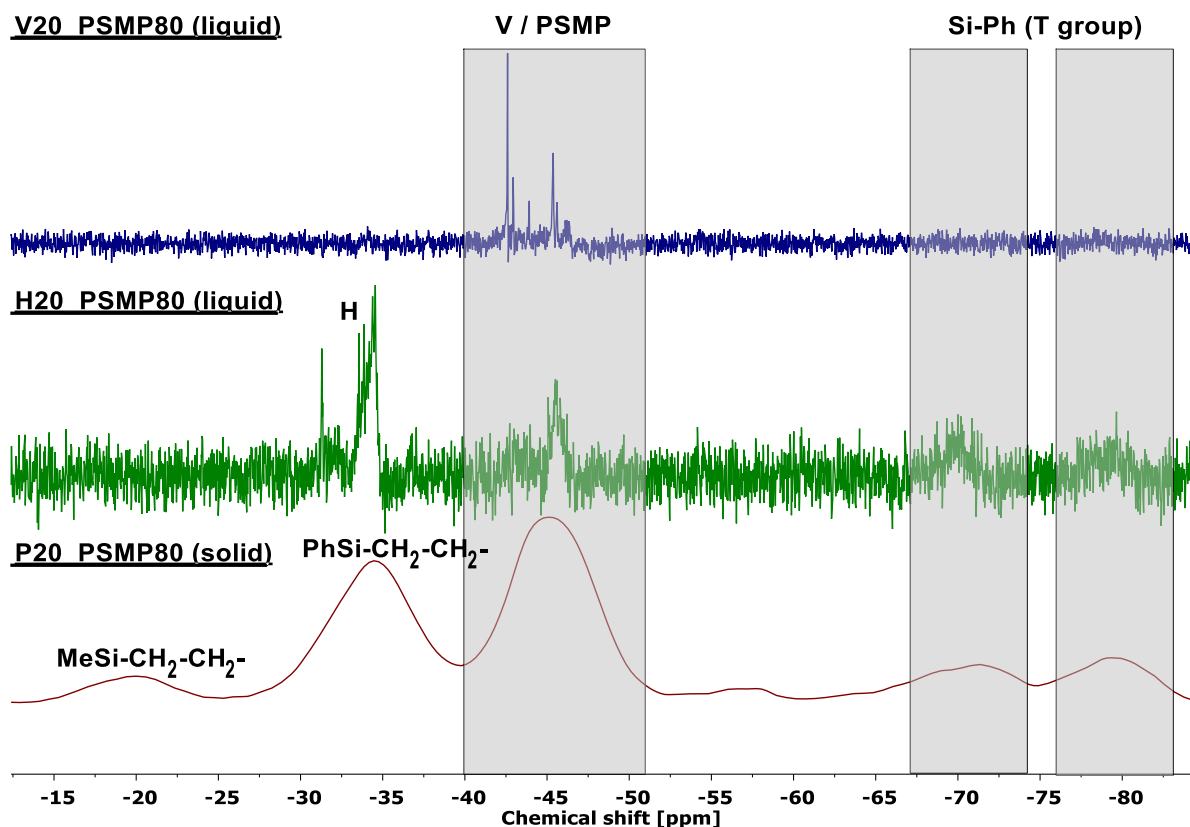
Figure 174: ^{29}Si NMR liquid (79 MHz, CDCl₃) and solid CP MAS NMR (80 MHz, 13 kHz) of X20_PSMP80.

In the ^{29}Si NMR of the vinyl-group containing copolymer are two groups of signals present, one at −43 ppm referring to the vinylphenylsiloxane[331, 368] (Si-V) and the other one at −45 ppm that relates to the 4-(methylthio)phenylphenylsiloxane (Si-PSMP), which is located close to the

diphenylsiloxane one.[331, 368] In the spectrum of the hydride copolymer, the hydridomethylsiloxane (Si-H) signals at −34 ppm are visible,[323-324, 331] as well as the 4-(methylthio)phenylphenylsiloxane (Si-PSMP) signal at −45 ppm.[331, 368] Also, some T groups are visible which, can be assigned to phenylsiloxane T groups with the help of ^{1}H ^{29}Si HMBC NMR (Figure 387). A phenylsiloxane-group with one hydroxyl-group is present at −70 ppm[321] and a fully condensed one is visible at −80 ppm.[321, 324, 368] These groups are derived from the impurities in the PSMP monomer. In an investigation of the vinyl copolymers with ^{1}H ^{29}Si HMBC NMR (experimental section, Figure 380) revealed that a small amount of phenylsiloxane T groups are also present, but only at around −80 ppm which relates to the fully condensed T^{3} ones.[321, 324, 368] The cured polysiloxane also shows the Si-PSMP signal at −45 ppm as well as the phenylsiloxane T groups at −71 ppm (T^{2}) and −80 ppm (T^{3}).[321, 324, 368] Two new signals at −20 ppm and −34 ppm are present, which relate to the hydrosilylation reaction between the <u>hydride-</u> and *vinyl*-group. The newly formed Me<u>Si</u>-CH$_2$-CH$_2$-*Si*Ph bridge shows signals at −20 ppm for the Me<u>Si</u>(OR)$_2$-CH$_2$- unit[61,64] and at −34 ppm for the Ph*Si*(OR)$_2$-CH$_2$- unit.[331, 368] The other two present groups in the copolymers are the MM and PM one, which are located at −17 ppm to −22 ppm[321-324] and at −27 ppm to −33 ppm[331, 368], respectively.

4.5.2.3.3 <u>Refractive index of the cured phenylthiomethyl-group containing polysiloxanes</u>

The RIs of the doctor bladed polysiloxanes (Table 41) were measured in reflection mode using 1-bromonaphthalene as contact fluid because of the high RI of the samples. Cinnamon oil cannot be use here, because it is only suitable for RIs below 1.590, while 1-bromonaphthalene can be used up to a RI of 1.657. The refractive index of P20_PSMP40_MM40 can be determined with 1.583. Substituting the dimethyl (MM) group *C* monomer with the phenylmethyl (PM) one increases the value by 0.016 to 1.599 (P20_PSMP40_PM40). A further methyl to phenyl substitution to the diphenyl monomer (PP) raises the value by 0.017 to 1.616 (P20_PSMP40_PP40). Switching the diphenyl monomer to the 4-(methylthio)phenylphenyl (PSMP) one increases the value by 0.019 up to 1.635 (P20_PSMP80).

Table 41: RI of the cured thioanisole-containing polysiloxanes.

Polysiloxane	RI at 20 °C and 589 nm
P20_PSMP40_MM40	1.583
P20_PSMP40_PM40	1.599
P20_PSMP40_PP40	1.616
P20_PSMP80	1.635

These outstanding high numbers of 1.635 even exceed the values reported by Mosley *et al.*, with 1.62 at 633 nm[136] which is close to the 589 nm of the Abbé refractometer. The RI increases with decreasing wavelength, this effect is called "normal dispersion".[500-501]

4.5.2.3.4 Thermogravimetric analyses of the cured phenylthiomethyl-group containing polysiloxanes

TGA measurements under oxygen and nitrogen atmosphere were performed for the four cured sulfur containing polysiloxanes (experimental section, Figures 393 – 394). The temperatures at 5 % mass loss are listed in Table 42. Comparing the decomposition temperatures under oxygen atmosphere shows an increasing value from 340 °C for the polysiloxane with the dimethyl-group *C* monomer (P20_PSMP40_MM40) up to 420 °C for the highly sulfurous one (P20_PSMP80). The $T_{95\%}$ temperature of the methylphenyl one (P20_PSMP40_PM40) is with 400 °C slightly higher than the 370 °C of the diphenyl-containing polysiloxane (P20_PSMP40_PP40), although a higher phenylic content should lead to a higher thermal stability.[222] The length of the hydride and vinyl copolymers as well as small cyclic siloxanes reduce the temperature at 5 % mass loss.[222, 502] The decomposition temperature ($T_{95\%}$) under nitrogen atmosphere increases with increasing phenyl content[222] starting from P20_PSMP40_MM40 with 330 °C. The value is slightly lower than under oxygen atmosphere, which can be explained because the activation energy as well as the thermal conductivity under oxygen is higher than under nitrogen resulting in an earlier decomposition under nitrogen.[376] The polymer with the methylphenyl-group *C* monomer (P20_PSMP40_PM40) has a $T_{95\%}$ value of 380 °C, which is 25 °C lower than the value under oxygen atmosphere. Here, other effects are also responsible for the difference, like the time of the measurement. The nitrogen samples were measured earlier, while the oxygen sample remained open in the cup for several hours until they could be measured. The diphenyl-containing one (P20_PSMP40_PP40) shows a decomposition temperature of 400 °C which is 25 °C higher than under nitrogen atmosphere. Substituting the diphenyl monomer with the phenylthiomethyl one even further increases the value up to 420 °C which equals the value under nitrogen atmosphere.

Table 42: $T_{95\%}$'s from the TGA analyses of the cured phenylthiomethyl-group containing polysiloxanes.

Polysiloxane	$T_{95\%}$, O_2 [°C]	$T_{95\%}$, N_2 [°C]
P20_PSMP40_MM40	341	334
P20_PSMP40_PM40	405	380
P20_PSMP40_PP40	375	400
P20_PSMP80	417	422

4.5.2.3.5 <u>DSC analyses of the cured phenylthiomethyl-group containing polysiloxanes</u>

DSC measurements of the cured polysiloxanes (experimental section, Figures 395 – 396) were recorded to determine the T_m's and the T_g's (Table 43). The T_g increases by around 15 °C by substitution a methyl with a phenyl-group or adding a sulfur atom. Starting from 1 °C for the P20_PSMP40_MM40 polymer with the dimethyl-group *C* monomer, the T_g increases to 14 °C for the P20_PSMP40_PM40 polysiloxane when a methyl-group is substituted. An additional substitution at the group *C* monomer leads to the P20_PSMP40_PP40 polymer with a T_g of 31 °C. The T_g can further be increased up to 47 °C by switching the diphenyl-group *C* monomer with the 4-(methylthio)phenylphenyl one (P20_PSMP80). The T_g values of the cured polysiloxanes are about 25 °C to 40 °C higher than the mean of the T_g values from the corresponding hydride and vinyl copolymers, which results from the cross-linking process.

The T_m also increase with increasing phenyl and sulfur content from P20_PSMP40_MM40 with 35 °C up to 87 °C for P20_PSMP80, respectively. By substituting the dimethyl-group *C* monomer with the methylphenyl one (P20_PSMP40_PM40) the value increases by around 10 °C, a further substitution to P20_PSMP40_PP40 or a formal addition of a methylthioether-group to P20_PSMP80 each increases the value by 20 °C. The amount of melting enthalpy although is very low with around 0.2 J/g to 0.5 J/g.

Table 43: T_g, T_m and the integrating melting energy E_m of the cured phenylthiomethyl polysiloxanes.

Polysiloxane	T_m [°C]	E_m [J/g]	T_g [°C]
P20_PSMP40_MM40	35.1	0.353	1.3
P20_PSMP40_PM40	46.5	0.516	14.1
P20_PSMP40_PP40	66.1	0.335	31.4
P20_PSMP80	86.8	0.176	47.5

4.5.2.3.6 <u>UV/Vis measurements of the cured phenylthiomethyl-group containing polysiloxanes</u>

UV/Vis measurements of the doctor bladed onto glass slides and cured samples are shown in Figure 175. The polysiloxanes are highly transparent and colourless, the polysiloxane film is about one centimetre wide and 50 µm thick after the curing and located in the middle of the glass slide. The UV/Vis measurements of the polysiloxanes (Figure 176) onto the glass slide were carried out with an integration sphere. The transmission measurements were corrected against the blank glass slide and the haze value was calculated from the transmission and scattering measurements. The values at 450 nm are reported in Table 44. Overall, the transmission decreases with increasing the phenyl content and reducing the methyl content. Brunchi *et al.* reported a reduction down to 95 % when using 50 % of phenyl side-groups.[228]
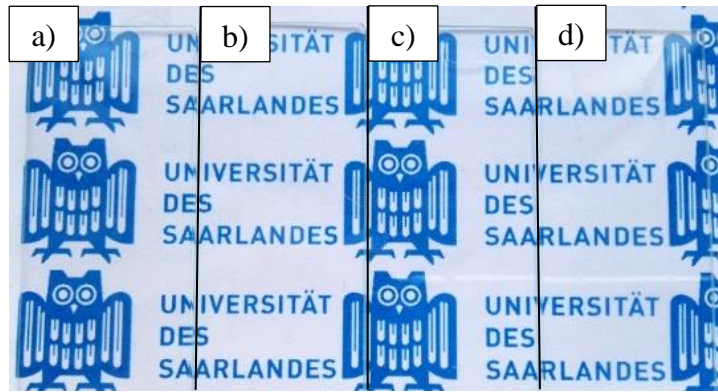
Figure 175: Images of cured phenylthiomethyl-group containing polysiloxanes, a) P20_PSMP40_MM40, b) P20_PSMP40_PM40, c) P20_PSMP40_PP40 and d) P20_PSMP80.

Here, the transmission of the highly methyl-group containing polysiloxane (P20_PSMP40_MM40) is around 100 % and it decreases by around 1 % per substitution of a methyl-group with a phenyl one or by adding the thiomethyl-group. The first substitution from MM to PM decreases the value to 99 % for P20_PSMP40_PM40.
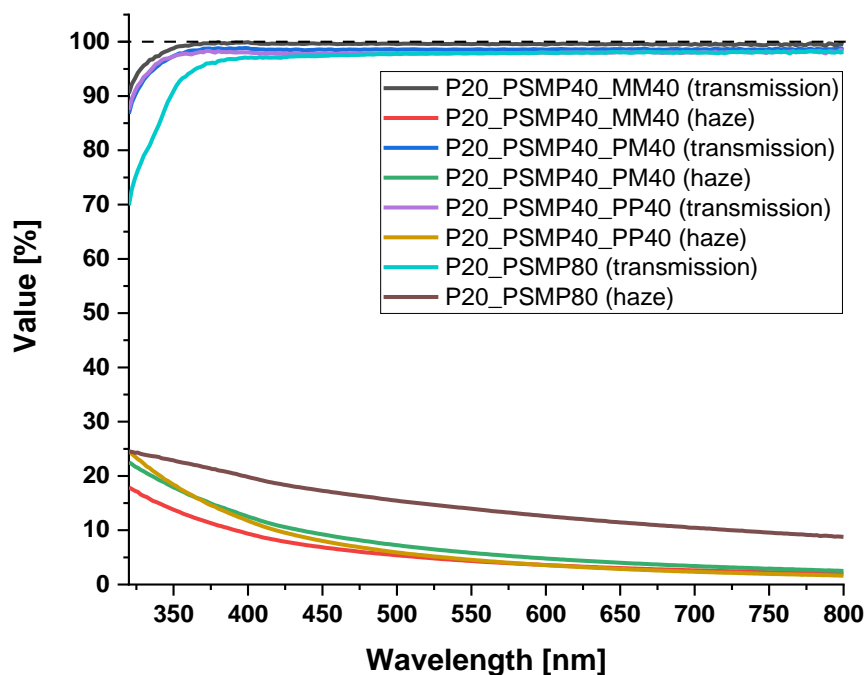
Figure 176: UV/Vis transmission measurements and haze value calculations for the cured phenylthiome-thyl-group containing polymers.

The second substitution from PM to PP decreases the transmission to 98 % for P20_PSMP40_PP40. Switching the diphenyl monomer (PP) with the 4-(methylthio)phe-nylphenyl one further reduces the value to 97 % for P20_PSMP80. Overall, even a 97 % trans-mission is outstanding for optoelectronic materials.

The haze values seem to mainly depend on the sulfur content. Varying the phenyl content from 50 % of the side-groups of P20_PSMP40_MM40 over 70 % of P20_PSMP40_PM40 to 90 %

of P20_PSMP40_PP40 slightly increases the haze value from 8 % to 10 %. Doubling the amount of sulfur from 20 % of the side-groups from P20_PSMP40_XX40 to 40 % for P20_PSMP80, also nearly doubles the haze to 17 %.[503-506]

Table 44: Transmission and haze values of the cured thioanisole-containing polysiloxanes at 450 nm.

Polysiloxane	T_{450} [%]	H_{450} [%]
P20_PSMP40_MM40	100	8
P20_PSMP40_PM40	99	9
P20_PSMP40_PP40	98	10
P20_PSMP80	97	17

The yellowness index (YI, Table 45) ranges from 0.1 to 0.7, indicating a slightly yellow colour. It rises with increasing phenyl content from 0.1 for the dimethyl-group *C* monomer containing P20_PSMP40_MM40 to 0.2 for P20_PSMP40_PM40. Introducing a further phenyl-group by replacing the PM monomer with the PP one, it drastically increases to 0.5 for P20_PSMP40_PP40. The substitution of a phenyl-group by the 4-(methylthio)phenylphenyl-group leads to a further increase to 0.7. The whiteness index (WI) shows the same trend, it decreases from marginally over 100.2 to 96.9, which indicates a light blue colour which weakens with increasing phenyl respectively sulfur content down to a slightly yellow colour with a WI of 96.9. It is close to the optimum of 100 which represents a nearly colourless sample. The WI of the dimethyl-group *C* monomer containing polysiloxane P20_PSMP40_MM40 is slightly over 100, substituting a methyl-group from the MM monomer to PM one (P20_PSMP40_PM40) further decreases the value to marginally under 100. Changing another methyl-group from PM to another phenyl (PP) one reduces the value to 97.4 for P20_PSMP40_PP40. Adding another sulfur atom in P20_PSMP80 decreases the value to 96.9, which is still a very good value, the yellow colouration cannot be seen with the bare eye. Overall, the trend that an increase of the phenyl content increases the yellow colour is observable.[474] The P20_PSMP40_MM40 shows the least amount of yellowing because of the lowest amount of phenyl-groups, but the difference in the calculated numbers, especially compared to P20_PSMP40_PM40, is very small and therefore negligible. Other reasons for the yellow colour besides the increasing phenyl content is the formation of small yellow to brown platinum nanoparticles around a diameter of 3 nm to 5 nm, which can be produced by the reaction of the platinum catalyst with the Si-H group.[474, 507]

Table 45: Yellowness and whiteness indices of the cured phenylthiomethyl-group containing polysiloxanes.

Polysiloxane	YI	WI
P20_PSMP40_MM40	0.1	100.2
P20_PSMP40_PM40	0.2	99.9
P20_PSMP40_PP40	0.5	97.4
P20_PSMP80	0.7	96.9

4.5.2.3.7 Thermal aging test of the cured phenylthiomethyl-group containing polysiloxanes

The glass slides with the doctor bladed and cured phenylthiomethyl-group containing polysiloxanes (Figure 177) were placed in an oven at 180 °C for 63 days (1512 h) to simulate the heat generated from the LED chip during the operation of the LED while the humidity was not changed artificially. The higher phenylic samples P20_PSMP40_PP40 and P20_PSMP80 show cracks after the thermal heating, because these side-groups increase the viscosity of the hydride and vinyl copolymers and therefore also the one of the cured polymers. Mosley *et al.* also reported a buckling of their sample under heat exposure.[136]
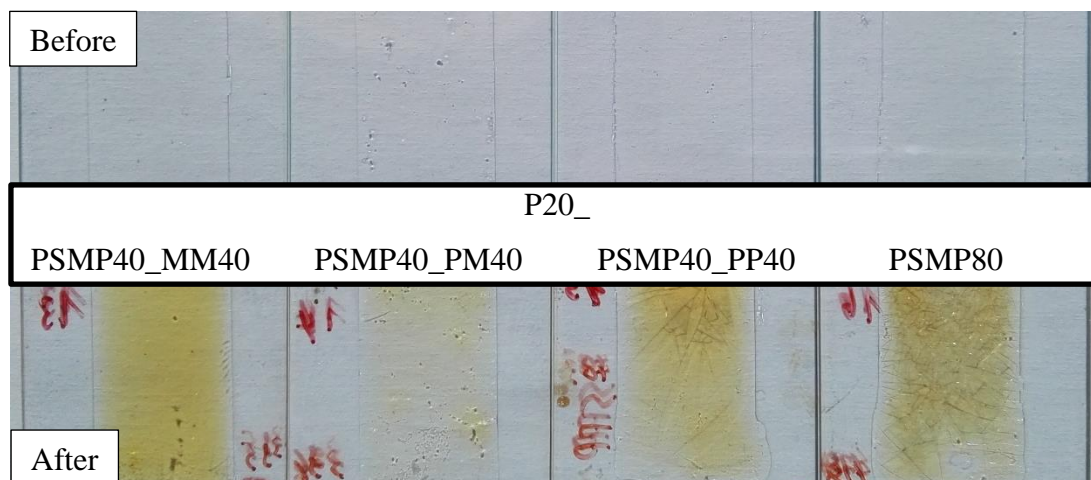
Figure 177: Methylthiophenyl-group containing polysiloxanes before (top) and after (bottom) the thermal heat treatment at 180 °C for 63 days under air atmosphere.

The change of the material was evaluated using UV/Vis measurements in transmission and scattering mode to calculate the corrected transmission and haze spectra. Both values at 450 nm are displayed in Figure 178. The transmission of the highly methyl-group containing P20_PSMP40_MM40 starts with the highest value of around 100 %, but after four days it drops under 90 % and remains below all other values. The constant decrease slows down after 41 days with 63 % transmission, but still drops down to 59 %. The P20_PSMP40_PM40 shows the second highest transmission in the beginning with 99 % and after a drop during the first seven days down to 92 %, the transmission slightly decreases during the next 56 days to 87 % which

is the highest value achieved after the completed test. P20_PSMP40_PP40 and P20_PSMP80 show the second lowest respectively lowest transmission in the beginning and after a drop down to 90 % respectively 84 %, both curves stay close to each other. After 63 days, a transmission of 64 % for P20_PSMP40_PP40 and P20_PSMP80 was reached and stayed above the transmission of P20_PSMP40_MM40. Mosley *et al.* reported a 90 % transmission after 70 days under 200 °C and oxygen atmosphere in the UV region for their 4-(phenylthio)phenylphenyl-group containing polysiloxane and claimed it onto the only 96 % purity of the 4-(phenylthio)phenylphenyldimethoxysilane monomer.[136] 90 % transmission of the best sulfur containing polysiloxane could nearly remained after 63 days under 180 °C and oxygen atmosphere. The haze values drop in the first seven days and remain at the value without change. The three P20_PSMP40_XX40 samples have an initial value of around 10 % which drops between 7 % and 8 %. The P20_PSMP80 shows an initial value of 17 % which drops to 11 %.
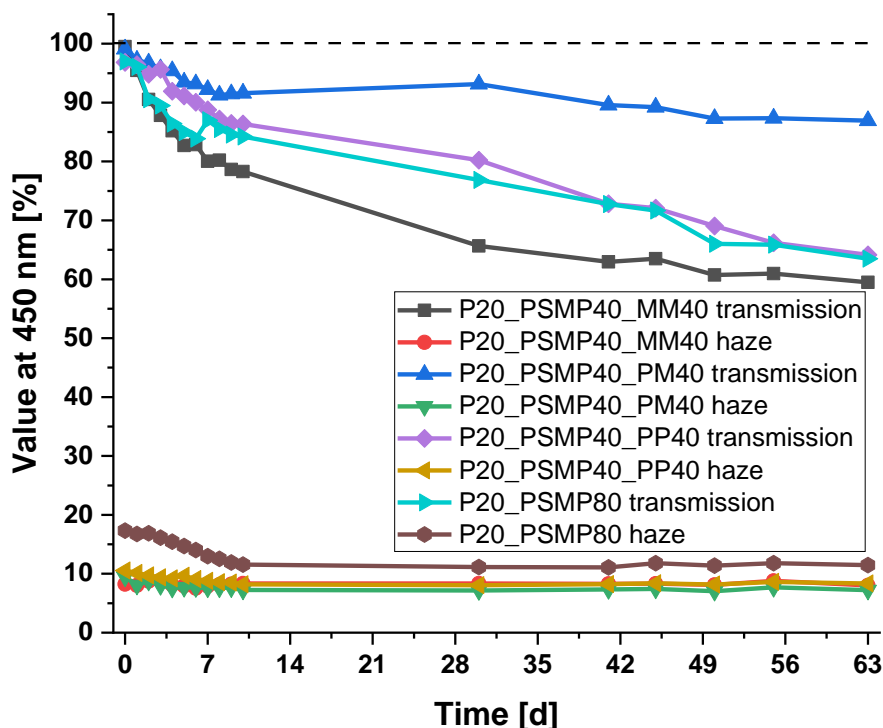
Figure 178: Transmission and Haze value at 450 nm for the thioanisole-containing polysiloxanes during a heat treatment of 180 °C for 63 days (1512 h).

To evaluate the amount of colouration by the yellowing of the samples, the yellowness and whiteness indices were calculated and are displayed in Table 46. The yellowness index increases for all polymers, which supports the visual strong yellow colouration (Figure 177). The yellow colouration is inversely proportional to the transmission because the yellow colour absorbs photons.[7, 316] P20_PSMP40_MM40 shows the highest value with 35.3, which is in agreement with the transmission measurement, where it has the lowest value. The P20_PSMP40_PP40 shows the second highest value with 30.7 and the highly sulfuric

P20_PSMP80 has a value of 26.1. These high values around 30 imply a strong yellow colour. The P20_PSMP40_PM40 shows a drastically lower value of 11.5, which is agreement with the images and the transmission measurements. The whiteness index supports the statement of the YI and indicates a strong yellow colour. The lowest value of −11.2 for P20_PSMP40_MM40 displays a very strong yellow colour, which increases for P20_PSMP40_PP40 with a WI of 1.3 and therefore the amount of the yellow colouration decreases. P20_PSMP80 shows the second highest value of 12.7 which indicates a lower yellow colouration. The least amount of yellowing has P20_PSMP40_PM40 with a value of 66.6, which is the closest one to 100 and supports the transmission measurements.

Table 46: Yellowness and whiteness indices after synthesis and after 63 days under 180 °C.

	YI after synthesis	YI after 63 d	WI after synthesis	WI after 63 d
P20_PSMP40_MM40	0.1	35.3	100.2	−11.2
P20_PSMP40_PM40	0.2	11.5	99.9	66.6
P20_PSMP40_PP40	0.5	30.7	97.4	1.3
P20_PSMP80	0.7	26.1	96.9	12.7

4.5.2.4 *Conclusion for the phenylthiomethyl-group containing polysiloxanes*

With the newly sulfur containing high refractive index monomer 4-(methylthio)phenylphenyl-dimethoxysilane (PSMP) novel hydride- and vinyl-group containing copolymers were synthe-sised (Figure 179). These show high refractive indices from 1.564 to 1.623 and, for linear co-polymers, already high thermal stabilities up to 360 °C under nitrogen and oxygen atmosphere. The different monomer compositions allow a tuneable glass transition temperature from −28 °C to 13 °C. These hydride and vinyl copolymers were then thermally cross-linked using *Ossko*'s platinum catalyst.
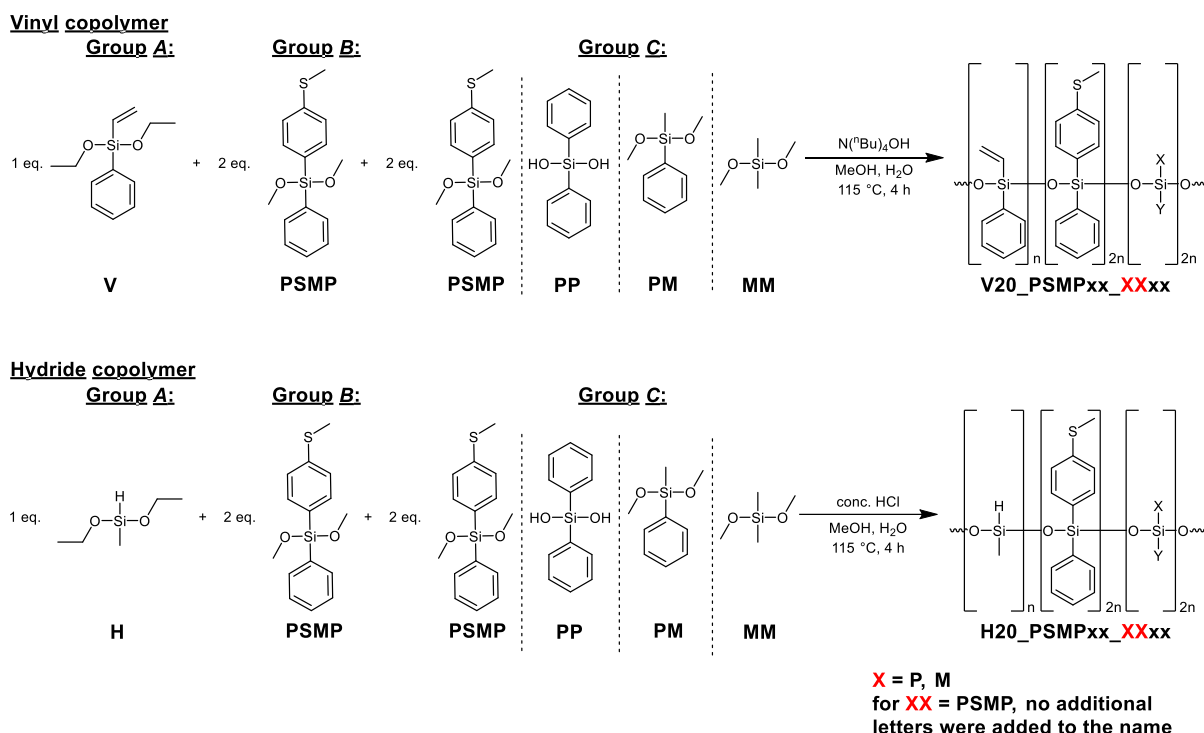
Figure 179: Overview of the synthesis of the phenylthiomethyl-group containing polysiloxanes from mono-mers.

These new materials show a very high refractive index of 1.583 to 1.635 depending on the used monomers and copolymers which is significantly higher than the 1.552 of the OE-6630. A very high transmission of over 97 % can be achieved for all sulfur containing polysiloxanes, which is close to the 99 % of the OE-6630 system. The calculated colouration from the yellowness and whiteness indices are close to the optimal value of zero for the YI and 100 of the WI. The sulfur containing polysiloxanes show YIs ranging from 0.1 to 0.7, while the OE-6630 has a comparably high value of 0.5. The WIs range from 96.9 to 100.2 and the OE-6630 is inside this range with a value of 99.0. The thermal stability of the systems reached around 420 °C for P20_PSMP80 under both nitrogen and oxygen atmosphere when using the $T_{95\%}$ criteria, the OE-6630 polysiloxane shows a marginally higher temperature of up to 430 °C. The additional thermal aging test showed a high transmission of 90 % for the P20_PSMP40_PM40 system

after 63 days under 180 °C while the OE-6630 remained a 99 % transmission over this period. Here, small residues and a too high platinum content drastically reduce the transmission under thermal aging, which was also investigated by Mosley *et al.*[136] The YI and WI indices of the sulfur containing cured polysiloxanes are drastically increased or reduced during the long thermal treatment which already can be seen in the optical images (Figure 177), respectively. Another reason could be the sulfur because the raw product of the phenylthiomethyl-group containing monomer also shows a light-yellow colour, which disappears after distillation. This observation is also reported by Mosley *et al.*[136] After several months, the purified monomer stored under argon atmosphere, shows again a slight yellow colour. Additionally, because of the catalyst poisoning effect of the sulfur towards the platinum,[386, 463] the reaction between the hydride- and vinyl-groups is slower respectively more platinum has to be used. Too high amounts of platinum result in the formation of yellow platinum nanoparticles,[136, 474, 507] this effect is increased when free Si-H groups are present.[507] Overall, the self-prepared polymers not only matches the properties of the commercial OE-6630 system but excels them. But during the long thermal treatment, some impurities lead to a bigger problem of a yellow colouration which has still to be solved.

4.5.3 Synthesis and characterisation of phenanthrenyl-group containing polysiloxanes

Besides the introduction of oxygen or sulfur atoms into the side-groups of the polysiloxane, Mosley *et al.* simultaneously used a higher aromatic content to increase the refractive index with formally seen three phenyl rings per silicon D monomer.[136] Another approach to introduce more phenyl-groups is the use of conjugated aryl-groups like the naphthyl[297-298], anthracenyl[299] or phenanthrenyl one. Because these side-groups are larger and not as flexible as the previously used phenyl-, 4-(phenoxy)phenyl- or 4-(methylthio)phenyl-group, a methyl-group on the D silicon atom of the newly synthesised monomers was also used instead of only the phenyl one. Therefore 9-bromophenanthrenyl (PH) was used in a Grignard reaction with methyl- or phenyltrimethoxysilane to receive both phenanthren-9-ylmethyldimethoxysilane (Figure 180, PHM) and phenanthren-9-ylphenyldimethoxysilane (PHP).
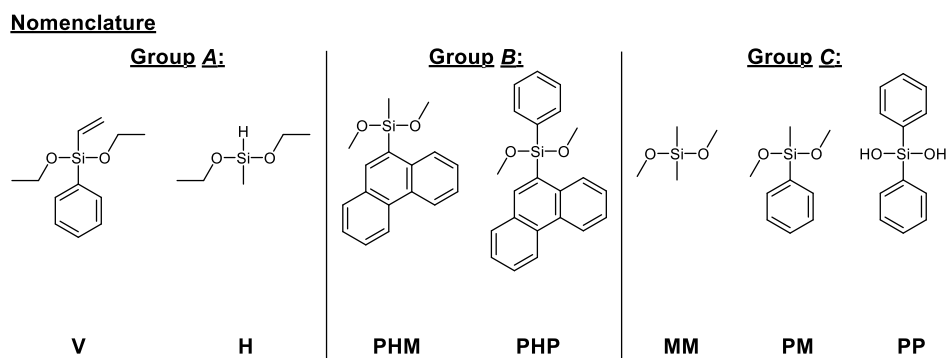
Figure 180: Overview of the used monomers for the phenanthrenyl-group containing polysiloxanes and their abbreviation.

These novel high refractive index group *B* monomers were polymerised with hydride- or vinyl-group *A* monomers and a group *C* monomer, which consists of either dimethyl- (MM), methylphenyldimethoxysilane (PM) or diphenylsilanediol (PP). These linear hydride and vinyl copolymers were thermally cured using *Ossko*'s platinum catalyst. Additionally, polysiloxanes with a general monomer composition of group *A*: hydride/vinyl (H/V), *B*: phenanthrenylmethyl (PHM) and *C*: diphenyl (PP) were polymerised using different amounts of these groups to be able to compare the effects of these groups among themselves.

4.5.3.1 *Synthesis and characterisation of the phenanthrenyl-group containing monomers*

For the investigation of the influence of conjugated electron rich substituents, which according to the calculations of the Lorentz-Lorenz equation[136, 227-228] increase the RI, new monomers have to be synthesised. Since these groups are known to significantly increase the viscosity of the copolymers because of their sterical demand[508-509] and the resulting brittleness of the cured films, two variants of the dimethoxysilane monomer were prepared. One with an additional methyl-group (PHM) and one with a phenyl-group (PHP). The Grignard syntheses (Figure 181) start from 9-bromophenanthrene with magnesium granules which were reacted with methyltrimethoxysilane (PHM) or phenyltrimethoxysilane (PHP), respectively. Both syntheses are based on published procedures of Mosley *et al.*[136] and Kondo *et al.*[510-511]
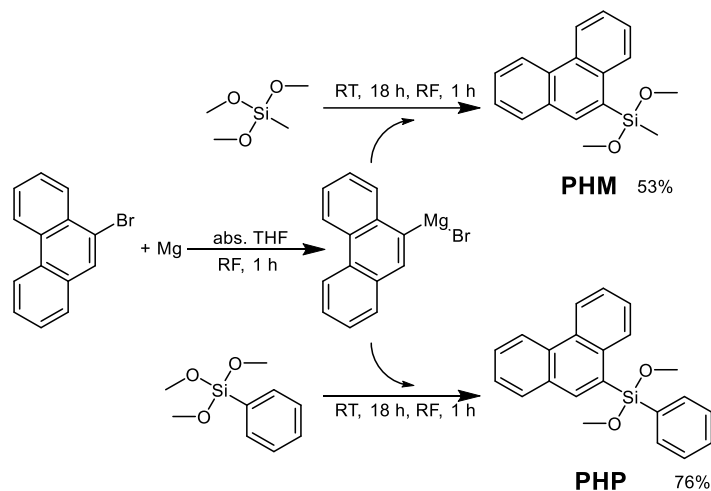
Figure 181: Grignard syntheses for phenanthren-9-ylmethyldimethoxysilane (PHM) and phenanthren-9-ylphenyldimethoxysilane (PHP).

In the first few syntheses, the magnesium organyl and the trimethoxysilane were reacted in a ratio of about 1:1, which leads to various side products of multiple substitutions. Unreacted educts can be removed at low temperatures under high vacuum. The double reacted species, especially in the PHP synthesis, remain in the flask during distillation due to its extreme high boiling point. The synthesis was modified to increase the methyl- or phenyltrimethoxysilane to 9-bromophenanthrene ratio to approximately 4:1. This nearly prevents the formation of the double substituted product and the unreacted trimethoxysilane can be removed by high vacuum distillation under room temperature.

The PHM monomer was synthesised as colourless oil in 53 % yield, therefore a refractive index of 1.631 at 20 °C and 589 nm can be determined. Comparing this value with three cyclic aromatics with the 1.544 for the two phenyl-group containing diphenyldimethoxyislane (PP) or the 1.479 for the one phenyl-group containing methylphenyldimethoxysilane (MM), an increase of

around 0.070 per additional cyclic aromatic can be calculated.[419] After some months crystal could be grown directly out of the pure monomer.

The purified PHP monomer was obtained as a colourless solid in 76 % yield and crystals could also be grown. A refractive index could not be measured because the melting point is above 80 °C and the refractometer could be damaged using higher temperatures. With the estimation of an increase of around 0.070 per aromatic, a theoretical value of ~1.700 for the PHP monomer with four aromatic rings can be assigned. Since purification by distillation takes a long time and remains incomplete, the synthesis was optimised. After the crude product has been dried and the phenyltrimethoxysilane was removed, it can be recrystallised in hexane for purification.

4.5.3.1.1 FT-IR spectra of the phenanthrenyl-group containing monomers

FT-IR measurements of the two monomers were recorded (Figure 182). The monomer shows the C-H bands at 2962 cm^{-1}, at 2935 cm^{-1}, at 1257 cm^{-1}, at 960 cm^{-1}, at 742 cm^{-1} and at 667 cm^{-1}.[346-347] The aromatic C=C vibrations are located around 1612 cm^{-1}, 1583 cm^{-1} and 1489 cm^{-1}.[495] The Si-O-C vibration from the methoxy-group (dark grey area) is clearly visible at 2835 cm^{-1} and at 1184 cm^{-1}.[346] Both monomers show the Si-O vibrations in the region of 1170 cm^{-1}.[346-347] The Si-C bands are located at 1445 cm^{-1}, at 1251 cm^{-1} as well as at 1170 cm^{-1} and in the area of 680 cm^{-1} till 780 cm^{-1} which is in the region of C-H bands.[346]
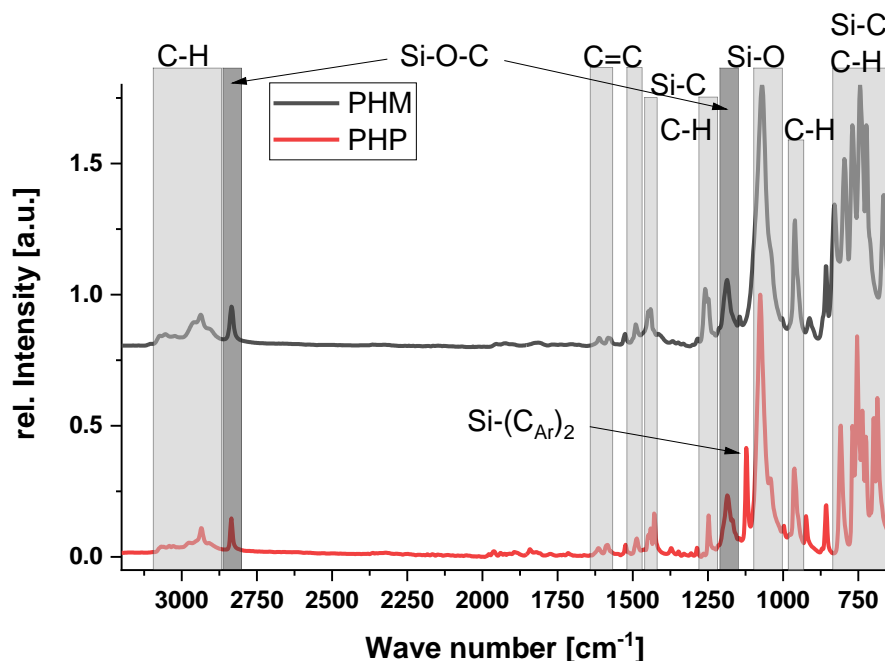
Figure 182: FT-IR spectra of phenanthren-9-ylmethyldimethoxysilane (PHM) and phenanthren-9-ylphenyldimethoxysilane (PHP).

The additional signal at 1120 cm^{-1} in the PHP spectrum also refers to the Si-C$_{Ar}$ group. This Si-C$_{Ar}$ vibration at 1170 cm^{-1} splits into a doublet when two aromatic groups are attached on

one silicon atom, according to Launer.[346] The second PHP signal and the single PHM signal are around 1170 cm^{-1} and under the Si-O signal.[346]

4.5.3.1.2 NMR spectra of the phenanthrenyl-group containing monomers

^{1}H, ^{13}C and ^{29}Si NMRs of the monomers were recorded (Figures 183 – 185 and 398 – 400), but only the ^{1}H NMR and ^{29}Si NMR are shown here. In both ^{1}H NMRs (Figures 183 – 184) all signals are assignable to PHM and PHP, respectively. In the PHM spectrum, small unknown signals in the aromatic area are also visible, they do not belong to the educt 9-bromophenan-threne or to solvent residuals like toluene. The signals can also not be assigned to phenanthrene because of the very low field shift, but they have to belong to a phenanthrene species.[426-428, 512] In the ^{29}Si NMR (Figure 185), one signal is visible at −13.1 ppm which belongs to PHM.
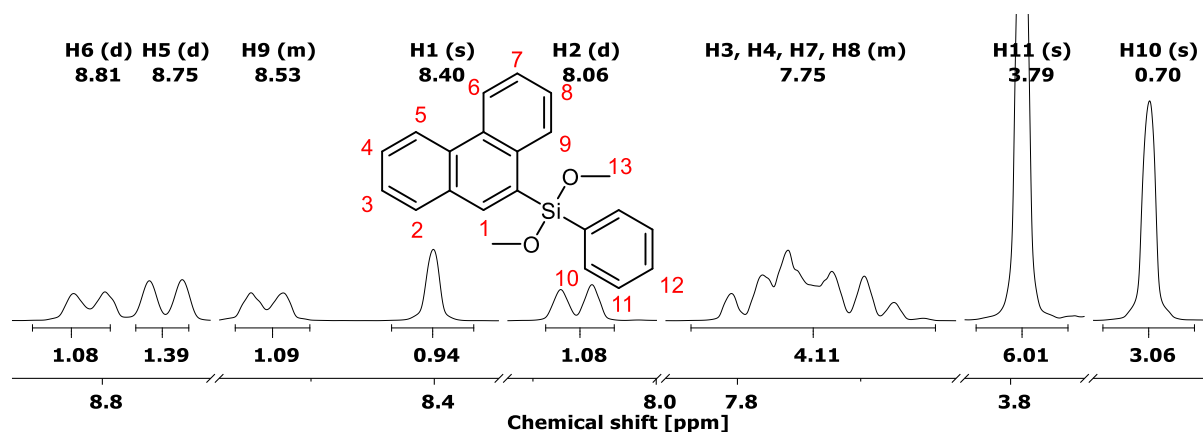
Figure 183: ^{1}H NMR (300 MHz, CDCl$_3$) of phenanthren-9-ylmethyldimethoxysilane.

In the ^{1}H NMR spectrum of PHP (Figure 184), small aromatic signals in the range from 7.3 ppm to 7.7 ppm are visible, which most likely belong to the unreacted educt phenyltrimethoxysilane.
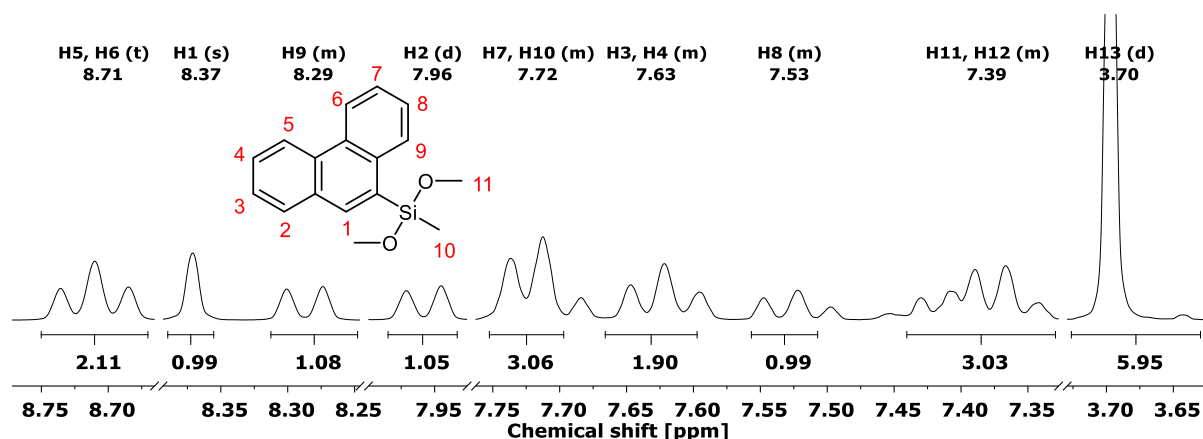
Figure 184: ^{1}H NMR (300 MHz, CDCl$_3$) of phenanthren-9-ylphenyldimethoxysilane.

In the ^{29}Si NMR (Figure 185) the product signal of PHP at −29.7 ppm is visible. No additional signal for the educt phenyltrimethoxysilane was separately measured and shows a signal at around −54.5 ppm, which cannot be observed here.
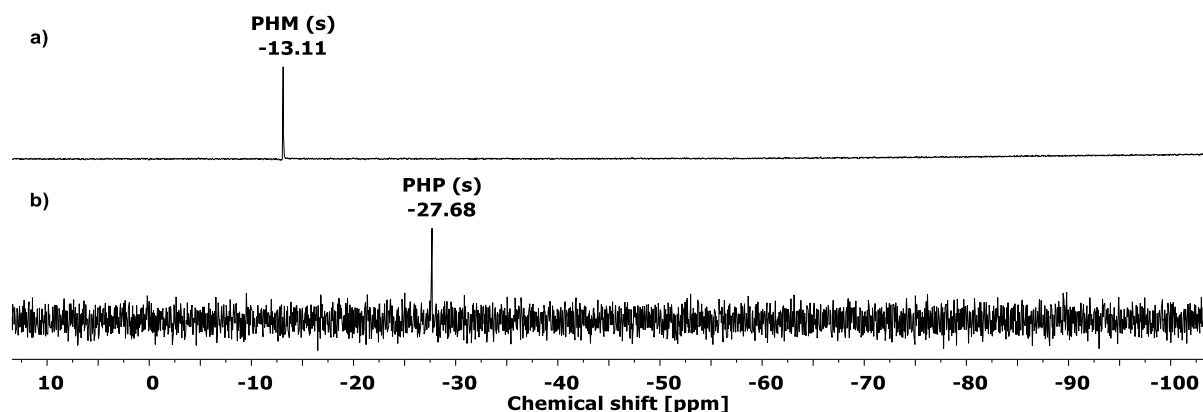
Figure 185: ^{29}Si NMR (60 MHz, CDCl$_3$) of a) phenanthren-9-ylmethyldimethoxysilane (PHM) and b) phenanthren-9-ylphenyldimethoxysilane (PHP).

4.5.3.1.3 Crystal structure of the phenanthrenyl-group containing monomers

From the synthesised PHM and PHP monomers, single crystals and thus a single crystal structure analysis (Figure 186) were obtained. The crystal data (Table 47), the bond lengths, and angles (Table 48) are discussed in the following section.
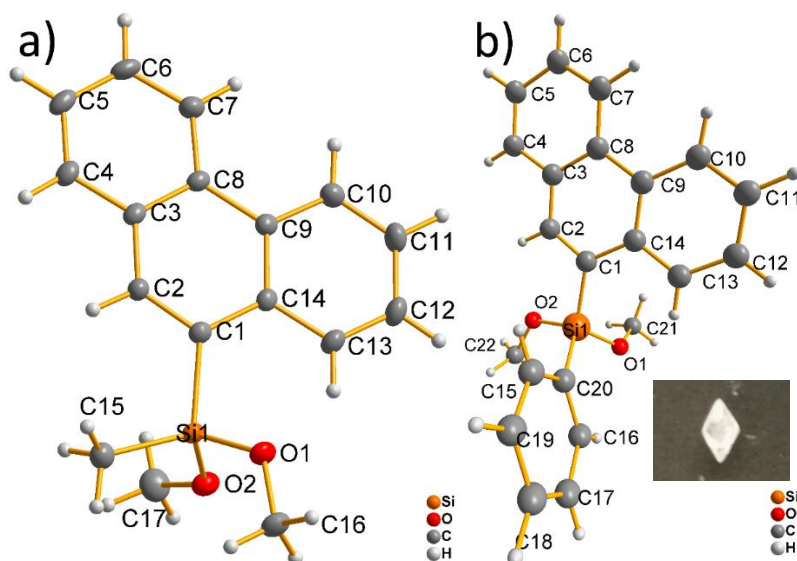
**Figure 186: Crystal structure of a) phenanthren-9-ylmethyldimethoxysilane (PHM)
and b) phenanthren-9-ylphenyldimethoxysilane (PHP).**

The methyl-group containing PHM monomer crystallises in the monoclinic space group *P2$_1$/c*, while the phenyl-group containing PHP monomer crystallises in the orthorhombic space group *Pbca*. The packing diagrams are shown in Figure 187.
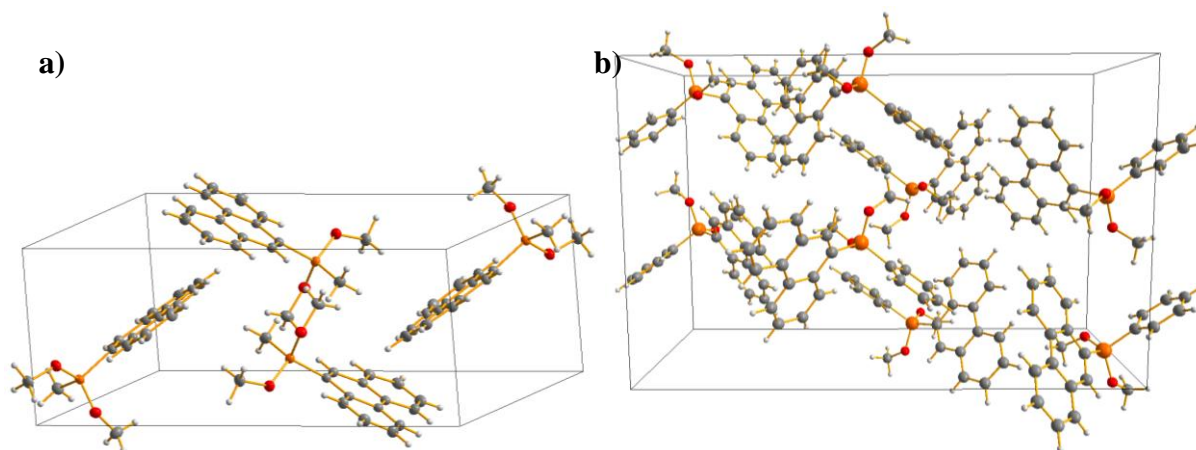
Figure 187: Packing diagrams of a) phenanthren-9-ylmethyldimethoxysilane (PHM) and b) phenanthren-9-ylphenyldimethoxysilane (PHP).

Table 47: Crystal data of the synthesised PHM and PHP monomers.

Monomer	PHM	PHP
Space group	*P2₁/c* (14)	*Pbca* (61)
	monoclinic	orthorhombic
a	1018.25(18) pm	1013.11(3) pm
b	746.59(13) pm	1531.34(5) pm
c	2005.6(4) pm	2393.66(7) pm
α	90°	90°
β	100.688(9)°	90°
γ	90°	90°
V	1.4983(5) nm³	3.7136(2) nm³

The important bond lengths and angles are shown in Table 48. The length of the bond between the phenanthrenyl carbon atom (C1) and the silicon atom is with 186.75(1) pm for PHM monomer and 186.52(11) pm for the PHP monomer marginally larger than the usually observed Si-C bond with around 185 pm.[492] The distance between the silicon atom and the carbon atom of the methyl- and phenyl-group (C15) is with 184.96(1) pm for PHM identical with the general literature value and with 185.57(12) pm for the PHP slightly larger than in the literature, respectively.[492] The bond length between the silicon atom and the two oxygen atoms is with 163.80(1) pm and 164.33(1) pm for the PHM molecule in the typical range of these bonds.[491] The Si-O distances for PHP is with 162.81(10) pm and 163.11(10) pm almost identical with the standard reported in literature.[491]

A torsion angle between the two aromatic planes of phenanthren-9-ylphenyldimethoxysilane of 87.28(3)° indicates a slight distortion compared to the ideal 90° angle. The phenanthrenyl-group shows an angle of 111.70(0)° between the methyl and an angle of 113.37(5)° between the sterical more demanding phenyl-group of PHP. Because of the large phenanthrenyl-group, both values exceed the tetrahedral angle of 109.5°. The angle between the C1 atom and one of the oxygen atoms for PHM is with 107.90(0)° for C1-Si-O1 and 109.33(0)° for C1-Si-O2 smaller than the tetrahedral one, while for PHP, one angle is with 102.72(5)° (C1-Si-O1) much smaller and the other one with 112.49(5)° (C1-Si-O2) larger than the tetrahedral one. This results in a smaller angle between the oxygen atoms for PHM, while for PHP the angle is slightly larger. The angle between the methyl or phenyl carbon atom and one of the oxygen atoms therefore is 112.20(0)° or 109.67(0)° for PHM and 103.94(5)° or 112.49(5)° for PHP.

Table 48: Selected bond lengths and angles of both phenanthrenyl-group containing monomers.

	PHM	PHP
Angle: C1-Si-C15	111.705(2)°	113.37(5)°
Angle: C1-Si-O1	107.904(3)°	113.67(5)°
Angle: C1-Si-O2	109.330(3)°	102.72(5)°
Angle: C15-Si-O1	112.200(3)°	103.94(5)°
Angle: C15-Si-O2	109.676(3)°	112.49(5)°
Angle: O1-Si-O2	105.824(3)°	110.93(6)°
Torsion angle between planes: phenanthrenyl and Me/Ph	−	87.282(32)°
Distance: Si-C1	186.75(1) pm	186.52(11) pm
Distance: Si-C15	184.96(1) pm	185.57(12) pm
Distance: Si-O1	163.80(1) pm	162.81(10) pm
Distance: Si-O2	164.33(1) pm	163.11(10) pm

4.5.3.2 Synthesis and characterisation of the hydride or vinyl and phenanthrenyl-group containing copolymers

With the two novel phenanthrenyl-group containing monomers, various hydride- and vinyl-group containing copolymers were synthesised based on the earlier described modified synthetic routes (Figure 188) reported by Mosley *et al.*[136] and Kim *et al.*[138, 317] The hydride polymerisation was carried out using concentrated hydrochloric acid as catalyst and tetra-*n*-butyl ammonium hydroxide was used for the vinyl polymerisation. The polycondensation reaction was performed in an aqueous methanol solution for three hours at 85 °C for the first hour and 115 °C for the last two ones.
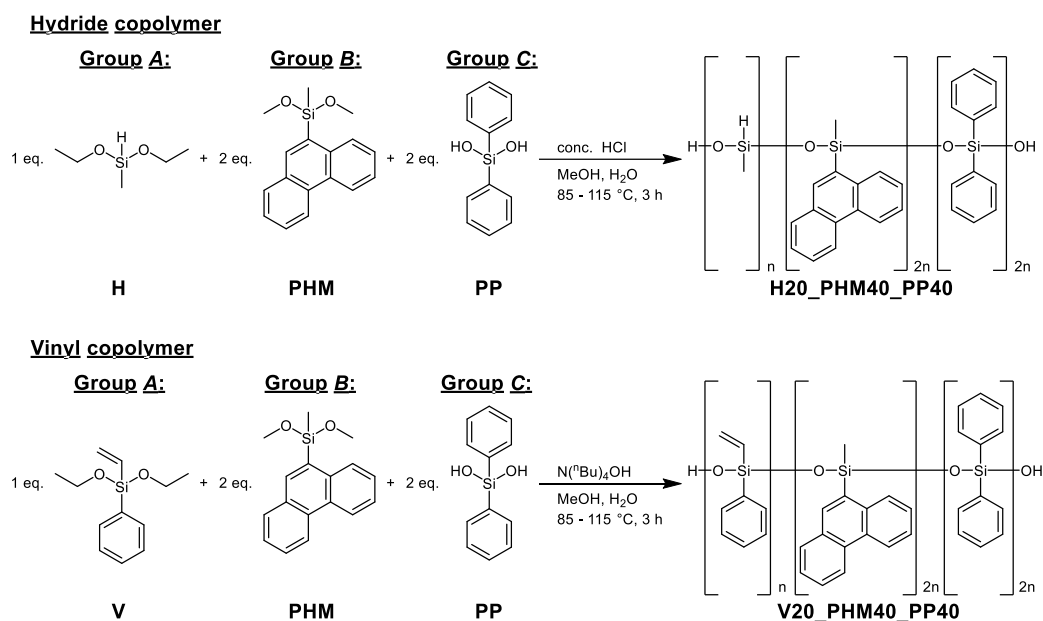
Figure 188: General hydride- or vinyl- and phenanthrenyl-group containing copolymer syntheses, exemplarily shown for X20_PHM40_PP40.

For the copolymers usually 20 mol% of cross-linking group *A* monomer, 40 mol% of high RI group *B* monomer and 40 mol% of lower RI group *C* monomers like dimethyl- (MM), phenylmethyl- (PM) and diphenylsiloxane (PP) were used in a sol-gel reaction. Additionally, a composition with different amounts of H/V, PHM and PP are used for the syntheses of Xm0_PHMn0_PPo0. The nomenclature is exemplarily shown (Figure 188) for H20_PHM40_PP40 and V20_PHM40_PP40, which consists of 20 mol% of H or V, 40 mol% of PHM and 40 mol% of PP referred to the total silicon atom content. All synthesised hydride and vinyl and phenanthrenyl-group containing copolymers are listed in Table 49.

Table 49: Overview of all synthesised phenanthrenyl-group containing copolymers.

Group *A*	Group *B*	Group *C*	Copolymer
20 % H	40 % PHM	40 % MM	H20_PHM40_MM40
20 % V	40 % PHM	40 % MM	V20_PHM40_MM40
20 % H	40 % PHM	40 % PM	H20_PHM40_PM40
20 % V	40 % PHM	40 % PM	V20_PHM40_PM40
20 % H	40 % PHM	40 % PP	H20_PHM40_PP40
20 % V	40 % PHM	40 % PP	V20_PHM40_PP40
40 % H	20 % PHM	40 % PP	H40_PHM20_PP40
40 % V	20 % PHM	40 % PP	V40_PHM20_PP40
40 % H	40 % PHM	20 % PP	H40_PHM40_PP20
40 % V	40 % PHM	20 % PP	V40_PHM40_PP20
20 % H	40 % PHP	40 % MM	H20_PHP40_MM40
20 % V	40 % PHP	40 % MM	V20_PHP40_MM40
20 % H	40 % PHP	40 % PM	H20_PHP40_PM40
20 % V	40 % PHP	40 % PM	V20_PHP40_PM40
20 % H	40 % PHP	40 % PP	H20_PHP40_PP40
20 % V	40 % PHP	40 % PP	V20_PHP40_PP40

4.5.3.2.1 <u>FT-IR spectra of the phenanthrenyl-group containing copolymers</u>

FT-IR analyses were recorded for all 16 copolymers (experimental section, Figures 405 – 412), but only one hydride and one vinyl spectrum from the PHM or PHP group containing polymers are shown here (Figure 189). The copolymers show slightly different FT-IR spectra compared to the PHM or PHP monomers ones because of the copolymerisation with other monomers. The already mentioned groups and bands are not described here, see 4.5.3.2.1. The methoxy signals are no longer present due to the sol-gel reaction, also additional bands for the Si-O backbone are visible from 1000 cm^{-1} to 1150 cm^{-1}.[346-347] Because of the copolymerisation of group *A* and *C* monomers with PHM or PHP, new signals are present. The vinyl copolymers V20_PHM40_PM40 and V20_PHP40_PM40 have signals at 1404 cm^{-1} and at 962 cm^{-1} representing the vinyl-group (yellow).[234-235, 319, 370] The hydride polymers H20_PHM40_PM40 and H20_PHP40_PM40 in contrast show Si-H signals (dark grey) at 2164 cm^{-1} and at 897 cm^{-1}.[234-235, 319, 346-347]
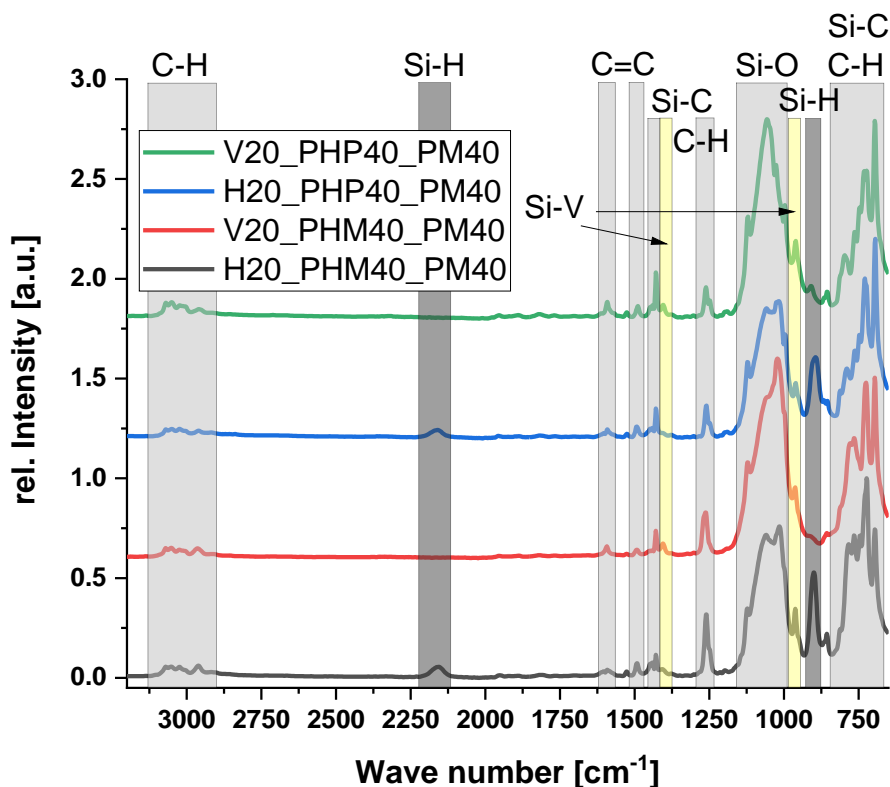
Figure 189: FT-IR spectra of hydride or vinyl and phenanthrenyl-containing linear copolymers X20_PHM40_PM40 and X20_PHP40_PM40.

4.5.3.2.2 Fluorescence spectroscopy of the phenanthrenyl-group containing copolymers

Because larger conjugated π-systems can be excited at lower wavelengths,[513] fluorescence measurements of V20_PHM40_PP40 in tetrahydrofuran were performed to evaluate if these side-groups show unwanted fluorescence when excited at 450 nm (Figure 190). The emission spectrum shows the highest fluorescence at 457 nm when excited at 370 nm.
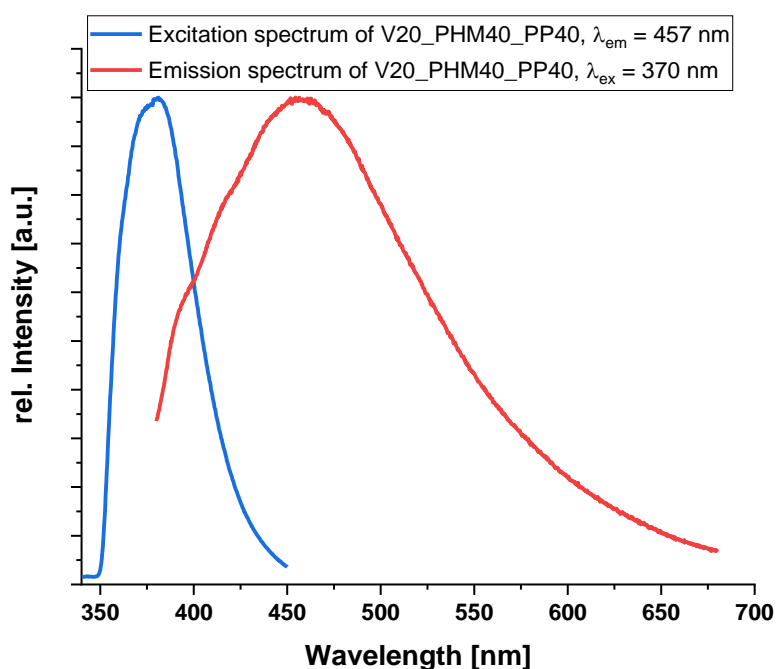
Figure 190: Excitation and emission spectrum of V20_PHM40_PP40.

In the excitation spectrum the intensity at 450 nm is almost zero, which means no significant fluorescence is present and these groups are suitable for blue LED applications.

4.5.3.2.3 NMR spectra of the phenanthrenyl-group containing copolymers

^{1}H, ^{13}C and ^{29}Si NMR were recorded for all copolymers (experimental section, Figures 413 – 428) and show all the desired signals. The CDCl$_3$ signal cannot be used as reference for the ^{1}H NMR spectra, because the phenanthrenyl and the phenyl-groups are present over a large area in the aromatic region. Therefore, the toluene CH$_3$ signal at 2.36 ppm is used here. The toluene is present in all samples because it could not completely be removed by the purification. Exemplarily the ^{1}H and ^{29}Si NMR spectra of V20_PHP40_PM40 and H40_PHM20_PP40 are shown below (Figures 191 and 192), because they represent all but the dimethylsiloxane-group in the ^{29}Si NMR.
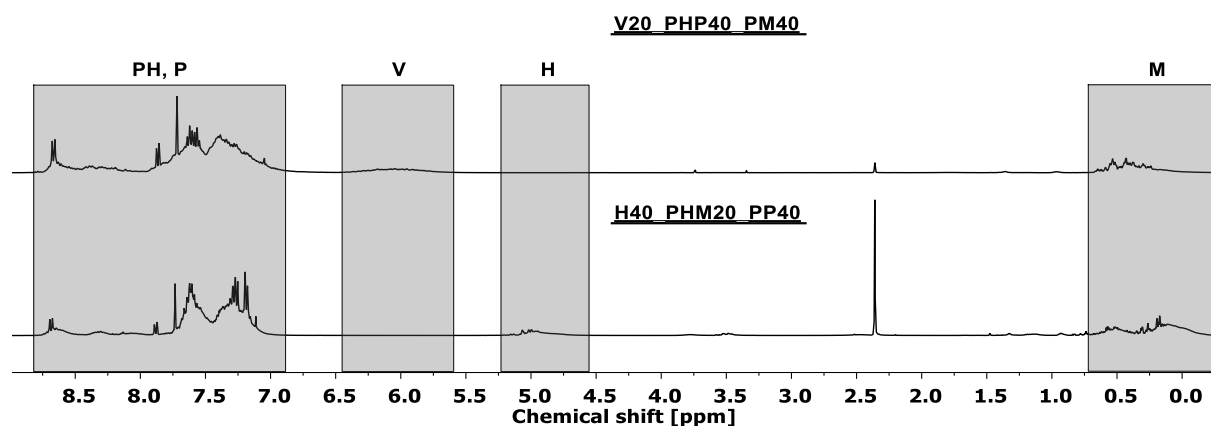
Figure 191: ^{1}H NMR (400 MHz, CDCl$_3$) of V20_PHP40_PM40 and H40_PHM20_PP40 to show all important regions.

The ^{1}H NMRs show the signals of the methyl (M, −0.5 – 0.5 ppm), the hydride (H: 4.6 – 5.3 ppm), the vinyl (V: 5.6 – 6.4 ppm) and the phenanthrenyl (PH) as well as the phenyl (P) groups in the region of 6.9 ppm to 8.8 ppm.

The ^{29}Si NMR spectra show a low signal-to-noise ratio because only 400 mg of sample were used and left, respectively. In the ^{29}Si NMRs there are seven regions of D signals referring to the seven silicon atoms with different side-groups. The lowest chemical shift signal relates to the MM group at around −17 ppm to −22 ppm,[321-324] but neither V20_PHP40_PM40 nor H40_PHM20_PP40 consists of these groups, therefore no signals are present in the spectra. The PM group shows signals at −27 ppm to −33 ppm[331, 368] and the PP group is located at −42 ppm to −46 ppm.[234-235, 319, 324, 331, 368] The signal from the methylsiloxane- (H) group can be seen at −34 ppm to −38 ppm[323-324, 331] and the signal of vinylphenylsiloxane (V) at −41 ppm to −43 ppm.[53,61,83] The phenanthren-9-ylmethylsiloxane (PHM) signal is in the region of −29 ppm to −37 ppm, the phenanthren-9-ylphenylsiloxane (PHP) one is located at −43 ppm to −50 ppm.

Both groups show slightly high-field shifted values compared to PM or PP, because of the larger aromatic system.[431, 490] The large signal range compared to molecules results from the impact of the neighboured groups inside the polymer as well as at the end of the chain to the chemical shift.[138] In the hydride polymerisations, the Piers-Rubinsztajn reaction can always occur, which is the formation of a Si-O-Si bond from Si-H and Si-OR.[514]
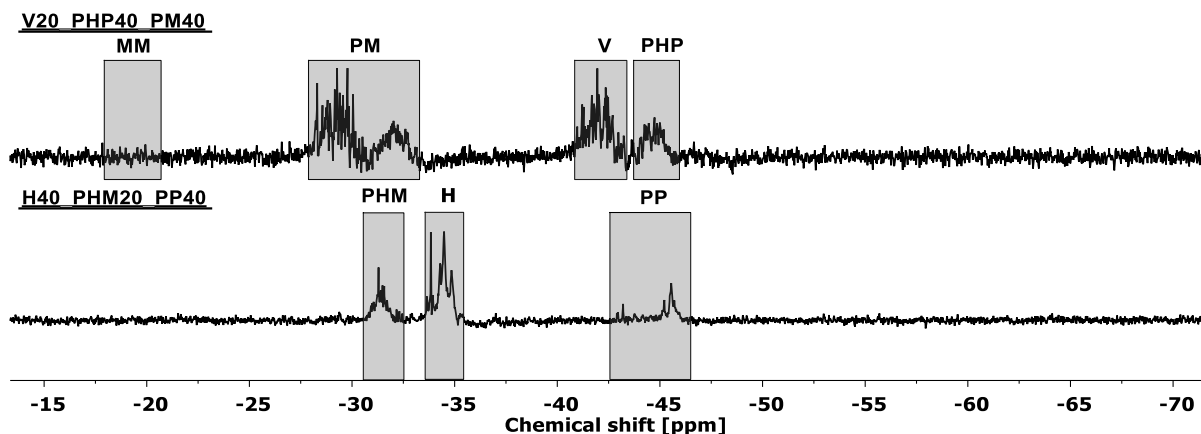
Figure 192: ^{29}Si NMR (101 MHz, CDCl₃) of V20_PHP40_PM40 and H40_PHM20_PP40 to show all important regions.

For H20_PHM40_PP40, additional signals in the 2D ^{1}H ^{29}Si HMBC NMR at around −19.5 ppm are visible (experimental section, Figure 403) that cannot observed in the 1D ^{29}Si NMR and therefore the amount is very small. Nevertheless, these signals are in an area where this copolymer should not have any signals, because it does not contain any dimethylsiloxane-groups (MM). Further analysis showed that these peaks belong to the methoxylated phenanthren-9-ylmethyl (MeO-SiPHM-O-) end group and indicates an uncompleted condensation process. Also, at 3.5 ppm in the ^{1}H NMR the methoxy signals are visible and can be assigned to the phenanthren-9-ylmethyl-group and the methylphenyl one via 2D ^{1}H ^{29}Si HMBC NMR (Figure 403). The integration at 3.4 ppm can be calculated to 0.5 methoxy-groups per hydride-group.

In the ^{29}Si NMR of H20_PHP40_PM40 are signals at around −20 ppm, which cannot be assigned to one of the three used monomers. Therefore, also a 2D ^{1}H ^{29}Si HMBC NMR was recorded (Figure 404), it showed, that the silicon atom is close to phenyl and methyl-groups, but not in the coupling range of phenanthren-9-yl- or hydride- groups. An explanation can be the reaction of the -MeSiH- group to a -MeSiC$_x$- one, because these aliphatic D groups like dimethylsiloxane (MM) show signals in this region. In the ^{1}H NMR about 0.3 methoxy groups at 3.5 ppm per hydride atom are also visible, which can be assigned to the -MeSiH-O- group applying 2D NMR spectroscopy. This group is in neighbourhood of one PHP group, which can

be seen by the highly low field shifted ^{1}H NMR signals at 8.5 ppm. The ethoxy-group intro-duced by the hydride monomer is no longer present, because no signals are visible in the ^{1}H and ^{13}C NMR. Instead, the methoxy signals are present in both NMRs. Therefore, during the polycondensation reaction the ethoxy-groups react before the methoxy-groups which was also observed in the kinetic study.

4.5.3.2.4 <u>Molecular weight determination of the phenanthrenyl-group containing copoly-mers</u>

The molecular weights of the linear hydride- or vinyl- and phenanthren-9-yl-containing copol-ymers were estimated using ^{1}H NMR spectroscopy and SEC analyses. For the ^{1}H NMR, the synthesised polysiloxanes were treated with *tert*-butyldimethylchlorosilane to introduce a ter-minal group which can be recognized in the spectrum (Figure 193). The OH end groups of the synthesized polysiloxanes were reacted with a high excess of the chlorosilane using triethyla-mine as catalyst. The introduced *tert*-butyl-group has a chemical shift of 0.9 ppm to 1.0 ppm with an integration of 18 protons for the two end groups and the dimethyl-groups are visible at 0.4 ppm revealing an integration of twelve protons for both end groups. The estimated mass of the hydride polymers is most likely slightly smaller than the real value, because of the possible reaction of the Si-H group with *tert*-butyldimethylchlorosilane under the basic conditions and the resulting polysiloxane might not be linear anymore. This side reaction is concluded from a lower integration of the hydride proton or from a T signal in the ^{29}Si NMR at −65 ppm,[321, 324] for example in the spectrum of H20_PHP40_PP40.
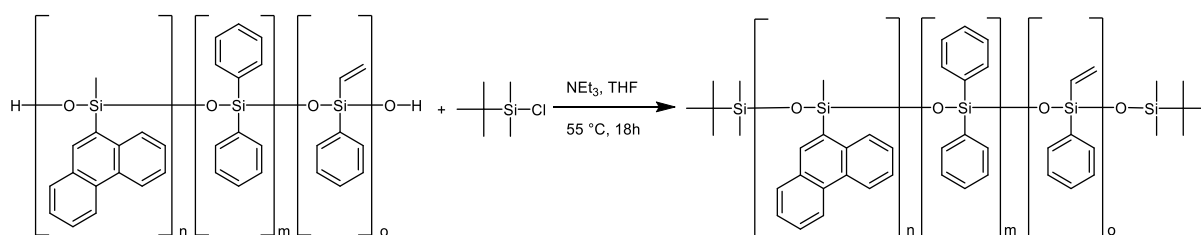
Figure 193: End group capping reaction of poly[vinylphenyl-*co*-phenanthren-9-ylmethyl-*co*-diphenyl]si-loxane (Vn0_PHMm0_PPo0) using *tert*-butyldimethylchlorosilane.

All calculated average molecular weights range from 6000 g/mol to 41000 g/mol (Table 50). The M$_W$ of the vinyl copolymers is higher or equal than the one of hydride copolymers, except H20_PHM40_MM40 and H40_PHM40_PP20. They also should show lower values compared to the vinyl compound, because of the lower reaction speed for hydride-containing ethoxides compared to vinyl ones.[515] The measured SEC masses vary between 800 g/mol and 2200 g/mol. Nearly all values are significantly lower than estimated by ^{1}H NMR spectroscopy. Potential problems in the NMR estimation method are unreacted and small molecules as well as the po-tential Si-H side reaction with the chlorosilane leading to non-linear molecules, which overall

Table 50: Molecular weight and PDI of hydride- respectively vinyl- and phenanthrenyl-group containing copolymers using ^{1}H NMR integration and SEC measurements.

Hydride H20_	Mw NMR [g/mol]	Mw SEC [g/mol]	PDI SEC	Vinyl V20_	Mw NMR [g/mol]	Mw SEC [g/mol]	PDI SEC
PHM40_MM40	27200	21900	3.12	PHM40_MM40	2200	2500	1.24
PHM40_PM40	8300	6300	1.74	PHM40_PM40	35200	8900	2.76
PHM40_PP40	15200	1200	1.26	PHM40_PP40	18800	8300	2.38
PHP40_MM40	6200	11800	3.05	PHP40_MM40	27100	12100	2.68
PHP40_M40	9100	3100	1.44	PHP40_PM40	8800	800	1.09
PHP40_PP40	10100	11900	3.67	PHP40_PP40	12800	1100	1.20
H40_				**V40_**			
PHM20_PP40	9500	3400	1.43	PHM20_PP40	13900	2700	1.38
PHM40_PP20	40700	4900	1.50	PHM40_PP20	27300	3000	1.47

lead to a different value than determined by SEC analyses. These small molecules cannot be detected by SEC because they eluate with the solvent front. The SEC method is very sensitive to the environment and the chemical composition of the polymer, leading to two obstructions. First, the SEC instrument was calibrated using polystyrene standards and therefore the masses cannot be directly compared to the polysiloxane masses and second, all polysiloxanes have different amounts of specific side-groups, which results in different interactions with the columns. For both methods, cyclic polysiloxanes are problematic for having no end groups which leads to a higher M_W estimation and being non-linear, which results in a chemically different environment.

The trend of the PDI values follow the length of the polysiloxane chains, higher M_Ws cause an increase of the PDI due to the broader mass distribution like seen in the kinetic analyses. The comparison of the SEC analysis of hydride- and phenanthren-9-ylmethyl-containing polymers (H20_PHM40_XX40) show a rapid decrease of M_W and PDI with increasing the size of the group *C* monomer, which can result from an increased activation energy due to steric hindrance. While the vinyl- and phenanthren-9-ylmethyl-containing polymers (V20_PHM40_XX40) display a small molecular weight for the dimethyl (MM) monomer; the phenylmethyl (PM) and

the diphenyl (PP) monomers have equal M_Ws. Here, the chemical environment may be important. In the reaction with PM or PP monomers, all educts have phenyl-groups which increase the miscibility of each other. The comparison of H20_PHP40_XX40 shows an increasing M_W from 6200 g/mol to 10100 g/mol in ^{1}H NMR studies from smaller to larger group C monomers. In the SEC measurements, the MM and PP containing polymers show an equally high M_W of 11800 g/mol while the PM polymer shows a M_W of only 3100 g/mol. For the V20_PHP40_XX40 polymers, the MM containing one has the highest M_W and PDI, while the larger group C monomers show lower values in the SEC and ^{1}H NMR.

The variation of the composition of the H, PHM and PP group containing copolymers, named Hm0_PHMn0_PPo0 and Vm0_PHMn0_PPo0, shows the smallest M_W and PDI for the 20 mol% H containing sample. The highest M_W and PDI shows the for the 20 mol% V containing sample. For the 40 mol% vinyl respectively hydride polysiloxanes containing low amounts of phenanthren-9-ylmethyl (PHM) or diphenyl (PP), the M_W as well as the PDI are higher for the X40_PHM40_PP20 than the X40_PHM20_PP40 which shows a reduced reaction speed when using higher amounts of PP compared to PHM monomers. The reason may be because of the two phenyl-groups, despite being smaller than the phenanthrenyl one, shield the silicon atom from two sides, while for the PHM monomer, only one sterically demanding group (PH) is present. The M group is very flexible and small and therefore has only a very small impact.

Overall, the observed results are difficult to interpret because of the chemical different monomers and catalysts, as well as the various analytical methods SEC and ^{1}H NMR giving different results. An explanation for these results can be the chemical difference between the small aliphatic methylsilane (H) and sterically large aromatic vinylphenylsilane (V) and their interaction with the small aliphatic dimethylsilane (MM) and sterically large aromatic diphenylsilane (PP) and phenanthren-9-yl (PH), as well as the used catalyst and the usage of diols and dialkoxides with their different reactivity towards each other and the catalysts.

4.5.3.2.5 Refractive index of the phenanthrenyl-group containing copolymers

RIs of the liquid copolymers vary from 1.521 to 1.633 (Table 51). All values, despite for PHP with PM or PP, are higher for the hydride copolymers. Because the RI depends both on molar refraction and molar volume according to the Lorentz-Lorentz equation,[136, 227-228, 516] the size of the side-group plays an important role. The sterically smaller monomer methyldiethoxysilane can lead to a denser network compared to the sterically more demanding vinylphenyldiethoxysilane. This leads to a higher impact of the phenanthren-9-yl-groups, as can be seen in the study of the different compositions of Xm0_PHMn0_PPo0. The RI rises with increasing the

amount of phenyl (P) groups, precisely substituting a methyl one with a phenyl one. For every group, the RI increases by about 0.015 for the hydride copolymers despite H20_PHP40_PP40. For the vinyl ones on the other side, no correlation can be observed as some polymers, despite having a higher phenyl content, show no or only a slight increase which can be caused by residual solvent seen in the NMR data. The V20_PHM40_PX40 show only a small RI change of 0.009 when switching the methyl-groups with the phenyl ones (X=M $\rightarrow$ X=P), while others like the V20_PHP40_XM40 show a large difference of 0.060.

Reducing the amount of PP groups and increasing the amount of PHM groups from X40_PHM20_PP40 to X40_PHM40_PP20 increases the RI approximately by a value of 0.020, which is within the earlier agreement, that every "ring" (phenyl-group) raises the value by 0.015. Increasing the hydride content from H20_PHM40_PP40 reduces the RI by 0.010 or 0.030 for H40_PHM20_PP40 or H40_PHM40_PP20. When increasing the vinyl content, the difference is very small because the V monomer already consists out of a phenyl-group and a vinyl one, which also has an RI impact close to the phenyl one according to the Lorentz-Lorentz equation.[136, 227-228, 516] This effect can be seen when substituting the V group with the PP one by comparing V40_PHM40_PP20 and V20_PHM40_PP40 which shows identical values around 1.558. The V40_PHM40_PP20 with one "ring" (P) more therefore has a 0.020 higher value than the other two.

Table 51: Refractive indices of hydride- or vinyl- and phenanthrenyl-group containing copolymers measured in transmission mode at 20 °C and 589 nm.

Hydride	RI	Vinyl	RI
H20_PHM40_MM40	1.593	V20_PHM40_MM40	1.521
H20_PHM40_PM40	1.612	V20_PHM40_PM40	1.569
H20_PHM40_PP40	1.627	V20_PHM40_PP40	1.578
H20_PHP40_MM40	1.602	V20_PHP40_MM40	1.573
H20_PHP40_PM40	1.618	V20_PHP40_PM40	1.633
H20_PHP40_PP40	1.603	V20_PHP40_PP40	1.630
H40_PHM20_PP40	1.599	V40_PHM20_PP40	1.596
H40_PHM40_PP20	1.616	V40_PHM40_PP20	1.576

4.5.3.2.6 <u>Thermogravimetric analyses of the phenanthrenyl-group containing copolymers</u>

Thermogravimetric analyses (TGA) were carried out for each vinyl and hydride copolymer under oxygen and nitrogen atmosphere up to 900 °C (experimental section, Figures 429 – 444).

The two different conditions in the TGA analyses help to verify the difference between the depolymerisation of the polysiloxanes which is mainly occurring under inert atmosphere and the pyrolytic decomposition of the organic groups which is observable under oxidative atmosphere.[217, 351, 353-354, 356, 359, 376, 517] In the inert gas measurements the atmosphere was switched to oxygen above 900 °C to decompose pyrolytic graphite, which was obtained from the organic groups and oxidise the silicon moieties to SiO_2 and also to clean the oven. To compare the start of the decomposition, again the $T_{95\%}$ value was used, which is the temperature at 5 % mass loss and 95 % residual mass, respectively.[518-521]

The temperatures at 95 % residual mass for the hydride and vinyl copolymers are shown in Table 52 and vary between 180 °C to 280 °C. These low numbers result in two special decomposition mechanisms named "intramolecular back biting mechanism" (IBBM) and "preliminary hydrolysis" (PLH).[119, 353, 522] PLH occurs when the terminal OH group of a linear polysiloxane reacts with the silicon atom inside its own chain to form a cyclotrisiloxane or a cyclotetrasiloxane. IBBM is similar, but the ring formation takes place inside the chain without opening it.

Table 52: Temperatures of the hydride- respectively vinyl- and phenanthrenyl-group containing polysiloxanes at 95 % residual mass under oxygen respectively under nitrogen atmosphere.

Hydride copolymer	$T_{95\%}$ O_2 [°C]	$T_{95\%}$ N_2 [°C]	Vinyl copolymer	$T_{95\%}$ O_2 [°C]	$T_{95\%}$ N_2 [°C]
H20_PHM40_MM40	234	248	V20_PHM 40_MM40	190	193
H20_PHM40_PM40	254	228	V20_PHM 40_PM40	202	207
H20_PHM40_PP40	246	247	V20_PHM 40_PP40	198	191
H20_PHP40_MM40	221	237	V20_PHP 40_MM40	213	202
H20_PHP40_PM40	210	211	V20_PHP 40_PM40	254	244
H20_PHP40_PP40	184	184	V20_PHP 40_PP40	193	177
H40_PHM20_PP40	269	282	V40_PHM 20_PP40	218	220
H40_PHM40_PP20	218	224	V40_PHM 40_PP20	202	202

These mechanisms occur at very low temperatures because of its low activation energy (167 kJ). While using PHM or PHP and MM the decomposition temperatures are higher for the hydride polysiloxanes than their relating vinyl polymers. An explanation can be the better miscibility due to chemical more similar side-groups between the methyl-groups during the synthesis, resulting in a higher molecular weight. Every monomer consists of at least one methyl-

group, including the hydride component. The vinyl monomer only consists of electron rich and sterically more demanding side-groups (V and P), which results in a lower reaction rate of vinyl-containing ethoxides compared to hydride ones[515] and overall to a lower molecular weight.

The onset temperature of degradation depends on the type and amount of end groups and the resulting molecular weight.[217-218, 222, 523] Under oxygen the degradation of shorter or longer polymer chains shows no difference. Under nitrogen atmosphere the smaller polymers show a higher onset temperature, because the unzipping mechanism (PLH) is dominant due to the larger relative amount of hydroxyl-groups.[218] For longer polysiloxanes, the intramolecular backbiting (IBBM) is faster than the preliminary hydrolysis (PLH) and therefore dominant.[67-70] When using a very high phenyl content like in the X20_PHP40_PP40, the $T_{95\%}$ temperature can, according to Chou and Yang, decrease.[402]

4.5.3.2.7 <u>Differential scanning calorimetry of the phenanthrenyl-group containing copolymers</u>

DSC measurements were carried out from −60 °C to 150 °C in two cycles (Figures 445 – 448). The first heating cycle was used to determine T_m (Table 53) of crystalline areas of the copolymers. The second heating cycle was used to detect the T_g (Table 53) and additional T_m's which could not observed in the first heating. The T_g is an indicator of the steric claim of the side-groups and their degree of freedom, whereas larger groups like phenanthren-9-yl or phenyl increase the value and smaller groups like hydride and methyl or more flexible groups like propyl decrease it.[119] In Table 53, T_m and T_g of the hydride and the vinyl copolymers are shown, T_{m1} was identified using the first cycle, the T_g values and additional observable melting temperatures (T_{m2} and T_{m3}) were determined using the second heating cycle. T_{m3} is just shown for completeness and, if observable, equals T_{m1} but with a lower energy. The T_g varies between −42 °C and 42 °C for these phenanthren-9-yl-containing copolymers. Overall, the T_g of the hydride compounds rises with increasing phenyl content from −17 °C to 7 °C. When substituting one methyl-group from H20_PHM40_MM40 with a phenyl one to H20_PHM40_PM40 and H20_PHP40_MM40, the temperature rises from −17 °C to 3 °C. Switching another group further raises the value to 7 °C. The highest phenyl-containing copolymer H20_PHP40_PP40 although has a lower T_g of 4 °C. Increasing the amount of the H monomer from H20_PHM40_PP40 reduces the T_g from 7 °C to −7 °C for H40_PHM20_PP40 and to 3 °C for H40_PHM40_PP20. Values around 0 °C can be referred to poly[diphenyl-*co*-dimethyl]siloxane (80:20, $T_g = 4$ °C) or polyphenylsiloxane with a flexible sidechain at the phenyl-group polydi-(4-propyl)phenylsiloxane, $T_g = −5$ °C).

Table 53: Melting and glass transition temperatures as well as the integrated energy of the melting temperatures of hydride- or vinyl- and phenanthrenyl-group containing copolymers.

Copolymer	Cycle 1				Cycle 2			
	T_{m1}	E_{m1}	T_{g1}	T_{g2}	T_{m2}	E_{m2}	T_{m3}	E_{m3}
	[°C]	[J/g]	[°C]	[°C]	[°C]	[J/g]	[°C]	[J/g]
H20_PHM40_MM40	47.1	3.300	−17.2					
H20_PHM40_PM40			2.1					
H20_PHM40_PP40			7.0					
H20_PHP40_MM40			3.3					
H20_PHP40_PM40	81.4	0.041	6.7		12.5	0.388		
H20_PHP40_PP40	83.7	24.49	4.2		58.8	3.706	82.2	12.89
H40_PHM20_PP40			−6.5					
H40_PHM40_PP20			3.5					
V20_PHM40_MM40	93.0	37.73	−42.3		90.0	31.56		
V20_PHM40_PM40	91.5	30.32	−18.3		86.6	26.04		
V20_PHM40_PP40	92.0	30.22	5.8		89.6	28.99		
V20_PHP40_MM40	85.9	27.52	−22.3	41.6	59.8	1.311	84.7	14.92
V20_PHP40_PM40	68.0	0.818	14.1					
V20_PHP40_PP40	70.3	11.92	−4.4		54.1	0.401	62.9	1.035
V40_PHM20_PP40	83.4	7.515	−18.2		−13.8	0.381		
V40_PHM40_PP20	87.3	31.33	−17.2		83.3	27.72		

Polymethylphenylsiloxanes with a phenyl and methyl content of 50 mol% each show a reduced T_g value of −28 °C. Polysiloxanes with hydride atoms, like polymethylhydridosiloxane, show a much smaller value of −138 °C compared to pure polydimethylsiloxane with a value of −123 °C because of the hydride-group being much smaller than the methyl one.[119]

The T_g of the vinyl copolymers ranges from −42 °C to 42 °C. Staring from the highly methylic V20_PHM40_MM40 with a T_g of −42 °C, a substitution of a methyl-group with a phenyl one increases the value to −18 °C for V20_PHM40_PM40. For V20_PHP40_MM40, a second glass transition temperature was observed, indicating the existence of a kind of block-polymer structure[399, 404, 524] with a highly methyl side-group containing region and a T_g of −22 °C and a highly phenyl side-group containing region with a T_g of 42 °C. In comparison with other polysilox-

anes, a T_g value of 50 °C refers to polydi-(p-tolyl)siloxane, whereas the less sterical polydiphenylsiloxane shows a lower value of 40 °C.[119] Another substitution of methyl-groups with phenyl ones drastically increases the values and shows, that it is important where the substitution is made. While switching a group at the group C monomer to V20_PHM40_PP40 rises the value to 6 °C, the substitution at the phenanthren-9-yl-group B monomer to V20_PHP40_PM40 leads to a greater increase to 14 °C, showing the larger sterical impact of the phenanthren-9-ylphenyl-group. The only exception, likewise in the hydride series, is the V20_PHP40_PP40 with a low T_g of −4 °C. Increasing the amount of V monomer and decreasing the amount of PHM or PP decreases the T_g to around −18 °C, respectively.

Some of the hydride copolymers show a melting temperature, for H20_PHM40_MM40 a T_{m1} of 47 °C and for H20_PHP40_PX40 a T_{m1} of around 82 °C is observable, while only the highly phenylic H20_PHP40_PP40 shows a significant amount of energy. All vinyl copolymers display a T_m which is in the range of 68 °C to 93 °C and decreases with increasing phenyl content.

4.5.3.3 Syntheses and characterisations of the cured phenanthrenyl-group containing polysiloxanes

The appropriate linear copolymers were mixed in a 1:1 ratio with 6.00 ppm of platinum catalyst, doctor bladed onto microscope glass slides with 120 µm and thermally cured in a hydrosilylation reaction at 100 °C for one hour and 150 °C for six hours (Figure 194). The resulting cured films are 50 µm to 60 µm thick.
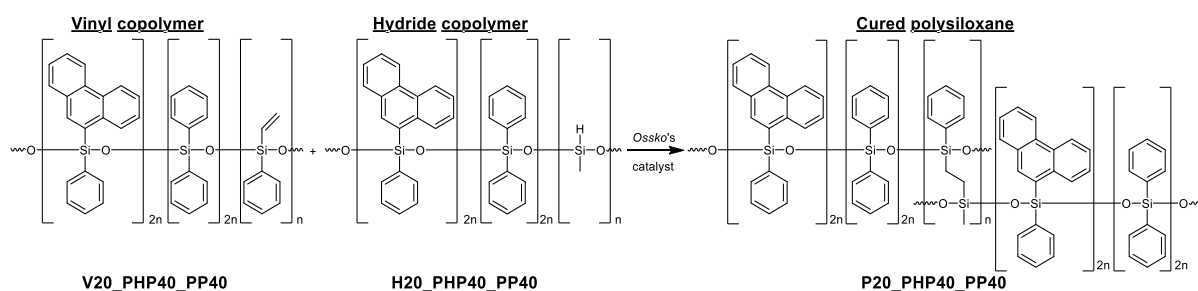
Figure 194: Curing reaction of a vinyl and the appropriate hydride copolymers exemplarily shown for V20_PHP40_PP40 and H20_PHP40_PP40 to P20_PHP40_PP40.

4.5.3.3.1 <u>FT-IR spectra of the cured phenanthrenyl-containing polysiloxanes</u>

All recorded FT-IR spectra of the cured phenanthrenyl-containing polysiloxanes are shown in Figure 195. Only the typical regions for the hydride and vinyl signals are marked because all signals of the copolymers were assigned earlier. All cured polymers show a reduced intensity for these bands. P40_PHM20_PP40 shows a small Si-H signal at 2164 cm^{-1} and a larger one at 897 cm^{-1},[234-235, 319, 346-347] which indicates an incomplete hydrosilylation reaction maybe caused by the high amount of diphenyl (PP) monomer. Also, the higher amount of cross-linkable hydride- or vinyl-groups may not find each other at some point during the formation of the dense network, because they are not able to move and react anymore.[396, 463] Despite there being unreacted-groups, a rigid, non-sticky material was obtained. P20_PHP40_MM40 shows a very small signal at 2162 cm^{-1} and at 893 cm^{-1} from the unreacted Si-H group. The other polymers show a negligible signal at 2160 cm^{-1} and at 900 cm^{-1}, but at 900 cm^{-1} other signals also overlap. The vinyl-group signals are located at 1406 cm^{-1} [26,27,48,85] and at 966 cm^{-1},[26,27,48,85] but they overlap with other aromatic signals from the phenyl or phenanthrenyl-groups and therefore can only hardly be used as an identification for residual vinyl-groups.

Overall, besides P40_PHM20_PP40, the polysiloxanes are almost fully condensed,[396] a full reaction cannot be achieved most of the time due to the increasing viscosity and reduced immobility of the reactive groups during the curing process,[136, 318, 395] especially here when the sterical demanding phenanthren-9-yl-groups are present. Post-curing processes are possible when the hydride-groups react in presence of platinum and oxygen or moisture.[525]
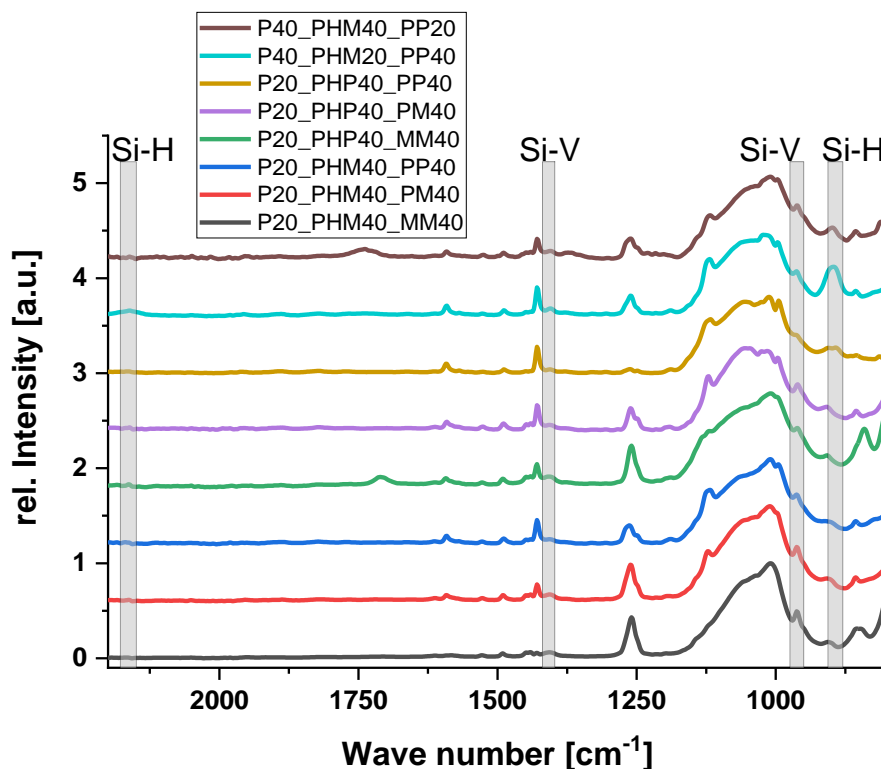
Figure 195: FT-IR spectra of the cured phenanthrenyl-containing polysiloxanes.

4.5.3.3.2 CP MAS NMR spectra of the cured phenanthrenyl-containing polysiloxanes

One ^{13}C and one ^{29}Si CP MAS NMR of P20_PHP40_MM40 were recorded as example of the cured phenanthrenyl-group containing polysiloxanes. In the carbon NMR (Figure 196), two regions of signals are visible. One for the aliphatic carbon of the methyl atoms[322, 332] and the one of the ethyl bridge[333] at −5 ppm to 10 ppm and one for the aromatic atoms of the phenyl and phenanthrenyl atoms at 120 ppm to 140 ppm.[369]
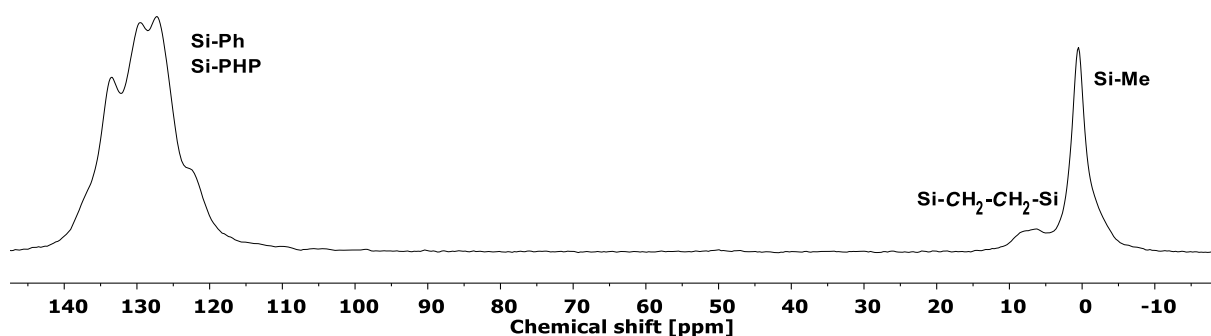
Figure 196: ^{13}C solid-state CP MAS NMR (101 MHz, 13 kHz) of P20_PHP40_MM40.

The silicon atom NMR is displayed in Figure 197. The signal at −20 ppm can be referred to the dimethyl silicon atom (MM)[321-324] as well as the MeSi(OR)$_2$-CH$_2$-CH$_2$-X silicon atom,[331, 333] which was verified by using a ^{1}H ^{29}Si HMBC measurement of the related H20_PHP40_MM40 polymer. The peak at around −35 ppm is caused by the PhSi(OR)$_2$-CH$_2$-CH$_2$-X atom,[331, 368] which was also confirmed with liquid ^{1}H ^{29}Si HMBC measurements of V20_PHP40_MM40.

The signal at −47 ppm can be referred to the D silicon atom with the self-synthesised phenanthren-9-ylphenyl- (PHP) group, which can be compared to a high field shifted diphenyl silicon atom,[324, 331, 368] because of the larger conjugated polycyclic aromatic.
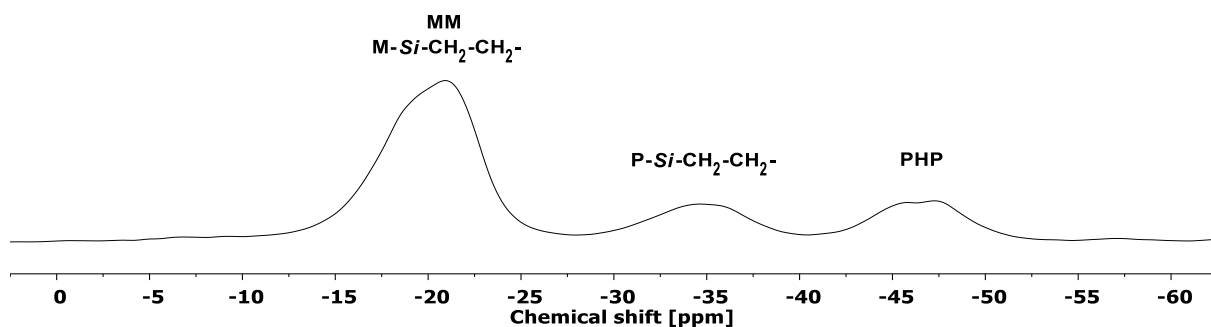
Figure 197: ^{29}Si solid-state CP MAS NMR (80 MHz, 13 kHz) of P20_PHP40_MM40.

4.5.3.3.3 Refractive index of the cured phenanthrenyl-containing polysiloxanes

RIs of the cured phenanthrenyl-group containing polysiloxanes were determined in reflection mode using the high RI 1-bromonaphthalene as contact fluid at 20.0 °C and 589 nm and varies from 1.569 to 1.630 (Table 54). For the comparison between the P20_PHX40_XX40 polymers, the methyl and phenyl-group from the H and V monomer as well as the phenanthrenyl-group were neglected, because they are present in all polysiloxanes in a constant amount. With increasing phenyl content starting from P20_PHM40_MM40 with three methyl-groups and zero phenyl-groups and a RI of 1.569, a substitution of one M group with a P one increases the RI to 1.599 for P20_PHM40_PM40 and 1.590 for P20_PHP40_MM40. This supports previous observations, at least for P20_PHM40_PM40, that one more phenyl-group increases the RI by about 0.020. The impact of a phenyl-group at a different silicon atom than the phenanthrenyl one is here slightly higher and results in an increase of 0.030. A further M group substitution to two P groups and one M one increases the RI to 1.614 for P20_PHM40_PP40 which is an increase of 0.015 to 0.024 depending on whether it is compared to P20_PHP40_MM40 and P20_PHM40_PM40. P20_PHP40_PM40, however shows a RI of 1.627 which is only 0.013 higher than P20_PHM40_PP40 with the same amount of phenyl and methyl-groups. The smaller increase shows that in the region of 1.63 the lower RI contributing groups like phenyl only have a smaller overall impact. Particularly, when taken the RI of P20_PHP40_PP40 with 1.630 into account, which is 0.016 higher than the P20_PHM40_PP40 or 0.003 higher than the P20_PHP40_PM40, both with one less phenyl side-group.

Comparing the polysiloxanes with different monomer content (Pm0_PHMn0_PPo0), the one with the lowest amount of cross-linkers, P20_PHM40_PP40, has the highest RI with 1.614. Comparing the increase of the amount of PP groups (P40_PHM20_PP40) while reducing the amount of the PHM ones in P40_PHM40_PP40 shows a slight increase of the RI from 1.603 to

1.605 and therefore has no significant impact. Overall, one substitution of a methyl-group with a phenyl one increases the RI by around 0.020 and the refractive index increment of the PHM group is comparable to the PP one.

Table 54: Refractive indices of the cured phenanthrenyl-containing polysiloxanes.

Cured polymer	RI
P20_PHM40_MM40	1.569
P20_PHM40_PM40	1.599
P20_PHM40_PP40	1.614
P20_PHP40_MM40	1.590
P20_PHP40_PM40	1.627
P20_PHP40_PP40	1.630
P40_PHM20_PP40	1.603
P40_PHM40_PP20	1.605

4.5.3.3.4 <u>**Thermogravimetric analyses of the cured phenanthrenyl-containing polysiloxanes**</u>

TGA measurements were carried out to analyse the thermal stability of the cured phenanthrenyl-group containing polysiloxanes (experimental section, Figures 429 – 444) under the same conditions as the copolymers. The decomposition temperatures ($T_{95\%}$, Table 55) for the cured polysiloxanes under oxygen vary between 300 °C and 370 °C, while the temperatures under nitrogen atmosphere range up to 420 °C with decreasing methylic and increasing phenylic content, which is agreement with the literature.[218, 234, 317, 402] P20_PHM40_MM40 shows a $T_{95\%}$ of 309 °C under oxygen atmosphere. Switching a methyl-group with a phenyl one increases the temperature to 329 °C for P20_PHP40_MM40 and 347 °C for P20_PHM40_PM40. A further substitution with a phenyl-group raises the temperatures to 364 °C for P20_PHP40_PM40, while for the phenanthrenylmethyl-containing polymer P20_PHM40_PP40 no increase is observable. The highly phenylic P20_PHP40_PP40 shows the highest value with 366 °C under oxygen. Under nitrogen atmosphere the $T_{95\%}$ value is with 341 °C about 30 °C higher than the one under oxygen atmosphere. P20_PHP40_MM40 shows a decomposition temperature of 342 °C, which is only marginally higher despite the methyl to phenyl substitution.

Table 55: TGA values of the cured phenanthrenyl-group containing polysiloxanes under oxygen and nitrogen atmosphere.

Cured polymer	$T_{95\%}$ O_2 [°C]	$T_{95\%}$ N_2 [°C]
P20_PHM40_MM40	309	341
P20_PHM40_PM40	347	301
P20_PHM40_PP40	346	335
P20_PHP40_MM40	329	342
P20_PHP40_PM40	364	367
P20_PHP40_PP40	366	416
P40_PHM20_PP40	350	377
P40_PHM40_PP20	340	396

For P20_PHM40_PM40, a $T_{95\%}$ of only 301 °C can be measured, which is probably due to residual solvent like toluene or an uncompleted sol-gel reaction, because in the graph in Figure 430 (red) the mass loss starts already at 150 °C, which is very unusual for cross-linked polysiloxanes. With a $T_{95\%}$ of 335 °C, P20_PHM40_PP40 is in the range of the previously mentioned phenanthrenyl polymers under nitrogen. P20_PHP40_PM40 however shows an increased temperature with 367 °C and shows the impact of the high amount of phenyl-groups.

The highest value under nitrogen has the highly aromatic P20_PHP40_PP40 with 416 °C. Overall, the phenanthrenylphenyl-group containing polysiloxanes show a higher $T_{95\%}$ value than phenanthrenylmethyl ones with the same amount of phenyl-groups.[24,48,122] Besides the variation of monomers, different monomer contents for Pm0_PHMn0_PPo0 were also studied. The cured polysiloxanes show little difference in their decomposition behaviour under oxygen atmosphere with temperatures ranging from 340 °C to 350 °C. Under nitrogen an increasing stability for the higher cross-linked polysiloxanes P40_PHMx0_PPx0 is observable.[218] The P20_PHM40_PP40 has a $T_{95\%}$ value of 335 °C while the one with the increased phenanthrenylmethyl content, P40_PHM40_PP20, shows the highest value with 396 °C. The polymer with the high diphenyl content, P40_PHM20_PP40, has a 20 °C lower decomposition temperature of 377 °C.

The thermal stability is independent of the aromatic content when the amount of P or PH side-groups is in between 30 % to 70 % with a $T_{95\%}$ value of 300 °C to 350 °C. With higher aromatic

content over 70 %, the thermal stability ranges from 360 °C to 416 °C. For nearly all polysilox-anes the decomposition temperature is higher or equal under nitrogen compared to the values under oxygen, which is the case when comparing low molecular weight polymers.[218, 356]

4.5.3.3.5 Differential scanning calorimetry of the cured phenanthrenyl-containing pol-ysiloxanes

DSC measurements of the cured phenanthren-9-yl-group containing polysiloxanes were carried out from −60 °C to 150 °C in two cycles analogously to the DSC measurements of the copoly-mers (experimental section, Figures 449 – 450). Curing generally increases the T_g compared to the ones obtained from the relating copolymers, because the increased cross-linking decreases the mobility of the polymer chain and the side-groups.[273, 526] The measurements of the cured polymers were carried out although cross-linking decreases the ability of crystallisation and therefore, smaller respectively no signals can be observed.[273, 460, 526-532] The integrated energy of the melting area therefore can be used as an indirect measurement of cross-linking.[526, 532] Also, a shift of the melting temperatures to lower values is visible which was already reported by Bac et al.[529] The T_m of the cured polysiloxanes (Table 56) are consequently lower than the ones of the linear polymers with the relating monomer composition,[529] despite the highly me-thylic H20_PHM40_MM40.

Table 56: Differential scanning calorimetry of the cured phenanthrenyl-group containing polysiloxanes.

Cured polymer	T_g [°C]	T_m [°C]	E_m [J/g]
P20_PHM40_MM40	17.0	−	−
P20_PHM40_PM40	49.0	59.0	3.688
P20_PHM40_PP40	39.2	52.5	2.597
P20_PHP40_MM40	33.6	55.5	0.043
P20_PHP40_PM40	51.3	61.3	3.956
P20_PHP40_PP40	25.3	60.6	0.401
P40_PHM20_PP40	41.7	53.6	2.014
P40_PHM40_PP20	43.2	53.4	1.819

The T_g's of all cured polysiloxanes are significantly higher than their relating hydride and vinyl copolymers. The T_g first ascends with increasing phenyl content from 17.0 °C for P20_PHM40_MM40 to 51.3 °C for P20_PHP40_PM40, but no clear side-group correlation can be made because P20_PHM40_PM40, despite having a low amount of phenyl-groups shows

the second highest T_g with 49.0 °C. Also, P20_PHP40_PP40, which is the polymer with the highest aromatic content, has a comparably low T_g value of 25.3 °C.

The T_m of all cured polysiloxanes vary between 52 °C and 61 °C where a higher phenyl content tendentially leads to higher temperatures. The polysiloxane with high amounts of methyl-groups, P20_PHM40_MM40, shows no T_m.

Varying the amount of monomers for the cured PHM and PP group containing polysiloxanes, named Pm0_PHMn0_PPo0, only shows a slight difference in the melting temperature around 53 °C. The energy of the integrated area although increases from P40_PHM40_PP20 over P40_PHM20_PP40 to P20_PHM40_PP40 and shows the increased mobility of the polymer when reducing the amount of PHM and increasing the amount of the sterical less demanding PP group and reducing the cross-linking from P40_PHMn0_PPo0 to P20_PHM40_PP40. The T_g shows the opposite trend, the increasing mobility and reduced cross-linking from P40_PHM40_PP20 over P40_PHM20_PP40 to P20_PHM40_PP40 decreases the T_g from 43.2 °C over 41.7 °C to 39.3 °C.[162,163]

4.5.3.3.6 <u>UV/Vis measurements of the cured phenanthrenyl-group containing polysiloxanes</u>

The cured films on microscope slides (Figure 198) are all highly transparent and colourless or slightly yellow.

P20_PHM40_			P20_PHP40_		Pn0_PHMm0_PPo0		
MM40	PM40	PP40	MM40	PM40	2-4-4	4-2-4	4-4-2
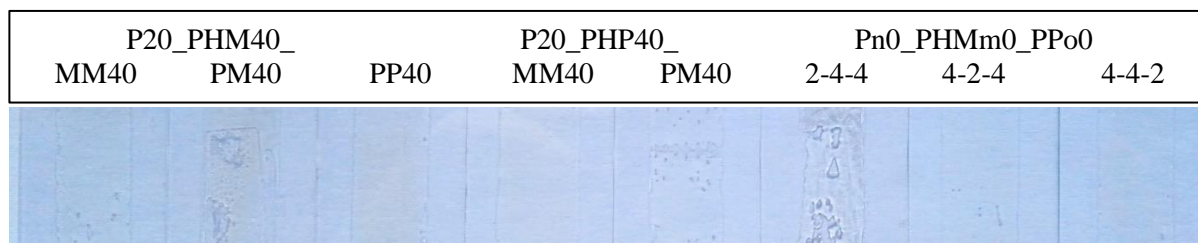
Figure 198: Optical pictures of the cured phenanthrenyl-containing polysiloxanes onto glass slides on blue paper to increase the visibility of the yellow colour.

The polysiloxanes were analysed using an UV/Vis spectrometer with an integrating sphere to consider the dispersion of the films (Figure 199), the calculated haze curve is reported in the experimental section (Figure 451). At 450 nm, all polysiloxanes show a transmission from 96 % up to 99 % (Table 57). The transmission decreases with increasing phenyl content and increasing RI.[18, 533-534] The highly methylic P20_PHM40_MM40 reveals the highest value of 99 %. Replacing one methyl-group with a phenyl one to P20_PHM40_PM40 shows no change and to P20_PHP40_MM40 slightly reduces the transmission down to 98 %. By further increasing the aromatic content the transmission is reduced to 97 % for P20_PHP40_PM40 or remains at 98 %

for P20_PHM40_PP40. The highly phenylic sample P20_PHP40_PP40 shows the lowest but still very high transmission of 96 %.
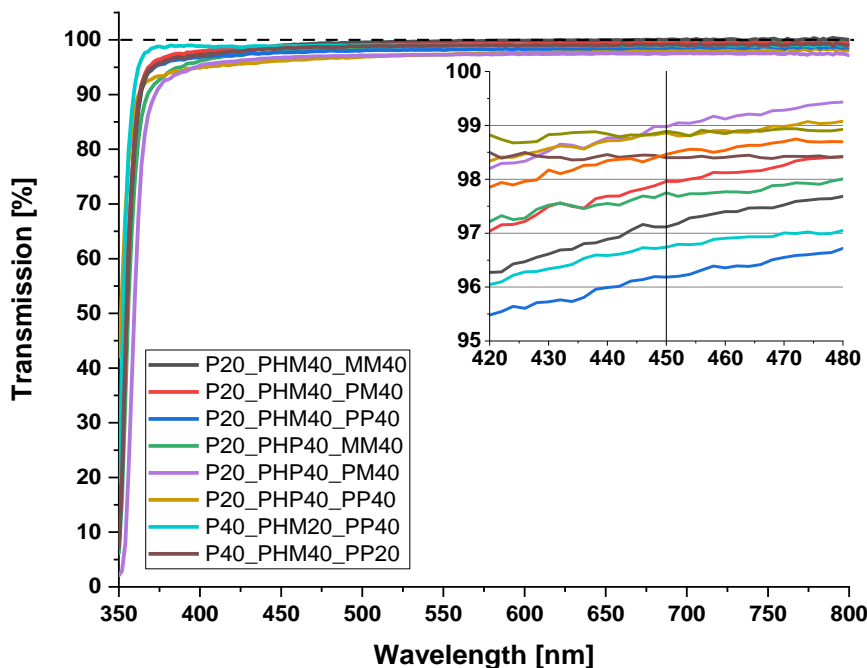
Figure 199: Transmission spectra of cured phenanthrenyl-group containing polysiloxanes onto microscope slides.

The same trend can also be observed when varying the composition of Pm0_PHMn0_PPo0. The sample with the highest aromatic content, P20_PHM40_PP40, shows the lowest transmission value with 98 %. The difference between the high amounts of PHM compared to the high amounts of PP is very small. Nonetheless, the P40_PHM20_PP40 shows 99 % transmission while the P40_PHM40_PP20 shows 98 %.

To evaluate the amount of light, which is diverted by passing through the samples, the haze values were calculated. Therefore, the transmission values and the measured diffusion values are required. The haze value at 450 nm varies from 8 % to 9 % for the low phenyl-containing polysiloxanes like P20_PHM40_XX40 or P20_PHP40_MM40. P20_PHP40_PM40 and P20_PHP40_PP40 with higher aromatic content show values of 15 % respectively 19 %. The comparison of Pm0_PHMn0_PPo0 shows a haze values of around 9 % for the 40 mol% PHM containing ones and 15 % for P40_PHM20_PP40.

The WI's and YI's[535-537] were calculated using the spectrometer software, the values are shown in Table 57. YI values larger than zero are implying yellow probes, negative values blue ones. A WI value of 100 is achievable, higher values imply bluish and lower values yellowish samples. YIs vary from 0.0 to 1.7 and imply a slightly yellow colour. However, these amounts are

so small that they can only barely be seen in the thin films. The values are increasing with higher phenyl content, which was already observed in literature.[12, 273, 538-540]

Table 57: Transmission and haze values at 450 nm and yellowness and whiteness indexes of the cured phenanthrenyl-group containing polysiloxanes.

Polysiloxane	T_{450} [%]	H_{450} [%]	YI	WI
P20_PHM40_MM40	99	9	0.8	97.0
P20_PHM40_PM40	99	8	0.6	97.5
P20_PHM40_PP40	98	9	0.8	97.1
P20_PHP40_MM40	98	8	1.1	97.0
P20_PHP40_PM40	97	15	0.9	96.2
P20_PHP40_PP40	96	19	1.7	93.6
P40_PHM20_PP40	99	15	0.0	98.7
P40_PHM40_PP20	98	9	0.5	97.6

The phenanthrenylmethyl-group containing polymers show a value below 0.8. The samples with the phenanthrenylphenyl-group containing monomer show higher values of 0.9 to 1.7. WIs between 96.2 and 97.5 were observed for nearly all samples, only P20_PHP40_PP40 shows a lower value of 93.6. The value can be increased using low amounts of phenyl and high amount of methyl-groups in the polysiloxanes.[12, 273, 538-540] The P40_PHM20_PP40 sample, with the lowest amount of phenanthrenyl side-groups shows the highest WI of all samples with 98.7. This clearly shows the direct correlation of delocalised electrons and the yellow colour.[12, 273, 538-540]

4.5.3.3.7 <u>**Thermal aging test of the cured phenanthrenyl-group containing polysiloxanes**</u>

To simulate the thermal aging inside the LED, the cured polysiloxanes were treated under operating temperatures of high energy LEDs, which is in the range of 150 °C to 200 °C.[364, 394] The thermal stability was verified by calculating the colouration of the samples using UV/Vis measurements. The synthesised polysiloxanes were thermally treated for 63 days at 180 °C in air atmosphere and ambient humidity (Figure 200) while UV/Vis measurements were carried out regularly and the transmission values at 450 nm are displayed (Figure 201). YI and WI were compared before and after the thermal treatment (Figure 202). The phenanthrenylmethyl-group containing samples show a decreasing transmission after 63 days with increasing phenyl content down from 94 % for P20_PHM40_MM40 over 91 % for P20_PHM40_PM40 down to

82 % for P20_PHM40_PP40. The phenanthrenylphenyl-group containing polysiloxanes show a more rapid decrease with increasing phenyl content. The transmission of P20_PHP40_MM40 decreases to 83 % after the thermal treatment. P20_PHP40_PM40 shows a linear reduction of the transmission down to 66 %.
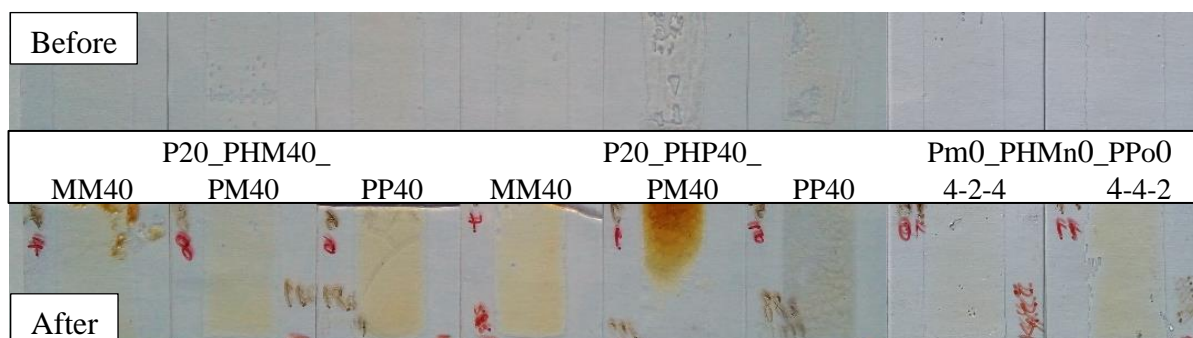
Figure 200: Transmission of the phenanthrenyl-group containing polysiloxanes after the synthesis (top) and after the thermal treatment (bottom).

The polysiloxane with the highest aromatic content, P20_PHP40_PP40 still remains at 88 %. The varied composition of Pm0_PHMn0_PPo0 also shows a decreasing transmission during the 63 days with increasing phenyl content down to 94 % for P40_PHM20_PP40, to 86 % for P40_PHM40_PP20 and to 82 % for P20_PHM40_PP40.
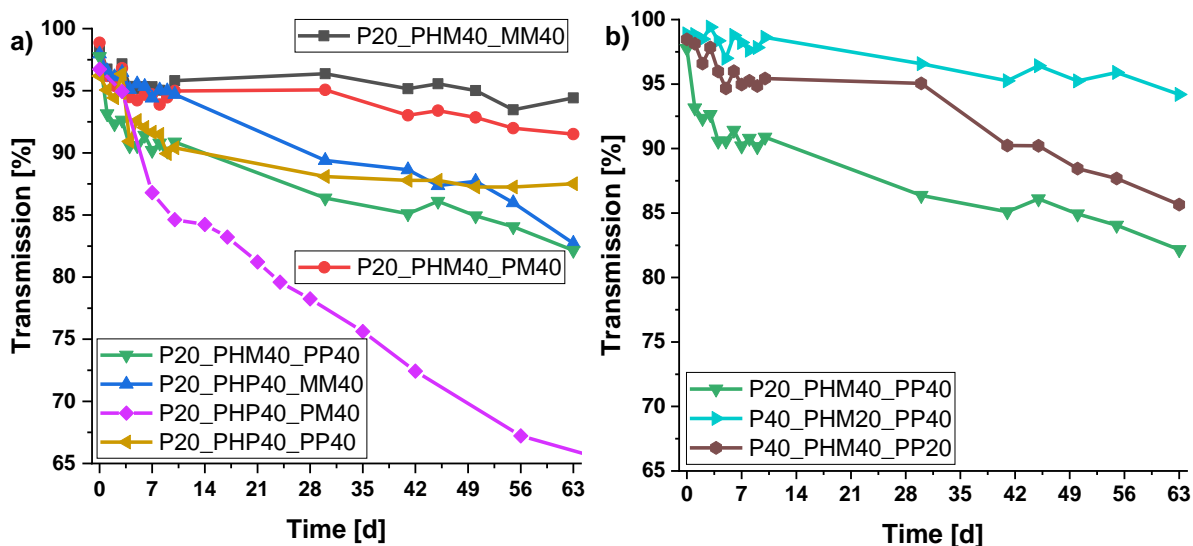
Figure 201: Transmission at 450 nm of cured phenanthrenyl-group containing polysiloxanes during thermal treatment at 180 °C under air atmosphere, a) P20_PHX40_XX40 and b) Pm0_PHMn0_PPo0.

The calculated yellowness and whiteness indices implicate a yellowing of the polysiloxanes (Figure 202) which can already be seen in the optical images.[535-537] With increasing phenyl content from P20_PHM40_MM40 to P20_PHM40_PP40 the yellowing increases linear, from around 0.8 YI for the as synthesised polysiloxanes up to 18.7 YI and from 97.1 WI down to 41.9 WI. The phenanthrenylphenyl-group containing samples P20_PHP40 _MM40 and

P20_PHP40_PM40 display a strong yellow colour which increases with increasing phenyl content, the YI increases from around 1.0 to 17.0 respectively 27.5. The WI shows the same tendency by decreasing from 96.5 down to 48.3 for P20_PHP40 _MM40 respectively to 5.8 for P20_PHP40_PM40 in the first M to P switch. Interestingly, the sample with the highest phenyl content, P20_PHP40_PP40, only shows very little yellowing, which is comparable to the highly methyl-containing sample P20_PHM40_MM40. The YI increases from 1.7 to 4.4, while the WI decreases from 93.6 to 79.9.

Varying the composition of the monomers for Pm0_PHMn0_PPo0 shows little to no difference, for the YI from 0.0 to 0.8 and for the WI from 97.1 to 98.7. The yellowing increases with increasing aromatic content from P40_PHM20_PP40 over P40_PHM40_PP20 to P20_PHM40_PP40 with 4.2 over 11.0 to 18.7. The WI shows the same trend by decreasing from 87.5 over 65.8 down to 41.9. The yellowing most likely occurs due to the formation of phenyl radicals, which are produced from cleaving of backbone chains.[12, 541]
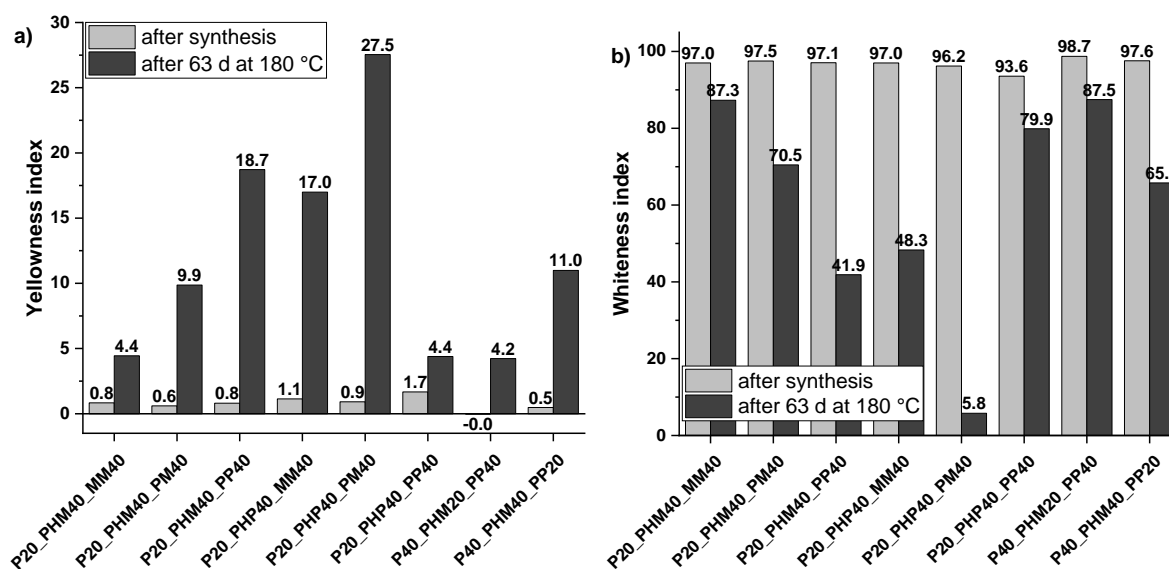
Figure 202: Yellowness (a)) and whiteness (b)) indices bevor and after thermal treatment at 180 °C for 63 days under air atmosphere of the cured phenanthrenyl-group containing polysiloxanes onto microscope glass slides.

4.5.3.4 Conclusion for the phenanthrenyl containing polysiloxanes

We synthesised two new novel phenanthrenyl-containing monomers which show very high RI values of 1.631 for the phenanthren-9-ylmethyldimethoxysilane (PHM) and an approximated value of ~1.700 for the phenanthren-9-ylphenyldimethoxysilane (PHP). With these monomers and the usual V, H, MM, PM and PP monomers new hydride- and vinyl-group containing co-polymers were synthesised (Figure 203). Besides the usual 20 mol% group *A* and 40 mol% group *B* as well as *C* monomers, for Xm0_PHMn0_PPo0 different amounts were used to study the impact of the individual monomers. These linear polymers have a tuneable RI of 1.521 to 1.633, which is a slightly larger range compared to the thioanisole ones. The thermal stability although reaches a maximum of 280 °C, which is lower than the maximum value of the thioanisole copolymers or the commercial ones. The glass transition temperature ranges from −42 °C to 14 °C when neglecting V20_PHP40_MM40, because it shows two T_g signals. Nonetheless, the T_g region is slightly larger than for the thioanisole-group containing polymers. These novel hydride and vinyl copolymers were thermally cross-linked using *Ossko's* platinum catalyst.
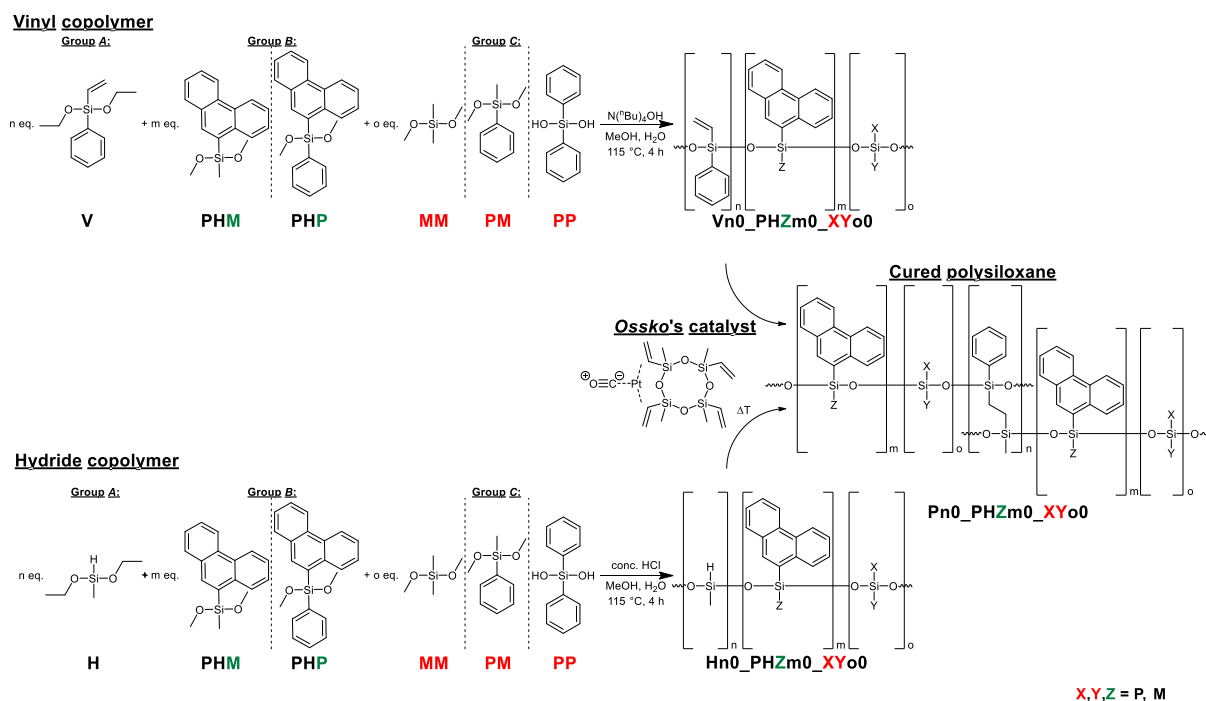
Figure 203: Overview of the synthesis of phenanthrenyl-group containing polysiloxanes from monomers.

These new solid materials show a very high refractive index of 1.569 to 1.630 depending on the used copolymers, which is identical to the range of the thioanisole-group containing ones but significantly higher than the 1.552 of the OE-6630. A very high transmission of 96 % to 99 % with reducing phenyl content can be achieved for the polysiloxanes, which is slightly lower than the one for the thioanisole ones or the commercial systems. The calculated colouration from the yellowness and whiteness indices are close to the optimal value of zero for the YI

and 100 of the WI. The self-prepared phenanthrenyl-containing polysiloxanes show YIs of 0.0 to 1.7 for the highly aromatic ones, but most of the values are in the range of the OE-6630 and the thioanisole-group containing polymers. The WIs range from 94 to 97 and therefore are lower than the 97 to 100 for the sulfur polymers respectively the OE-6630 system. The glass transition temperatures can be tuned from 17 °C to 51 °C with increasing the arylic and decreasing the methylic content. The thermal stability of the systems can be increased up to 416 °C for the highly aromatic P20_PHP40_PP40 when using the $T_{95\%}$ criteria, which is in the range of the thioanisole-containing PPSMPS with 420 °C or the OE-6630 polysiloxane with 430 °C. The simulated thermal aging test showed a high transmission of over 94 % for P20_PHM40_MM40 and P40_PHM20_PP40 which is larger than the 90 % for the P20_PSMP40_PM40 system after the 63 days under 180 °C while the commercial OE-6630 remained at 99 % transmission over this period. Here again, small residuals from the synthesis and a relatively high content of platinum of 6.00 ppm reduces the transmission under the thermal aging. The platinum catalyst can form yellow Pt nanoparticles[136, 474, 507] and the effect is even increased when free Si-H groups are present. Therefore, the content was lowered to 1.63 ppm for the phenoxyphenyl and phenylthiomethyl-group containing polymers. Additionally, aromatic side-groups, which here are represented in large numbers, lead to yellowing of the cured polysiloxanes.

Overall, novel cured polysiloxanes with the newly synthesised monomers could be prepared which show comparable properties like the commercial OE-6630 system but have a drastically increased refractive index like the self-synthesised thioanisole-group containing polymers. For some compositions, the long thermal treatment leads to a reduced transmission which is caused by yellowing of the samples. Some impurities and a relatively high amount of platinum caused this problem, which has to be solved. Nonetheless, these materials are very suitable for high-energy LED encapsulation when slightly improving the synthesis progress.

4.6 Results obtained from *OSRAM Opto Semiconductors*

In cooperation with *OSRAM Opto Semiconductors*, some well-chosen copolymer systems (H and V) were tested directly on LED chips. The selection of the chips and the reference systems as well as the performed measurements were carried out by OSRAM employees. First, blue LED chips (Duris S5) which emit at 450 nm were used because the focus was on white LEDs in the beginning of the project.[542-543] The chip of blue LEDs often consists of GaN with a RI of 2.49[544] or InGaN with a RI of 2.59[545-546] both at 450 nm. After the first test from OSRAM, they shifted to red LED chips (Oslon[2] Hyper Red) which emit at 660 nm.[547] The chip consists of InGaAlP with a refractive index of 3.59 at 660 nm.[548] This change was made because the energetically weaker radiation and the lower thermal stress of these LEDs should provide better testing results with the self-synthesised materials. For red emitting LEDs the impact of a high refractive index is more important in receiving a high lumen output because the LED chip has a higher RI than blue LED chips.

4.6.1   Testing of P20_PHM40_PP40 with the Duris S5 LED

Several LEDs (Duris S5,[542-543] Figure 204) were casted with the self-prepared polysiloxane P20_PHM40_PP40. The mould is 3 mm x 3 mm and the here used blue fluorescing chip has a dimension of 2 mm x 2 mm, electrical details cannot be described because the chips are available in different versions. A 1:1 mixture of H20_PHM40_PP40 and V20_PHM40_PP40 with *Ossko*'s platinum catalyst was casted into the mould by hand with a syringe. The moulds were placed on a hot plate to reduce the viscosity and receive a bubble-free film.
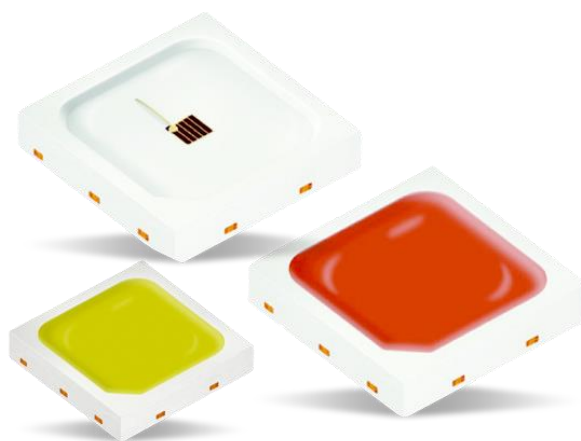
Figure 204: OSRAM Duris S5 mould with a small exemplarily shown chip and coloured encapsulation material.[549]

Besides the P20_PHM40_PP40, a reference polymer LPS5547S-1,[550] was used as well as a chip without casting. The LPS5547S-1 was manufactured by Shin-Etsu and has a refractive index of 1.51 to 1.53[550] and therefore is a methyl- and phenyl-group containing polysiloxane comparable to the OE-6630 system. Different currents from 10 mA to 250 mA were applied (Figure 205) and the lumen were measured. These correlate to the brightness and the light extraction of the chip. The LED chip without encapsulant always shows the highest lumen with 9.45 lm at 250 mA. The second highest is always the LPS5547S-1 for example with 8.50 lm at 250 mA. The self-synthesised P20_PHM40_PP40 always shows the lowest value and only reaches 7.10 lm at 250 mA. According to a personal communication with OSRAM, the main advantage of the high refractive index polymer P20_PHM40_PP40 can only be seen in combination with a fluorescent dye and a lens. Therefore, no additional tests or explanations were made, and the further testing was optimised.
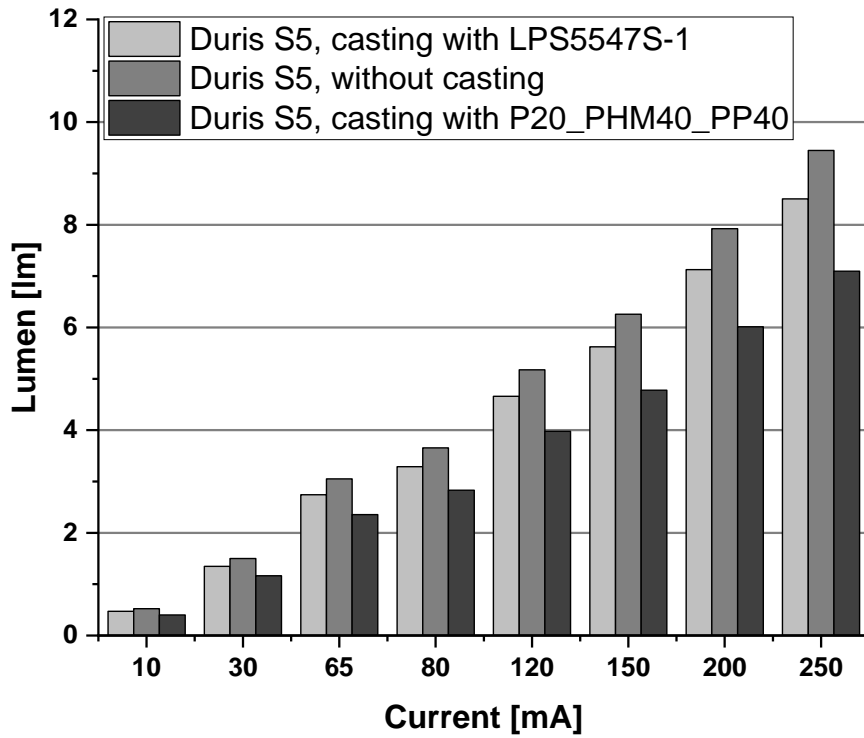
Figure 205: Comparison of the lumen output from the Duris S5 chip without and with casting of LPS5547S-1 or P20_PHM40_PP40.

4.6.2 Testing of various polysiloxanes with the Oslon² Hyper Red LED

For further and extended testing, a different LED chip was chosen by OSRAM employees, because the advantages of high RI polysiloxanes can be better evaluated using high RI chips. The longer wavelength of 660 nm of the Oslon² Hyper Red[547] also leads to a radiation with lower energy which should increases the lifetime of the self-synthesised polysiloxanes. The Oslon² Hyper Red (Figure 206) has no TiO_2 reflector and a "giant lens", the chip is 2 mm x 2 mm large and has a beam angle of 120°. The InGaAlP chip has a light current of 905 mW using 700 mA and about 2000 mW when applying 1800 mA for a 1000 hour steady-state lifetime test, where the surrounding air is also heated to 150 °C to simulate fast aging.
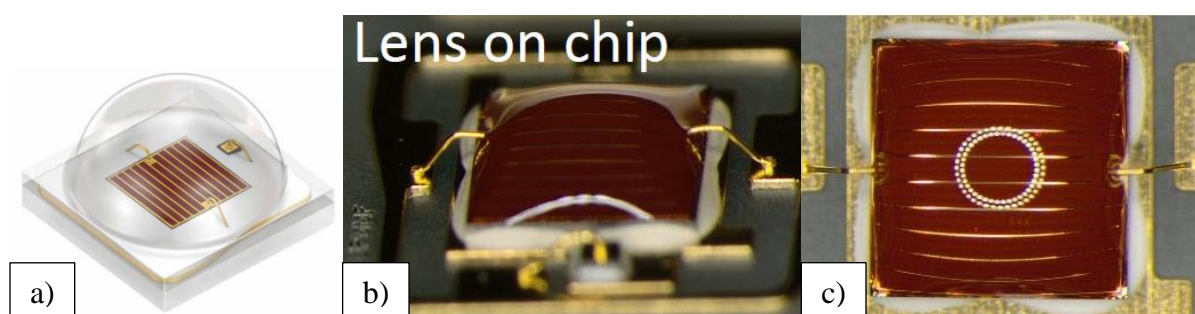
Figure 206: Oslon² Hyper Red LED, a) schematic image with giant lens, b) side view, c) top view.[547]

Eight self-synthesised polymers were selected for further testing (Table 58, Figure 208). Besides the 4-(phenoxy)phenyl-group containing one (P20_POPP40_PP40), two phenanthrenyl-containing polymers P20_PHM40_PX40 were chosen by OSRAM. For the 4-(methylthio)phenyl-group containing polysiloxanes all four (P20_PSMP40_XX40 and P20_PSMP80) were tested as well as the epoxide-group containing polymethylphenylsiloxane (EP = EP6.3_MM37.5_PP37.5_TP18.7) with 10.0 wt% of zirconium dioxide nanoparticles. Also, a commercial high refractive index polysiloxane (RI = 1.61 at 633 nm) was used. This ILE501 polymer was manufactured by INKRON and is a two component system which can be cured thermally using a platinum catalyst.[551] The phenylic polysiloxane with nanoparticle fillers can be used as encapsulation material because of its high transmission of 99 % for a 70 µm thick film.[552] It has a low water and air permeability compared to a standard polymethylphenylsiloxane like the OE-6630 system.[551] The ILE501 was only used by OSRAM and therefore no own investigations were made.

The hydride and matching vinyl copolymers were mixed and hand casted onto the chip and cured. Afterwards an additional "giant lens" with a refractive index of around 1.54 was applied onto the self-synthesised silicone using compression moulding. This led to delamination because of the stiff lens as well as bubbles or cracks at the wire bonds (Figure 207).

P20_POPP40_PP40	P20_PHM40_PP40	P20_PSMP40_MM40	P20_PSMP40_PM40
P20_PSMP40_PP40	P20_PSMP80	EP with 10.0 w% ZrO$_2$	ILE501
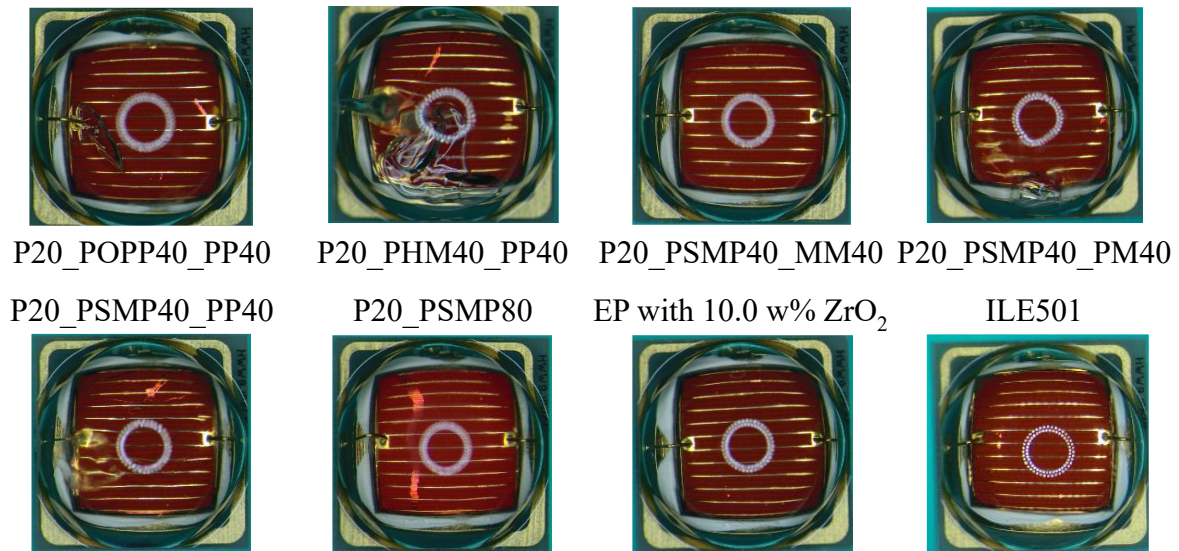
Figure 207: Images of the Oslon^2 Hyper Red LED encapsulated with the selected polymers and the "giant lens", EP = EP6.3_MM37.5_PP37.5_TP18.7, P20_PHM40_PM40 is not shown here because OSRAM did not provide an image.

Nevertheless, the best chips from each polymer set were used to compare the brightness difference from the bare chip and the reference polysiloxane (Figure 208).
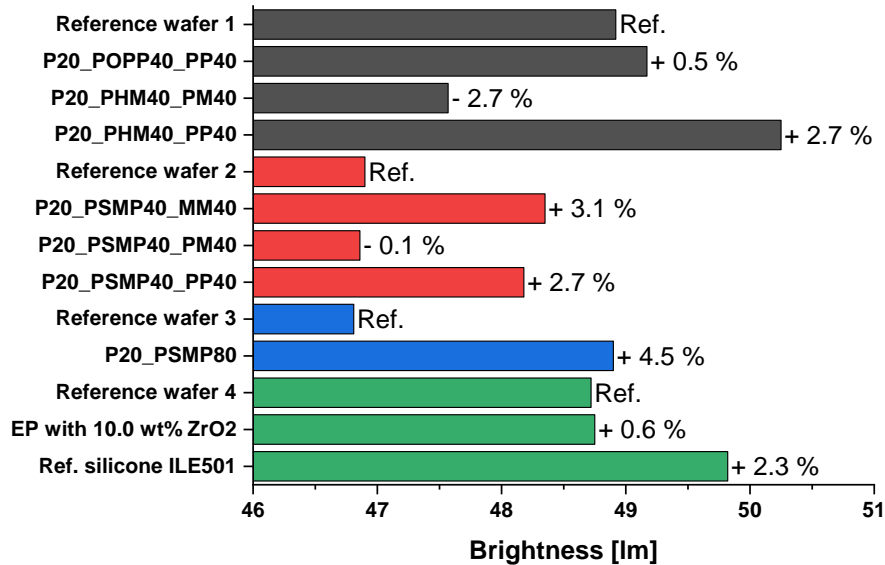
Figure 208: Brightness comparison of the eight selected self-synthesised as well as the reference polysiloxane in the wafers. They are split into four different groups because the chips were produced in different batches, LoC with "giant lens" compression moulding.

Because the chips are from four different wafer batches which has a huge effect on the brightness, the reference wafer are also displayed for every set. The percentage difference between the self-synthesised polymers and the pure chip is given in percent to be able to compare the different batches. In addition, the reference silicone ILE501 was casted in the fourth batch. In Table 58, the polymers are arranged with increasing refractive index, which shows that the RI

increase also leads to a percentage increase in the brightness independent from the used side-groups or fillers. The reference siloxane ILE501 has a RI of 1.61 and shows an increase of 2.3 % compared to the pure chip. Therefore, P20_PHM40_PP40, P20_PSMP40_PP40 and P20_PSMP80, which have a higher RI than 1.61 display an increased brightness and show the potential of the newly synthesised polysiloxanes. Noteworthy, P20_PSMP40_MM40 shows the second highest brightness increase with 3.1 % despite having the lowest RI. A higher the RI should always result in a higher brightness, which is described in the theoretical background. Also, when comparing P20_PHM40_PM40 and P20_PSMP40_PM40, which have an identical RI, show a large difference in the relative brightness change. Very small residues from the syntheses as well as the handmade build-up quality has a high influence on the brightness output as stated by OSRAM employees and therefore results in these errors.

Table 58: The eight selected polysiloxanes with a high RI and a reference silicone, which are used in the Oslon² Hyper Red LED with a "giant lens" are shown and their refractive indices as well as the percentage increase in brightness.

Polysiloxane	Refractive index at 589 nm	Brightness increase [%]
P20_PSMP40_MM40	1.583	+ 3.1
P20_PHM40_PM40	1.599	- 2.7
P20_PSMP40_PM40	1.599	- 0.1
EP with 10.0 wt% ZrO_2	1.607	+ 0.6
Ref. silicone ILE501	*~1.61 (633 nm)*	*+ 2.3*
P20_POPP40_PP40	1.613	+ 0.5
P20_PHM40_PP40	1.614	+ 2.7
P20_PSMP40_PP40	1.616	+ 2.7
P20_PSMP80	1.635	+ 4.6

Therefore, in the next test, the "giant lens" compression moulding is not applied for a better brightness comparison. Only the "Lens on Chip" approach (LoC) is used here, which also reduces the appearance of bubbles or cracks and prevents the delamination. The brightness values are shown in Figure 209 with the percentage difference to the reference siloxane ILE501, the self-synthesised polymers are sorted again by increasing RI for a better comparison. For every polysiloxane eight to ten chips were encapsulated and measured which is the reason why error bars are displayed here. Without the additional giant lens, no clear brightness to refractive index correlation can be made. The lower RI polysiloxanes P20_PSMP40_MM40,

P20_PSMP40_PM40 and P20_PHM40_PM40 show a raise in brightness of about 2 %. EP 10.0 wt% ZrO_2 and P20_POPP40_PP40 show lower values, which is congruent with the general explanation, although P20_POPP40_PP40 shows large error bars because the measured brightness ranges from 40.6 lm to 43.9 lm. Out of the three polysiloxanes with a higher RI than ILE501, P20_PHM40_PP40 shows 0.7 % less brightness, while the two sulfur containing P20_PSMP40_PP40 and P20_PSMP80 show higher values. Out of all tested polysiloxanes P20_PSMP40_PP40 has the highest increase with 3.4 % despite only having a slightly higher RI than the reference.
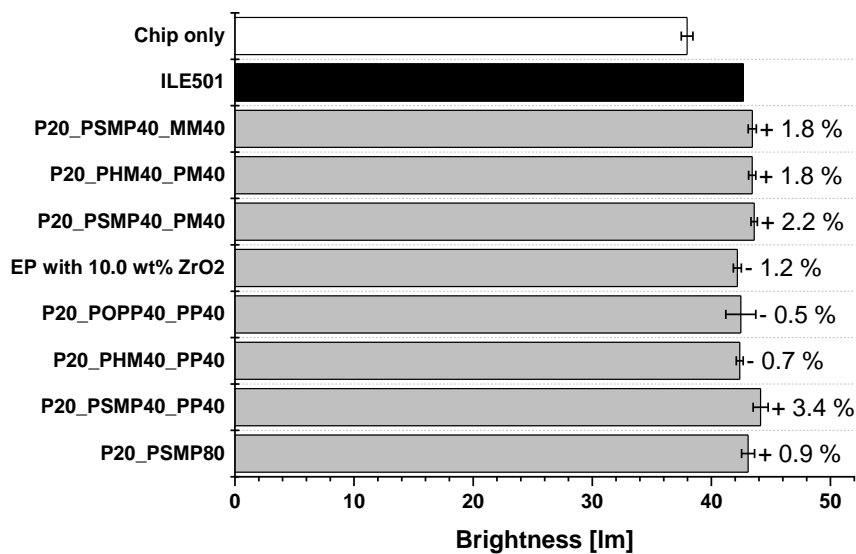
Figure 209: Brightness comparison of the eight selected self-synthesised as well as the reference polysiloxane sorted by increasing RI, only LoC approach.

To simulate the durability of the materials, a steady-state lifetime (SSLT) test for 1000 hours at 150 °C with 1800 mA was performed and the relative brightness change from 100 % was compared. The humidity was not artificially increased. Seven out of the eight polysiloxanes showed cracks and strong discolouration's before the 1000 h were reached (Figure 210). EP with 10.0 wt% ZrO_2, P20_PHM40_PP40 and P20_PSMP40_PP40 show a strong decomposition after 24 h. P20_PSMP40_MM40, P20_PHM40_PM40 and P20_PSMP80 showed failures after 96 h, while P20_PSMP40_PM40 lasted for 168 h. Some LEDs show cracks and deformations of the encapsulant while staying transparent, others turned black.

| P20_PSMP40_MM40 96 h | P20_PHM40_PM40 96 h | P20_PSMP40_PM40 168 h | EP/ZrO$_2$ 24 h |

| P20_PHM40_PP40 24 h | P20_PSMP40_PP40 24 h | P20_PSMP80 96 h |
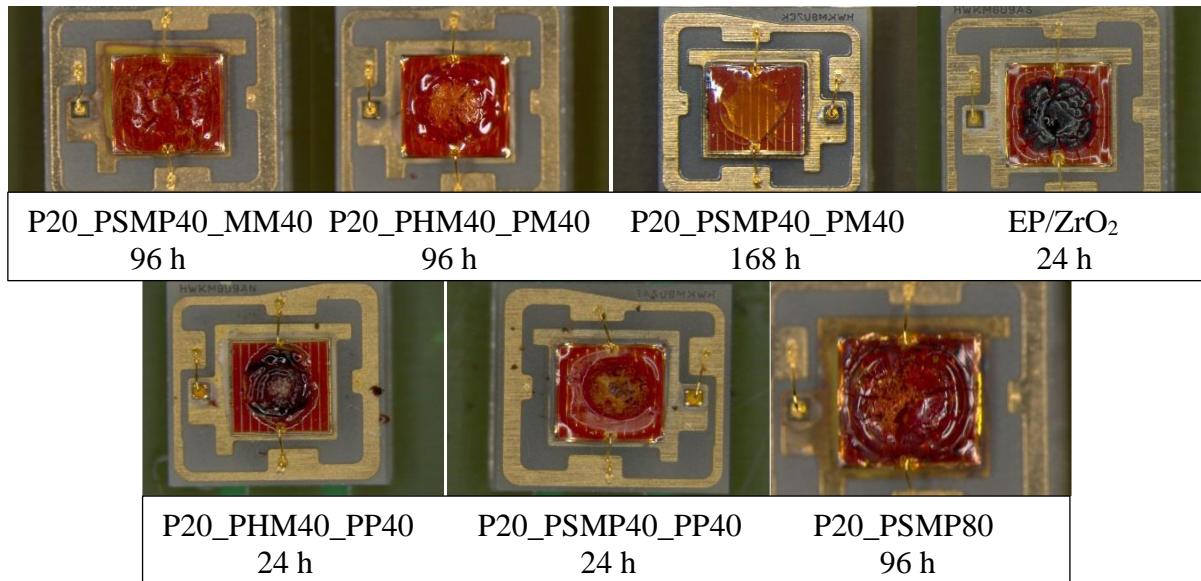
Figure 210: Images of LED chips whit the seven self-synthesised polysiloxanes, which broke down during the steady-state lifetime test, the successful operating time is shown under the name in hours.

After 1000 h, pictures of the LED chips were taken again (Figure 211). The two-dark brown to black coloured samples EP with 10.0 wt% ZrO$_2$ and P20_PHM40_PP40 were not further investigated and therefore only six samples are shown. The five different polymers which showed cracks after 24 h to 168 h, were continuously operated until the 1000 h were reached. P20_PSMP40_MM40, P20_PHM40_PM40, P20_PHM40_PP40 and P20_PSMP40_PP40 show a strong yellow colour and an increased number of larger cracks after the full SSLT test.

| P20_PSMP40_MM4 | P20_PHM40_PM40 | P20_PSMP40_PM40 | P20_PHM40_PM40 |

| P20_PSMP40_PP40 | P20_POPP40_PP40 | ILE 501 | chip only |
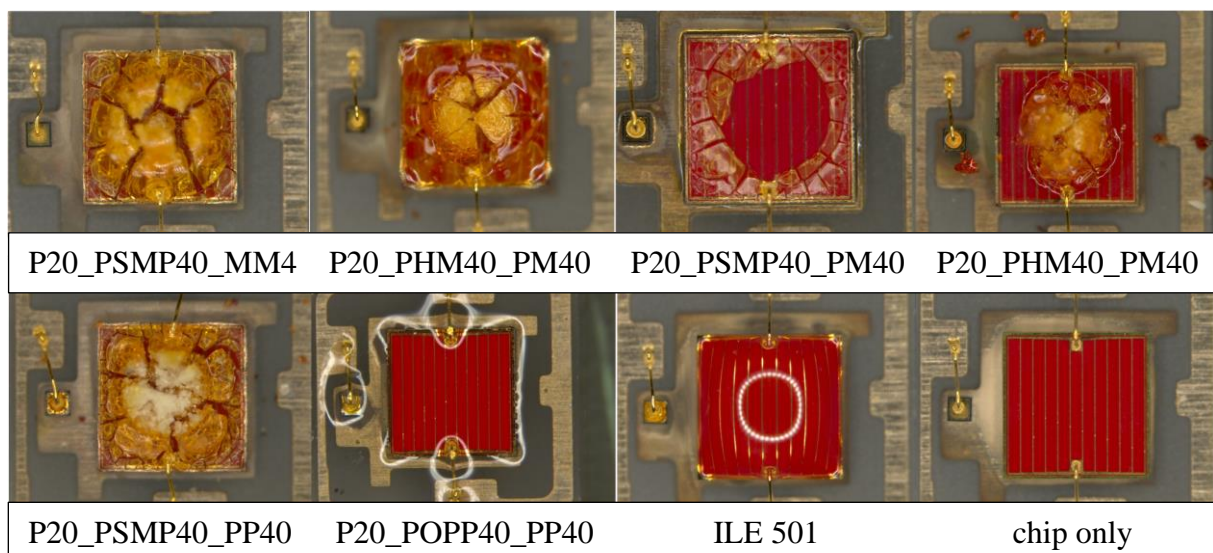
Figure 211: Images of five of the seven damaged chips, the two still operating chips with P20_POPP40_PP40 respectively ILE501 and the bare chip after 1000 h of SSLT treatment under 150 °C and 1800 mA.

The encapsulant P20_PSMP40_PM40 detached from the chip with only remaining small amounts at the edges. Synthesising polysiloxanes suitable for these high energy LED applications is very difficult in a small scale, because very small residues have a large impact under these conditions. Also, the amount of platinum is critical, commercial manufacturers can use very low amounts because of the reduced amount of side reactions resulting from the purer materials from the more advanced synthesis process. Additionally, no additives were used which commonly manufactures use in their commercial polysiloxanes. The only self-synthesised polysiloxane which tolerated the hard conditions is P20_POPP40_PP40 which showed no colouration, no bubbles, and no cracks. The commercial reference polysiloxane also withstands the SSLT test as well as the pure chip.

The relative change in brightness at 150 °C and 700 mA for the three remaining systems over the whole time period is shown in Figure 212. Three LEDs for P20_POPP40_PP40 are shown and four for the ILE501 and the chip alone. The aim of this measurement is the consistent light extraction of the chip, the graph should ideally run horizontally, because a rise could be due to scattering effects and a drop due to material decomposition, according to OSRAM employees.[23] After a strong increase from 100.0 % to 105.5 % after the first 24 h, one LED maintains the power output, while the other two slightly increase to 106.4 % and 107.5 %, respectively.
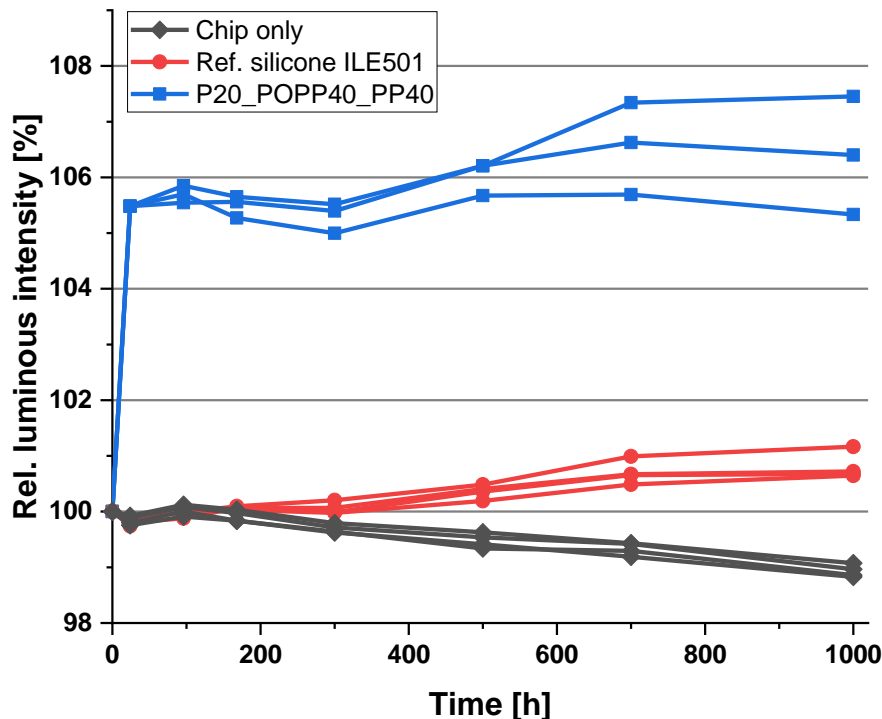
Figure 212: Relative brightness of the Oslon[2] Hyper Red during 1000 h of a SSLT test under 150 °C and 700 mA (The graph was redrawn using WebPlotDigitizer[410] from the curve OSRAM received from another institution).

Therefore, P20_POPP40_PP40 showed good results in the SSLT test and is suitable for LED applications. Mosley *et al.* tested their phenoxyphenyl-group containing polysiloxane with a Luxeon K2 1000 mA LEDs from Philips Lumileds Lighting Company where they removed the silicone and the lens and casted their self-made silicone onto it.[136] They cycled the temperature from −10 °C to 85 °C every twelve hours while maintaining 50 % humidity for 5400 h.[136] Starting from 100 % relative brightness, it decreased to 98 % after 1000 h down to 86 % after the full 225 days.[136] While the cycling does improve the mechanical stress especially towards highly cross-linked polymers, Mosley *et al.* used more ampere and about 53 % of the temperature compared to the SSTL test.[136] The system shows no drop in relative brightness, on the contrary, even neglecting the initial increase in the first 24 h, the relative brightness increases by 1 % to 2 %.

Overall, despite the other seven tested polysiloxanes not surviving the fast aging process, with an improved synthesis procedure they can still be used as an encapsulation material for LEDs, which do not operate at high current like shown for the P20_POPP40_PP40. In literature, chips which operate at lower currents of 10 mA to 50 mA were often used to test the durability in hindsight to low energy LEDs.[25, 469, 553-561]

5 Conclusions and perspective

The aim of this thesis was the development of novel polysiloxanes, which can serve as encapsulation material for high energy LEDs. The focus was in the increase of the refractive index compared to the commercially used systems. An increase of the refractive index results in a higher light output of the LED chip and therefore increased efficiency. Additionally, less backscattered photons lead to lower thermal and photon stress for the chip.

First, the two commercial materials provided by *OSRAM Opto Semiconductor* were analysed. The KJR-9022E-1 system from Shin-Etsu is a LRI ($n = 1.410$) polydimethylsiloxane. The polymer consists of two components: a vinyl- and methyl-group terminated polydimethylsiloxane with Q groups and a cross-linked hydride-group terminated poly[dimethyl-*co*-hydridomethyl]siloxane with T and Q groups. The analysis was performed by using FT-IR and NMR spectroscopy to determine the completeness of the polymerisation and cross-linking reactions, respectively. TG and TG-FT-IR measurements were used to evaluate the thermal stability under oxygen and nitrogen atmosphere as well as the decomposition products, respectively. DSC measurements were performed to determine the glass transition temperature which also depends on the amount of cross-linking. The refractive index was determined for comparing it with the commercial systems as well as the self-prepared materials. The viscosity using a rheometer and the molecular weight using a SEC of the copolymers were ascertained for comparing the processability compared to the commercial systems. UV/Vis measurements were performed to determine the transmission, haze values, yellowness, and whiteness indices at 450 nm after the synthesis and during a thermal treatment to evaluate their use as LED encapsulation material. The cured polysiloxane shows a high thermal stability ($T_{95\%}$ value) of 399 °C in an oxygen atmosphere and 471 °C in a nitrogen atmosphere. The high transmission of around 100 % is maintained after 69 days at 180 °C. The OE-6630 system from Dow Corning is a high refractive index ($n = 1.552$) polymethylphenylsiloxane. The polymer consists of two components: A being a linear vinyl terminated polymethylphenylsiloxane and B being a cross-linked hydride and vinyl terminated poly[dimethyl-*co*-diphenyl]siloxane. The thermal stability ($T_{95\%}$ values) of the cured polysiloxane is 425 °C under oxygen and 430 °C under nitrogen. The high transmission of around 100 % is maintained under 180 °C for over 1600 h.

The second part of this thesis focused on investigating the use ZrO_2 and HfO_2 nanoparticles produced by different ambient pressure and high-pressure synthesis. The zirconium dioxide nanoparticles were synthesised using an alkoxide, basic carbonate, and acetate precursor. The

self-prepared nanoparticles were analysed using TEM, XRD and DLS measurements to determine the particle size. The received particle sizes determined by TEM images are 4.1 ± 0.8 nm, 4.3 ± 0.7 nm, and 8.1 ± 4.0 nm. The hafnium dioxide nanoparticles were prepared using an alkoxide, chlorine, and acetate precursor. The received particle sizes determined by TEM images are 5.1 ± 1.5 nm, 5.6 ± 1.6 nm, and 4.8 ± 1.2 nm. The trifluoroacetate route cannot be recommend, although it is very fast, because of larger elongated particles and agglomerates which was observed in the TEM images. These particles increase the scattering and therefore lead to opaque samples. The basic carbonate and the *n*-propoxide route resulted in identical particle diameters determined by TEM images with around 4.2 nm and a crystallite size of 4.6 ± 0.1 nm and 3.7 ± 0.2 nm. The autoclave reaction of the *n*-propoxide shows a smaller crystallite size of 3.3 ± 0.1 nm making them all suitable. The diameter as well as the deviations of the HfO_2 nanoparticles measured by TEM images are comparable between 3.5 nm and 7.2 nm considering the standard deviation. The crystallite size increases from *iso*-propoxide over trifluoroacetate to the chloride precursor reaction from 2.0 ± 0.1 nm over 3.2 ± 0.1 nm to 5.0 ± 0.1 nm. Therefore, the trifluoroacetate synthesis is the most suitable one because it is the fastest. The particles were incorporated into the KJR-9022E-1, OE-6630 and a self-prepared polydiphenylsiloxane. The RI could not be increased significantly with only a maximum increase of 0.45 %. The transmission often dropped drastically from 99 % of the pure polymer to 85 % when using 10 wt% HfO_2. Therefore, the particles were surface modified with methacrylate-groups and a new methacrylate-group containing polysiloxane was prepared to be able to covalently cross-link the particles with the matrix. The RI could be increased by adding up to 20 wt% ZrO_2 nanoparticles to 1.617, but the transmission as well as the thermal stability dropped to 80 % and 261 °C under oxygen atmosphere, respectively. Also, the thermal curing process resulted in a yellowing of the material which was prevented by substituting the methacrylate-groups with epoxide ones. The RI could be increased to 1.604 with 10 wt% ZrO_2 nanoparticles and a transmission of 100 % could be achieved. The thermal stability is also lower than the one of the commercial systems. It is rather time-consuming to synthesise the nanoparticles in a suitable amount. Additionally, a surface-modification has to be carried out to enhance the miscibility of the particles with the matrix material. In contrast to these aspects, the incorporation of 10 wt% nanoparticles have a rather small effect on the refractive index and is therefore not efficient in terms of possible industry scale production processes.

The third part has focused on studying the increase of the RI by substituting silicon atoms with metal atoms in the polymer backbone using zirconium, hafnium, tin, and tantalum. The alkoxide or chlorine precursors were copolymerised with methyl-, phenyl-, hydride-, and vinyl-group

containing D silicon monomers which were then curing in a hydrosilylation reaction. The metal content was varied between 0.0 mol% and 15.0 mol%. The RI varied between 1.570 and 1.593 but did not correlate with the metal content. A transmission of over 97 % for nearly all metal atom containing polysiloxanes could be achieved after the synthesis which is comparable to the commercial systems. The yellowness and whiteness indices showed colourless samples. The thermal stability roughly decreases with increasing metal content between 247 °C and 390 °C, which is lower as the commercial systems. The effect of backbone-insertion of metal atoms in polysiloxanes is rather small towards the increase of the RI and the thermal stability compared to an analogue metal-free system. The syntheses revealed some difficulties, which are the reactivity of the metal centres towards Si-H groups. As a result, the vinyl components with the twofold metal content have to be synthesised and combined with metal-free hydrogen compounds. Also, the metal centres are potential places for additional cross-linking during the synthesis, leading to very high viscous and brittle products. An attempt to reduce this problem using chelating ligands was not successful and also led to coloured products.

In the fourth part, the dependency of the achieved molecular weight on the reaction method, the reaction time, and the pH value were investigated. To this end, model copolymers were synthesised in an acidic and a basic polycondensation reaction. For the acidic reaction methyldiethoxysilane, methylphenyldimethoxysilane and diphenylsilanediol were used and for the basic reaction phenylvinyldiethoxysilane, methylphenyldimethoxysilane and diphenylsilanediol. In the hydride-group containing polymerisation the molecular weight increased exponentially with increasing reaction time while in the vinyl-group containing polymerisation the molecular weight increased nearly linearly when excluding the last two samples due to them being bimodal. The acidic catalysis revealed a linear decrease of the integration of methoxy and ethoxy protons in the ^{1}H NMR, while the basic catalysed reaction showed a "S" shape, which are both reported in the literature. The molecular weight was calculated using ^{1}H NMR measurements and SEC analyses, which are both afflicted with errors. The M_W calculations using ^{1}H NMR revealed MW's of 22500 g/mol after five hours, while the SEC showed masses of around 1800 g/mol. For the vinyl polymerisation the initially used five hours of reaction time for the hydride polymerisation was extended for an additional hour because after five hours the M_W curves in the acidic polymerisation have a strong slope. According to the NMR calculations this additional hour leads to a strong increase of the molecular weight up to 37000 g/mol when calculating the masses with ^{1}H NMR and 3800 g/mol when using the SEC analysis. The SEC data shows that the M_W also rises but due to the equilibrium reactions these numbers are maybe afflicted with errors, which occurred because the sample could not be measured the next day.

In conclusion the reaction time should be long enough to let hydrolysis occur completely, and to let the released alcohols be distilled or evaporated completely in dependence on the used alcohols as well as the sterical hindrance of the side-groups.

The fifth part of the thesis investigated the modification of the organic side-groups to increase the refractive index. First the phenoxyphenyl side-groups were investigated and the monomer 4-(phenoxy)phenylphenyldimethoxysilane was synthesised in a Grignard reaction. This new monomer was the copolymerised with diphenylsilanediol and methyldiethoxysilane or phenyl-vinyldiethoxysilane to receive a hydride- and vinyl-group containing copolymer. The cured polysiloxane has a high RI of 1.613 compared to the 1.552 of OE-6630 and a high transmission of 95 % compared to the 100 %. The thermal stability is slightly lower but still high with 400 °C compared to the 425 °C of the OE-6630 independently of the atmosphere. Next the 4-(methyl-thio)phenyl side-group was investigated. The new monomer 4-(methylthio)phenylphenyl-dimethoxysilane was synthesised in an analogous way. Four hydride- and vinyl-group contain-ing copolymers were synthesised each while the diphenylsilanediol-group was substituted with dimethyldimethoxylsilane, methylphenyldimethoxysilane and 4-(methylthio)phenylphenyl-dimethoxysilane, later one to double the amount of sulfur atoms. The refractive index could be increased between 1.583 to 1.635 depending on the amount of methyl, phenyl and 4-(methyl-thio)phenyl side-groups which is higher than the 1.552 of OE-6630. A transmission of 97 % could be achieved for all polysiloxanes which is close to the 100 % of OE-6630. A thermal stability of 380 °C to 420 °C could be reached for all but the dimethyldimethoxysilane mono-mer containing polysiloxane with around 340 °C, which is lower than the 420 °C of OE-6630 independently of the atmosphere. The next side-group was investigated is the phenanthrene one. The monomer synthesis was analogously but phenanthren-9-ylmethyldimethoxysilane and phenanthren-9-ylphenyldimethoxysilane were synthesised. The hydride- and vinyl-group con-taining copolymers were synthesised using one of the self-prepared monomers, either methyl-diethoxysilane or phenylvinyldiethoxysilane and one of dimethyldimethoxysilane, methylphenyldimethoxysilane or diphenylsilanediol. A high refractive index of the cured ma-terials between 1.569 and 1.630 could be reached compared to the 1.552 of OE-6630. A trans-mission between 96 % to 99 % could be obtained which decreases with increasing phenyl con-tent compared to the 100 % of the OE-6630. The thermal stability ranges from 300 °C to 420 °C rising with increasing phenyl content compared to the 420 °C of the OE-6630 independently of the atmosphere. The synthesis is more complex and expensive for large scales because at the novel monomers had to be synthesised via Grignard reaction. Contrary to the other attempts, a notable increase of the refractive index of the produced siloxanes can be observed. An increase

to values above 1.6 is possible using various organic side-groups. Higher values would also be possible, but the aromatic moieties tend to stack or crystallise which results in very viscous and brittle products. For this reason, a higher content of methyl-groups realised by the thiomethyl- or methyl-group at the phenanthrenyl-group containing silicon atom was introduced in the polymers to enhance the flexibility and reduce viscosity at the expense of a slightly lowered refractive index.

The sixth part focused on the study of eight selected encapsulation materials on the Oslon[2] Hyper Red LED with an InGaAlP chip which was driven with 1800 mA an emitted a light at 660 nm. The test was performed by *OSRAM Opto Semiconductors*. The selected materials were the 10 wt% ZrO_2 and epoxide-group containing polysiloxane, the 4-(phenoxy)phenyl- and all four 4-(methylthio)phenyl-group containing ones as well as the phenanthren-9-ylmethyl- and methylphenyl- or diphenyl-group containing ones. The casting with poly[4-(methylthio)phenylphenyl]siloxane increased the brightness of the bare chip with a giant lens compression moulding by 4.6 %, poly[4-(methylthio)phenylphenyl-*co*-dimethyl]siloxane by 3.1 %, poly[4-(methylthio)phenylphenyl-*co*-diphenyl]siloxane by 2.7 % and poly[phenanthrene-9-ylmethyl-*co*-diphenyl]siloxane by 2.7 % while the reference silicone ILE 501 increased it only by 2.3 %. Without the giant lens compression moulding most of the polymers showed a higher brightness with poly[4-(methylthio)phenylphenyl-*co*-diphenyl]siloxane being superior with an increase of 16.3 % compared to the bare chip and 3.4 % compared to the reference silicone. The last performed test was a steady-state lifetime investigation for 1000 hours at 150 °C with a forward current of 1800 mA. Only the reference silicone and poly[4-(phenoxy)phenylphenyl-*co*-diphenyl]siloxane passed the test. The other seven polymers probably did not pass the test because very small syntheses impurities strongly affect the performance of them.

Despite not passing the test, some of the materials appear promising, by showing a thermal stability and a transmission comparable to the commercial OE-6630 system. Overall, the addition of nanoparticles and the modification of the polysiloxane backbone using metal atoms lead to unsatisfactory results, the modification of the side-groups was very successful. The main advantage of the self-prepared polysiloxanes using self-synthesised monomers is the greatly increased refractive index without losing the advantages of the silicone as encapsulant. With further synthesis optimisations, the materials can be used as commercial encapsulation materials showing that the project goal was successfully reached.

252

6 Experimental details

6.1 Instruments and methods

6.1.1 Thermogravimetry

Thermogravimetric analyses (TGA) of the samples were measured on a Netzsch TG 209C F1 Iris (Netzsch-Gerätebau GmbH, Germany) with 10 K/min heating rate. The measurements under oxygen were performed using 20 mL/min oxygen and 20 mL/min nitrogen gas up to 1000 °C. The analyses under inert atmosphere were performed using 40 mL/min nitrogen gas up to 900 °C, switching to 20 mL/min oxygen and 20 mL/min nitrogen from 900 °C to 1000 °C. The thermal stability was estimated using $T_{95\%}$ value, indicating the temperature at 5 % mass loss. The polymer samples were cut into small pieces and 5 mg to 30 mg were placed into a corundum crucible. The collected data were analysed by standard procedures using the Netzsch Proteus program package.

6.1.2 Differential scanning calorimetry

DSC measurements were conducted in a DSC 204 F1 Phoenix (Netzsch-Gerätebau GmbH, Germany) in a range from −160 °C to 160 °C depending on the substance with a rate of 10 K/min under nitrogen atmosphere. The apparatus has an active cooling via liquid/gaseous nitrogen and samples of 4 mg to 15 mg were measured in aluminium crucibles with pierced lids. The collected data were analysed by standard procedures using the Netzsch Proteus program package.

6.1.3 Infrared spectroscopy

Infrared spectra were recorded in total reflectance mode on a Bruker Vertex 70 ATR Spectrometer (Bruker Corporation, USA) from 400 cm^{-1} to 4500 cm^{-1} performing 16 scans with a resolution of 4 cm^{-1}. The collected data were analysed using the Bruker OPUS program package.

6.1.4 Rheology (viscosity)

The rheological measurements were performed on a MCR-301 rheometer with a CTD-450 convection heating system (Anton Paar GmbH, Austria) at 25 °C in oscillatory mode with a plate–plate geometry using a 25 mm PP25-SN0 measuring plate, a frequency of 1 Hz, a normal force value of 0 N and an amplitude of 5 %. The measurements were performed for 10 min and were recorded every 0.1 min using the RHEOPLUS/32 V3.21 software.

6.1.5 Nuclear magnetic resonance

The liquid NMR spectra (Table 59) were recorded on a Bruker Avance III 300 (300 MHz) or Bruker Avance III HD with a 400 UltraShield core (400 MHz) spectrometer (Bruker Corporation, USA). Deuterated chloroform was used as internal standard for ^{1}H (7.26 ppm) and ^{13}C (77.00 ppm) spectra. Tetramethylsilane was used as internal standard for ^{29}Si (0.00 ppm) spectra. The solid-state NMR spectra were recorded on a Bruker Avance III HD with an Ascend 400 WB (400 MHz) core (Bruker Corporation, USA).

Table 59: Core frequencies of the NMR spectrometer.

NMR core	Frequency at 300 MHz	Frequency at 400 MHz
^{1}H	300.13	400.13
^{13}C	75.47	100.61
^{29}Si	59.63	79.50
^{31}P	121.50	161.98
^{119}Sn	111.92	149.21
^{195}Pt	64.52	86.02

Some ^{29}Si NMR experiments were performed with a PTFE NMR tube (Figure 213) from Rototec-Spintec GmbH (Germany) which consists of three parts, a PTFE inlet for measuring the silicon containing probes, a PTFE plug for closing the inlet and a glass holder to match the diameter of this special NMR tube with standard spinners.
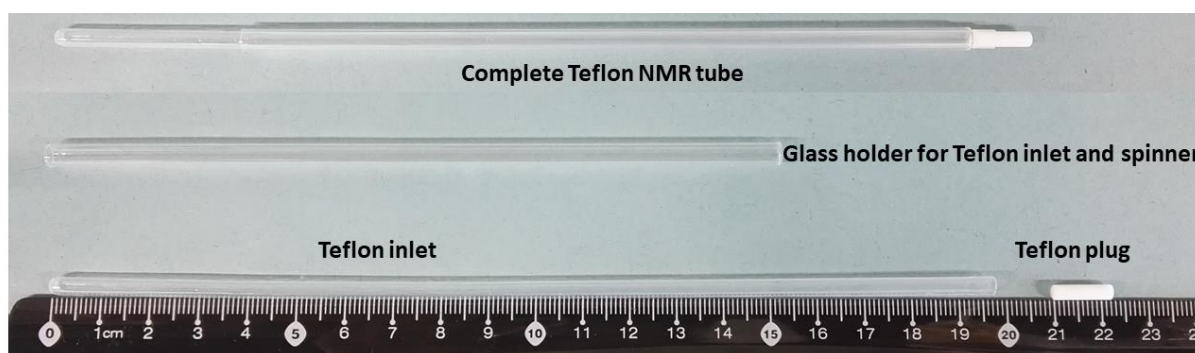
Figure 213: PTFE NMR tube.

Solid state NMR of elastic polysiloxanes like Shin-Etsu KJR-9022E-1 and Dow Corning OE-6630 were measured using a polysiloxane rod (Figure 214) which was produced by curing the mixed components A and B inside a Teflon mould with different diameters from 5 mm to 10 mm. One end of the mould has a screw thread where a screw is placed to seal one side of the form. After filling the mould bubble-free with the liquid polysiloxane through a syringe, it

is placed inside an oven at 150 °C for 18 hours to receive a cured polysiloxane rod, which can be removed by unscrewing the bolt and pushing out the cylinder. The idea as well as the appearance of the system was developed in the group of Prof. Dr. Guido Kickelbick.

Figure 214: Teflon mould for curing elastic polysiloxanes to receive a rod which can be placed inside the zirconia solid-state NMR rotor.

6.1.6 Refractive index

Refractive indices (RI) were measured using an AR4 Abbé refractometer with a PT31 Peltier thermostat (A. KRÜSS Optronic GmbH, Germany) at 20.0 °C, with 589 nm wavelength and 1-bromonaphthalene respectively cinnamon oil as contact fluid for solid samples. Cinnamon oil can only be used up to a RI of 1.5902, while 1-bromonaphthalene is usable up to a RI of 1.6570.

6.1.7 Plasma Etching

Plasma etching of the microscope slides was carried out applying a Plasma-Surface-Technology Femto (Diener electronic GmbH + Co. KG, Germany) with 15 mL/min oxygen and 100 % power for 10 minutes. The microscope glass slides were cleaned with acetone and dried using pressurised air before the plasma etching.

6.1.8 UV/Vis spectroscopy

UV/Vis spectra were recorded using a Lambda 750 (Perkin Elmer, USA) and a 100 mm integrating sphere with an InGaAs detector. The polysiloxanes were doctor bladed with 120 µm onto a plasma etched glass slide, which was corrected by blank measurements. The samples are measured from 320 nm to 800 nm using a scan speed of 2 nm/sec.

The yellowness index (YI) and the whiteness index (WI) of the doctor bladed samples were determined with the UV/Vis spectrometer in an integration sphere and were calculated using PerkinElmer UV Winlab (6.4.0.973) software. The higher the yellowness index is, the more yellow the sample appears. A negative value indicates a blue colour and the optimum value is zero. The whiteness index indicates the whiteness of a sample, the optimum is 100. A value

below 100 indicates a yellowish and a value above 100 a bluish sample. The glass slide is included in the baseline correction so that the samples can be measured in transmission. The measurements are performed from 380 nm to 780 nm with 5 nm increment. The yellowness index is measured according to ASTM D 1925-88 and the whiteness index according to ASTM E 313-96.

6.1.9 Fluorescence spectroscopy

Fluorescence spectroscopy was performed on a FluoroMax 4 Spectrofluorometer (Horiba Scientific, Japan) using different excitation and emission wavelengths and a quartz cuvette.

6.1.10 SEC measurements

SEC measurements were performed using a Viscotek VE1121 Pump (Malvern Instruments, United Kingdom), two PSS SDV 10^3 and 10^5 columns. Three detectors were used, a Shodex RID org udc 2 (refractive index, Showa Denko, Japan), a UV Waters 2487 (UV/Vis, Waters GmbH, Germany) and a PSS SLD 7000/BI-MwA (light scattering, PSS Polymer Standards Service GmbH, Germany). Measurements were carried out in THF, the system was calibrated with polystyrene. Stock solutions of 8 mg of polysiloxane in 4 mL of THF were prepared and eluted at 0.95 mL/min. The detection wavelength was the absorption maximum of the phenyl-groups at 264 nm.

6.1.11 Film applicator

A 4-fold film applicator MODEL 360 15078 with various gap heights at 30 µm, 60 µm, 90 µm and 120 µm from Erichsen GmbH & Co. KG PrüfMasch.Bau (Germany) was used for the doctor-blading onto the microscope slides (Figure 215).
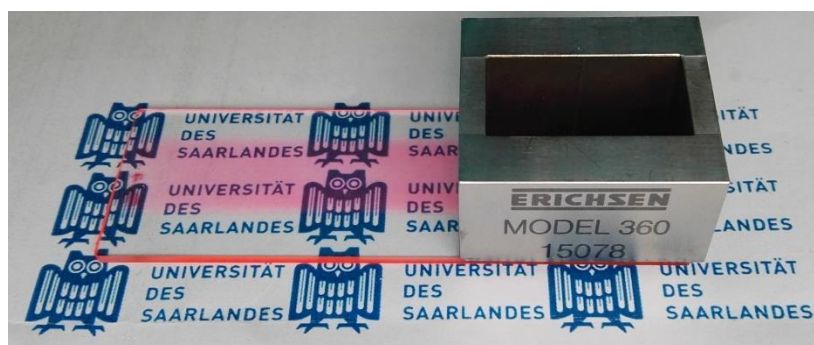
Figure 215: 4-fold film applicator MODEL 360 15078 onto an inked polysiloxane film cured on a microscope glass slide.

6.1.12 Used chemicals

All chemicals were used as received. The solvents were dried using a solvent purification system from M.Braun Inertgas-Systeme GmbH (Germany). Dow Corning OE-6630 two component system and Shin-Etsu KJR-9022E-1 two component system were obtained from *OSRAM Opto Semiconductors*. 3-Methacryloxypropyl trimethoxysilane (98 %), dimethyldimethoxysilane (97 %), diphenyldimethoxysilane (97 %), diphenylsilanediol (98 %), hafnium (IV) *iso*-propoxide (99 %), *Karstedt*'s catalyst ([Pt] = 2.1 – 2.4 % in xylene), methyldiethoxysilane (95 %), methyltrimethoxysilane (97 %), *Ossko*'s catalyst ([Pt] = 1.85 – 2.1 % in Cyclomethylvinylsiloxane), phenylmethyldimethoxysilane (97 %), phenyltrimethoxysilane (97 %), polydimethylsiloxane, α-*n*-butyl, ω-carboxylate, polydimethylsiloxane, α-*n*-butyl, ω-phosphate, polydimethylsiloxane, α-*n*-butyl, ω-phosphonate, triphenylsilanol (98 %), vinylphenyldiethoxysilane (95 %), vinyltrimethoxysilane (99 %) and zirconium(IV) chloride (99.5 % Zr) were bought from ABCR (Germany). 4-Bromophenyl phenyl ether (99 %), 9-bromophenanthrene (96 %), acetylacetone (99 %), benzyl alcohol (98 %), diphenylphosphinic acid (99 %), dodecanoic acid (99 %), oleylamine (80 % – 90 %), stearic acid (97 %), tin(IV) chloride (anhydrous, 99 %) and trifluoroacetic acid (99 %) were bought from ACROS Organics B.V.B.A. (Belgium). Butyric acid (99 %) and tetra-*n*-butylammonium hydroxide (40 wt% in water) were bought from fisher scientific (United States). Tantalum(V) ethoxide (98 %) was bought from Gelest (United States). 3-Glycidyloxypropyl trimethoxysilane (98 %), 4-bromothioanisole (97 %), barium hydroxide monohydrate (98 %), barium hydroxide octahydrate (98 %), benzoyl peroxide (98 %), hafnium (IV) *n*-butoxide (99 %), hafnium(IV) chloride (98 %), zirconium(IV) carbonate basic (≥ 40 % ZrO_2 basis), zirconium(IV) *iso*-propoxide *iso*-propanol complex (99.9 % trace metals basis) and zirconium(IV) *n*-propoxide solution (70 wt% in 1-propanol) were bought from Merck Group (Germany). Polydiphenylsiloxane two component system was synthesised by Patrick Wenderoth. Acetone (99 %), benzene (99.5 %), chloroform (99 %), concentrated hydrochloric acid (37 %), dichloromethane (97 %), diethyl ether (97 %), ethanol (99 %), ethyl acetate (97 %), *iso*-propanol (97 %), magnesium turnings, methanol (98 %), *n*-hexane (99 %), *n*-pentane (95 %), potassium bicarbonate (98 %), sodium hydroxide (98 %), tetrahydrofuran (99 %), toluene (99.8 %) and xylene (98 %) were bought from zentrales Chemikalienlager der Universität des Saarlandes (Germany).

6.2 Syntheses

6.2.1 Commercial silicones

The two commercial silicon systems were obtained from *OSRAM Opto Semiconductors*.

6.2.1.1 KJR-9022E-1

KJR-9022E-1 from Shin-Etsu (Tokio, Japan) consists of two components, A (KJR-9022E) and B (C-9022E), which are mixed in a 10:1 ratio. After degassing for 30 minutes at 2 mbar the polymer is cured at 150 °C for four hours, as described by the manufacturer.[13]

6.2.1.1.1 Shin-Etsu KJR-9022E-1 component A (KJR-9022E)

^{1}H NMR (400 MHz, CDCl$_3$): δ = 6.19 − 5.72 (m, 3H, vinyl), 0.24 − −0.05 (m, 426H, methyl) ppm.

^{13}C NMR (101 MHz, CDCl$_3$): δ = 139.54 (vinyl), 131.82 (vinyl), 1.63 (methyl), 1.62 (methyl), 1.36 (methyl), 1.26 (methyl), 1.16 (methyl), 0.89 (methyl), 0.46 (methyl) ppm.

^{29}Si NMR (79 MHz, CDCl$_3$): δ = 11.88 (Me$_3$Si-), −4.15 (Me$_2$VSi-), −20.96 − −22.44 (-Me$_2$Si-), −109.8 (-Si-) ppm.

RI: 1.4086.

Viscosity: 2790 ± 4 mPa·s.
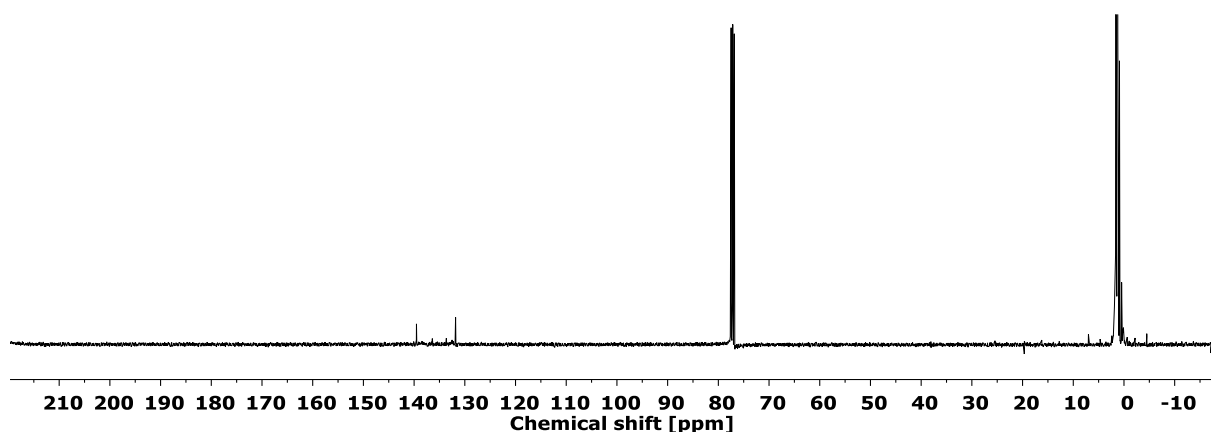
Figure 216: ^{13}C NMR (101 MHz, CDCl$_3$) of Shin-Etsu KJR-9022E.

6.2.1.1.2 Shin-Etsu KJR-9022E-1 component B (C-9022E)

^{1}H NMR (400 MHz, CDCl$_3$) δ = 4.78 − 4.63 (m, 1H, hydride), 3.70 (ddd, J = 11.5 Hz 3.2 Hz, 1.8 Hz, 0.13H), 3.63 − 3.54 (m, 0.28H), 3.44 (s, 0.45H), 3.13 (ddd, J = 5.8 Hz, 4.0 Hz, 2.8 Hz, 0.12H), 2.77 (t, J = 4.6 Hz, 0.13H), 2.58 (dd, J = 5.1 Hz, 2.7 Hz, 0.13H), 1.74 − 1.58 (m, 0.26H), 0.68 − 0.54 (m, 0.27H), 0.35 − −0.12 (m, 16.3H, methyl) ppm.

^{13}C NMR (101 MHz, CDCl$_3$) δ = 49.81 – 43.15 (methoxy), 0.37 – −2.20 (methyl) ppm.

^{29}Si NMR (79 MHz, CDCl$_3$) δ = −4.71 – −7.00 (Me$_2$HSi-), −17.08 – −22.49 (-Me$_2$Si-), −32.21 – −37.57 (-MeHSi-), −65.09 (-MeSi-), −75.29 (-MeOSi-), −110.43 (-Si-) ppm.

RI: 1.4062.

Viscosity: 108 ± 3 mPa·s.
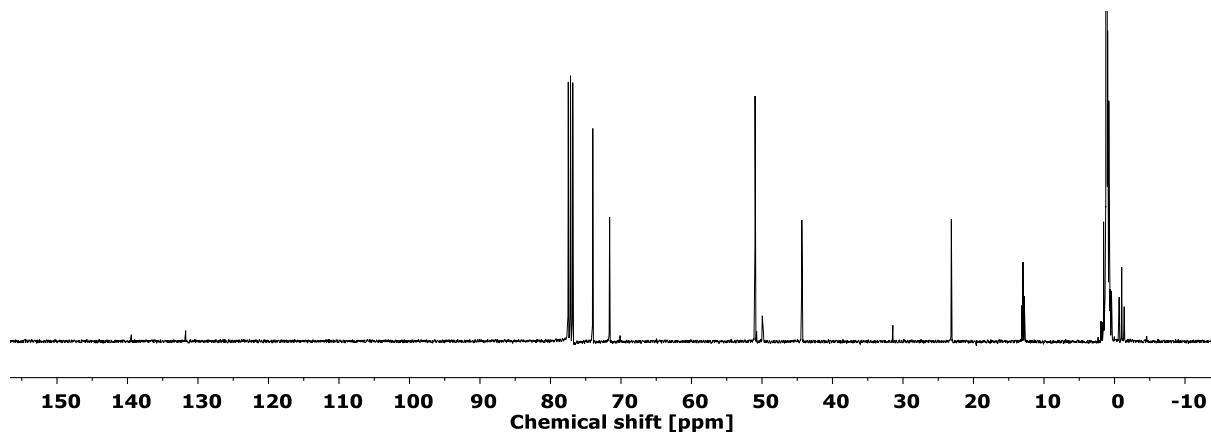
Figure 217: ^{13}C NMR (101 MHz, CDCl$_3$) of Shin-Etsu C-9022E.
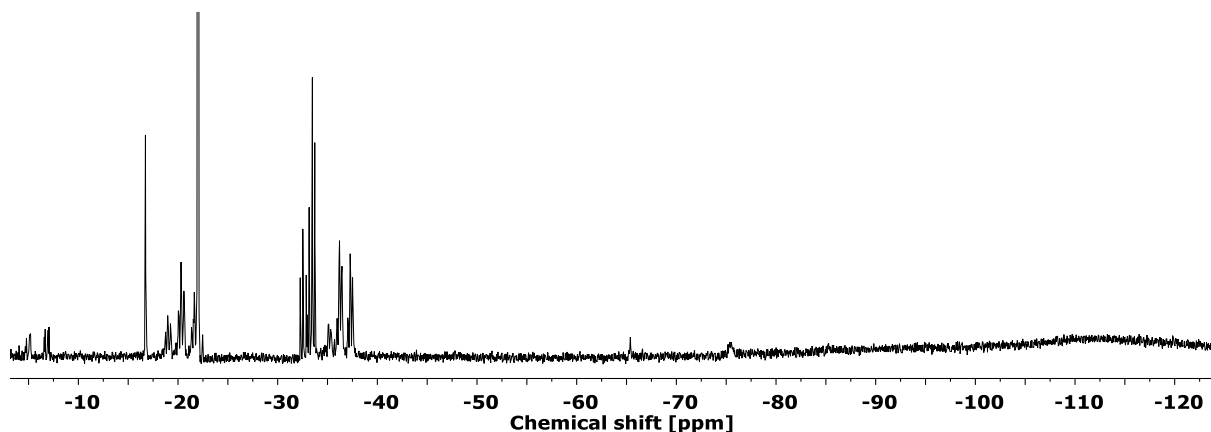
Figure 218: ^{29}Si NMR (79 MHz, CDCl$_3$) of C-9022E measured in the PTFE tube.

6.2.1.1.3 Shin-Etsu KJR-9022E-1 cured
^{13}C CP MAS NMR (101 MHz, 13 kHz) δ = 8.63 (ethyl), 1.09 (methyl), −1.17 (methyl) ppm.

^{29}Si CP MAS NMR (80 MHz, 13 kHz) δ = 11.04 (Me3Si-, -Me2EtSi-), −4.01 (Me$_2$VSi-, Me$_2$HSi-), −22.71 (-MeEtSi-, -Me2Si-), −35.91 – −38.81 (-MeHSi-), −67.78 (-MeSi-), −110.68 (-Si-) ppm.

RI: 1.4100.

6.2.1.2 OE-6630

OE-6630 from Dow Corning (Michigan, United States of America) consisting of two components, A (OE-6630 A) and B (OE-6630 B), which are mixed in a 1:4 ratio. After degassing for 30 minutes at two mbar the polymer is cured at 150 °C for four hours, although the manufacturer suggested two hours.[14]

6.2.1.2.1 Dow Corning OE-6630 component A

^{1}H NMR (400 MHz, CDCl$_3$) δ = 7.89 – 7.28 (m, 50H, phenyl), 6.44 – 5.98 (m, 3H, vinyl), 0.65 – 0.34 (m, 36H, methyl) ppm.

^{13}C NMR (101 MHz, CDCl$_3$) δ = 139.01 – 127.39 (phenyl, vinyl), 0.39 – −0.63 (methyl) ppm.

^{29}Si NMR (79 MHz, CDCl$_3$) δ = −2.34 (Me2VSi-), −32.05 – −33.61 (-MePhSi-) ppm.

RI: 1.5420.

Viscosity: 2960 ± 60 mPa·s (manufacturer: 2975 mPa·s).
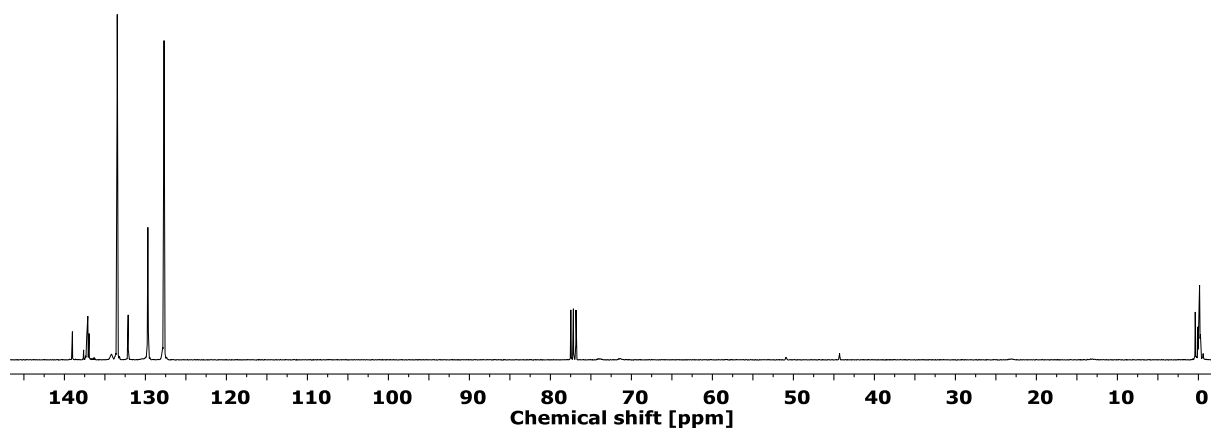
Figure 219: ^{13}C NMR (101 MHz, CDCl$_3$) of Dow Corning OE-6630 component A.

6.2.1.2.2 Dow Corning OE-6630 component B

^{1}H NMR (400 MHz, CDCl$_3$) δ = 7.93 – 6.89 (m, 22.5H, phenyl), 6.31 – 5.51 (m, 3H, vinyl), 5.03 – 4.90 (m, 1H, hydride), 0.47 – −0.25 (m, 13.5H, methyl) ppm.

^{13}C NMR (101 MHz, CDCl$_3$) δ = 139.03 – 127.60 (phenyl, vinyl), 1.19 – 0.00 (methyl) ppm.

^{29}Si NMR (79 MHz, CDCl$_3$) δ = −0.47 – −2.27 (Me$_2$VSi-, Me$_2$HSi-), −3.51 – −4.41 (-Me$_2$Si-), −44.70 (-Ph$_2$Si-), −77.40 – −82.09 (-PhSi-) ppm.

RI: 1.5336.

Viscosity: 2530 ± 30 mPa·s (manufacturer: 2775 mPa·s).
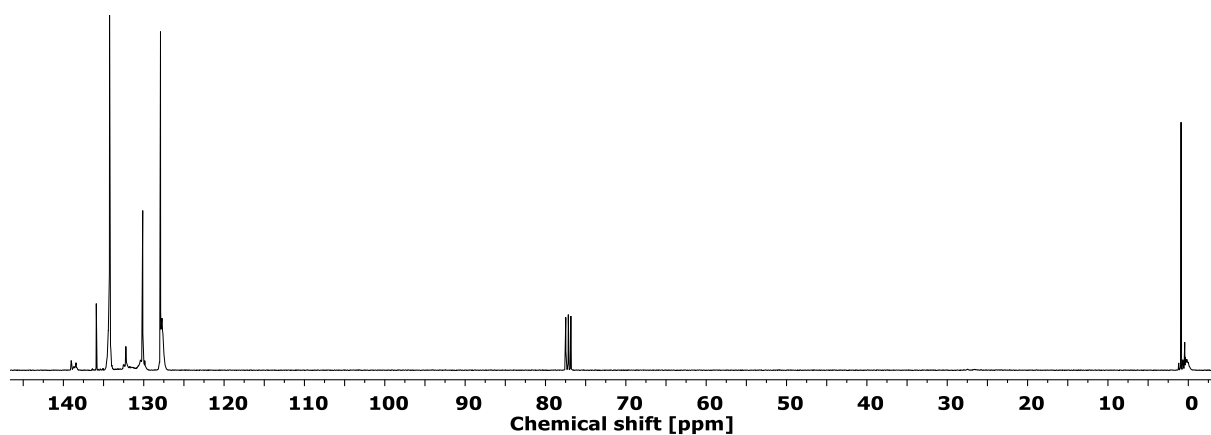
Figure 220: ^{13}C NMR (101 MHz, CDCl$_3$) of Dow Corning OE-6630 component B.

6.2.1.2.3 Dow Corning OE-6630 cured

^{13}C CP MAS NMR (101 MHz, 13 kHz) δ = 133.84 − 127.47 (phenyl, vinyl), 9.32 (ethyl), −0.60 (methyl) ppm.

^{29}Si CP MAS NMR (80 MHz, 13 kHz) δ = 11.11 (-Me$_2$EtSi-), −4.32 (-Me$_2$HSi-), −19.38 (-Me$_2$Si-), −33.08 (-MePhSi-), −46.29 (-Ph$_2$Si-), −79.08 (-PhSi-) ppm.

RI: 1.5515.

FT-IR measurements:

Figure 222: FT-IR spectrum of the unmodified and modified ZrO₂ nanoparticles.

TG measurements:
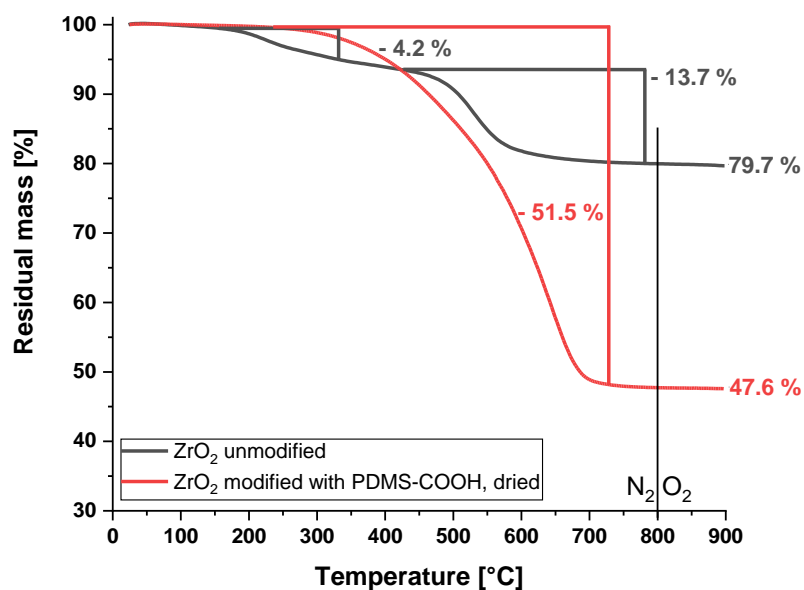
Figure 223: TG analysis of the ZrO₂ nanoparticles with and without surface modification synthesised from Zr(OⁿPr)₄ under nitrogen atmosphere.

6.2.2.1.2 ZrO₂ for the cross-linking with polysiloxanes by the ring opening reaction of epoxides

The particles received after the autoclave synthesis inside the benzyl alcohol were mixed with 5.0 g (21.2 mmol) of 3-glycidyloxypropyl trimethoxysilane and 0.5 mL of sulfuric acid. After heating the suspension at 70 °C for one hour, the particles were precipitated with 100 mL of

distilled water and centrifuged. The resulting particles were dried under high vacuum ($2 \cdot 10^{-3}$ mbar) and dispersed in toluene.

NMR measurements:

^{1}H NMR (300 MHz, CDCl$_3$) δ = 3.65 (s, 1H, H5), 3.56 (m, 2H, H4, H5'), 3.18 (s, 1H, H4'), 2.74 (m, 1H, H6), 2.57 (s, 1H, H7), 2.15 (s, 1H, H7'), 1.57 (m, 2H, H3), 0.94 (tr, J = 7.4 Hz, 2H, H2) ppm.

DLS measurements:
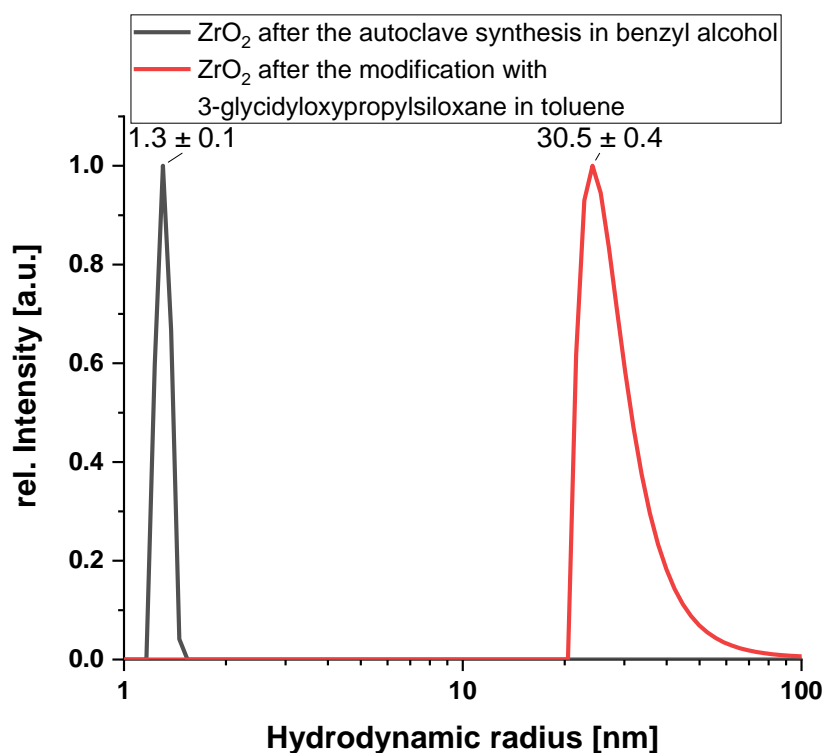
Figure 224: DLS curves of ZrO₂ nanoparticles after the synthesis in benzyl alcohol and after the surface modification with 3-glycidyloxypropylsiloxane in toluene.

TG measurements:
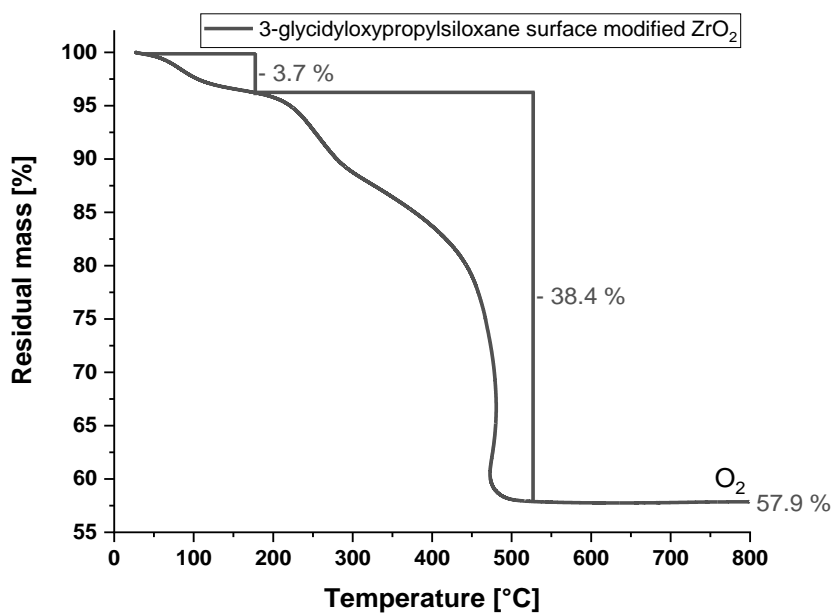
Figure 225: TGA of 3-glycidyloxypropylsiloxane surface modified ZrO₂ with residual methanol, toluene, and benzyl alcohol.

6.2.2.1.3 HfO₂

DLS measurements:
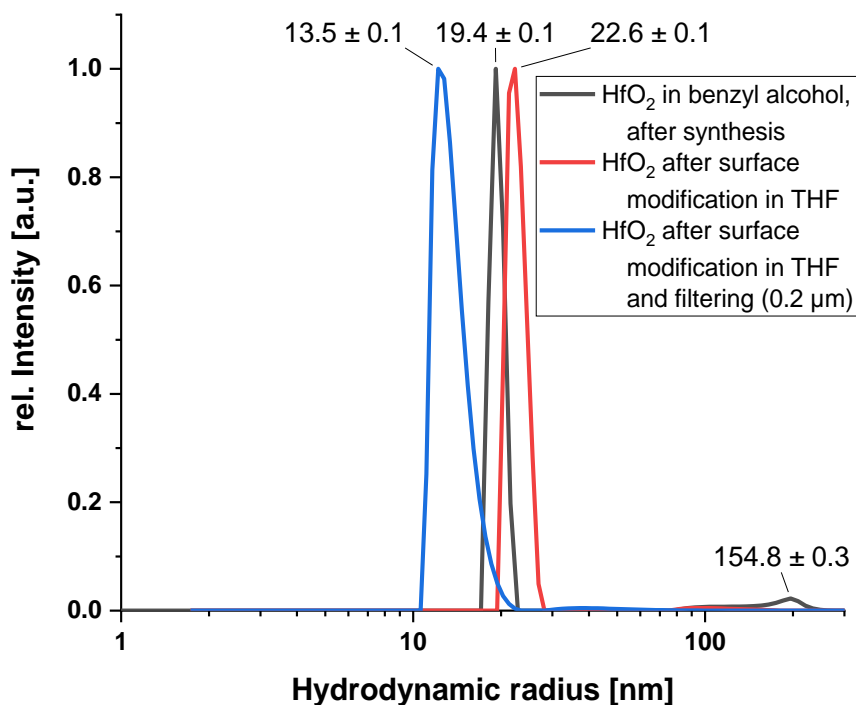
Figure 226: DLS measurement of hafnium dioxide nanoparticles synthesised from Hf(O^{i}Pr)₄ in benzyl alcohol respectively THF and surface modified with PDMS-COOH (1500 g/mol).

FT-IR measurements:
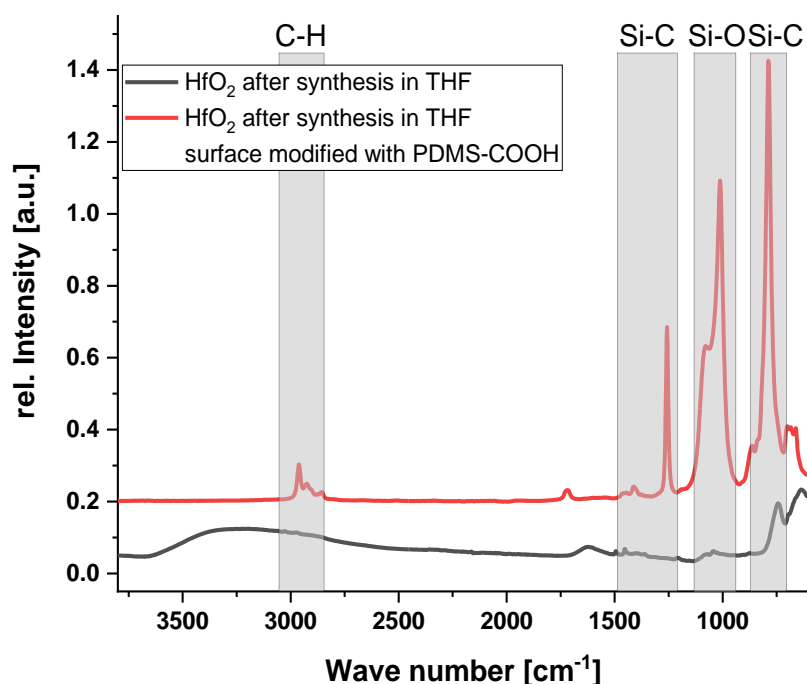
Figure 227: FT-IR spectrum of HfO₂ nanoparticles in THF, dried on the spectrometer.

TG measurements:
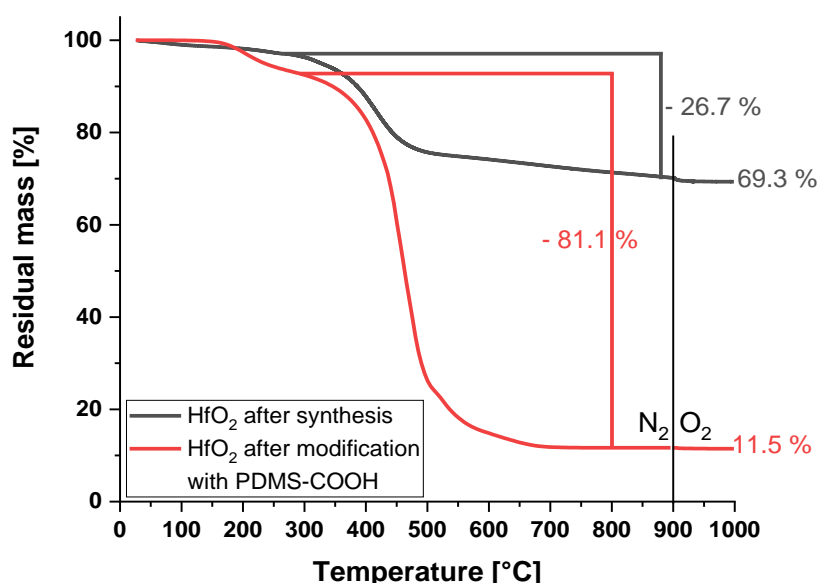
Figure 228: TG analysis of the HfO₂ nanoparticles with and without surface modification synthesised from Hf(OⁱPr)₄ under nitrogen atmosphere.

6.2.2.2 Synthesis of HfO₂ from chlorine precursor

The synthesis was carried out by mixing 200 mg (0.624 mmol) of HfCl₄ with 45 mL of benzyl alcohol in a 200 mL stainless steel autoclave with a closed 110 mL Teflon inlet. After the suspension was heated to 220 °C for three days, it was washed twice with ethanol and diethyl ether and filtered with a 0.2 µm syringe filter. The residue was dispersed in 6.94 ml of chloroform

and for post modification, 40 mg of dodecanoic acid were added and stirred for 5 min. Subsequently, 64 µL oleylamine were added and an opaque suspension was obtained.

DLS measurements:
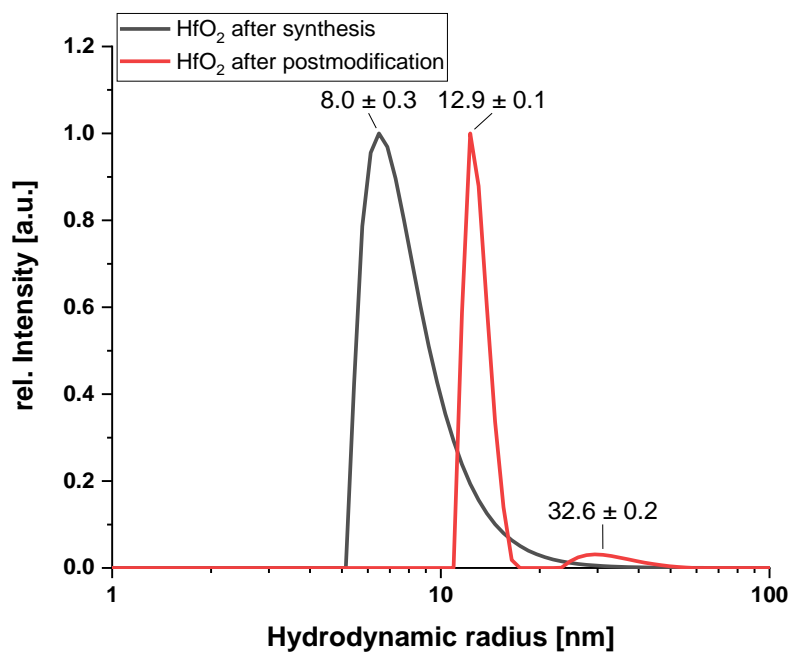
Figure 229: DLS measurement of HfO₂ nanoparticles synthesized from HfCl₄ in THF and surface modified with dodecanoic acid and oleylamine.

FT-IR measurements:
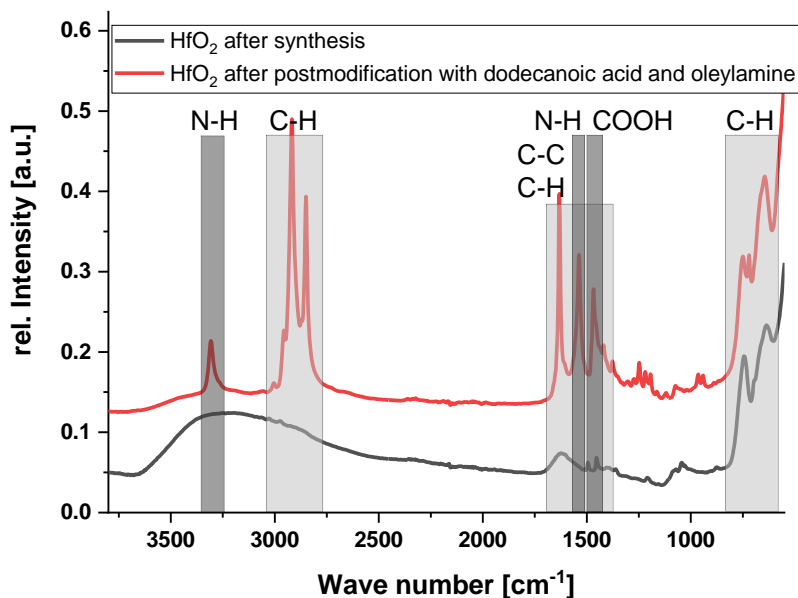
Figure 230: FT-IR spectrum of HfO₂ nanoparticles synthesised from HfCl₄.

TG measurements:
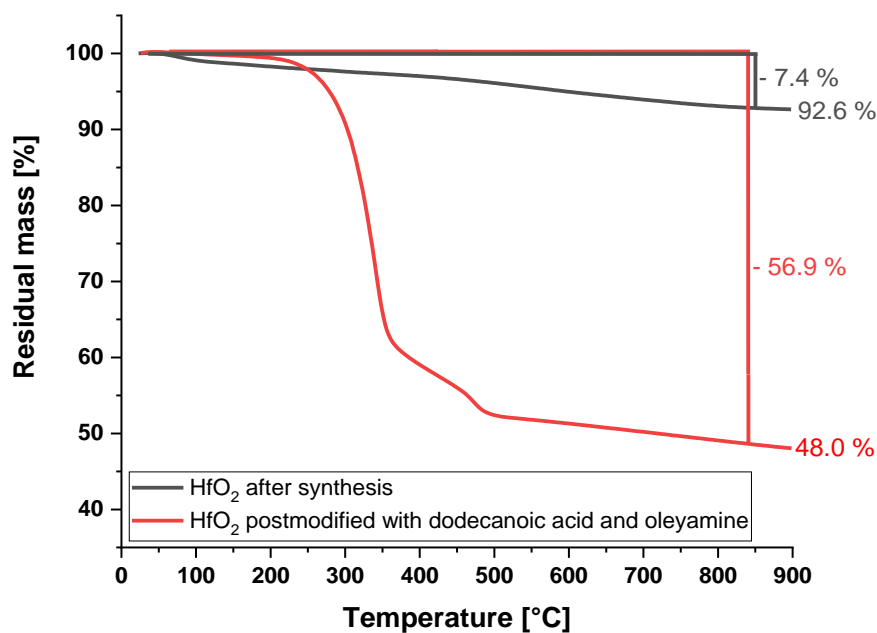
Figure 231: TG analysis of HfO₂ nanoparticles synthesised by HfCl₄.

6.2.2.3 Synthesis of MetO₂ from trifluoroacetate precursor

Precursor synthesis:

50 mL (~ 650.0 mmol) of trifluoroacetic acid were slowly added to 30.0 mmol of $MetCl_4$ (9.60 g of $HfCl_4$, 6.99 g of $ZrCl_4$). After the solution was heated at 40 °C for five hours, the solvent was removed under reduced pressure. The product was obtained as a white solid (14.44 g, 25.5 mmol, 85 % $HfCl_4$, 15.33 g, 28.2 mmol, 94 % of $ZrCl_4$).

Nanoparticle synthesis:

4.00 mmol (2.52 g $Hf(CF_3COO)_4$, 2.17 g $Zr(CF_3COO)_4$) of the metal trifluoroacetate precursor were added to 52.6 mL (160.0 mmol) of oleylamine and high vacuum ($2 \cdot 10^{-3}$ mbar) was applied for 30 min at 110 °C. Afterwards, the now transparent solution was heated under argon atmosphere for 1 h at 330 °C. After the solution was cooled down to room temperature. 150 mL of acetone were added, and the precipitated particles were collected by centrifugation. By redissolving three times with toluene and precipitating in ethanol followed by centrifuging, clean particles were obtained. Thereafter, the particles are redissolved in 20 mL of toluene to form a clear suspension.

6.2.2.3.1 ZrO$_2$

DLS measurements:
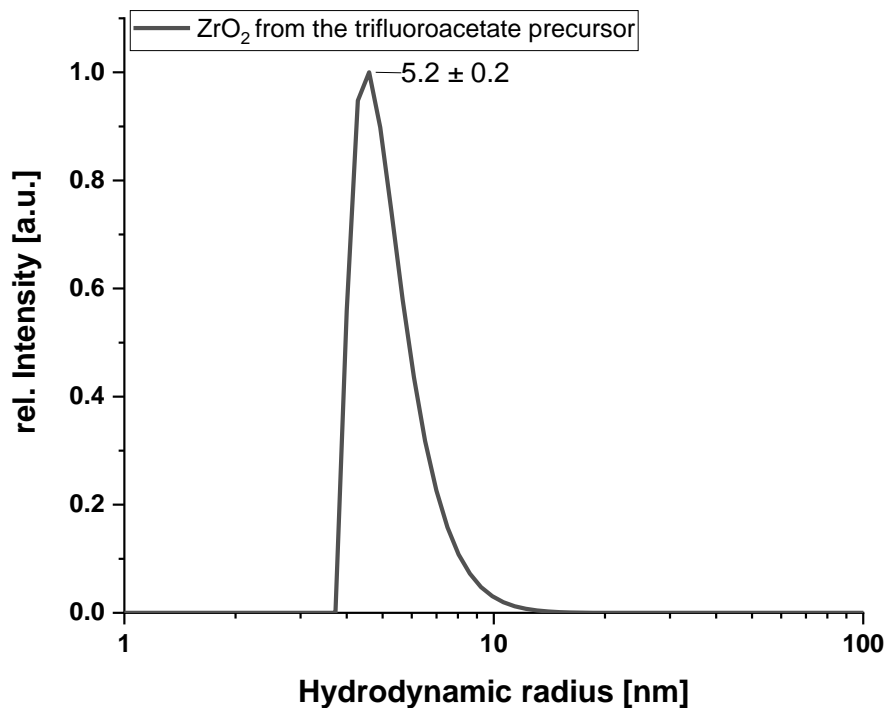
Figure 232: DLS measurement of ZrO$_2$ nanoparticles in THF after the synthesis from the trifluoroacetate route.
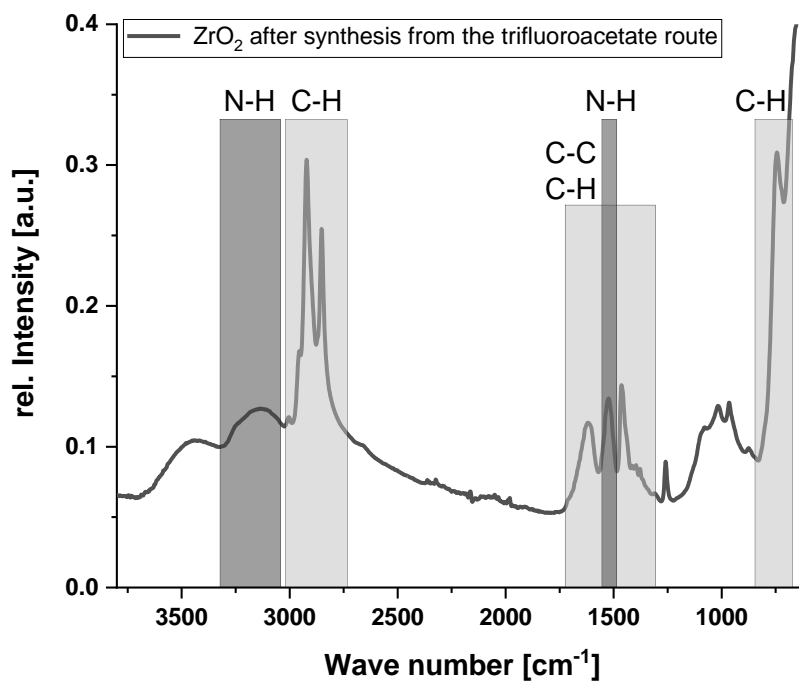
FT-IR measurements:

Figure 233: FT-IR spectrum of the ZrO$_2$ nanoparticles after the synthesis from the trifluoroacetate route.

TGA measurements:
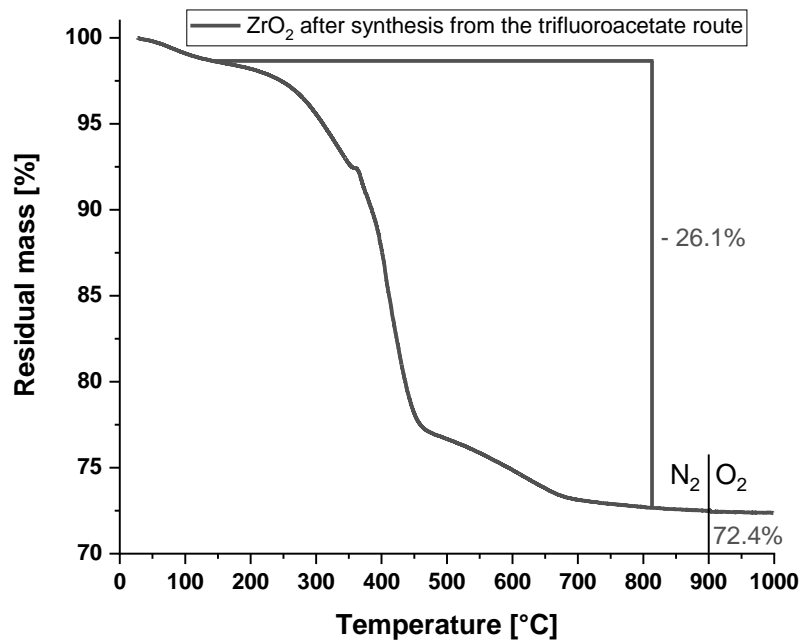
Figure 234: TG analysis of ZrO₂ nanoparticles synthesised by Zr(CF₃COO)₄.

6.2.2.3.2 HfO₂

DLS measurements:
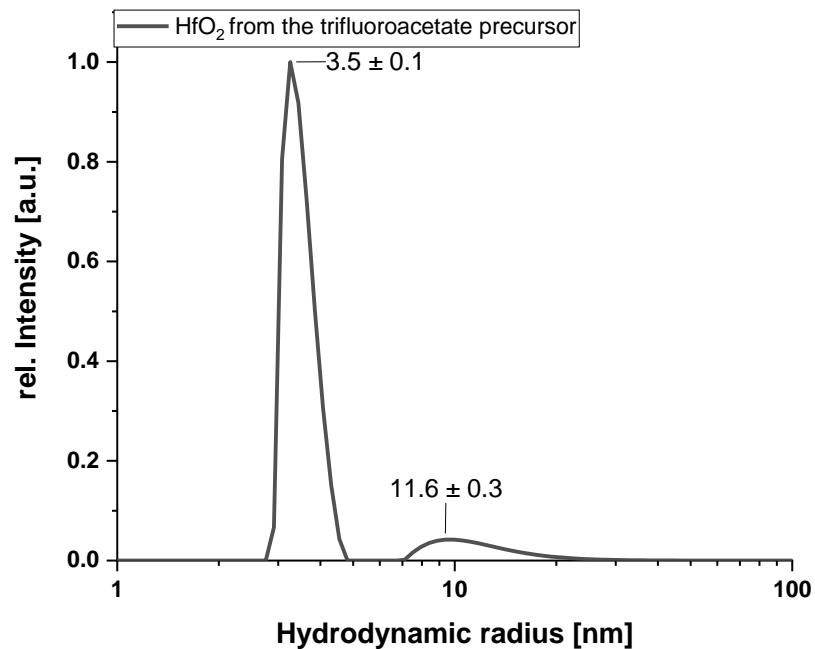
Figure 235: DLS measurement of HfO₂ nanoparticles in THF after the synthesis from the trifluoroacetate route.
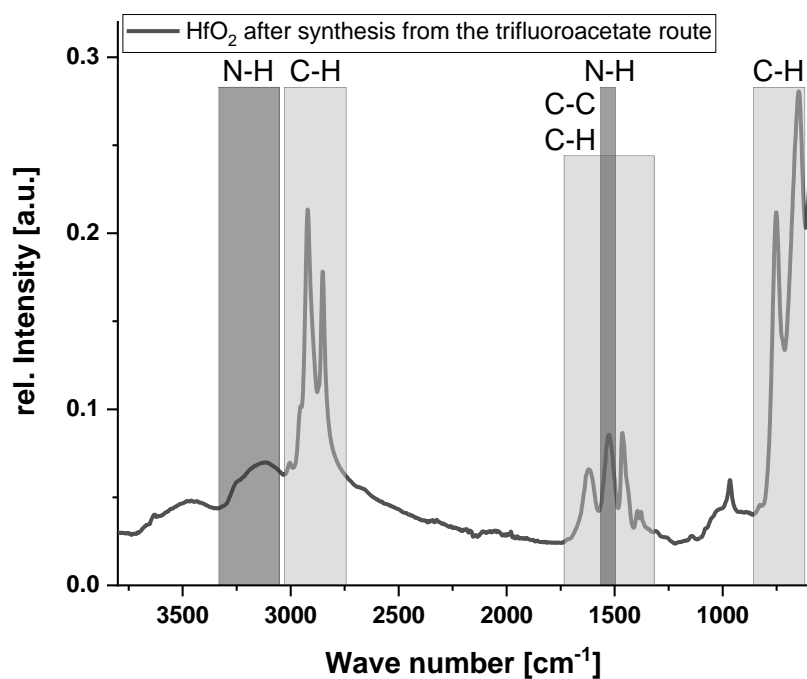
FT-IR measurements:

Figure 236: FT-IR spectrum of the HfO₂ nanoparticles after the synthesis from the trifluoroacetate route.

TG measurements:
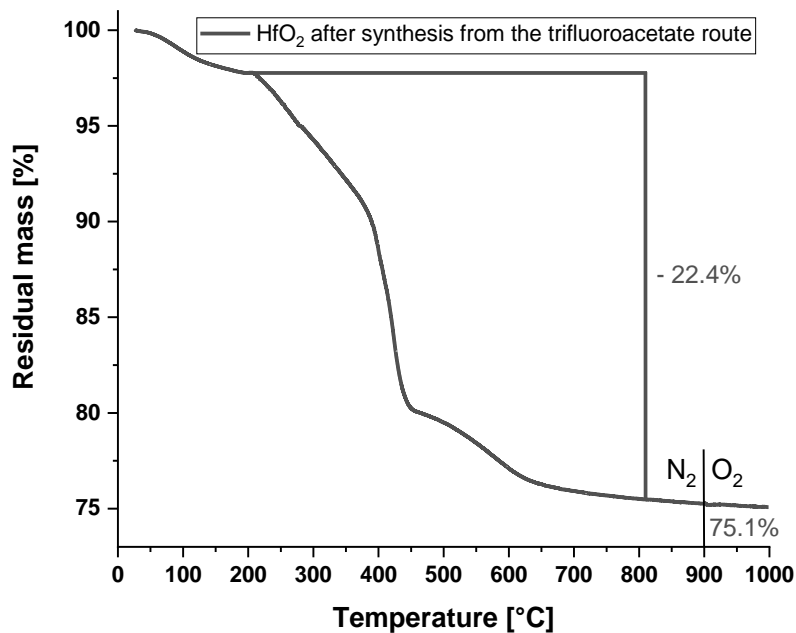
Figure 237: TG analysis of HfO₂ nanoparticles synthesised by Hf(CF₃COO)₄.

6.2.2.4 Synthesis of ZrO₂ from basic carbonate precursor

50.0 g (47.2 wt% ZrO_2) zirconium basic carbonate ($3ZrO_2 \cdot CO_2 \cdot yH_2O$), 35.0 g (1943 mmol) distilled water and 9.4 g (235 mmol) sodium hydroxide were heated at 110 °C for twelve hours.

After the supernatant was discarded, the particles were washed twice with 2 M ammonium bicarbonate solution and once with distilled water. The particles were mixed with 80 mL of distilled water and 100 mL of butyric acid and then heated at 70 °C for four hours. After the sediment was centrifuged, it was washed twice with distilled water to remove the free acid. The postmodified particles were dried for 48 hours at 5 mbar and 200 °C. These were then redispersed in 96 mL ethyl acetate and 8.0 g (32.3 mmol) of 3-methacryloxypropyl trimethoxysilane and heated at 70 °C for one hour. The particles were precipitated with 100 mL of distilled water and centrifuged. The resulting particles were dried under high vacuum ($2 \cdot 10^{-3}$ mbar) and redispersed in toluene.

DLS measurement:
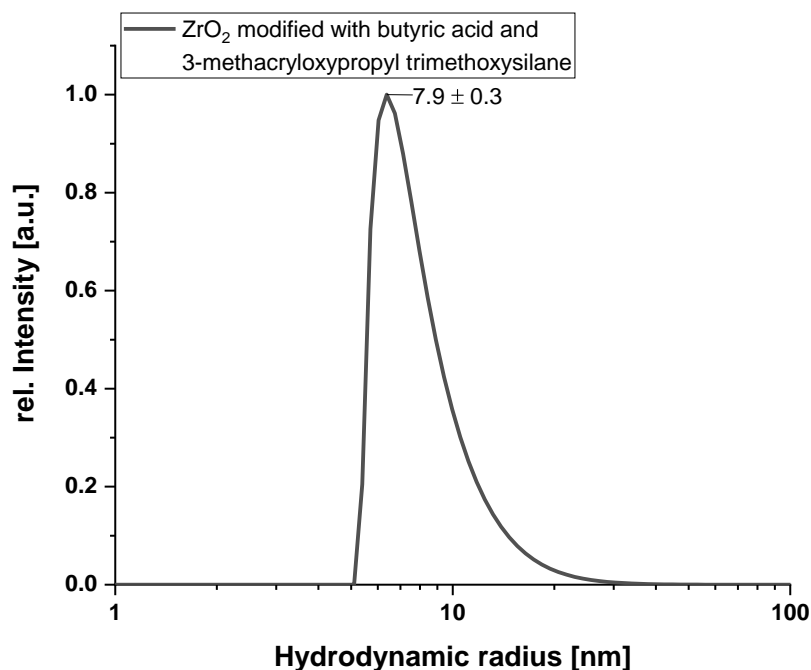
Figure 238: DLS measurement of the ZrO₂ nanoparticles in THF after the post-modification with butyric acid and 3-methacryloxypropyl trimethoxysilane.

FT-IR measurement:
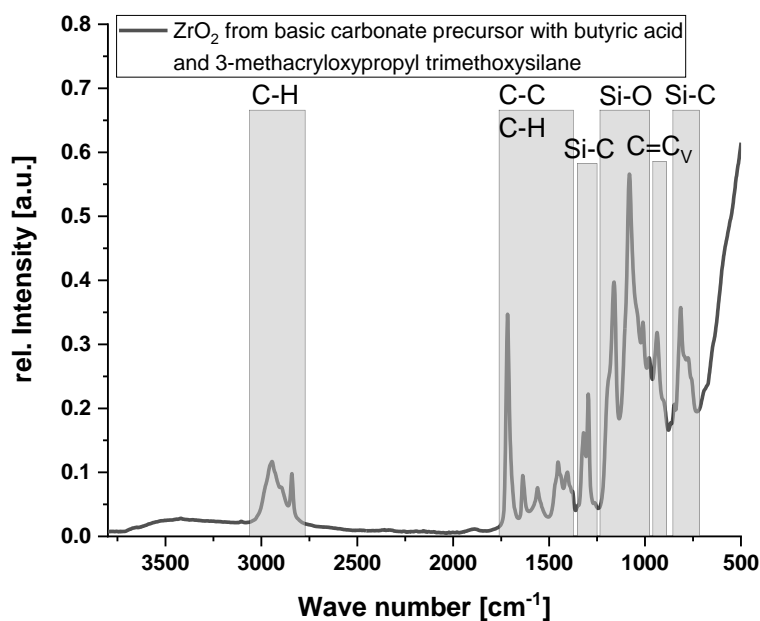
Figure 239: FT-IR spectra of the dried ZrO₂ nanoparticles after the post-modification with butyric acid and 3-methacryloxypropyl trimethoxysilane.

TGA measurement:
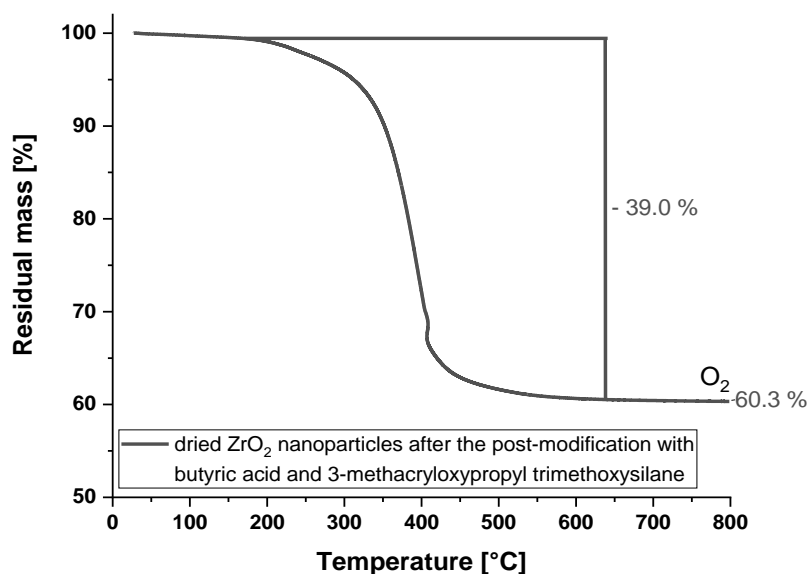
Figure 240: TG analyses of the dried ZrO₂ nanoparticles after the post-modification with butyric acid and 3-methacryloxypropyl trimethoxysilane.

NMR measurements:

^{1}H NMR (400 MHz, CDCl₃) δ = 6.08 (s, 1H, H5), 5.52 (s, 1H, H6), 4.10 (tr, J = 6.8 Hz, 2H, H4), 3.55 (s, 5.7H, H1), 1.92 (s, H7, 3H), 1.75 (m, 2H, H3), 0.67 (m, 2H, H2) ppm.

^{13}C NMR (101 MHz, CDCl₃) δ = 167.50 (C-CO-O), 136.59 (C₂-C=C), 125.27 (C=C), 66.63 (O-C-C), 50.64 – 50.41 (CH₃-O-, 22.24 (C-C₂=C), 6.83 (C-C-Si), 5.43 (C-C-C-Si) ppm.

^{29}Si NMR (79 MHz, CDCl$_3$) δ = −42.53 (SiOMeOH), −50.78 (Si-OMe$_2$) ppm.
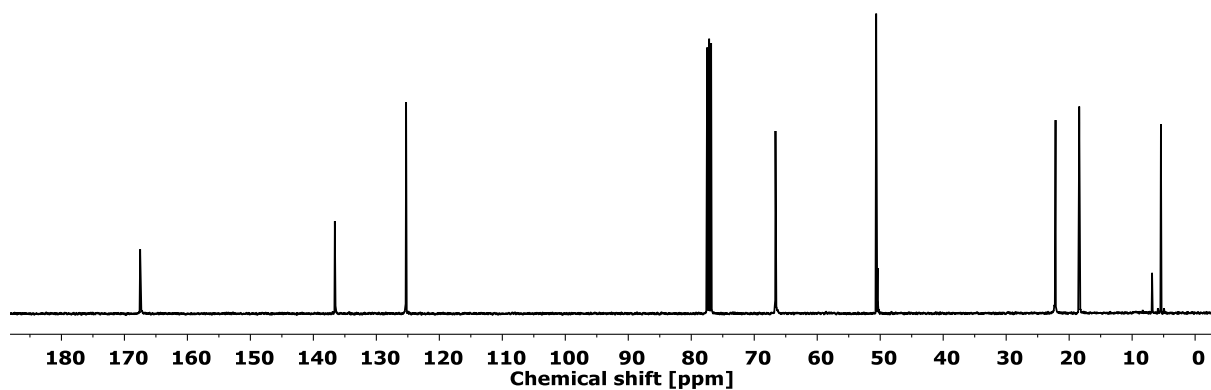
Figure 241: ^{13}C NMR (101 MHz, CDCl$_3$) of ZrO$_2$ nanoparticles after the postmodification with butyric acid and 3-methacryloxypropyl trimethoxysilane
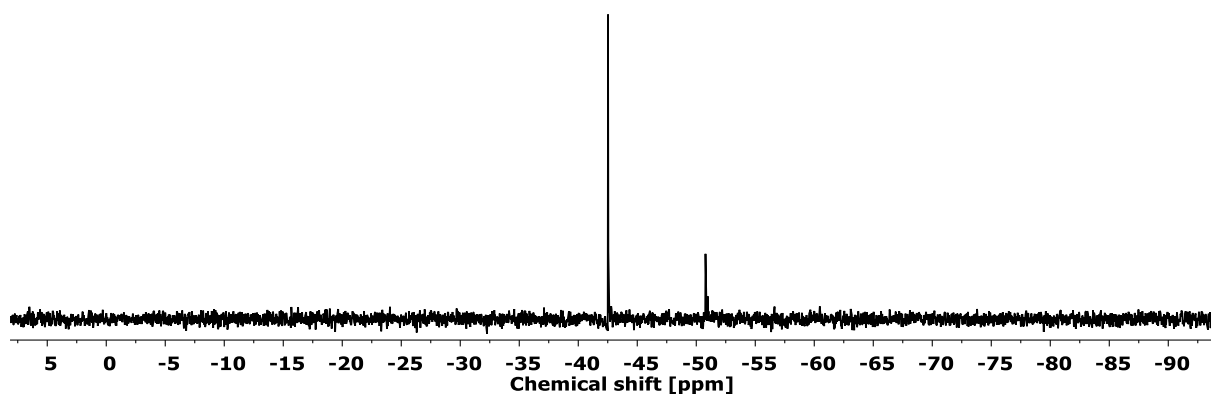
Figure 242: ^{29}Si NMR (79 MHz, CDCl$_3$) of ZrO$_2$ nanoparticles after the postmodification with butyric acid and 3-methacryloxypropyl trimethoxysilane

6.2.3   Metal dioxide nanoparticles incorporated into polysiloxane

General procedure for surface-modification of nanoparticles after the synthesis and mixing of the particles into the polysiloxane polymers:

The wet particles were mixed with the surfactant and stirred for three hours at room temperature. Subsequently, ethanol was added to precipitate the modified particles. After centrifugation, the supernatant was discarded to remove the liberated oleylamine and benzyl alcohol depending on the synthesis route. The still wet particles were suspended in toluene until a clear and homogeneous suspension was obtained. The polysiloxane component A and B for KJR-9022-E1, OE-6630 or PDPS (including adding the *Ossko*'s platinum catalyst for PDPS) were added in relation to the wanted particle content. The solvent was removed under stirring and reduced pressure (2 mbar). The polymer was doctor bladed with a film thickness of 120 μm or spread thinly onto a cleaned microscope glass slide and cured at 150 °C for four hours.

FT-IR measurements:
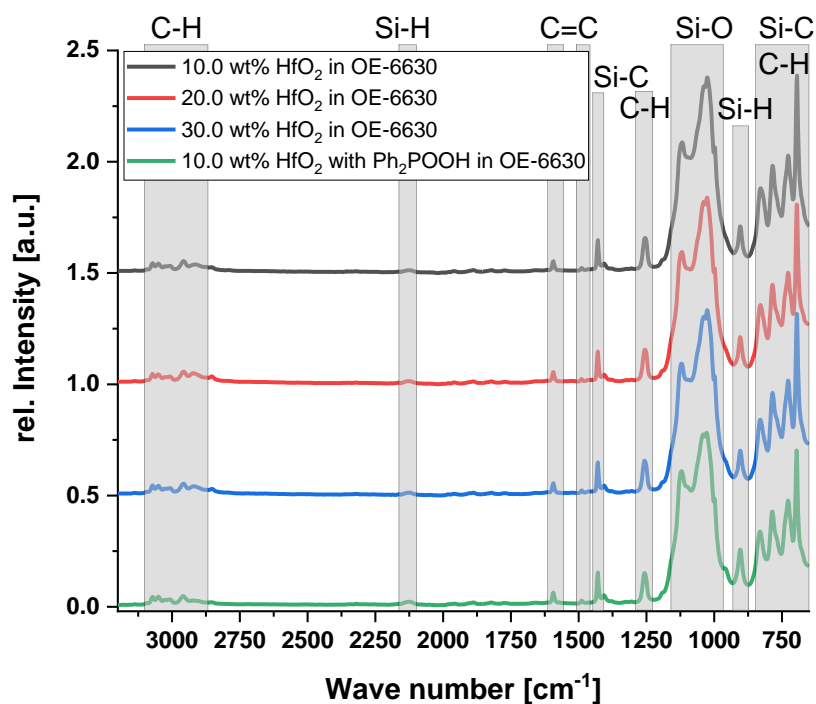
Figure 243: FT-IR spectra of HfO₂ nanoparticles synthesised with the trifluoroacetate precursor mixed in OE-6630 and cured.

UV/Vis measurements:
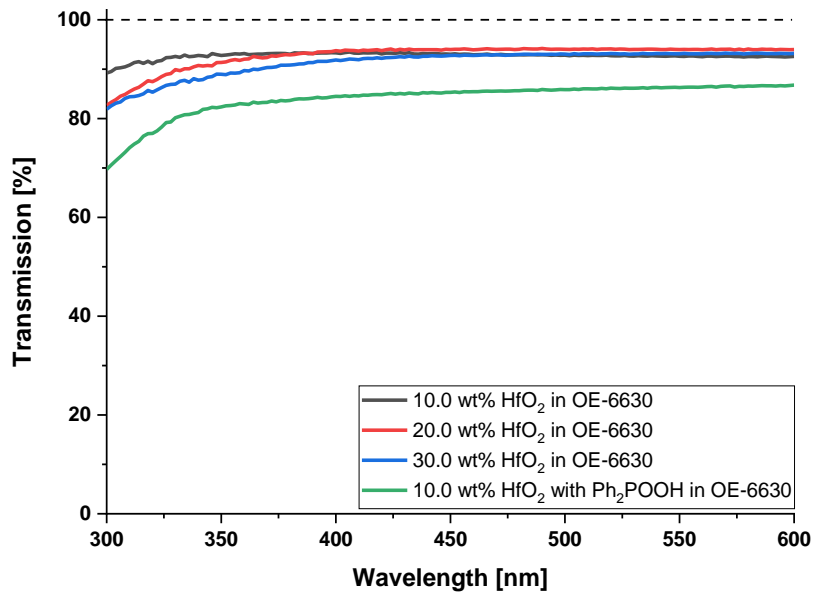
Figure 244: UV/Vis spectra of HfO₂ nanoparticles synthesised with the trifluoroacetate precursor mixed in OE-6630 and cured.

TGA measurements:
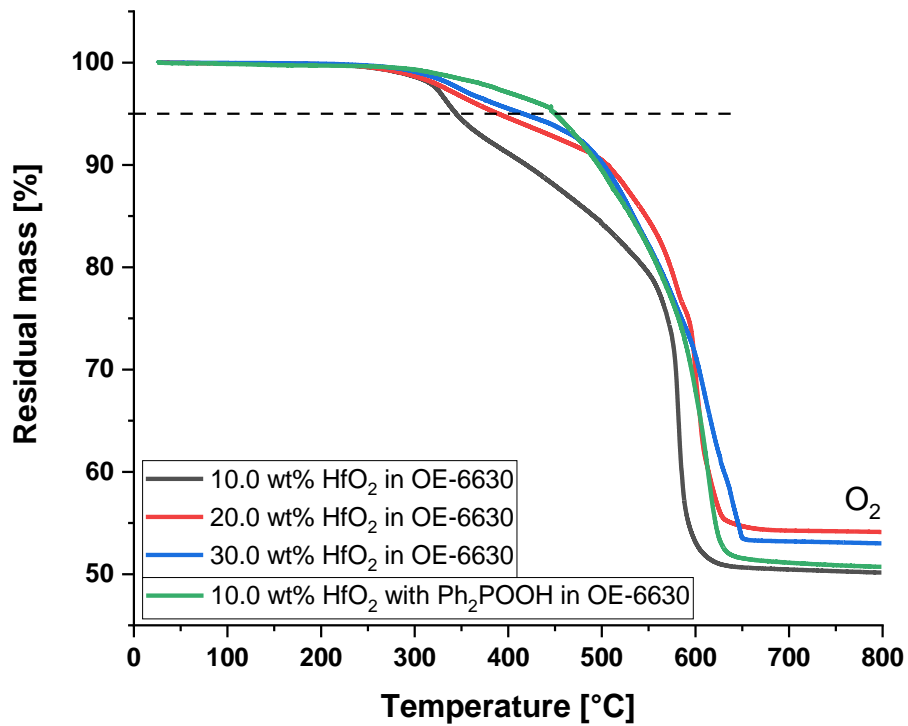
Figure 245: TGA curves of HfO₂ nanoparticles synthesised with the trifluoroacetate precursor mixed in OE-6630 and cured.

FT-IR measurements:
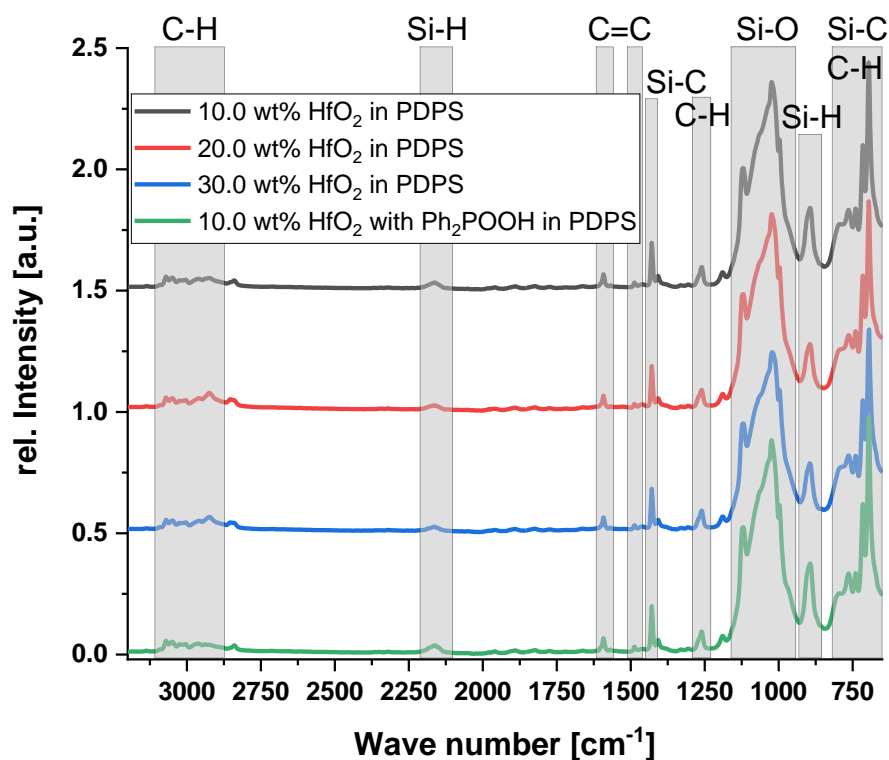
Figure 246: FT-IR spectra of HfO₂ nanoparticles synthesised with the trifluoroacetate precursor mixed in polydiphenylsiloxane and cured.

UV/Vis measurements:
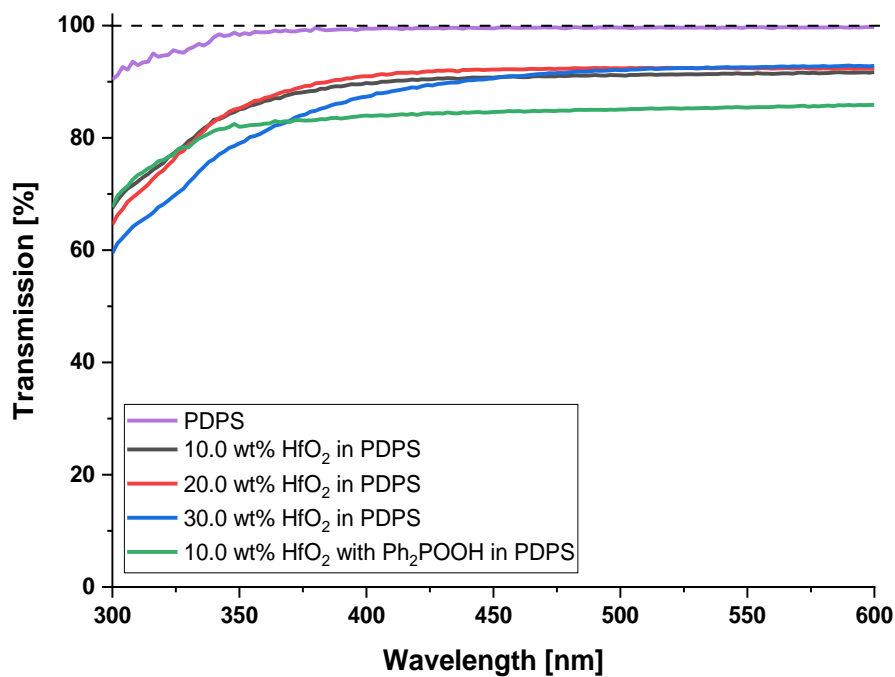
Figure 247: UV/Vis spectra of HfO₂ nanoparticles synthesised with the trifluoroacetate precursor mixed in polydiphenylsiloxane and cured.

TGA measurements:
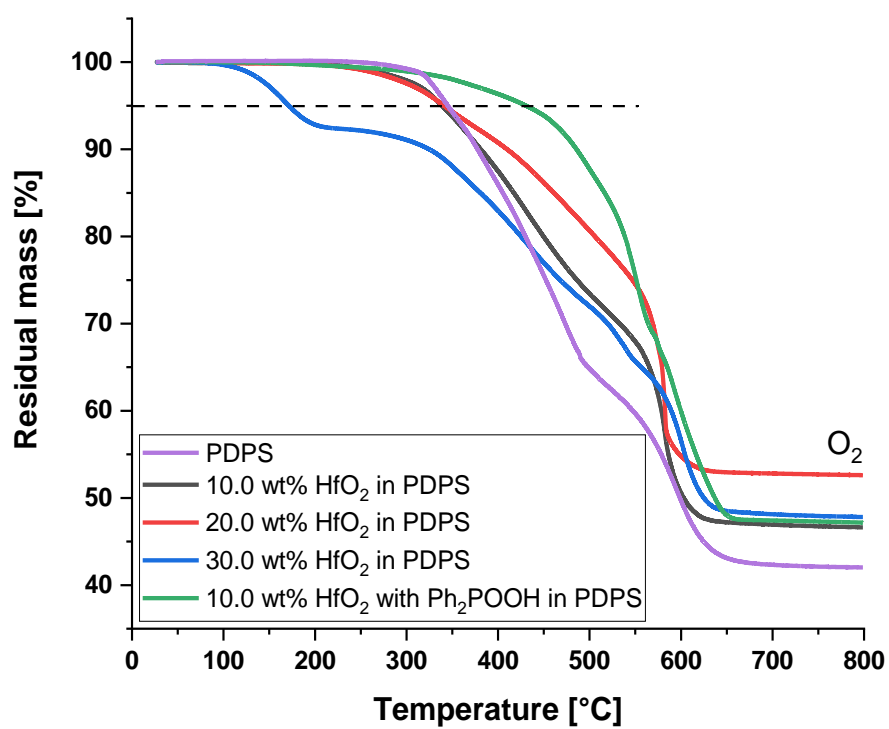
Figure 248: TGA curves of HfO₂ nanoparticles synthesised with the trifluoroacetate precursor mixed in polydiphenylsiloxane and cured.

6.2.4 Synthesis of methacrylate-group containing polysiloxane for cross-linking with 10.0 wt%, 20.0 wt% and 30.0 wt% methacrylate surface modified ZrO₂ nanoparticles

6.2.4.1 Synthesis of triphenylsiloxane terminated poly[(3-methacryloxypropyl)-co-dimethyl-co-diphenyl]siloxane

Polymer synthesis:

898.5 mg (3.25 mmol, 1 eq.) 3-methacryloxypropyl trimethoxysilane, 4696.0 mg (21.71 mmol, 6 eq.) diphenylsilanediol, 2610.0 mg (21.71 mmol, 6 eq.) dimethoxydimethylsilane, 3000.0 mg (10.85 mmol, 3 eq.) triphenylsilanol and 18.1 mg (0.06 mmol) barium hydroxide octahydrate were added to 50 mL of ethyl acetate and refluxed for 24 h at 60 °C. The cold suspension was filtered with a 0.45 µm syringe filter to remove the catalyst. After removing the solvent and the emerging methanol under reduced pressure, a clear polymer (9060.4 mg, 97 %) was obtained.
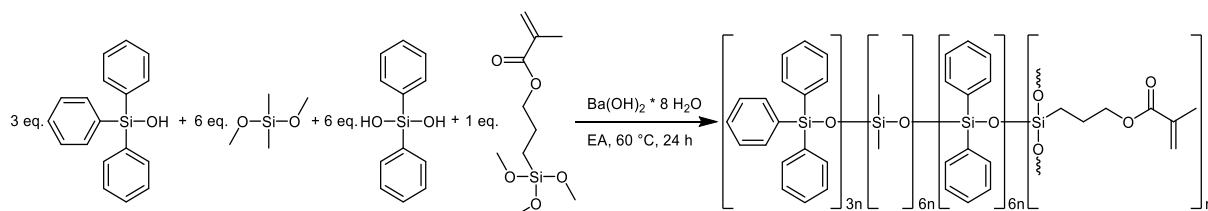
Figure 249: Synthesis of triphenylsiloxane terminated poly[(3-methacryloxypropyl)-*co*-dimethyl-*co*-diphenyl]siloxane.

Curing:

1000.0 mg of the polymer were mixed without or with the butyric acid and 3-methacryloxypropyl trimethoxysilane surface modified zirconium dioxide nanoparticles with 17 µL of a suspension of 10.0 mg (0.04 mmol) of benzoyl peroxide in 100 µL ethyl acetate. After degassing at 2 mbar for one hour the polymer was doctor bladed and cured at 150 °C for four hours.

NMR spectra:

^{1}H NMR (400 MHz, CDCl₃) δ = 7.73 – 7.46 (m, 42H, Ph), 7.45 – 7.08 (m, 63H, Ph), 6.58 – 6.18 (m, 2H, C=CH₂), 4.16, (m, 2H, C-CH₂-O), 2.27 – 2.16 (m, 3H, C-CH₃), 1.81 – 1.72 (m, 2H, C-CH₂-C), 0.38 – 0.31 (m, 2H, Si-CH₂-C), 0.30 – −0.26 (m, 36H, Me) ppm.

^{13}C NMR (101 MHz, CDCl₃) δ = 171.24 (C-*C*O-O), 136.15 (C₂-*C*=C), 135.92 – 129.79 (Ph), 127.80 (*C*=C), 60.46 (O-*C*-C), 22.97 (*C*-C₂=C), 14.23 (C-*C*-Si), 11.36 (C-*C*-C-Si), 1.13 – −1.58 (methyl) ppm.

^{29}Si NMR (79 MHz, CDCl$_3$) δ = −8.13 – −11.04 (Me/HO- Me$_2$Si-), −14.57 – −15.33 (Ph$_3$Si-), −19.05 – −21.22 (-Me$_2$Si-), −37.84 – −39.15 (HO-Ph$_2$Si-), −42.81 – −47.95 (-Ph$_2$Si-), −64.50 – −65.52 (-MASi-) ppm.
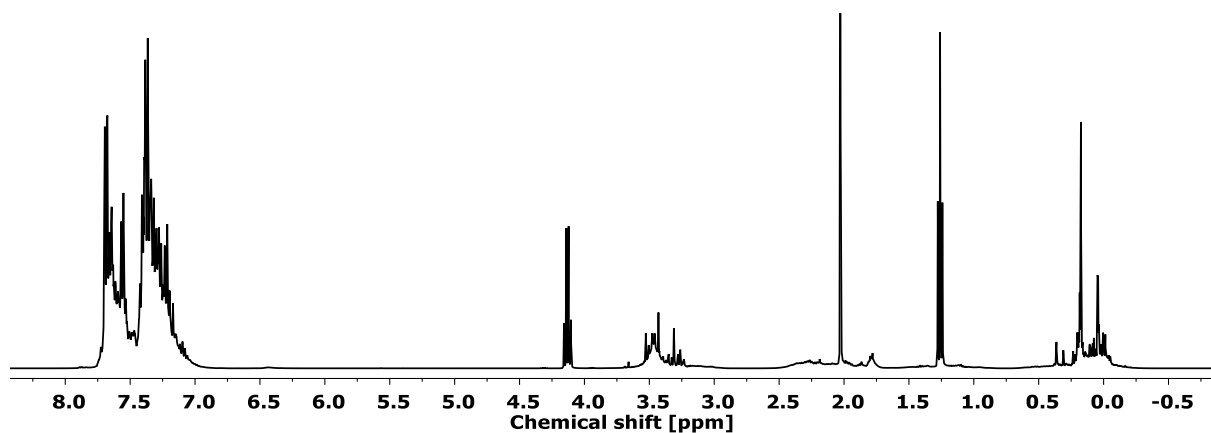
Figure 250: ^{1}H NMR (400 MHz, CDCl$_3$) of triphenylsiloxane terminated poly[(3-methacryloxypropyl)-*co*-dimethyl-*co*-diphenyl]siloxane.
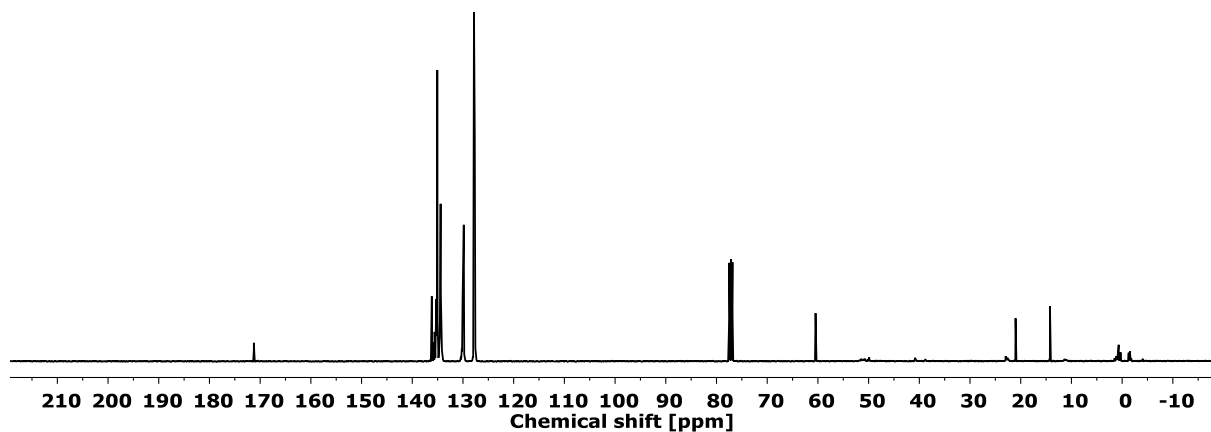
Figure 251: ^{13}C NMR (101 MHz, CDCl$_3$,) of triphenylsiloxane terminated poly[(3-methacryloxypropyl)-*co*-dimethyl-*co*-diphenyl]siloxane.

RI:

After synthesis: 1.5840.

After curing: 1.6041.

FT-IR measurements:
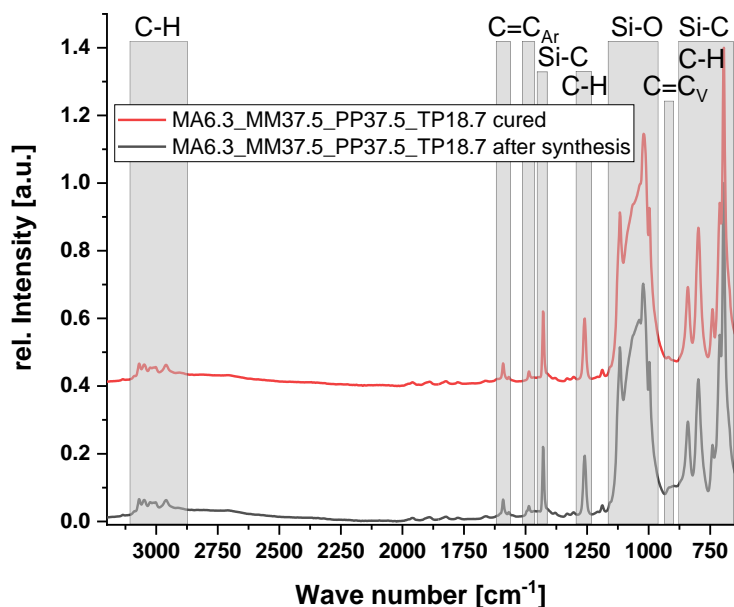
Figure 252: FT-IR spectra of MA6.3_MM37.5_PP37.5_TP18.7 after the synthesis and after curing.

UV/Vis measurements:
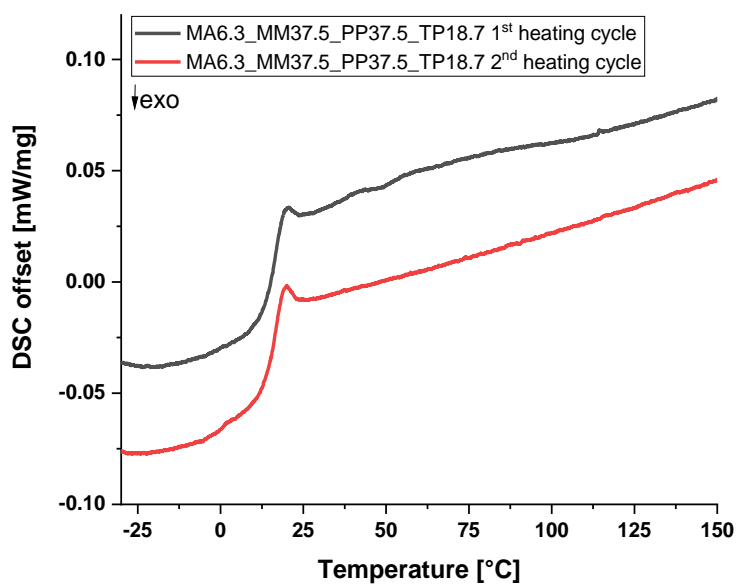
Figure 253: 1st and 2nd heating cycle of the cured MA6.3_MM37.5_PP37.5_TP18.7.

6.2.4.2 Synthesis of a ZrO₂/polysiloxane nanocomposite cross-linked by methacrylate-groups

RI:

RI cured, with 10.0 wt% ZrO_2: 1.6041.

RI cured, with 20.0 wt% ZrO_2: 1.6157.

RI cured, with 30.0 wt% ZrO_2: 1.6167.

FT-IR measurements:
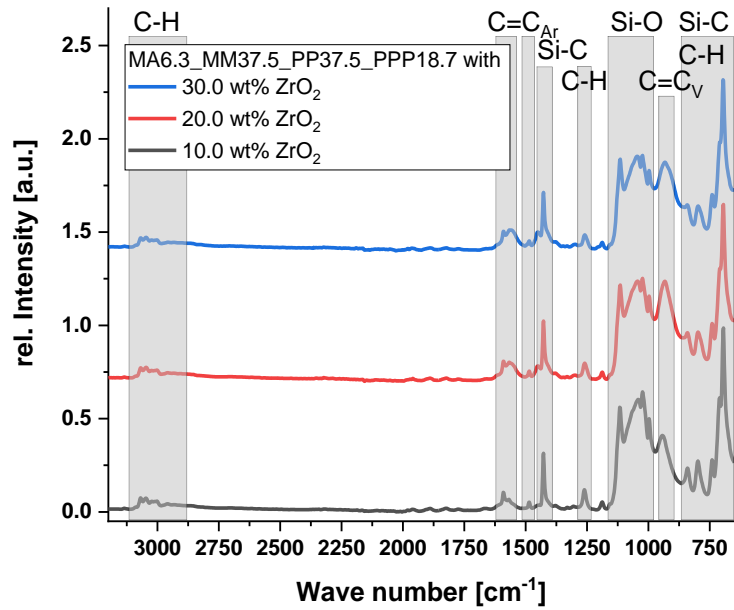
Figure 254: FT-IR spectra of cured MA6.3_MM37.5_PP37.5_TP18.7 with 10.0 wt%, 20.0 wt% and 30.0 wt% surface modified nanoparticles.

DSC curves:
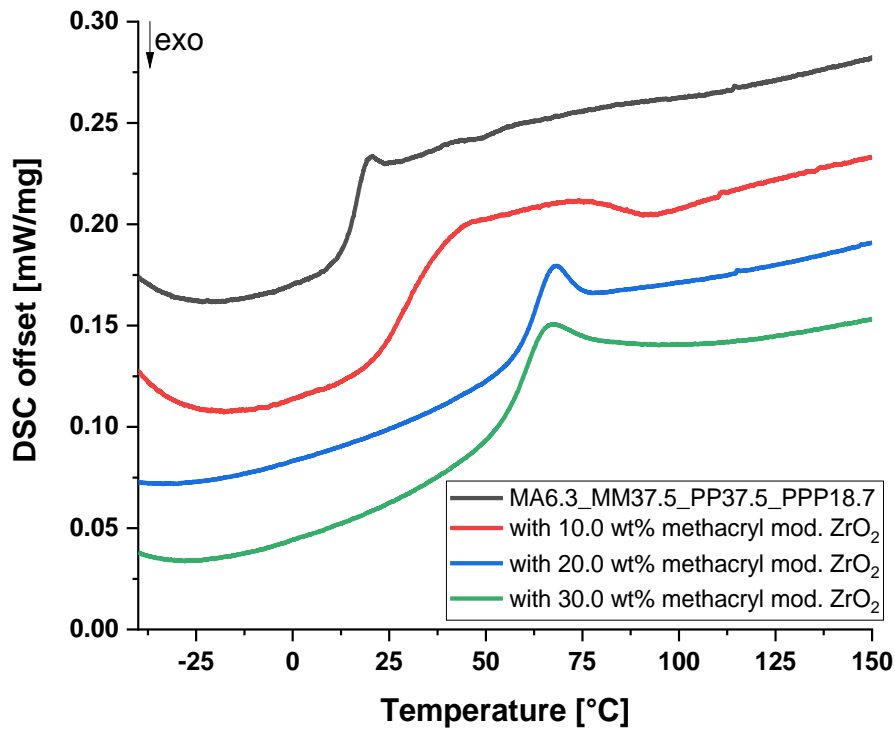
Figure 255: 1st DSC heating curve of cured MA6.3_MM37.5_PP37.5_TP18.7 with 0.0 wt%, 10.0 wt%, 20.0 wt% and 30.0 wt% surface modified nanoparticles.
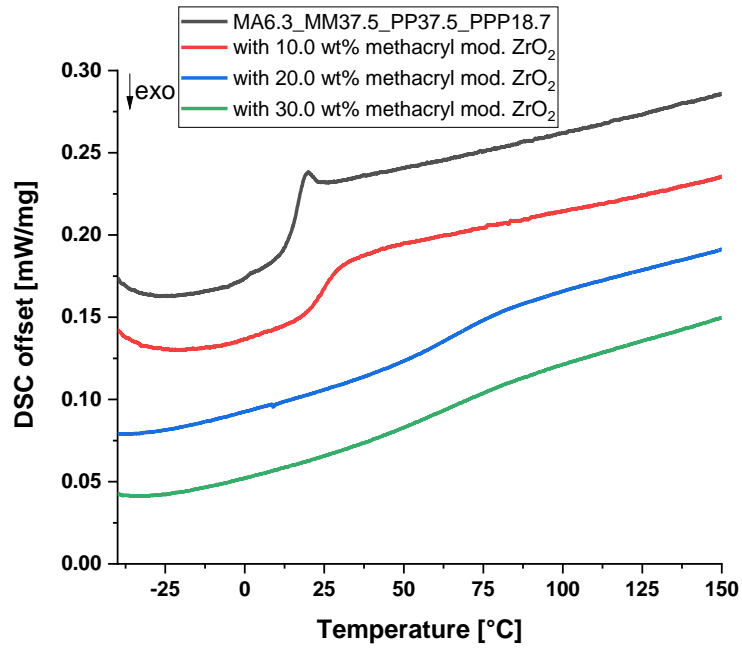
Figure 256: 2nd DSC heating curve of cured MA6.3_MM37.5_PP37.5_TP18.7 with 0.0 wt%, 10.0 wt%, 20.0 wt% and 30.0 wt% surface modified nanoparticles.

UV/Vis measurements:
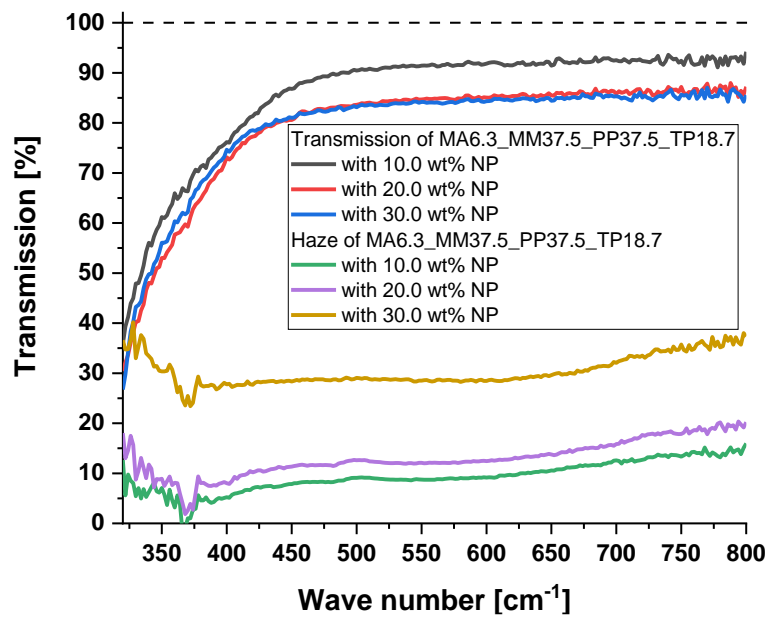
Figure 257: UV/Vis spectra and the calculated haze curves of cured MA6.3_MM37.5_PP37.5_TP18.7 with 0.0 wt%, 10.0 wt%, 20.0 wt% and 30.0 wt% surface modified nanoparticles.

6.2.5 Synthesis of epoxide-group containing polysiloxane for cross-linking with 10.0 wt% epoxide-surface modified ZrO$_2$ nanoparticles

Polymer synthesis:

768.1 mg (3.25 mmol, 1 eq.) 3-glycidyloxypropyl trimethoxysilane, 4696.0 mg (21.71 mmol, 6 eq.) diphenylsilanediol, 2610.0 mg (21.71 mmol, 6 eq.) dimethoxydimethylsilane, 3000.0 mg (10.85 mmol, 3 eq.) triphenylsilanol and 18.1 mg (0.06 mmol) barium hydroxide octahydrate were added to 50 mL of ethyl acetate and refluxed for 24 h at 60 °C. The cold suspension was filtered with a 0.45 µm syringe filter to remove the catalyst. After removing the solvent and the emerging methanol under reduced pressure, a clear polymer (6722.7 mg, 94 %) was obtained.
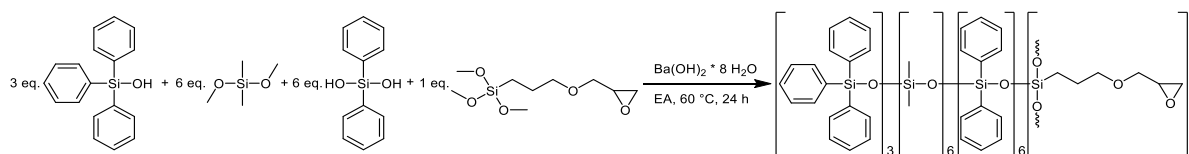
Figure 258: Synthesis of triphenylsiloxane terminated poly[(3-glycidyloxypropyl)-*co*-dimethyl-*co*-diphenyl]siloxane.

Curing:

1000.0 mg of the polymer EP6.3_MM37.5_PP37.5_TP18.7 were mixed with the 100.0 mg 3-glycidyloxypropyl trimethoxysilane surface modified zirconium dioxide nanoparticles. After degassing at 2 mbar for one hour the polymer was doctor bladed and cured at 150 °C for four hours.

NMR spectra:

^{1}H NMR (400 MHz, CDCl$_3$) δ = 7.92 – 7.55 (m, 42H, Ph), 7.55 – 7.14 (m, 63H, Ph), 3.60 – 3.40 (m, 3H, H4, H5, H5'), 3.16 – 3.00 (s, 1H, H4'), 2.77 – 2.65 (m, 1H, H6), 2.61 – 2.43 (s, 1H, H7), 1.93 – 2.03 (s, 1H, H7'), 1.88 – 1.46 (m, 2H, H3), 0.87 – 0.58 (m, 2H, H2), 0.05 – 0.31 (m, 36H, Me) ppm.

^{13}C NMR (101 MHz, CDCl$_3$) δ = 135.79 – 127.67 (phenyl), 77.48 (-O-*C*-C-C), 76.84 (O-*C*-C$_2$-O-C), 49.99 (*C*-O-C$_2$-C), 44.25 (O-*C*-C$_2$), 23.12 (C-*C*-C-Si-), 14.73 (C-C-*C*-Si-), 0.53 – −1.71 (methyl) ppm.

^{29}Si NMR (79 MHz, CDCl$_3$) δ = −4.84 (MeO-Me$_2$Si-), −7.18 – −9.67 (HO-Me$_2$Si-), −13.35 (Ph$_3$Si-), −15.24 – −20.88 (-Me$_2$Si-), −33.58 (MeO-Ph$_2$Si-), −35.10 – −38.39 (HO-Ph$_2$Si-), −41.39 – −46.52 (-Ph$_2$Si-), −54.61 (EPSiOH-), −64.52 (EPSi-) ppm.
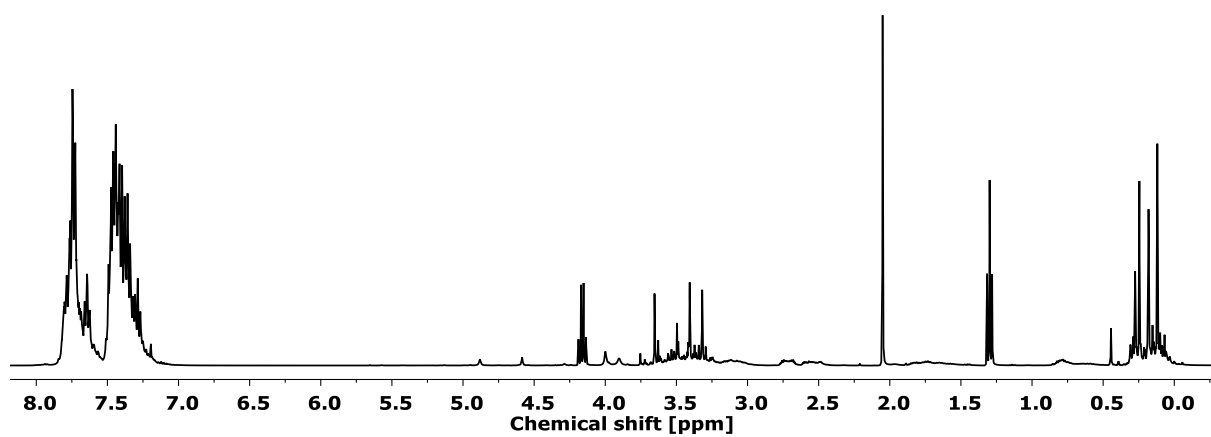
Figure 259: ^{1}H NMR (400 MHz, CDCl$_3$) of triphenylsiloxane terminated poly[(3-glycidyloxypropyl)-*co*-dimethyl-*co*-diphenyl]siloxane.
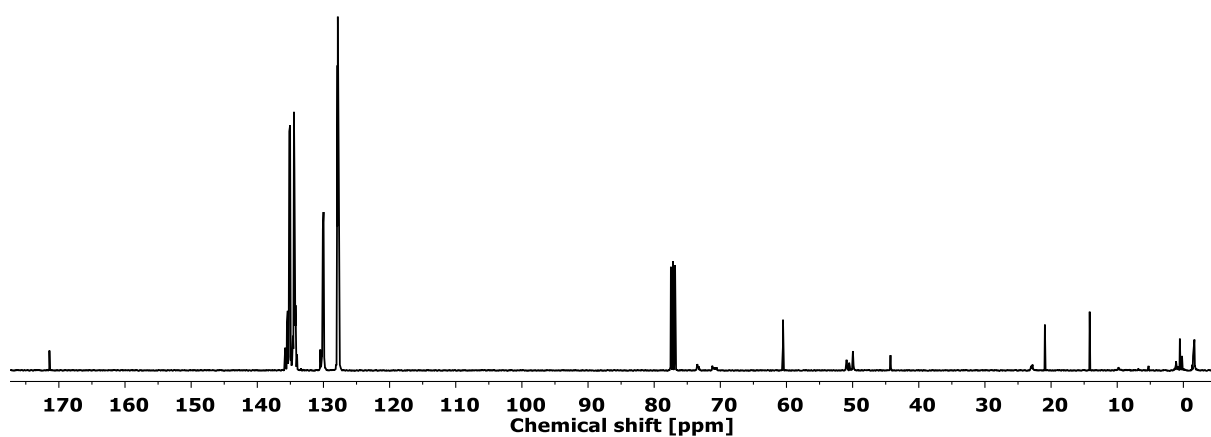
Figure 260: ^{13}C NMR (101 MHz, CDCl$_3$) of triphenylsiloxane terminated poly[(3-glycidyloxypropyl)-*co*-dimethyl-*co*-diphenyl]siloxane.

RI:

RI uncured: 1.5815.

RI cured, with 10.0 wt% ZrO$_2$: 1.6075.

FT-IR measurements:
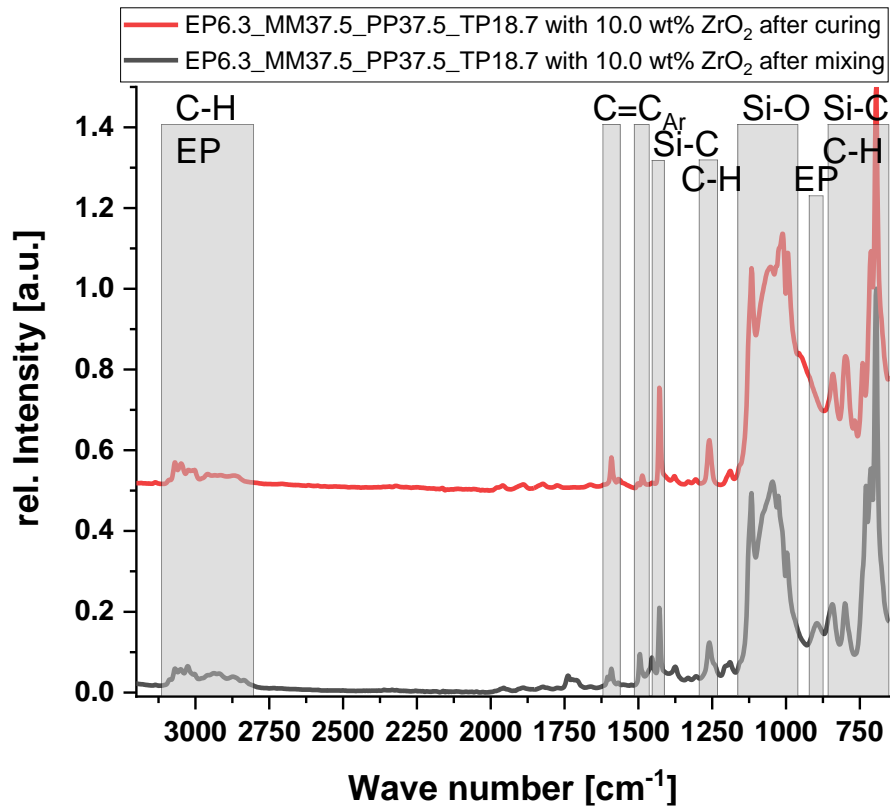
Figure 261: FT-IR spectra of mixed and cured EP6.3_MM37.5_PP37.5_TP18.7 with 10.0 wt% epoxide-group surface modified ZrO₂ nanoparticles.

TGA curves:
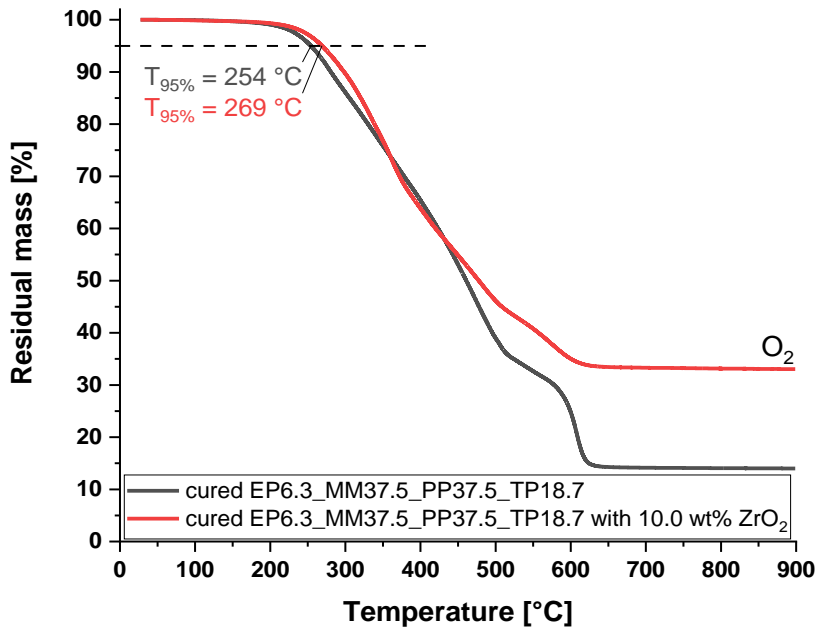
Figure 262: TGA curves of cured EP6.3_MM37.5_PP37.5_TP18.7 without and with 10.0 wt% epoxide-group surface modified ZrO₂ nanoparticles under oxygen atmosphere.
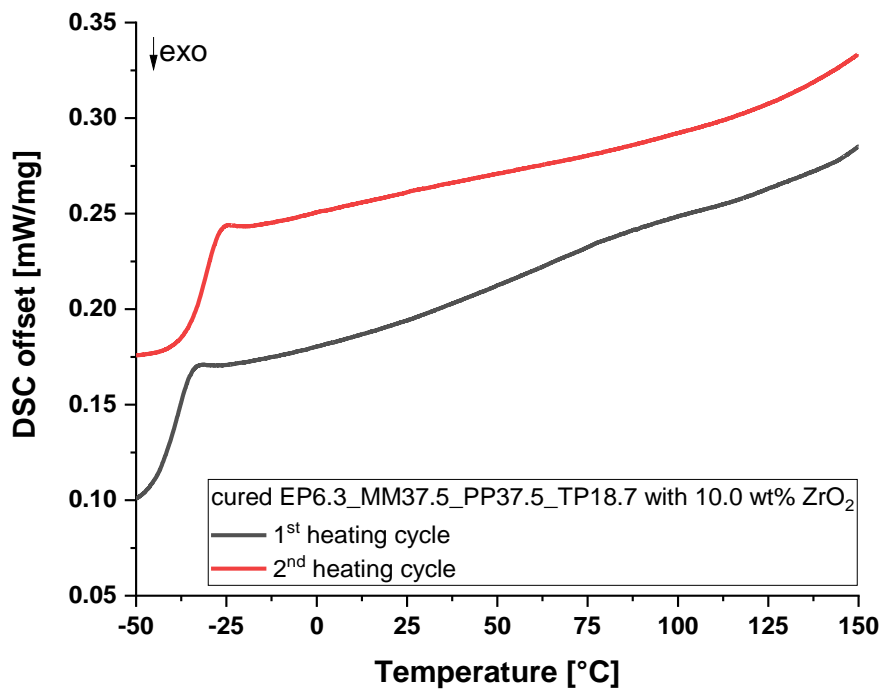
DSC curves:

Figure 263: DSC curves of the first and second heating cycle of cured EP6.3_MM37.5_PP37.5_TP18.7 with 10.0 wt% epoxide-group surface modified ZrO₂ nanoparticles.

UV/Vis measurements:
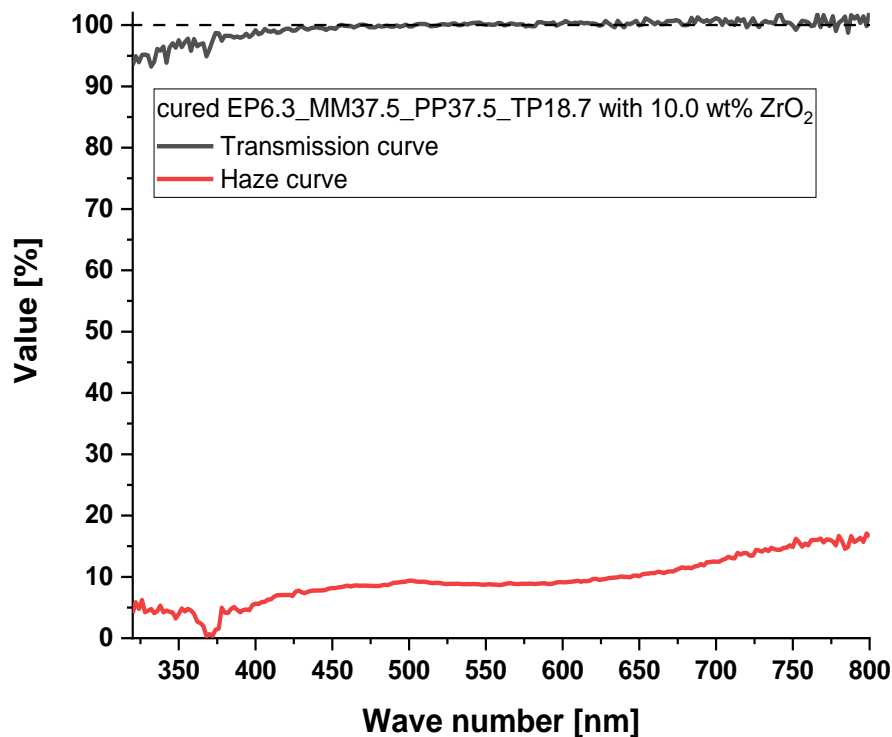
Figure 264: Transmission and haze curves of cured EP6.3_MM37.5_PP37.5_TP18.7 with 10.0 wt% epoxide-group surface modified ZrO₂ nanoparticles.

6.2.6 Syntheses of metal atom containing polysiloxanes

6.2.6.1 Hydride and metal atom containing polysiloxanes

General synthesis for hydride and metal atom containing polysiloxanes:

The percentages refer to the accumulated amount of silicon and metal atoms. To 40 % (2.50 g, 11.56 mmol) of diphenylsilanediol, (40-X) % (40 %: 2.10 g, 11.56 mmol) of methylphenyl-dimethoxysilane, X % of the metal monomer, 3 mL of xylene and 0.1 % (4.37 mg, 0.02 mmol) of barium hydroxide monohydrate were heated to 110 °C for 24 h with an equipped distillation head. A ^{1}H NMR measurement was performed to check if the reaction is finished. After the addition of 100 µL conc. $HCl_{(aq)}$ at room temperature the solution was stirred for 10 min, then 20 % (0.78 g, 5.78 mmol) of methyldiethoxysilane were added. The solution was heated to 80 °C for one hour and to 110 °C for two additional hours. After cooling down and adding 2 mL of distilled water and 2 mL of toluene, the polymer was extracted using a centrifuge at 8000 rpm for one minute. After washing the organic phase once with potassium bicarbonate solution and four times with distilled water, it was filtered with a 0.45 µm syringe filter and the residual solvent was removed under high vacuum to receive a viscous clear to opaque polymer (theoretical: 100 % with solvent residuals). The synthesis of the reference hydride was performed in a larger scale using 296.2 mmol of silanes in total because every metal containing vinyl copolymer is cross-linked with this metal-free hydride.

For the tin containing samples, the $Sn(Cl)_4 \cdot 5\ H_2O$ was dissolved in absolute methanol first before it was added to the siloxanes. Also, additional amounts of barium hydroxide or sodium hydroxide were added to compensate the emerging HCl and remain a slightly basic solution.

The ^{1}H NMRs are referenced to the CH_3 signal of toluene at 2.36 ppm, the ^{13}C NMRs are referenced to the $CDCl_3$ signal at 77.16 ppm. The stated integration of the groups is based on the theoretical values because of overlapping solvent and alkoxy signals.

H20_Met0_PP40_PM40:
Yield: 40.49 g.
^{1}H NMR (400 MHz, $CDCl_3$): δ = 7.75 – 7.06 (m, 30.00H, Ph), 5.08 – 4.67 (m, 1.00H, H), 0.61 – −0.31 (m, 9.00H, Me) ppm.

^{13}C NMR (101 MHz, $CDCl_3$): δ = 134.51 – 125.45 (Ph), 1.22 – −0.30 (Me) ppm.

^{29}Si NMR (79 MHz, $CDCl_3$): δ = −29.22 – −32.45 (-MePhSi-), −33.87 – −35.24 (-HMeSi-), −43.12 – −46.28 (-Ph2Si-) ppm.

Refractive index: 1.5625.

Viscosity: 2800 ± 170 mPa·s.

6.2.6.1.1 Zirconium

H20_Zr1_PP40_PM39:

Yield: 3.88 g.

^{1}H NMR (400 MHz, CDCl$_3$): δ = 7.82 – 6.83 (m, 29.75H, Ph), 5.24 – 4.64 (m, 1.00H, H), 0.56 – −0.20 (m, 8.85H, Me) ppm.

^{13}C NMR (101 MHz, CDCl$_3$): δ = 134.72 – 127.55 (Ph), 1.05 – −1.97 (Me) ppm.

^{29}Si NMR (79 MHz, CDCl$_3$): δ = −29.20 – −32.64 (-MePhSi-), −33.15 – −36.03 (-HMeSi-), −42.89 – −47.07 (-Ph$_2$Si-) ppm.

Refractive index: 1.5668.

Viscosity: 25200 ± 350 mPa·s.

H20_Zr3_PP40_PM37:

Yield: 3.54 g.

^{1}H NMR (400 MHz, CDCl$_3$): δ = 7.84 – 6.83 (m, 29.25H, Ph), 5.06 – 4.01 (m, 1.00H, H), 0.57 – −0.12 (m, 8.55H, Me) ppm.

^{13}C NMR (101 MHz, CDCl$_3$): δ = 134.79 – 127.55 (Ph), −0.14 – −4.05 (Me) ppm.

^{29}Si NMR (79 MHz, CDCl$_3$): −29.98 – −32.49 (-MePhSi-), −33.47 – −34.64 (-HMeSi-), −42.81 – −47.04 (-Ph$_2$Si-) ppm.

Refractive index: 1.5606.

Viscosity: 7220 ± 90 mPa·s.

H20_Zr5_PP40_PM35:

Yield: 3.19 g.

^{1}H NMR (400 MHz, CDCl$_3$): δ = 7.80 – 6.87 (m, 28.75H, Ph), 5.02 – 4.16 (m, 1.00H, H), 0.61 – −0.10 (m, 8.25H, Me) ppm.

^{13}C NMR (101 MHz, CDCl$_3$): δ = 135.00 – 127.54 (Ph), −0.30 – −1.99 (Me) ppm.

^{29}Si NMR (79 MHz, CDCl$_3$): −25.51 – −29.78 (-MePhSi-), −32.47 – −33.61 (-HMeSi-), −42.78 – −47.07 (-Ph$_2$Si-) ppm.

Refractive index: 1.5560.

Viscosity: 7090 ± 80 mPa·s.

H20_Zr10_PP40_PM30:

Yield: 3.70 g.

^{1}H NMR (400 MHz, CDCl$_3$): δ = 7.73 – 6.98 (m, 27.50H, Ph), 4.79 – 4.09 (m, 1.00H, H), 0.49 – −0.18 (m, 7.50H, Me) ppm.

^{13}C NMR (101 MHz, CDCl$_3$): δ = 135.04 – 125.44 (Ph), −0.25 – −4.12 (Me) ppm.

^{29}Si NMR (79 MHz, CDCl$_3$): −25.18 – −32.73 (-MePhSi-), −33.30 – −39.65 (-HMeSi-), −42.92 – −46.84 (-Ph$_2$Si-) ppm.

Refractive index: 1.5506.

Viscosity: 30200 ± 1600 mPa·s.

H20_Zr15_PP40_PM25:

Yield: 2.29 g.

^{1}H NMR (400 MHz, CDCl$_3$): δ = 7.81 – 6.86 (m, 26.25H, Ph), 4.61 – 4.05 (m, 1.00H, H), 0.59 – −0.17 (m, 6.75H, Me) ppm.

^{13}C NMR (101 MHz, CDCl$_3$): δ = 135.04 – 125.43 (Ph), −0.25 – −5.56 (Me) ppm.

^{29}Si NMR (79 MHz, CDCl$_3$): −29.24 – −32.63 (-MePhSi-), −33.18 – −39.40 (-HMeSi-), −42.93 – −47.20 (-Ph$_2$Si-) ppm.

Refractive index: 1.5770.

Viscosity: 680000 ± 24000 mPa·s.

6.2.6.1.2 **Hafnium**
H20_Hf1_PP40_PM39:

Yield: 3.94 g.

^{1}H NMR (400 MHz, CDCl$_3$): δ = 7.76 – 6.92 (m, 29.75H, Ph), 5.31 – 4.54 (m, 1.00H, H), 0.58 – −0.23 (m, 8.85H, Me) ppm.

^{13}C NMR (101 MHz, CDCl$_3$): δ = 134.99 – 125.45 (Ph), −0.23 – −0.30 (Me) ppm.

^{29}Si NMR (79 MHz, CDCl$_3$): δ = −29.21– −32.66 (-MePhSi-), −33.08 – −33.75 (-HMeSi-), −42.91 – −47.18 (-Ph$_2$Si-) ppm.

Refractive index: 1.5657.

Viscosity: 20000 ± 220 mPa·s.

H20_Hf3_PP40_PM37:

Yield: 3.22 g.

^{1}H NMR (400 MHz, CDCl$_3$): δ = 7.81 – 6.83 (m, 29.25H, Ph), 5.13 – 4.64 (m, 1.00H, H), 0.64 – −0.21 (m, 8.55H, Me) ppm.

^{13}C NMR (101 MHz, CDCl$_3$): δ = 134.98 – 125.43 (Ph), 0.14 – −2.86 (Me) ppm.

^{29}Si NMR (79 MHz, CDCl$_3$): −29.16 – −32.52 (-MePhSi-), −33.13 – −34.66 (-HMeSi-), −42.85 – −47.23 (-Ph$_2$Si-) ppm.

Refractive index: 1.5589.

Viscosity: 26600 ± 110 mPa·s.

H20_Hf5_PP40_PM35:

Yield: 3.66 g.

^{1}H NMR (400 MHz, CDCl$_3$): δ = 7.85 – 6.87 (m, 28.75H, Ph), 5.01 – 4.28 (m, 1.00H, H), 0.61 – −0.10 (m, 8.25H, Me) ppm.

^{13}C NMR (101 MHz, CDCl$_3$): δ = 135.00 – 127.54 (Ph), −0.30 – −4.12 (Me) ppm.

^{29}Si NMR (79 MHz, CDCl$_3$): −24.94 – −31.12 (-MePhSi-), −32.30 – −33.59 (-HMeSi-), −42.77 – −47.06 (-Ph$_2$Si-) ppm.

Refractive index: 1.5560.

Viscosity: 3120000 ± 470000 mPa·s.

H20_Hf10_PP40_PM30:

Yield: 3.17 g.

^{1}H NMR (400 MHz, CDCl$_3$): δ = 7.82 – 6.85 (m, 27.50H, Ph), 4.96 – 4.27 (m, 1.00H, H), 0.53 – −0.13 (m, 7.50H, Me) ppm.

^{13}C NMR (101 MHz, CDCl$_3$): δ = 135.04 – 125.44 (Ph), −0.25 – −4.15 (Me) ppm.

^{29}Si NMR (79 MHz, CDCl$_3$): −25.16 – −32.68 (-MePhSi-), −33.07 – −39.72 (-HMeSi-), −42.91 – −47.20 (-Ph$_2$Si-) ppm.

Refractive index: 1.5520.

Viscosity: 54000 ± 750 mPa·s.

H20_Hf15_PP40_PM25:

Yield: 3.93 g.

^{1}H NMR (400 MHz, CDCl$_3$): δ = 7.82 – 6.85 (m, 26.25H, Ph), 4.96 – 4.27 (m, 1.00H, H), 0.53 – −0.13 (m, 6.75H, Me) ppm.

^{13}C NMR (101 MHz, CDCl$_3$): δ = 135.04 – 125.44 (Ph), −0.25 – −4.15 (Me) ppm.

^{29}Si NMR (79 MHz, CDCl$_3$): −25.16 – −32.68 (-MePhSi-), −33.07 – −39.72 (-HMeSi-), −42.91 – −47.20 (-Ph$_2$Si-) ppm.

Refractive index: 1.5365.

Viscosity: 6640 ± 360 mPa·s.

6.2.6.1.3 <u>Tin</u>

H20_Sn1_PP40_PM39:

Yield: 3.67 g.

^{1}H NMR (400 MHz, CDCl$_3$): δ = 7.84 – 6.83 (m, 29.75H, Ph), 5.12 – 4.63 (m, 1.00H, H), 0.57 – −0.24 (m, 8.85H, Me) ppm.

^{13}C NMR (101 MHz, CDCl$_3$): δ = 137.88 – 125.94 (Ph), 1.03 – −0.28 (Me) ppm.

^{29}Si NMR (79 MHz, CDCl$_3$): δ = −29.11 – −32.53 (-MePhSi-), −33.02 – −35.84 (-HMeSi-), −42.80 – −47.11 (-Ph$_2$Si-) ppm.

Refractive index: 1.5654.

Viscosity: 30600 ± 470 mPa·s.

H20_Sn3_PP40_PM37:

Yield: 4.05 g.

^{1}H NMR (400 MHz, CDCl$_3$): δ = 7.83 – 6.89 (m, 29.25H, Ph), 4.89 – 4.67 (m, 1.00H, H), 0.62 – −0.13 (m, 8.55H, Me) ppm.

^{13}C NMR (101 MHz, CDCl$_3$): δ = 134.98 – 125.94 (Ph), 1.01 – −0.30 (Me) ppm.

^{29}Si NMR (79 MHz, CDCl$_3$): −28.97 – −32.87 (-MePhSi-), −33.59 – −37.73 (HMeSi-), −41.43 – −46.72 (-Ph$_2$Si-) ppm.

Refractive index: 1.5674.

Viscosity: 276000 ± 1700 mPa·s.

H20_Sn5_PP40_PM35:

Yield: 4.14 g.

^{1}H NMR (400 MHz, CDCl$_3$): δ = 7.77 – 6.88 (m, 28.75H, Ph), 5.07 – 4.64 (m, 1.00H, H), 0.62 – −0.12 (m, 8.25H, Me) ppm.

^{13}C NMR (101 MHz, CDCl$_3$): δ = 134.79 – 125.45 (Ph), 1.03 – −0.31 (Me) ppm.

^{29}Si NMR (79 MHz, CDCl$_3$): −29.04 – −32.51 (-MePhSi-), −33.11 – −35.49 (-HMeSi-), −42.73 – −47.22 (-Ph$_2$Si-) ppm.

Refractive index: 1.5729.

Viscosity: 26800 ± 580 mPa·s.

H20_Sn10_PP40_PM30:

Yield: 3.11 g.

^{1}H NMR (400 MHz, CDCl$_3$): δ = 7.89 – 7.16 (m, 27.50H, Ph), 5.19 – 4.83 (m, 1.00H, H), 0.67 – −0.23 (m, 7.50H, Me) ppm.

^{13}C NMR (101 MHz, CDCl$_3$): δ = 134.49 – 125.44 (Ph), 1.32 – −0.51 (Me) ppm.

^{29}Si NMR (79 MHz, CDCl$_3$): −29.04 – −32.55 (-MePhSi-), −33.58 – −36.63 (-HMeSi-), −43.36 – −46.30 (-Ph$_2$Si-) ppm.

Refractive index: not determinable.

Viscosity: not determinable.

H20_Sn15_PP40_PM25:

Yield: 4.30 g.

^{1}H NMR (400 MHz, CDCl$_3$): δ = 7.75 – 6.80 (m, 26.25H, Ph), 5.03 – 4.61 (m, 1.00H, H), 0.51 – −0.23 (m, 6.75H, Me) ppm.

^{13}C NMR (101 MHz, CDCl$_3$): δ = 134.66 – 125.92 (Ph), −0.25 (Me) ppm.

^{29}Si NMR (79 MHz, CDCl$_3$): −28.93 – −32.81 (-MePhSi-), −33.24 – −38.93 (-HMeSi-), −42.98 – −46.81 (-Ph$_2$Si-) ppm.

Refractive index: not determinable.

Viscosity: not determinable.

6.2.6.1.4 Tantalum

H20_Ta1_PP40_PM39:

Yield: 3.74 g.

^{1}H NMR (400 MHz, CDCl$_3$): δ = 7.79 – 6.87 (m, 29.75H, Ph), 5.01 – 4.69 (m, 1.00H, H), 0.58 – −0.11 (m, 8.85H, Me) ppm.

^{13}C NMR (101 MHz, CDCl$_3$): δ = 134.97 – 125.94 (Ph), 1.07 – −1.90 (Me) ppm.

^{29}Si NMR (79 MHz, CDCl$_3$): δ = −24.83 – −32.98 (-MePhSi-), −33.45 – −39.27 (-HMeSi-), −42.62 – −46.91 (-Ph$_2$Si-) ppm.

Refractive index: 1.5718.

Viscosity: 16700 ± 190 mPa·s.

H20_Ta3_PP40_PM37:

Yield: 4.16 g.

^{1}H NMR (400 MHz, CDCl$_3$): δ = 7.77 – 6.90 (m, 29.25H, Ph), 4.99 – 4.65 (m, 1.00H, H), 0.44 – −0.12 (m, 8.55H, Me) ppm.

^{13}C NMR (101 MHz, CDCl$_3$): δ = 134.78 – 125.93 (Ph), 1.05 – −1.93 (Me) ppm.

^{29}Si NMR (79 MHz, CDCl$_3$): −24.87 – −32.79 (-MePhSi-), −33.38 – −39.31 (-HMeSi-), −42.72 – −46.98 (-Ph$_2$Si-) ppm.

Refractive index: 1.5677.

Viscosity: 2160 ± 30 mPa·s.

H20_Ta5_PP40_PM35:

Yield: 3.76 g.

^{1}H NMR (400 MHz, CDCl$_3$): δ = 7.74 – 6.88 (m, 28.75H, Ph), 5.02 – 4.66 (m, 1.00H, H), 0.57 – −0.16 (m, 8.25H, Me) ppm.

^{13}C NMR (101 MHz, CDCl$_3$): δ = 134.96 – 125.93 (Ph), 1.06 – −1.93 (Me) ppm.

^{29}Si NMR (79 MHz, CDCl$_3$): −29.02 – −32.97 (-MePhSi-), −33.48 – −39.28 (-HMeSi-), −42.70 – 46.92 (-Ph$_2$Si) ppm.

Refractive index: 1.5750.

Viscosity: 20300 ± 300 mPa·s.

H20_Ta10_PP40_PM30:

Yield: 3.95 g.

^{1}H NMR (400 MHz, CDCl$_3$): δ = 8.21 – 6.92 (m, 27.50H, Ph), 5.16 – 4.61 (m, 1.00H, H), 0.59 – −0.28 (m, 7.50H, Me) ppm.

^{13}C NMR (101 MHz, CDCl$_3$): δ = 134.98 – 125.42 (Ph), 1.03 – −1.94 (Me) ppm.

^{29}Si NMR (79 MHz, CDCl$_3$): −24.66 – −32.60 (-MePhSi-), −33.22 – −39.29 (-HMeSi-), −43.83 – −46.73 (-Ph$_2$Si-) ppm.

Refractive index: 1.5635.

Viscosity: 25200 ± 460 mPa·s

H20_Ta15_PP40_PM25:

Yield: 4.13 g.

^{1}H NMR (400 MHz, CDCl$_3$): δ = 7.72 – 6.82 (m, 26.25H, Ph), 5.07 – 4.51 (m, 1.00H, H), 0.52 – −0.16 (m, 6.75H, Me) ppm.

^{13}C NMR (101 MHz, CDCl$_3$): δ = 134.96 – 125.92 (Ph), −0.24 – −0.28 (Me) ppm.

^{29}Si NMR (79 MHz, CDCl$_3$): −29.19 – −32.56 (-MePhSi-), −33.00 – −39.11 (-HMeSi-), −42.89 – −47.15 (-Ph$_2$Si-) ppm.

Refractive index: 1.5820.

Viscosity: 10600000 ± 960000 mPa·s.

6.2.6.2 *Vinyl and metal atom containing polysiloxanes*

General synthesis for vinyl and metal atom containing polysiloxanes:

The percentages refer to the accumulated amount of silicon and metal atoms. To 40 % (2.50 g, 11.56 mmol) of diphenylsilanediol, (40-X) % (40 %: 2.10 g, 11.56 mmol) of methylphenyl-dimethoxysilane, X % of the metal monomer, 3 mL of xylene and 0.1 % (4.37 mg, 0.02 mmol) of barium hydroxide monohydrate were heated to 110 °C for 24 h with an equipped distillation head. A ^{1}H NMR measurement was performed to check if the reaction is finished. After the addition of 100 µL conc. HCl$_{(aq)}$ at room temperature the solution was stirred for 10 min, then 20 % (1.29 g, 5.78 mmol) of vinylphenyldiethoxysilane were added. The solution was heated to 80 °C for one hour and to 110 °C for two additional hours. After cooling down and adding

2 mL of distilled water and 2 mL of toluene, the polymer was extracted using a centrifuge at 8000 rpm for one minute. After washing the organic phase once with potassium bicarbonate and four times with distilled water, it was filtered with a 0.45 µm syringe filter and the residual solvent was removed under high vacuum to receive a viscous clear to opaque polymer (theoretical: 100 % with solvent residuals).

For the tin containing samples, the $Sn(Cl)_4 \cdot 5\ H_2O$ was dissolved in absolute methanol first before it was added to the siloxanes. Also, additional amounts of barium hydroxide or sodium hydroxide were added to compensate the emerging HCl and remain a slightly basic solution.

The ^{1}H NMRs are referenced to the CH_3 signal of toluene at 2.36 ppm, the ^{13}C NMRs are referenced to the $CDCl_3$ signal at 77.16 ppm. The stated integration of the groups is based on the theoretical values because of overlapping solvent and alkoxy signals.

V20_Met0_PP40_PM40:

Yield: 4.90 g.

^{1}H NMR (400 MHz, $CDCl_3$): δ = 7.82 – 6.84 (m, 35.00H, Ph), 6.24 – 5.47 (m, 3.00H, V), 0.55 – −0.19 (m, 6.00H, Me) ppm.

^{13}C NMR (101 MHz, $CDCl_3$): δ = 134.57 – 125.45 (Ph, V), −0.17 – −0.26 (Me) ppm.

^{29}Si NMR (79 MHz, $CDCl_3$): δ = −29.09 – −32.75 (-MePhSi-), −42.77 – −47.59 (-Ph_2Si-, -PhVSi-) ppm.

Refractive index: 1.5731.

Viscosity: 508000 ± 10000 mPa·s.

6.2.6.2.1 <u>Zirconium</u>

V20_Zr1_PP40_PM39:

Yield: 5.34 g.

^{1}H NMR (400 MHz, $CDCl_3$): δ = 7.81 – 6.84 (m, 34.75H, Ph), 6.25 – 5.80 (m, 3.00H, V), 0.48 – −0.25 (m, 5.85H, Me) ppm.

^{13}C NMR (101 MHz, $CDCl_3$): δ = 134.65 – 127.53 (Ph, V), −0.30 – −2.47 (Me) ppm.

^{29}Si NMR (79 MHz, $CDCl_3$): δ = −22.89 – −32.77 (-MePhSi-), −42.47 – −46.91 (-Ph_2Si-, -PhVSi-) ppm.

Refractive index: 1.5639.

Viscosity: 330 ± 10 mPa·s.

V20_Zr3_PP40_PM37:

Yield: 5.43 g.

^{1}H NMR (400 MHz, CDCl$_3$): δ = 7.82 – 6.86 (m, 34.25H, Ph), 6.37 – 6.00 (m, 3.00H, V), 0.64 – −0.13 (m, 5.55H, Me) ppm.

^{13}C NMR (101 MHz, CDCl$_3$): δ = 134.76 – 127.53 (Ph, V), −0.16 – −4.12 (Me) ppm.

^{29}Si NMR (79 MHz, CDCl$_3$): δ = −23.05 – −32.40 (-MePhSi-), −42.70 – −46.94 (-Ph$_2$Si-, -PhVSi-) ppm.

Refractive index: 1.5580.

Viscosity: 320 ± 10 mPa·s.

V20_Zr5_PP40_PM35:

Yield: 6.13 g.

^{1}H NMR (400 MHz, CDCl$_3$): δ = 7.63 – 6.72 (m, 33.75H, Ph), 6.14 – 5.84 (m, 3.00H, V), 0.38 – −0.29 (m, 5.25H, Me) ppm.

^{13}C NMR (101 MHz, CDCl$_3$): δ = 135.00 – 127.54 (Ph, V), −0.17 – −4.14 (Me) ppm.

^{29}Si NMR (79 MHz, CDCl$_3$): δ = −24.76 – −32.65 (-MePhSi-), −42.64 – −46.86 (-Ph$_2$Si-, -PhVSi-) ppm.

Refractive index: 1.5526.

Viscosity: 500 ± 370 mPa·s.

V20_Zr10_PP40_PM30:

Yield: 6.35 g.

^{1}H NMR (400 MHz, CDCl$_3$): δ = 7.65 – 6.85 (m, 32.50H, Ph), 6.15 – 5.85 (m, 3.00H, V), 0.34 – −0.24 (m, 4.50H, Me) ppm.

^{13}C NMR (101 MHz, CDCl$_3$): δ = 134.98 – 127.51 (Ph, V), −0.30 – −4.16 (Me) ppm.

^{29}Si NMR (79 MHz, CDCl$_3$): δ = −25.20 – −32.47 (-MePhSi-), −42.57 – −46.82 (-Ph$_2$Si-, -PhVSi-) ppm.

Refractive index: 1.5510.

Viscosity: 830 ± 30 mPa·s.

V20_Zr15_PP40_PM25:

Yield: 6.63 g.

^{1}H NMR (400 MHz, CDCl$_3$): δ = 7.66 – 6.72 (m, 31.25H, Ph), 6.16 – 5.87 (m, 3.00H, V), 0.37 – −0.24 (m, 3.75H, Me) ppm.

^{13}C NMR (101 MHz, CDCl$_3$): δ = 134.96 – 127.50 (Ph, V), −0.22 – −4.18 (Me) ppm.

^{29}Si NMR (79 MHz, CDCl$_3$): δ = −24.92 – −32.78 (-MePhSi-), −42.45 – −46.69 (-Ph$_2$Si-, -PhVSi-) ppm.

Refractive index: 1.5474.

Viscosity: 260 ± 10 mPa·s.

6.2.6.2.2 <u>Hafnium</u>

V20_Hf1_PP40_PM39:

Yield: 5.26 g.

^{1}H NMR (400 MHz, CDCl$_3$): δ = 7.74 – 6.88 (m, 34.75H, Ph), 6.25 – 5.95 (m, 3.00H, V), 0.39 – −0.13 (m, 5.85H, Me) ppm.

^{13}C NMR (101 MHz, CDCl$_3$): δ = 134.69 – 127.53 (Ph, V), −0.16 – −2.50 (Me) ppm.

^{29}Si NMR (79 MHz, CDCl$_3$): δ = −25.46 – −32.97 (-MePhSi-), −42.64 – −46.86 (-Ph$_2$Si-, -PhVSi-) ppm.

Refractive index: 1.5592.

Viscosity: 1430 ± 10 mPa·s.

V20_Hf3_PP40_PM37:

Yield: 5.63 g.

^{1}H NMR (400 MHz, CDCl$_3$): δ = 7.64 – 6.87 (m, 34.25H, Ph), 6.19 – 5.85 (m, 3.00H, V), 0.36 – −0.19 (m, 5.55H, Me) ppm.

^{13}C NMR (101 MHz, CDCl$_3$): δ = 134.72 – 127.54 (Ph, V), −0.17 – −4.14 (Me) ppm.

^{29}Si NMR (79 MHz, CDCl$_3$): δ = −24.95 – −32.95 (-MePhSi-), −42.62 – −46.81 (-Ph$_2$Si-, -PhVSi-) ppm.

Refractive index: 1.5561.

Viscosity: 300 ± 20 mPa·s.

V20_Hf5_PP40_PM35:

Yield: 6.15 g.

^{1}H NMR (400 MHz, CDCl$_3$): δ = 7.78 – 6.78 (m, 33.75H, Ph), 6.17 – 5.81 (m, 3.00H, V), 0.40 – −0.14 (m, 5.25H, Me) ppm.

^{13}C NMR (101 MHz, CDCl$_3$): δ = 134.69 – 127.52 (Ph, V), −0.34 – −4.17 (Me) ppm.

^{29}Si NMR (79 MHz, CDCl$_3$): δ = −24.82 – −32.75 (-MePhSi-), −42.35 – −46.57 (-Ph$_2$Si-, -PhVSi-) ppm.

Refractive index: 1.5518.

Viscosity: 290 ± 10 mPa·s.

V20_Hf10_PP40_PM30:

Yield: 7.24 g.

^{1}H NMR (400 MHz, CDCl$_3$): δ = 7.71 – 6.68 (m, 32.50H, Ph), 6.15 – 5.86 (m, 3.00H, V), 0.36 – −0.30 (m, 4.50H, Me) ppm.

^{13}C NMR (101 MHz, CDCl$_3$): δ = 135.00 – 127.51 (Ph, V), −0.19 – −4.16 (Me) ppm.

^{29}Si NMR (79 MHz, CDCl$_3$): δ = −29.03 – −32.80 (-MePhSi-), −42.68 – −46.92 (-Ph$_2$Si-, -PhVSi-) ppm.

Refractive index: 1.5460.

Viscosity: 140 ± 10 mPa·s.

V20_Hf15_PP40_PM25:

Yield: 7.37 g.

^{1}H NMR (400 MHz, CDCl$_3$): δ = 7.87 – 6.83 (m, 31.25H, Ph), 6.24 – 5.93 (m, 3.00H, V), 0.47 – −0.24 (m, 3.75H, Me) ppm.

^{13}C NMR (101 MHz, CDCl$_3$): δ = 135.03 – 127.60 (Ph, V), −0.26 – −4.14 (Me) ppm.

^{29}Si NMR (79 MHz, CDCl$_3$): δ = −25.16 – −33.18 (-MePhSi-), −42.93 – −46.86 (-Ph$_2$Si-, -PhVSi-) ppm.

Refractive index: 1.5364.

Viscosity: 61600 ± 3800 mPa·s.

6.2.6.2.3 Tin

V20_Sn1_PP40_PM39:

Yield: 5.99 g.

^{1}H NMR (400 MHz, CDCl$_3$): δ = 7.88 – 6.92 (m, 34.75H, Ph), 6.39 – 5.72 (m, 3.00H, V), 0.62 – 0.02 (m, 5.85H, Me) ppm.

^{13}C NMR (101 MHz, CDCl$_3$): δ = 134.63 – 125.45 (Ph, V), −0.13 – −0.32 (Me) ppm.

^{29}Si NMR (79 MHz, CDCl$_3$): δ = −29.13 – −33.65 (-MePhSi-), −42.82 – −47.06 (-Ph$_2$Si-, -PhVSi-) ppm.

Refractive index: 1.5728.

Viscosity: 5260 ± 170 mPa·s.

V20_Sn3_PP40_PM37:

Yield: 3.24 g.

^{1}H NMR (400 MHz, CDCl$_3$): δ = 7.81 – 7.02 (m, 34.25H, Ph), 6.15 – 5.61 (m, 3.00H, V), 0.55 – 0.00 (m, 5.55H, Me) ppm.

^{13}C NMR (101 MHz, CDCl$_3$): δ = 134.63 – 125.45 (Ph, V), −0.12 – −0.38 (Me) ppm.

^{29}Si NMR (79 MHz, CDCl$_3$): δ = −29.10 – −33.62 (-MePhSi-), −42.79 – −47.04 (-Ph$_2$Si-, -PhVSi-) ppm.

Refractive index: 1.5805.

Viscosity: 1170000 ± 38000 mPa·s.

V20_Sn5_PP40_PM35:

Yield: 4.42 g.

^{1}H NMR (400 MHz, CDCl$_3$): δ = 7.61 – 6.74 (m, 33.75H, Ph), 6.15 – 5.84 (m, 3.00H, V), 0.31 – −0.20 (m, 5.25H, Me) ppm.

^{13}C NMR (101 MHz, CDCl$_3$): δ = 134.69 – 127.51 (Ph, V), −0.16 – −2.47 (Me) ppm.

^{29}Si NMR (79 MHz, CDCl$_3$): δ = −29.03 – −33.54 (-MePhSi), −42.70 – −46.95 (-Ph$_2$Si-, -PhVSi-) ppm.

Refractive index: 1.5588.

Viscosity: 330 ± 10 mPa·s.

V20_Sn10_PP40_PM30:

Yield: 4.84 g.

^{1}H NMR (400 MHz, CDCl$_3$): δ = 7.87 – 6.87 (m, 32.50H, Ph), 6.41 – 5.81 (m, 3.00H, V), 0.63 – −0.10 (m, 4.50H, Me) ppm.

^{13}C NMR (101 MHz, CDCl$_3$): δ = 136.02 – 125.93 (Ph, V), 0.00 – −0.27 (Me) ppm.

^{29}Si NMR (79 MHz, CDCl$_3$): δ = −32.33 – −33.42 (-MePhSi-), −42.61 – −46.52 (-Ph$_2$Si-, -PhVSi-) ppm.

Refractive index: 1.5757.

Viscosity: 541000 ± 120000 mPa·s.

V20_Sn15_PP40_PM25:

Yield: 6.34 g.

^{1}H NMR (400 MHz, CDCl$_3$): δ = 7.78 – 6.88 (m, 31.25H, Ph), 6.45 – 5.76 (m, 3.00H, V), 0.49 – −0.10 (m, 3.75H, Me) ppm.

^{13}C NMR (101 MHz, CDCl$_3$): δ = 136.52 – 125.90 (Ph, V), −0.17 – −0.31 (Me) ppm.

^{29}Si NMR (79 MHz, CDCl$_3$): δ = −32.20 – −33.55 (-MePhSi-), −42.70 – −46.96 (-Ph$_2$Si-, -PhVSi-) ppm.

Refractive index: 1.5641.

Viscosity: 80 ± 20 mPa·s.

6.2.6.2.4 **Tantalum**

V20_Ta1_PP40_PM39:

Yield: 4.53 g.

^{1}H NMR (400 MHz, CDCl$_3$): δ = 7.66 – 6.78 (m, 34.75H, Ph), 6.15 – 5.85 (m, 3.00H, V), 0.42 – −0.25 (m, 5.85H, Me) ppm.

^{13}C NMR (101 MHz, CDCl$_3$): δ = 134.70 – 127.64 (Ph, V), 0.04 – −2.49 (Me) ppm.

^{29}Si NMR (79 MHz, CDCl$_3$): δ = −30.24 − −33.45 (-MePhSi-), −42.63 − −46.83 (-Ph$_2$Si-, -PhVSi-) ppm.

Refractive index: 1.5620.

Viscosity: 4490 ± 2020 mPa·s.

V20_Ta3_PP40_PM37:

Yield: 3.94 g.

^{1}H NMR (400 MHz, CDCl$_3$): δ = 7.66 – 6.74 (m, 34.25H, Ph), 6.15 – 5.82 (m, 3.00H, V), 0.42 – −0.17 (m, 5.55H, Me) ppm.

^{13}C NMR (101 MHz, CDCl$_3$): δ = 134.73 – 127.55 (Ph, V), 0.04 – −2.44 (Me) ppm.

^{29}Si NMR (79 MHz, CDCl$_3$): δ = −30.26 − −30.45 (-MePhSi-), −42.65 − −46.86 (-Ph$_2$Si-, -PhVSi-) ppm.

Refractive index: 1.5620.

Viscosity: 340 ± 10 mPa·s.

V20_Ta5_PP40_PM35:

Yield: 4.22 g.

^{1}H NMR (400 MHz, CDCl$_3$): δ = 7.60 – 6.78 (m, 33.75H, Ph), 6.15 – 5.80 (m, 3.00H, V), 0.30 – −0.26 (m, 5.25H, Me) ppm.

^{13}C NMR (101 MHz, CDCl$_3$): δ = 134.70 – 127.52 (Ph, V), −0.04 – −2.50 (Me) ppm.

^{29}Si NMR (79 MHz, CDCl$_3$): δ = −31.30 − −33.62 (-MePhSi), −42.75 − −46.98 (-Ph$_2$Si-, -PhVSi-) ppm.

Refractive index: 1.5675.

Viscosity: 890 ± 20 mPa·s.

V20_Ta10_PP40_PM30:

Yield: 5.16 g.

^{1}H NMR (400 MHz, CDCl$_3$): δ = 8.17 – 6.75 (m, 32.50H, Ph), 6.37 – 5.61 (m, 3.00H, V), 0.78 – −0.12 (m, 4.50H, Me) ppm.

^{13}C NMR (101 MHz, CDCl$_3$): δ = 134.76 – 125.41 (Ph, V), −0.06 – −1.90 (Me) ppm.

^{29}Si NMR (79 MHz, CDCl$_3$): δ = −31.95 − −33.45 (-MePhSi-), −39.73 − −46.47 (-Ph$_2$Si-, -PhVSi-) ppm.

Refractive index: 1.5773.

Viscosity: 159000 ± 3000 mPa·s.

V20_Ta15_PP40_PM25:

Yield: 4.66 g.

^{1}H NMR (400 MHz, CDCl$_3$): δ = 7.65 – 6.89 (m, 31.25H, Ph), 6.15 – 5.85 (m, 3.00H, V), 0.41 – −0.24 (m, 3.75H, Me) ppm.

^{13}C NMR (101 MHz, CDCl$_3$): δ = 134.69 – 127.61 (Ph, V), 0.03 – −0.36 (Me) ppm.

^{29}Si NMR (79 MHz, CDCl$_3$): δ = −30.84 – −33.49 (-MePhSi-), −42.65 – −46.97 (-Ph$_2$Si-, -PhVSi-) ppm.

Refractive index: 1.5680.

Viscosity: 2310 ± 80 mPa·s.

6.2.6.3 *Additional experimental data for the hydride- or vinyl-group and metal atom containing copolymers*

6.2.6.3.1 FT-IR spectra of the hydride- or vinyl-group and metal atom containing copolymers
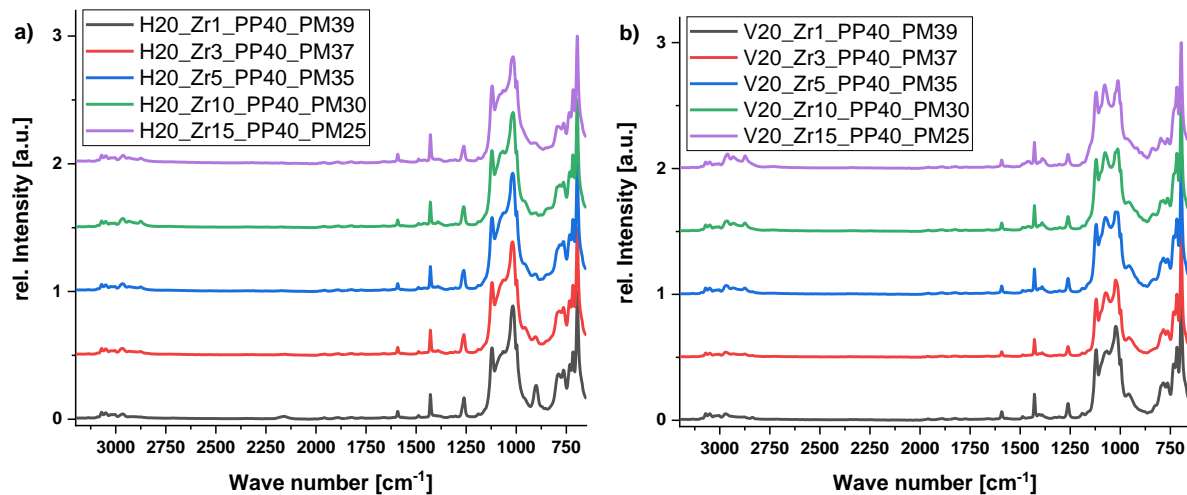
Figure 265: FT-IR spectra of the a) hydride- and b) vinyl-group and zirconium atom containing copolymers.
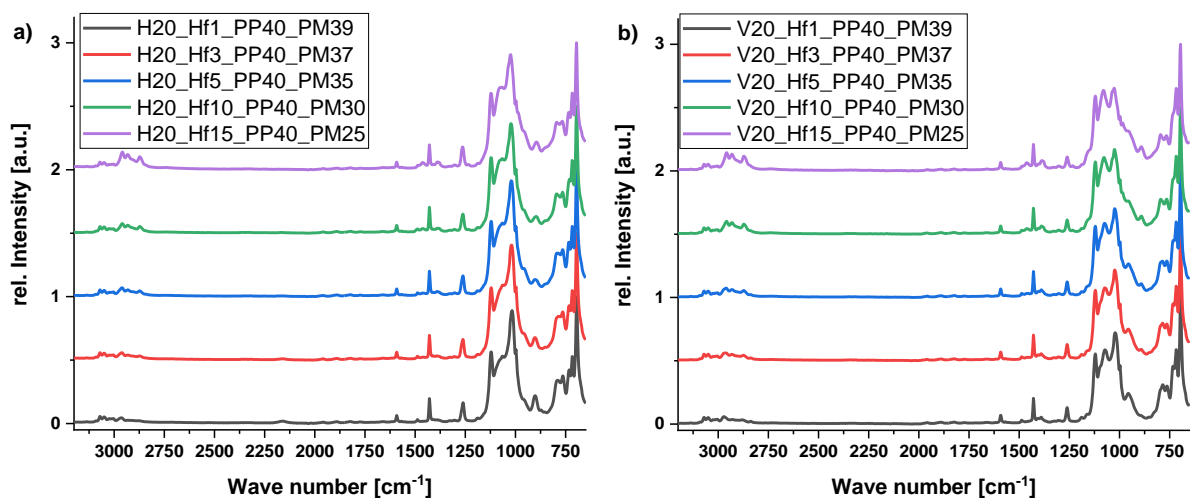
Figure 266: FT-IR spectra of the a) hydride- and b) vinyl-group and hafnium atom containing copolymers.
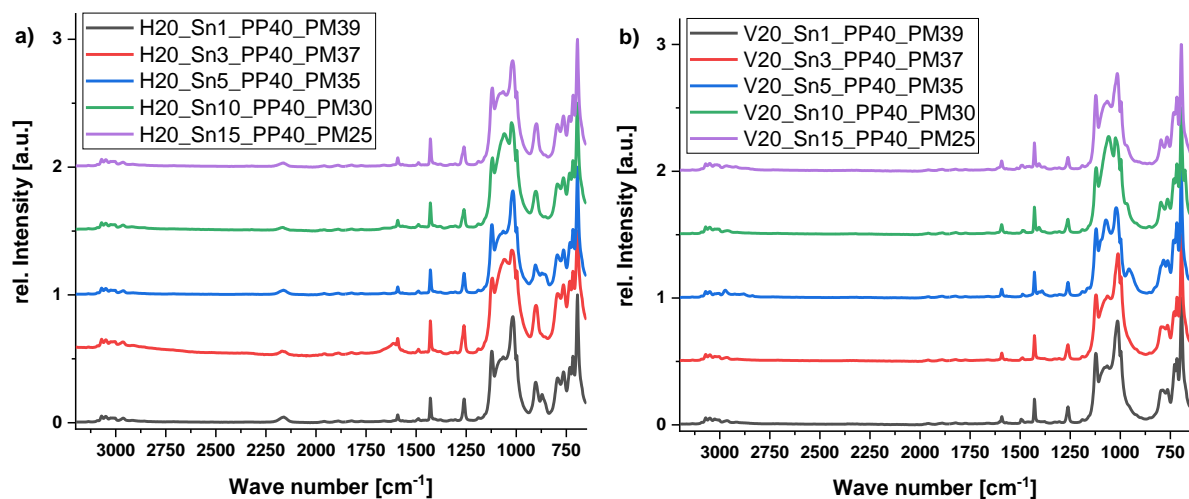
Figure 267: FT-IR spectra of the a) hydride- and b) vinyl-group and tin atom containing copolymers.
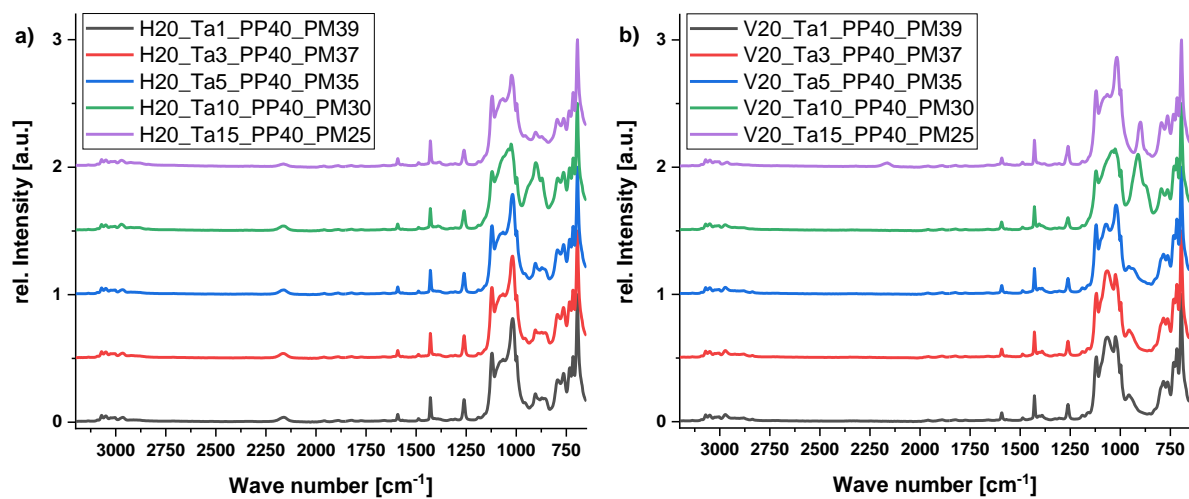
Figure 268: FT-IR spectra of the a) hydride- and b) vinyl-group and tantalum atom containing copoly-mers.

6.2.6.3.2 NMR spectra of the hydride- or vinyl-group and metal atom containing copolymers

6.2.6.3.2.1 Metal free copolymers
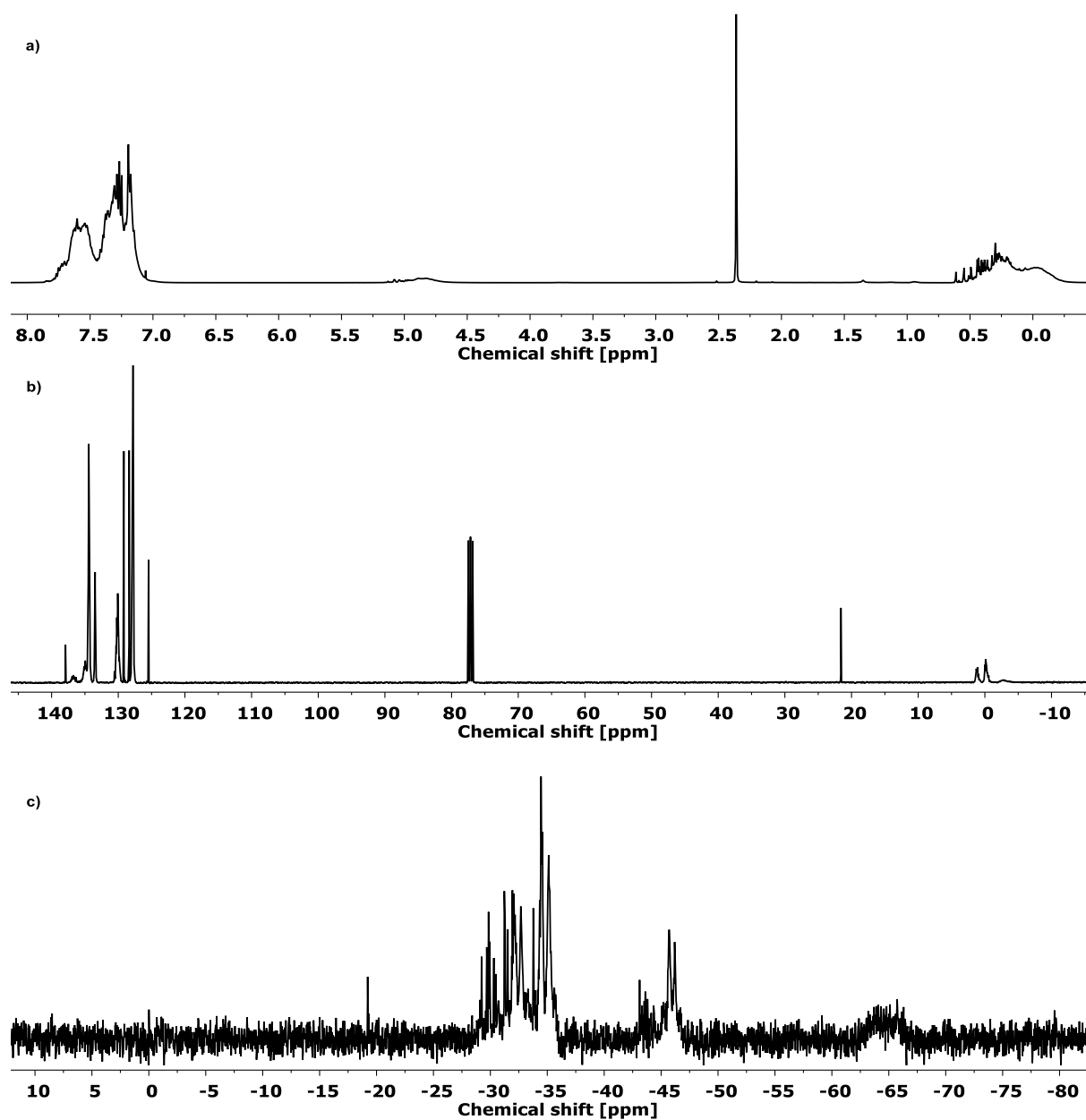
Figure 269: a) ^{1}H (400 MHz, CDCl$_3$), b) ^{13}C (101 MHz, CDCl$_3$) and c) ^{29}Si NMR (79 MHz, CDCl$_3$) of **H20_Met0_PP40_PM40.**
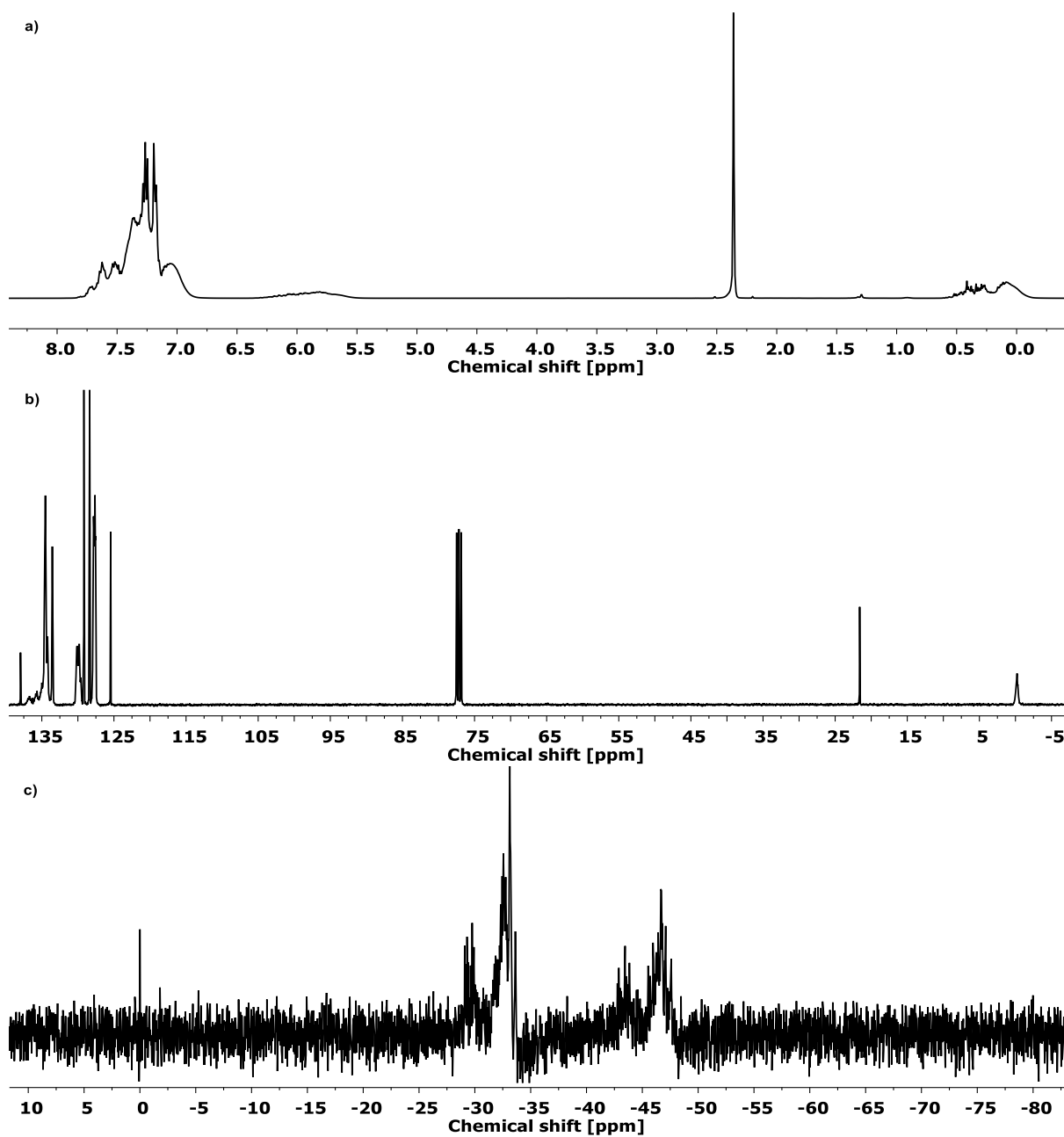
Figure 270: a) ^{1}H (400 MHz, CDCl$_3$), b) ^{13}C (101 MHz, CDCl$_3$) and c) ^{29}Si NMR (79 MHz, CDCl$_3$) of V20_Met0_PP40_PM40.

6.2.6.3.2.2 Zirconium containing copolymers
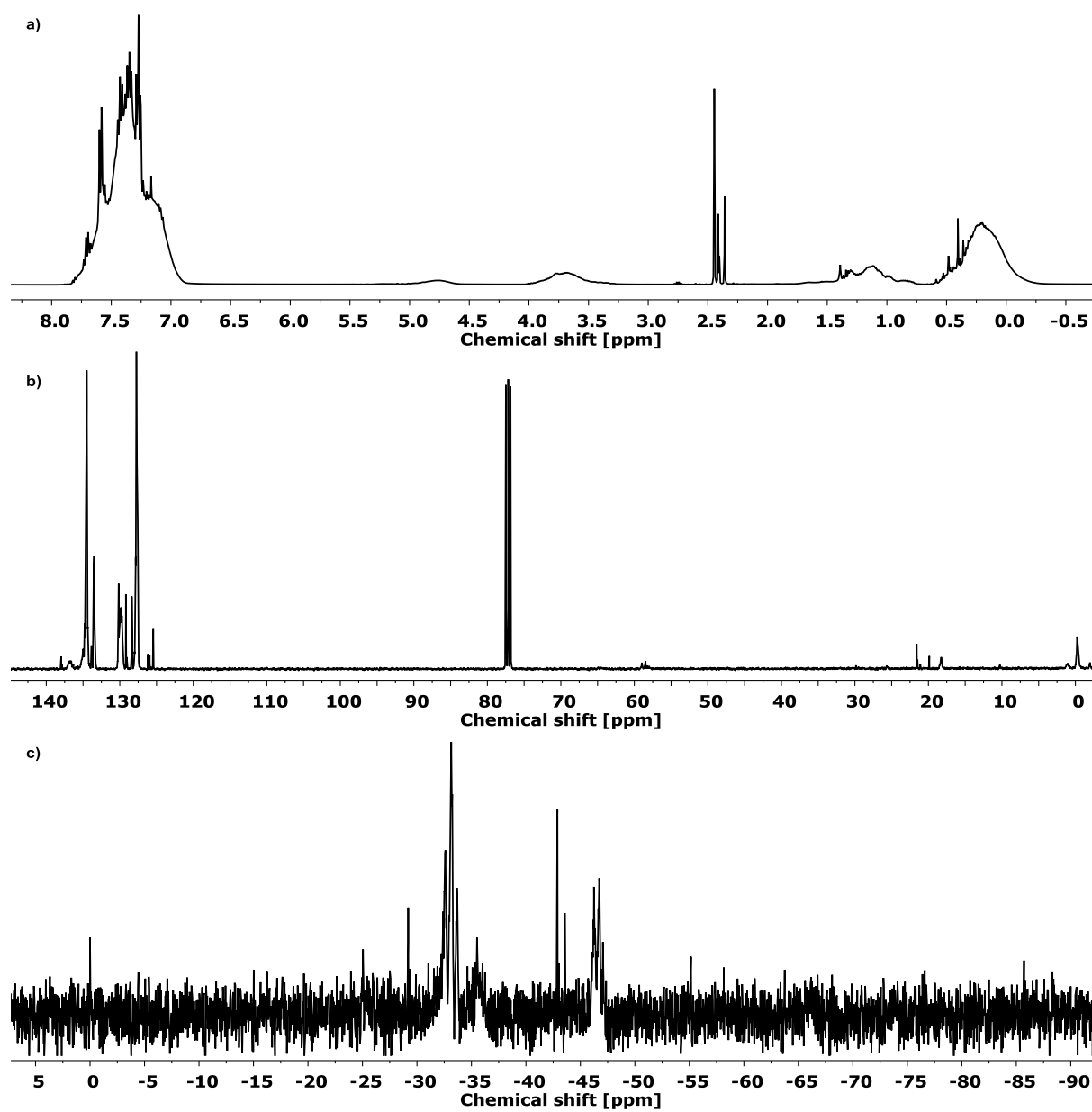
Figure 271: a) ^{1}H (400 MHz, CDCl$_3$), b) ^{13}C (101 MHz, CDCl$_3$) and c) ^{29}Si NMR (79 MHz, CDCl$_3$) of H20_Zr1_PP40_PM39.
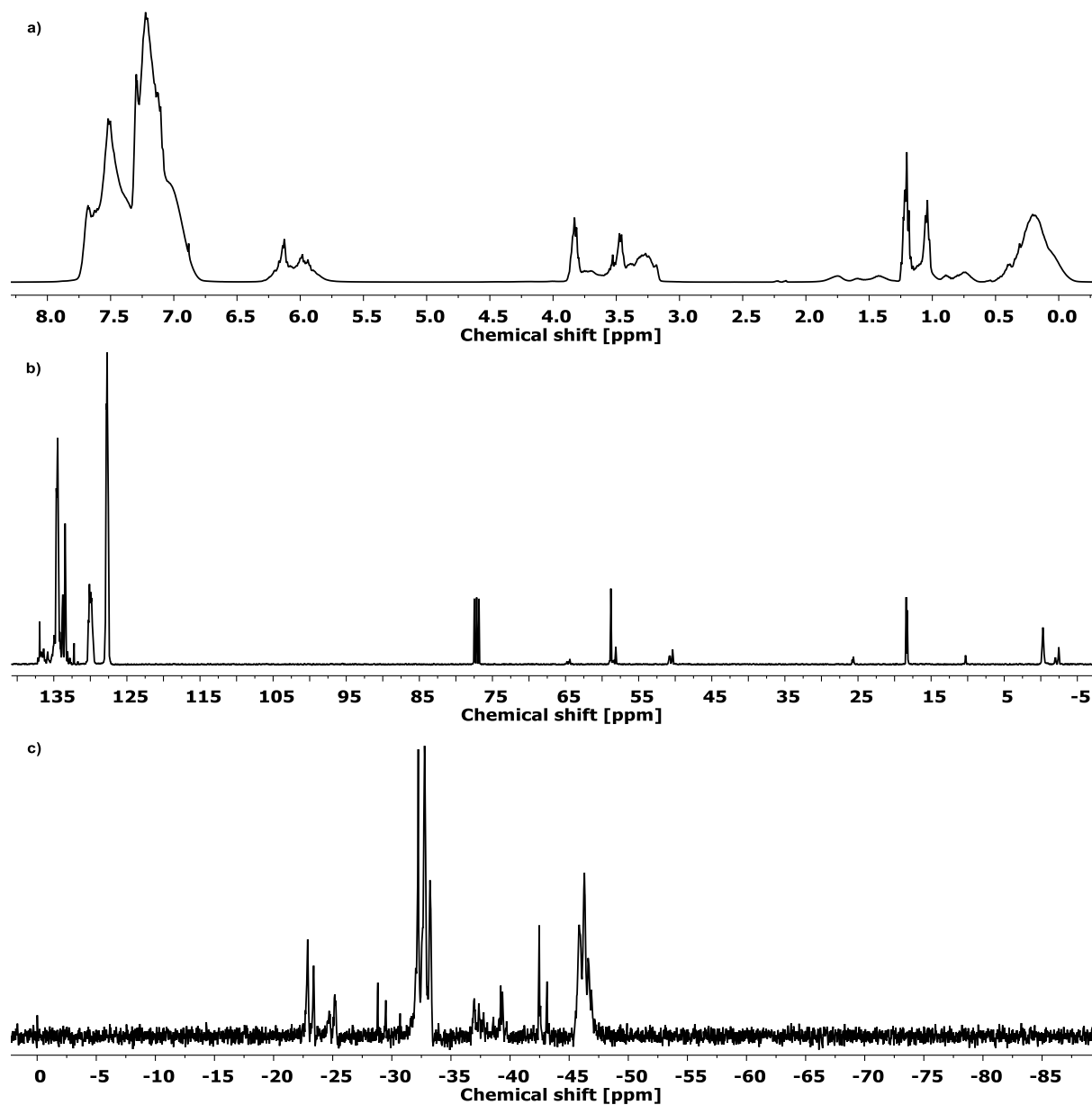
Figure 272: a) ^{1}H (400 MHz, CDCl$_3$), b) ^{13}C (101 MHz, CDCl$_3$) and c) ^{29}Si NMR (79 MHz, CDCl$_3$) of V20_Zr1_PP40_PM39.
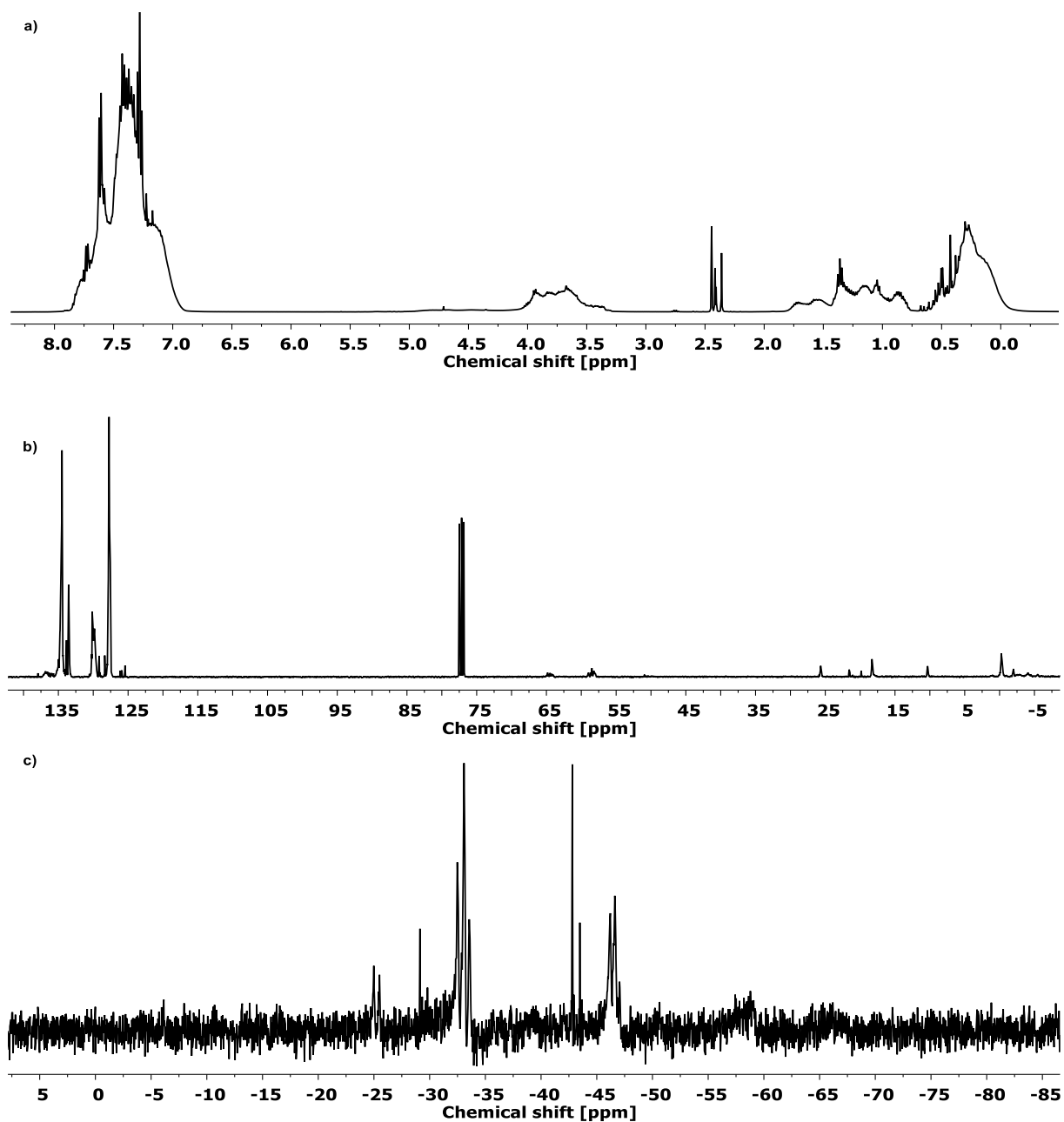
Figure 273: a) ^{1}H (400 MHz, CDCl$_3$), b) ^{13}C (101 MHz, CDCl$_3$) and c) ^{29}Si NMR (79 MHz, CDCl$_3$) of H20_Zr3_PP40_PM37.
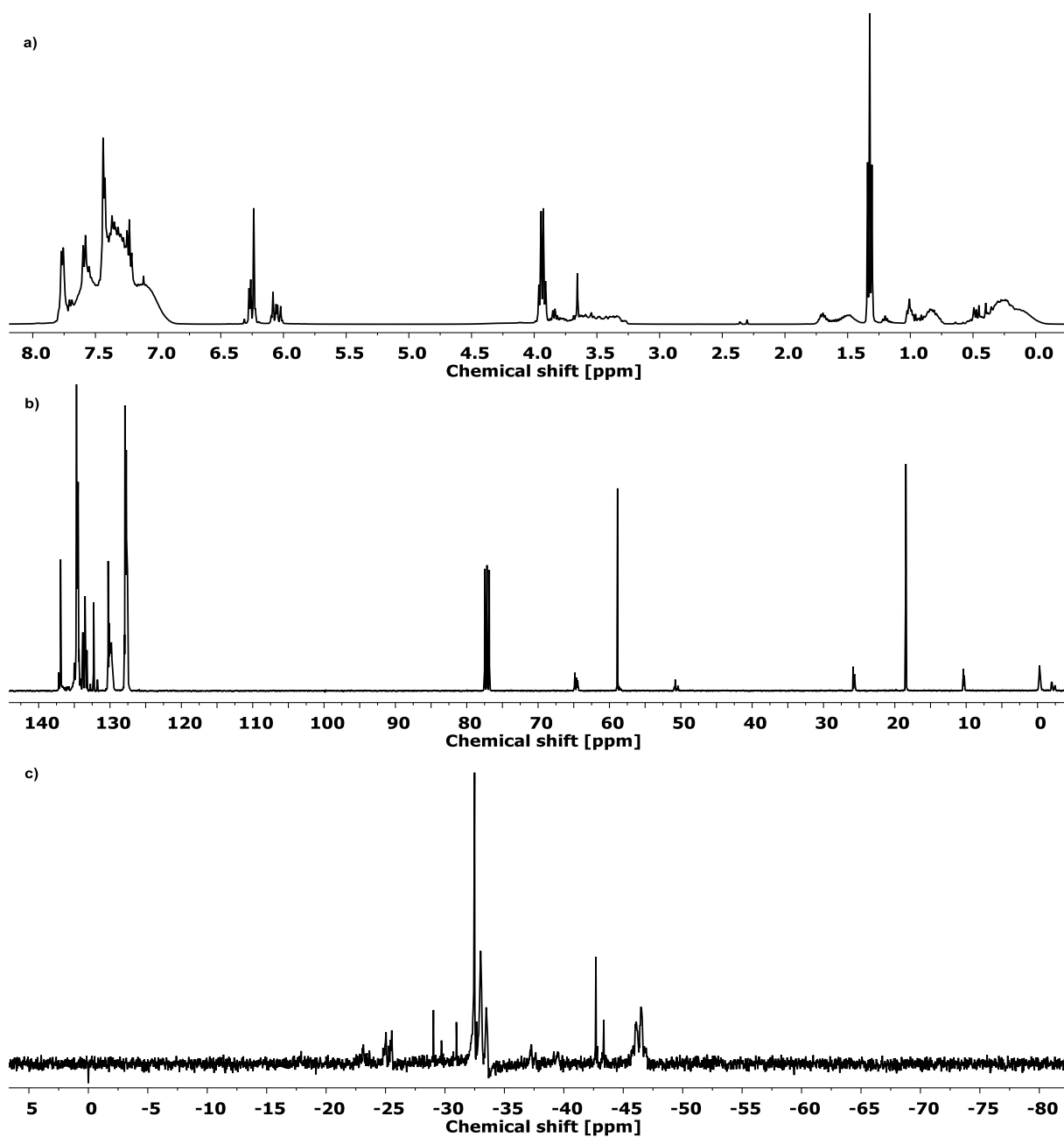
Figure 274: a) ^{1}H (400 MHz, CDCl$_3$), b) ^{13}C (101 MHz, CDCl$_3$) and c) ^{29}Si NMR (79 MHz, CDCl$_3$) of V20_Zr3_PP40_PM37.

a)

b)

c)
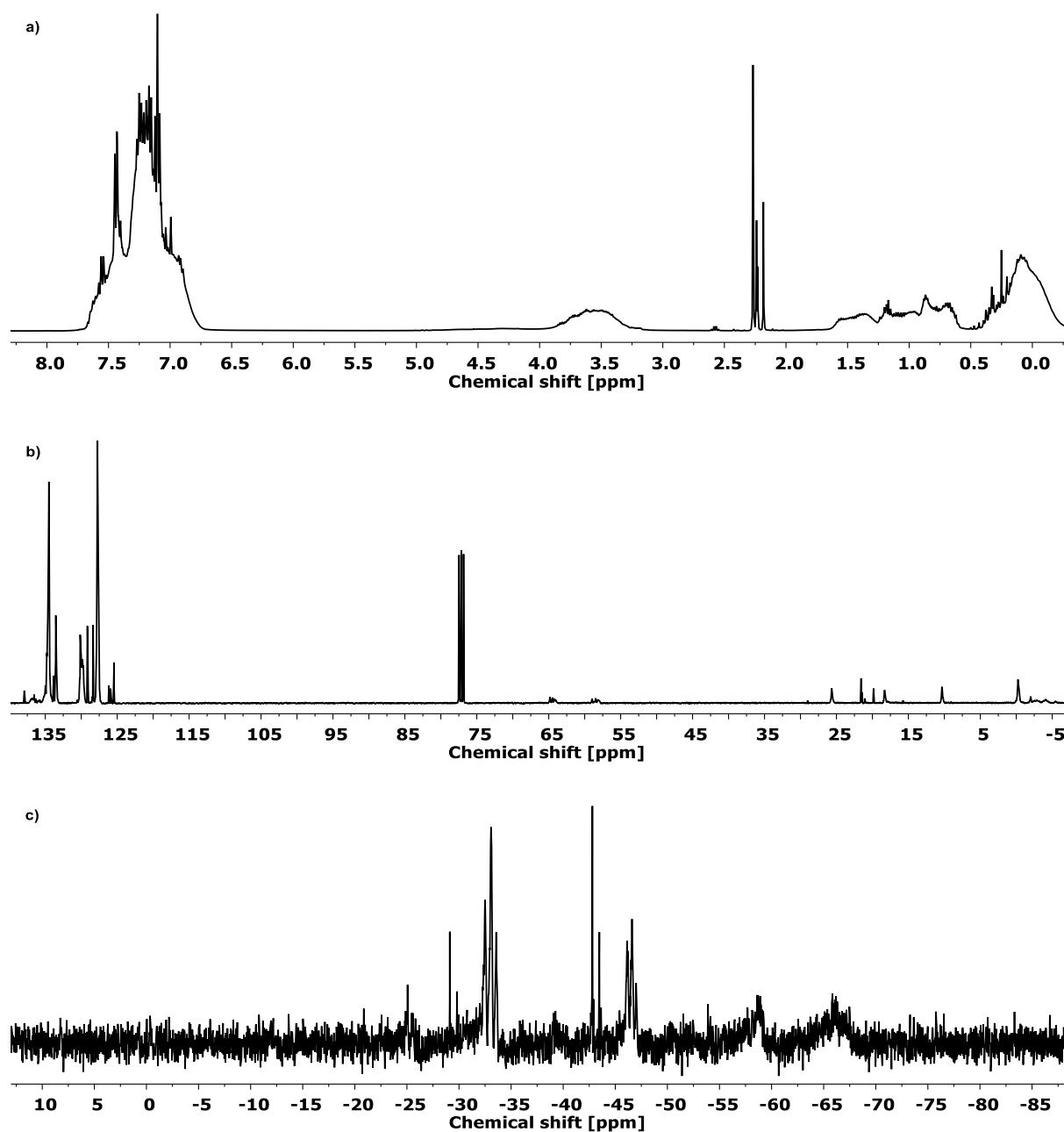
Figure 275: a) ^{1}H (400 MHz, CDCl$_3$), b) ^{13}C (101 MHz, CDCl$_3$) and c) ^{29}Si NMR (79 MHz, CDCl$_3$) of H20_Zr5_PP40_PM35.

a)

b)

c)
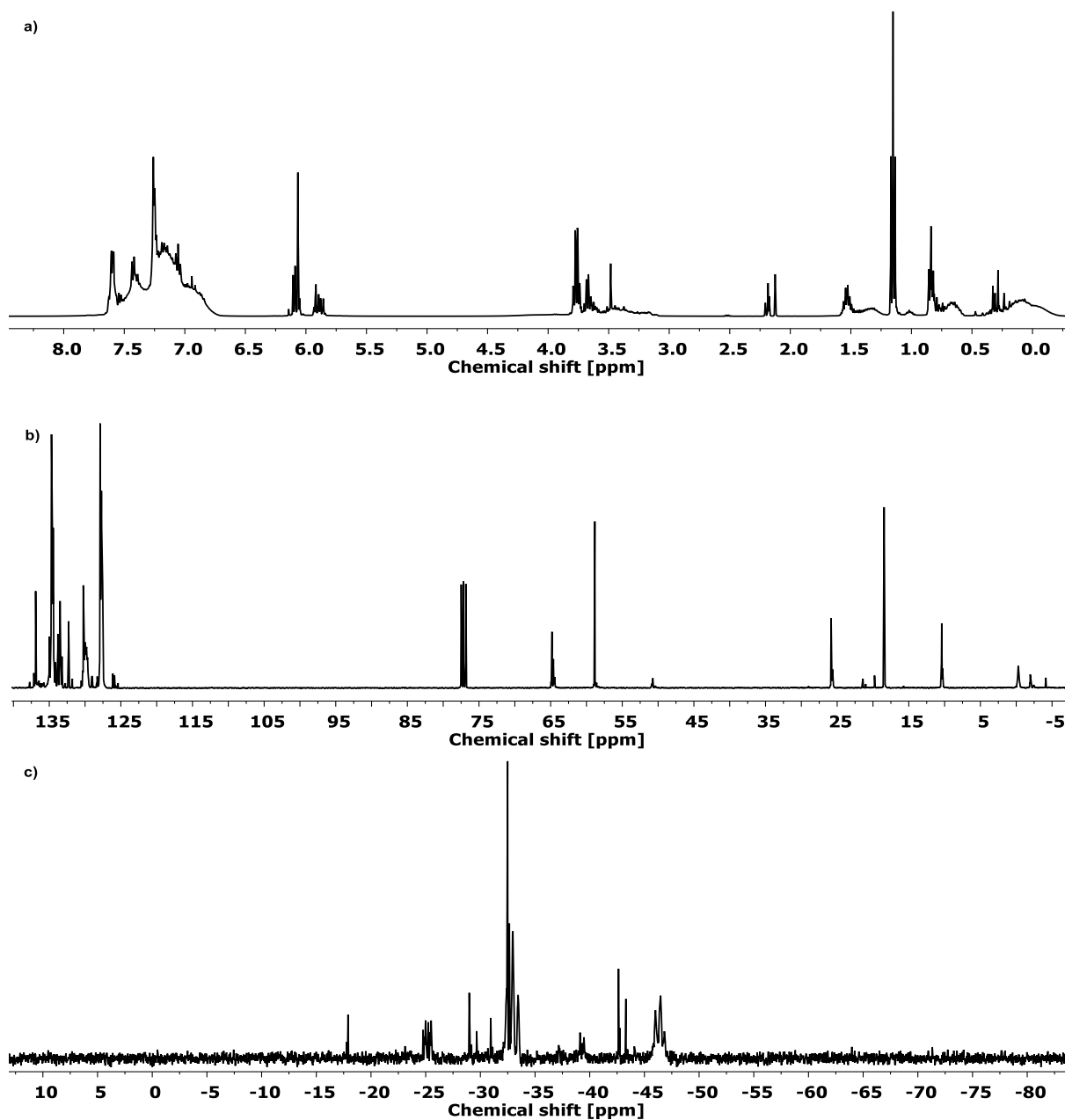
Figure 276: a) ^{1}H (400 MHz, CDCl$_3$), b) ^{13}C (101 MHz, CDCl$_3$) and c) ^{29}Si NMR (79 MHz, CDCl$_3$) of V20_Zr5_PP40_PM35.
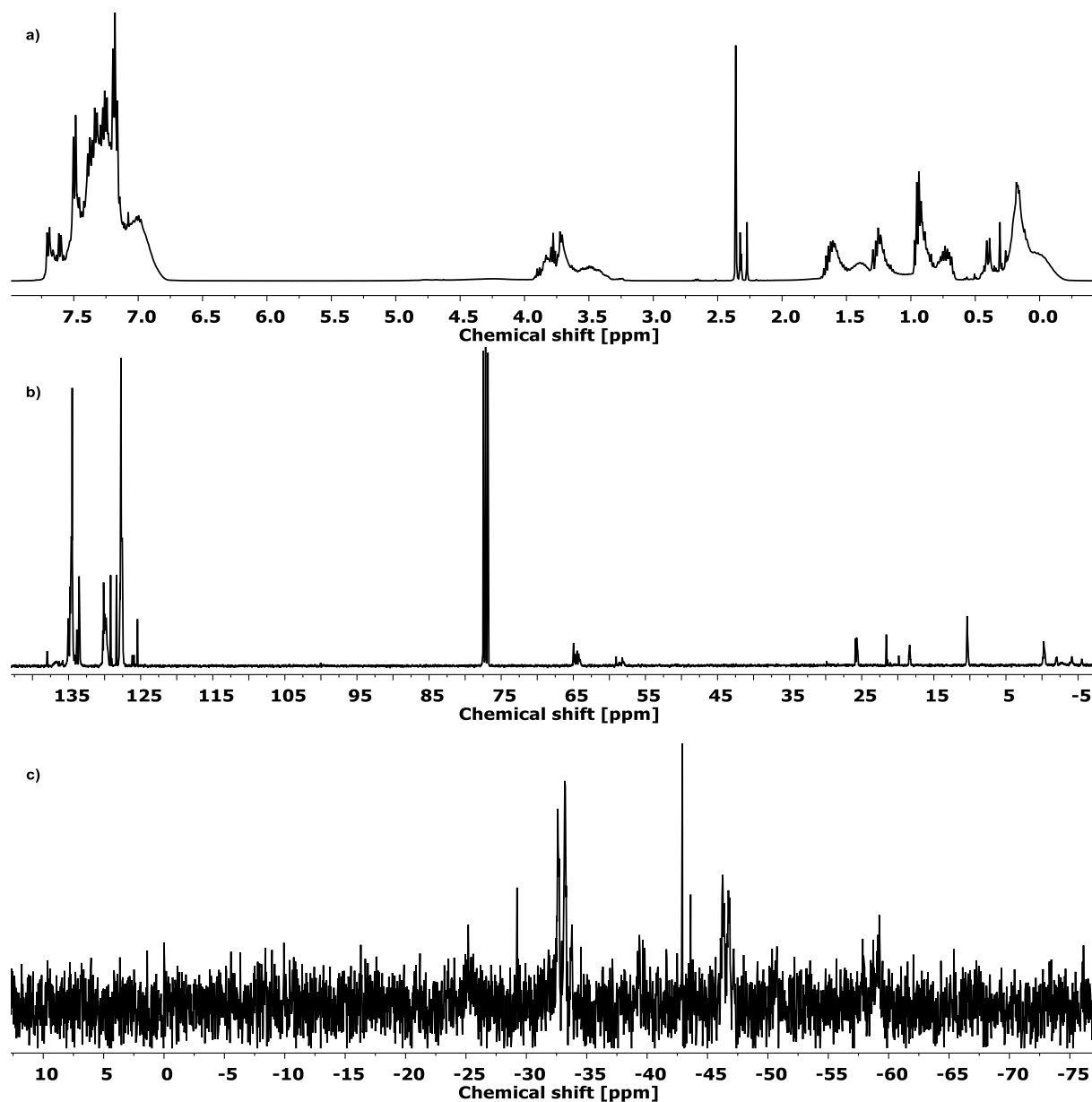
Figure 277: a) ^{1}H (400 MHz, CDCl$_3$), b) ^{13}C (101 MHz, CDCl$_3$) and c) ^{29}Si NMR (79 MHz, CDCl$_3$) of H20_Zr10_PP40_PM30.
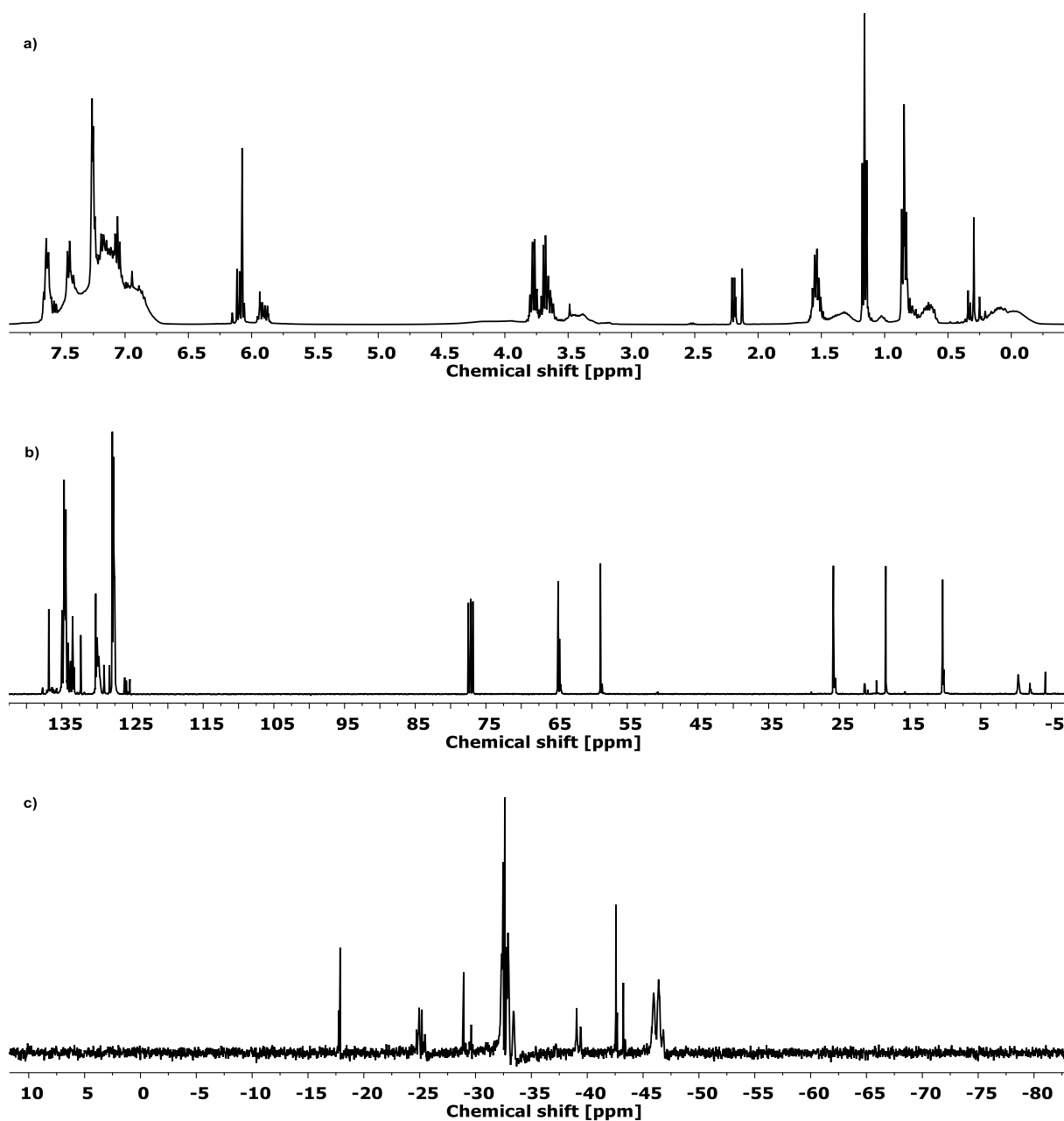
Figure 278: a) ^{1}H (400 MHz, CDCl$_3$), b) ^{13}C (101 MHz, CDCl$_3$) and c) ^{29}Si NMR (79 MHz, CDCl$_3$) of V20_Zr10_PP40_PM30.

a)

b)

c)
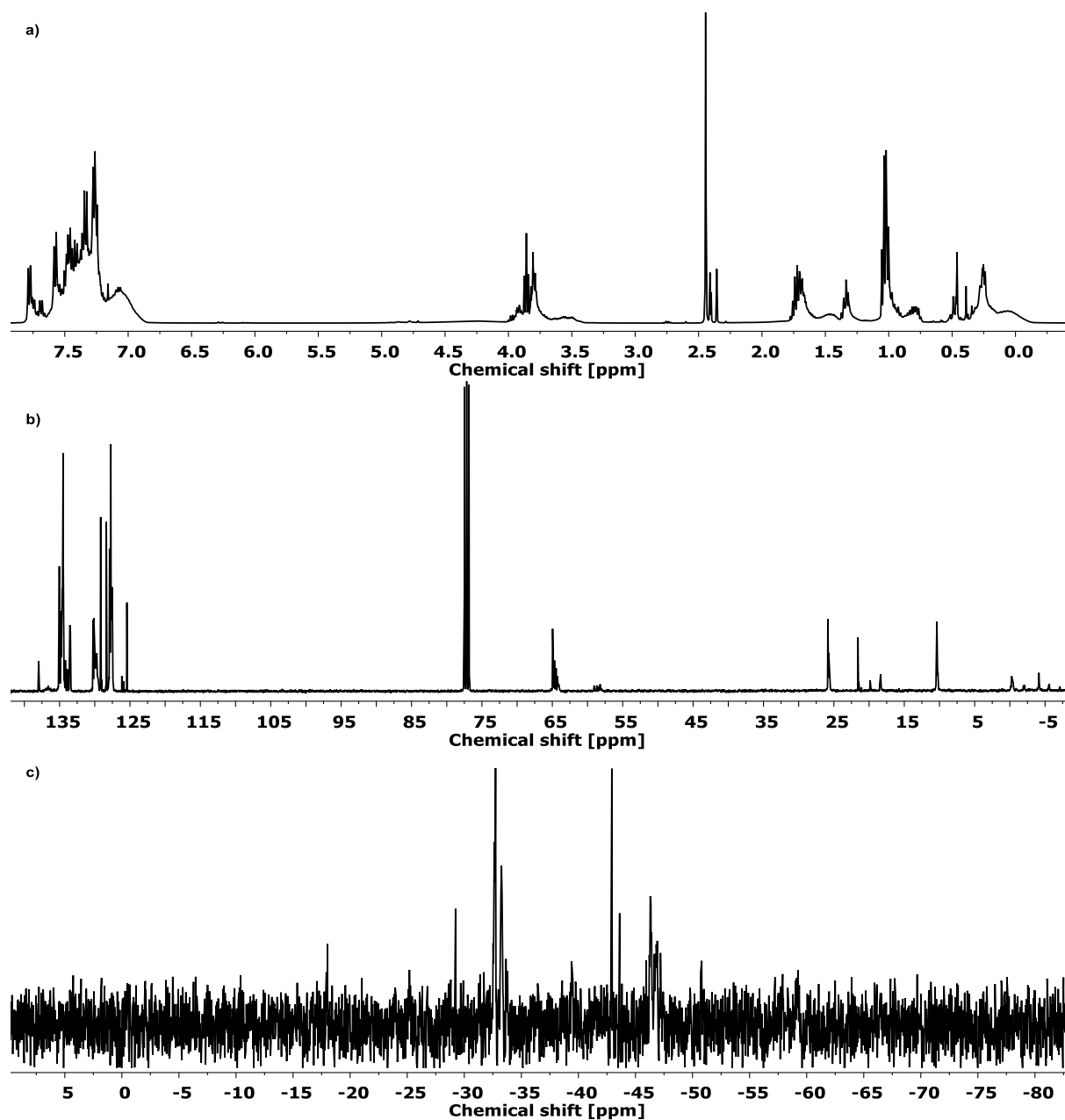
Figure 279: a) ^{1}H (400 MHz, CDCl$_3$), b) ^{13}C (101 MHz, CDCl$_3$) and c) ^{29}Si NMR (79 MHz, CDCl$_3$) of **H20_Zr15_PP40_PM25.**
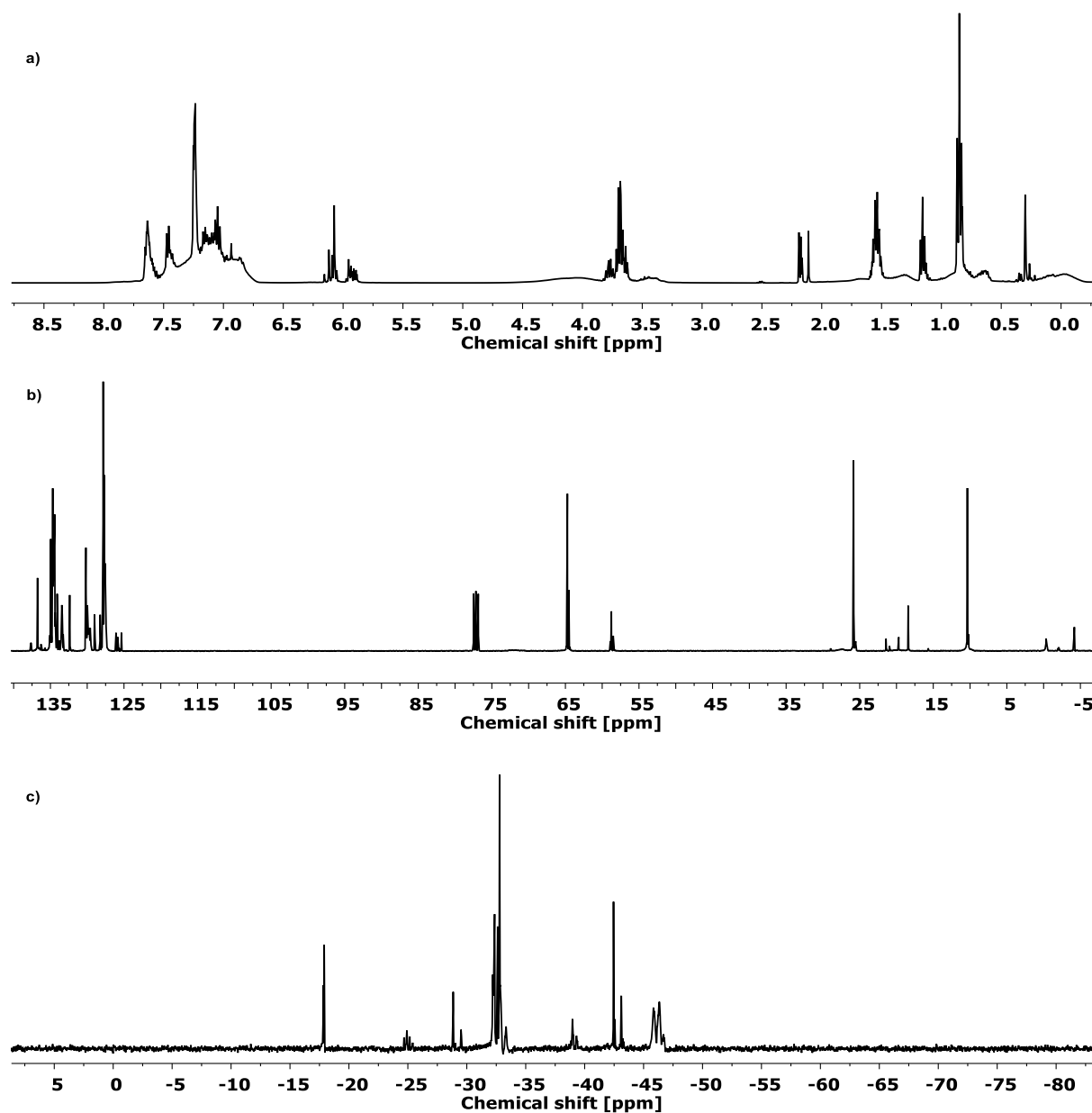
Figure 280: a) ¹H (400 MHz, CDCl₃), b) ¹³C (101 MHz, CDCl₃) and c) ²⁹Si NMR (79 MHz, CDCl₃) of V20_Zr15_PP40_PM25.

6.2.6.3.2.3 Hafnium containing copolymers
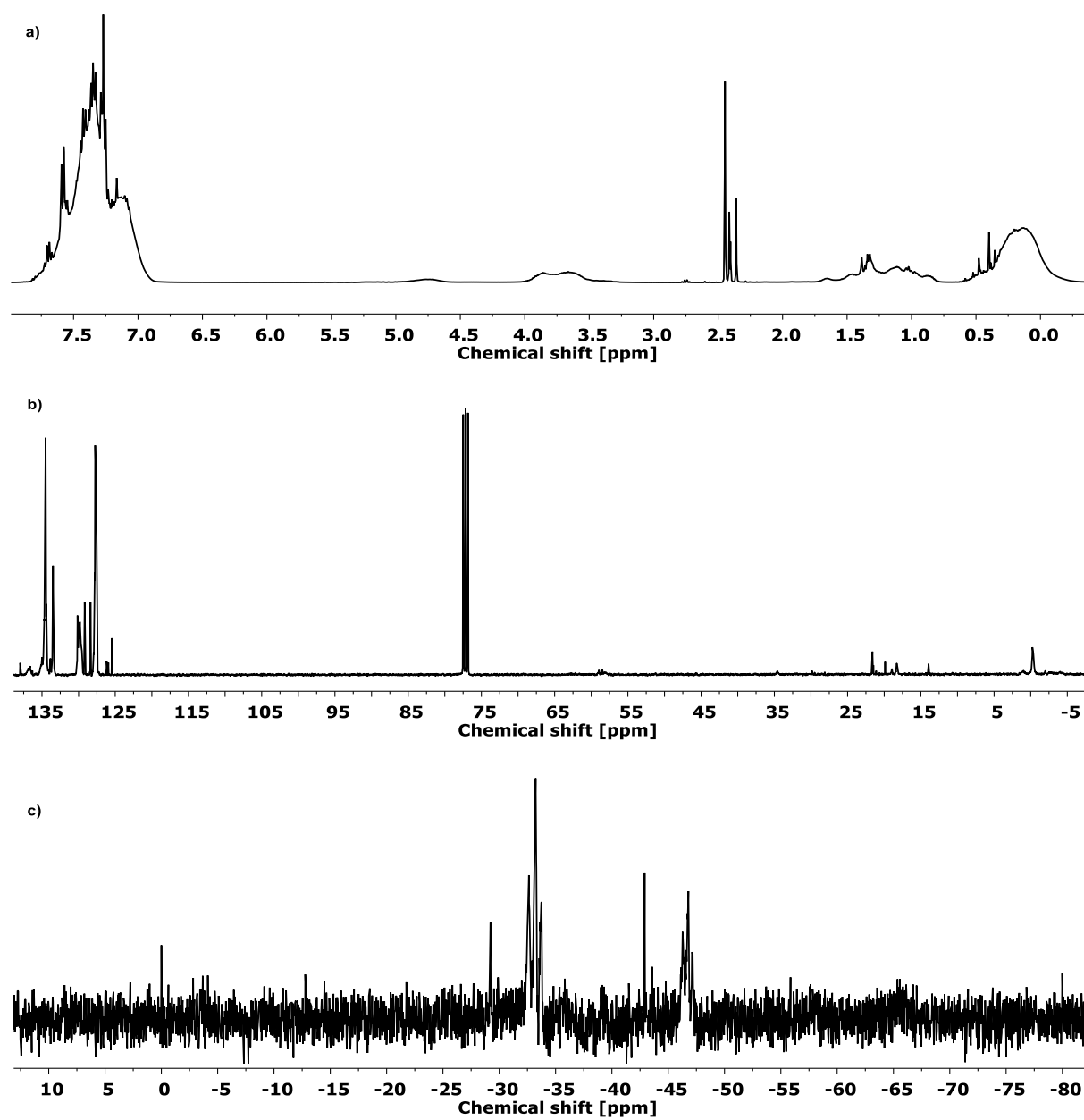
Figure 281: a) ^{1}H (400 MHz, CDCl$_3$), b) ^{13}C (101 MHz, CDCl$_3$) and c) ^{29}Si NMR (79 MHz, CDCl$_3$) of H20_Hf1_PP40_PM39.
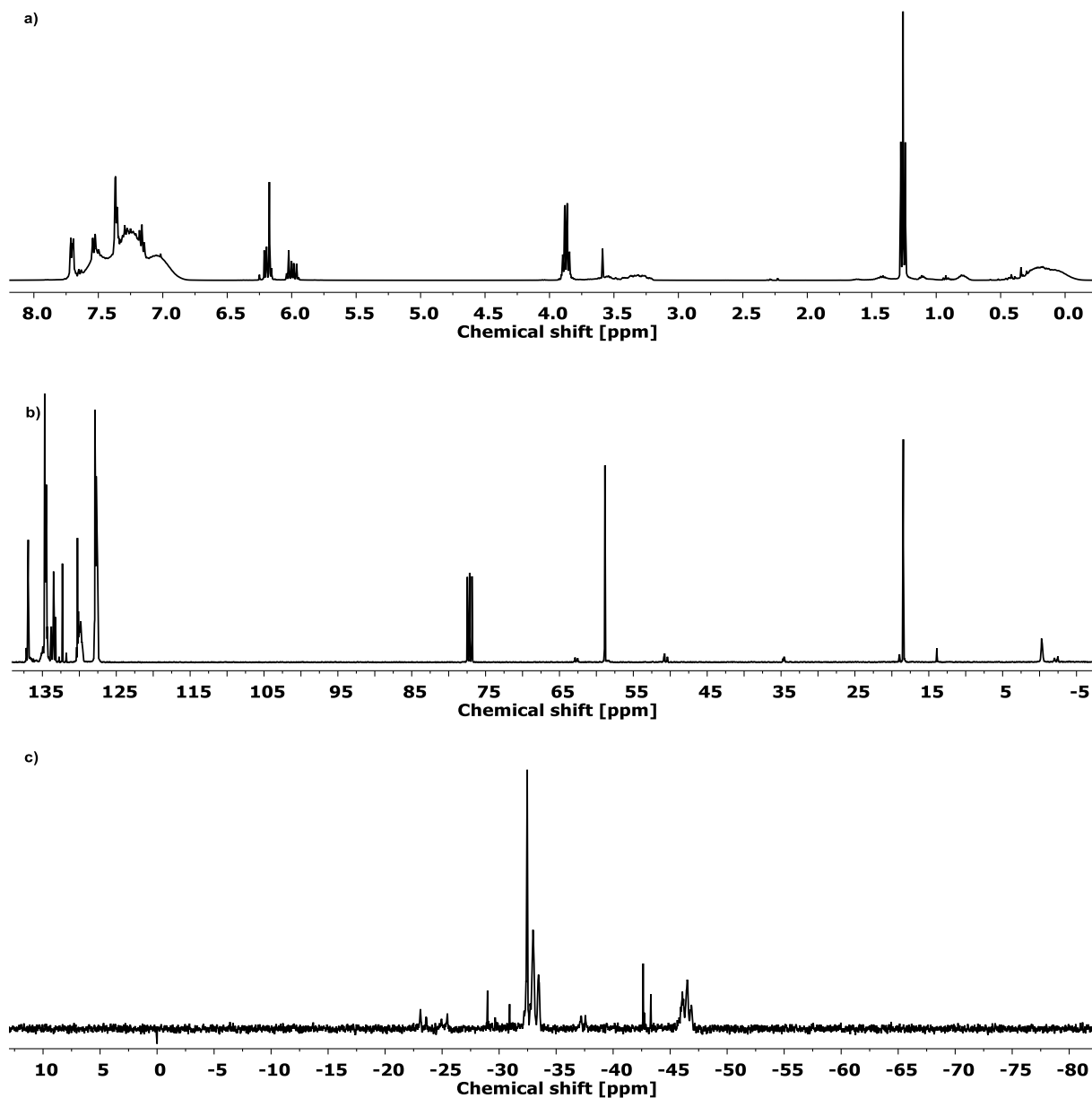
Figure 282: a) ^{1}H (400 MHz, CDCl$_3$), b) ^{13}C (101 MHz, CDCl$_3$) and c) ^{29}Si NMR (79 MHz, CDCl$_3$) of V20_Hf1_PP40_PM39.
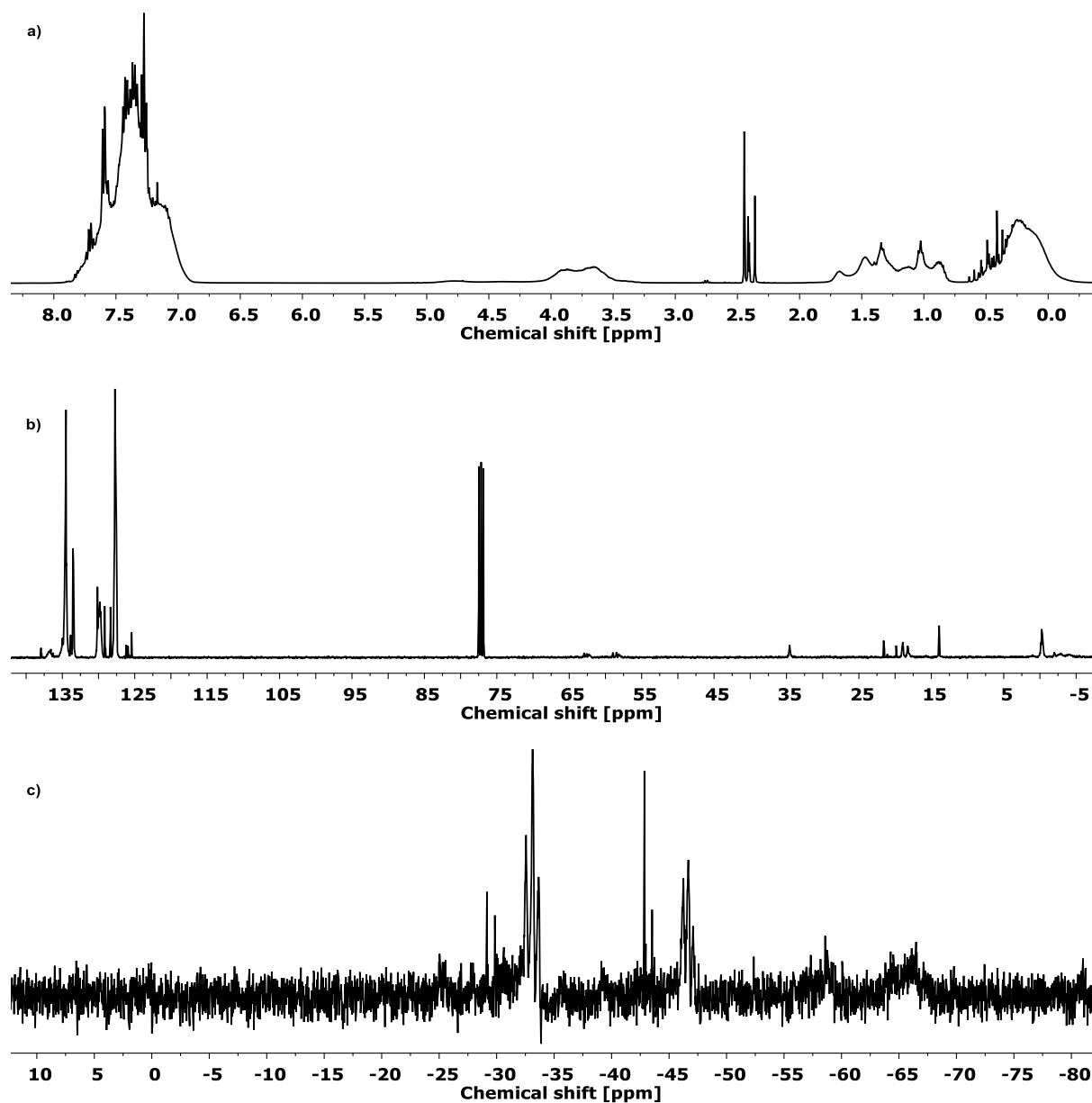
Figure 283: a) ^{1}H (400 MHz, CDCl$_3$), b) ^{13}C (101 MHz, CDCl$_3$) and c) ^{29}Si NMR (79 MHz, CDCl$_3$) of H20_Hf3_PP40_PM37.
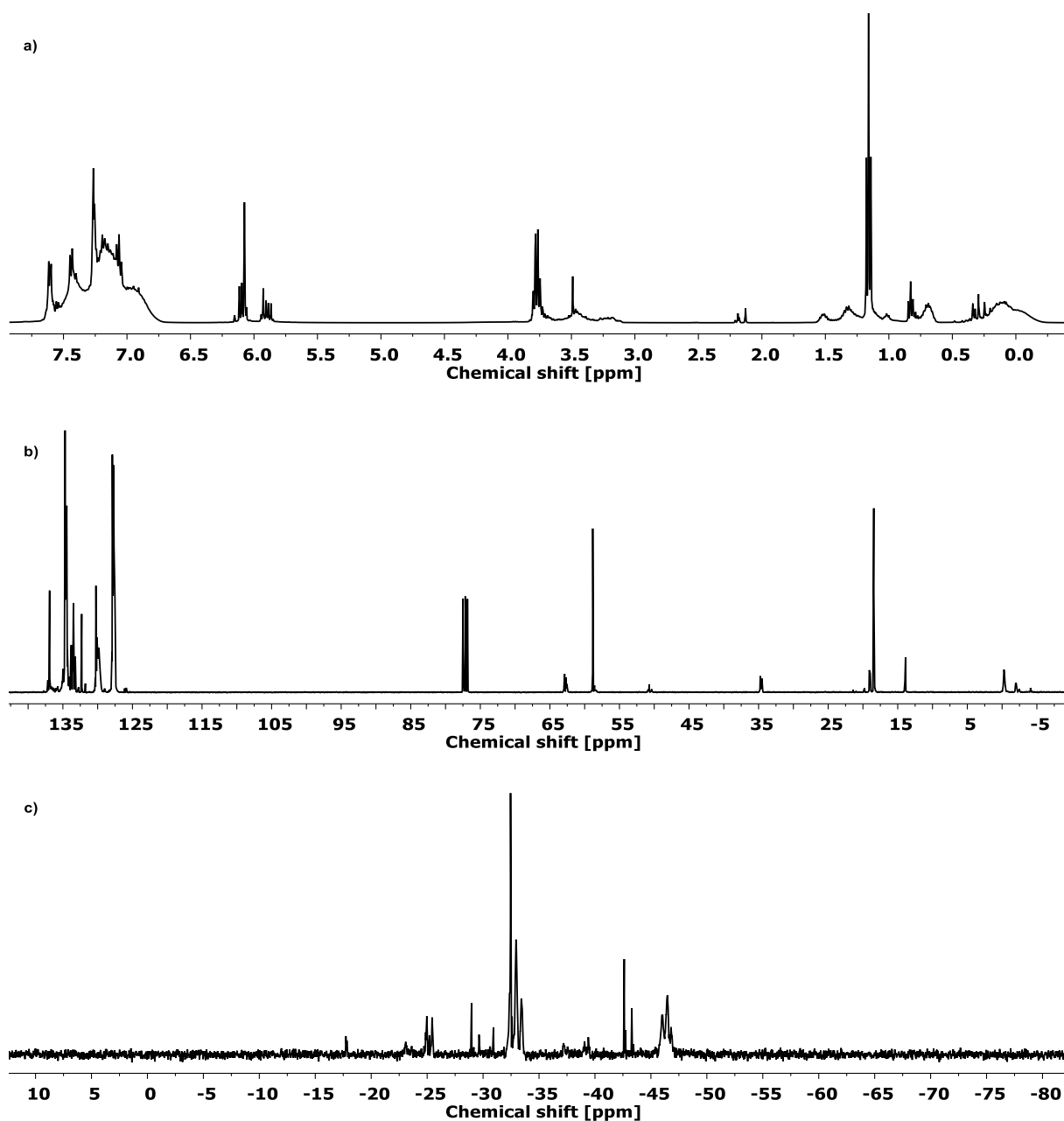
Figure 284: a) ^{1}H (400 MHz, CDCl$_3$), b) ^{13}C (101 MHz, CDCl$_3$) and c) ^{29}Si NMR (79 MHz, CDCl$_3$) of V20_Hf3_PP40_PM37.
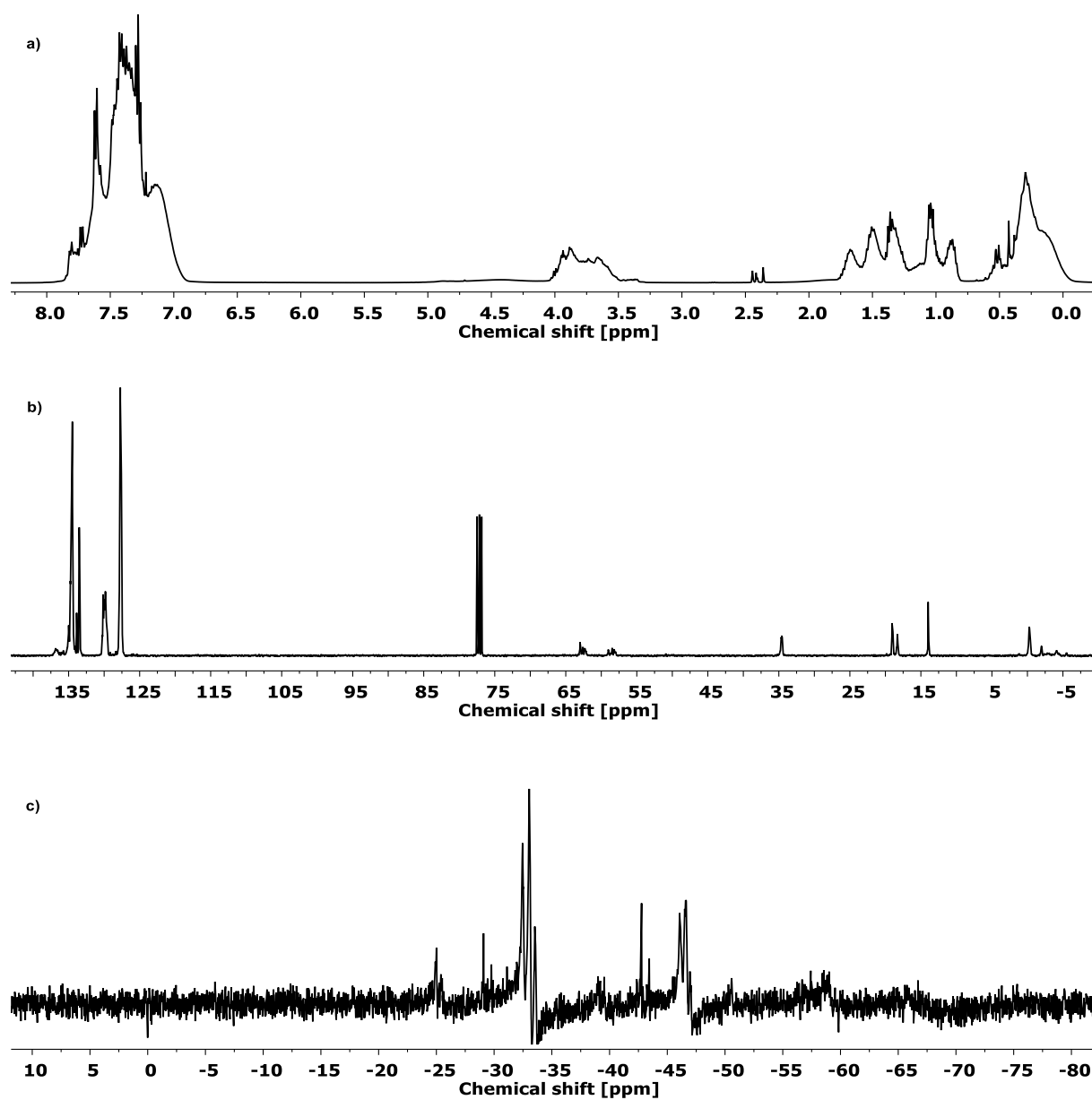
Figure 285: a) ¹H (400 MHz, CDCl₃), b) ¹³C (101 MHz, CDCl₃) and c) ²⁹Si NMR (79 MHz, CDCl₃) of H20_Hf5_PP40_PM35.
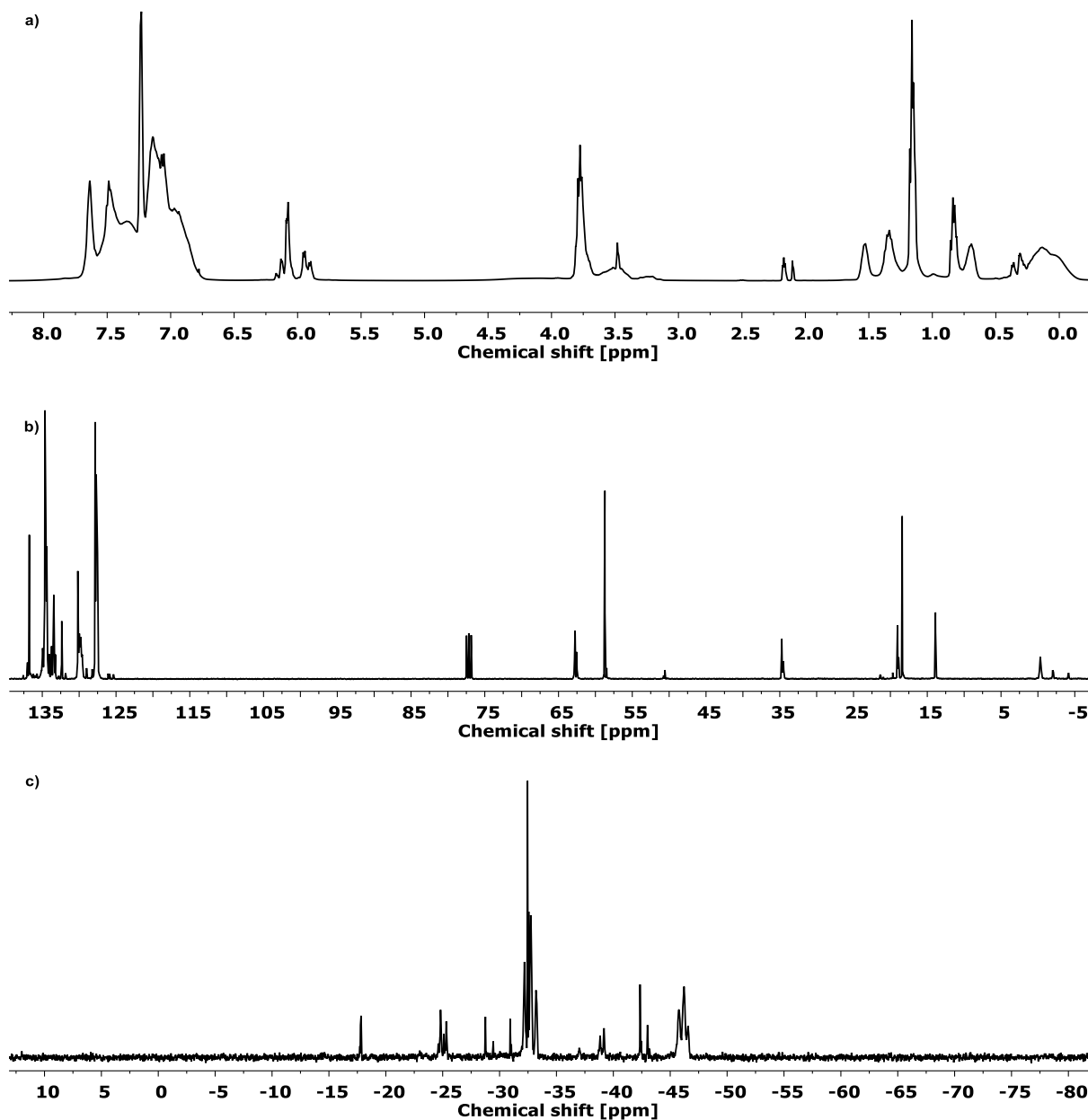
Figure 286: a) ^{1}H (400 MHz, CDCl$_3$), b) ^{13}C (101 MHz, CDCl$_3$) and c) ^{29}Si NMR (79 MHz, CDCl$_3$) of V20_Hf5_PP40_PM35.
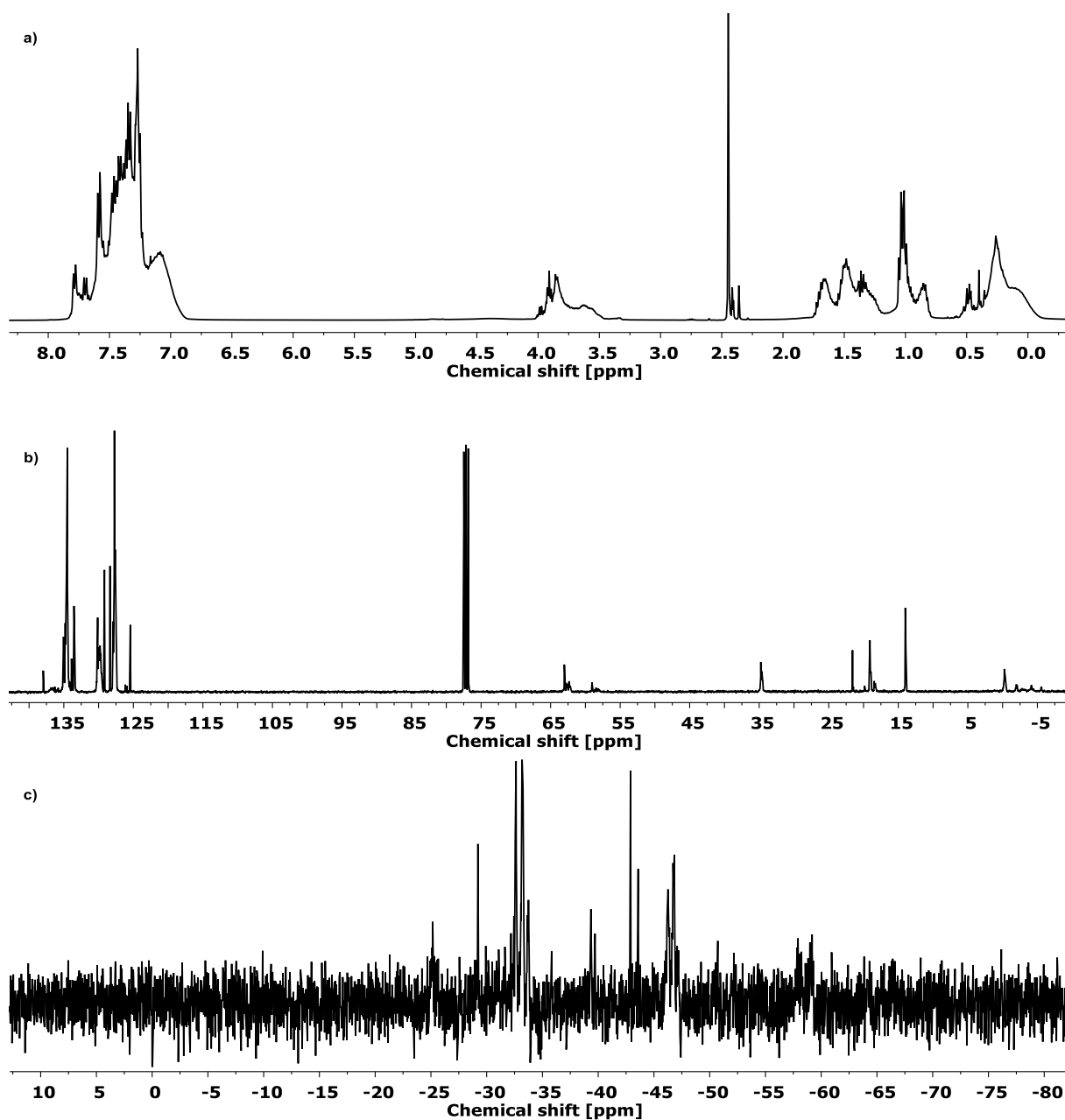
Figure 287: a) ¹H (400 MHz, CDCl₃), b) ¹³C (101 MHz, CDCl₃) and c) ²⁹Si NMR (79 MHz, CDCl₃) of H20_Hf10_PP40_PM30.
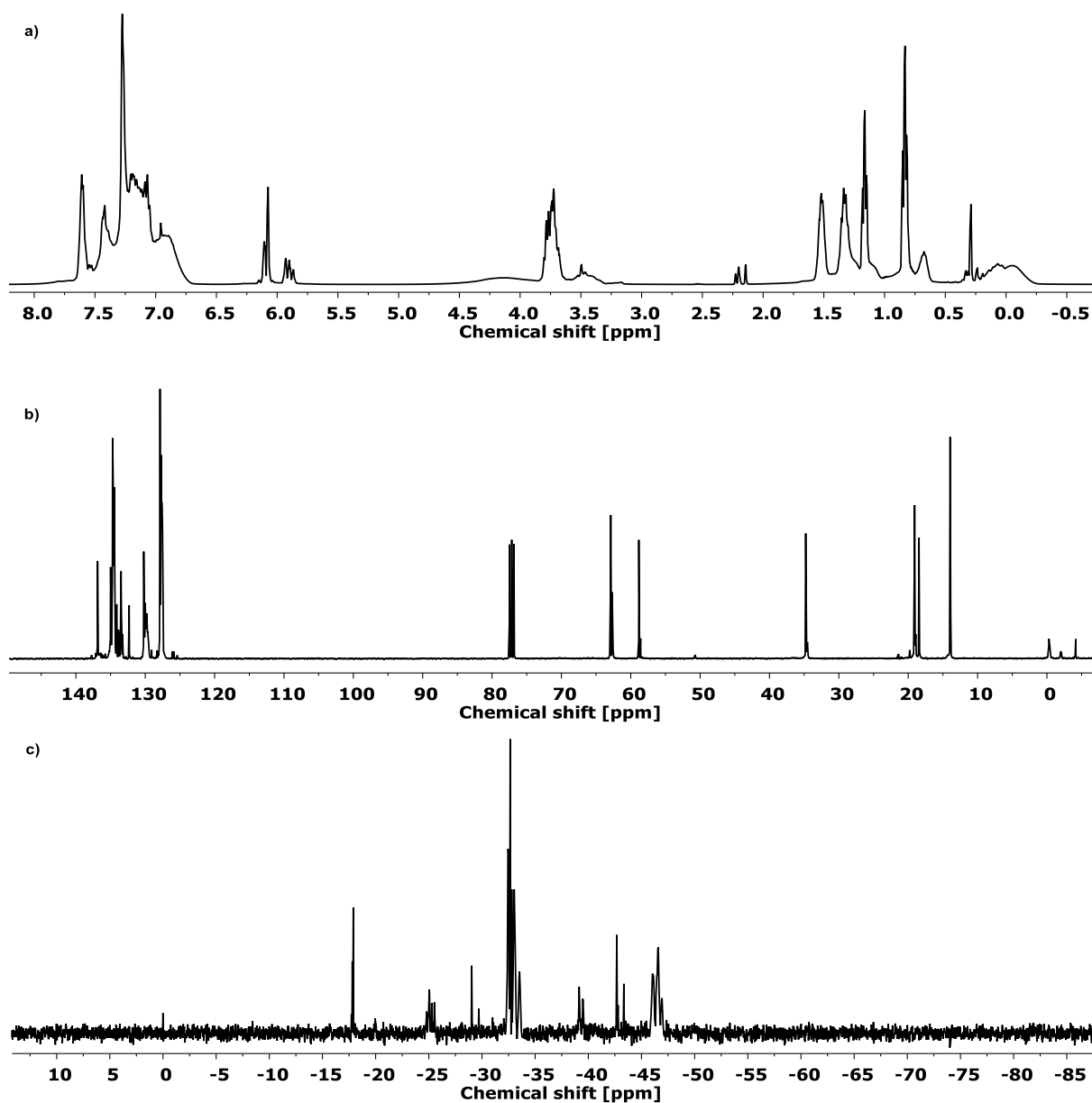
Figure 288: a) ^{1}H (400 MHz, CDCl$_3$), b) ^{13}C (101 MHz, CDCl$_3$) and c) ^{29}Si NMR (79 MHz, CDCl$_3$) of V20_Hf10_PP40_PM30.
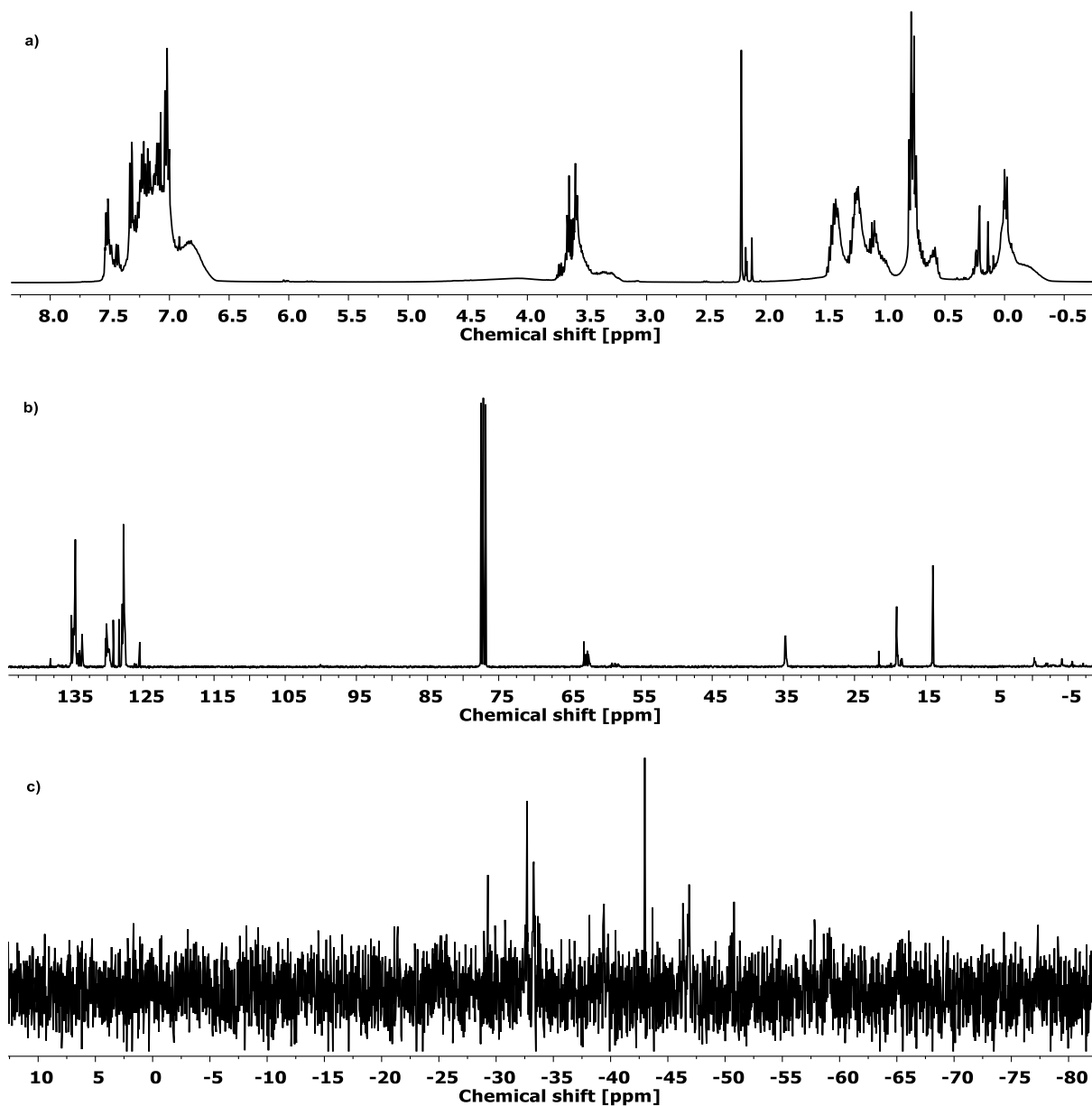
Figure 289: a) ^{1}H (400 MHz, CDCl$_3$), b) ^{13}C (101 MHz, CDCl$_3$) and c) ^{29}Si NMR (79 MHz, CDCl$_3$) of H20_Hf15_PP40_PM25.
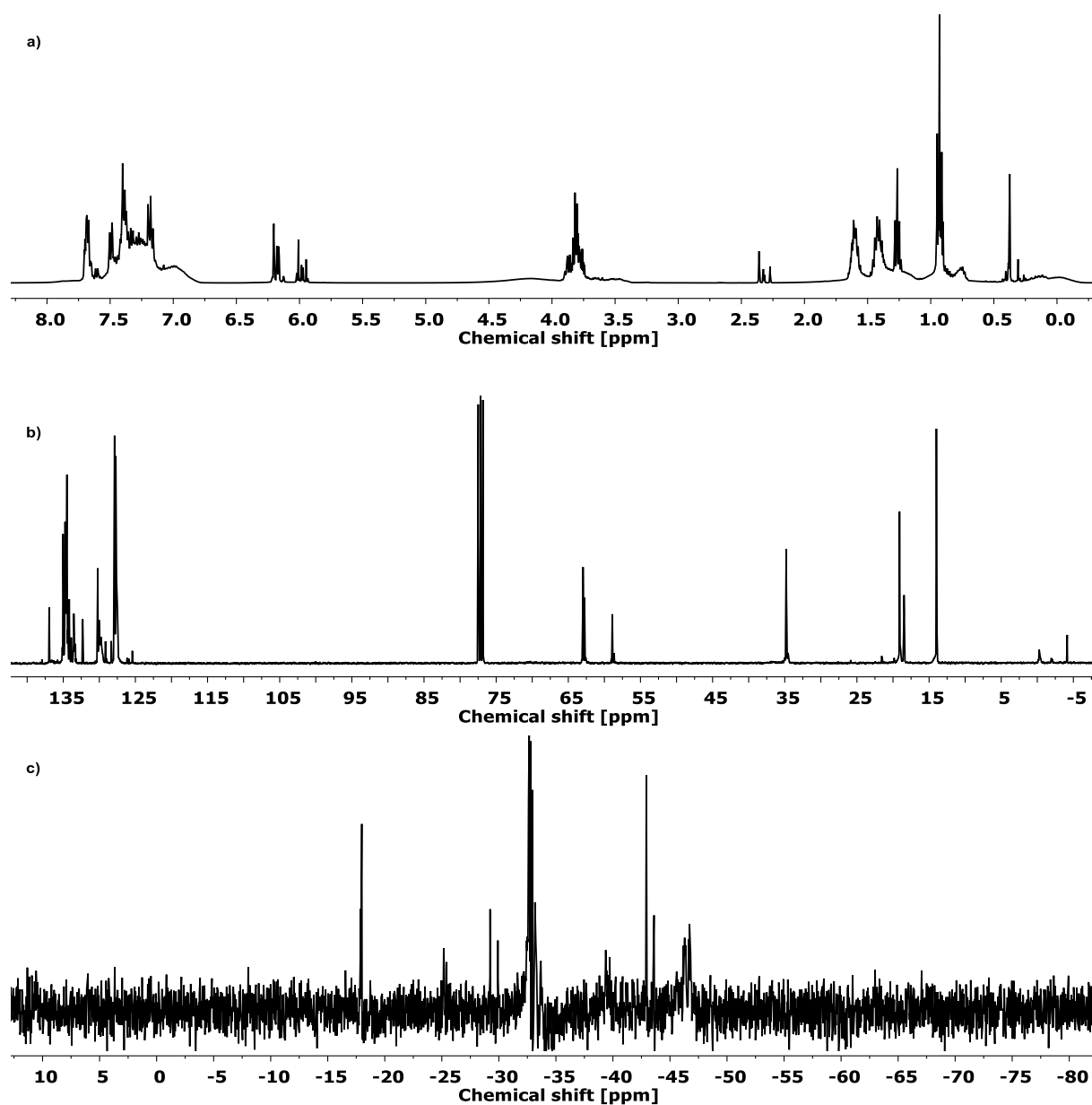
Figure 290: a) ¹H (400 MHz, CDCl₃), b) ¹³C (101 MHz, CDCl₃) and c) ²⁹Si NMR (79 MHz, CDCl₃) of V20_Hf15_PP40_PM25.

6.2.6.3.2.4 Tin containing copolymers
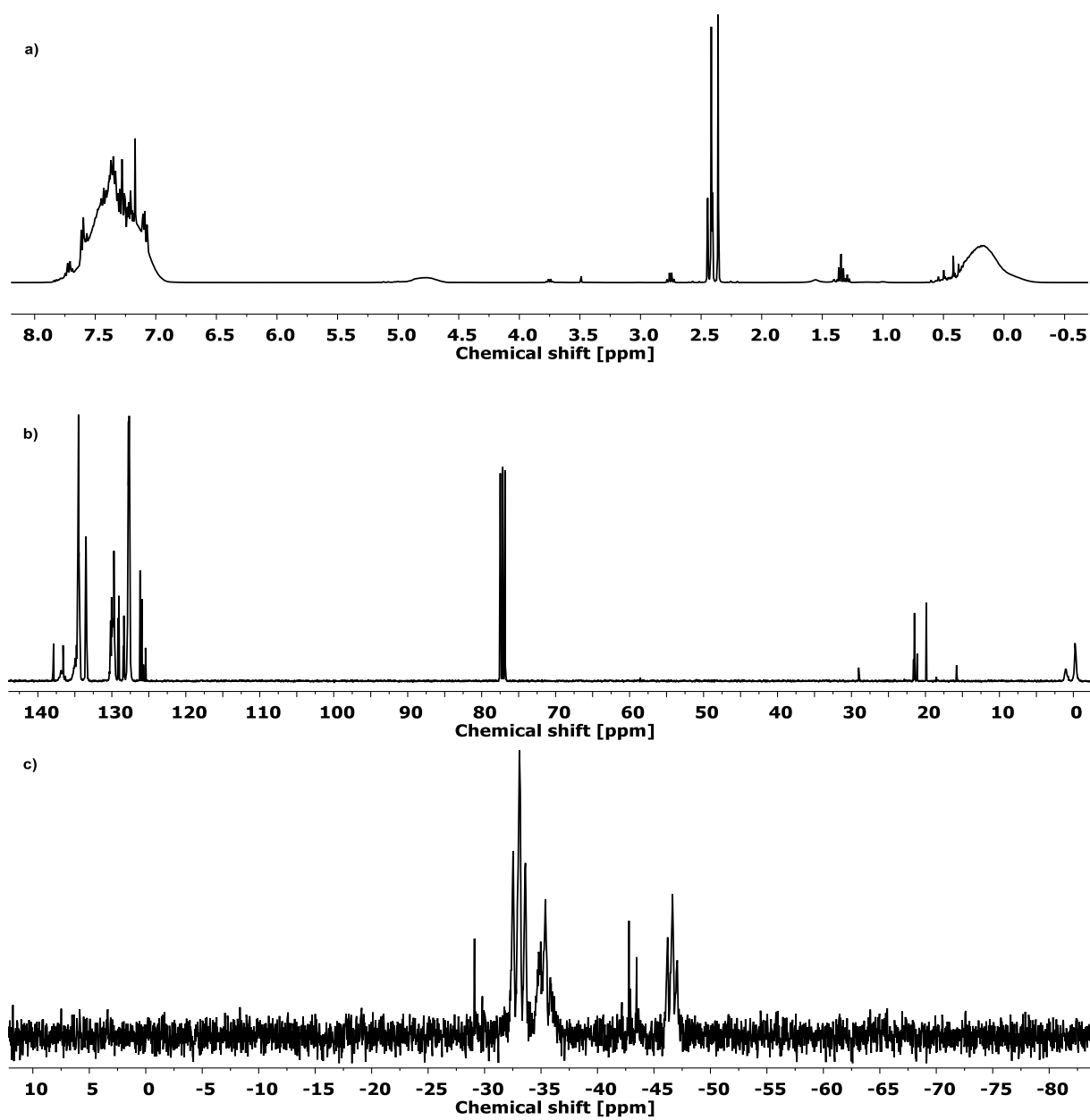
Figure 291: a) ¹H (400 MHz, CDCl₃), b) ¹³C (101 MHz, CDCl₃) and c) ²⁹Si NMR (79 MHz, CDCl₃) of H20_Sn1_PP40_PM39.
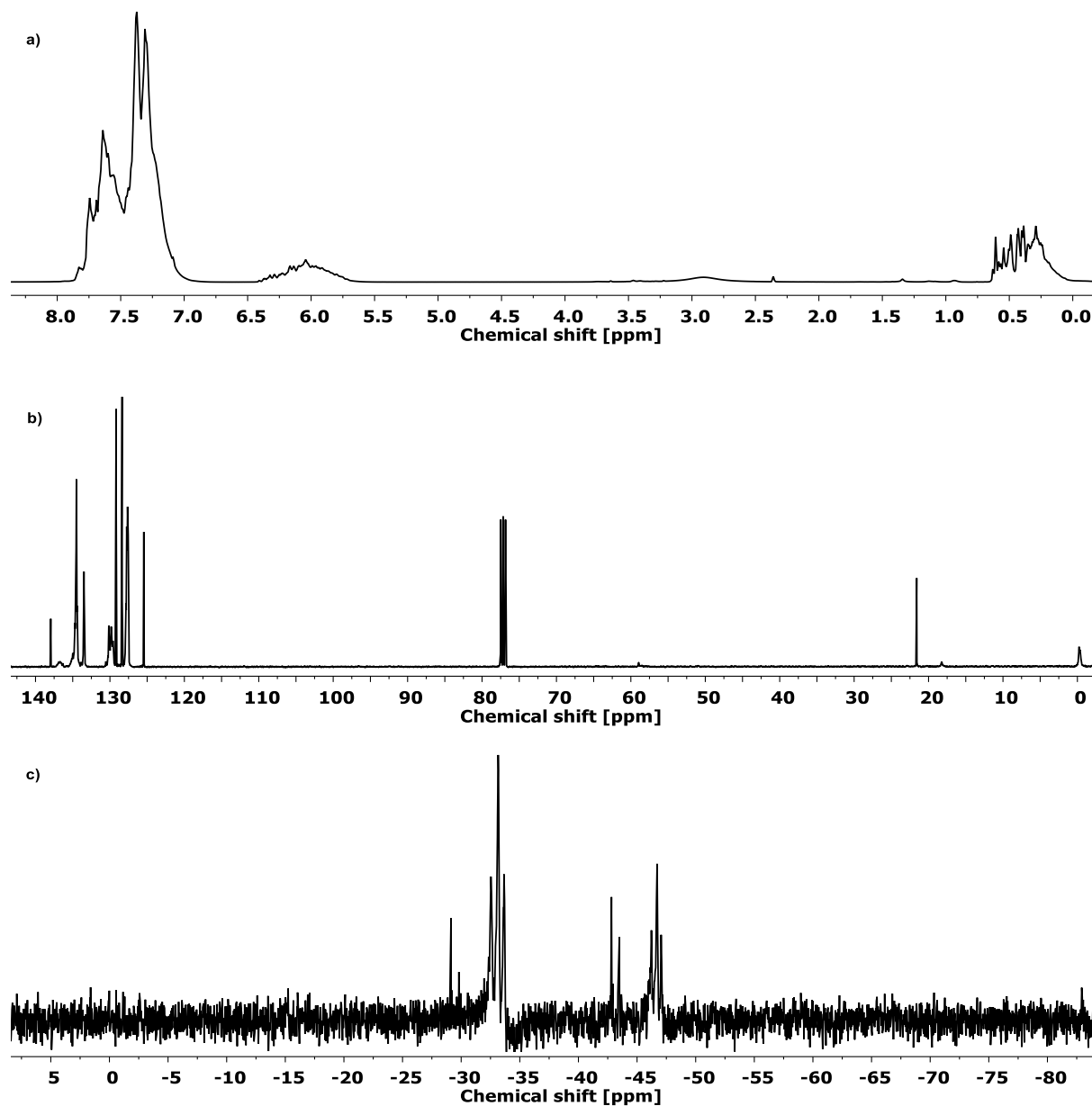
Figure 292: a) ¹H (400 MHz, CDCl₃), b) ¹³C (101 MHz, CDCl₃) and c) ²⁹Si NMR (79 MHz, CDCl₃) of V20_Sn1_PP40_PM39.
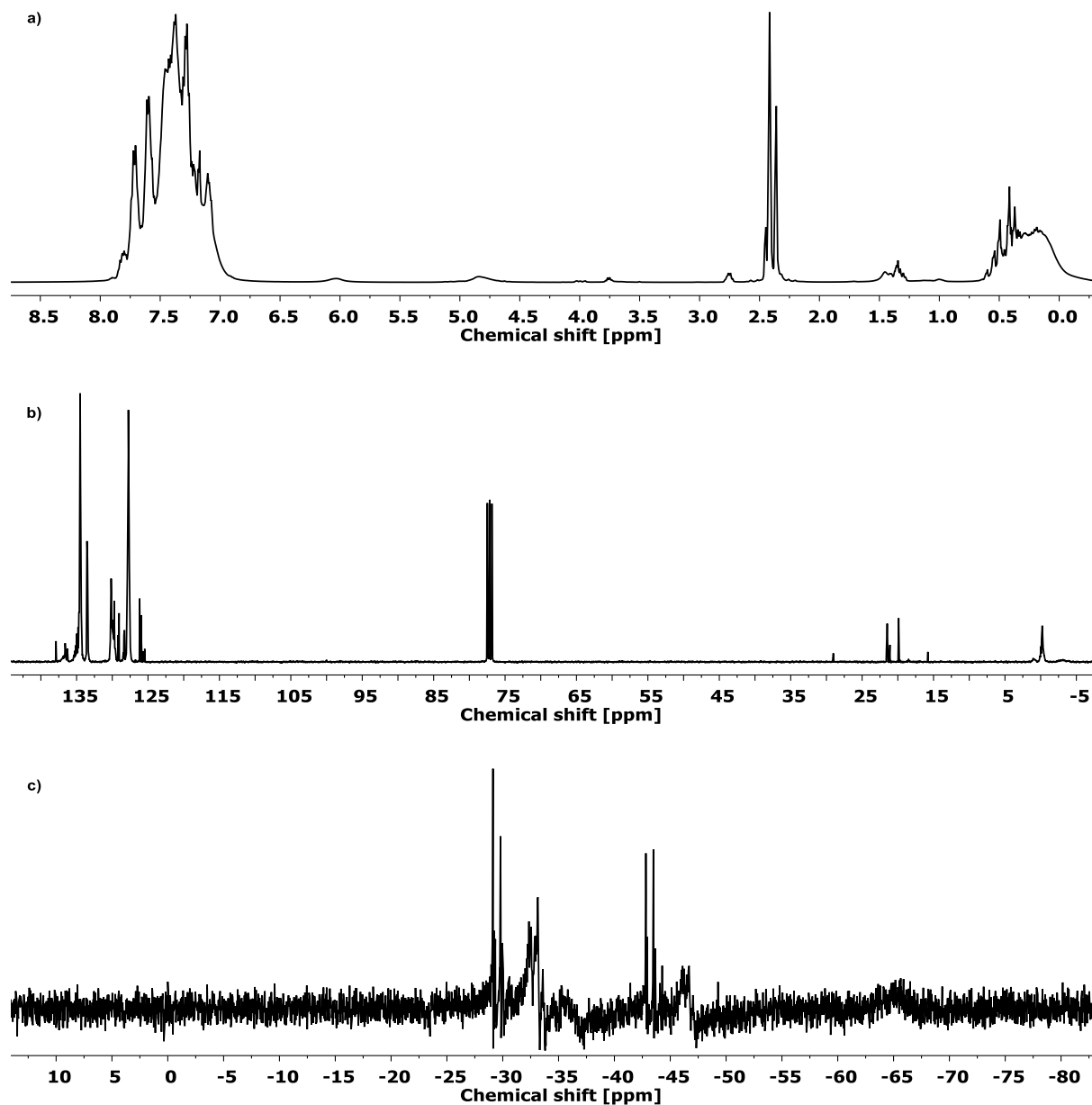
Figure 293: a) ¹H (400 MHz, CDCl₃), b) ¹³C (101 MHz, CDCl₃) and c) ²⁹Si NMR (79 MHz, CDCl₃) of H20_Sn3_PP40_PM37.
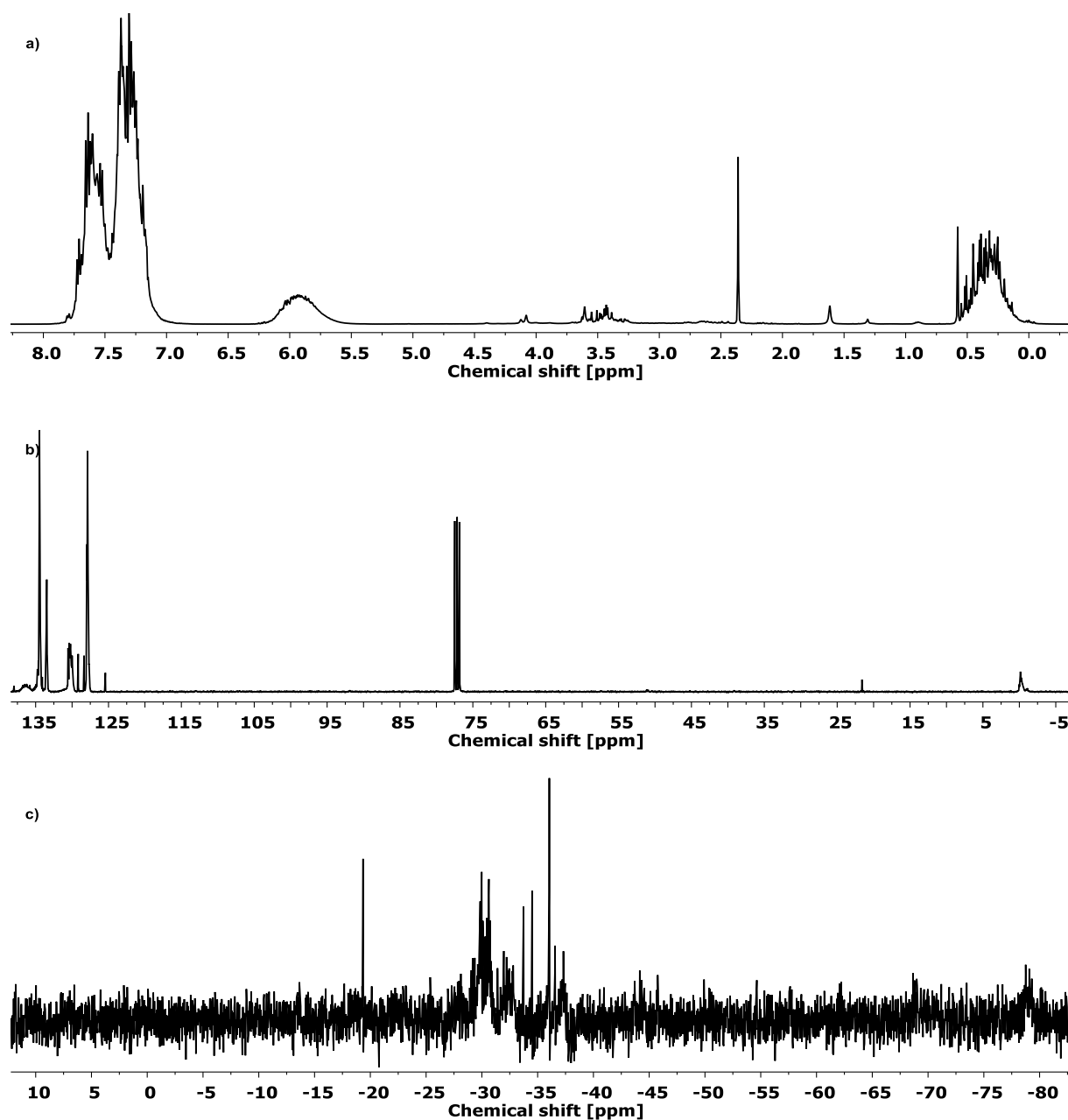
Figure 294: a) ^{1}H (400 MHz, CDCl$_3$), b) ^{13}C (101 MHz, CDCl$_3$) and c) ^{29}Si NMR (79 MHz, CDCl$_3$) of V20_Sn3_PP40_PM37.
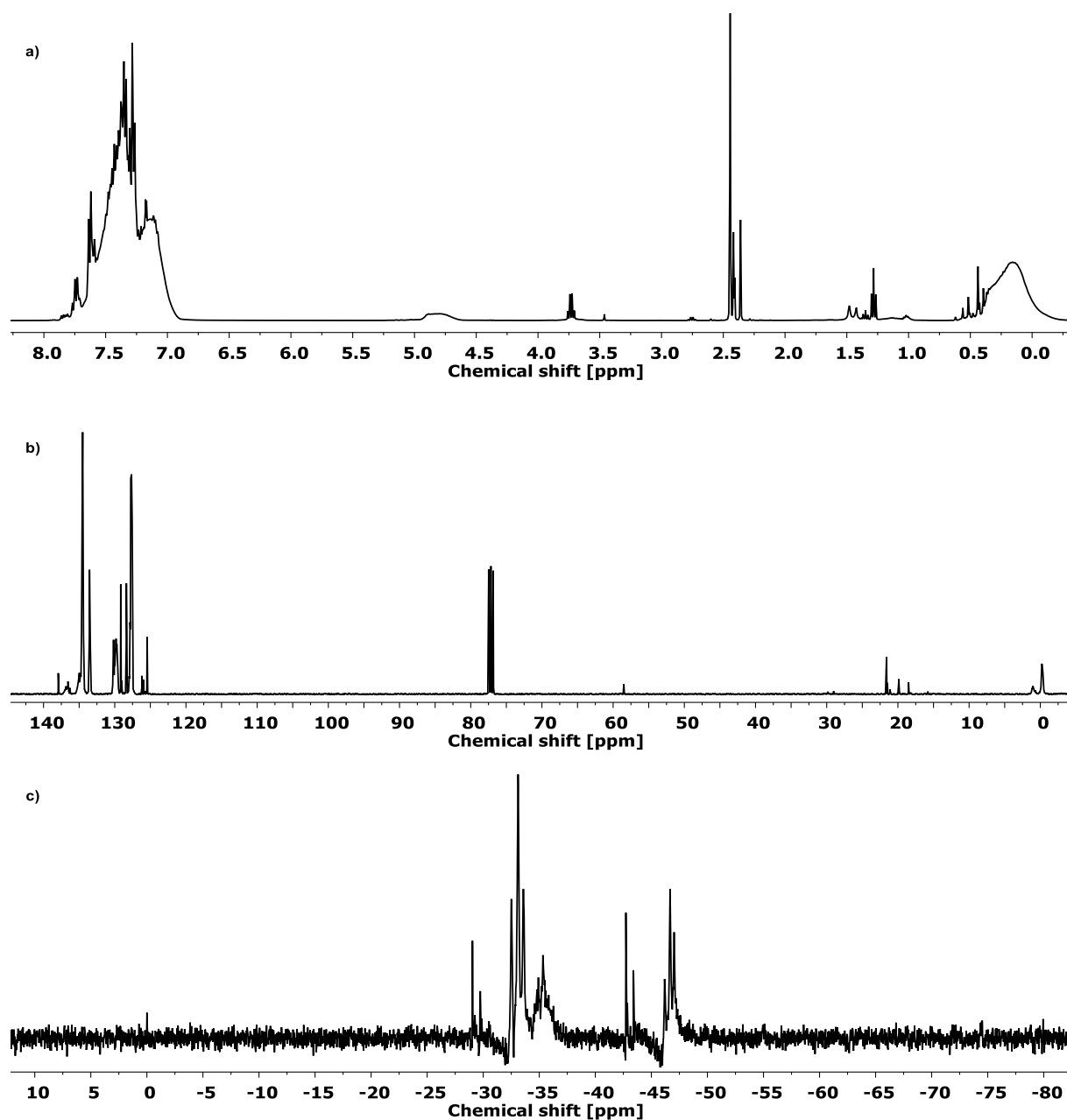
Figure 295: a) ^{1}H (400 MHz, CDCl$_3$), b) ^{13}C (101 MHz, CDCl$_3$) and c) ^{29}Si NMR (79 MHz, CDCl$_3$) of H20_Sn5_PP40_PM35.
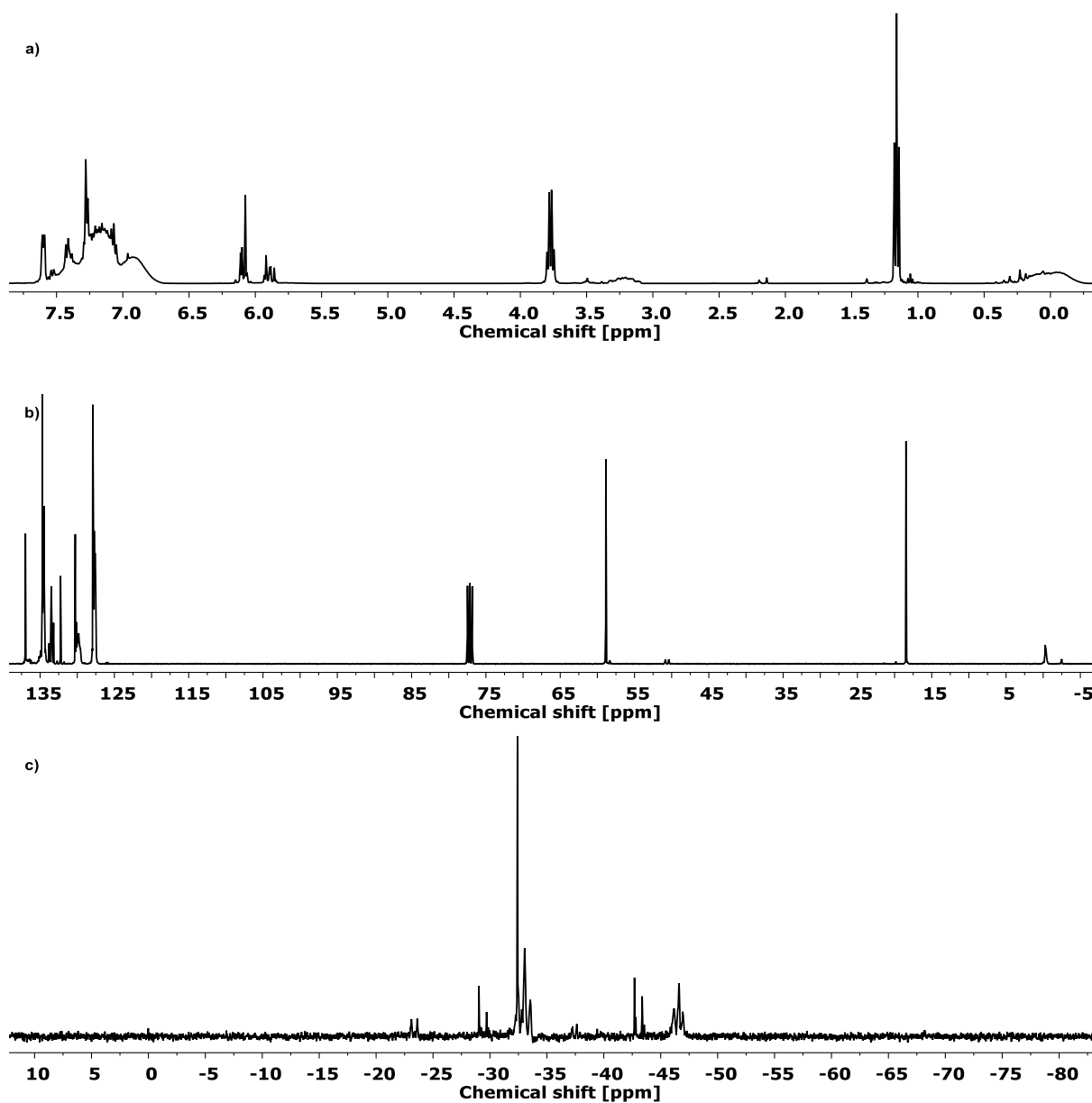
Figure 296: a) ¹H (400 MHz, CDCl₃), b) ¹³C (101 MHz, CDCl₃) and c) ²⁹Si NMR (79 MHz, CDCl₃) of V20_Sn5_PP40_PM35.
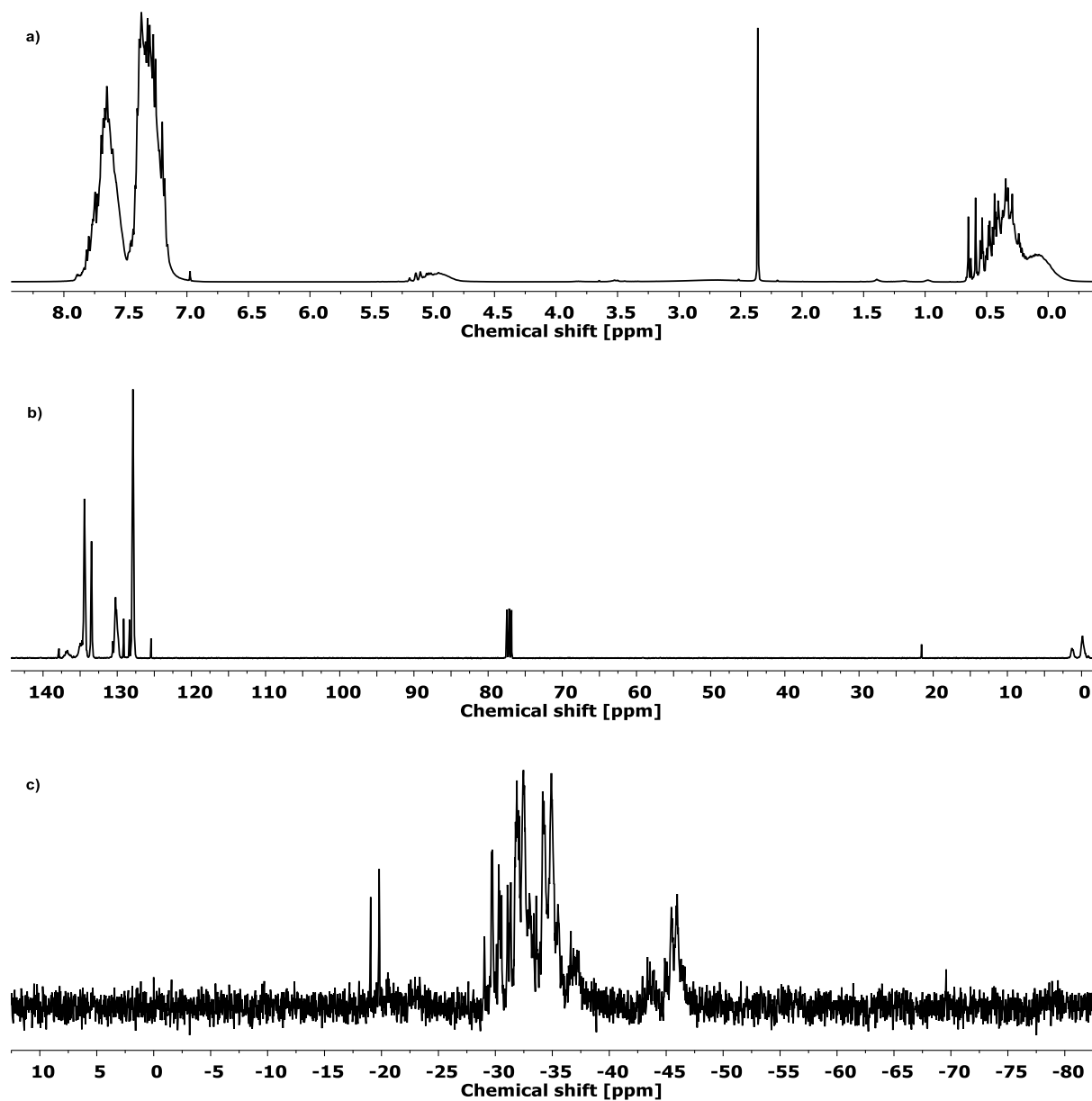
Figure 297: a) ^{1}H (400 MHz, CDCl$_3$), b) ^{13}C (101 MHz, CDCl$_3$) and c) ^{29}Si NMR (79 MHz, CDCl$_3$) of H20_Sn10_PP40_PM30.
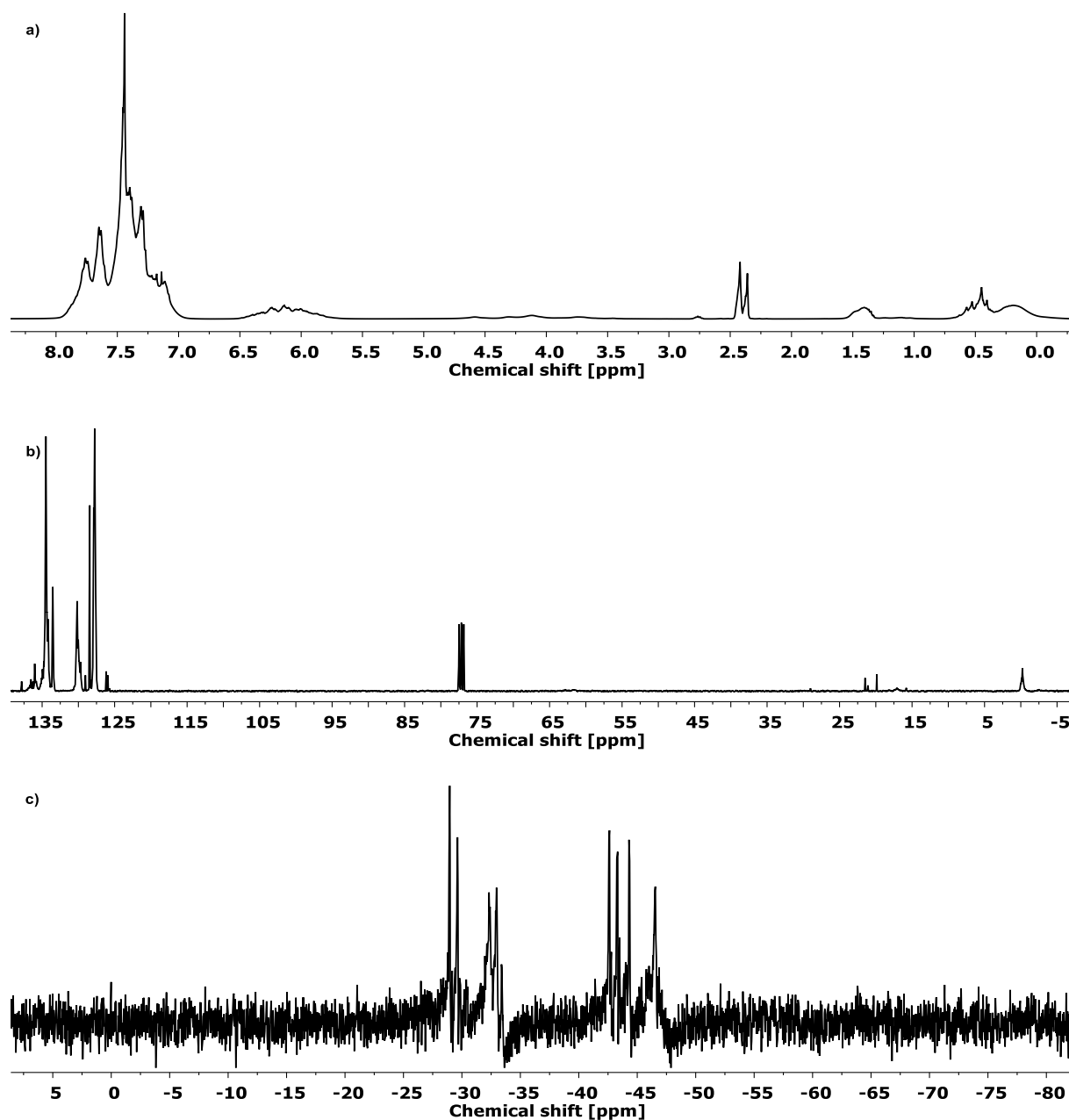
Figure 298: a) ^{1}H (400 MHz, CDCl$_3$), b) ^{13}C (101 MHz, CDCl$_3$) and c) ^{29}Si NMR (79 MHz, CDCl$_3$) of **V20_Sn10_PP40_PM30.**
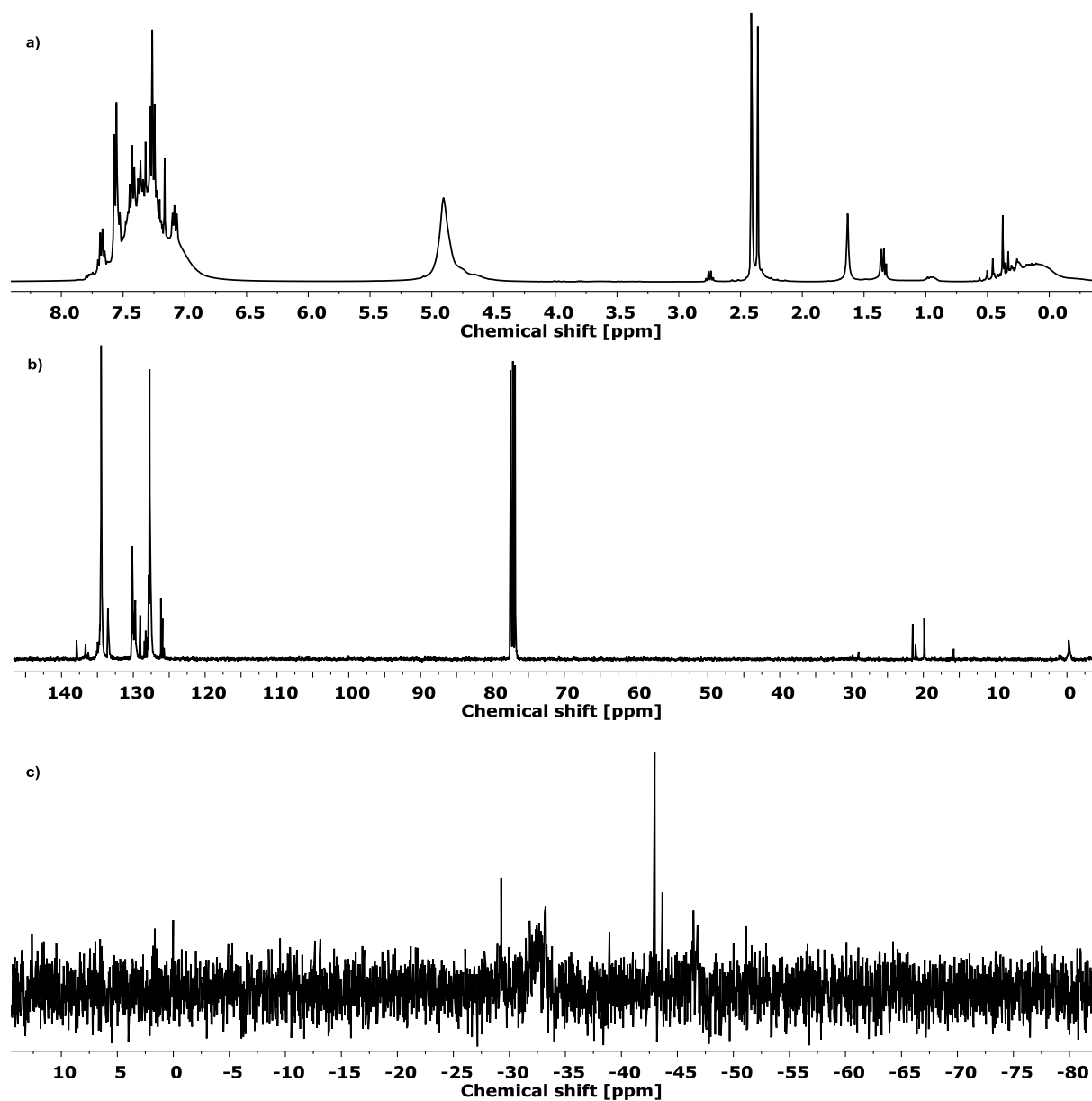
Figure 299: a) ^{1}H (400 MHz, CDCl$_3$), **b)** ^{13}C (101 MHz, CDCl$_3$) and **c)** ^{29}Si NMR (79 MHz, CDCl$_3$) of **H20_Sn15_PP40_PM25.**
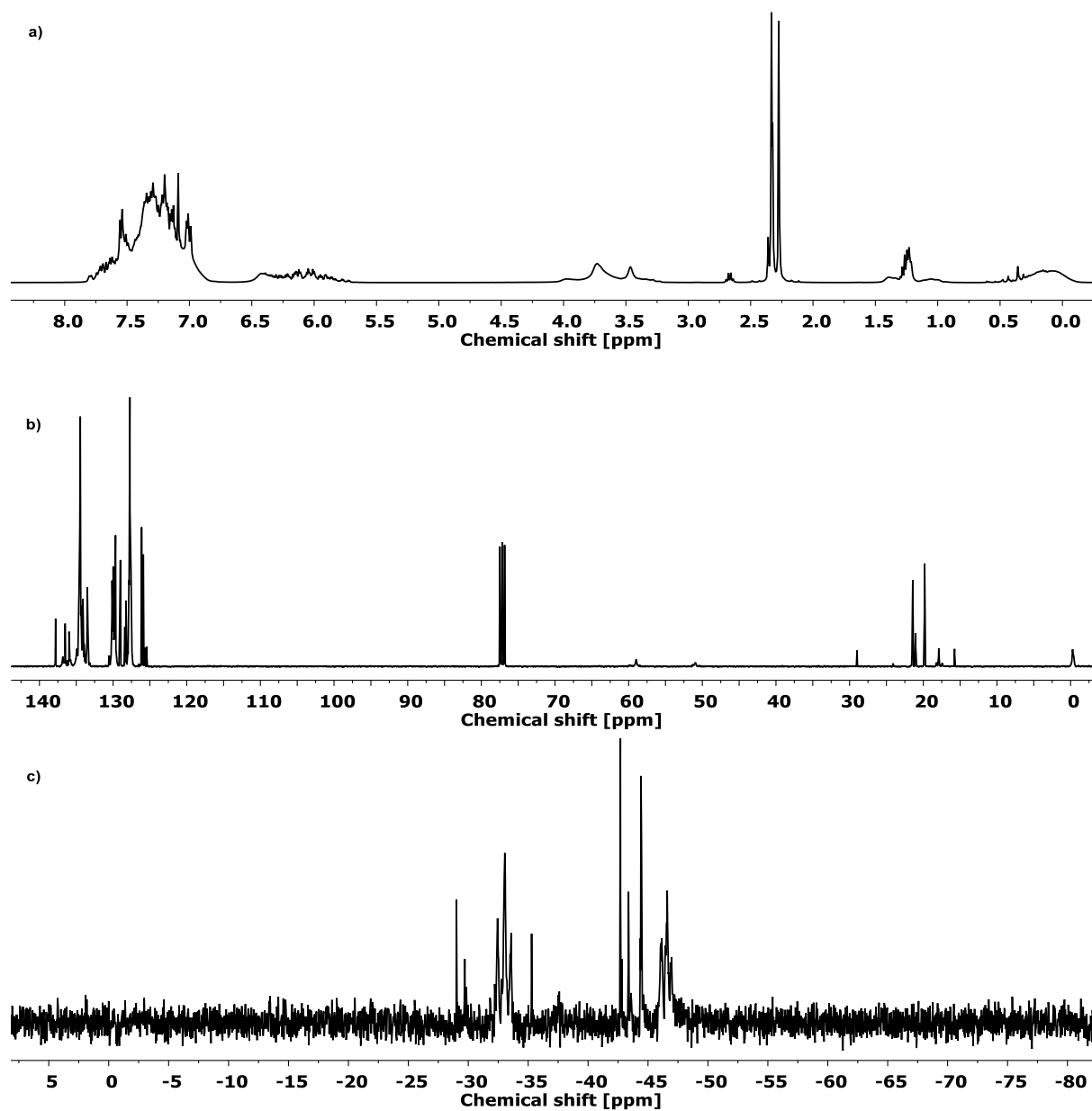
Figure 300: a) ^{1}H (400 MHz, CDCl$_3$), b) ^{13}C (101 MHz, CDCl$_3$) and c) ^{29}Si NMR (79 MHz, CDCl$_3$) of **V20_Sn15_PP40_PM25.**

6.2.6.3.2.5 Tantalum containing copolymers
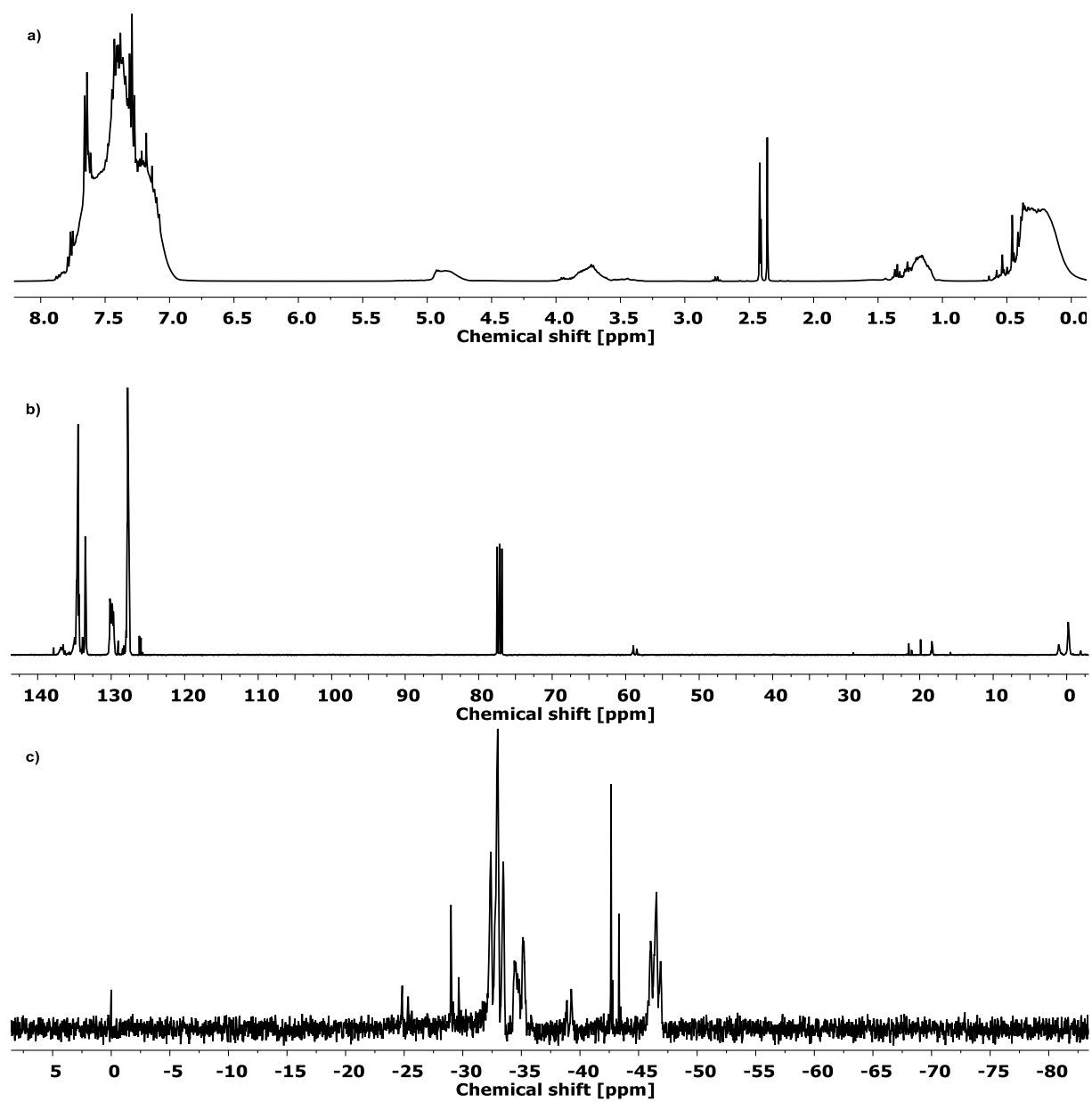
Figure 301: a) ¹H (400 MHz, CDCl₃), b) ¹³C (101 MHz, CDCl₃) and c) ²⁹Si NMR (79 MHz, CDCl₃) of H20_Ta1_PP40_PM39.
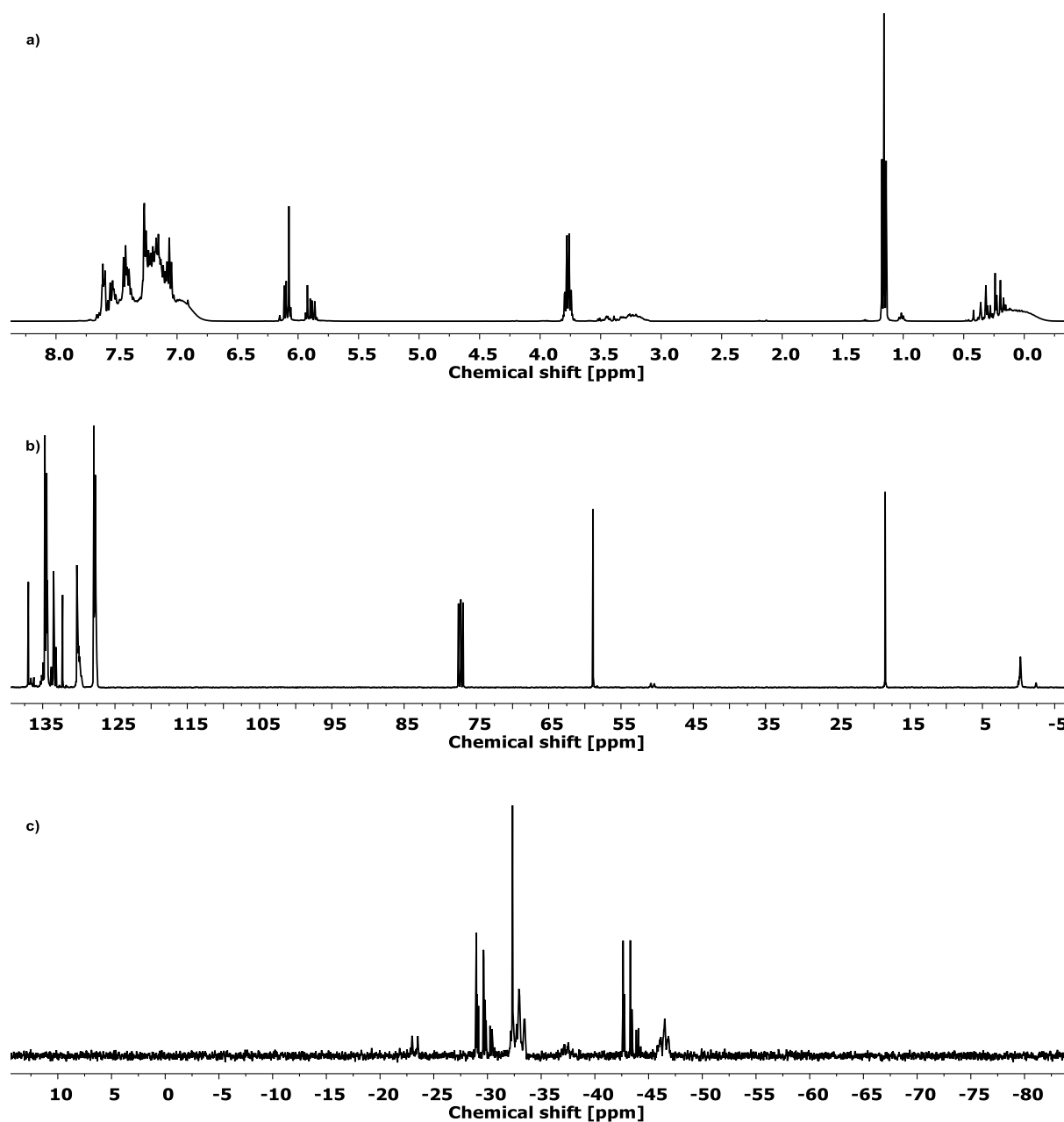
Figure 302: a) ^{1}H (400 MHz, CDCl$_3$), b) ^{13}C (101 MHz, CDCl$_3$) and c) ^{29}Si NMR (79 MHz, CDCl$_3$) of V20_Ta1_PP40_PM39.
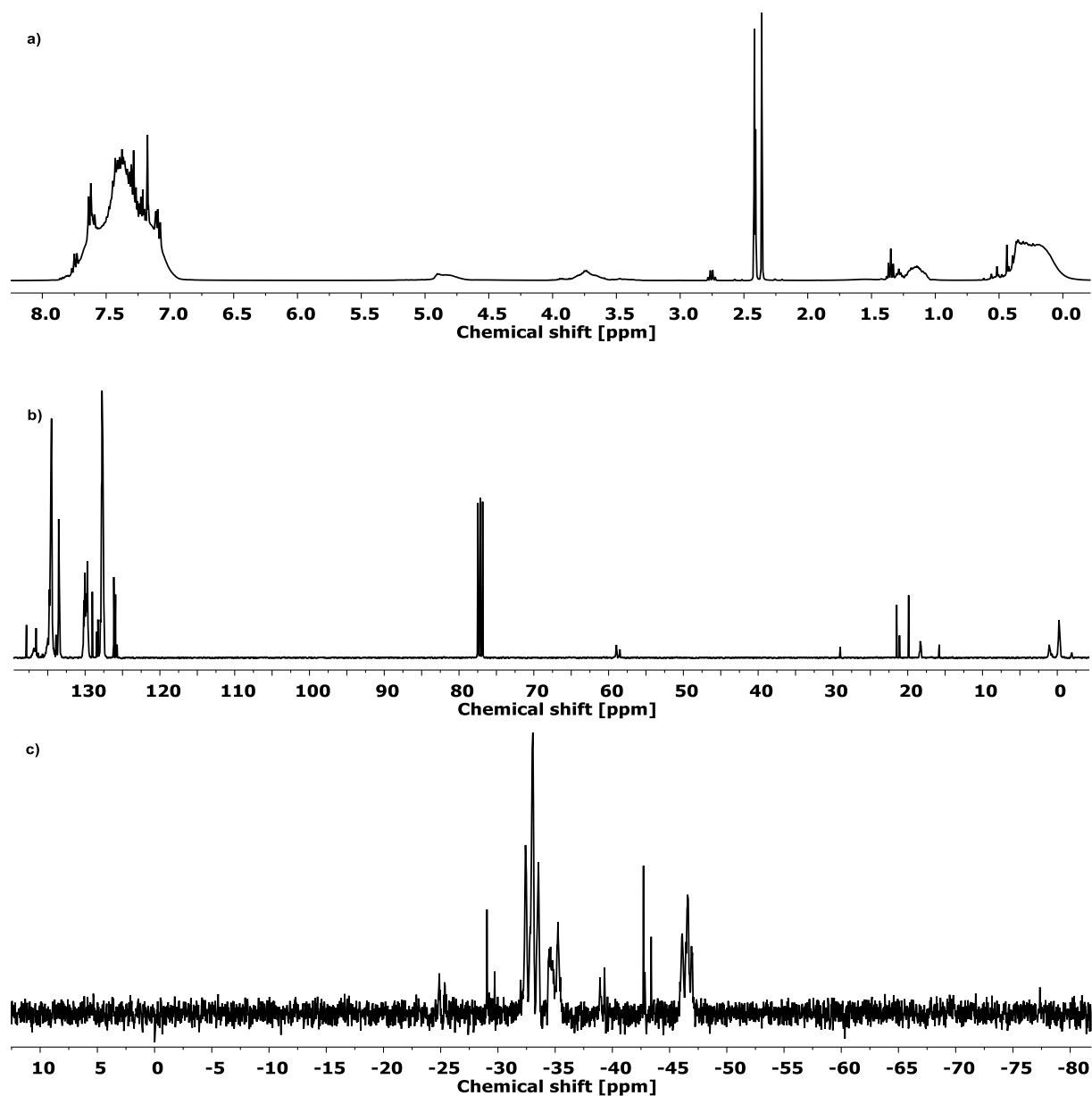
Figure 303: a) ^{1}H (400 MHz, CDCl$_3$), b) ^{13}C (101 MHz, CDCl$_3$) and c) ^{29}Si NMR (79 MHz, CDCl$_3$) of H20_Ta3_PP40_PM37.
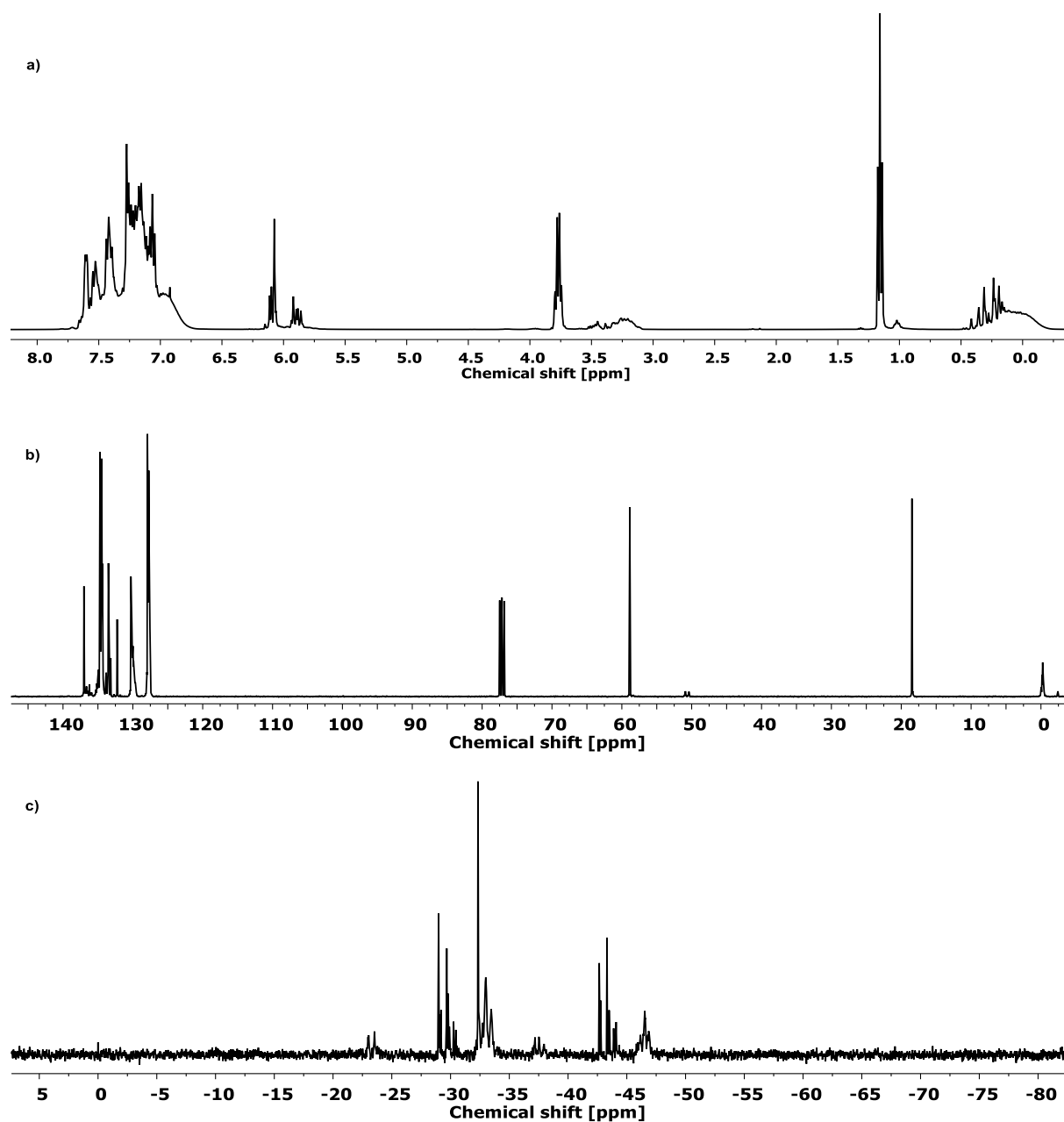
Figure 304: a) ^{1}H (400 MHz, CDCl$_3$), b) ^{13}C (101 MHz, CDCl$_3$) and c) ^{29}Si NMR (79 MHz, CDCl$_3$) of V20_Ta3_PP40_PM37.
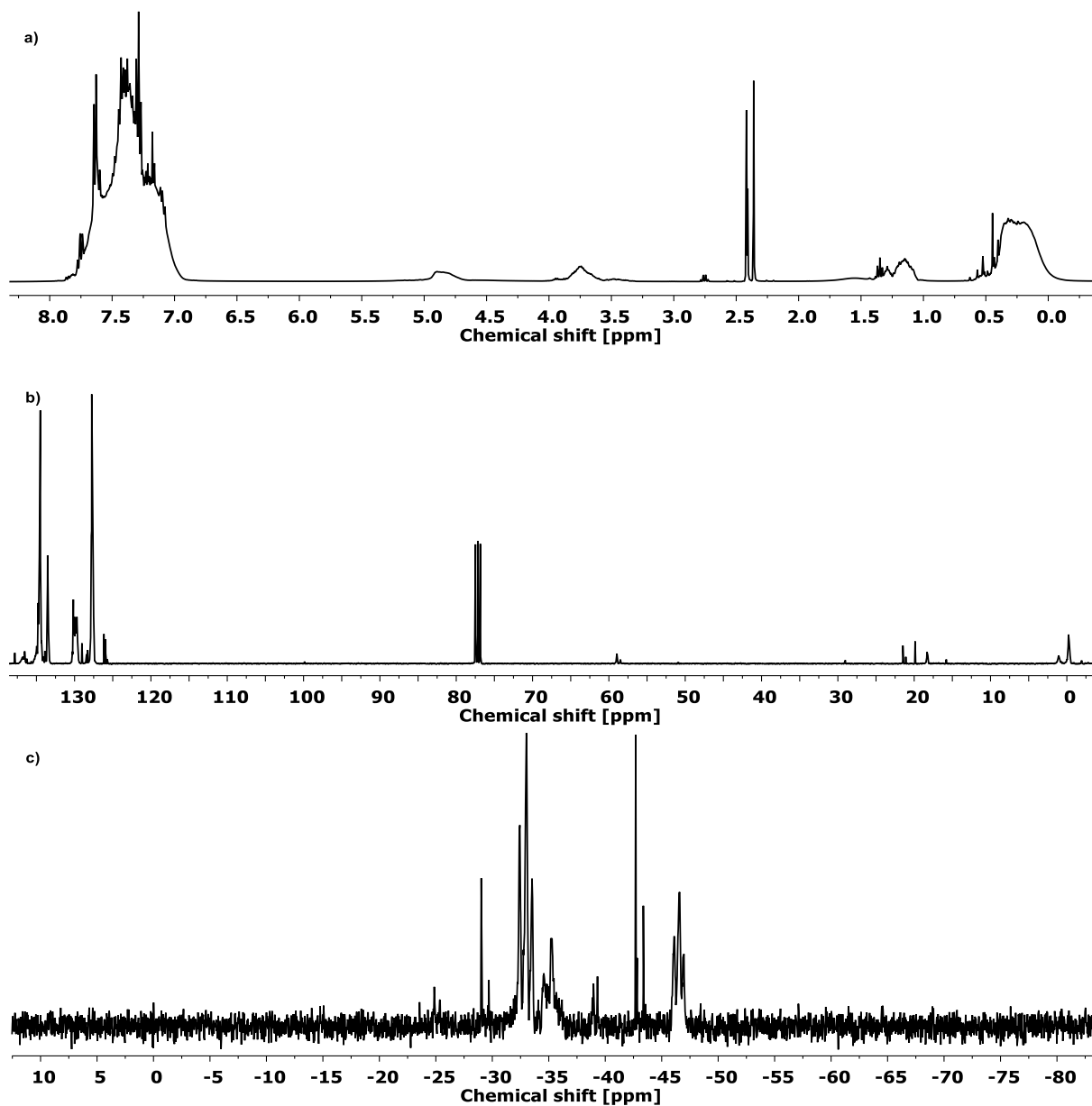
Figure 305: a) ^{1}H (400 MHz, CDCl$_3$), **b)** ^{13}C (101 MHz, CDCl$_3$) **and c)** ^{29}Si NMR (79 MHz, CDCl$_3$) of **H20_Ta5_PP40_PM35.**
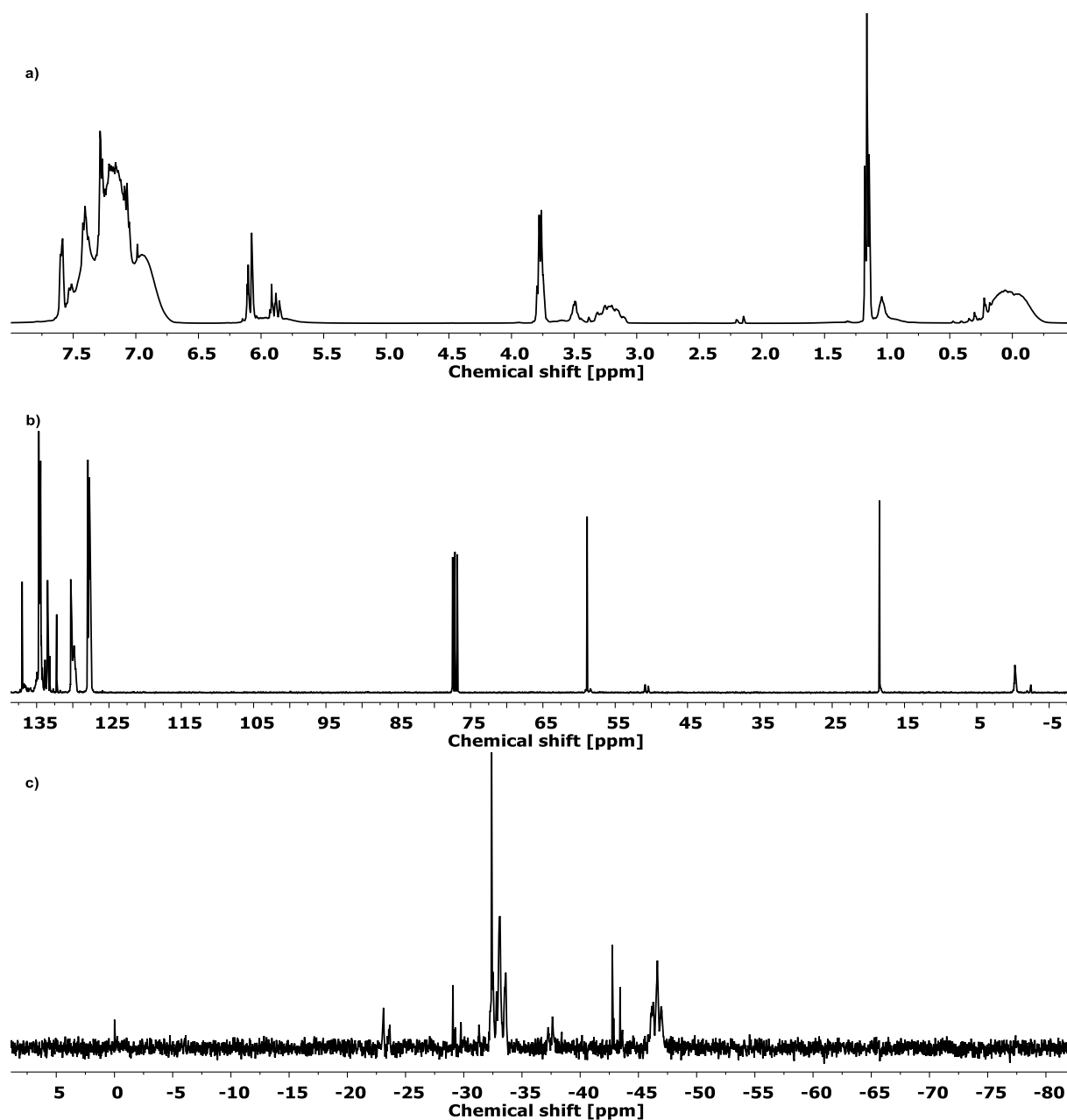
Figure 306: a) ¹H (400 MHz, CDCl₃), b) ¹³C (101 MHz, CDCl₃) and c) ²⁹Si NMR (79 MHz, CDCl₃) of V20_Ta5_PP40_PM35.
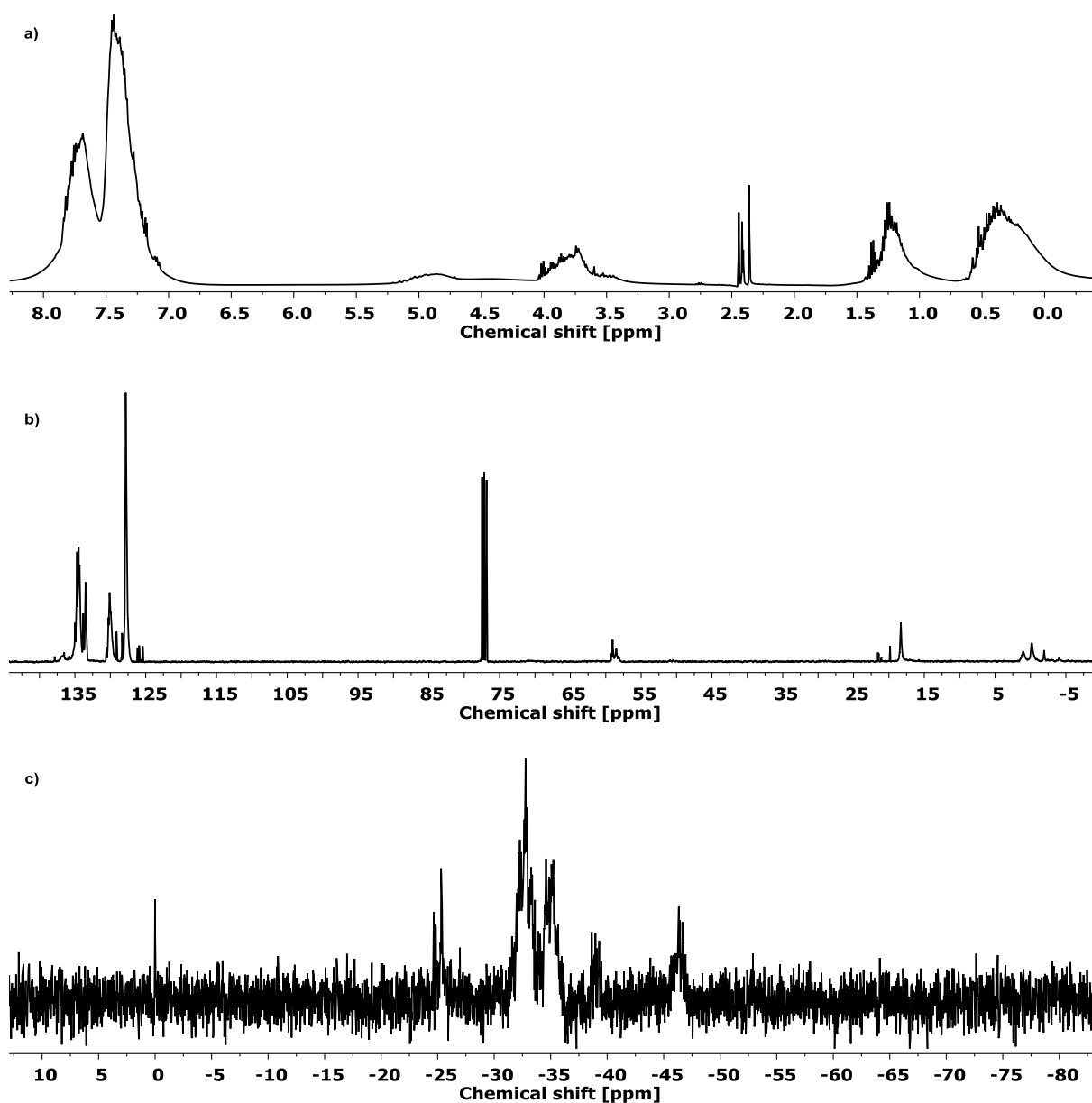
Figure 307: a) ^{1}H (400 MHz, CDCl$_3$), b) ^{13}C (101 MHz, CDCl$_3$) and c) ^{29}Si NMR (79 MHz, CDCl$_3$) of H20_Ta10_PP40_PM30.
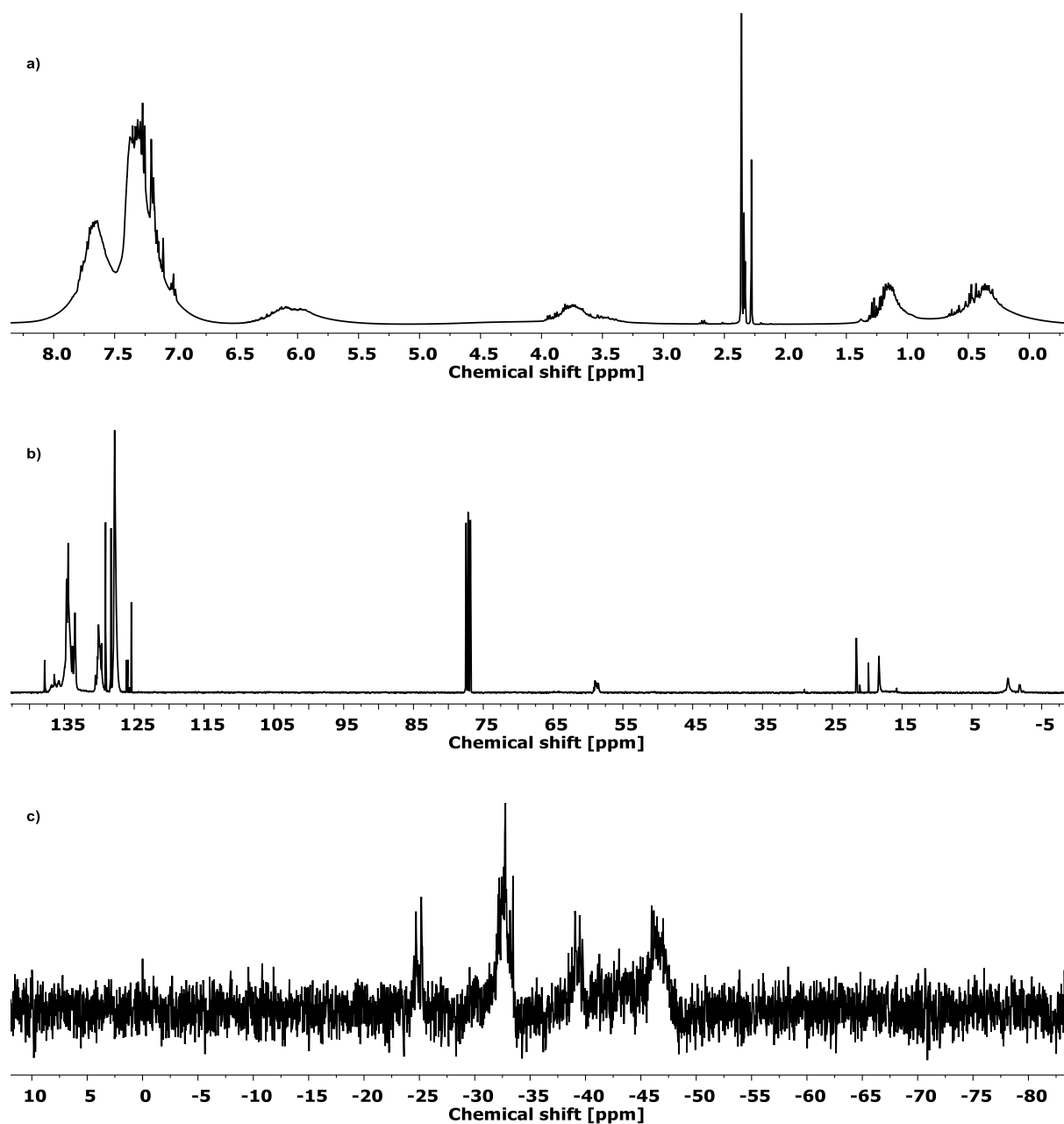
Figure 308: a) ^{1}H (400 MHz, CDCl$_3$), b) ^{13}C (101 MHz, CDCl$_3$) and c) ^{29}Si NMR (79 MHz, CDCl$_3$) of **V20_Ta10_PP40_PM30.**
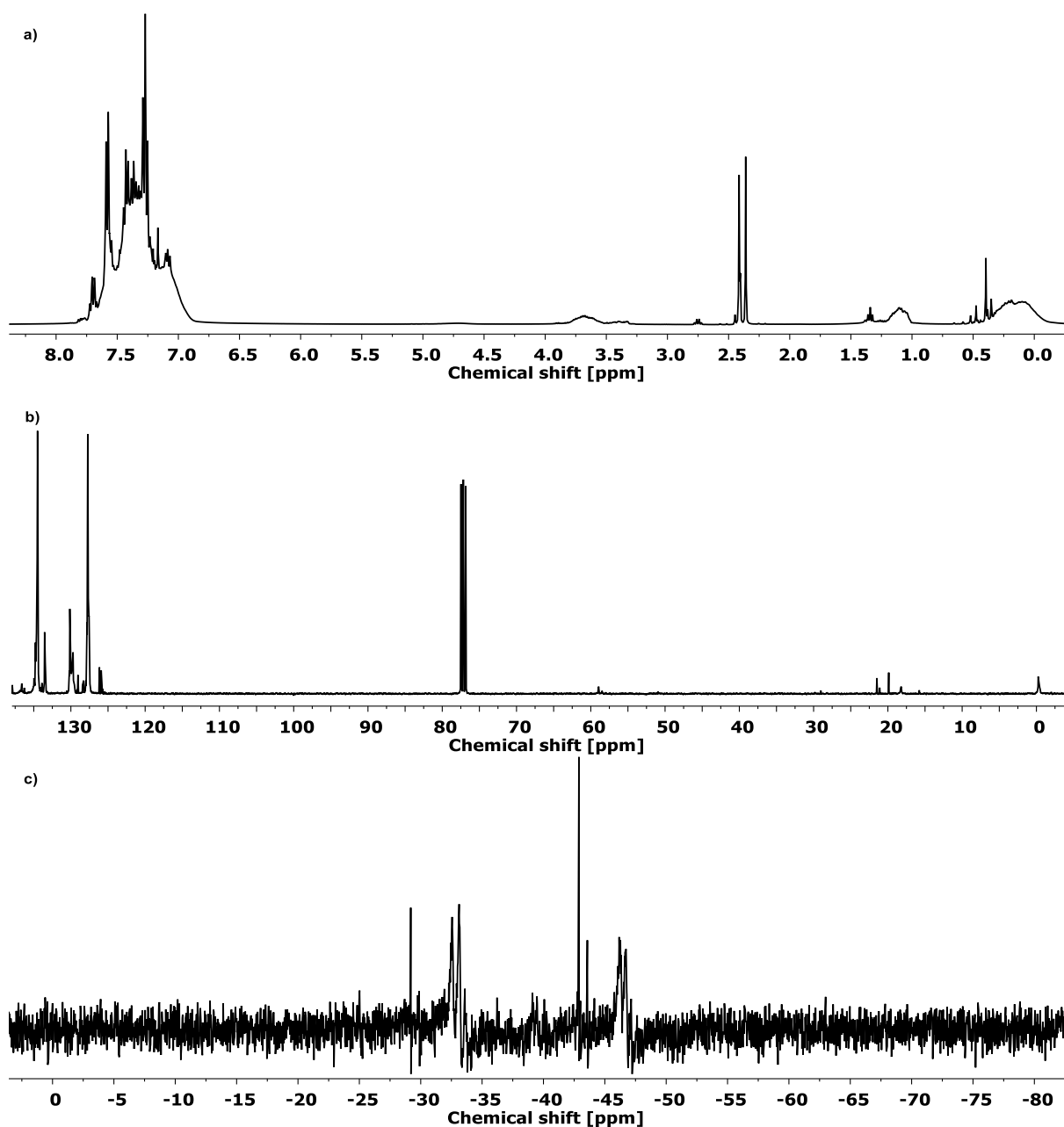
Figure 309: a) ^{1}H (400 MHz, CDCl$_3$), b) ^{13}C (101 MHz, CDCl$_3$) and c) ^{29}Si NMR (79 MHz, CDCl$_3$) of H20_Ta15_PP40_PM25.
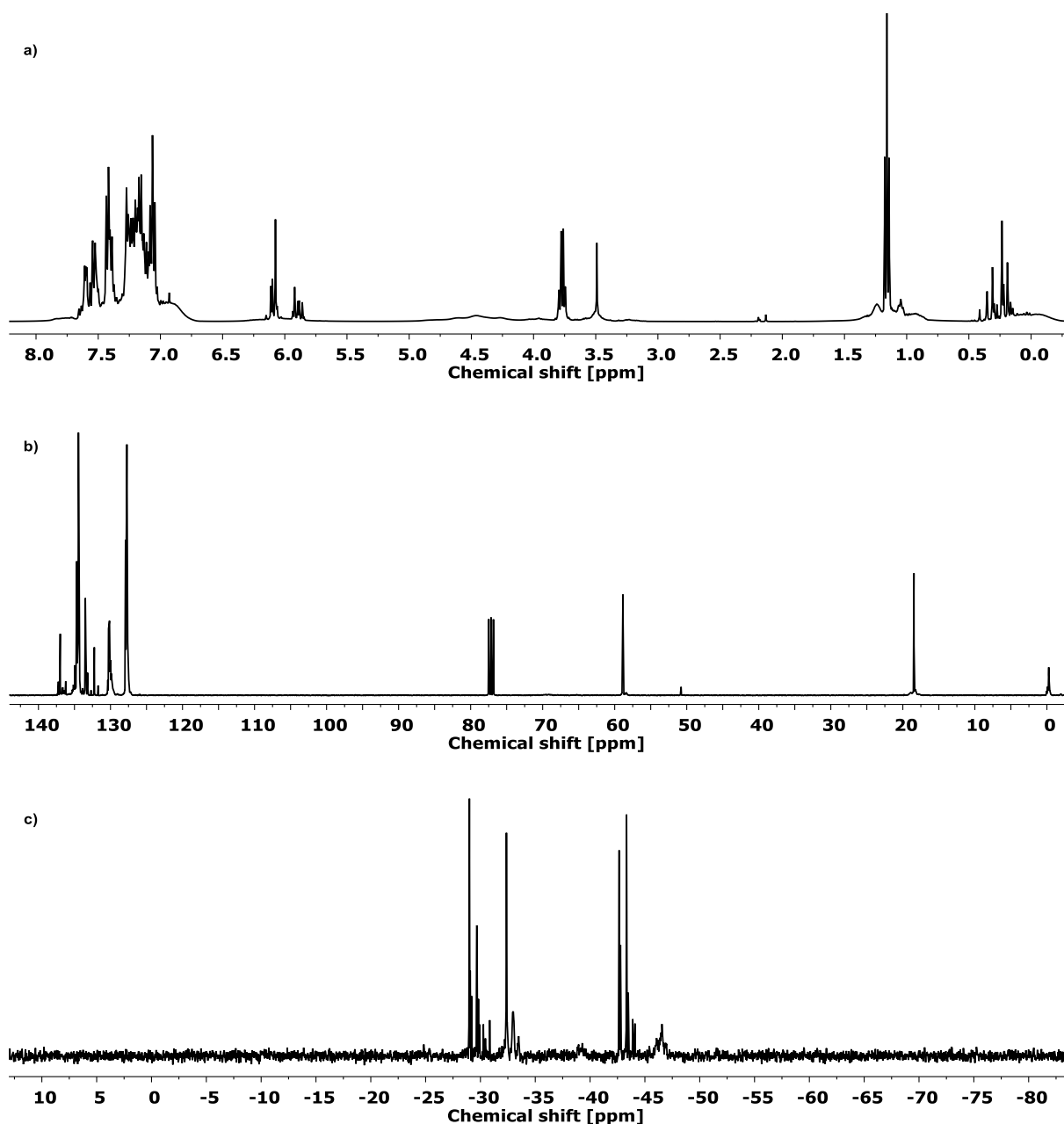
Figure 310: a) ^{1}H (400 MHz, CDCl$_3$), b) ^{13}C (101 MHz, CDCl$_3$) and c) ^{29}Si NMR (79 MHz, CDCl$_3$) of **V20_Ta15_PP40_PM25.**

6.2.6.3.3 TGA curves of the hydride- or vinyl-group and metal atom containing copolymers

All measured TGA curves from the metal atom containing copolymers are shown here, the thermogravimetric measurements under oxygen atmosphere up to 900 °C are shown on the left, and the one under inert atmosphere on the right. The nitrogen atmosphere was maintained up to 800 °C and then switched to oxygen atmosphere and the measurement was continued up to 900 °C.
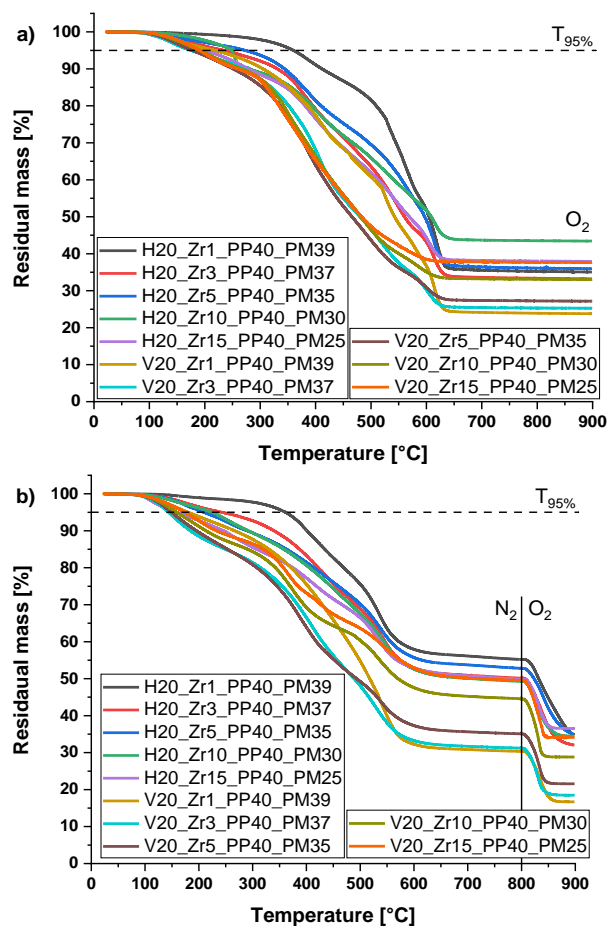
Figure 311: TGA curves of the hydride- or vinyl-group and zirconium atom containing copolymers under a) oxygen and b) nitrogen atmosphere.
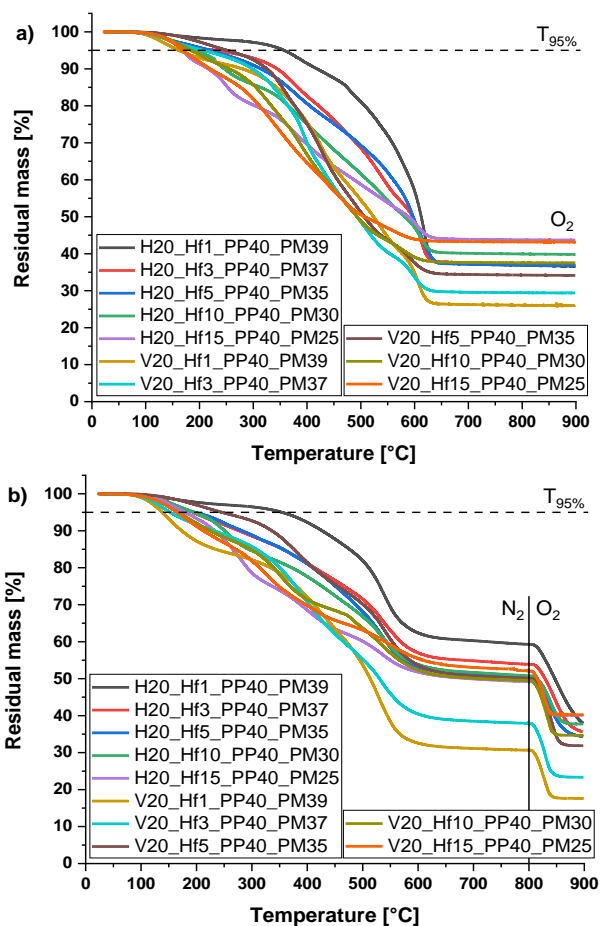
Figure 312: TGA curves of the hydride- or vinyl-group and hafnium atom containing copolymers under a) oxygen and b) nitrogen atmosphere.
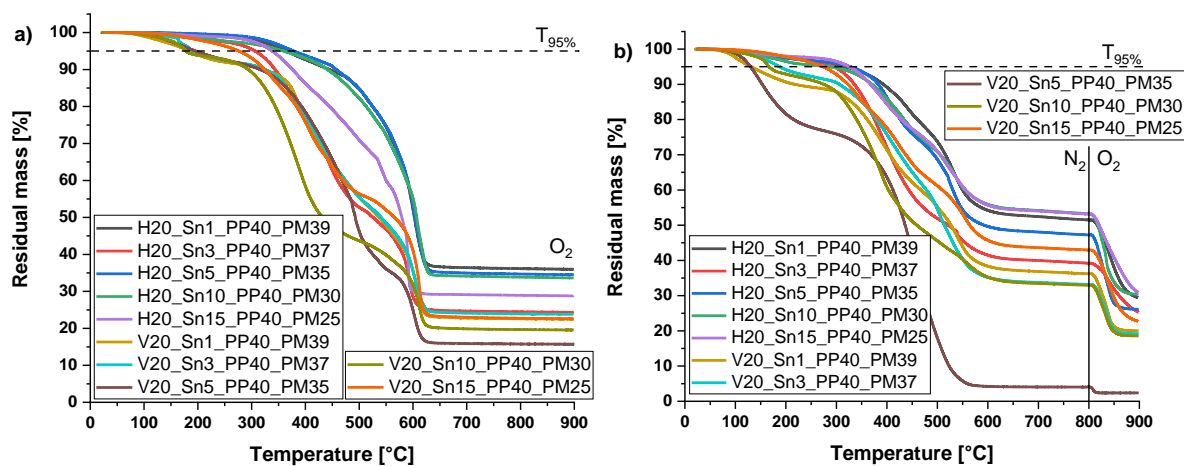
Figure 313: TGA curves of the hydride- or vinyl-group and tin atom containing copolymers under a) oxygen and b) nitrogen atmosphere.
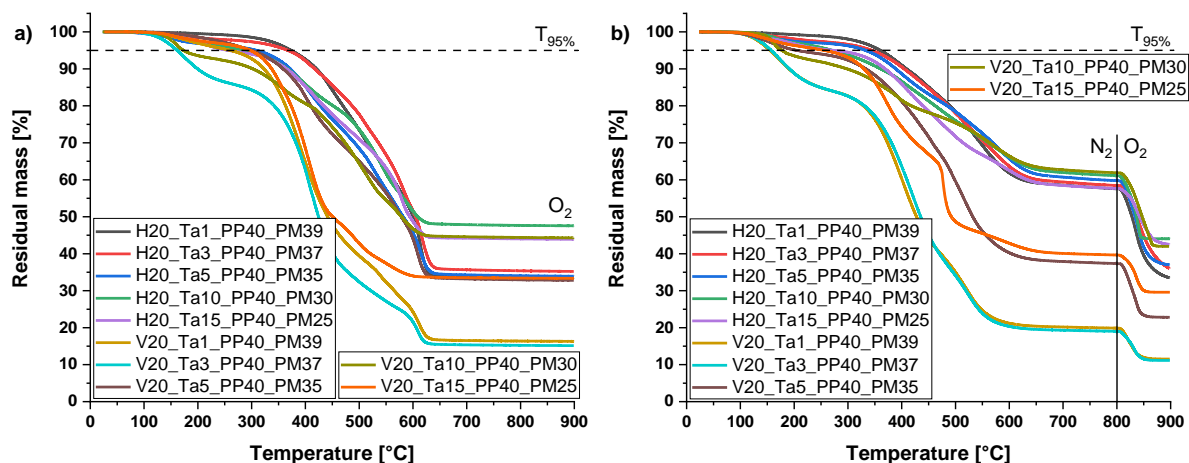
Figure 314: TGA curves of the hydride- or vinyl-group and tantalum atom containing copolymers under a) oxygen and b) nitrogen atmosphere.

6.2.6.3.4 <u>DSC curves of the hydride- or vinyl-group and metal atom containing copolymers</u>

From the DSC curves of the metal atom containing copolymers the first and second heating cycle (h. c.) are shown here. The measurements range from $-100\ °C$ or $-50\ °C$ to $150\ °C$ under nitrogen atmosphere depending on the copolymer.
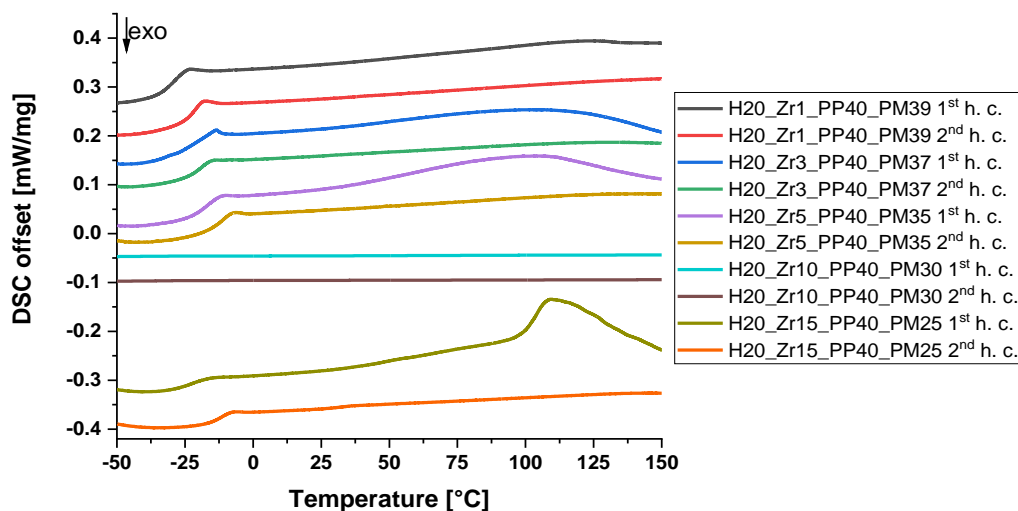
Figure 315: 1st and 2nd heating cycle (h. c.) from DSC curves of the hydride-group and zirconium atom containing copolymers.
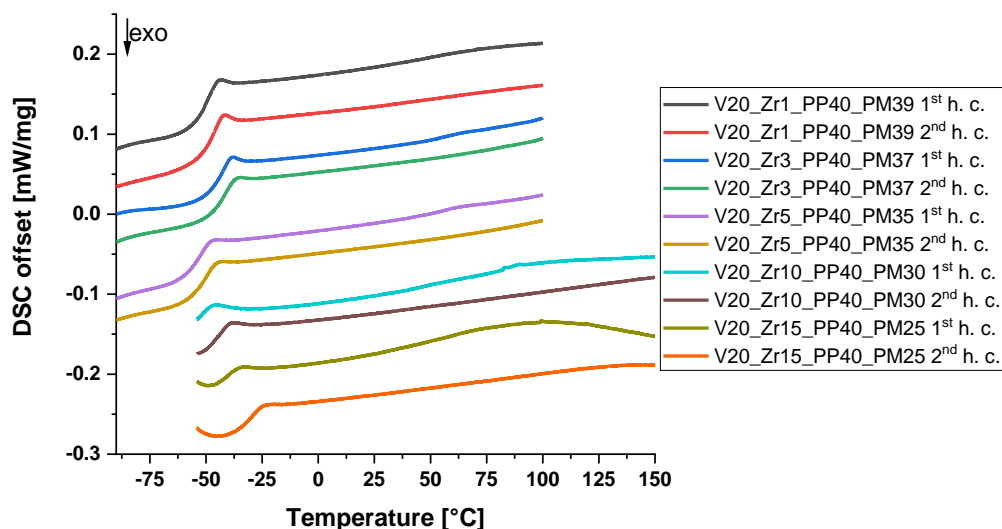
Figure 316: 1st and 2nd heating cycle (h. c.) from DSC curves of the vinyl-group and zirconium atom containing copolymers.
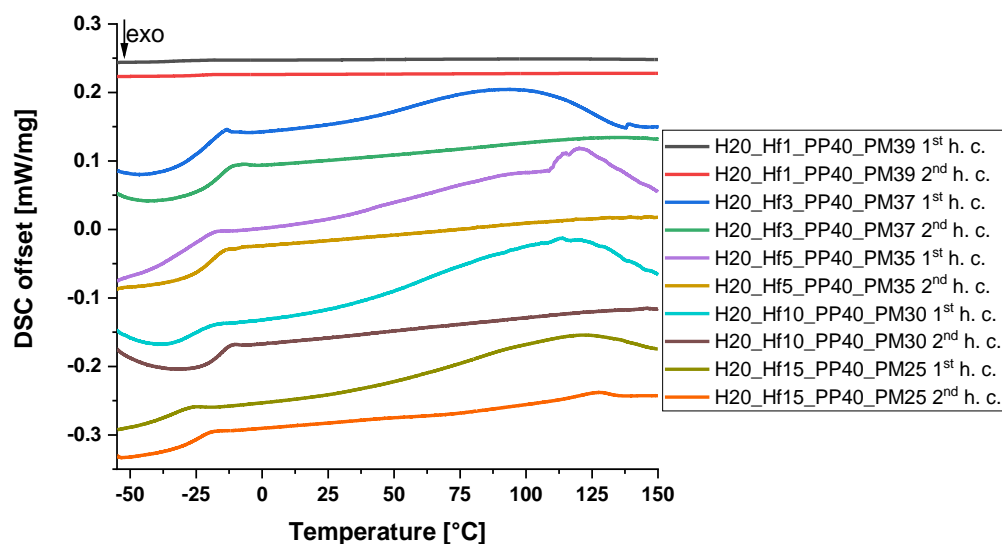
Figure 317: 1st and 2nd heating cycle (h. c.) from DSC curves of the hydride-group and hafnium atom containing copolymers.
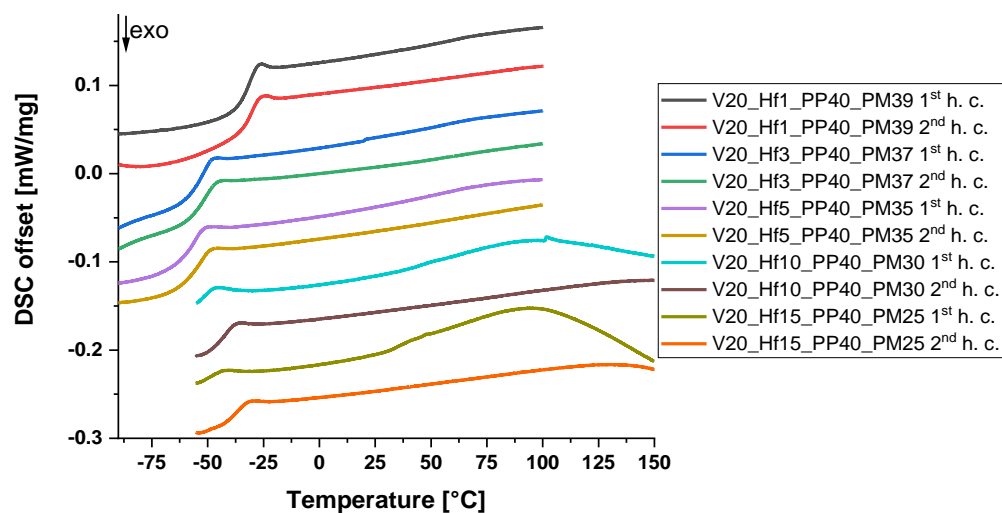
Figure 318: 1st and 2nd heating cycle (h. c.) from DSC curves of the vinyl-group and hafnium atom containing copolymers.
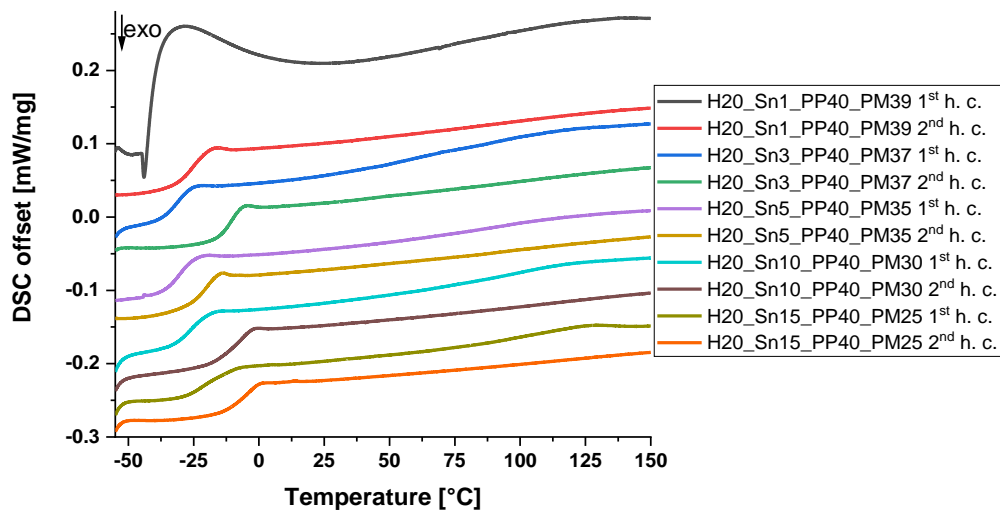
Figure 319: 1st and 2nd heating cycle (h. c.) from DSC curves of the hydride-group and tin atom containing copolymers.
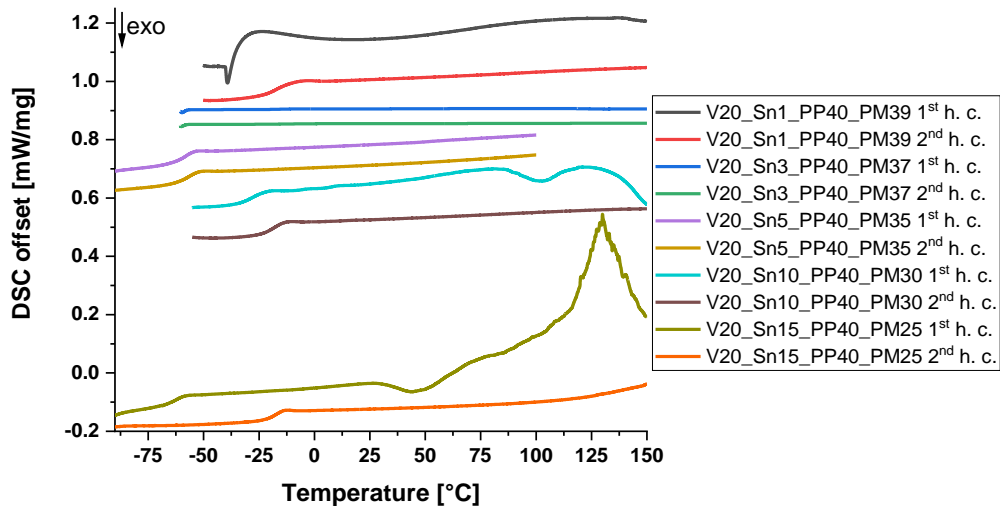
Figure 320: 1st and 2nd heating cycle (h. c.) from DSC curves of the vinyl-group and tin atom containing copolymers.
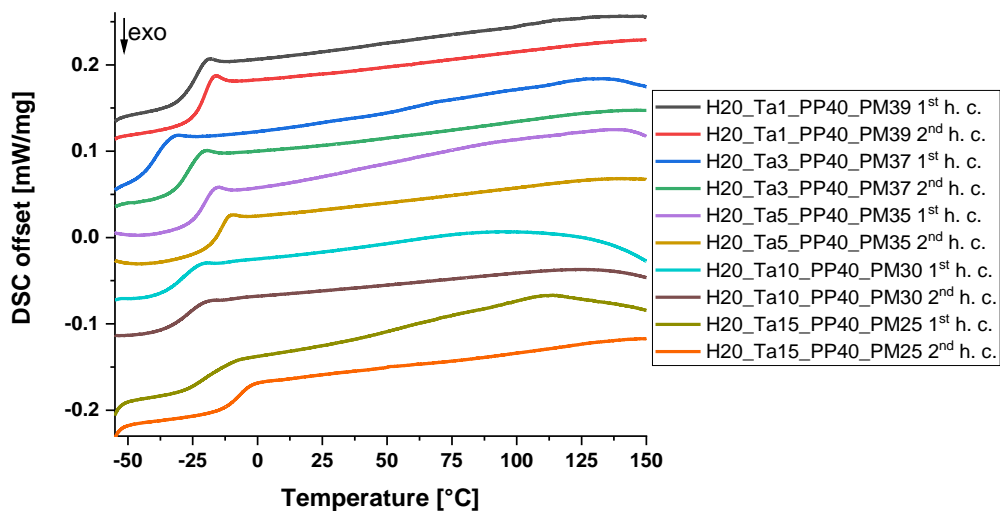
Figure 321: 1st and 2nd heating cycle (h. c.) from DSC curves of the hydride-group and tantalum atom containing copolymers.
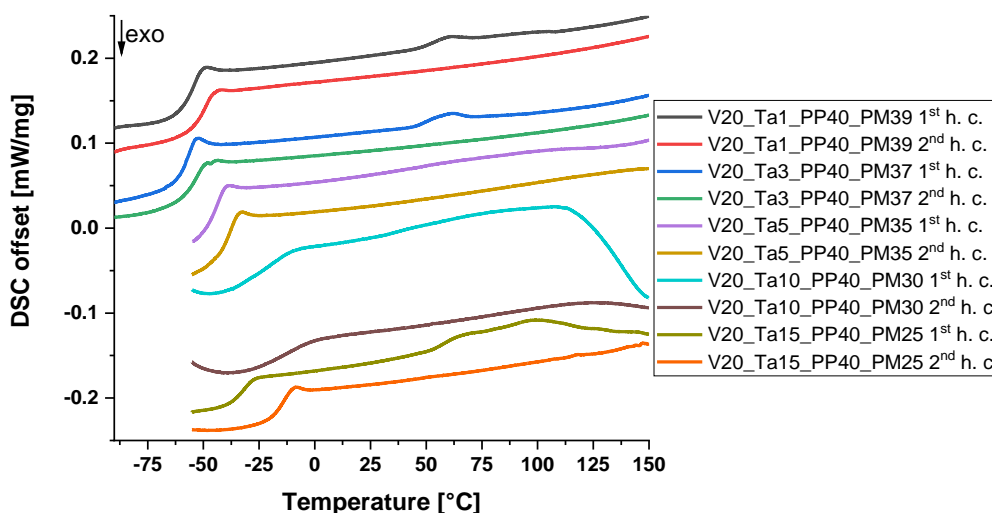
Figure 322: 1st and 2nd heating cycle (h. c.) from DSC curves of the vinyl-group and tantalum atom containing copolymers.

6.2.6.4 Cured metal atom containing polysiloxanes

400 mg each of a hydride and a vinyl copolymer were mixed with 2.5 µL of the platinum stock solution (1.63 ppm), which was prepared using 6 µL of *Ossko*'s platinum catalyst and 10 µL of xylene. After degassing for 30 min at 2 mbar, the polymer was doctor bladed onto a cleaned microscope glass slide. The polymer film was cured for one hour at 80 °C, one hour at 100 °C and six hours at 150 °C.

P20_Met0_PP40_PM40:
RI: 1.5833.

6.2.6.4.1 Zirconium
P20_Zr1_PP40_PM39:
RI: 1.5848.

P20_Zr1.5_PP40_PM38.5:
RI: 1.5820.

P20_Zr2.5_PP40_PM37.5:
RI: 1.5852.

P20_Zr3_PP40_PM37:
RI: 1.5879.

P20_Zr5_PP40_PM35:
RI: 1.5855.

P20_Zr5H_PP40_PM35:

RI: 1.5855.

P20_Zr7.5_PP40_PM32.5:

RI: not determinable.

P20_Zr10_PP40_PM30:

RI: not determinable.

P20_Zr15_PP40_PM25:

RI: not determinable.

6.2.6.4.2 <u>Hafnium</u>

P20_Hf1_PP40_PM39:

RI: 1.5856.

P20_Hf1.5_PP40_PM38.5:

RI: 1.5825.

P20_Hf2.5_PP40_PM37.5:

RI: 1.5730.

P20_Hf3_PP40_PM37:

RI: 1.5826.

P20_Hf5_PP40_PM35:

RI: not determinable.

P20_Hf5H_PP40_PM35:

RI: 1.5860.

P20_Hf7.5_PP40_PM32.5:

RI: 1.5850.

P20_Hf10_PP40_PM30:

RI: 1.5865.

P20_Hf15_PP40_PM25:

RI: not determinable.

6.2.6.4.3 Tin

P20_Sn1_PP40_PM39:

RI: 1.5821.

P20_Sn1.5_PP40_PM38.5:

RI: 1.5825.

P20_Sn2.5_PP40_PM37.5:

RI: 1.5820.

P20_Sn3_PP40_PM37:

RI: not determinable.

P20_Sn5_PP40_PM35:

RI: not determinable.

P20_Sn5H_PP40_PM35:

RI: not determinable.

P20_Sn7.5_PP40_PM32.5:

RI: not determinable.

P20_Sn10_PP40_PM30:

RI: not determinable.

P20_Sn15_PP40_PM25:

RI: not determinable.

6.2.6.4.4 Tantalum

P20_Ta1_PP40_PM39:

RI: 1.5864.

P20_Ta1.5_PP40_PM38.5:

RI: 1.5800.

P20_Ta2.5_PP40_PM37.5:

RI: 1.5815.

P20_Ta3_PP40_PM37:

RI: 1.5886.

P20_Ta5_PP40_PM35:

RI: 1.5930.

P20_Ta5H_PP40_PM35:

RI: 1.5750.

P20_Ta7.5_PP40_PM32.5:

RI: 1.5884.

P20_Ta10_PP40_PM30:

RI: 1.5700.

P20_Ta15_PP40_PM25:

RI: not determinable.

6.2.6.5 *Additional experimental data for the cured metal atom containing polysiloxanes*

6.2.6.5.1 FT-IR spectra of the metal atom containing and cured polysiloxanes
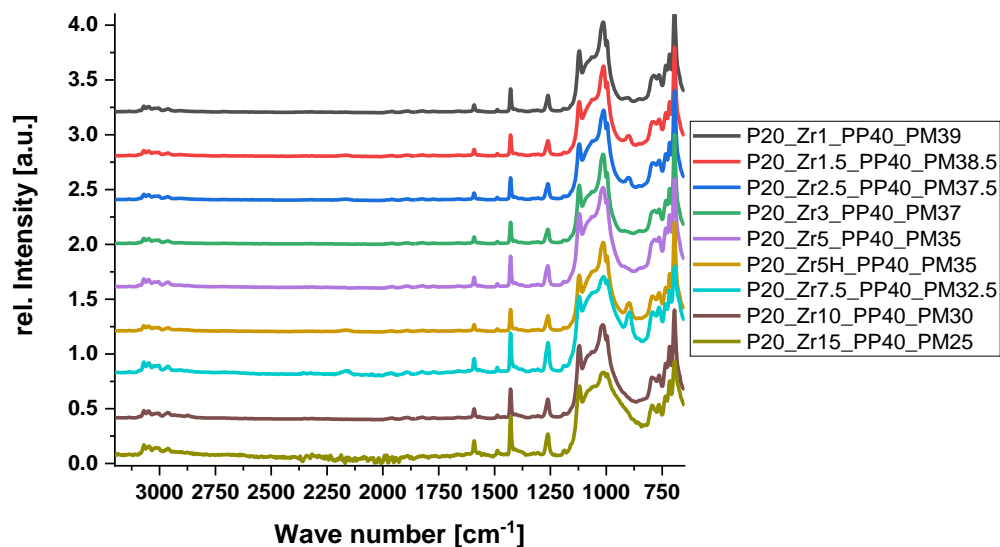
Figure 323: FT-IR spectra of the zirconium atom containing cured polysiloxanes.
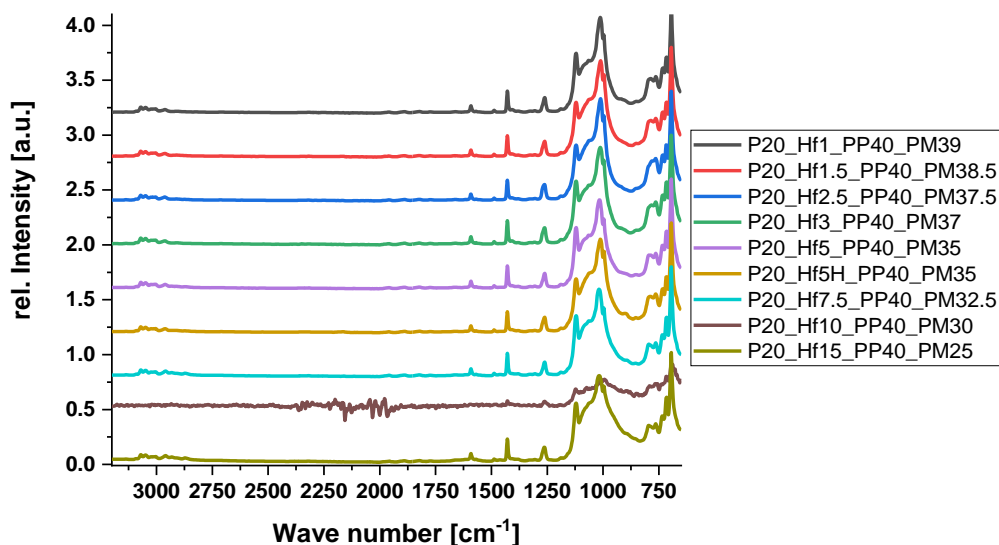
Figure 324: FT-IR spectra of the hafnium atom containing cured polysiloxanes.
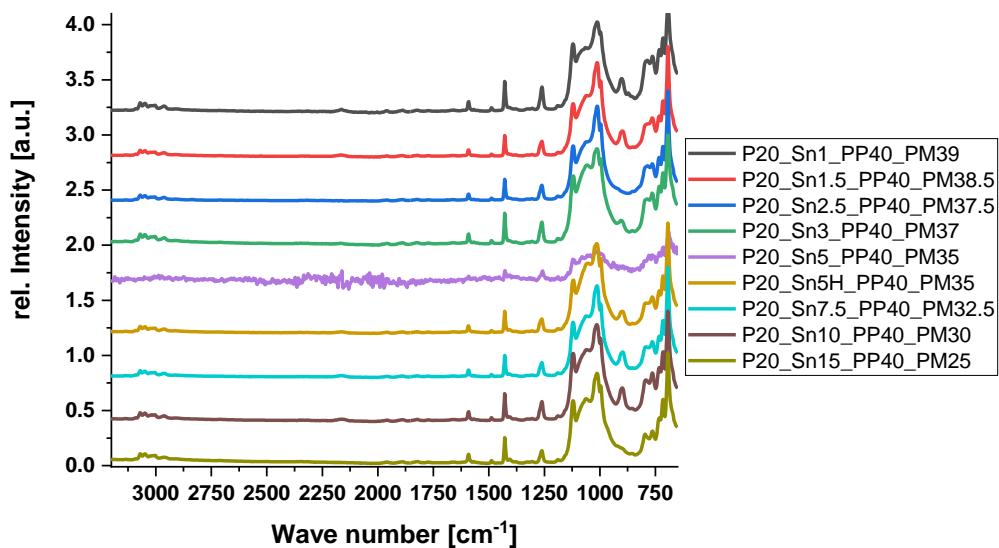
Figure 325: FT-IR spectra of the tin containing cured polysiloxanes.
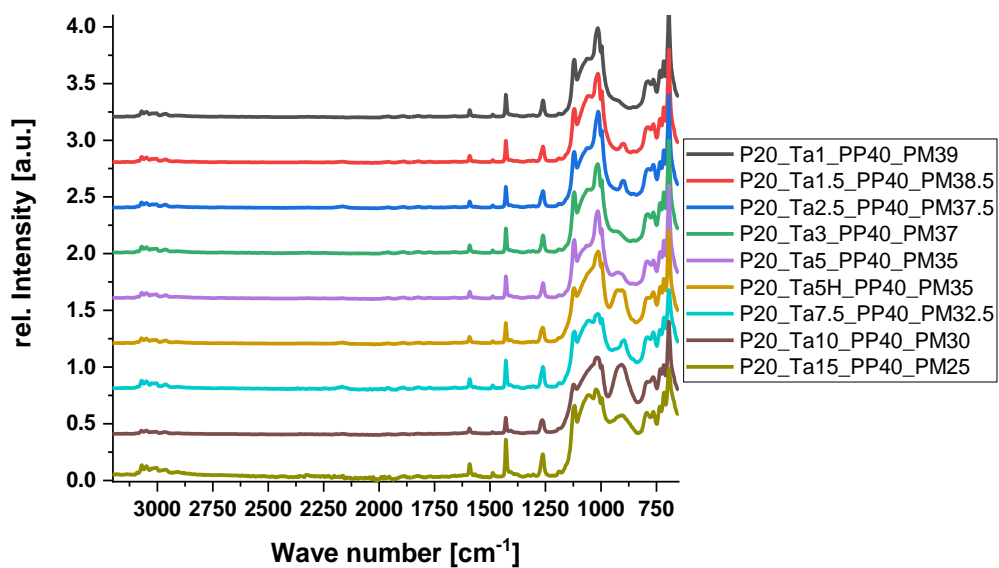
Figure 326: FT-IR spectra of the tantalum containing cured polysiloxanes.

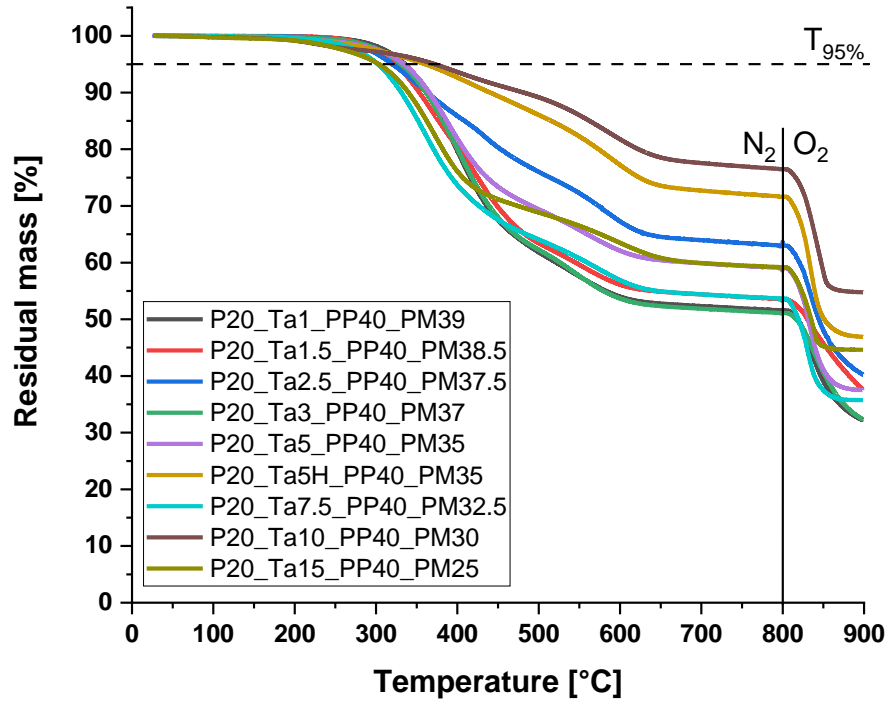**6.2.6.5.2 TGA curves of the metal atom containing polysiloxanes**
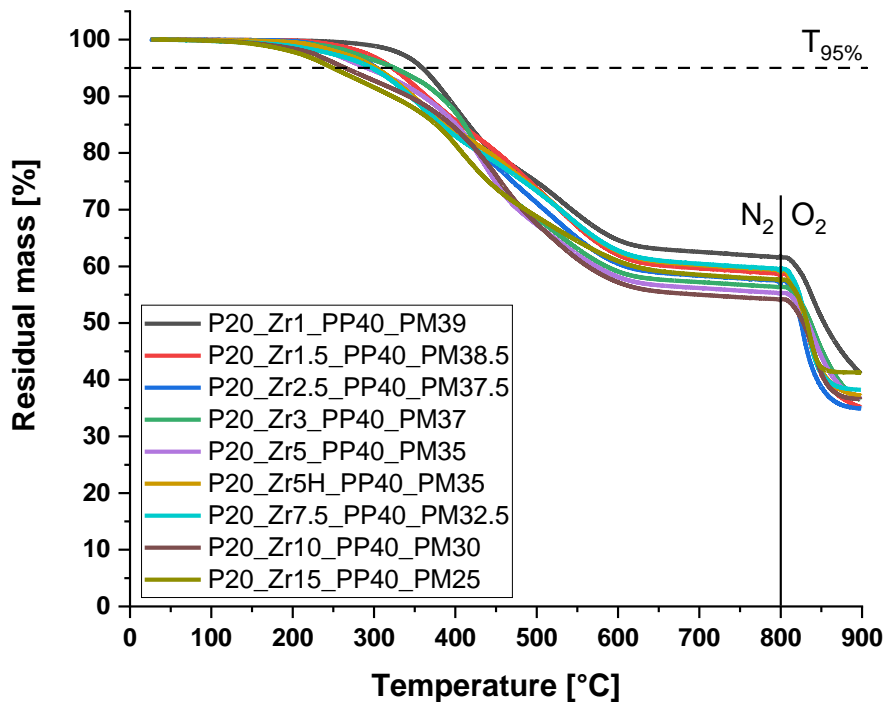
Figure 327: TGA curves of the zirconium atom containing polysiloxanes under nitrogen atmosphere.
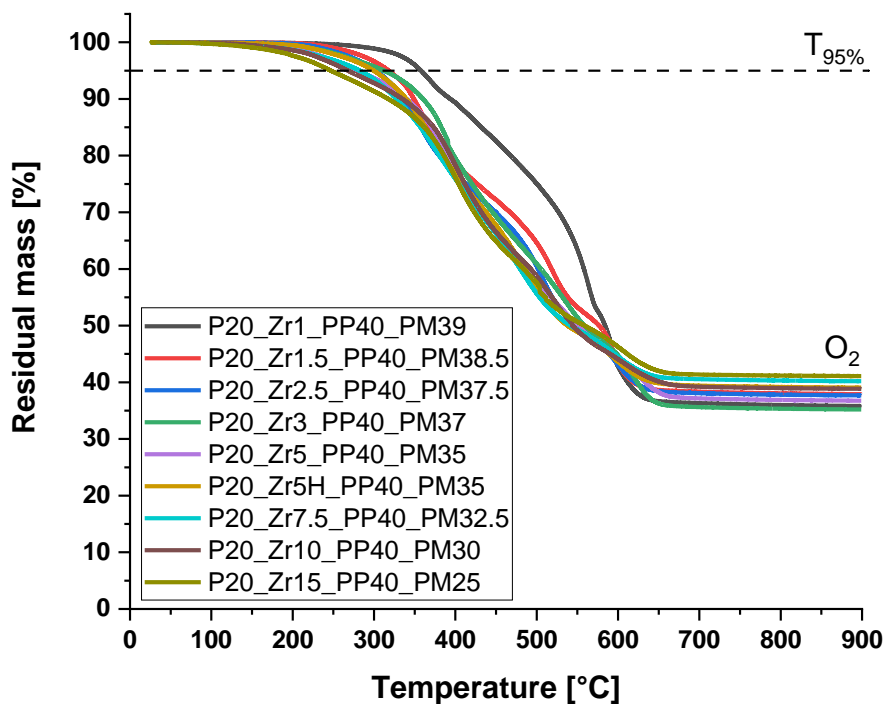
Figure 328: TGA curves of the zirconium atom containing polysiloxanes under oxygen atmosphere.
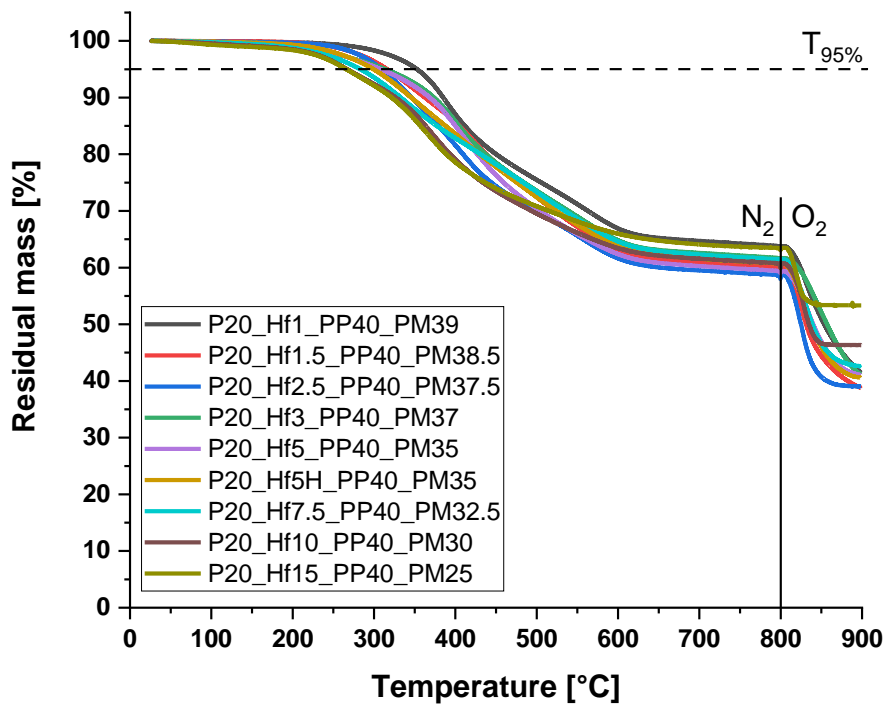
Figure 329: TGA curves of the hafnium atom containing polysiloxanes under nitrogen atmosphere.
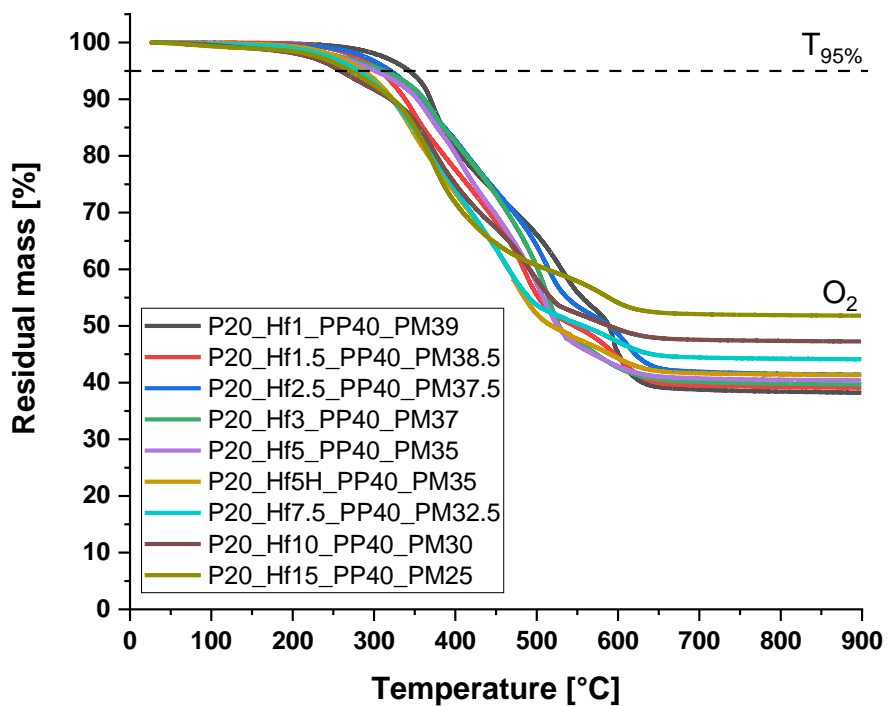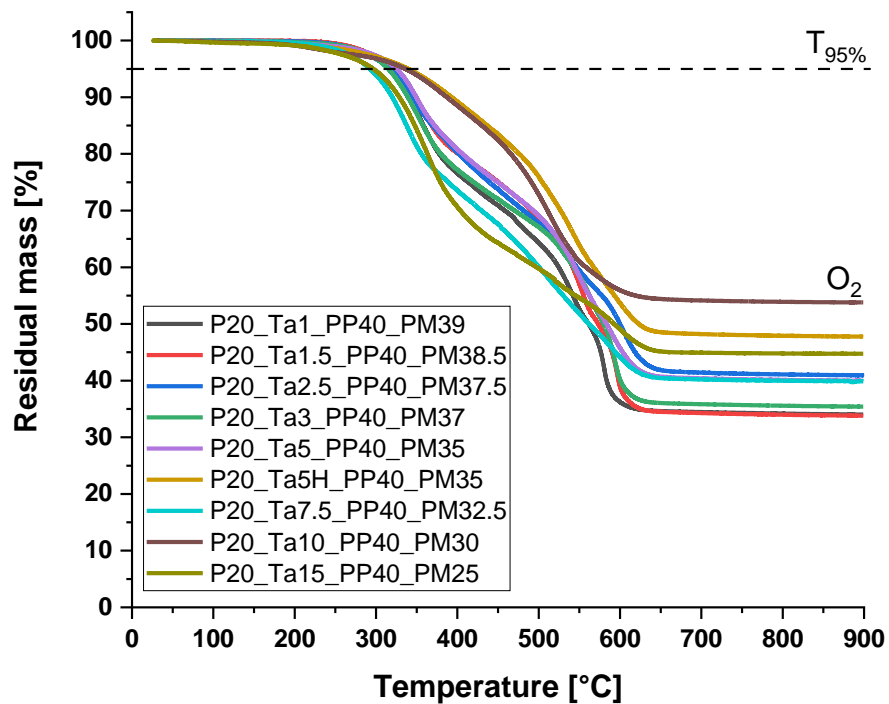

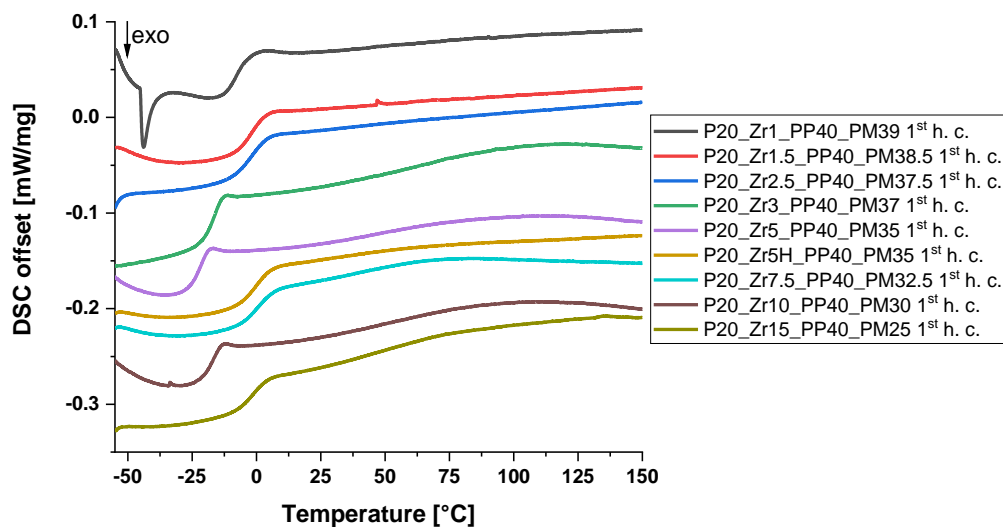**Figure 330: TGA curves of the hafnium atom containing polysiloxanes under oxygen atmosphere.**
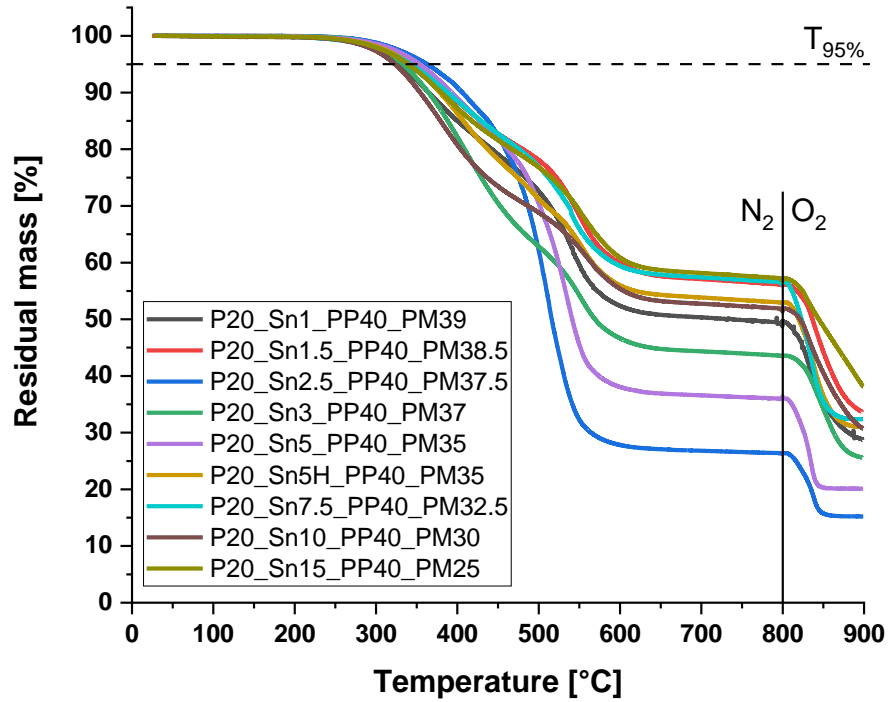
Figure 331: TGA curves of the tin atom containing polysiloxanes under nitrogen atmosphere.
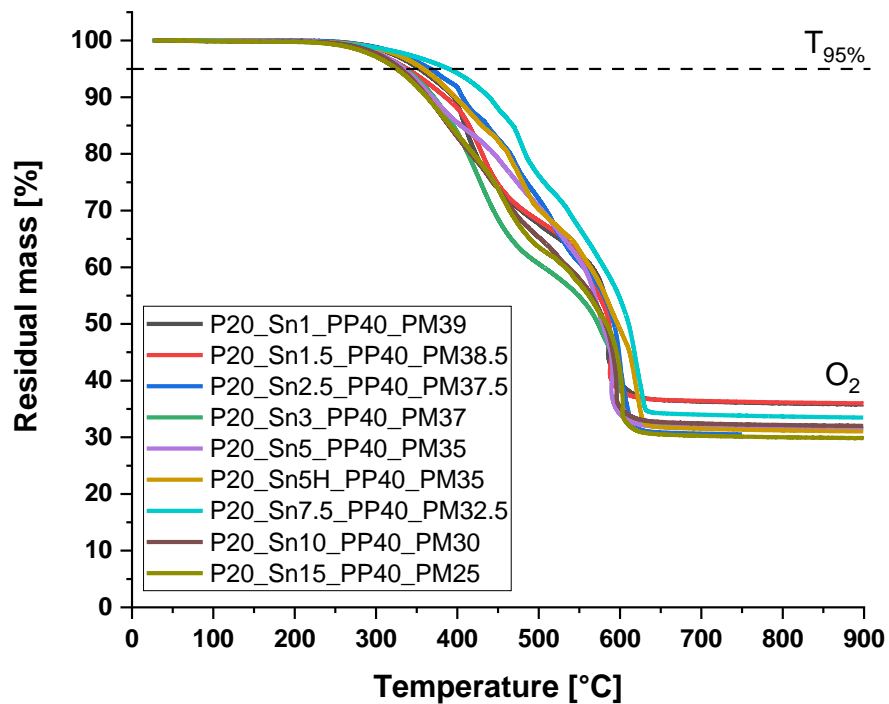
Figure 332: TGA curves of the tin atom containing polysiloxanes under oxygen atmosphere.

Figure 333: TGA curves of the tantalum atom containing polysiloxanes under nitrogen atmosphere.

Figure 334: TGA curves of the tantalum atom containing polysiloxanes under oxygen atmosphere.

6.2.6.5.3 DSC curves of the metal atom containing polysiloxanes

Figure 335: 1st heating cycle (h. c.) of the DSC curves of the cured zirconium atom containing polysiloxanes.
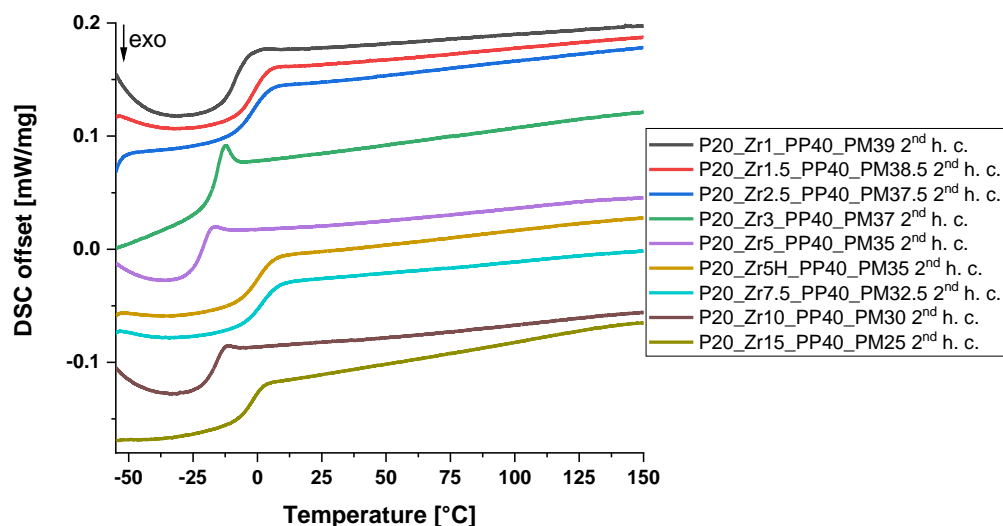
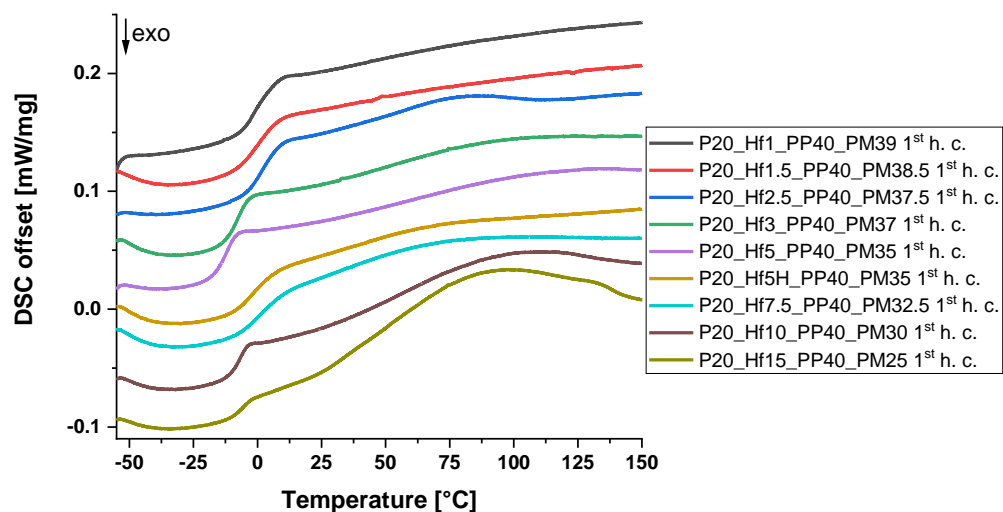**Figure 336: 2nd heating cycle (h. c.) of the DSC curves of the cured zirconium atom containing polysiloxanes.**

Figure 337: 1st heating cycle (h. c.) of the DSC curves of the cured hafnium atom containing polysiloxanes.
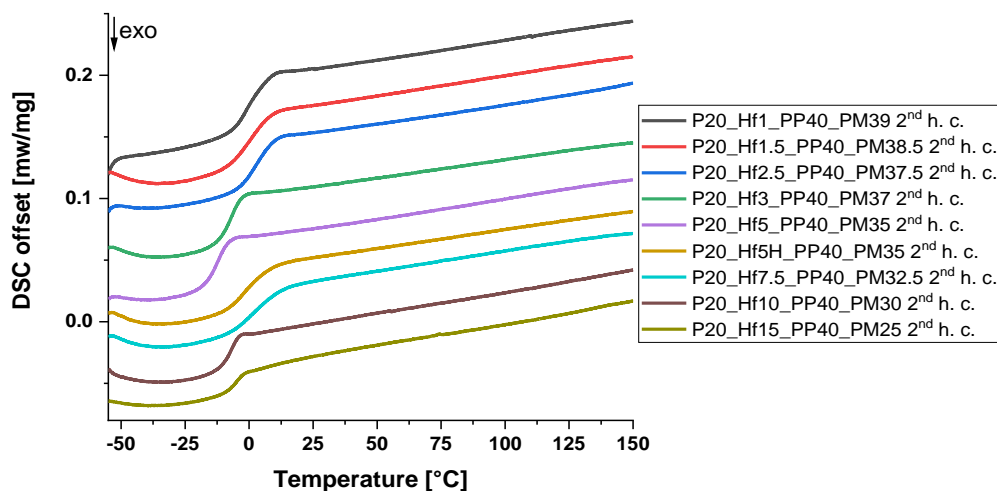
Figure 338: 2nd heating cycle (h. c.) of the DSC curves of the cured hafnium atom containing polysiloxanes.
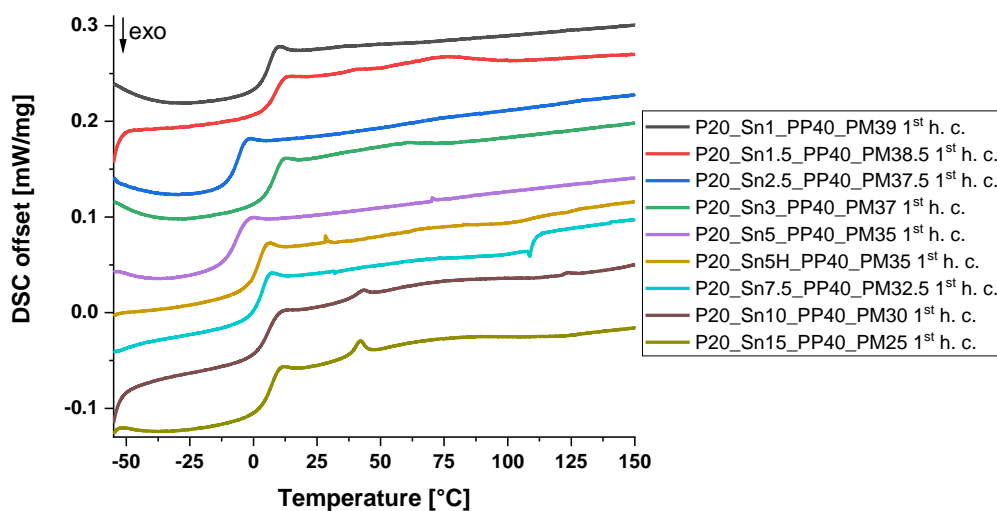

Figure 339: 1st heating cycle (h. c.) of the DSC curves of the cured tin atom containing polysiloxanes.
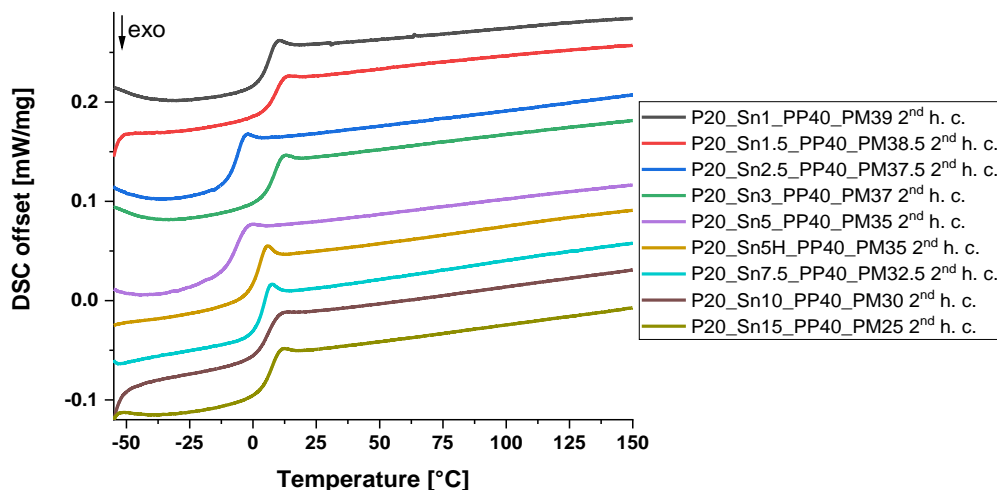

Figure 340: 2nd heating cycle (h. c.) of the DSC curves of the cured tin atom containing polysiloxanes.
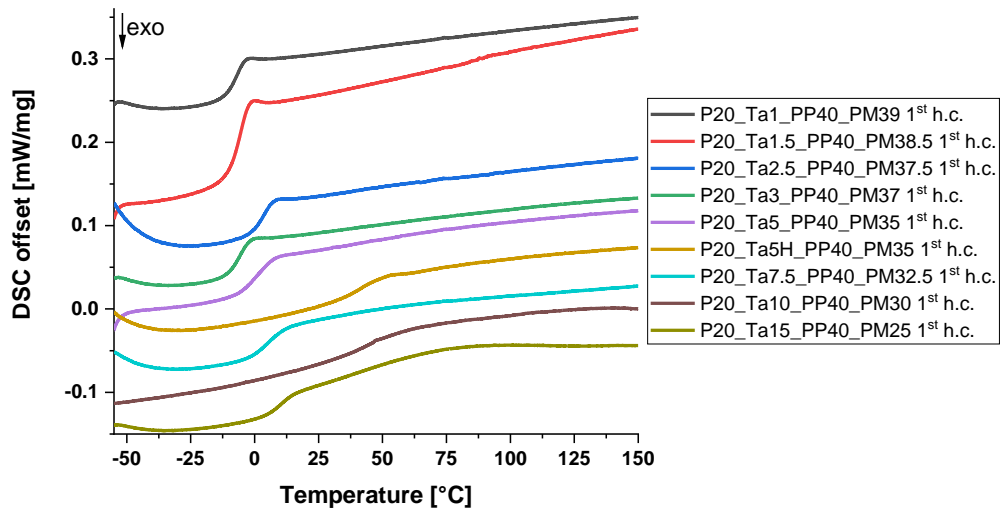
Figure 341: 1ˢᵗ heating cycle (h. c.) of the DSC curves of the cured tantalum atom containing polysiloxanes.
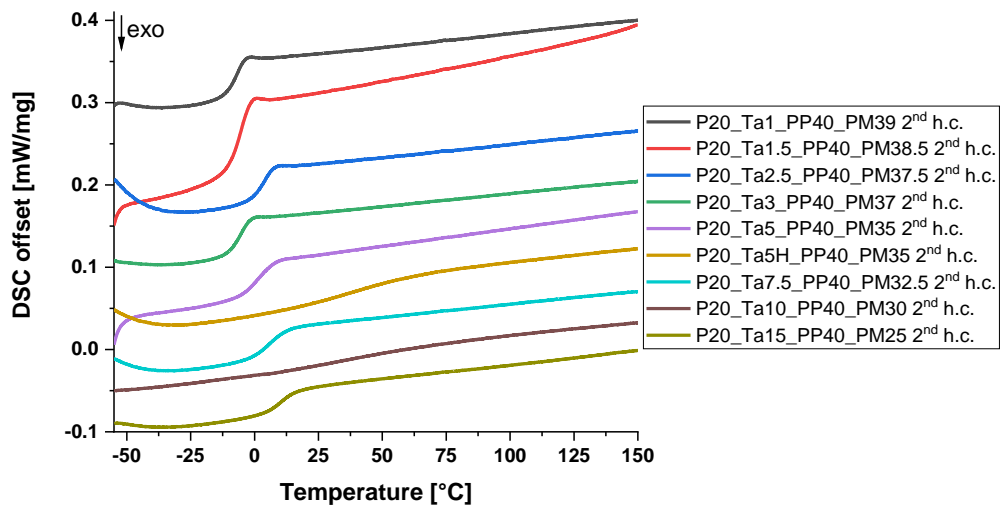

Figure 342: 2ⁿᵈ heating cycle (h. c.) of the DSC curves of the cured tantalum atom containing polysilox-anes.
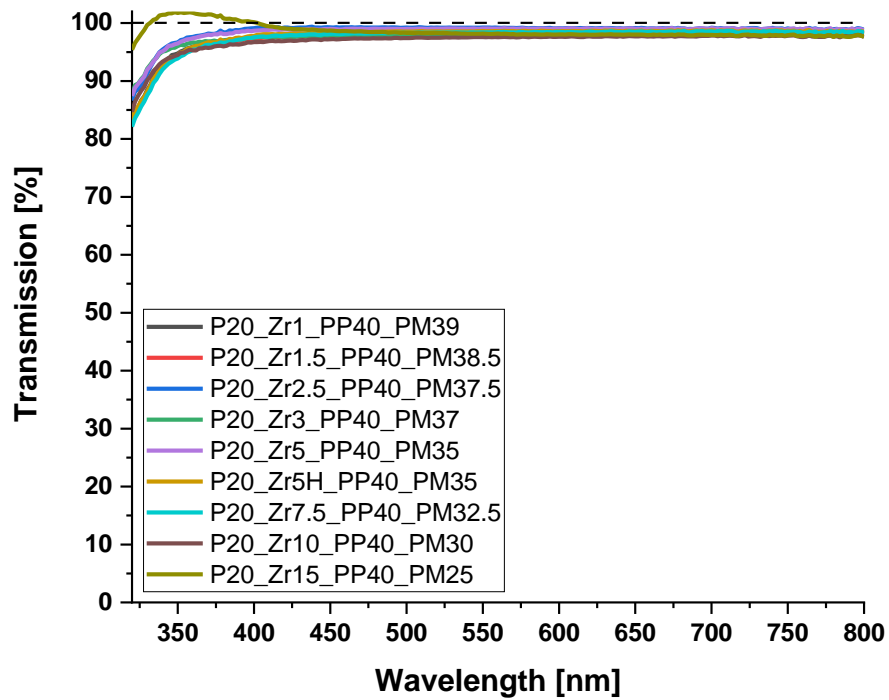
6.2.6.5.4 UV/Vis measurements

Figure 343: UV/Vis measurements curves of the zirconium atom containing polysiloxanes.

Figure 344: UV/Vis measurements curves of the hafnium atom containing polysiloxanes.
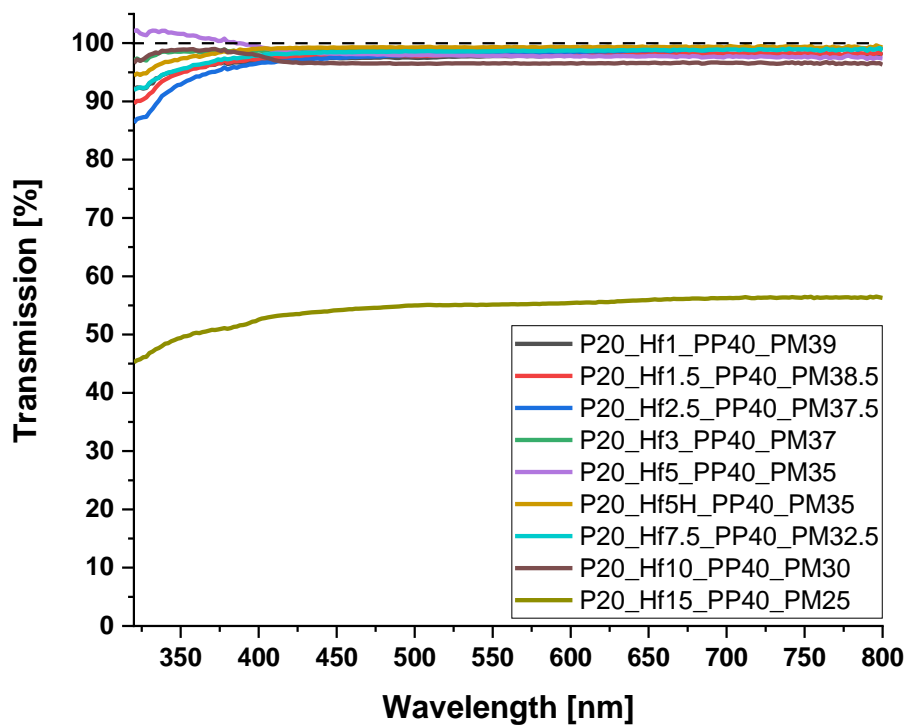
Figure 345: UV/Vis measurements curves of the tin atom containing polysiloxanes.

Figure 346: UV/Vis measurements curves of the tantalum atom containing polysiloxanes.
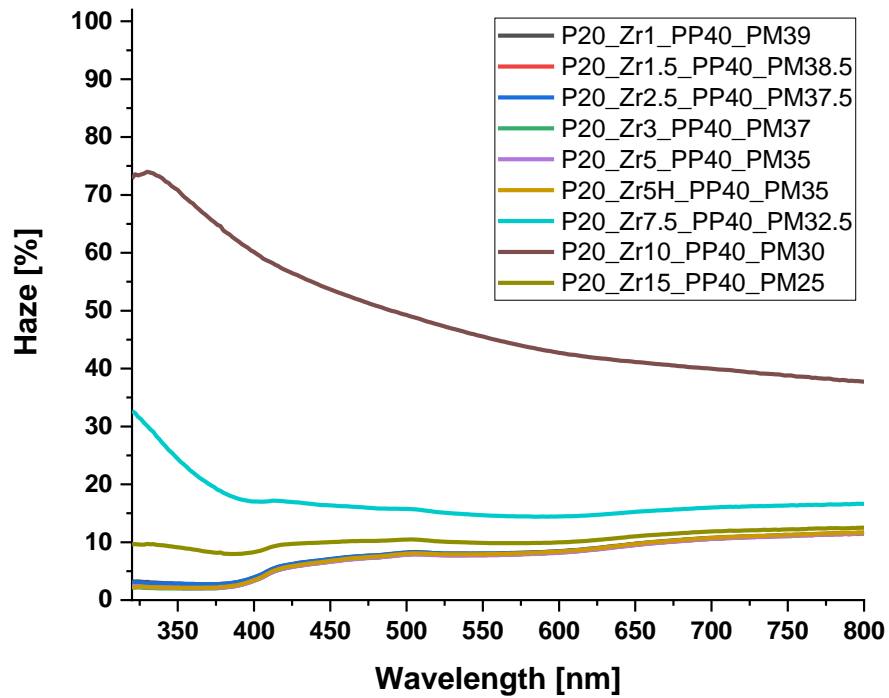
Figure 347: Calculated haze curves of the zirconium atom containing polysiloxanes.

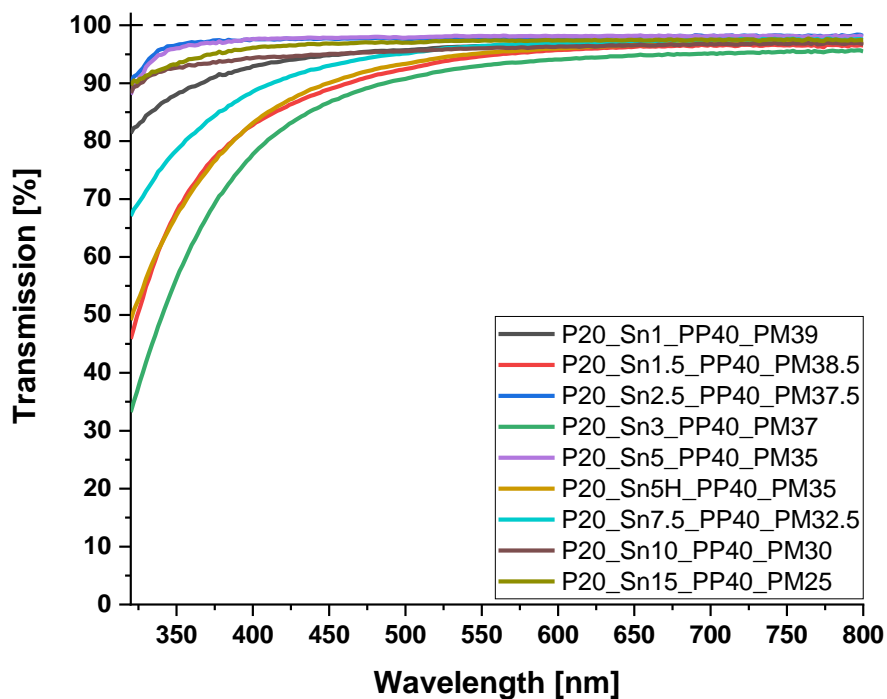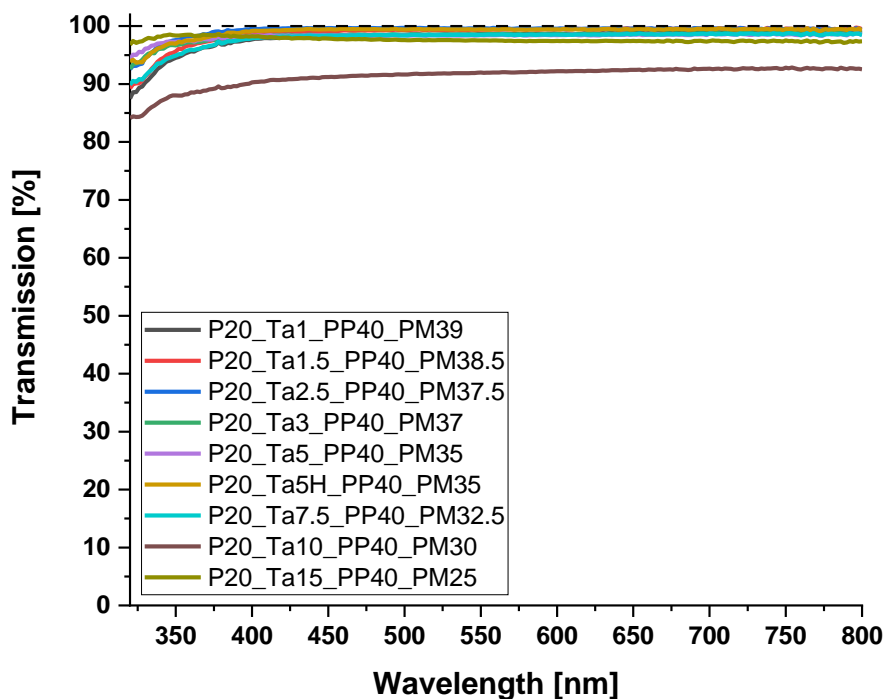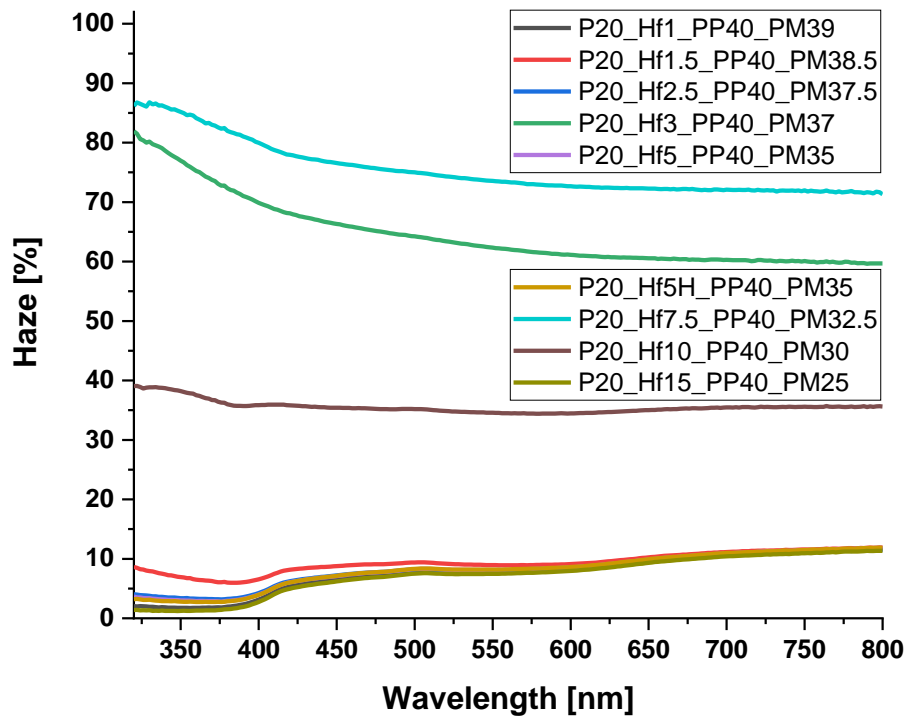**Figure 348: Calculated haze curves of the hafnium atom containing polysiloxanes.**
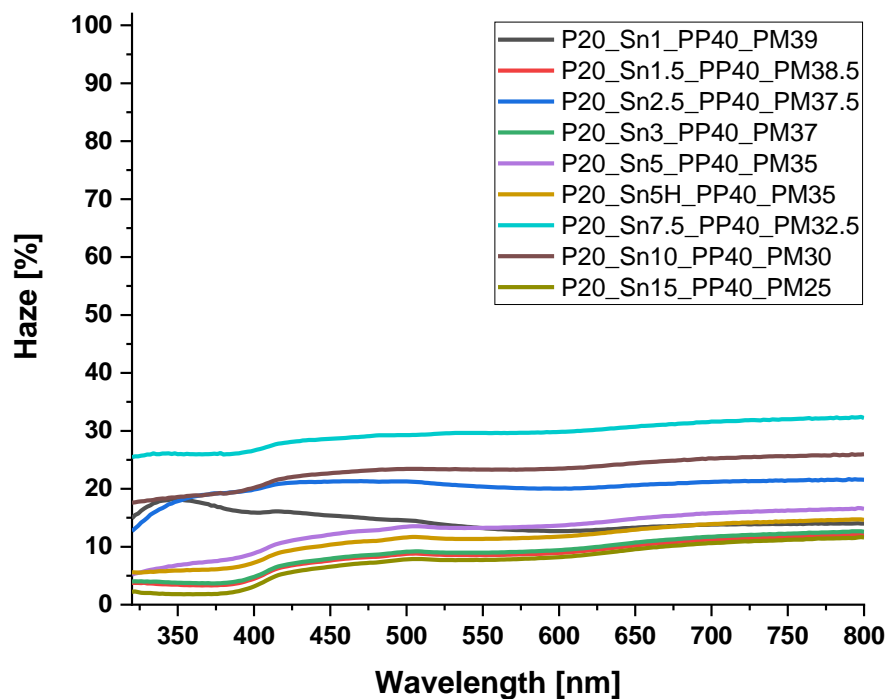
Figure 349: Calculated haze curves of the tin atom containing polysiloxanes.
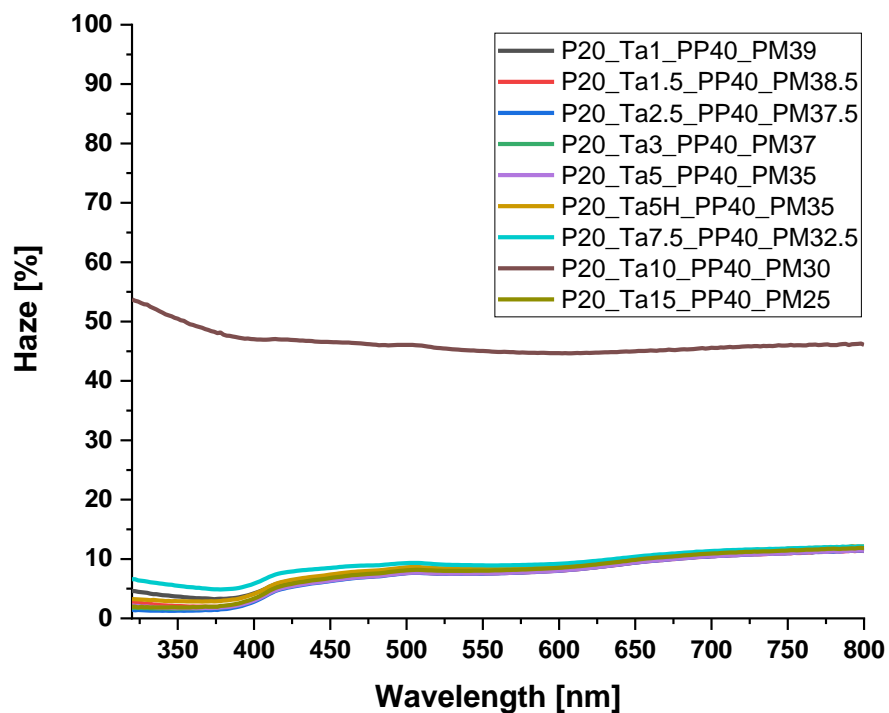
Figure 350: Calculated haze curves of the tantalum atom containing polysiloxanes.

6.2.6.5.5 Haze values during the thermal aging
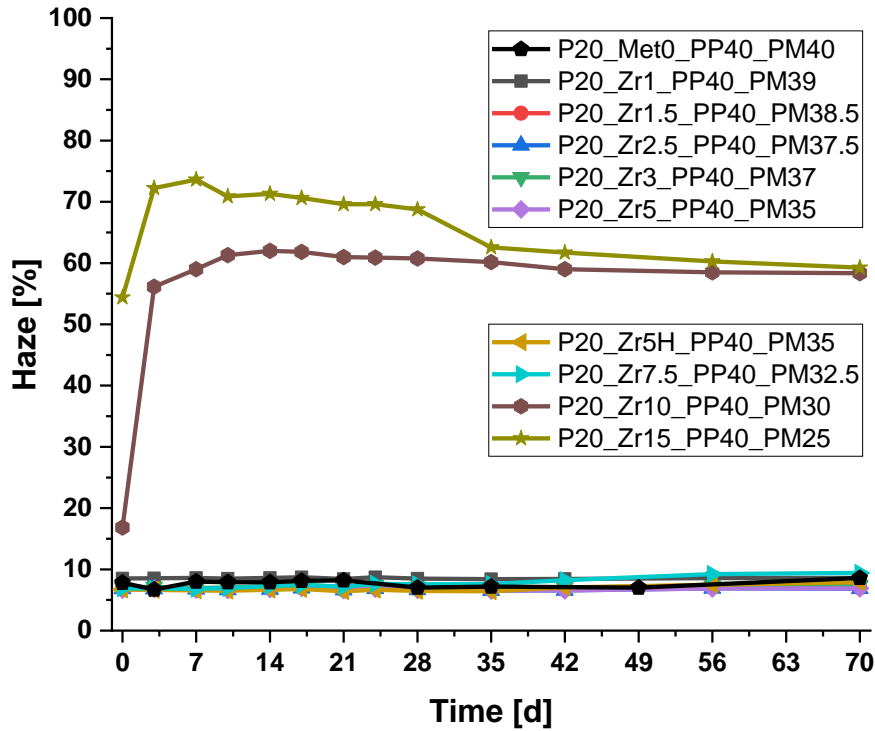
Figure 351: Haze values at 450 nm of the metal-free and the zirconium atom containing samples during the thermal treatment at 180 °C for 70 days.
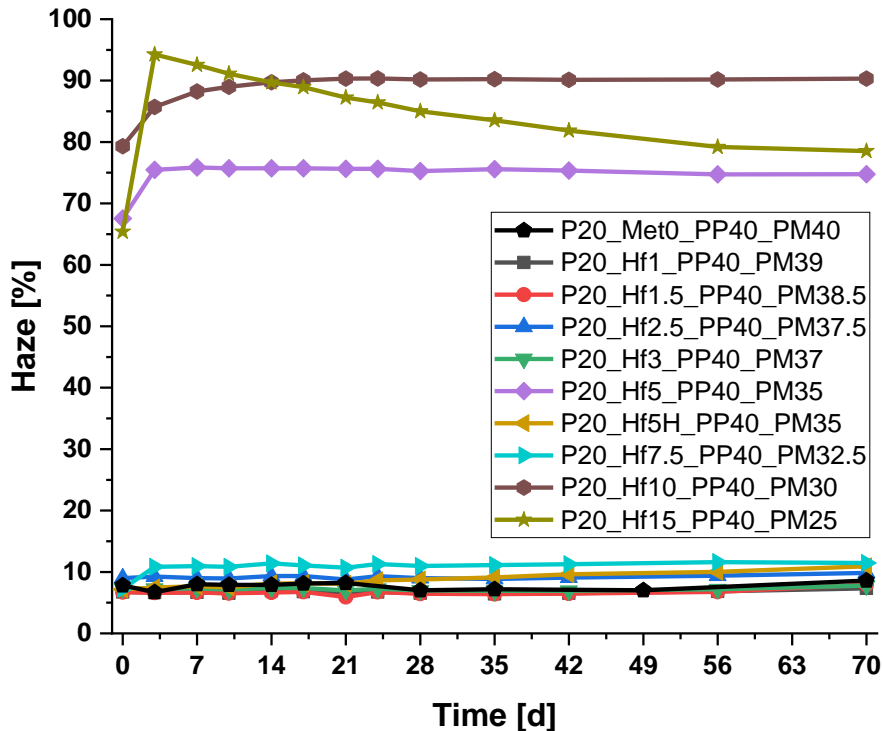
Figure 352: Haze values at 450 nm of the metal-free and the hafnium atom containing samples during the thermal treatment at 180 °C for 70 days.
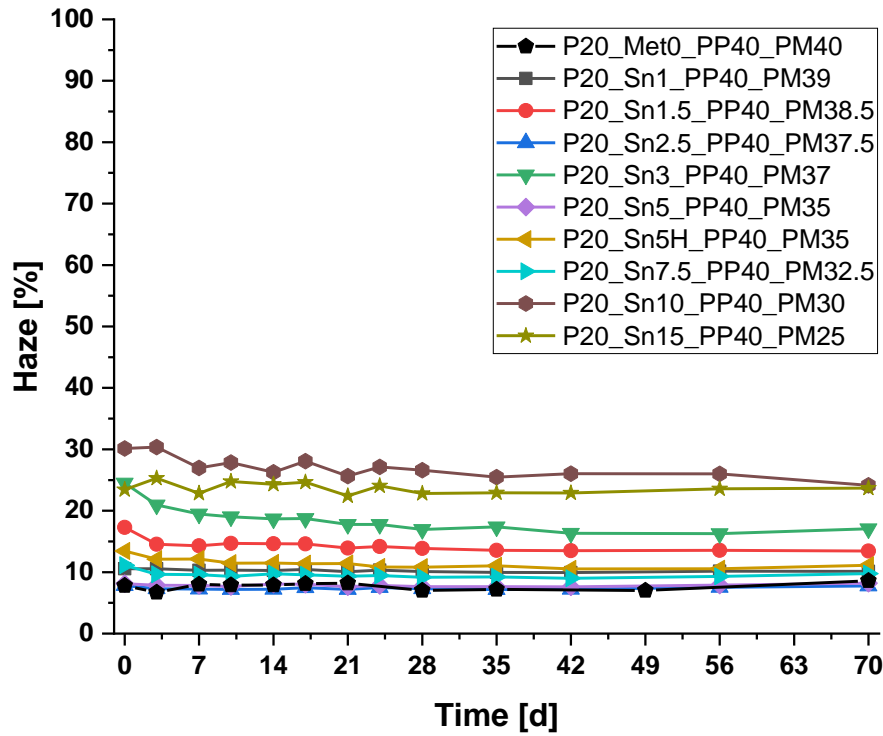
Figure 353: Haze values at 450 nm of the metal-free and the tin atom containing samples during the thermal treatment at 180 °C for 70 days.
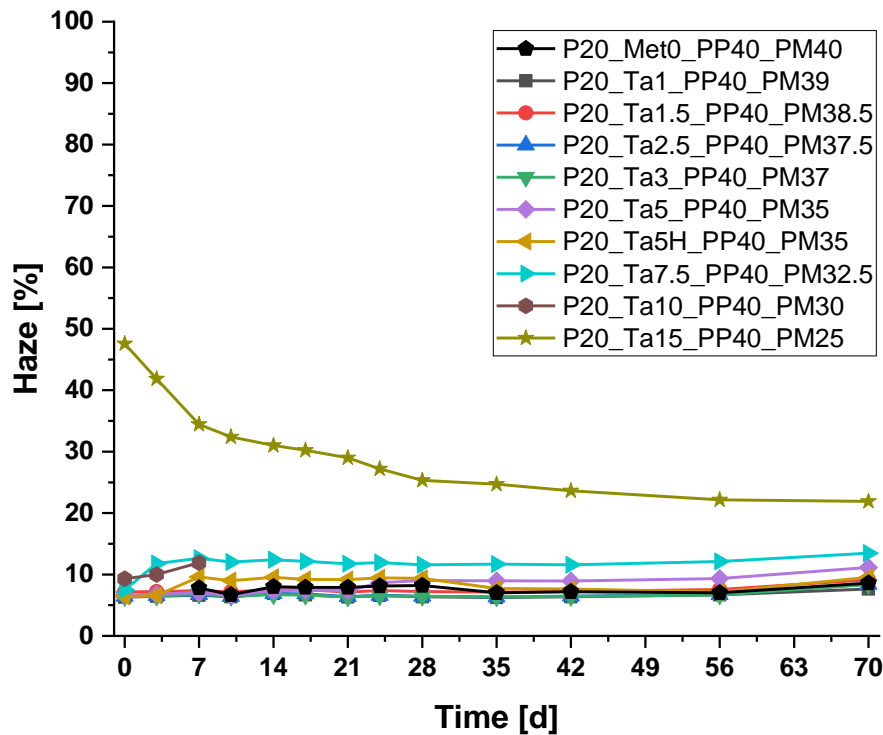
Figure 354: Haze values at 450 nm of the metal-free and the tantalum atom containing samples during the thermal treatment at 180 °C for 70 days.

6.2.7 Synthesis of hydride- or vinyl-group containing polymethylphenylsiloxanes for the kinetic investigations

6.2.7.1 Poly[hydridomethyl-co-methylphenyl-co-diphenyl]siloxane

The target polymer is poly[hydridomethyl-*co*-methylphenyl-*co*-diphenyl]siloxane, which was prepared by copolymerisation of methyldiethoxysilane, methylphenyldimethoxysilane and diphenylsilanediol (Figure 355) in methanolic-aqueous solution with concentrated hydrochloric acid as catalyst. The reaction (initial weights see Table 60) was carried out in a round bottom flask with a distillation head. The reaction was performed according to the following temperature profile (Figure 356).
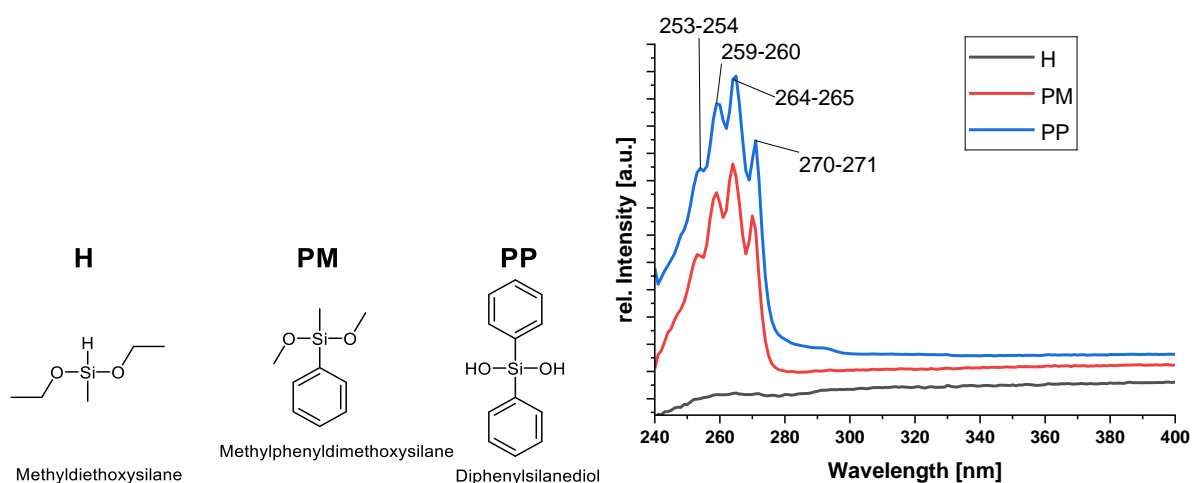
Figure 355: Left: structural formulas of the monomers, right: UV/Vis spectra with marked positions of the absorption maxima.

Table 60: Initial weights for the kinetics study of the hydride-group containing polysiloxanes from the kinetic reaction.

Substance	Equivalent	Weight [g]	Mol [mmol]	O-X/Si-H
Methyldiethoxysilane	20	0.736	5.48	2
Methylphenyldimethoxysilane	40	2.000	10.97	4
Diphenylsilanediol	40	2.373	10.97	4
Dist. Water		1.344	74.67	
Methanol		1.974	61.61	
conc. Hydrochloric acid	5.3 % rel. to Si	0.143	1.45	
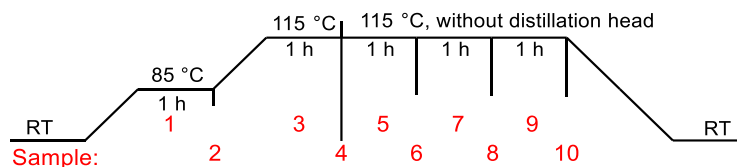
Figure 356: Temperature profile and nomenclature of the samples for the hydride-group containing polysiloxane from the kinetic reaction.

For the investigation, a sample was taken every 30 minutes, between 0.7 mL at the beginning and 0.4 mL at the end, depending on the present amount of solvent. Because during the reaction process the product concentration rises, the removed amount has to be lowered to remove approximately the same amount of polymer. The withdrawn sample was diluted with 1.5 mL saturated potassium bicarbonate and 2.0 mL toluene, shaken in a 5.0 mL centrifuge tube, and centrifuged for one minute at 8000 rpm. The aqueous phase was discarded, and 1.5 mL of distilled water was added, shaken and centrifuged again. After centrifuging, the aqueous phase was discarded. In total the sample was washed three times with water. The organic phase was transferred into a cylindrical glass and all volatiles were removed over two hours at 3 mbar, then at $5 \cdot 10^{-2}$ mbar under high vacuum.

FT-IR spectra, ^{1}H NMR spectra in CDCl$_3$ and SEC analyses in tetrahydrofuran (8 mg sample in 4 mL THF) were recorded of the ten obtained samples. ^{1}H NMR spectra are referenced to the CH$_3$ signal of toluene and normalized to an integration value of one for the Si-H group. For the SEC analyses, both a refractive index (RI) detector and a UV/Vis detector were used. For the UV/Vis detector adsorption spectra (Figure 355) of the monomers were recorded in tetrahydrofuran which also is the solvent for the SEC analysis to find the best wavelength for the detector. The absorption from 250 nm to 270 nm is characteristic for phenyl-groups.[562]

Figure 357: ^{1}H ^{29}Si HMBC NMR spectrum of sample one for the hydride-group containing polysiloxanes from the kinetic reaction.
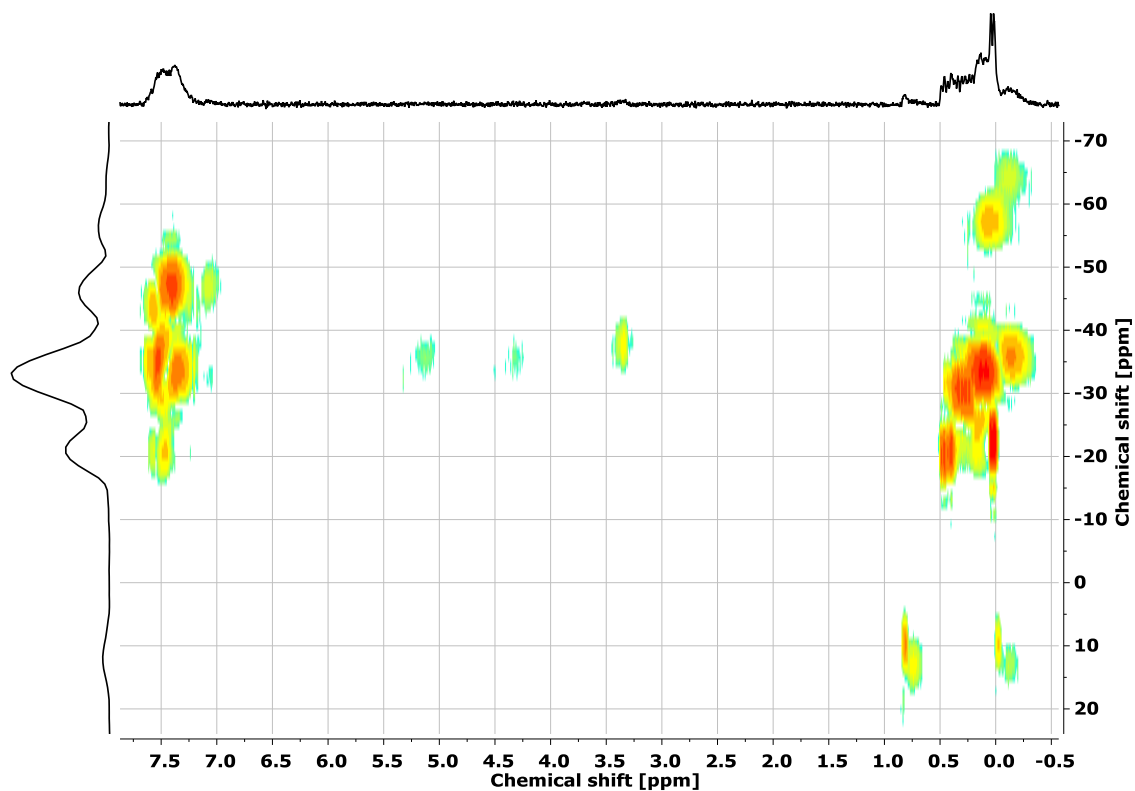
Figure 358: ^{1}H ^{29}Si HMBC NMR spectrum of sample nine for the hydride-group containing polysiloxanes from the kinetic reaction.
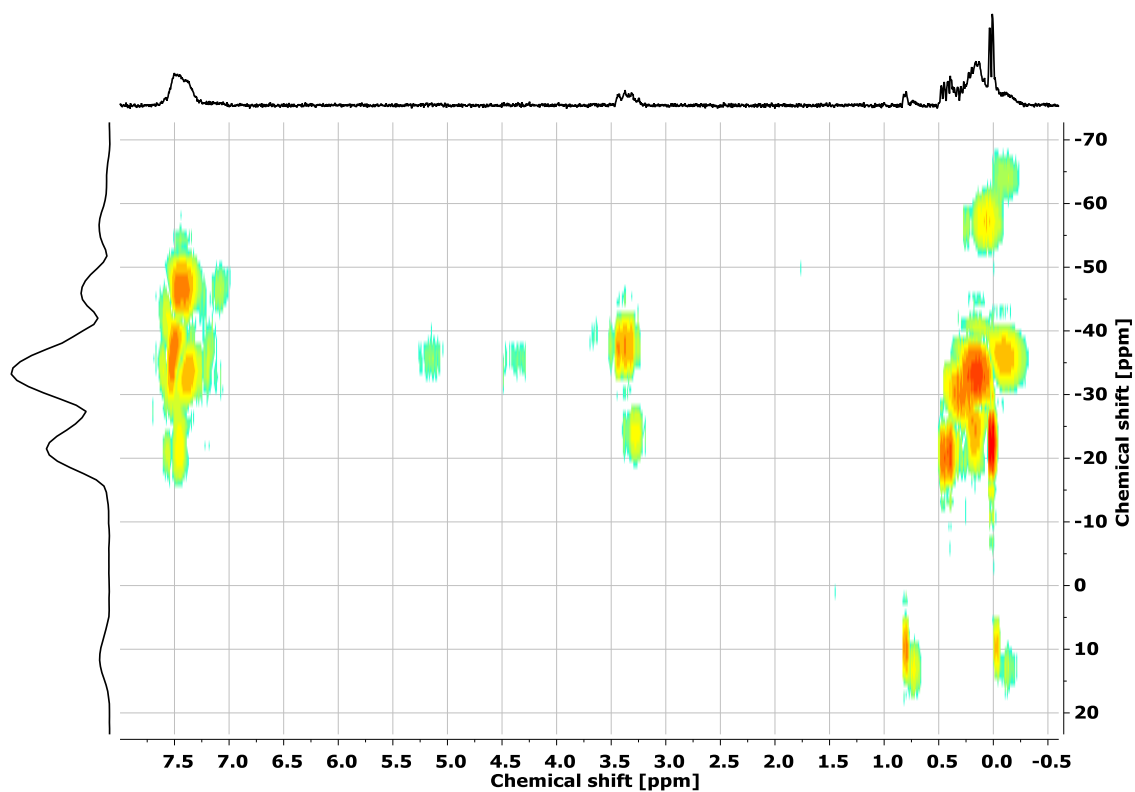
6.2.7.2 Poly[vinylphenyl-co-methylphenyl-co-diphenyl]siloxane

The target polymer is poly[vinylphenyl-*co*-methylphenyl-*co*-diphenyl]siloxane, which was prepared by copolymerisation of vinylphenyldiethoxysilane, methylphenyldimethoxysilane and diphenylsilanediol (Figure 359) in methanolic-aqueous solution with tetrabutylammonium hydroxide (40 wt% in water) as catalyst. The reaction (initial weights see Table 61) was carried out in a round bottom flask with a distillation head.
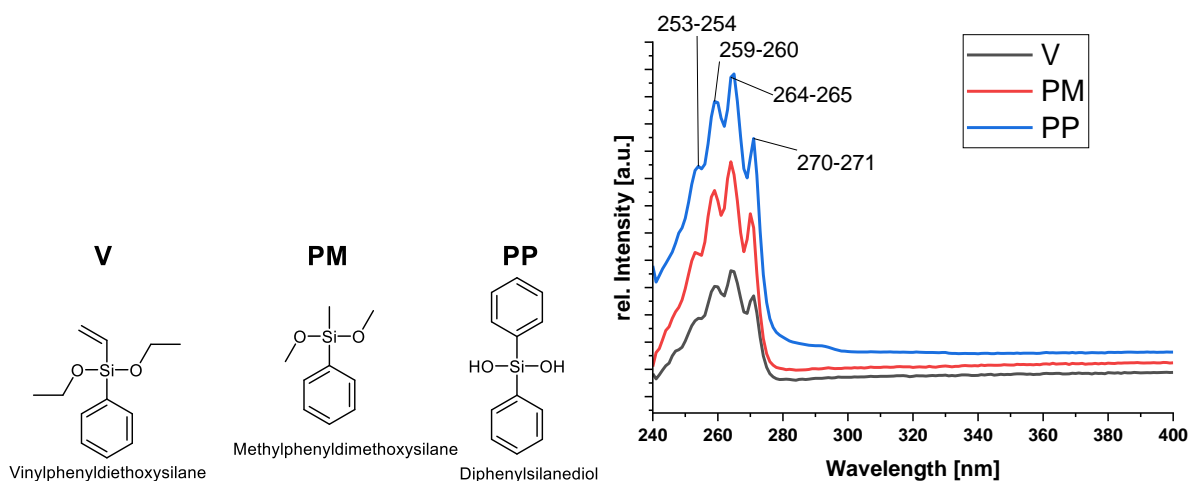
Figure 359: Left: structural formulas of the monomers, right: UV/Vis spectra with marked positions of the absorption maxima.

Table 61: Initial weights for the kinetics study for the vinyl-group containing polysiloxanes from the kinetic reaction.

Substance	Equivalent	Weight [g]	Mol [mmol]	O-X/Si-H
Vinylphenyldiethoxysilane	20	1.830	8.23	2
Methylphenyldimethoxysilane	40	3.000	16.46	4
Diphenylsilanediol	40	3.560	16.46	4
Dist. water		2.016	112.00	
Methanol		2.961	92.42	
Tetrabutylammonium hydroxide solution	1.5 % rel. to Si	0.039	0.06	

The reaction was performed according to the following temperature profile (Figure 360). For one hour at 85 °C, an isothermal step was applied for a prehydrolysis of the reactants without removing them by distillation because of their low boiling point (methyldiethoxysilane 94 – 95 °C). Although, this temperature is high enough to remove methanol (T_b = 64.7 °C). The second isothermal step at 115 °C allows the polymerisation of the now condensed and hydrolysed precursors. In a first step the polymerisation was carried out with a distillation head for

one hour. Afterwards the distillation head was removed to facilitate the removal of methanol, ethanol and water and the reaction was continued for three hours instead of the two hours for the hydride polymerisation because the M_W analyses showed a drastically increasing weight after five hours of total reaction time.
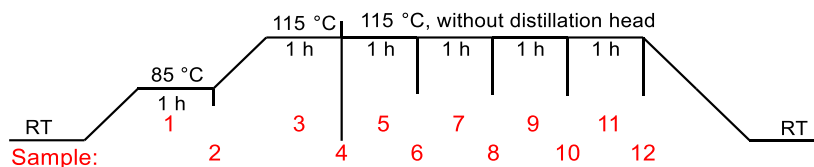
Figure 360: Temperature profile and nomenclature of the samples for the vinyl-group containing polysiloxanes from the kinetic reaction.

For the investigation, a sample was taken every 30 minutes, between 1.0 mL at the beginning and 0.3 mL at the end, depending on the present amount of solvent, because during the reaction process the product concentration rises, to remove approximately the same amount of polymer. The withdrawn sample was diluted with 1.5 mL 2 M HCl and 2.0 mL toluene, shaken in a 5.0 mL centrifuge tube and centrifuged for one minute at 8000 rpm. The aqueous phase was discarded and 1.5 mL of 2 M HCl was added, shaken, and centrifuged again, for a total of three times. Afterwards the sample was washed twice with 1.5 mL of distilled water, shaken, and centrifuged again. In total the sample was washed three times with 2 M HCl and twice with water. The organic phase was transferred into a cylindrical glass and all volatiles were removed over two hours at 3 mbar, then at $5 \cdot 10^{-2}$ mbar under high vacuum.

All analyses were performed identically as well as the sample preparation for SEC measurements, the ^{1}H NMR was integrated relative to the vinyl-group (integration of three) instead of the hydride-group (integration of one). For the UV/Vis detector adsorption spectra (Figure 359, right) of the monomers were recorded in tetrahydrofuran which also is the solvent for the SEC analysis to find the best wavelength for the detector. The absorption from 250 nm to 270 nm is characteristic for phenyl-groups.[562]

Figure 361: ^{1}H ^{29}Si HMBC NNMR spectra of sample one from the vinyl-group containing polysiloxanes from the kinetic reaction.

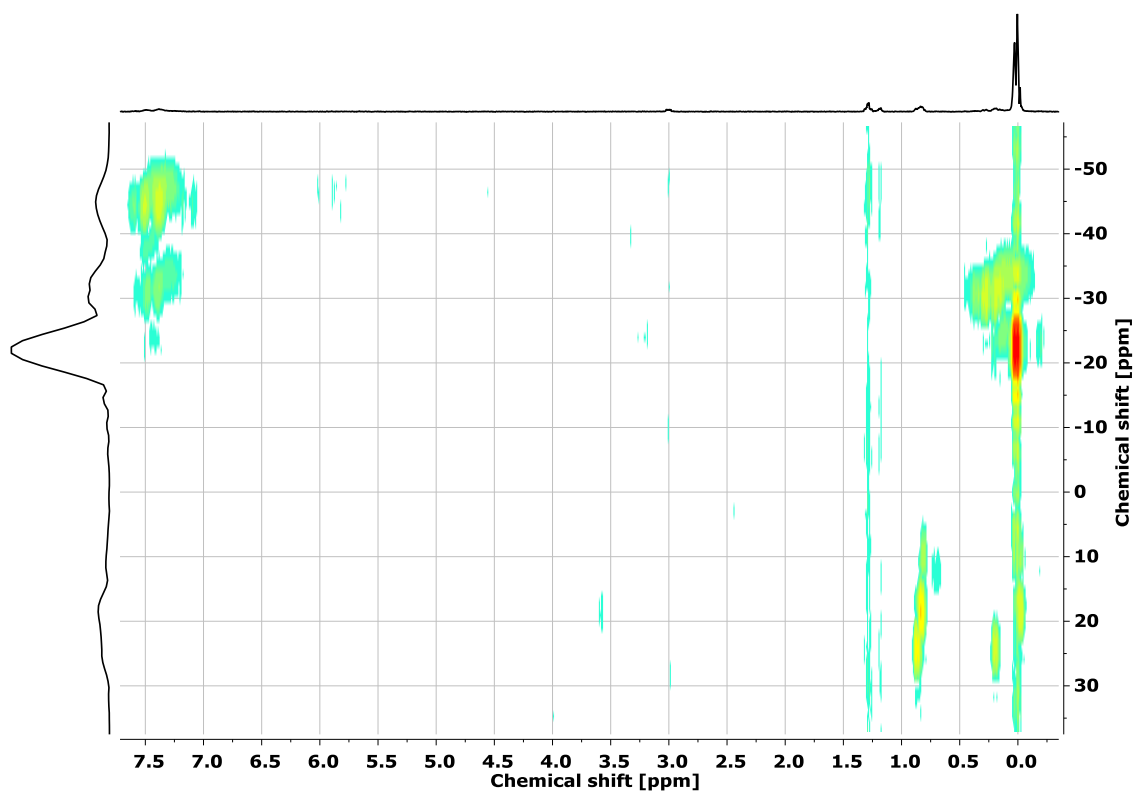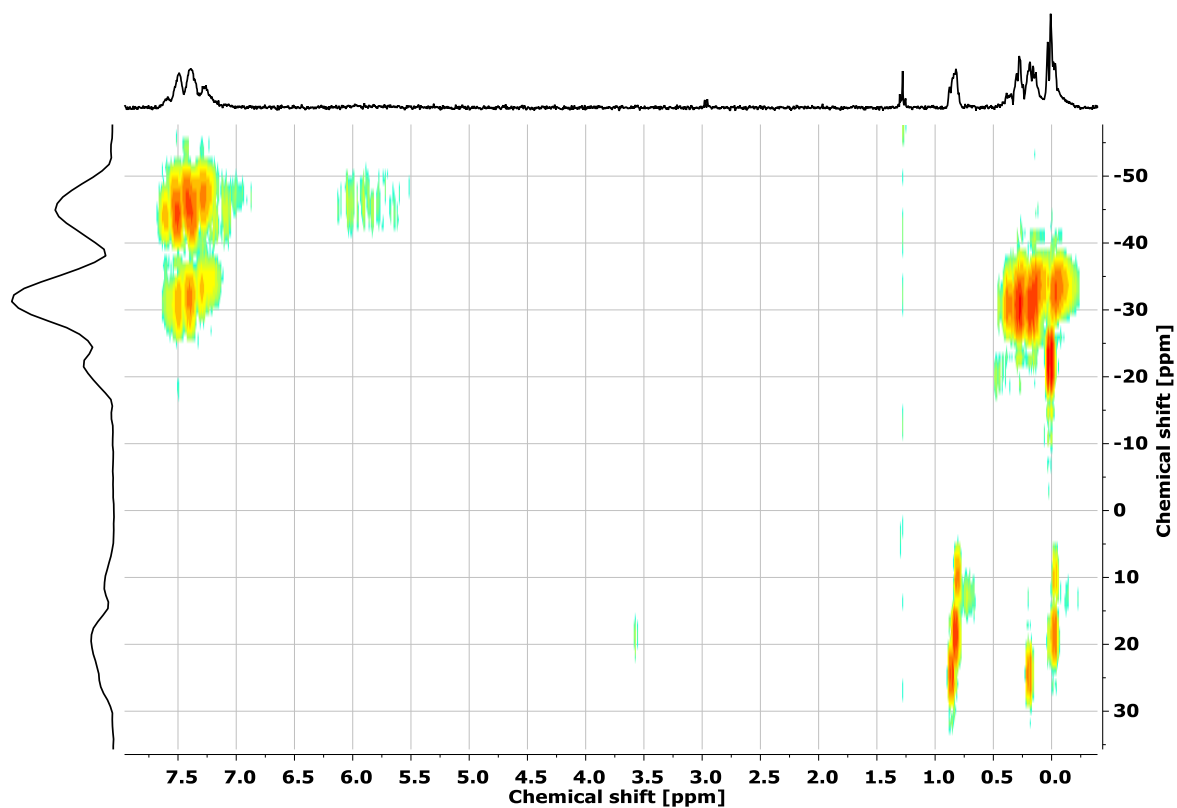**Figure 362:** ^{1}H ^{29}Si HMBC NNMR spectra of sample eleven from the vinyl-group containing polysiloxanes from the kinetic reaction.

6.2.8 Synthesis of phenoxyphenyl-group containing monomers and polymers

6.2.8.1 Synthesis of 4-(phenoxy)phenylphenyldimethoxysilane
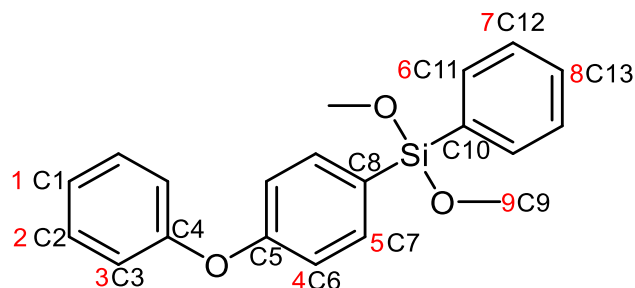
Figure 363: Chemical formula of 4-(phenoxy)phenylphenyldimethoxysilane.

To 3.22 g (132.4 mmol) of magnesium turnings in 50 mL of absolute THF, 30.00 g (120.4 mmol) of 4-bromodiphenylether in 100 mL of absolute tetrahydrofuran were added dropwise at room temperature and heated under reflux for one hour. In a second flask, 47.75 g (240.8 mmol) of phenyltrimethoxysilane was mixed in 50 ml of absolute tetrahydrofuran and the reactive Grignard species were added dropwise. After the mixture was stirred at room temperature overnight, it was refluxed for one hour. The cold suspension was filtered through a glass frit and the THF removed under reduced pressure. The crude product was dissolved in toluene and the precipitated salt was removed with a glass frit. After the solvent had been removed under reduced pressure, the crude product was distilled under high vacuum ($4 \cdot 10^{-3}$ mbar, 45 °C). The product was obtained as a clear oil (Figure 363, 29.21 g, 86.8 mmol, 72 %).

^{1}H NMR (300 MHz, CDCl$_3$): δ = 7.85 – 7.76 (m, 4H, H5, H6), 7.57 – 7.36 (m, 5H, H2, H7, H8), 7.27 – 7.11 (m, 5H, H1, H3, H4), 3.76 (s, 6H, H9) ppm.

^{13}C NMR (75 MHz, CDCl$_3$): δ = 159.64 (C5), 156.44 (C4), 136.67 (C10), 134.85 (C11), 132.37 (C7), 130.41 (C13), 129.83 (C12), 127.98 (C2), 126.19 (C8), 123.75 (C1), 119.59 (C3), 117.90 (C6), 50.87 (C9) ppm.

^{29}Si NMR (60 MHz, CDCl$_3$): δ = −28.78 (POPPSiOMe$_2$) ppm.

RI: 1.5701.

CHN C: 70.56 %, H: 5.94 %, N: 0.00 %; calc.: C: 71.40 %, H: 5.99 %, N: 0.00 %.

Figure 364: ¹³C NMR (75 MHz, CDCl₃) of 4-(phenoxy)phenylphenyldimethoxysilane.
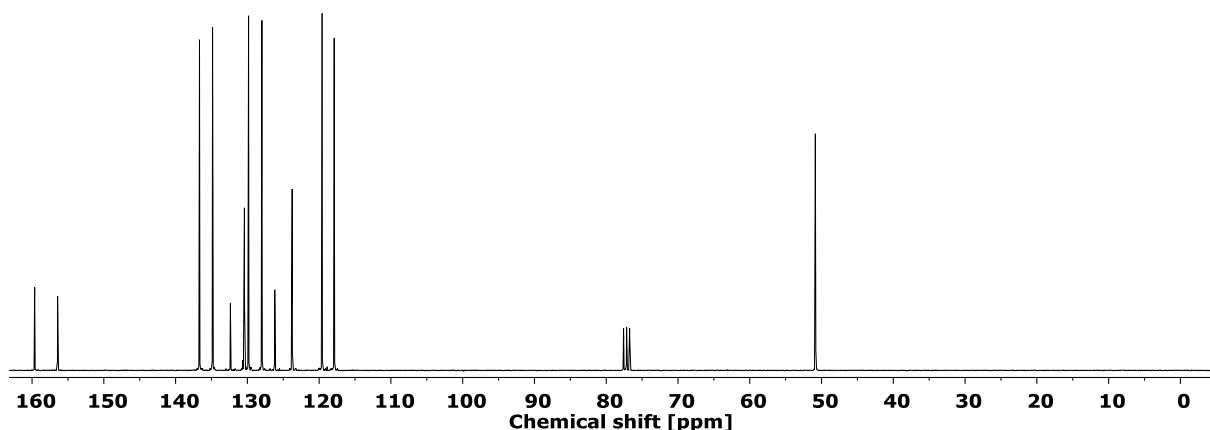
Figure 364: ^{13}C NMR (75 MHz, CDCl$_3$) of 4-(phenoxy)phenylphenyldimethoxysilane.

6.2.8.2 Synthesis of vinyl- and phenoxyphenyl-group containing polysiloxanes

Vinyl copolymer

Figure 365: Synthesis of vinyl- and phenoxyphenyl-group containing polysiloxanes

To 324.0 mg (1.45 mmol) vinylphenyldiethoxysilane, 975.7 mg (2.90 mmol) 4-(phenoxy)phenylphenyldimethoxysilane, 708.6 mg (2.90 mmol) diphenylsilanediol, 352.0 mg (19.60 mmol) distilled water and 0.5 mL of methanol, 22.6 mg (0.09 mmol) of tetra-n-butylammonium hydroxide (40 wt% in water) as catalyst was added and a fractionating column was attached onto the flask (Figure 365). After one hour at 85 °C, the temperature was raised to 115 °C for one hour. The distillation head was removed, and the reaction was continued for three additional hours. 8.0 mL of toluene and 4.0 mL of water were added and then centrifuged at 8000 rpm for one minute. The organic phase was washed three times with 6.0 mL of 2 M hydrochloric acid and two times with 6.0 ml of distilled water analogously. After filtering the organic phase with a 0.45 µm syringe filter, the organic phase was dried under vacuum. A slightly turbid, viscous polymer was obtained (1675.8 mg, 100 % with toluene).

^{1}H NMR (400 MHz, CDCl$_3$): δ = 7.71 – 6.70 (m, 53H, Ph), 6.19 – 5.63 (m, 3H, V) ppm.

^{13}C NMR (101 MHz, CDCl$_3$): δ = 156.70 – 117.66 (Ph, V, POPP) ppm.

^{29}Si NMR (79 MHz, CDCl$_3$): δ = −42.63 – −46.48 (-VPhSi-, -Ph$_2$Si-, -POPPSi-), −82.97 (-PhSi-) ppm.

Refractive index: 1.6104.
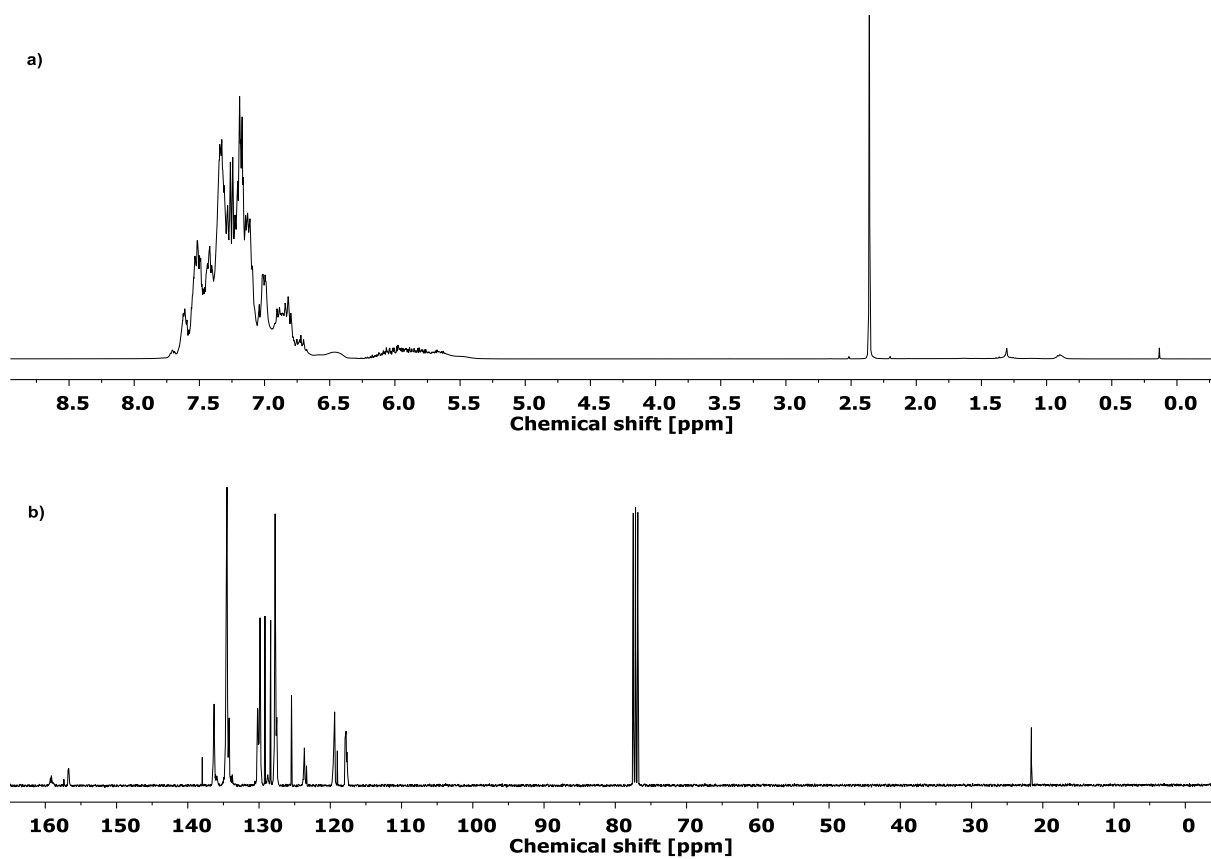
Figure 366: a) ^{1}H (400 MHz, CDCl$_3$) and b) ^{13}C (101 MHz, CDCl$_3$) of V20_POPP40_PP40.
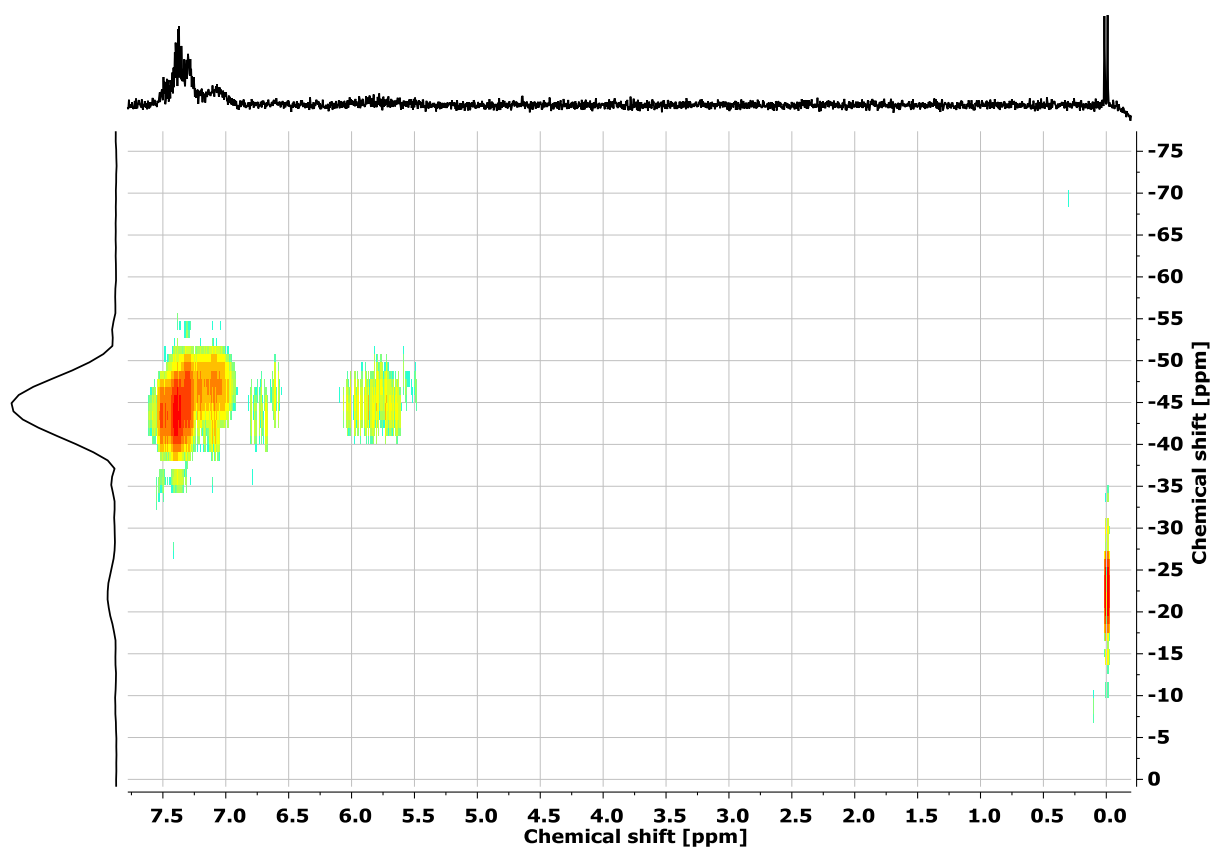
Figure 367: ^{1}H ^{29}Si HMBC NMR of V20_POPP40_PP40.

6.2.8.3 Synthesis of hydride- and phenoxyphenyl-group containing polysiloxanes

<u>Hydride copolymer</u>
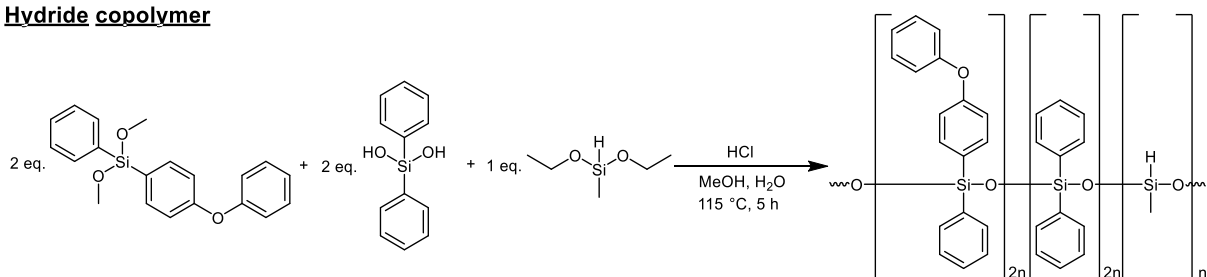
Figure 368: Synthesis of hydride- and phenoxyphenyl-group containing polysiloxanes

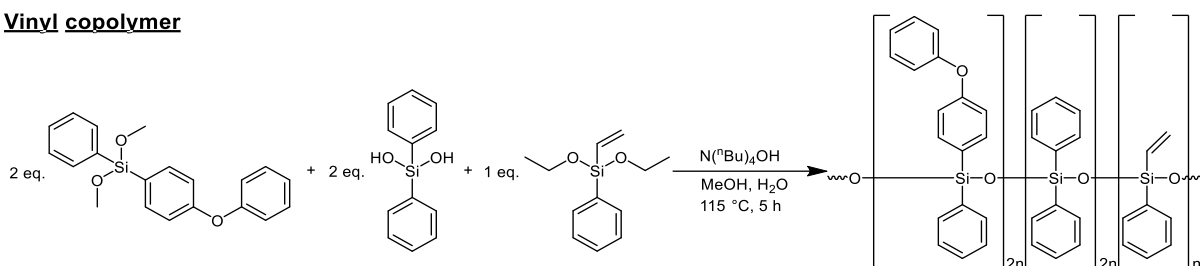To 195.0 mg (1.45 mmol) methyldiethoxysilane, 975.7 mg (2.90 mmol) 4-(phenoxy)phenylphenyldimethoxysilane, 708.6 mg (2.90 mmol) diphenylsilanediol, 352.0 mg (19.60 mmol) distilled water, 0.5 mL of methanol and 45.0 mg (1.23 mmol) of concentrated hydrochloric acid as catalyst was added and a fractionating column was attached onto the flask (Figure 368). After one hour at 85 °C, the temperature was raised to 115 °C for one hour. The distillation head was removed, and the reaction was continued for three additional hours. 8.0 mL of toluene and 4.0 mL of water were added and then centrifuged at 8000 rpm for one minute. The organic phase was washed once with 6.0 mL of saturated potassium bicarbonate and four times with 6.0 mL of distilled water analogously. After filtering the organic phase with a 0.45 µm syringe filter, the organic phase was dried under vacuum. A clear, viscous polymer was obtained (1602.6 mg, 100 % with toluene).

^{1}H NMR (400 MHz, CDCl$_3$): δ = 7.65 – 6.93 (m, 48H, Ph), 5.02 – 4.55 (m, 1H, H), 0.29 – −0.48 (m, 3H, Me) ppm.

^{13}C NMR (101 MHz, CDCl$_3$): δ = 134.49 – 119.01 (Ph, POPP), 1.20 – 0.70 (Me) ppm.

^{29}Si NMR (79 MHz, CDCl$_3$): δ = −31.40 – −34.52 (-HMeSi-), −45.84 (-Ph$_2$Si-, -POPPSi-), −69.62 (-PhOHSi-), −76.54 – −79.65 (-PhSi-) ppm.

Refractive index: 1.5953.

a)

b)
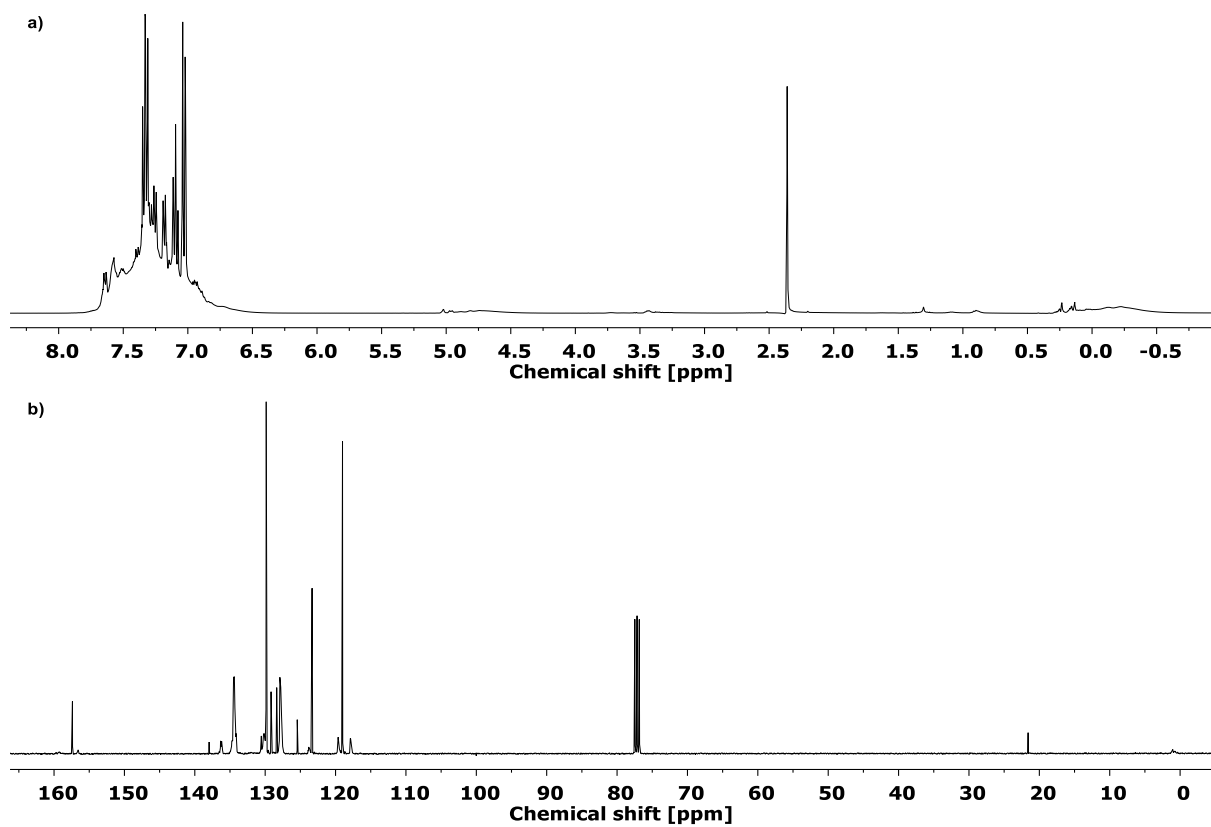
Figure 369: a) ¹H (400 MHz, CDCl₃) and b) ¹³C (101 MHz, CDCl₃) of H20_POPP40_PP40.
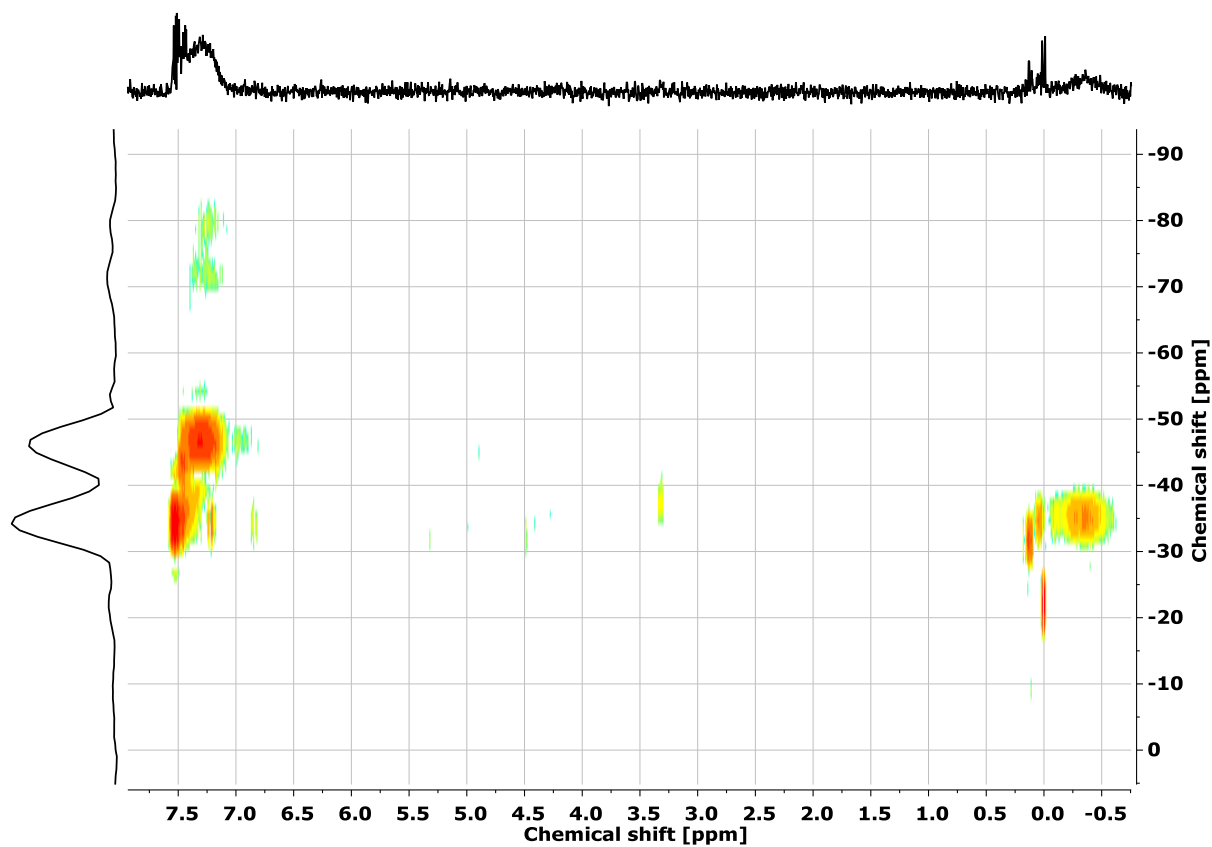
Figure 370: ¹H ²⁹Si HMBC NMR of H20_POPP40_PP40.

6.2.8.4 Synthesis of the cured phenoxyphenyl-group containing polysiloxane

400 mg of hydride (H20_POPP40_PP40) and vinyl (V20_POPP40_PP40) copolymers were mixed with 2.5 µL (1.63 ppm in siloxane) *Ossko*'s catalyst stock solution which was prepared using 10 µL of xylene isomers with 6 µL *Ossko*'s catalyst. The polymer was degassed at 2 mbar for one hour and doctor bladed with 120 µm onto a glass which was cleaned with *iso*-propanol and acetone and plasma etched at 100 % power for 15 minutes. The sample was cured at 80 °C for one hour and at 150 °C for four hours.

^{13}C CP MAS NMR (101 MHz, 13 kHz): δ = 158.24 – 156.11 (C_{Ph}-O-C_{Ph}), 133.67 –118.85 (Ph), 6.03 (Et), −1.96 (Me) ppm.

^{29}Si CP MAS NMR (80 MHz, 13 kHz): δ = −20.06 (-EtMeSi-), −34.17 (-EtPhSi-), −47.03 (-Ph$_2$Si-, -POPPSi-), −71.84 (-PhOHSi-), −80.25 (-PhSi-) ppm.

Refractive index: 1.6132.
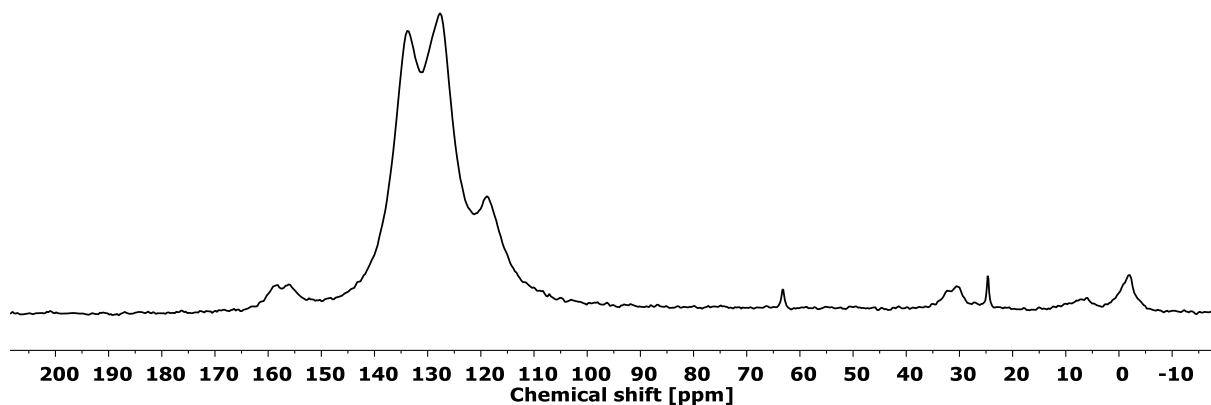
Figure 371: [13]**C CP MAS NMR (80 MHz, 13 kHz) of P20_POPP40_PP40.**

6.2.9 Synthesis of phenylthiomethyl-group containing monomers and polymers

6.2.9.1 Synthesis of 4-(methylthio)phenylphenyldimethoxysilane (PSMP)
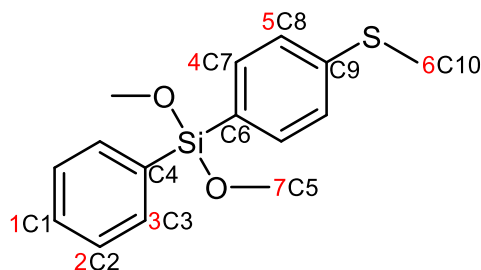
Figure 372: Chemical formula of 4-(methylthio)phenylphenyldimethoxysilane.

To 4.79 g (196.90 mmol) of magnesium chippings in 40 mL absolute THF, 20.00 g (98.48 mmol) bromothioanisole in 100 mL absolute THF were slowly added. After three hours under reflux, the suspension was added to a second flask with 87.87 g (443.12 mmol) phenyl-trimethoxysilane in 50 mL absolute THF over two hours. After stirring the solution overnight at room temperature, it was heated to reflux for three hours. Salts were filtered off and the solvent was evaporated. 200 mL of toluene were added, and the remaining salts were filtered off. The crude product was distilled under high vacuum (135 – 140 °C, $1 \cdot 10^{-2}$ mbar) to receive the desired product as clear oil (Figure 372, 19.11 g, 65.80 mmol, 67 %).

^{1}H NMR (300 MHz, CDCl$_3$): δ = 7.75 (dt, J = 7.6 Hz, 1.7 Hz, 2H, H3), 7.66 (d, J = 7.6 Hz, 2H, H4), 7.55 – 7.40 (m, 3H, H1, H2), 7.33 (d, J = 7.6 Hz, 2H, H5), 3.70 (s, 6H, H7), 2.50 (s, 3H, H6) ppm.

^{13}C NMR (75 MHz, CDCl$_3$): δ = 141.72 (C9), 135.18 (C3), 134.78 (C4, C7), 132.23 (C6), 130.37 (C1), 127.92 (C2), 125.31 (C8), 50.82 (C5), 14.88 (C10) ppm.

^{29}Si NMR (60 MHz, CDCl$_3$): δ = −28.80 (PSMPSiOMe$_2$) ppm.

RI: 1.5777.

CHN: C: 62.13 %, H: 6.59 %, N: 0.00 %; calc.: C: 62.03 %, H: 6.25 %, N: 0.00 %.
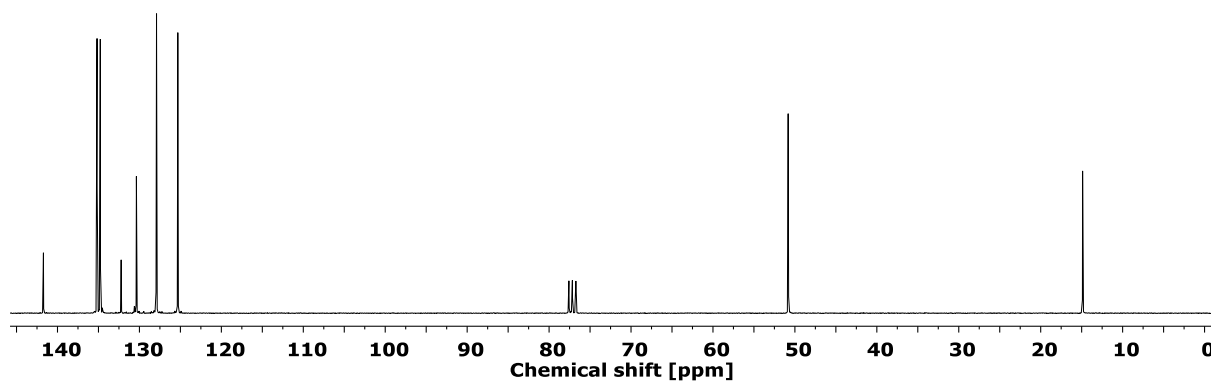
Figure 373: ^{13}C NMR (75 MHz, CDCl$_3$) of 4-(methylthio)phenylphenyldimethoxysilane (PSMP).

6.2.9.2 Synthesis of vinyl- and phenylthiomethyl-group containing polysiloxanes
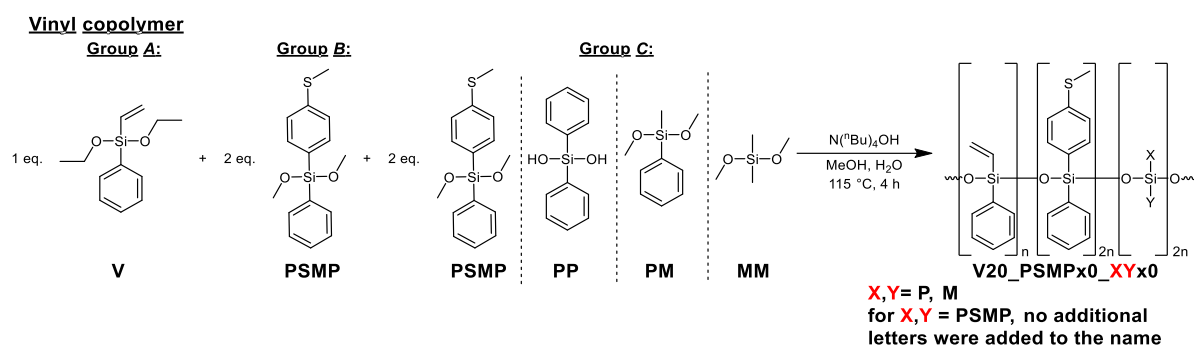
Figure 374: General synthesis of vinyl- and phenylthiomethyl-group containing polysiloxanes.

General synthesis for vinyl- and phenylthiomethyl-group containing polysiloxanes:

To 1 eq. (1.912 g, 8.6 mmol) vinylphenyldiethoxysilane, 2 eq. (5.000 g, 17.2 mmol) 4-(methyl-thio)phenylphenyldimethoxysilane, 2 eq. (17.2 mmol) group *C* monomer, 2.089 g (116.0 mmol) distilled water and 2.869 mL (70.9 mmol) of methanol, 134.0 µL (0.5 mmol) of 40 wt% tetra-*n*-butylammonium hydroxide solution in water as catalyst was added and a fractionating column was attached onto the flask (Figure 374). After one hour at 85 °C, the temperature was raised to 115 °C for one hour. The distillation head was removed, and the reaction was continued for two additional hours. 40 mL of toluene and 20 mL of water were added and then centrifuged at 8000 rpm for one minute. The organic phase was washed twice with 12 mL of 2 M hydrochloric acid and three times with 12 ml of distilled water analogously. After filtering the organic phase with a 0.45 µm syringe filter, the organic phase was dried under vacuum. A clear, viscous polymer was obtained (100 % with residual toluene).

V20_PSMP40_MM40:

Yield: 6.512 g

^{1}H NMR (400 MHz, CDCl$_3$): δ = 7.65 – 6.96 (m, 23H, Ph), 6.14 – 5.71 (m, 3H, V), 2.44 (s, 6H, S-Me), 0.23 – −0.10 (m, 12H, Me) ppm.

^{13}C NMR (101 MHz, CDCl$_3$): δ = 134.81 – 125.41 (Ph, V), 15.13 – 15.08 (SMe), 1.15 – 0.88 (SiMe) ppm.

^{29}Si NMR (79 MHz, CDCl$_3$): δ = −17.06 – −20.42 (-Me$_2$Si-), −44.43 – −48.15 (-PSMPSi-, -VPhSi-) ppm.

Refractive index: 1.5796.

Viscosity: 10000 ± 330 mPa·s.

V20_PSMP40_PM40:

Yield: 6.971 g

^{1}H NMR (400 MHz, CDCl$_3$): δ = 7.66 – 7.10 (m, 33H, Ph), 6.18 – 5.70 (m, 3H, V), 2.48 (s, 6H, S-Me), 0.57 – −0.02 (m, 6H, Me) ppm.

^{13}C NMR (101 MHz, CDCl$_3$): δ = 134.86 – 125.16 (Ph, V), 15.11 (SMe), −0.15 – −0.33 (SiMe) ppm.

^{29}Si NMR (79 MHz, CDCl$_3$): δ = −29.49 – −33.68 (-MePhSi-), −43.29 – −46.74 (-PSMPSi-, -VPhSi-) ppm.

Refractive index: 1.5992.

Viscosity: 87600 ± 5200 mPa·s.

V20_PSMP40_PP40:

Yield: 5.038 g

^{1}H NMR (400 MHz, CDCl$_3$): δ = 7.70 – 6.91 (m, 43H, Ph), 6.12 – 5.64 (m, 3H, V), 2.44 (s, 6H, S-Me) ppm.

^{13}C NMR (101 MHz, CDCl$_3$): δ = 134.88 – 125.09 (Ph, V), 15.14 – 15.12 (SMe) ppm.

^{29}Si NMR (79 MHz, CDCl$_3$): δ = −42.55 – −45.61 (-PSMPSi-, -Ph$_2$Si-, -PhVSi-) ppm.

Refractive index: 1.6160.

Viscosity: 1490000 ± 107000 mPa·s.

V20_PSMP80:

Yield: 5.837 g

^{1}H NMR (400 MHz, CDCl$_3$): δ = 7.70 – 6.91 (m, 43H, Ph), 6.12 – 5.64 (m, 3H, V), 2.44 (s, 6H, S-Me) ppm.

^{13}C NMR (101 MHz, CDCl$_3$): δ = 134.85 – 124.95 (Ph, V), 15.08 – 15.03 (SMe) ppm.

^{29}Si NMR (79 MHz, CDCl$_3$): δ = −42.56 – −45.60 (-PSMPSi-, -PhVSi-) ppm.

Refractive index: 1.6230.

Viscosity: 151000 ± 2300 mPa·s.

6.2.9.2.1 FT-IR spectra
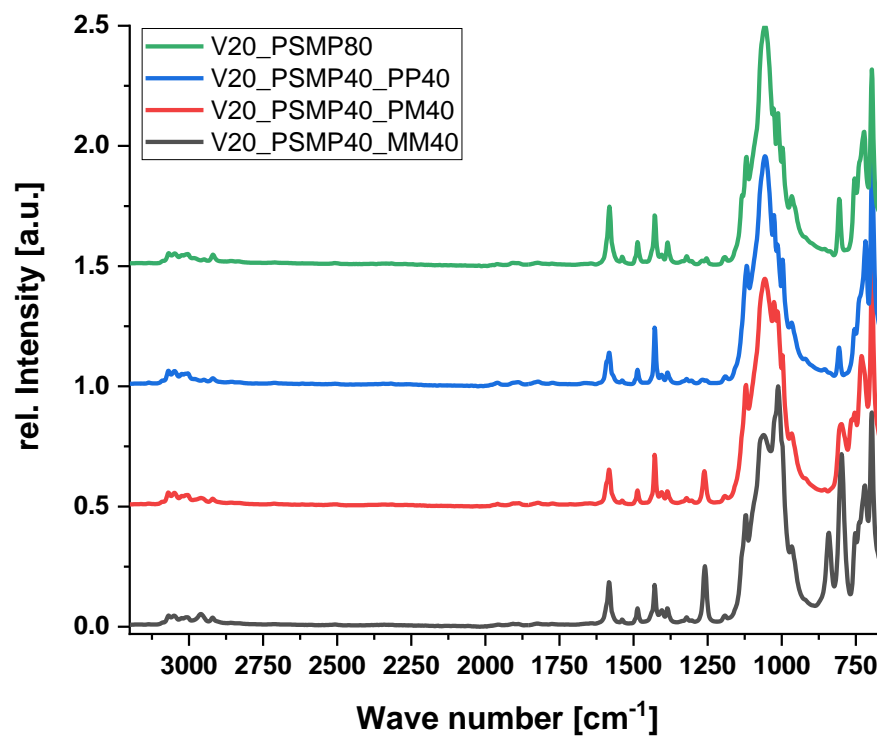
Figure 375: FT-IR spectra of the vinyl- and phenylthiomethyl-group containing copolymers.

6.2.9.2.2 NMR spectra

a)

b)

c)
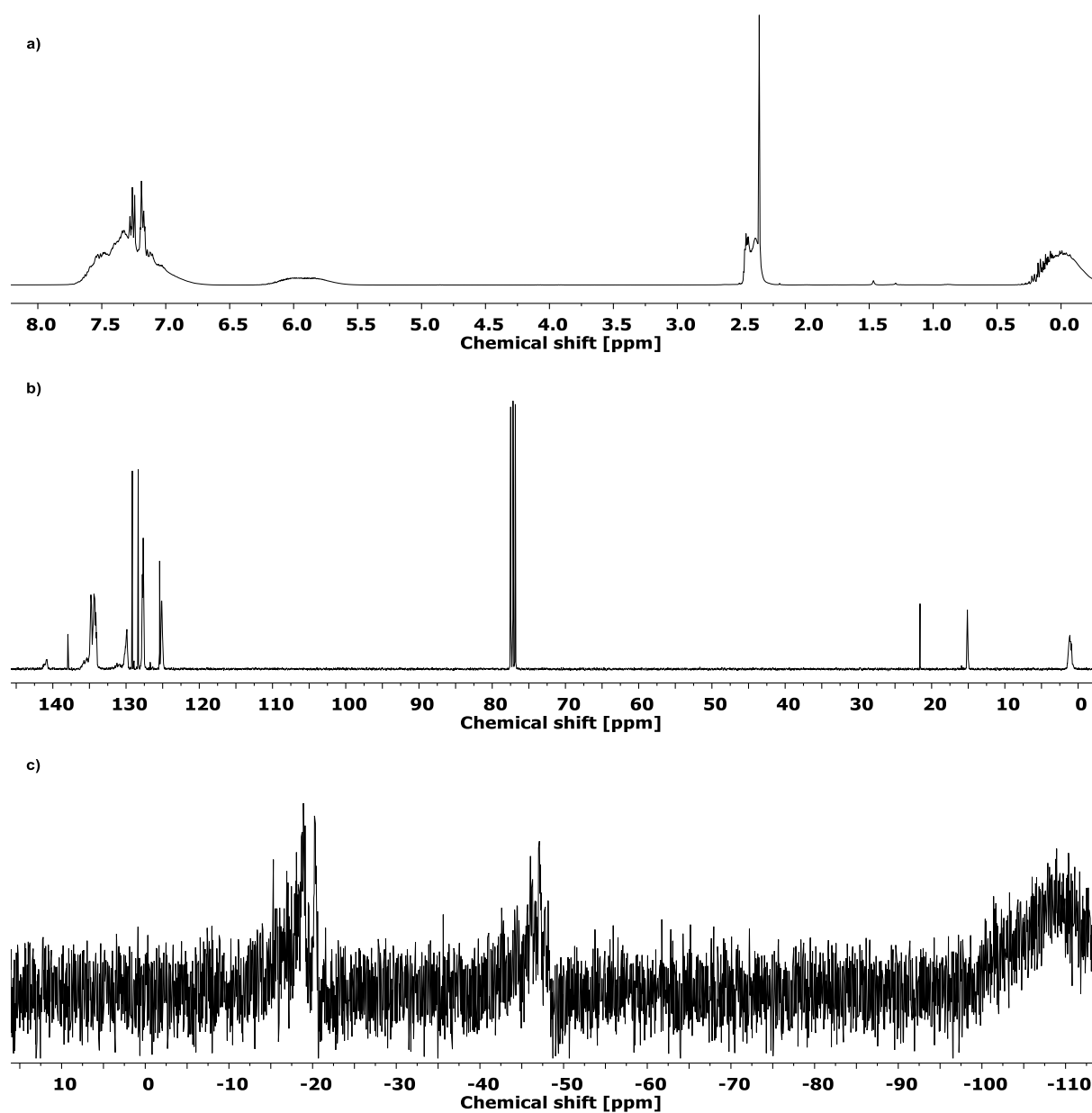
Figure 376: a) ^{1}H NMR (400 MHz, CDCl$_3$), b) ^{13}C NMR (101 MHz, CDCl$_3$) and c) ^{29}Si NMR (79 MHz, CDCl$_3$) of V20_PSMP40_MM40.
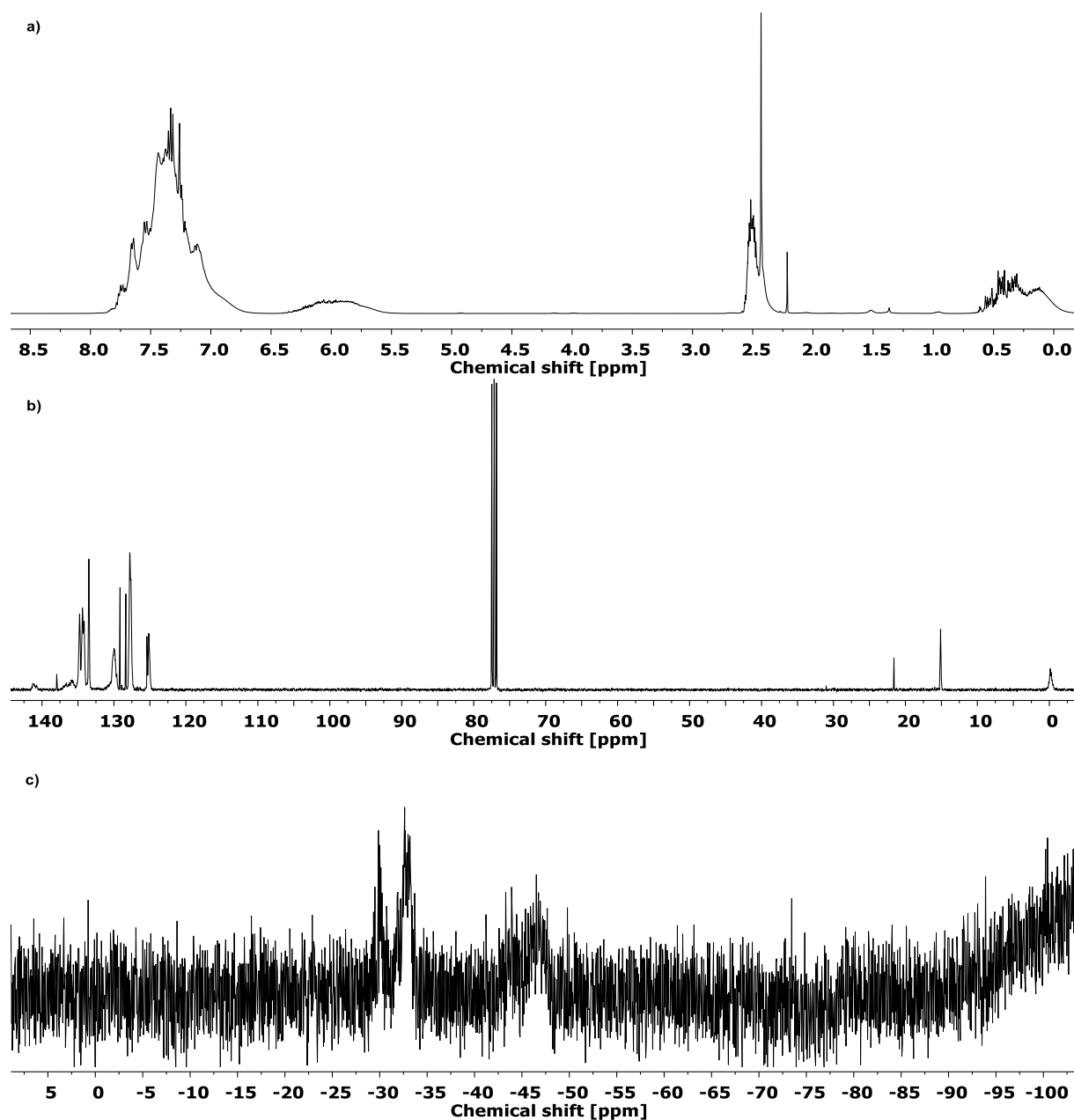
Figure 377: a) ^{1}H NMR (400 MHz, CDCl$_3$), b) ^{13}C NMR (101 MHz, CDCl$_3$) and c) ^{29}Si NMR (79 MHz, CDCl$_3$) of V20_PSMP40_PM40.

a)

b)

c)
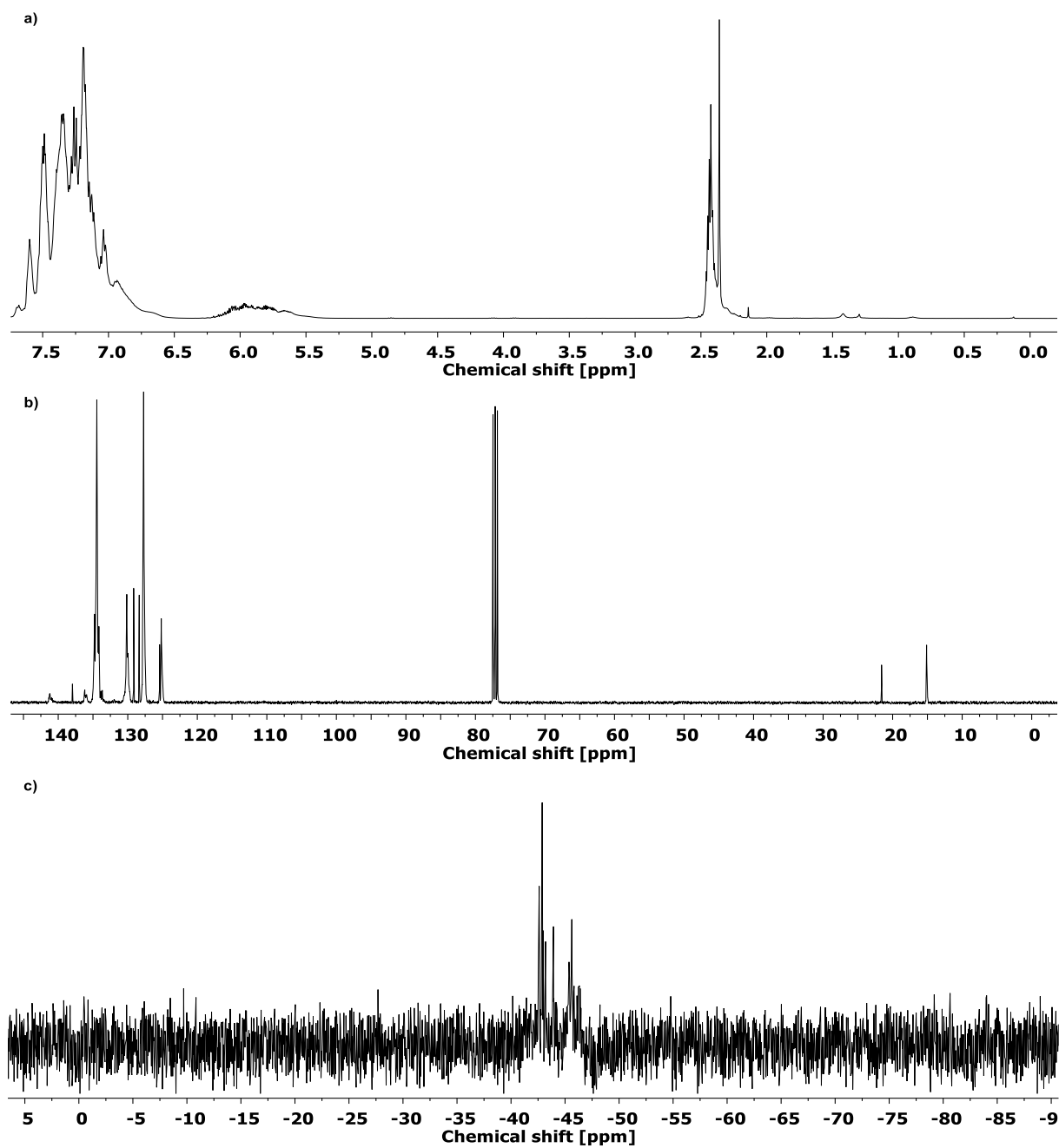
Figure 378: a) ^{1}H NMR (400 MHz, CDCl$_3$), b) ^{13}C NMR (101 MHz, CDCl$_3$) and c) ^{29}Si NMR (79 MHz, CDCl$_3$) of V20_PSMP40_PP40.

a)

b)

c)
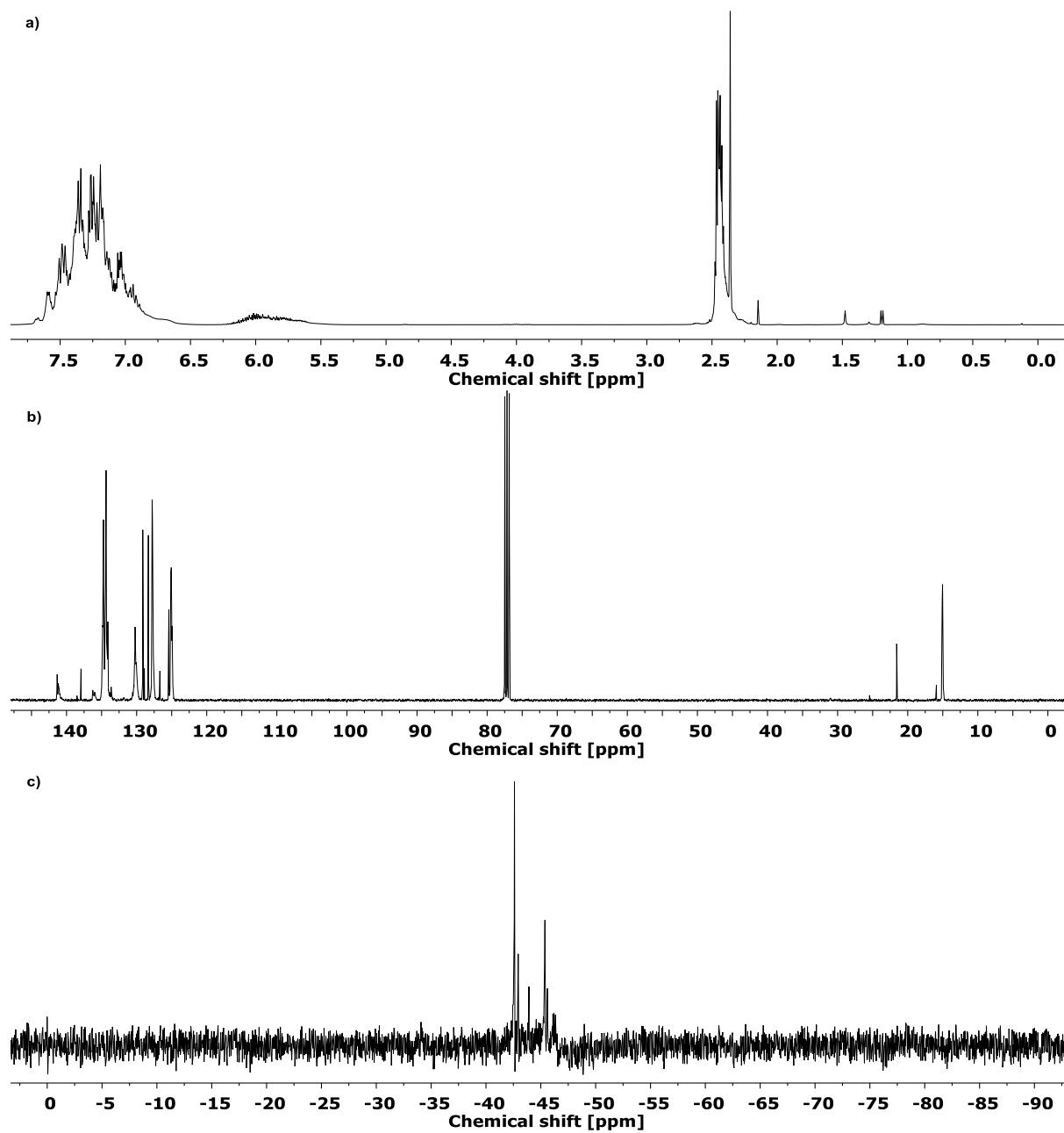
Figure 379: a) ¹H NMR (400 MHz, CDCl₃), b) ¹³C NMR (101 MHz, CDCl₃) and c) ²⁹Si NMR (79 MHz, CDCl₃) of V20_PSMP80.
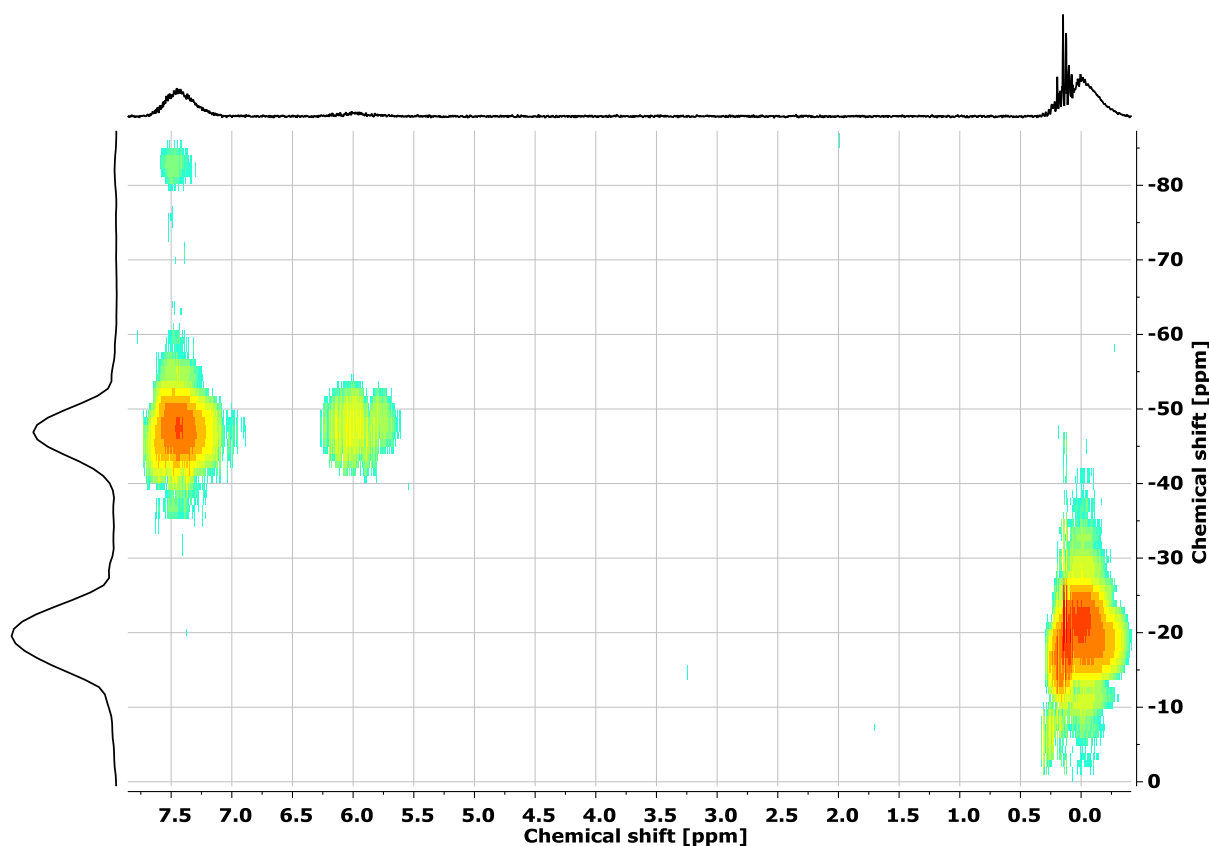
Figure 380: ¹H ²⁹Si HMBC NMR of V20_PSMO40_PM40 in CDCl₃.

6.2.9.3 Synthesis of hydride- and phenylthiomethyl-group containing polysiloxanes
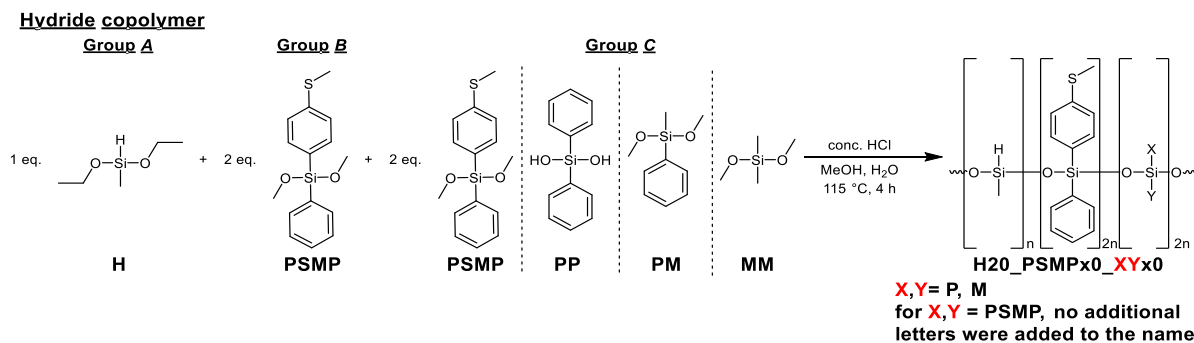
Figure 381: General synthesis of hydride- and phenylthiomethyl-group containing polysiloxanes.

General synthesis for hydride- and phenylthiomethyl-group containing polysiloxanes:

To 1 eq. (1.155 g, 8.6 mmol) methyldiethoxysilane, 2 eq. (5.000 g, 17.2 mmol) 4-(methyl-thio)phenylphenyldimethoxysilane, 2 eq. (17.2 mmol) group *C* monomer, 2.089 g (116.0 mmol) distilled water and 2.869 mL (70.9 mmol) of methanol, 258.2 µL (3.2 mmol) of concentrated hydrochloric acid as catalyst was added and a fractionating column was attached onto the flask (Figure 381). After one hour at 85 °C, the temperature was raised to 115 °C for one hour. The distillation head was removed, and the reaction was continued for two additional hours. 40 mL of toluene and 20 mL of water were added and then centrifuged at 8000 rpm for one minute. The organic phase was washed once with 12 mL of saturated potassium bicarbonate

and four times with 12 ml of distilled water analogously. After filtering the organic phase with a 0.45 µm syringe filter, the organic phase was dried under vacuum. A clear, viscous polymer was obtained (100 % with residual toluene).

H20_PSMP40_MM40:

Yield: 5.146 g

^{1}H NMR (400 MHz, CDCl$_3$): δ = 7.70 – 6.94 (m, 18H, Ph), 5.01 – 4.67 (m, 1H, H), 2.45 (s, 6H, S-Me), 0.31 – −0.18 (m, 15H, Me) ppm.

^{13}C NMR (101 MHz, CDCl$_3$): δ = 135.05 – 125.12 (Ph, V), 15.19 – 15.08 (SMe), 1.12 – 0.87 (SiMe) ppm.

^{29}Si NMR (79 MHz, CDCl$_3$): δ = −17.51 – −21.02 (-Me$_2$Si-), −31.80 – −35.67 (-HMeSi-), −45.73 – −46.81 (-PSMPSi-) ppm.

Refractive index: 1.5645.

Viscosity: 2190 ± 100 mPa·s.

H20_PSMP40_PM40:

Yield: 5.725 g

^{1}H NMR (400 MHz, CDCl$_3$): δ = 7.67 – 7.02 (m, 28H, Ph), 5.03 – 4.58 (m, 1H, H), 2.45 (s, 6H, S-Me), 0.58 – −0.05 (m, 9H, Me) ppm.

^{13}C NMR (101 MHz, CDCl$_3$): δ = 134.77 – 125.12 (Ph, V), 15.94 – 15.10 (SMe), −0.06 – −0.22 (SiMe) ppm.

^{29}Si NMR (79 MHz, CDCl$_3$): δ = −30.02 – −32.57 (-MePhSi-), −34.19 – −35.13 (-HMeSi-), −45.18 – −45.87 (-PSMPSi-) ppm.

Refractive index: 1.5795.

Viscosity: 5250 ± 260 mPa·s.

H20_PSMP40_PP40:

Yield: 6.654 g

^{1}H NMR (400 MHz, CDCl$_3$): δ = 7.64 – 7.11 (m, 38H, Ph), 5.02 – 4.75 (m, 1H, H), 2.44 (s, 6H, S-Me), 0.24 – −0.18 (m, 3H, Me) ppm.

^{13}C NMR (101 MHz, CDCl$_3$): δ = 134.81 – 125.23 (Ph, V), 15.91 – 15.05 (SMe), 1.10 (SiMe) ppm.

^{29}Si NMR (79 MHz, CDCl$_3$): δ = −31.34 – −36.70 (-HMeSi-), −43.05 – −45.47 (-PSMPSi-, -Ph$_2$Si-) ppm.

Refractive index: 1.5991.

Viscosity: 13800 ± 460 mPa·s.

H20_PSMP80:

Yield: 8.172 g

^{1}H NMR (400 MHz, CDCl$_3$): δ = 7.64 – 6.98 (m, 36H, Ph), 5.02 – 4.61 (m, 1H, H), 2.43 (s, 12H, S-Me), 0.29 – −0.31 (m, 3H, Me) ppm.

^{13}C NMR (101 MHz, CDCl$_3$): δ = 138.48 – 125.06 (Ph, V)), 15.86 – 14.95 (SMe), 1.03 (SiMe) ppm.

^{29}Si NMR (79 MHz, CDCl$_3$): δ = −31.29 – −34.44 (-HMeSi-), −45.53 – −45.80 (-PSMPSi-) ppm.

Refractive index: 1.5960.

Viscosity: 1400 ± 740 mPa·s.

6.2.9.3.1 FT-IR spectra
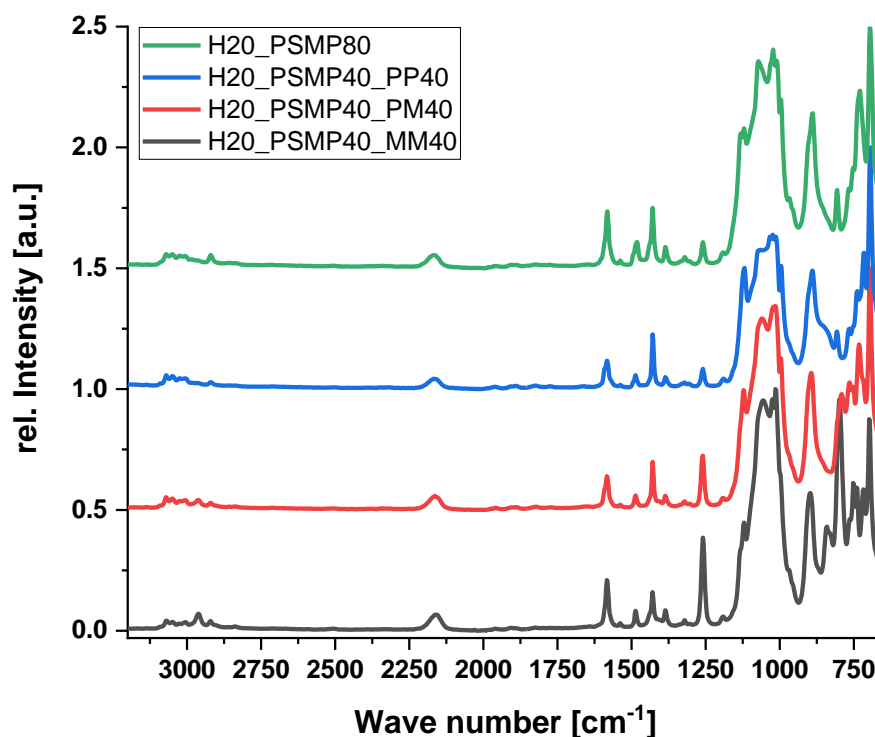
Figure 382: FT-IR spectra of the vinyl- and phenylthiomethyl-group containing copolymers.

6.2.9.3.2 NMR spectra

a)

b)

c)
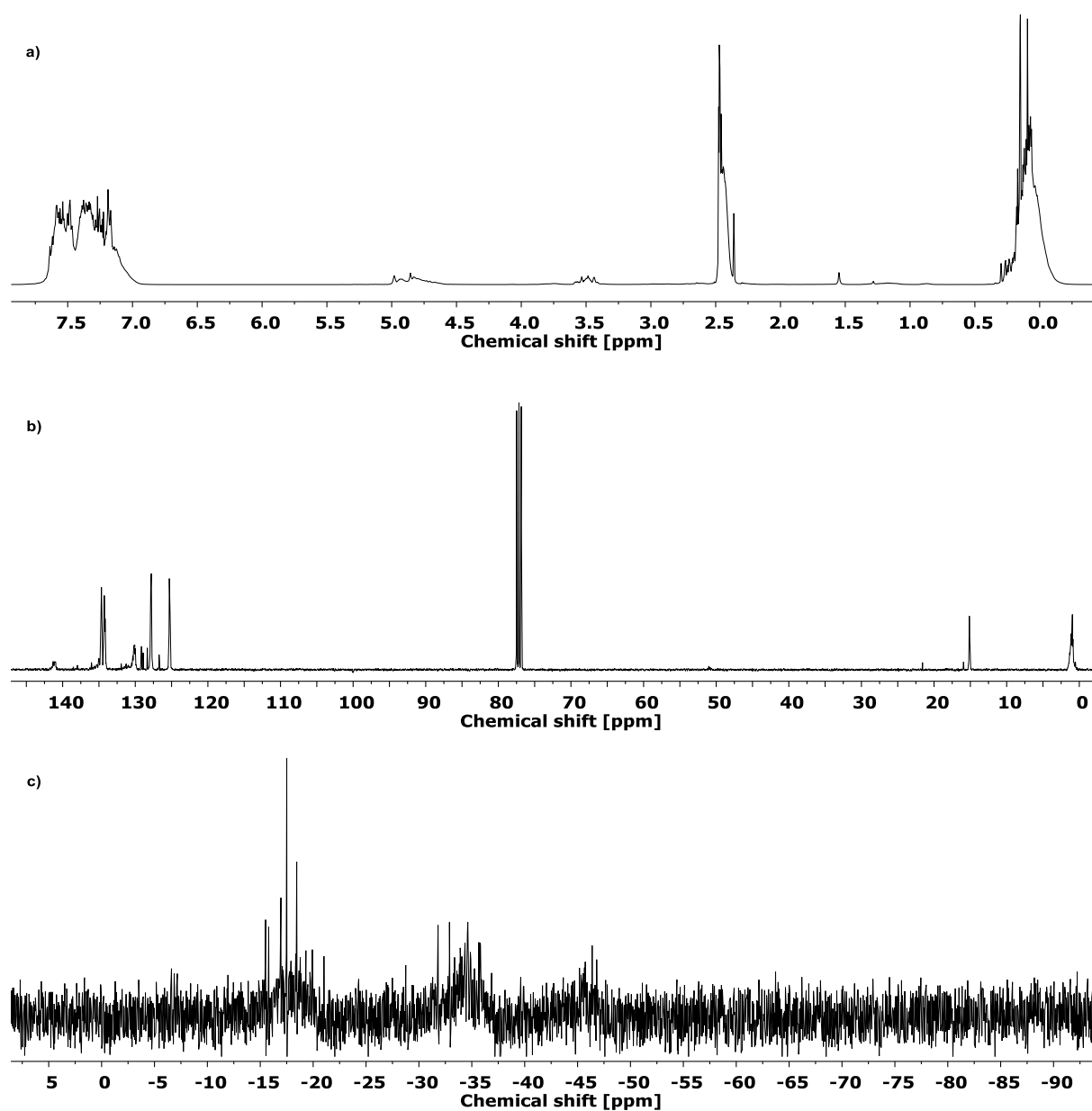
Figure 383: a) ^{1}H NMR (400 MHz, CDCl$_3$), b) ^{13}C NMR (101 MHz, CDCl$_3$) and c) ^{29}Si NMR (79 MHz, CDCl$_3$) of H20_PSMP40_MM40.
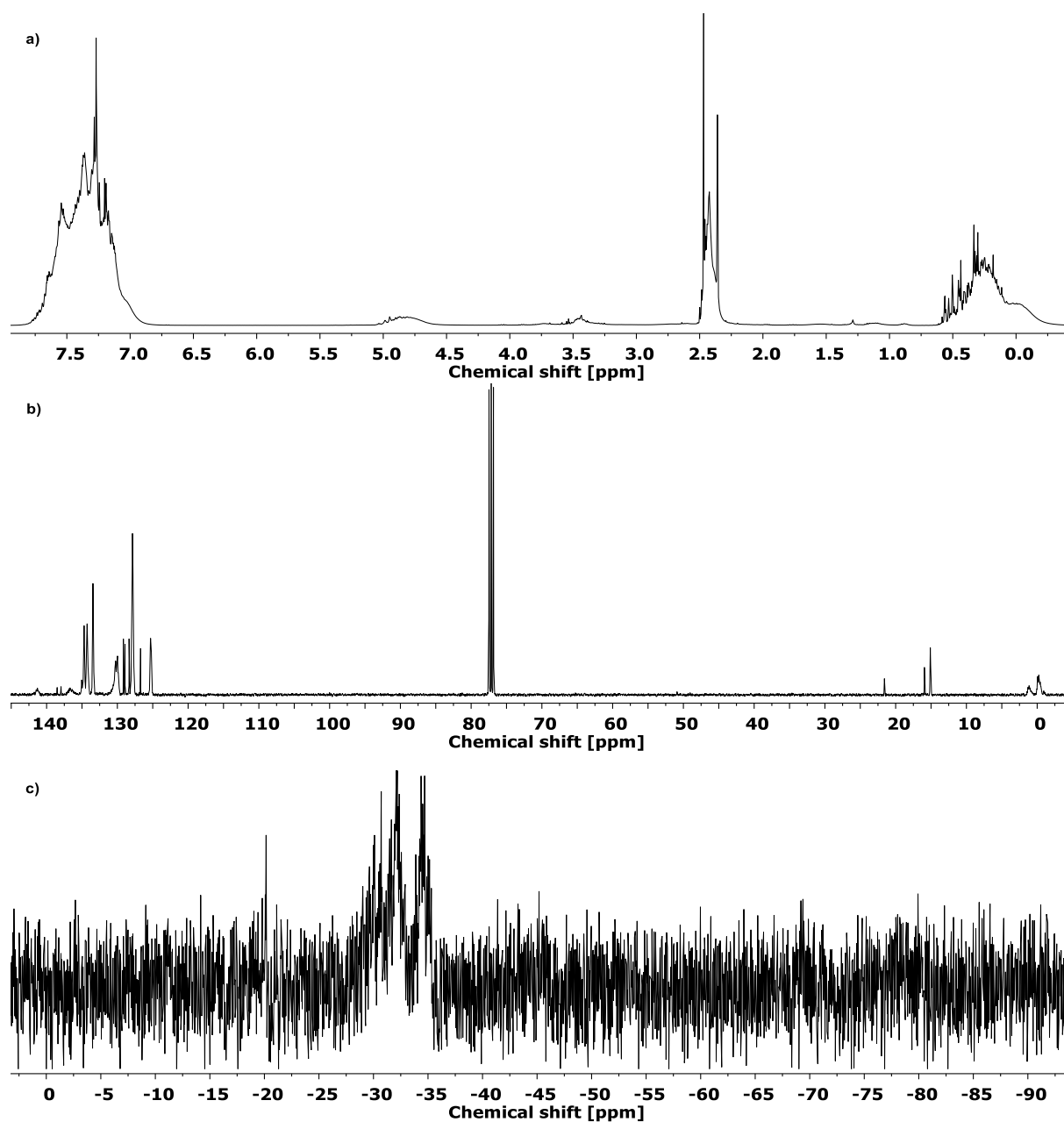
Figure 384: a) ^{1}H NMR (400 MHz, CDCl$_3$), b) ^{13}C NMR (101 MHz, CDCl$_3$) and c) ^{29}Si NMR (79 MHz, CDCl$_3$) of H20_PSMP40_PM40.

a)

b)

c)
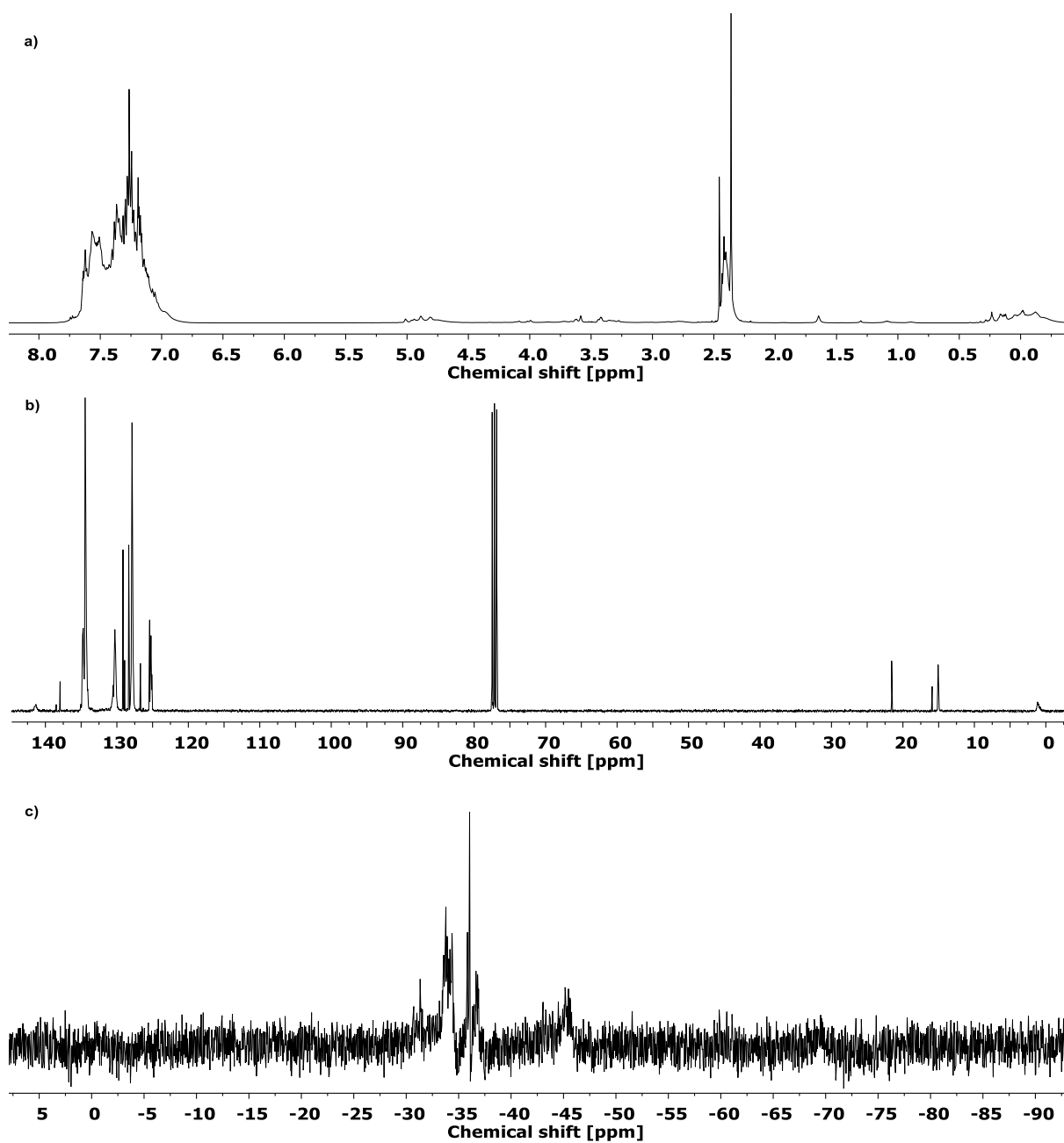
Figure 385: a) ^{1}H NMR (400 MHz, CDCl$_3$), b) ^{13}C NMR (101 MHz, CDCl$_3$) and c) ^{29}Si NMR (79 MHz, CDCl$_3$) of H20_PSMP40_PP40.
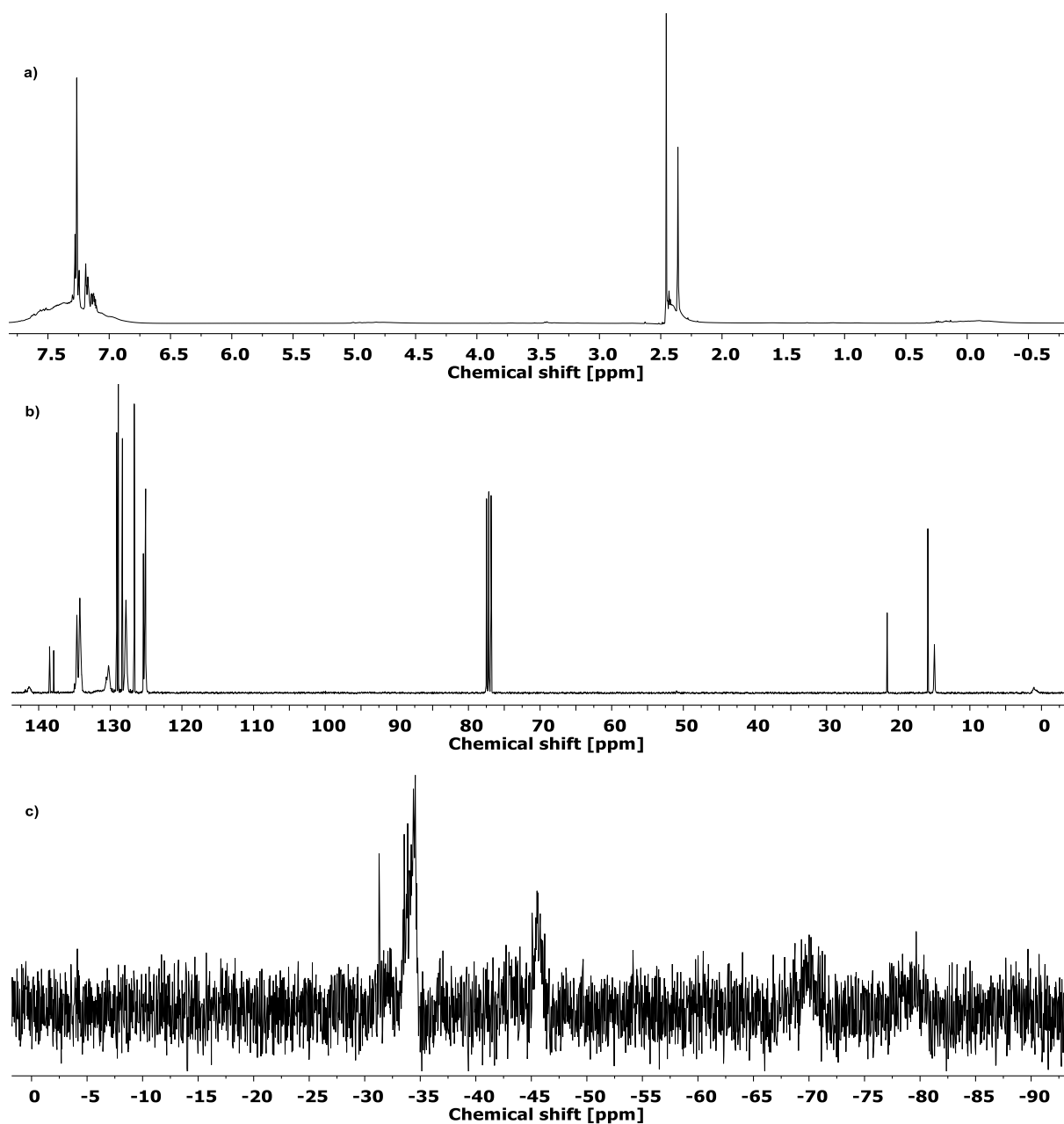
Figure 386: a) ^{1}H NMR (400 MHz, CDCl$_3$), b) ^{13}C NMR (101 MHz, CDCl$_3$) and c) ^{29}Si NMR (79 MHz, CDCl$_3$) of H20_PSMP80.
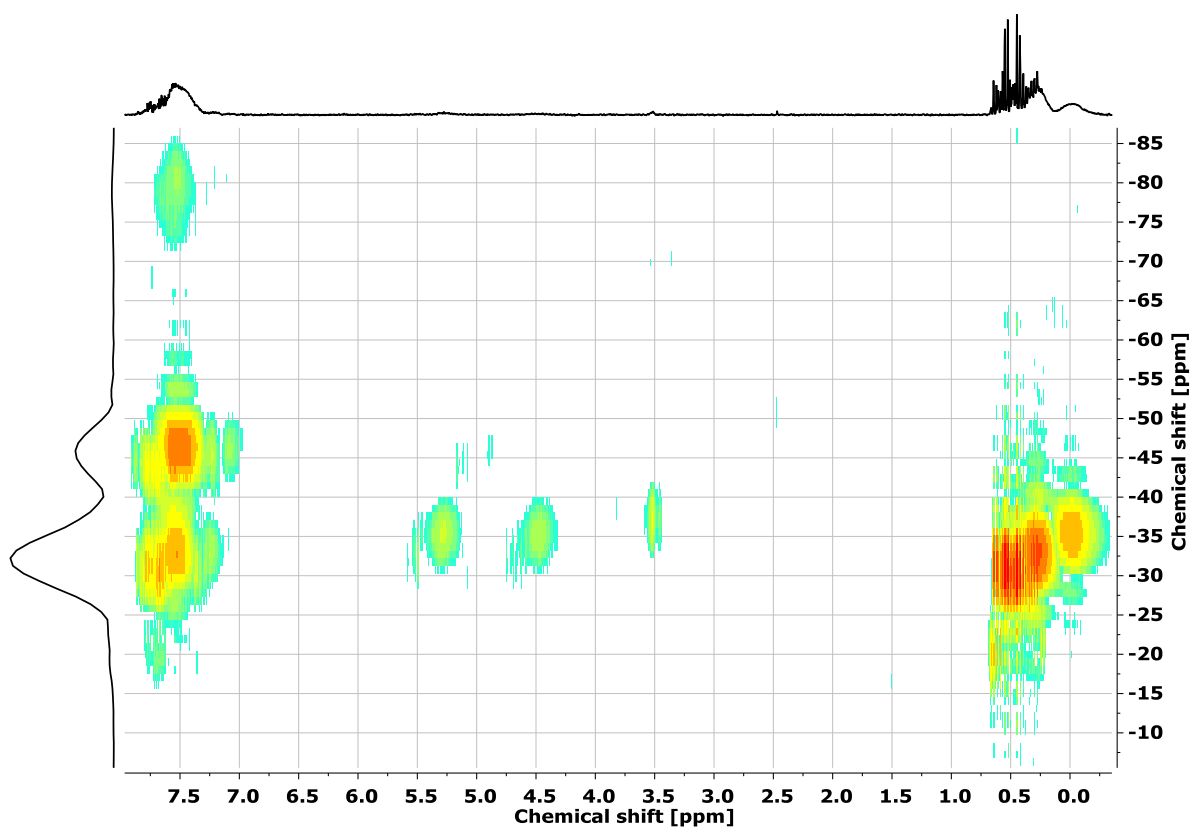
Figure 387: ¹H ²⁹Si HMBC NMR of H20_PSMO40_PP40 in CDCl₃.

6.2.9.4 Additional experimental data for the vinyl- or hydride- and phenylthiomethyl-group containing copolymers

6.2.9.4.1 TGA curves
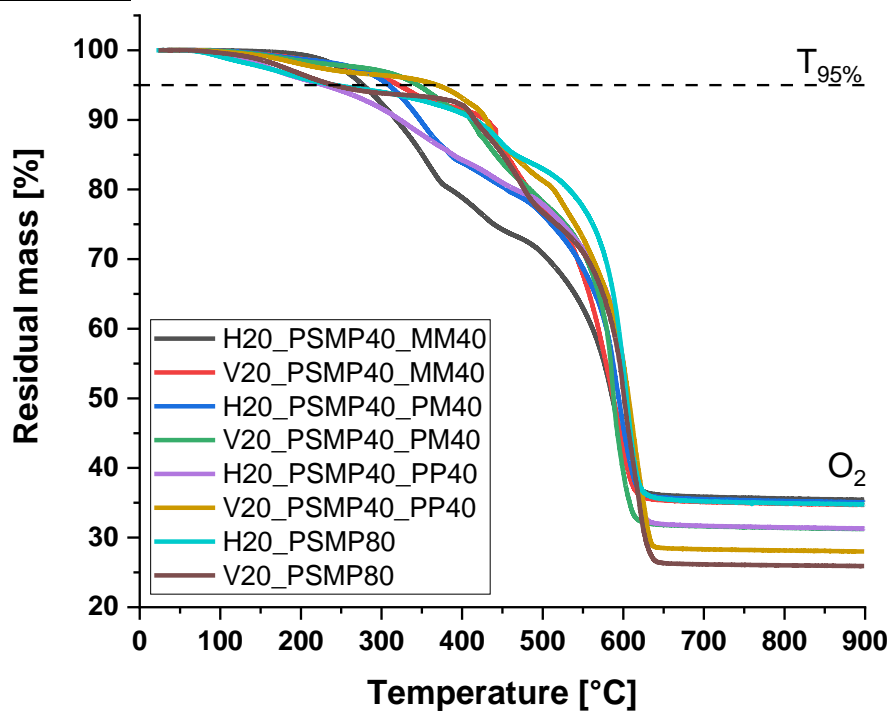
Figure 388: TGA curves of hydride- or vinyl- and phenylthiomethyl-group containing copolymers under oxygen atmosphere.
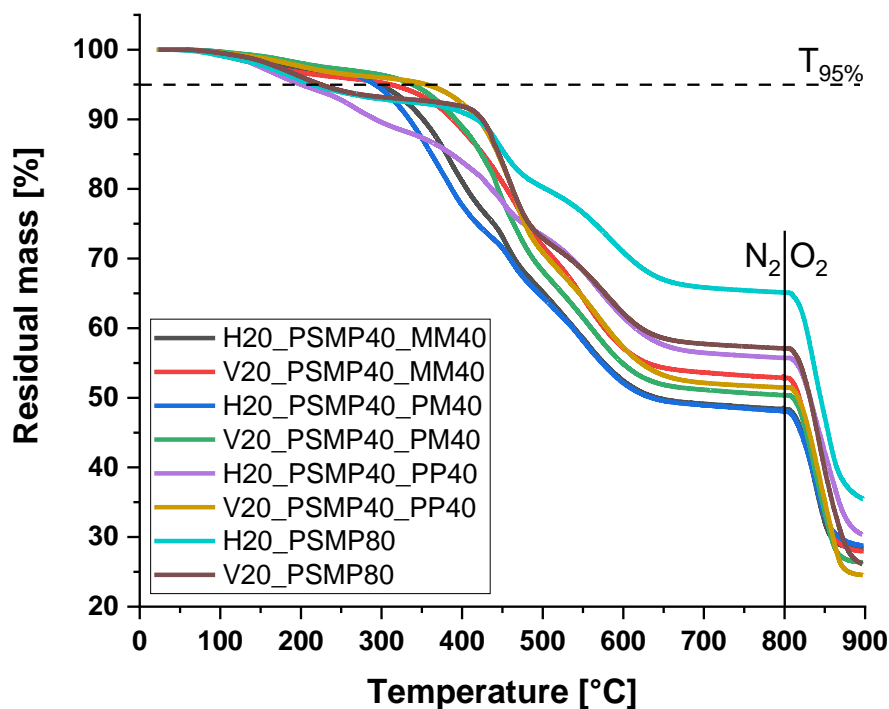
Figure 389: TGA curves of hydride- or vinyl- and phenylthiomethyl-group containing copolymers under nitrogen atmosphere.

6.2.9.4.2 DSC curves
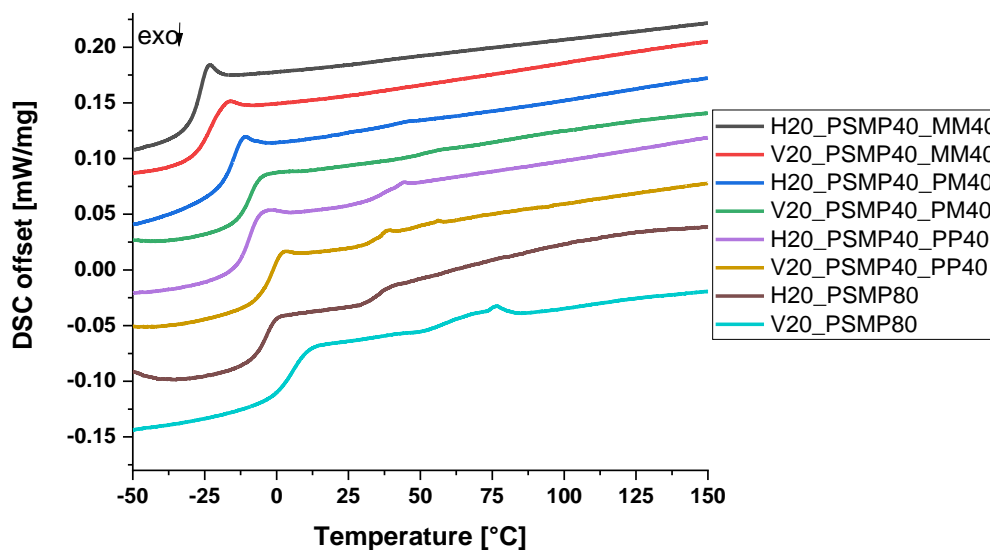
Figure 390: DSC curves of the first heating cycle of hydride- or vinyl- and phenylthiomethyl-group containing copolymers.
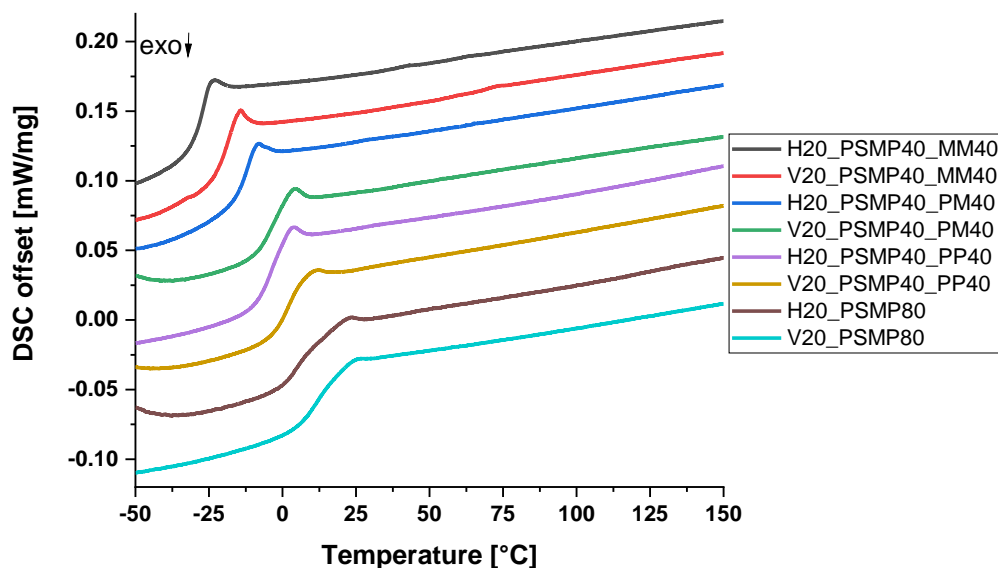
Figure 391: DSC curves of the second heating cycle of hydride- or vinyl- and phenylthiomethyl-group containing copolymers.

6.2.9.5 Synthesis of the cured phenylthiomethyl-group containing polysiloxanes

Typically 400 mg of hydride (H20_PSMP40_XY40) and vinyl (V20_PSMP40_XY40) copolymers are mixed with 2.5 µL (1.63 ppm in siloxane) *Ossko*'s catalyst stock solution which was prepared using 10 µL of xylene isomers with 6 µL *Ossko*'s catalyst. The polymer was degassed at two mbar for one hour and doctor bladed with 120 µm onto a glass which was cleaned with *iso*-propanol and acetone and plasma etched at 100 % power for 15 minutes. The sample was cured at 80 °C for one hour and at 150 °C for four hours.

For P20_PSMP80, ^{13}C and ^{29}Si CP MAS NMRs were exemplarily recorded.

P20_PSMP40_MM40:
Refractive index: 1.5830.

P20_PSMP40_PM40:
Refractive index: 1.5991.

P20_PSMP40_PP40:
Refractive index: 1.6156.

P20_PSMP80:
^{13}C CP MAS NMR (101 MHz, 13 kHz): δ = 141.64 – 124.48 (Ph), 14.01 (SMe), 5.02 (Et), 0.65 – −1.81 (SiMe) ppm.
^{29}Si CP MAS NMR (80 MHz, 13 kHz): δ = −19.98 (-EtMeSi-), −34.50 (-EtPhSi-), −45.12 (-PSMPSi-), −71.32 – −79.33 (-PhSi-) ppm.

Refractive index: 1.6348.
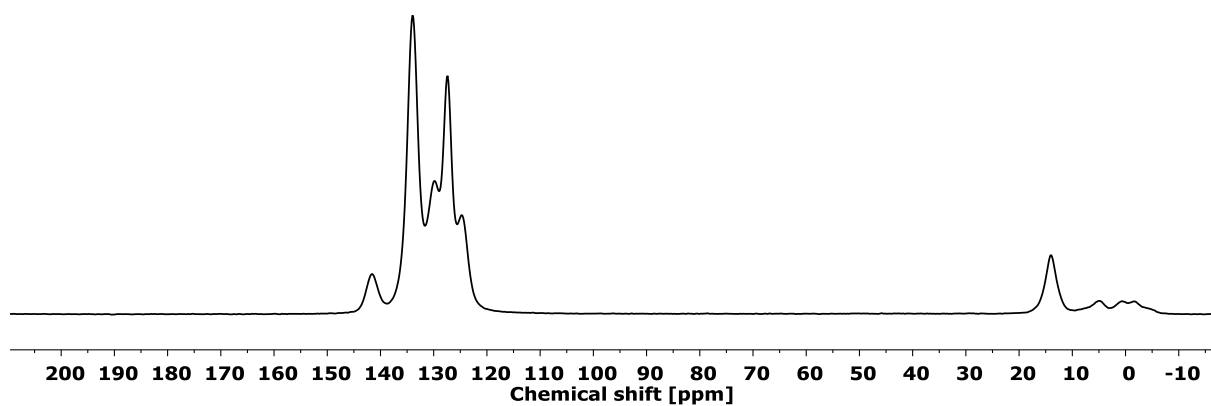
Figure 392: ^{13}C CP MAS NMR (101 MHz, 13 kHz) of P20_PSMP80.

6.2.9.5.1 TGA curves
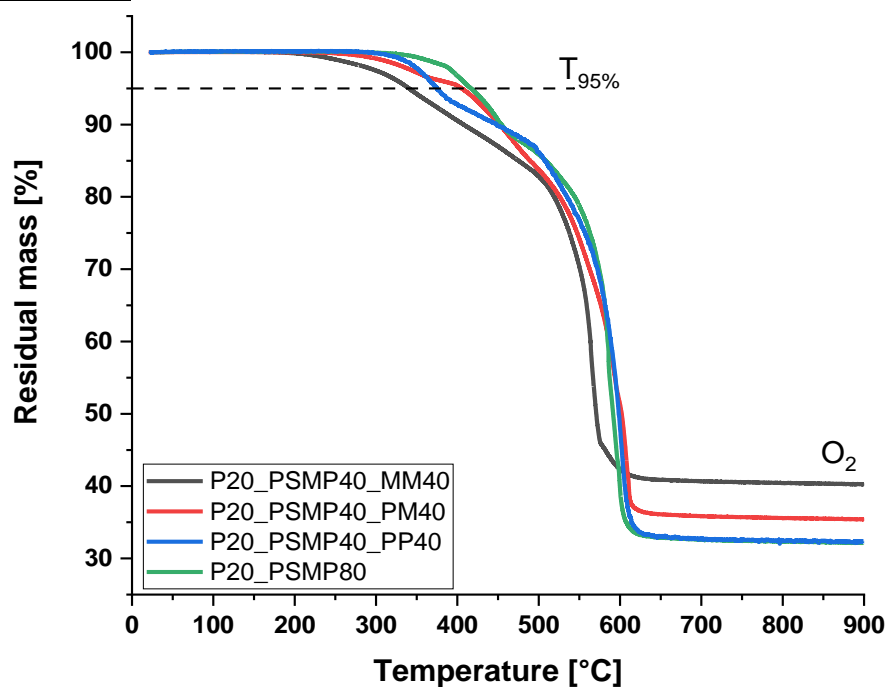
Figure 393: TGA curves of the cured phenylthiomethyl-group containing polymers under oxygen atmosphere.
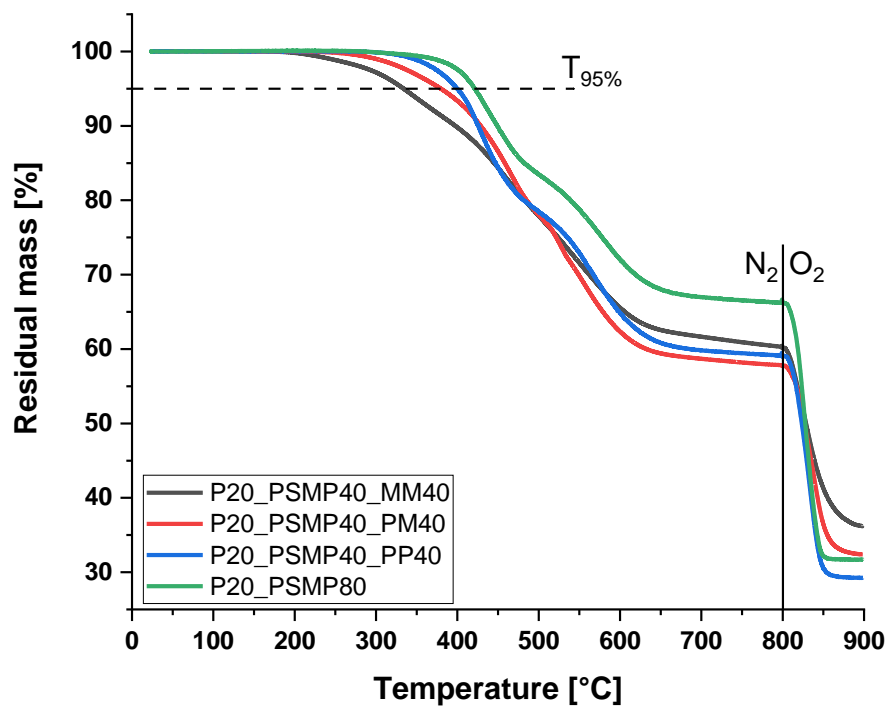
Figure 394: TGA curves of the cured phenylthiomethyl-group containing polymers under nitrogen atmosphere.

6.2.9.5.2 DSC curves
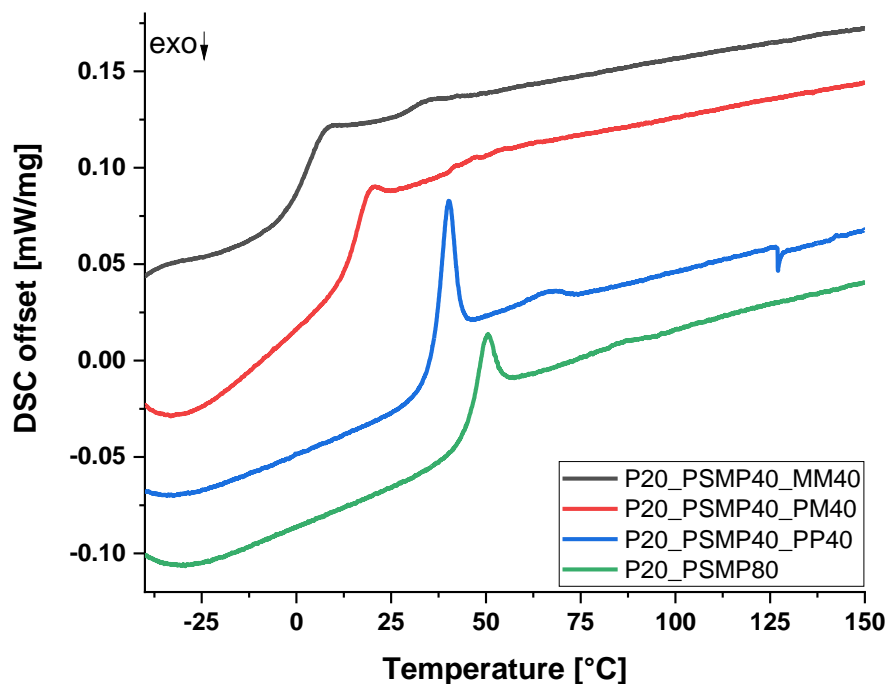
Figure 395: DSC curves of the first heating cycle of the cured phenylthiomethyl-group containing polysiloxanes.
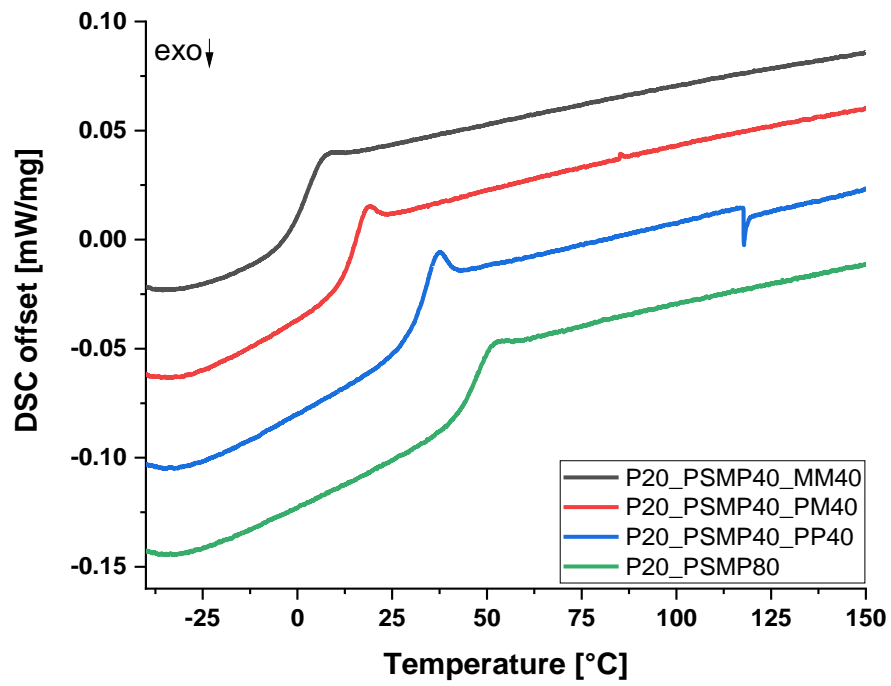
Figure 396: DSC curves of the second heating cycle of the cured phenylthiomethyl-group containing polysiloxanes.

6.2.10 Synthesis of phenanthrenyl-group containing monomers and polymers

6.2.10.1 Synthesis of phenanthrenyl-group containing monomers

6.2.10.1.1 Synthesis of phenanthren-9-ylmethyldimethoxysilane (PHM)
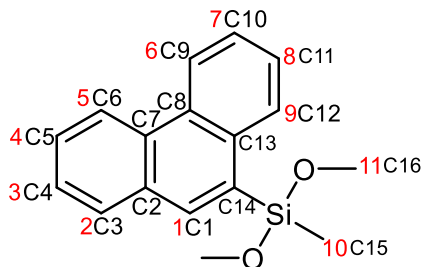
Figure 397: Chemical formula of phenanthren-9-ylmethyldimethoxysilane

20.00 g (77.78 mmol) of 9-bromophenanthrene in 100 mL of absolute tetrahydrofuran were added dropwise at room temperature to 2.00 g (82.29 mmol) of magnesium turnings in 40 mL of absolute tetrahydrofuran and were heated under reflux for one hour. 52.97 g (388.90 mmol) of methyltrimethoxysilane in 50 mL absolute tetrahydrofuran were mixed in a second flask and the reactive Grignard species was slowly added dropwise. After the mixture was stirred at room temperature overnight, it was refluxed for one hour. The cold solution was filtered through a glass frit and the tetrahydrofuran removed under reduced pressure. The crude product was dissolved in 200 mL of toluene and the precipitated salt was removed with a glass frit. After the solvent and the excess methyltrimethoxysilane had been removed under reduced pressure, the product is distilled under high vacuum ($8 \cdot 10^{-3}$ mbar at 152 °C). The clear colourless oil (11.61 g, 41.11 mmol, 53 %) crystallised after several months to form a white solid.

^{1}H NMR (300 MHz, CDCl$_3$): δ = 8.81 (d, J = 7.6 Hz, 1H, H6), 8.75 (d, J = 7.9 Hz, 1H, H5), 8.53 (d, J = 7.9 Hz, 1H, H9), 8.40 (s, 1H, H1), 8.06 (d, J = 7.6 Hz, 1H, H2), 7.75 (m, 4H, H3, H4, H7, H8), 3.79 (s, 6H, H11), 0.70 (s, 3H, H10) ppm.

^{13}C NMR (75 MHz, CDCl$_3$): δ = 137.75 (C14), 134.57 (C1), 131.55 (C2), 131.04 (C7), 130.66 (C13), 130.11 (C10), 129.27 (C3), 128.65 (C8), 127.73 (C11), 126.90 (C4), 126.68 (C5), 126.37 (C12), 123.17 (C9), 122.53 (C6), 50.62 (C16), −3.59 (C15) ppm.

^{29}Si NMR (60 MHz, CDCl$_3$): δ = −13.12 (PHMSiOMe$_2$) ppm.

RI: 1.6310.

CHN C: 72.30 %, H: 6.42 %, N: 0.00 %; calc.: C: 72.32 %, H: 6.45 %, N: 0.00 %.
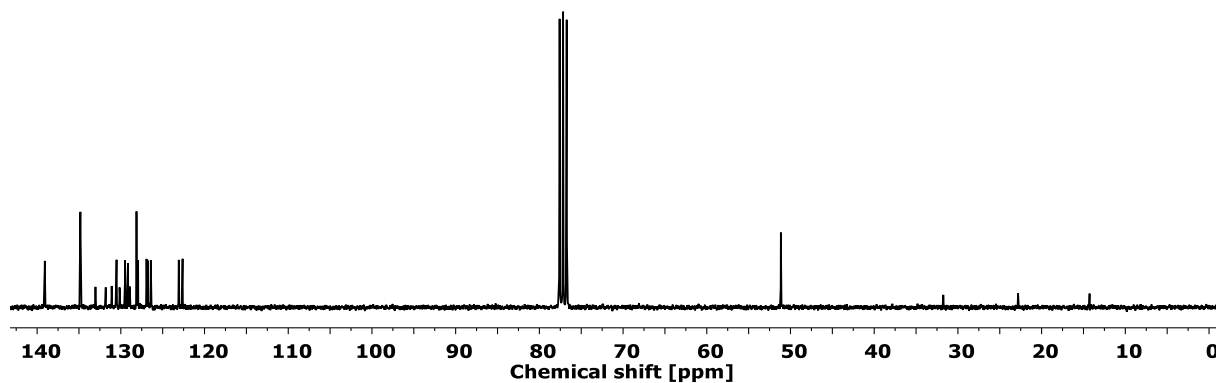
Figure 398: ^{13}C NMR (75 MHz, CDCl$_3$) of phenanthren-9-ylmethyldimethoxysilane (PHM).

6.2.10.1.2 Synthesis of phenanthren-9-ylphenyldimethoxysilane (PHP)
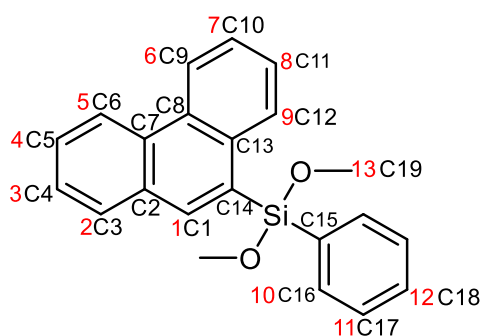
Figure 399: Chemical formula of phenanthren-9-ylphenyldimethoxysilane.

20.00 g (77.78 mmol) of 9-bromophenanthrene in 100 mL of absolute tetrahydrofuran were added dropwise at room temperature to 2.00 g (82.29 mmol) of magnesium turnings in 40 mL of absolute tetrahydrofuran and were heated under reflux for one hour. In a second flask, 30.85 g (155.56 mmol) of phenyltrimethoxysilane in 50 mL absolute tetrahydrofuran were mixed and the reactive Grignard species were slowly added dropwise. After the mixture was stirred at room temperature overnight, it was refluxed for one hour. The cold solution was filtered through a glass frit and the tetrahydrofuran removed under reduced pressure. The crude product was dissolved in 200 mL of toluene and the precipitated salt was removed with a glass frit. After the solvent had been removed under reduced pressure, the excess phenyltrimethoxysilane was removed under high vacuum by distillation (5·10^{-2} mbar at 25 °C). The product was recrystallized from hexane to give white crystals (20.31 g, 58.95 mmol, 76 %).

^{1}H NMR (300 MHz, CDCl$_3$) δ = 8.71 (tr, J = 7.6 Hz, 2H, H5, H6), 8.37 (s, 1H, H1), 8.29 (d, J = 8.1 Hz, 1H, H9), 7.96 (d, J = 7.7 Hz, 1H, H2), 7.72 (m, 3H, H7, H10), 7.63 (tr, J = 7.7 Hz, 2H, H3, H4), 7.53 (tr, J = 7.5 Hz, 1H, H8), 7.39 (m, 3H, H11, H12), 3.70 (s, 6H, H13) ppm.

^{13}C NMR (75 MHz, CDCl$_3$): δ = 139.09 (C14), 134.84 (C1), 134.76 (C16), 133.03 (C15), 131.81 (C2), 131.10 (C7), 130.52 (C18), 130.15 (C17), 129.50 (C13), 129.16 (C10), 128.94

(C3), 128.14 (C8), 127.95 (C11), 126.93 (C4), 126.76 (C12), 126.42 (C5), 123.08 (C9), 122.63 (C6), 51.15 (C19) ppm.

^{29}Si NMR (60 MHz, CDCl$_3$): δ = −27.68 (PHPSiOMe$_2$) ppm.

RI: could not be determined.

CHN C: 76.71 %, H: 5.85 %, N: 0.00 %; calc.: C: 76.73 %, H: 5.90 %, N: 0.00 %.
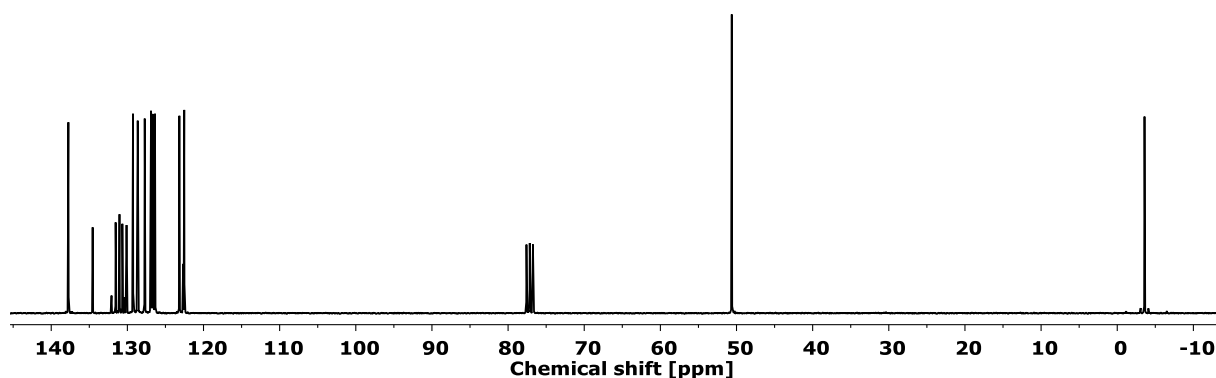
Figure 400: ^{13}C NMR (75 MHz, CDCl$_3$) of phenanthren-9-ylphenyldimethoxysilane (PHP).

6.2.10.2 Synthesis of phenanthrenyl-group containing copolymers

6.2.10.2.1 Vinyl- and phenanthrenyl-group containing polysiloxanes
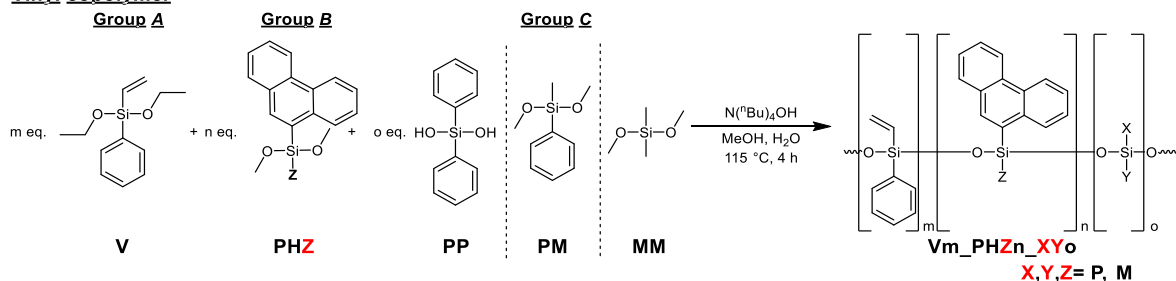
Figure 401: General synthesis of vinyl- and phenanthrenyl-group containing polysiloxanes.

General synthesis for vinyl- and phenanthrenyl-group containing polysiloxanes:

To 1 eq. (1.45 mmol) vinylphenyldiethoxysilane, 2 eq. (2.90 mmol) phenanthrenyl-group containing monomer of group *B*, 2 eq. (2.90 mmol) of group *C* monomer, 352 mg (19.60 mmol) distilled water and 396 mg (12.36 mmol) of methanol, 22.6 µL (0.09 mmol) of 40 wt% tetra-*n*-butylammonium hydroxide solution in water as catalyst was added and a fractionating column was attached onto the flask (Figure 401). After one hour at 85 °C, the temperature was raised to 115 °C for one hour. The distillation head was removed, and the reaction was continued for two additional hours. 7.0 mL of toluene and 3.5 mL of water were added and then centrifuged

at 8000 rpm for one minute. The organic phase was washed twice with 2.0 mL of 2 M hydrochloric acid and three times with 2.0 mL of distilled water analogously. After filtering the organic phase with a 0.45 µm syringe filter, the organic phase was dried under vacuum. A clear, viscous polymer was obtained (100 % with residual toluene).

V20_PHM40_MM40:

Yield: 1007.8 mg

^{1}H NMR (400 MHz, CDCl$_3$): δ = 8.72 – 7.14 (m, 23H, PHE, Ph), 6.25 – 5.94 (m, 3V, V), 0.27 – 0.14 (m, 18H, Me) ppm.

^{13}C NMR (101 MHz, CDCl$_3$): δ = 136.48 – 122.78 (Ph, PH, V), 1.04 – −3.34 (Me) ppm.

^{29}Si NMR (79 MHz, CDCl$_3$): δ = −17.60 – −21.91 (-Me$_2$Si-), −34.36 – −37.67 (-PHMSi-), −46.12 – −46.54 (-PhVSi-) ppm.

Refractive index: 1.5210.

V20_PHM40_PM40:

Yield: 1231.7 mg

^{1}H NMR (400 MHz, CDCl$_3$): δ = 8.68 – 7.13 (m, 33H, PHE, Ph), 6.18 – 5.81 (m, 3V, V), 0.56 – −0.01 (m, 12H, Me) ppm.

^{13}C NMR (101 MHz, CDCl$_3$): δ = 136.69 – 122.78 (Ph, PH, V), −0.02 – −2.42 (Me) ppm.

^{29}Si NMR (79 MHz, CDCl$_3$): δ = −30.14 – −34.92 (-MePhSi-, -PHMSi-), −42.19 – −43.39 (-PhVSi-) ppm.

Refractive index: 1.5689.

V20_PHM40_PP40:

Yield: 1368.6 mg

^{1}H NMR (400 MHz, CDCl$_3$): δ = 8.68 – 7.15 (m, 43H, PHE, Ph), 6.26 – 5.75 (m, 3V, V), 0.86 – 0.30 (m, 6H, Me) ppm.

^{13}C NMR (101 MHz, CDCl$_3$): δ = 136.87 – 122.42 (Ph, PH, V), 1.97 – 1.55 (Me) ppm.

^{29}Si NMR (79 MHz, CDCl$_3$): δ = −28.26 – −31.78 (-PHMSi-), −42.59 – −46.22 (-Ph$_2$Si-, -PhVSi-) ppm.

Refractive index: 1.5782.

V20_PHP40_MM40:

Yield: 1239.3 mg

^{1}H NMR (400 MHz, CDCl$_3$): δ = 8.70 – 7.17 (m, 33H, PHE, Ph), 6.11 – 5.84 (m, 3H, V), 0.24 – −0.25 (m, 12H, Me) ppm.

^{13}C NMR (101 MHz, CDCl$_3$): δ = 134.18 – 122.79 (Ph, PH, V), 0.99 (Me) ppm.

^{29}Si NMR (79 MHz, CDCl$_3$): δ = −17.93 – −20.33 (-Me$_2$Si-), −44.44 – −49.17 (-PHPSi-, -PhVSi-) ppm.

Refractive index: 1.5725.

V20_PHP40_PM40:

Yield: 1479.4 mg

^{1}H NMR (400 MHz, CDCl$_3$): δ = 8.68 – 7.05 (m, 43H, PHE, Ph), 6.18 – 5.90 (m, 3H, V), 0.65 – 0.17 (m, 6H, Me) ppm.

^{13}C NMR (101 MHz, CDCl$_3$): δ = 138.38 – 122.76 (Ph, PH, V), 0.14 – −0.40 (Me) ppm.

^{29}Si NMR (79 MHz, CDCl$_3$): δ = −28.30 – −32.71 (-MePhSi-), −40.97 – −45.47 (-PHPSi-, -PhVSi-) ppm.

Refractive index: 1.6334.

V20_PHP40_PP40:

Yield: 1683.0 mg

^{1}H NMR (300 MHz, CDCl$_3$): δ = 8.70 – 6.84 (m, 53H, PHE, Ph), 6.07 – 5.67 (m, 3H, V) ppm.

^{13}C NMR (75 MHz, CDCl$_3$): δ = 138.30 – 122.78 (Ph, PH, V) ppm.

^{29}Si NMR (60 MHz, CDCl$_3$): δ = −44.94 – −48.93 (-PHPSi-, -Ph$_2$Si-, -PhVSi-) ppm.

Refractive index: 1.6297.

V40_PHM20_PP40:

Yield: 1263.9 mg

^{1}H NMR (400 MHz, CDCl$_3$): δ = 8.69 – 7.18 (m, 39H, PHE, Ph), 6.14 – 5.75 (m, 6H, V), 0.63 – −0.18 (m, 3H, Me) ppm.

^{13}C NMR (101 MHz, CDCl$_3$): δ = 136.11 – 122.77 (Ph, PH, V), 1.74 – −3.44 (Me) ppm.

^{29}Si NMR (79 MHz, CDCl$_3$): δ = −28.24 – −29.50 (-PHMSi-), −42.74 – −47.27 (-Ph$_2$Si-, -PhVSi-) ppm.

Refractive index: 1.5960.

V40_PHM40_PP20:

Yield: 1409.5 mg

^{1}H NMR (400 MHz, CDCl$_3$): δ = 8.69 – 7.12 (m, 38H, PHE, Ph), 6.30 – 5.74 (m, 6H, V), 0.35 – 0.10 (m, 6H, Me) ppm.

^{13}C NMR (101 MHz, CDCl$_3$): δ = 137.96 – 122.46 (Ph, PH, V), 1.36 – −3.90 (Me) ppm.

^{29}Si NMR (79 MHz, CDCl$_3$): δ = −28.37 – −35.28 (-PHMSi-), −44.25 – −47.90 (-Ph$_2$Si-, -PhVSi-) ppm.

Refractive index: 1.5756.

6.2.10.2.2 Hydride- and phenanthrenyl-group containing polysiloxanes
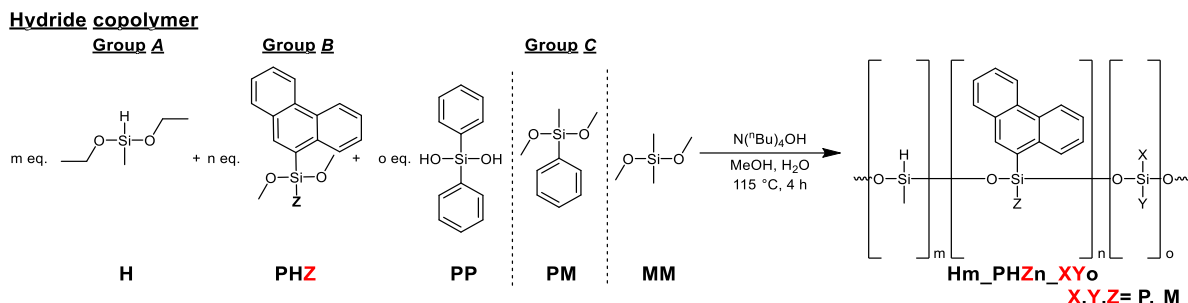
Figure 402: General synthesis of hydride- and phenanthrenyl-group containing polysiloxanes.

General synthesis for hydride- and phenanthrenyl-group containing polysiloxanes:

To 1 eq. (1.45 mmol) methyldiethoxysilane, 2 eq. (2.90 mmol) phenanthrenyl-group containing monomer of group *B*, 2 eq. (2.90 mmol) of group *C* monomer, 352 mg (19.60 mmol) distilled water and 396 mg (12.36 mmol) of methanol, 45 mg (1.12 mmol) of concentrated hydrochloric acid as catalyst was added and a fractionating column was attached onto the flask (Figure 402). After one hour at 85 °C, the temperature was raised to 115 °C for one hour. The distillation head was removed, and the reaction was continued for two additional hours. 7.0 mL of toluene and 3.5 mL of water were added and then centrifuged at 8000 rpm for one minute. The organic phase was washed once with saturated potassium bicarbonate and four times with 2.0 mL of distilled water analogously. After filtering the organic phase with a 0.45 µm syringe filter, the organic phase was dried under vacuum. A clear, viscous polymer was obtained (100 % with residual toluene).

H20_PHM40_MM40:

Yield: 1069.5 mg

^{1}H NMR (400 MHz, CDCl$_3$): δ = 8.71 – 7.15 (m, 18H, PHE), 5.11 – 4.76 (m, 1H, H), 0.61 – 0.04 (m, 21H, Me) ppm.

^{13}C NMR (101 MHz, CDCl$_3$): δ = 136.61 – 122.45 (PH), 1.56 – 0.84 (Me) ppm.

^{29}Si NMR (79 MHz, CDCl$_3$): δ = −17.42 – −21.73 (-Me$_2$Si-), −29.46 – −33.40 (-PHMSi-), −35.68 – −36.42 (-HMeSi-) ppm.

Refractive index: 1.5925.

H20_PHM40_PM40:

Yield: 1254.0 mg

^{1}H NMR (400 MHz, CDCl$_3$): δ = 8.69 – 7.08 (m, 28H, PHE, Ph), 5.24 – 4.87 (m, 1H, H), 0.85 – 0.04 (m, 15H, Me) ppm.

^{13}C NMR (101 MHz, CDCl$_3$): δ = 137.94 – 122.45 (Ph, PH), 1.67 – −0.53 (Me) ppm.

^{29}Si NMR (79 MHz, CDCl$_3$): δ = −29.37 – −32.86 (-MePhSi-, -PHMSi-), −35.26 – −35.87 (-HMeSi-) ppm.

Refractive index: 1.6120.

H20_PHM40_PP40:

Yield: 1321.1 mg

^{1}H NMR (400 MHz, CDCl$_3$): δ = 8.68 – 7.18 (m, 38H, PHE, Ph), 5.23 – 4.95 (m, 1H, H), 3.53 – 3.19 (m, 1.5H, Si-OMe), 0.69 – 0.08 (m, 9H, Me) ppm.

^{13}C NMR (101 MHz, CDCl$_3$): δ = 136.83 – 122.29 (Ph, PH), 2.31 – 0.64 (Me) ppm.

^{29}Si NMR (79 MHz, CDCl$_3$): δ = −29.29 – −31.51 (-PHMSi-), −33.59 – −36.76 (-HMeSi-), −45.03 – −45.41 (-Ph$_2$Si-) ppm.

Refractive index: 1.6274.
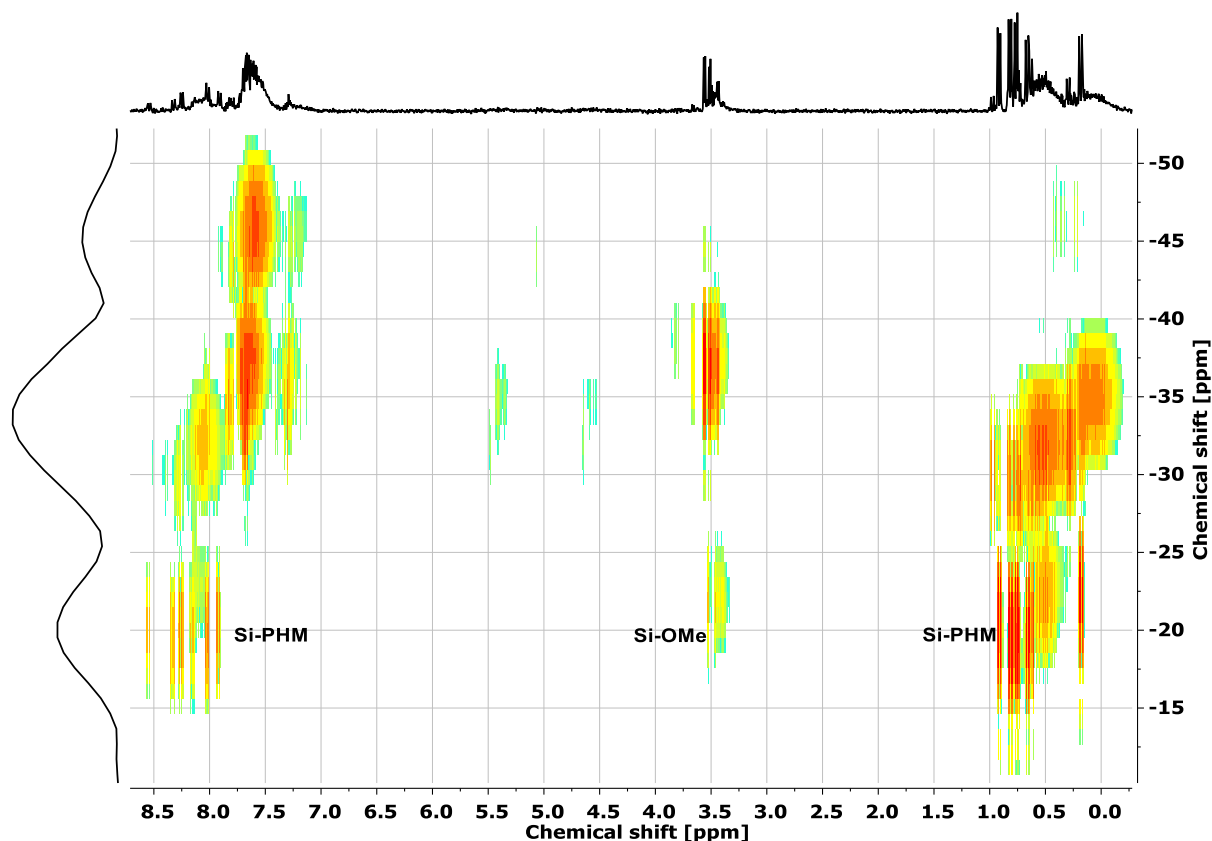
Figure 403: ^{1}H ^{29}Si HMBC NMR of H20_PHM40_PP40.

H20_PHP40_MM40:

Yield: 1206.6 mg

^{1}H NMR (400 MHz, CDCl$_3$): δ = 8.69 – 7.15 (m, 28H, PHE, Ph), 5.26 – 4.81 (m, 1H, H), 0.36 – −0.06 (m, 15H, Me) ppm.

^{13}C NMR (101 MHz, CDCl$_3$): δ = 137.83 – 122.42 (Ph, PH), 1.06 – 0.93 (Me) ppm.

^{29}Si NMR (79 MHz, CDCl$_3$): δ = −17.24 – −19.94 (-Me$_2$Si-), −31.40 – −35.84 (-HMeSi-), −43.21 – −46.06 (-PHPSi-) ppm.

Refractive index: 1.6024.

H20_PHP40_PM40:

Yield: 1479.3 mg

^{1}H NMR (400 MHz, CDCl$_3$): δ = 8.69 – 7.11 (m, 38H, PHE, Ph), 5.27 – 4.92 (m, 1H, H), 3.64 – 3.49 (m, 0.3 H, Si-OMe), 0.59 – 0.20 (m, 9H, Me) ppm.

^{13}C NMR (101 MHz, CDCl$_3$): δ = 138.58 – 122.50 (Ph, PH), 51.23 – 51.04 (OMe), 1.27 – −0.26 (SiMe) ppm.

^{29}Si NMR (79 MHz, CDCl$_3$): δ = −29.66 – −31.86 (-MePhSi-), −32.36 – −37.89 (-HMeSi-), −42.99 – −45.13 (-PHPSi-) ppm.

Refractive index: 1.6175.
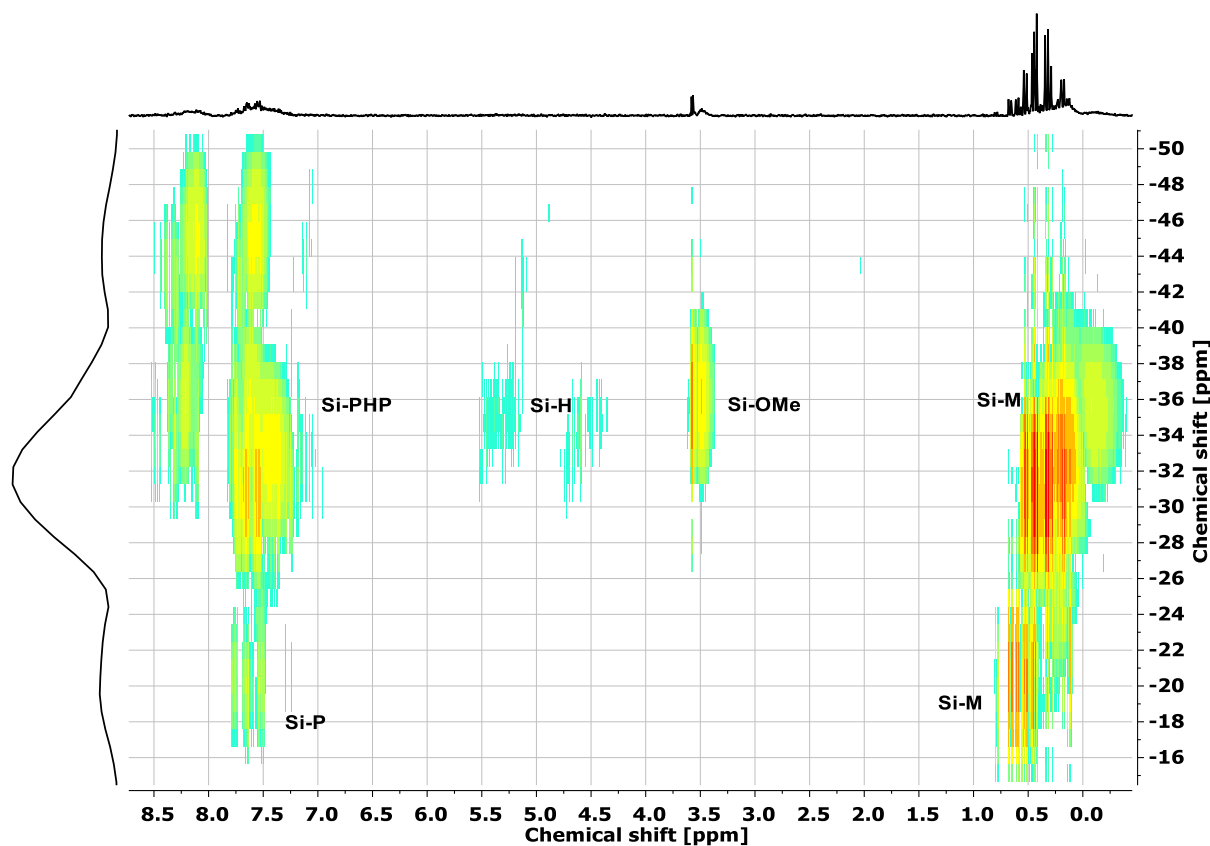
Figure 404: ^{1}H ^{29}Si HMBC NMR of H20_PHP40_PM40.

H20_PHP40_PP40:

Yield: 1531.9 mg

^{1}H NMR (300 MHz, CDCl3): δ = 8.69 – 6.78 (m, 48H, PHE, Ph), 5.06 – 4.27 (m, 1H, H), 0.17 –0.55 (m, 3H, Me) ppm.

^{13}C NMR (75 MHz, CDCl3): δ = 134.50 – 122.77 (Ph, PH), 0.58 (Me) ppm.

^{29}Si NMR (60 MHz, CDCl3): δ = −32.08 – −35.43 (-HMeSi-), −43.84 – −46.69 (-PHPSi-, -Ph$_2$Si-) ppm.

Refractive index: 1.6030.

H40_PHM20_PP40:

Yield: 927.8mg

^{1}H NMR (400 MHz, CDCl$_3$): δ = 8.74 – 7.00 (m, 29H, PHE, Ph), 5.16 – 4.73 (m, 2H, H), 0.64 – −0.11 (m, 9H, Me) ppm.

^{13}C NMR (101 MHz, CDCl$_3$): δ = 136.43 – 122.46 (Ph, PH), 1.44 – 1.04 (Me) ppm.

^{29}Si NMR (79 MHz, CDCl$_3$): δ = −30.93 – −34.85 (-HMeSi-, -PHMSi-), −42.91 – −45.80 (-Ph$_2$Si-) ppm.

Refractive index: 1.5985.

H40_PHM40_PP20:

Yield: 1225.8 mg

^{1}H NMR (400 MHz, CDCl$_3$): δ = 8.79 – 7.05 (m, 28H, PHE, Ph), 5.21 – 4.84 (m, 2H, H), 0.94 – −0.10 (m, 12H, Me) ppm.

^{13}C NMR (101 MHz, CDCl$_3$): δ = 137.96 – 122.44 (Ph, PH), 1.53 – 1.12 (Me) ppm.

^{29}Si NMR (79 MHz, CDCl$_3$): δ = −29.41 – −32.23 (-PHMSi-), −34.34 – −35.52 (-HMeSi-), −45.28 – −46.11 (-Ph$_2$Si-) ppm.

Refractive index: 1.6162.

6.2.10.3 Curing of the phenanthrenyl-containing polysiloxanes

330 mg from a vinyl and the appropriate hydride polysiloxane were mixed with 6 ppm of *Ossko*'s platinum catalyst. To handle such low concentrations, the as received 2 % *Ossko*'s catalyst in xylene was further diluted with xylene. The mixed copolymers were evacuated at two mbar for one hour and doctor bladed with 120 µm onto a microscope slide. The slide was cleaned with *iso*-propanol and acetone, then plasma etched for 15 minutes. Finally, the films were cured at 100 °C for one hour and 150 °C for six hours to ensure complete cross-linking.

P20_PHM40_MM40:

Refractive index: 1.5690.

P20_PHM40_PM40:

Refractive index: 1.5990.

P20_PHM40_PP40:

Refractive index: 1.6140.

P20_PHP40_MM40:

^{13}C CP MAS NMR (101 MHz, 13 kHz): δ = 140.00 – 120.00 (Ph, PH), 10.00 – −5.00 (Et, Me) ppm.

^{29}Si CP MAS NMR (80 MHz, 13 kHz): δ = −25.00 – −30.00 (-EtMeSi-), −32.00 – −38.00 (-EtPhSi-), −43.00 – −50.00 (-PHPSi-) ppm.

Refractive index: 1.5896.

P20_PHP40_PM40:
Refractive index: 1.6270.

P20_PHP40_PP40:
Refractive index: 1.6297.

P40_PHM20_PP40:
Refractive index: 1.6034.

P40_PHM40_PP20:

Refractive index: 1.6051.

6.2.10.4 Additional experimental data for the hydride- or vinyl- and phenanthrenyl-group containing copolymers and cured polysiloxanes

6.2.10.4.1 <u>FT-IR spectra of the phenanthrenyl-group containing polysiloxanes</u>
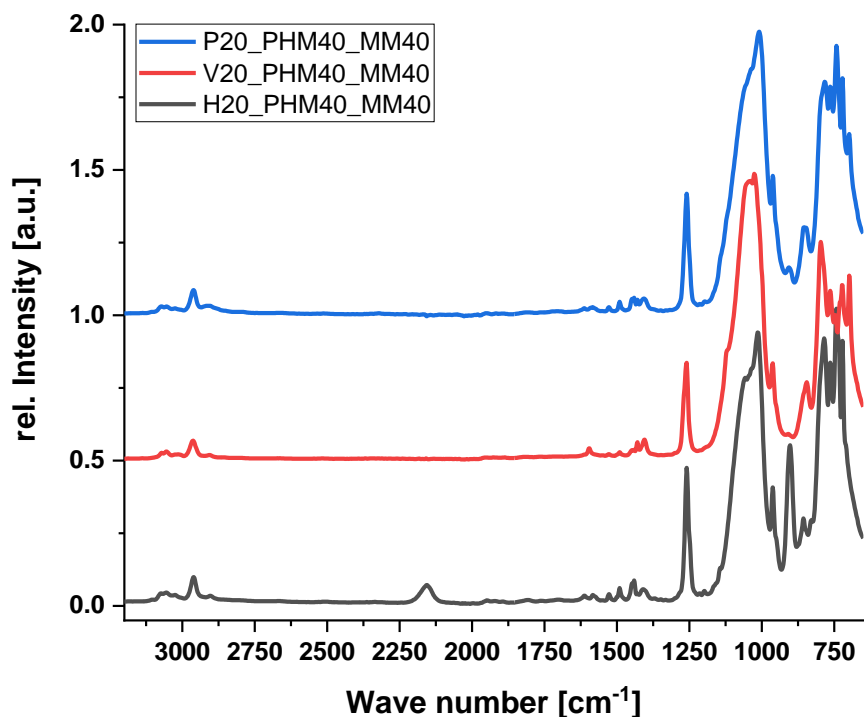
Figure 405: FT-IR spectra of X20_PHM40_MM40.
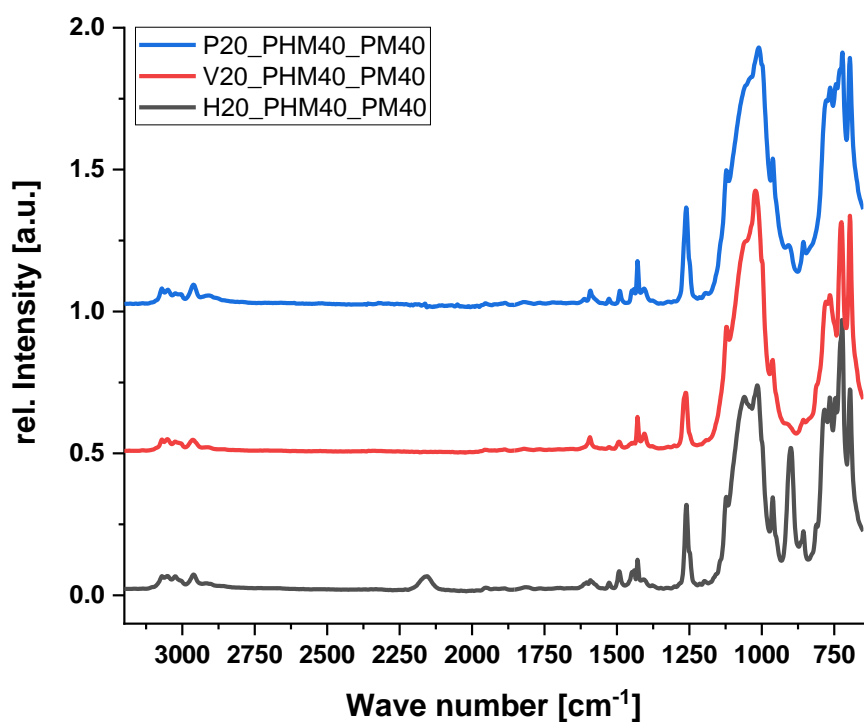
Figure 406: FT-IR spectra of X20_PHM40_PM40.
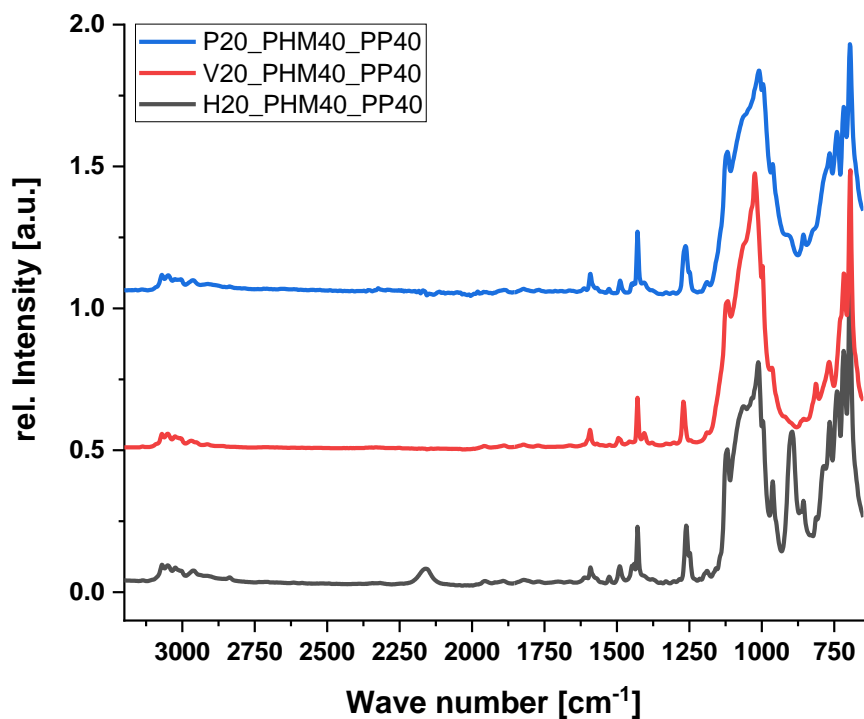
Figure 407: FT-IR spectra of X20_PHM40_PP40.
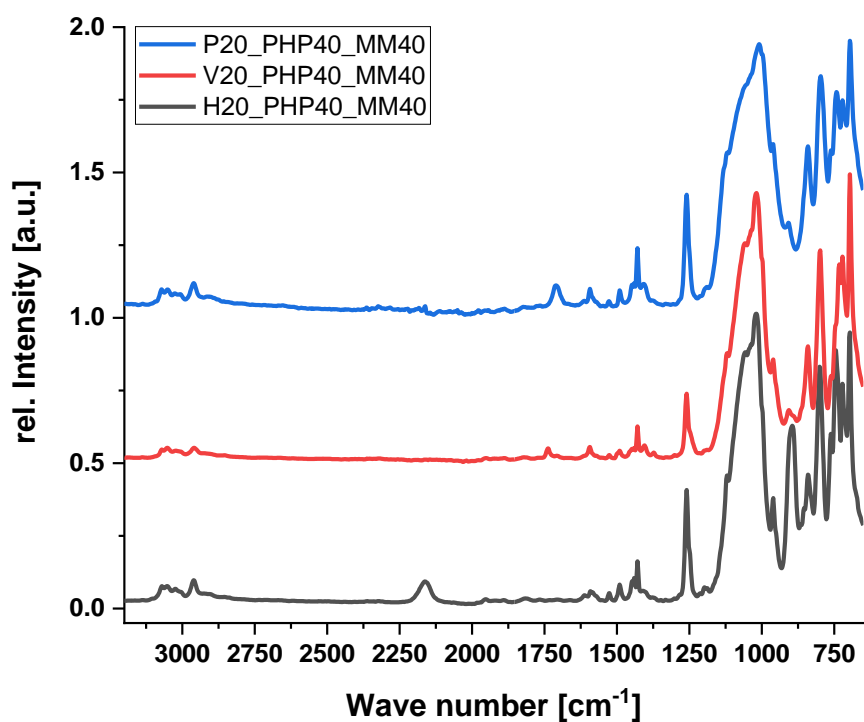
Figure 408: FT-IR spectra of X20_PHP40_MM40.
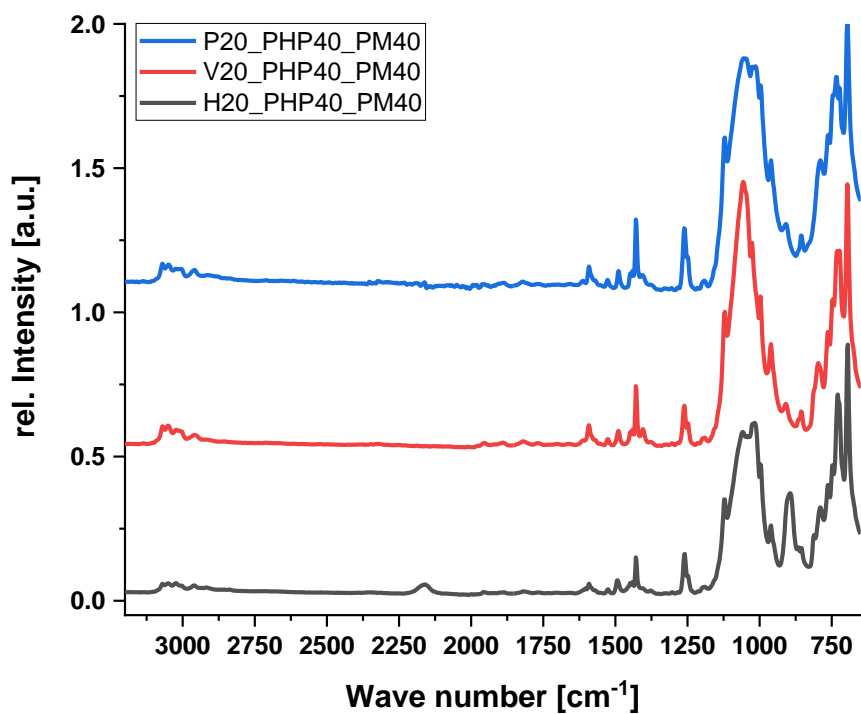
Figure 409: FT-IR spectra of X20_PHP40_PM40.
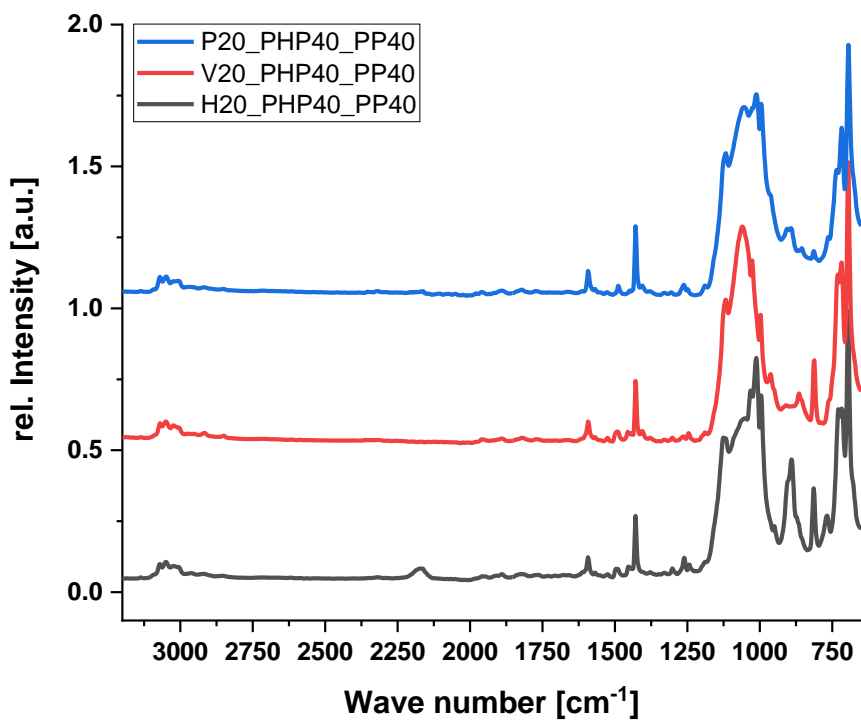
Figure 410: FT-IR spectra of X20_PHP40_PP40.
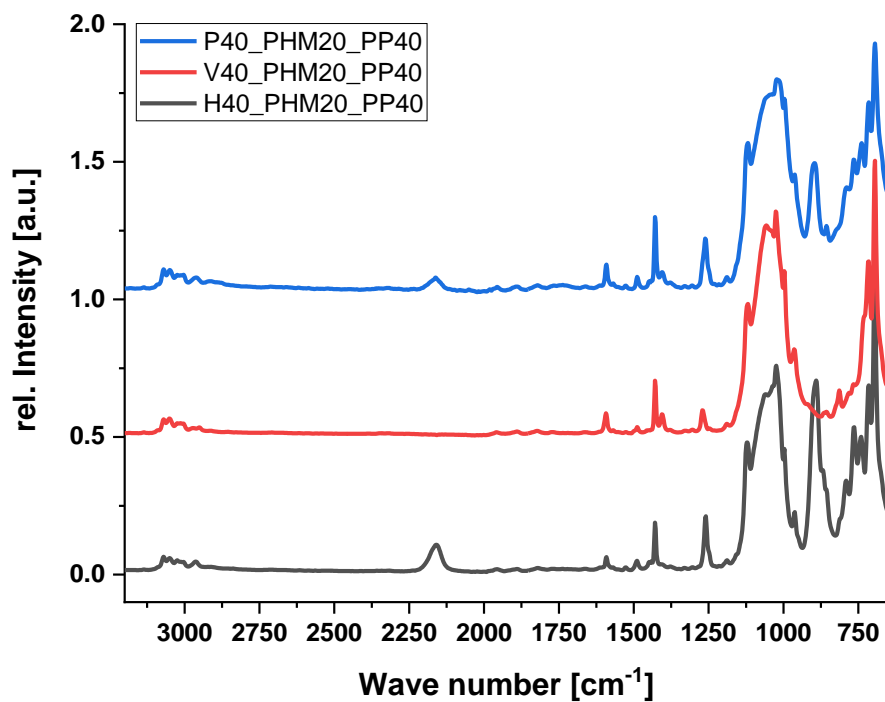
Figure 411: FT-IR spectra of X40_PHM20_PP40.
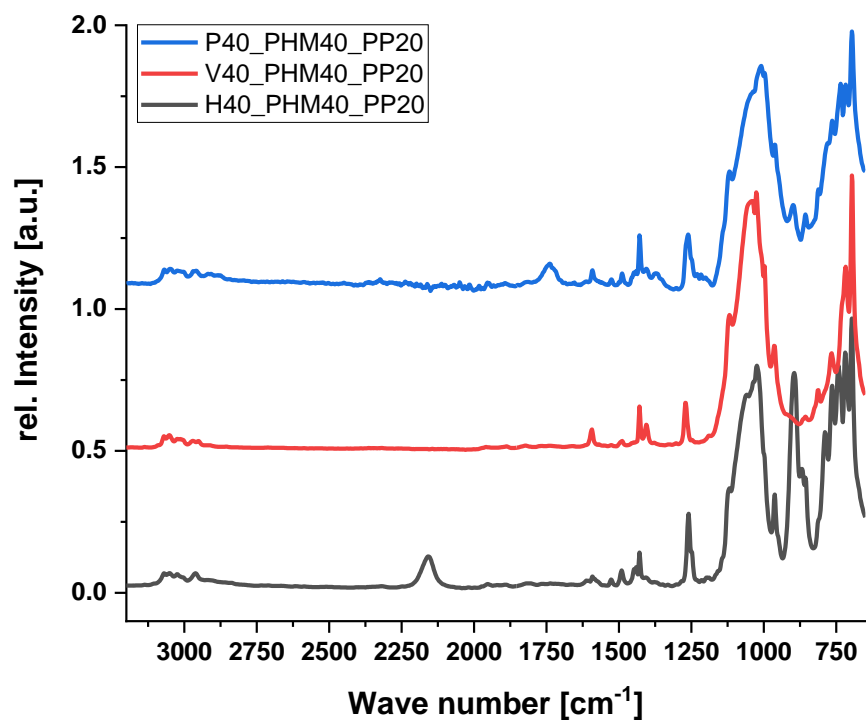
Figure 412: FT-IR spectra of X40_PHM40_PP20.

6.2.10.4.2 NMR spectra of the hydride- or vinyl- and phenanthrenyl-group containing polysiloxanes

a)

b)

c)
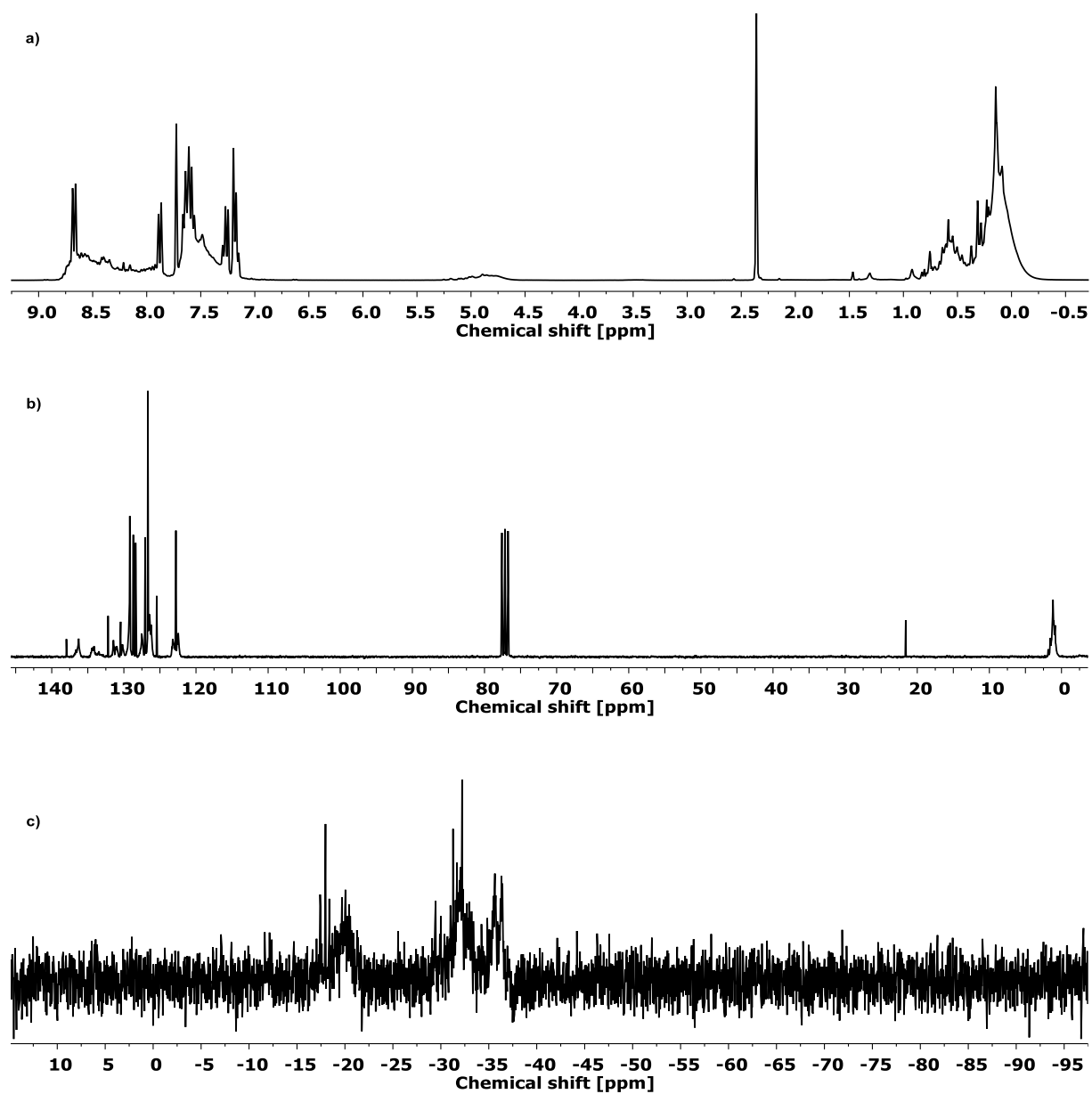
Figure 413: a) ^{1}H NMR (400 MHz, CDCl$_3$), b) ^{13}C NMR (101 MHz, CDCl$_3$) and c) ^{29}Si NMR (79 MHz, CDCl$_3$) of H20_PHM40_MM40.
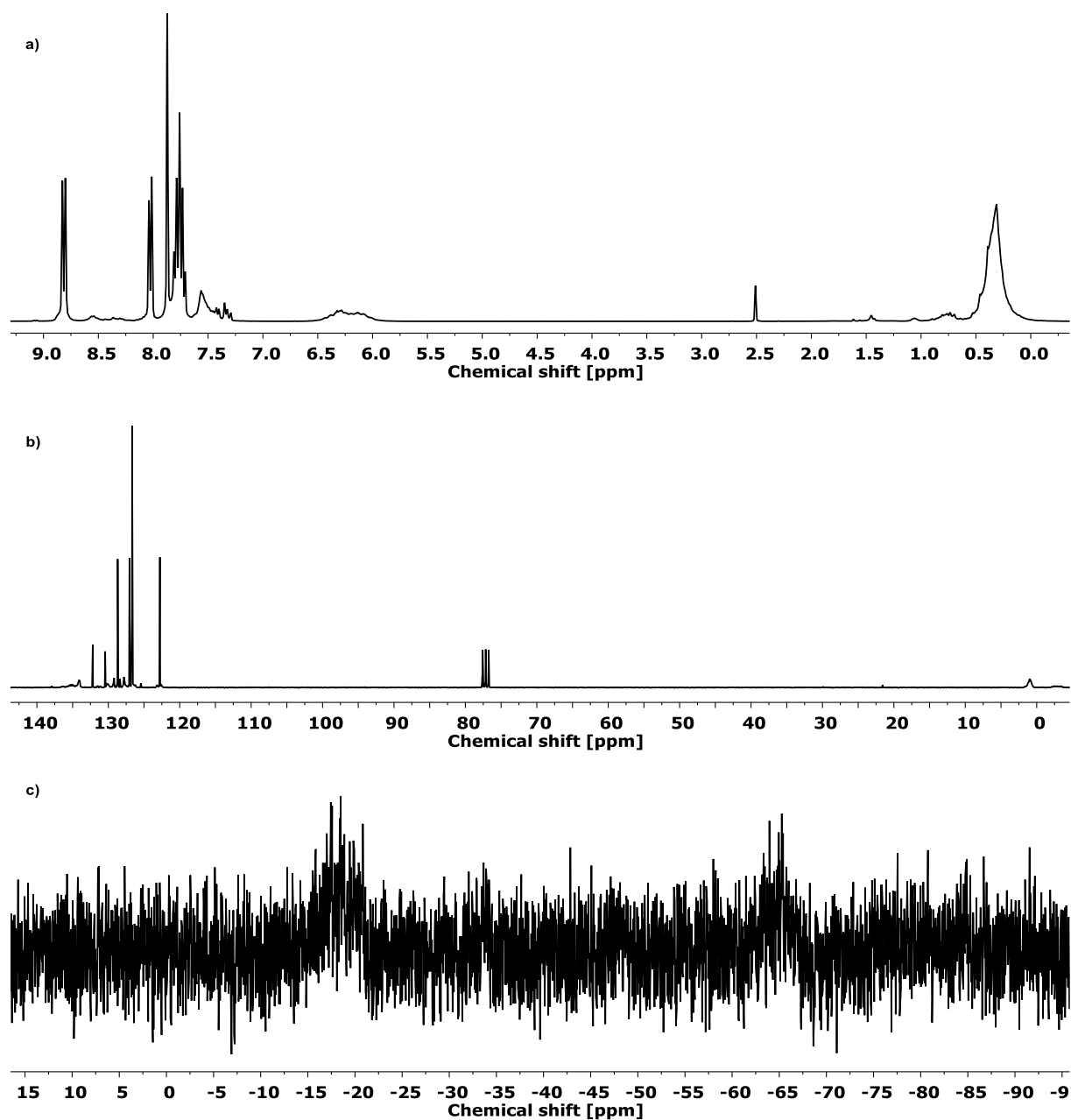
Figure 414: a) ^{1}H NMR (400 MHz, CDCl$_3$), b) ^{13}C NMR (101 MHz, CDCl$_3$) and c) ^{29}Si NMR (79 MHz, CDCl$_3$) of V20_PHM40_MM40.
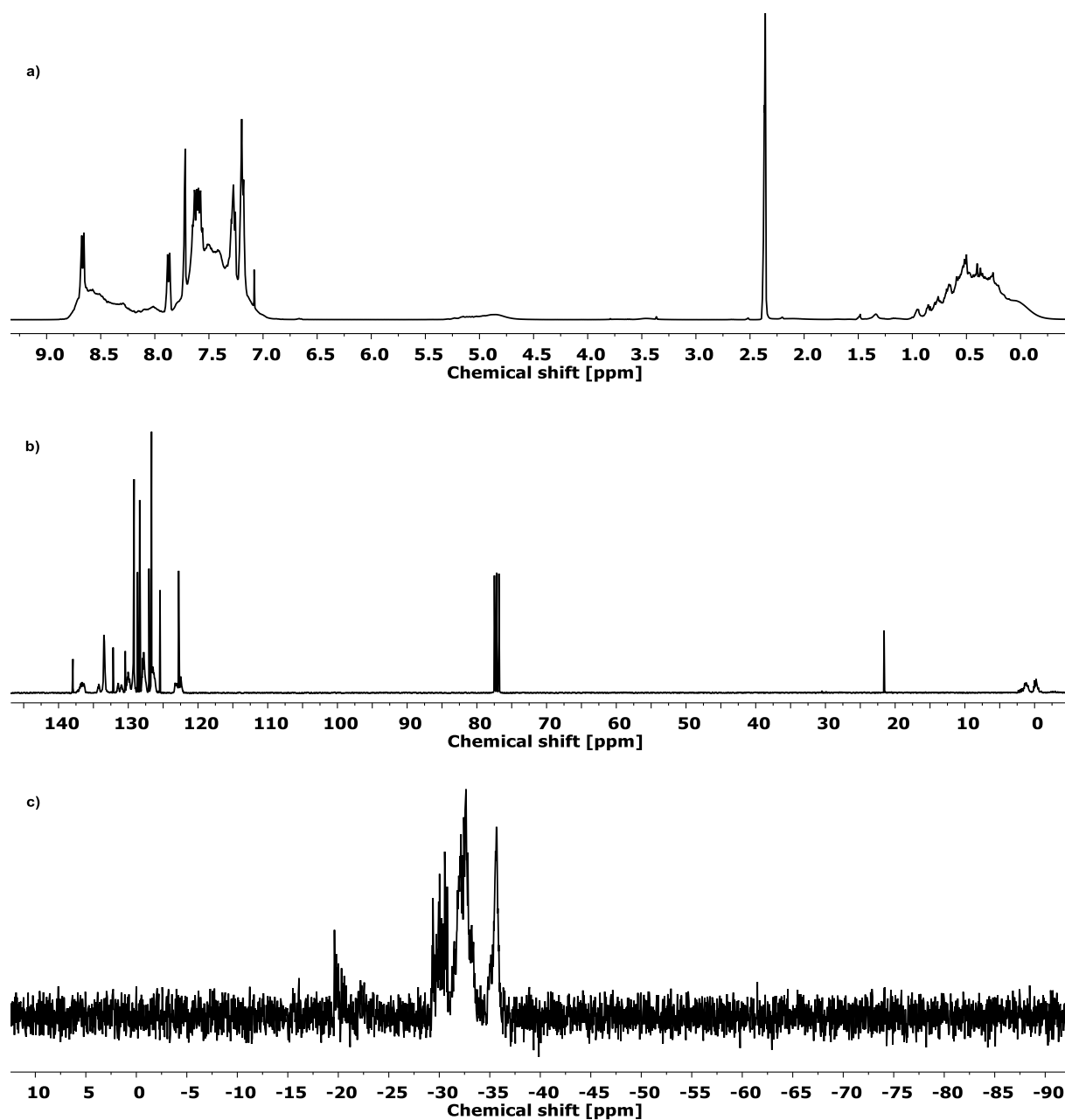
Figure 415: a) ^{1}H NMR (400 MHz, CDCl$_3$), b) ^{13}C NMR (101 MHz, CDCl$_3$) and c) ^{29}Si NMR (79 MHz, CDCl$_3$) of H20_PHM40_PM40.
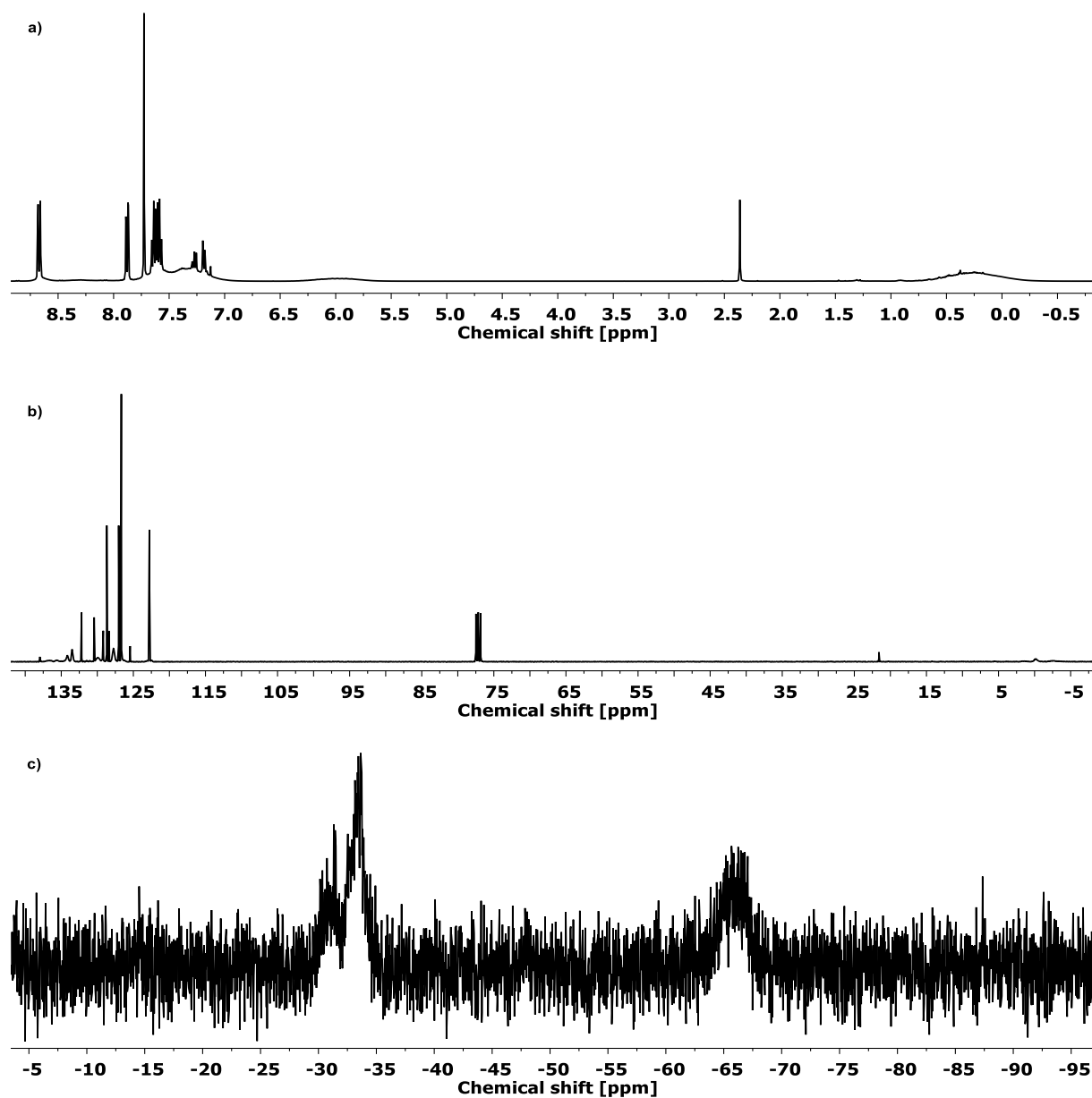
Figure 416: a) ^{1}H NMR (400 MHz, CDCl$_3$), b) ^{13}C NMR (101 MHz, CDCl$_3$) and c) ^{29}Si NMR (79 MHz, CDCl$_3$) of V20_PHM40_PM40.
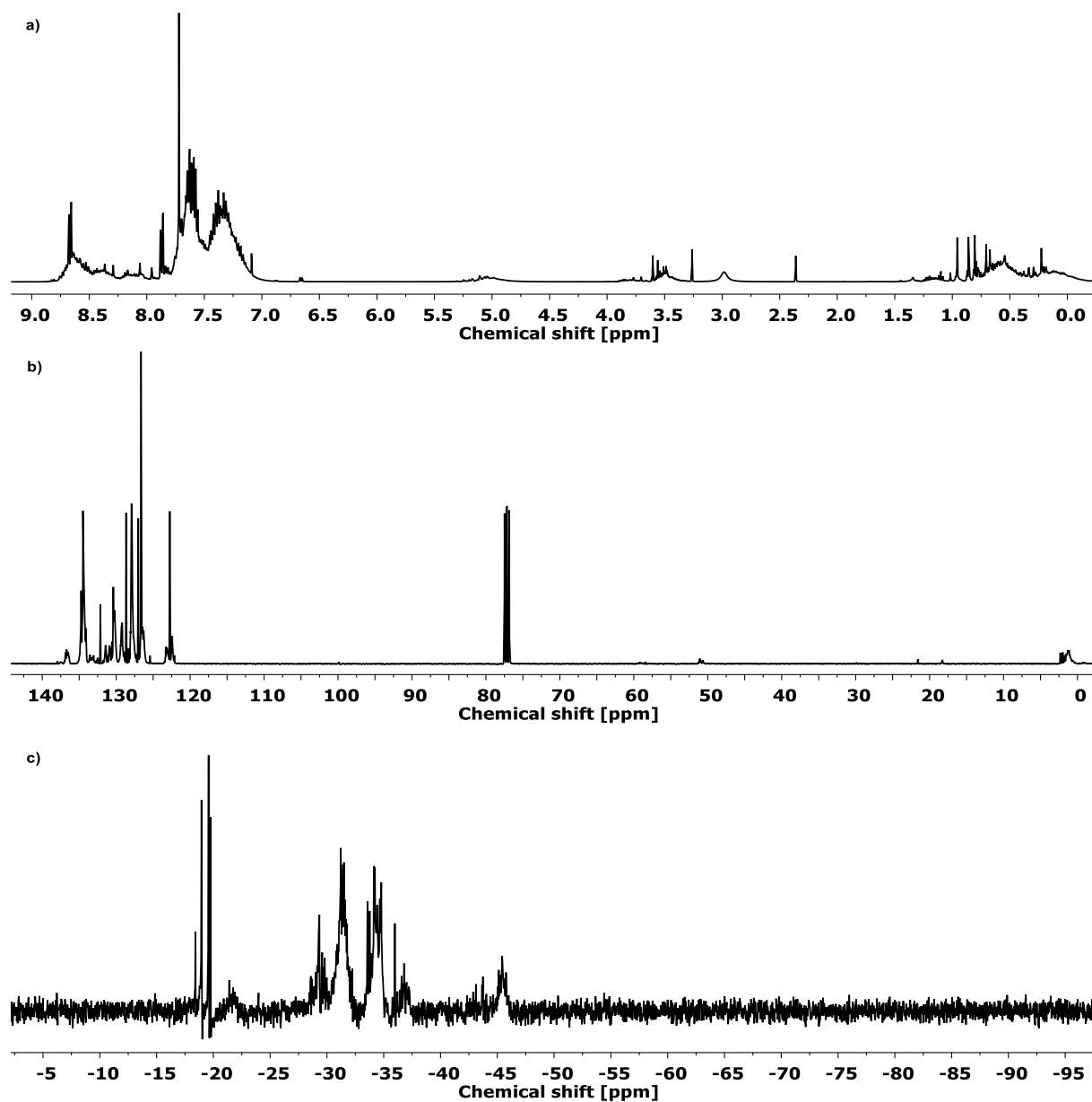
Figure 417: a) ¹H NMR (400 MHz, CDCl₃), b) ¹³C NMR (101 MHz, CDCl₃) and c) ²⁹Si NMR (79 MHz, CDCl₃) of H20_PHM40_PP40.
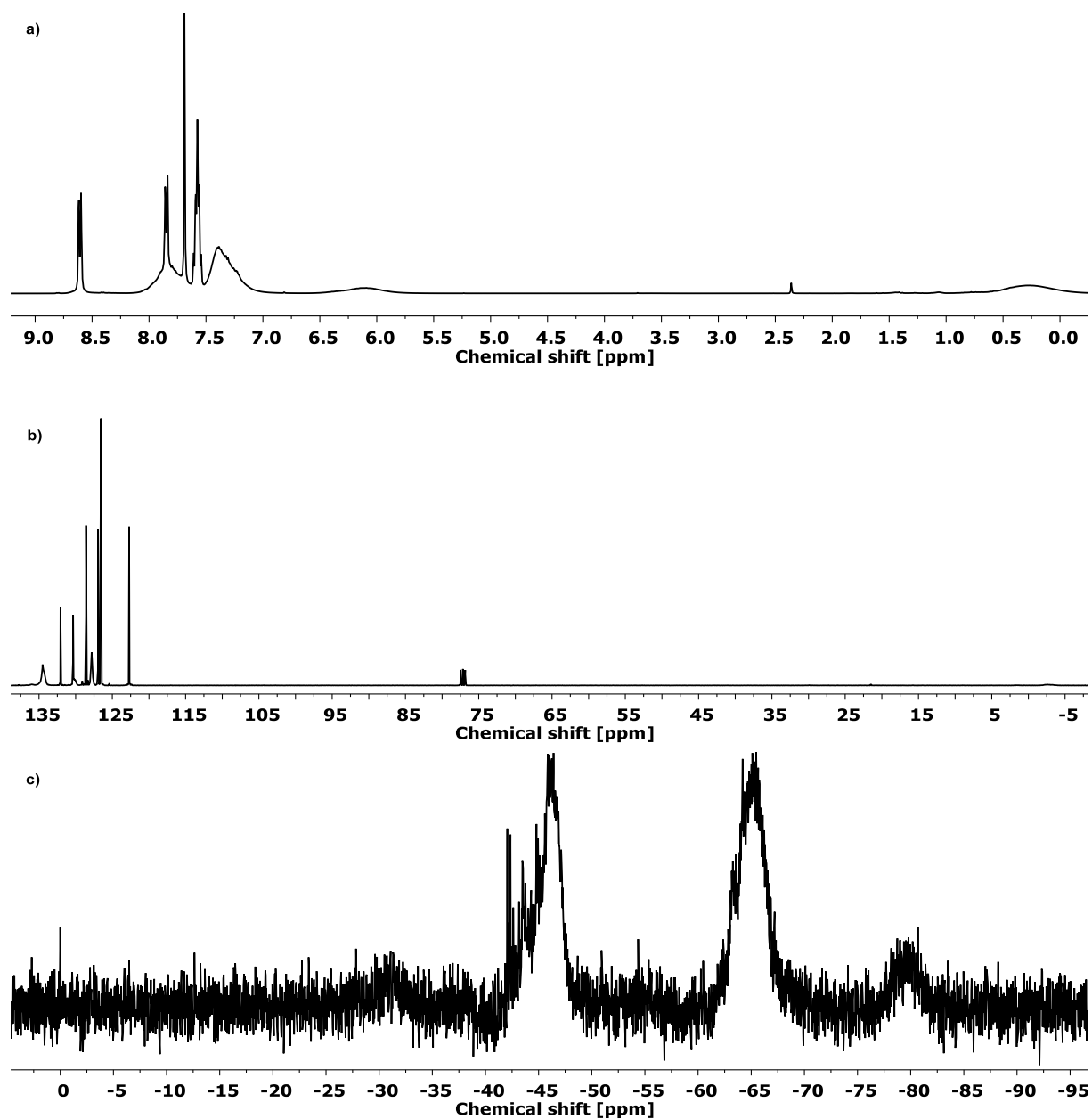
Figure 418: a) ^{1}H NMR (400 MHz, CDCl$_3$), **b)** ^{13}C NMR (101 MHz, CDCl$_3$) **and c)** ^{29}Si NMR (79 MHz, CDCl$_3$) **of V20_PHM40_PP40.**

a)

b)

c)
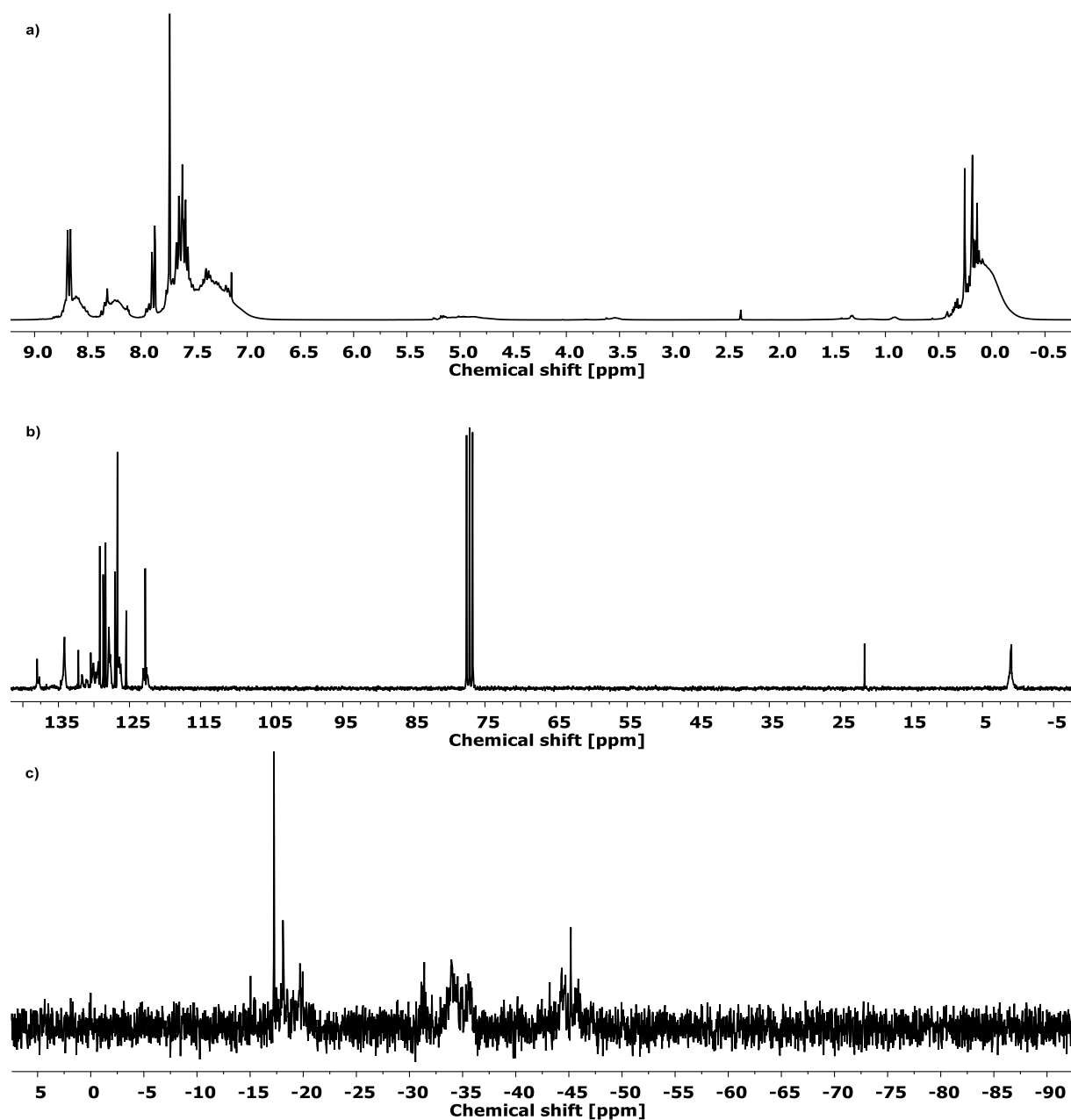
Figure 419: a) ^{1}H NMR (400 MHz, CDCl$_3$), b) ^{13}C NMR (101 MHz, CDCl$_3$) and c) ^{29}Si NMR (79 MHz, CDCl$_3$) of H20_PHP40_MM40.
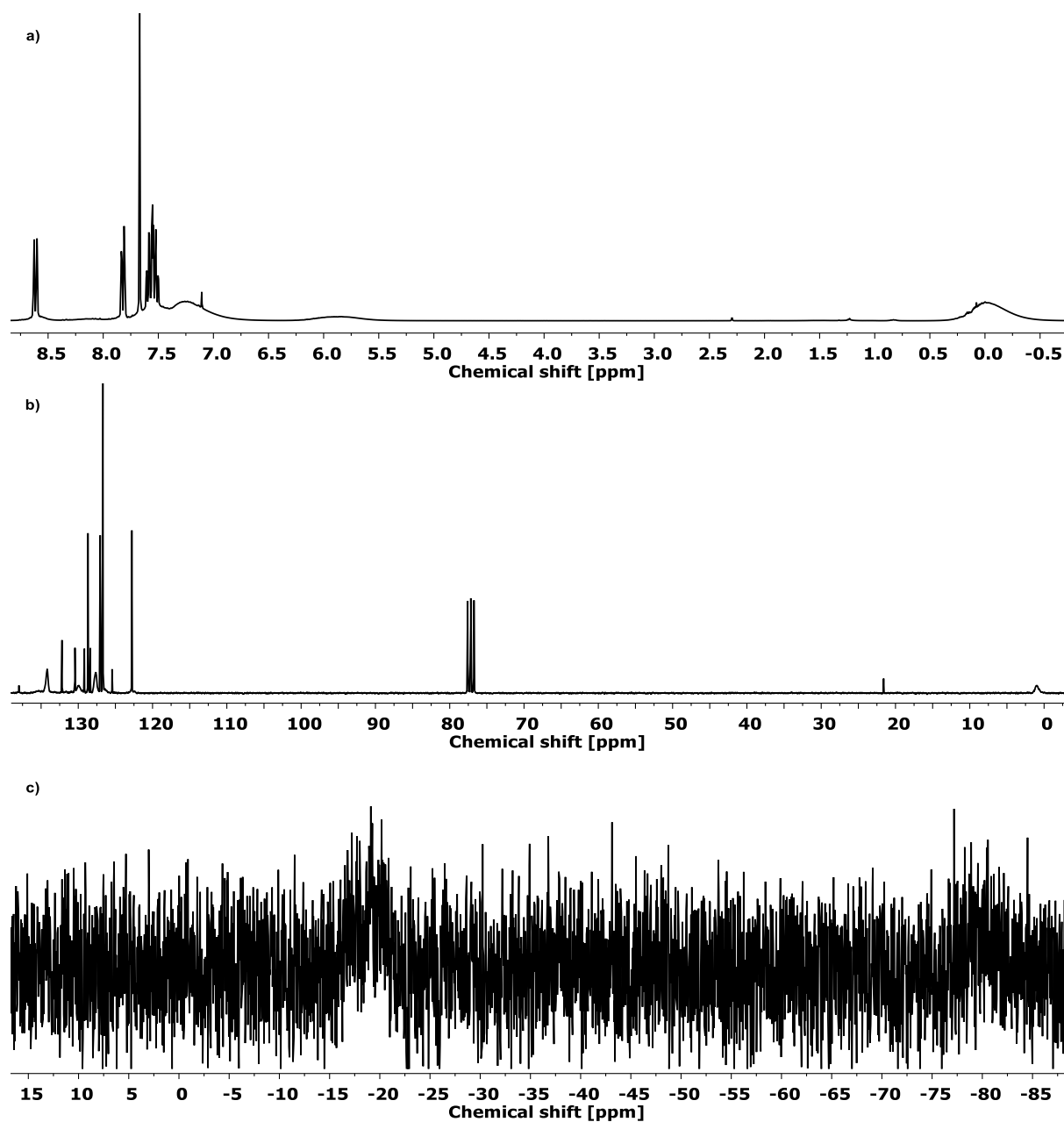
Figure 420: a) ^{1}H NMR (400 MHz, CDCl$_3$), b) ^{13}C NMR (101 MHz, CDCl$_3$) and c) ^{29}Si NMR (79 MHz, CDCl$_3$) of V20_PHP40_MM40.
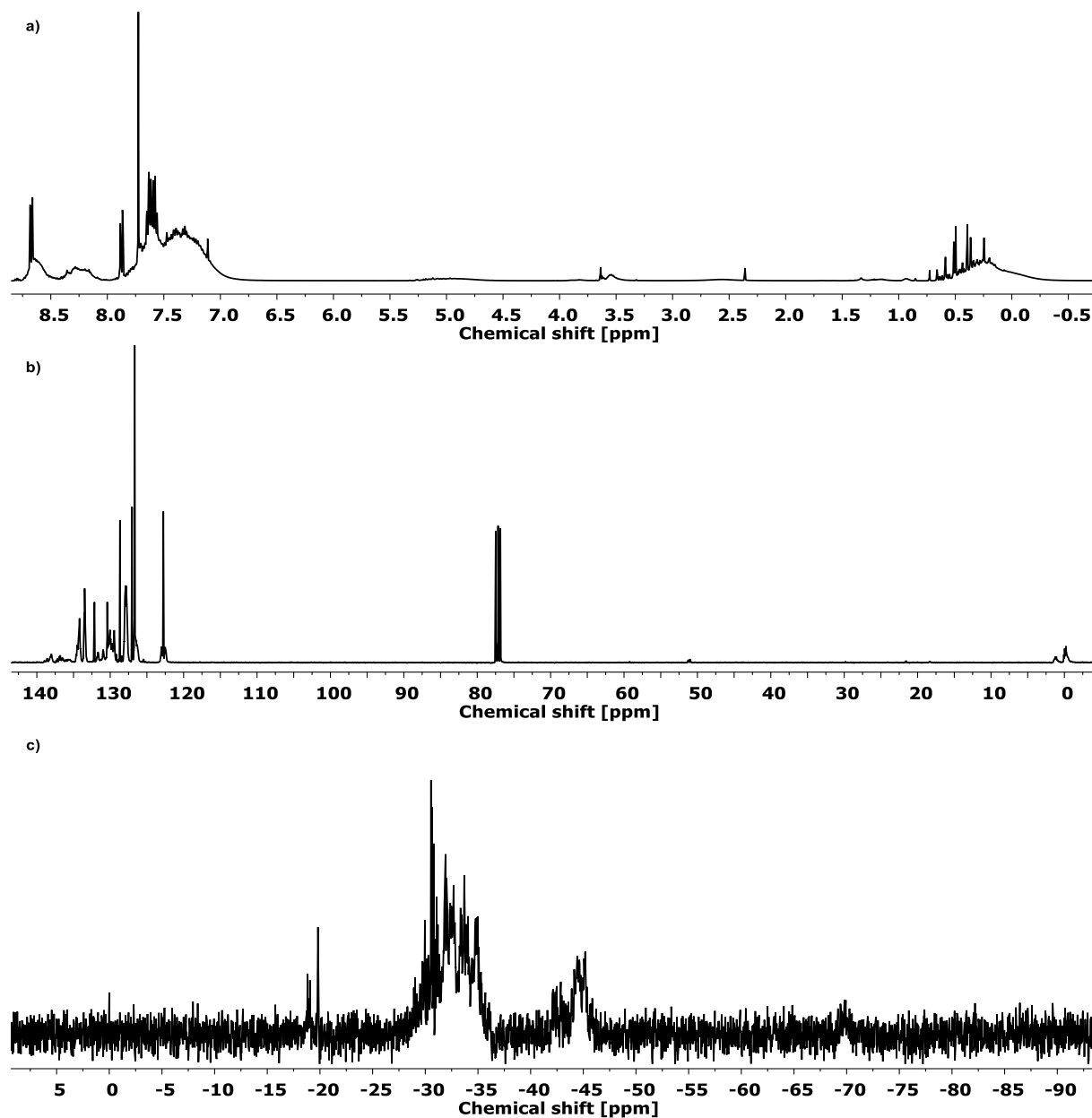
Figure 421: a) ^{1}H NMR (400 MHz, CDCl₃), b) ^{13}C NMR (101 MHz, CDCl₃) and c) ^{29}Si NMR (79 MHz, CDCl₃) of H20_PHP40_PM40.
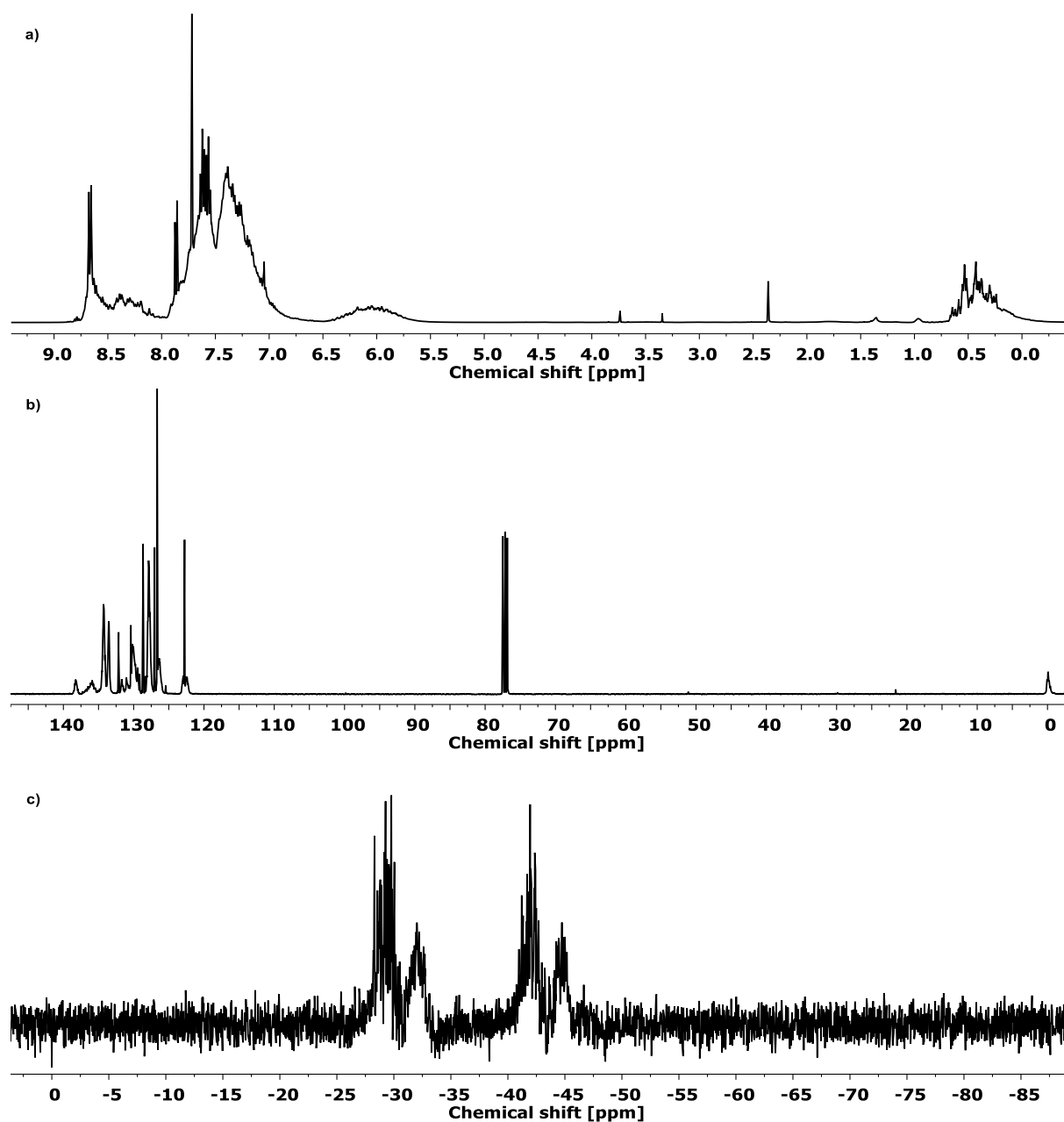
Figure 422: a) ^{1}H NMR (400 MHz, CDCl$_3$), b) ^{13}C NMR (101 MHz, CDCl$_3$) and c) ^{29}Si NMR (79 MHz, CDCl$_3$) of V20_PHP40_PM40.
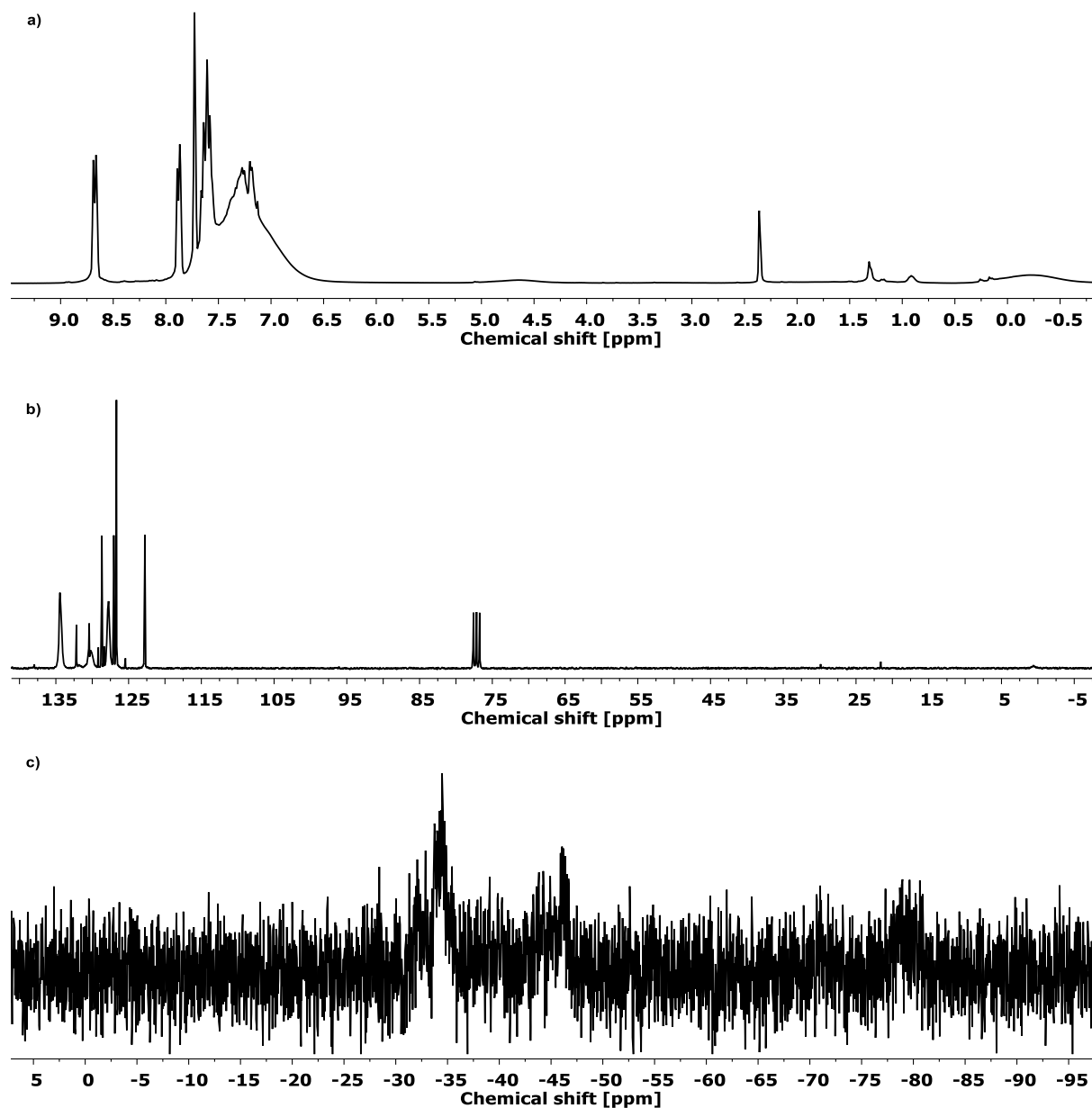
Figure 423: a) ^{1}H NMR (400 MHz, CDCl$_3$), b) ^{13}C NMR (101 MHz, CDCl$_3$) and c) ^{29}Si NMR (79 MHz, CDCl$_3$) of H20_PHP40_PP40.
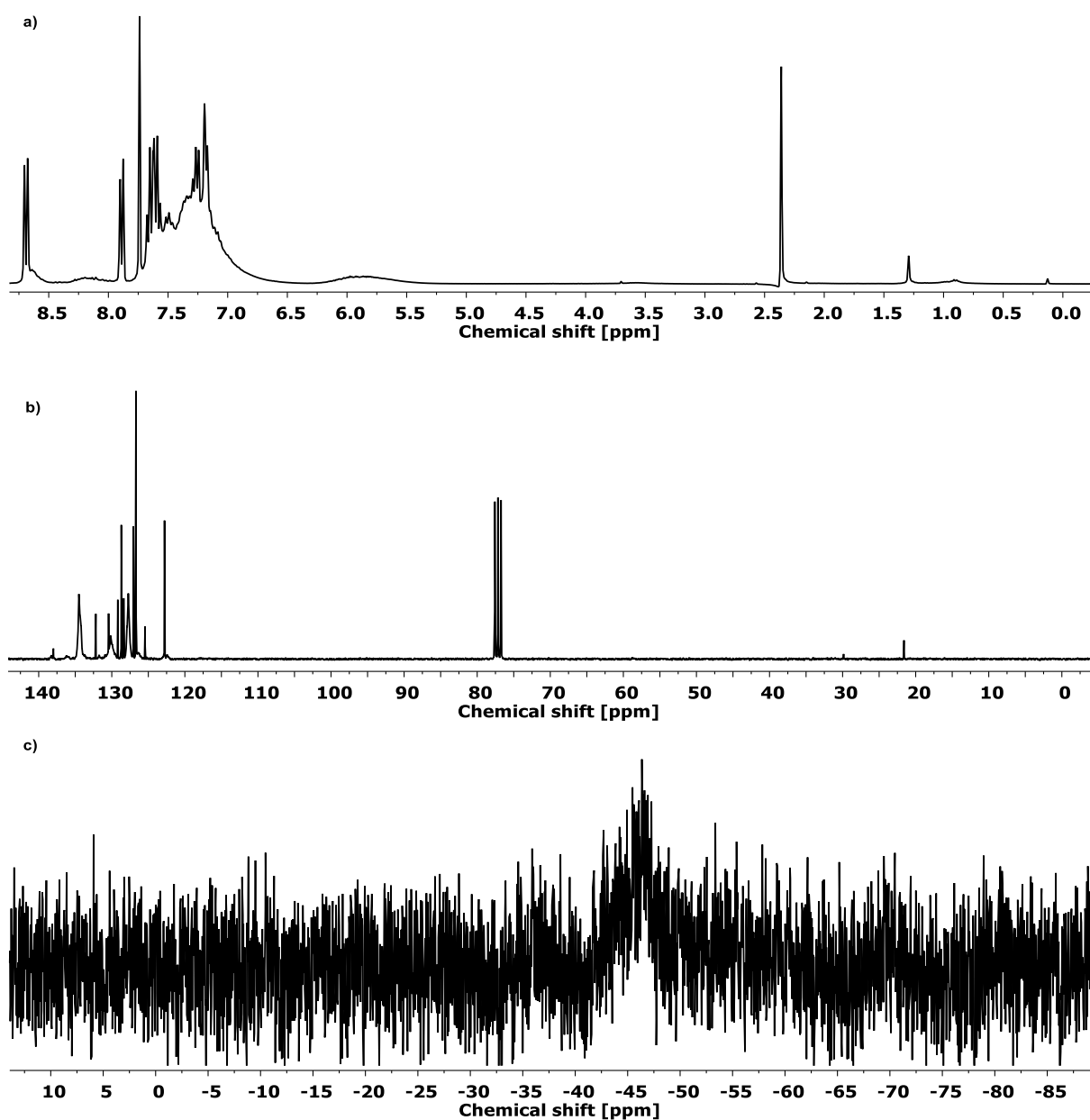
Figure 424: a) ^{1}H NMR (400 MHz, CDCl$_3$), b) ^{13}C NMR (101 MHz, CDCl$_3$) and c) ^{29}Si NMR (79 MHz, CDCl$_3$) of V20_PHP40_PP40.

a)

b)

c)
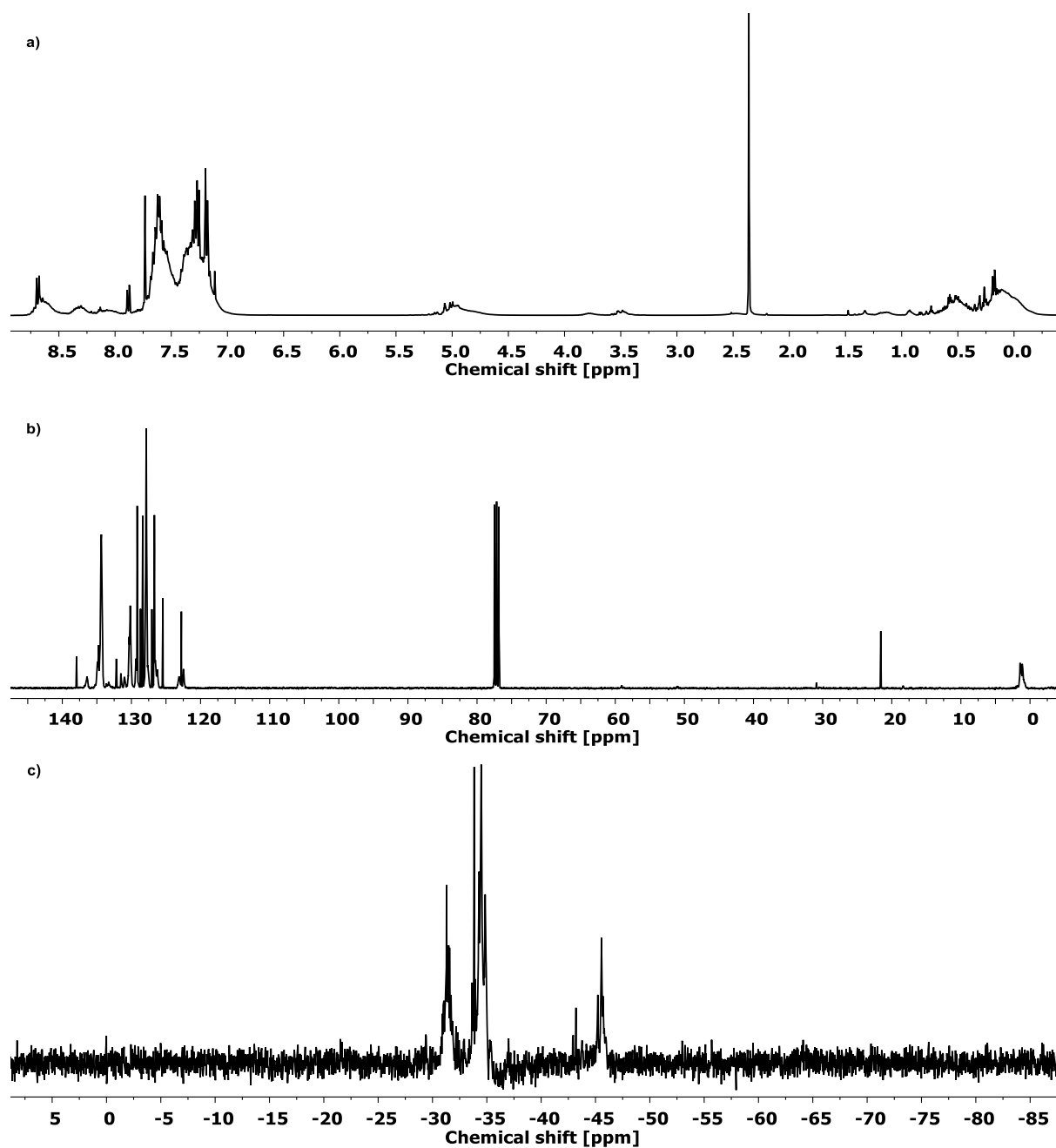
Figure 425: a) ^{1}H NMR (400 MHz, CDCl$_3$), b) ^{13}C NMR (101 MHz, CDCl$_3$) and c) ^{29}Si NMR (79 MHz, CDCl$_3$) of H40_PHM20_PP40.
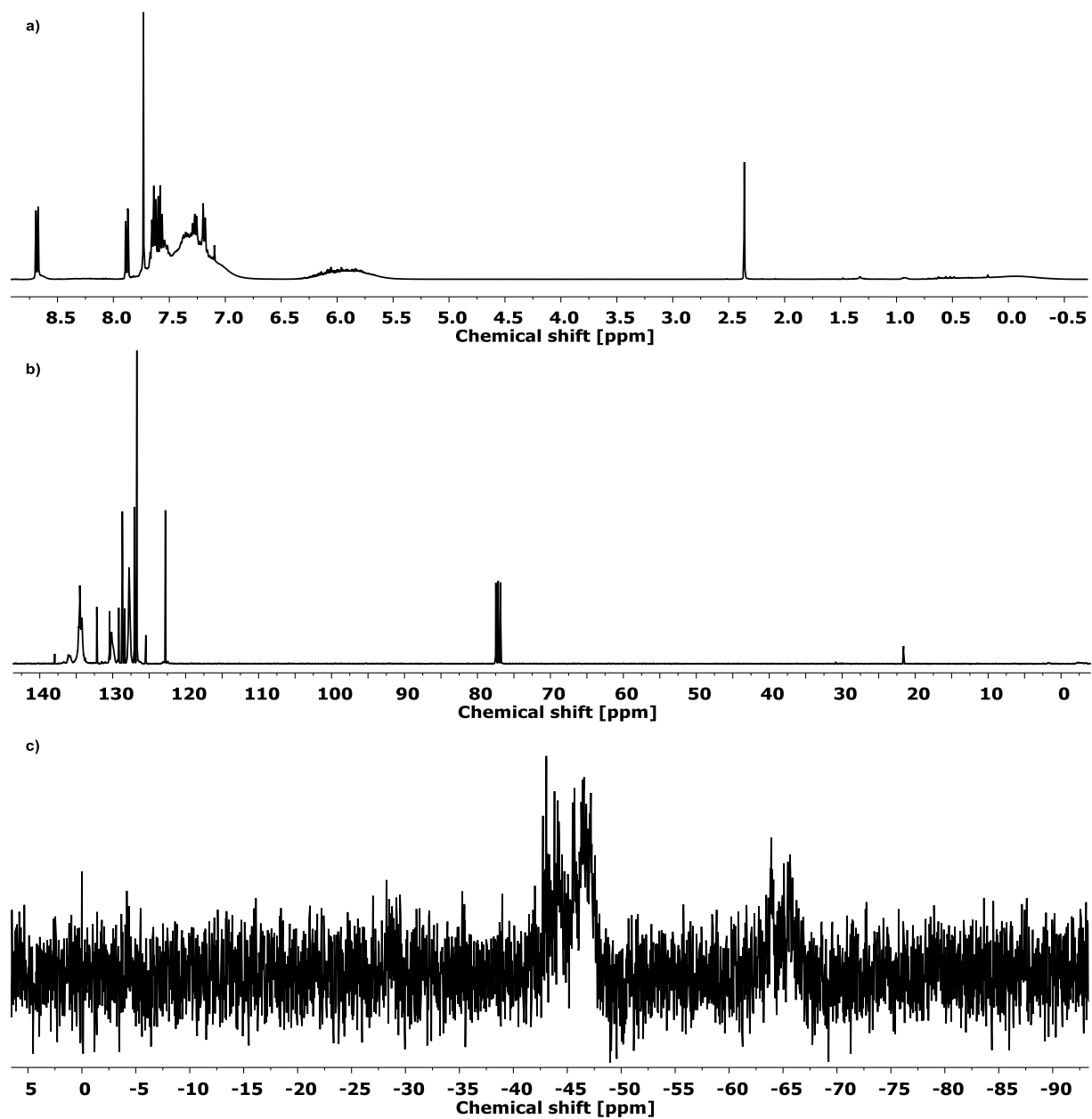
Figure 426: a) ¹H NMR (400 MHz, CDCl₃), b) ¹³C NMR (101 MHz, CDCl₃) and c) ²⁹Si NMR (79 MHz, CDCl₃) of V40_PHM20_PP40.

a)

b)

c)
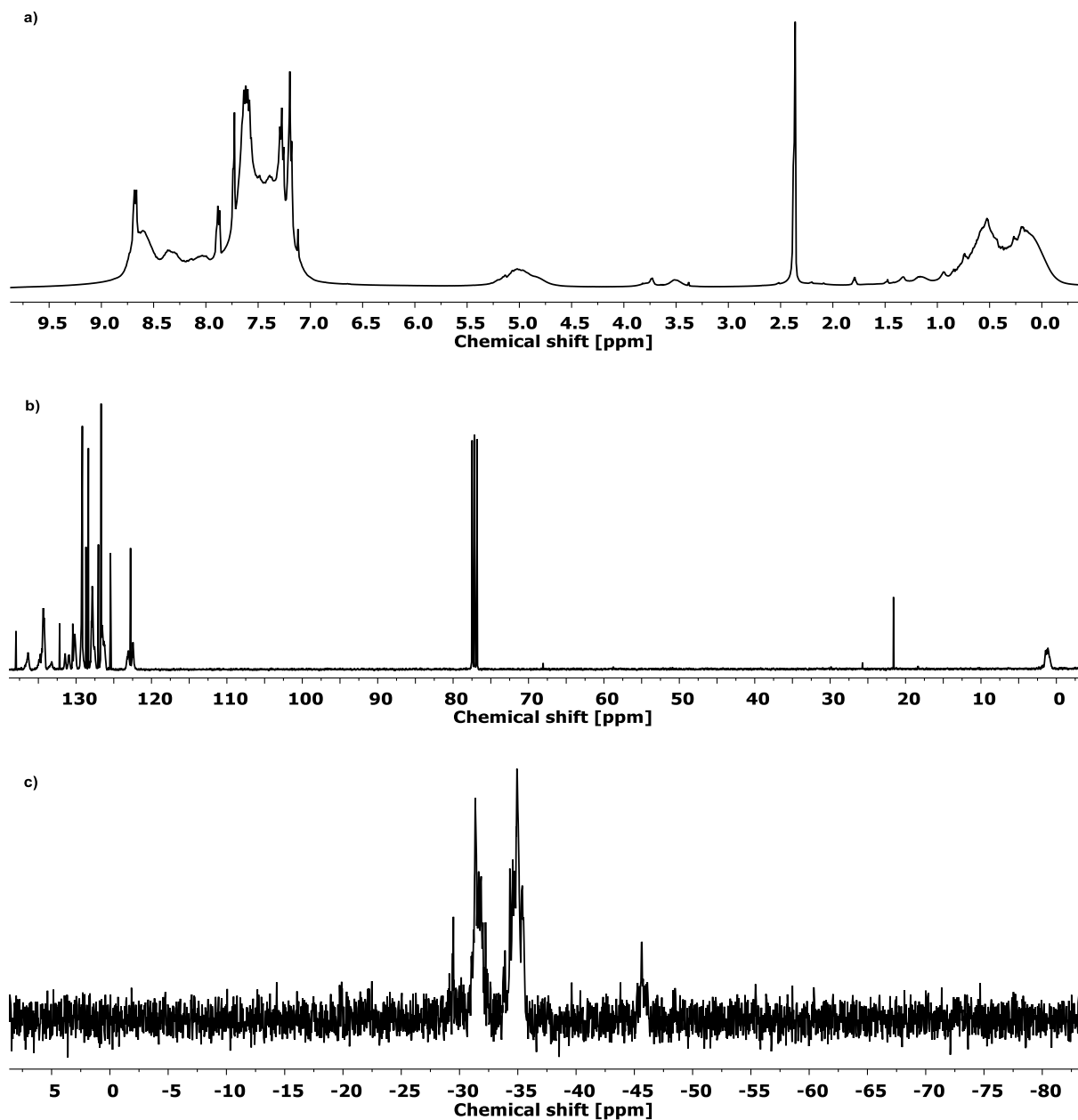
Figure 427: a) ^{1}H NMR (400 MHz, CDCl$_3$), b) ^{13}C NMR (101 MHz, CDCl$_3$) and c) ^{29}Si NMR (79 MHz, CDCl$_3$) of H40_PHM40_PP20.
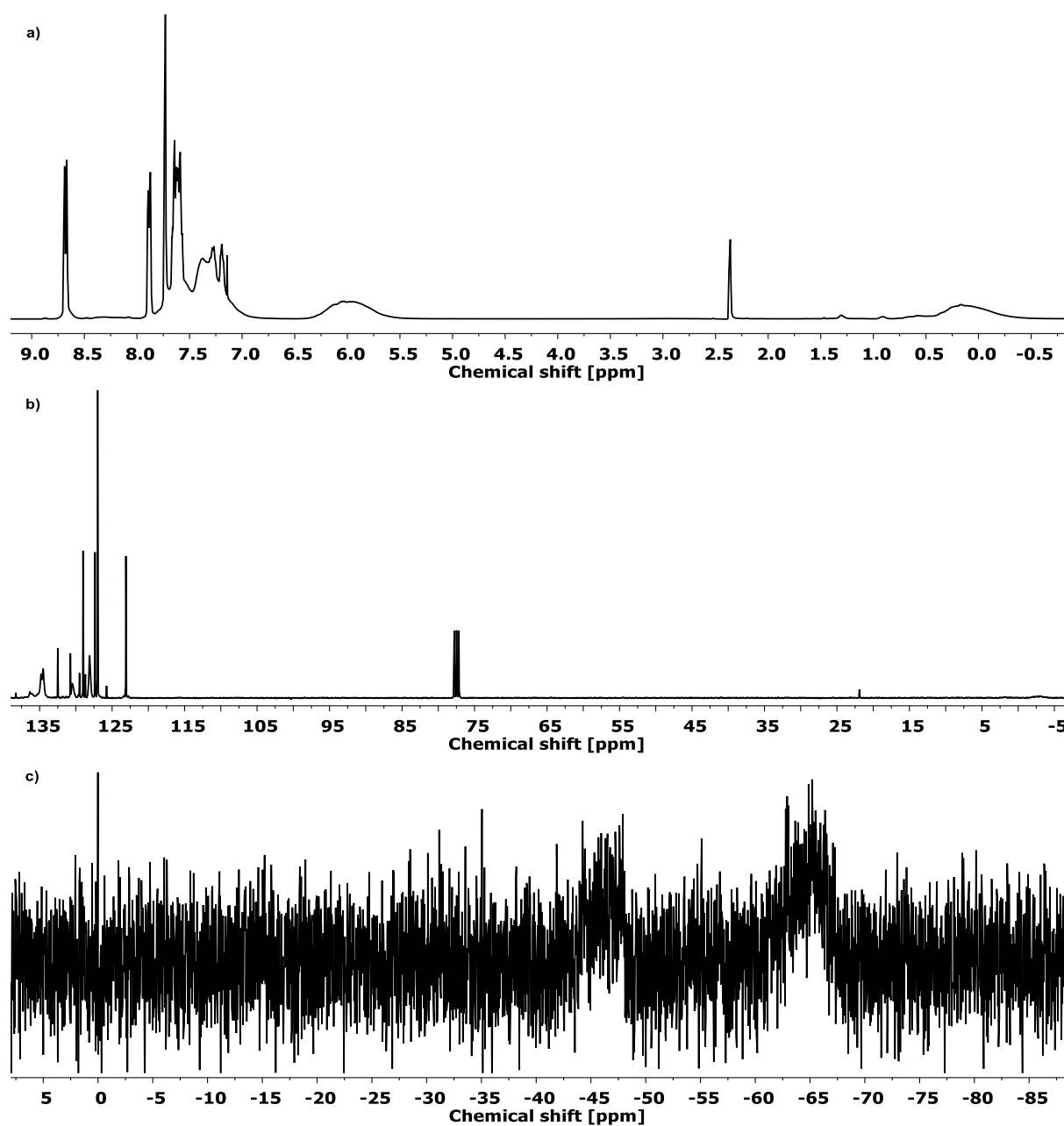
Figure 428: a) ^{1}H NMR (400 MHz, CDCl$_3$), b) ^{13}C NMR (101 MHz, CDCl$_3$) and c) ^{29}Si NMR (79 MHz, CDCl$_3$) of V40_PHM40_PP20.

6.2.10.4.3 TGA curves under oxygen atmosphere of the phenanthrenyl-group containing polymers
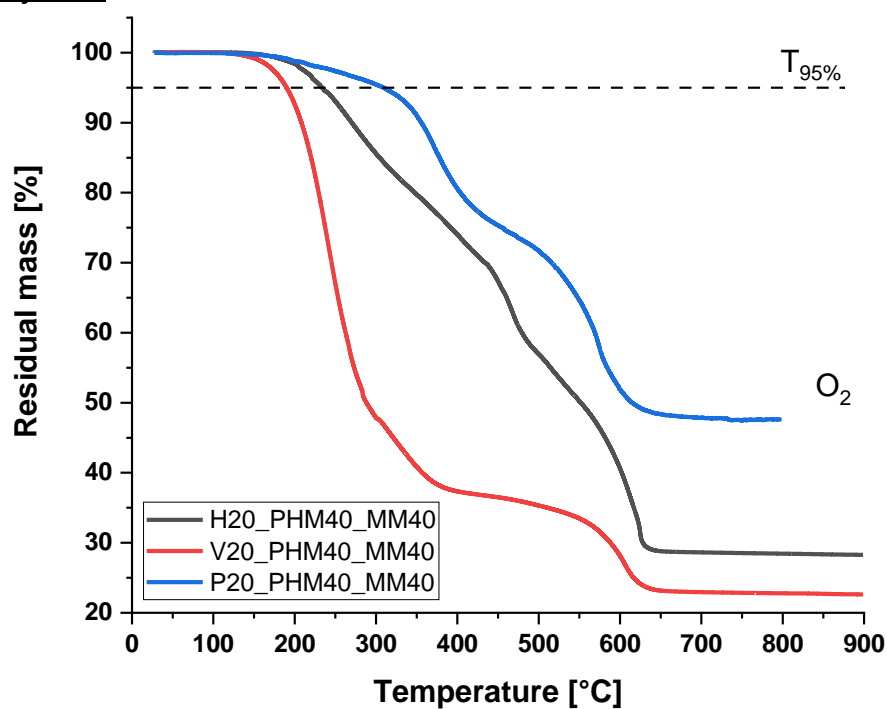
Figure 429: TGA curves under oxygen atmosphere of X20_PHM40_MM40.
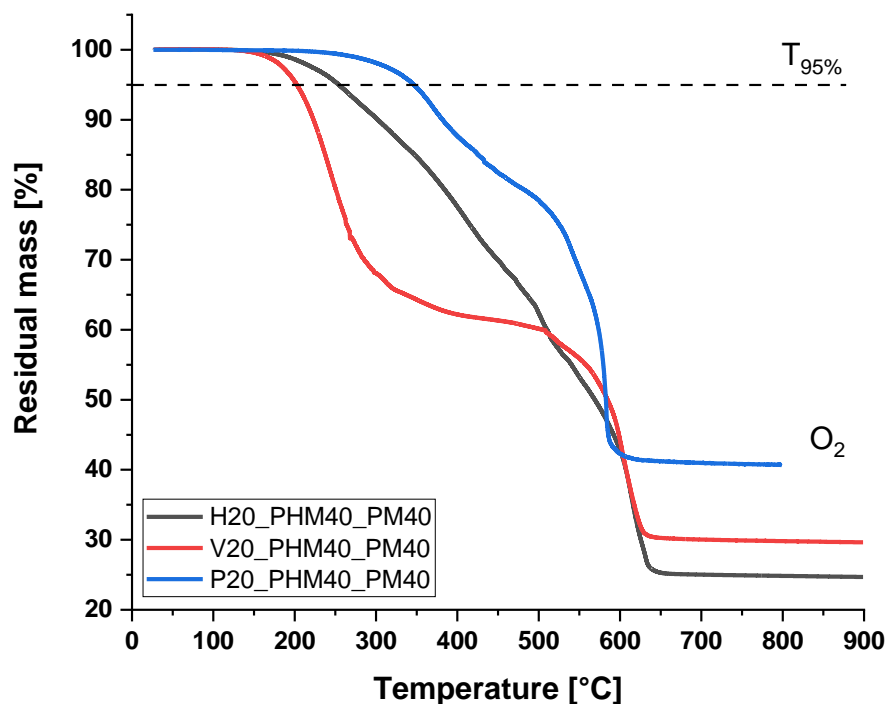
Figure 430: TGA curves under oxygen atmosphere of X20_PHM40_PM40.
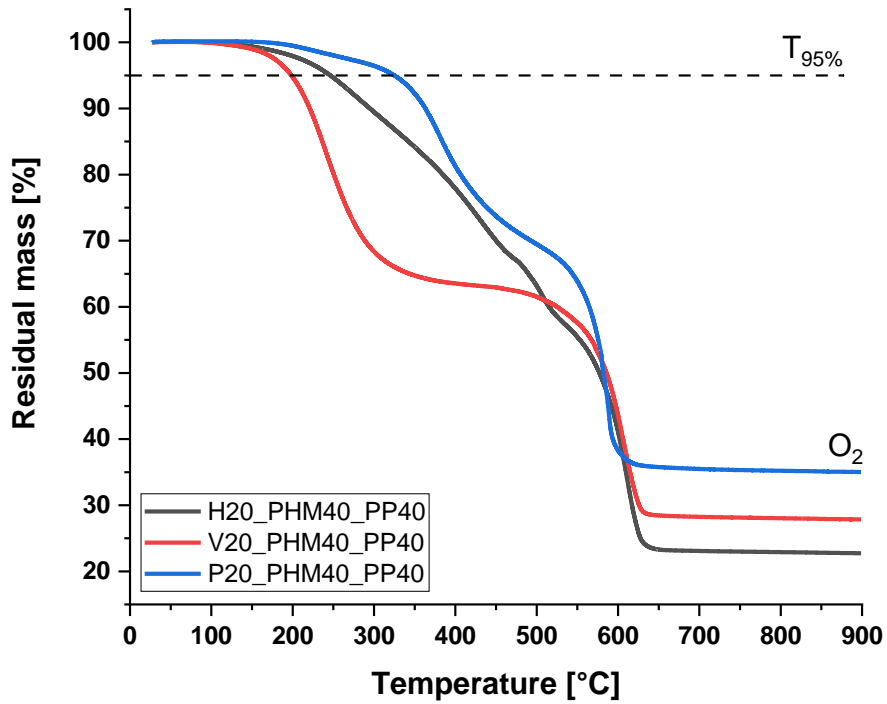
Figure 431: TGA curves under oxygen atmosphere of X20_PHM40_PP40.
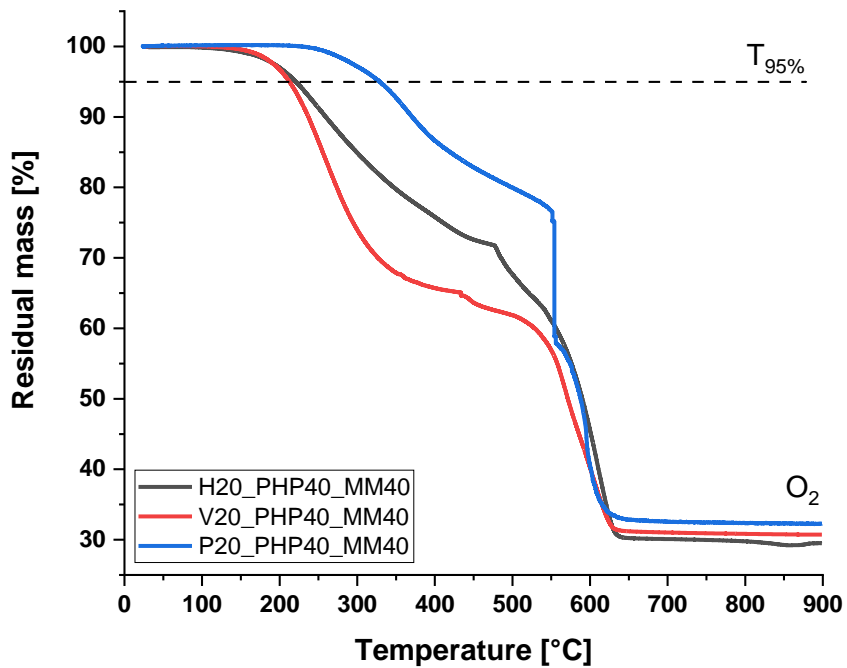
Figure 432: TGA curves under oxygen atmosphere of X20_PHP40_MM40.
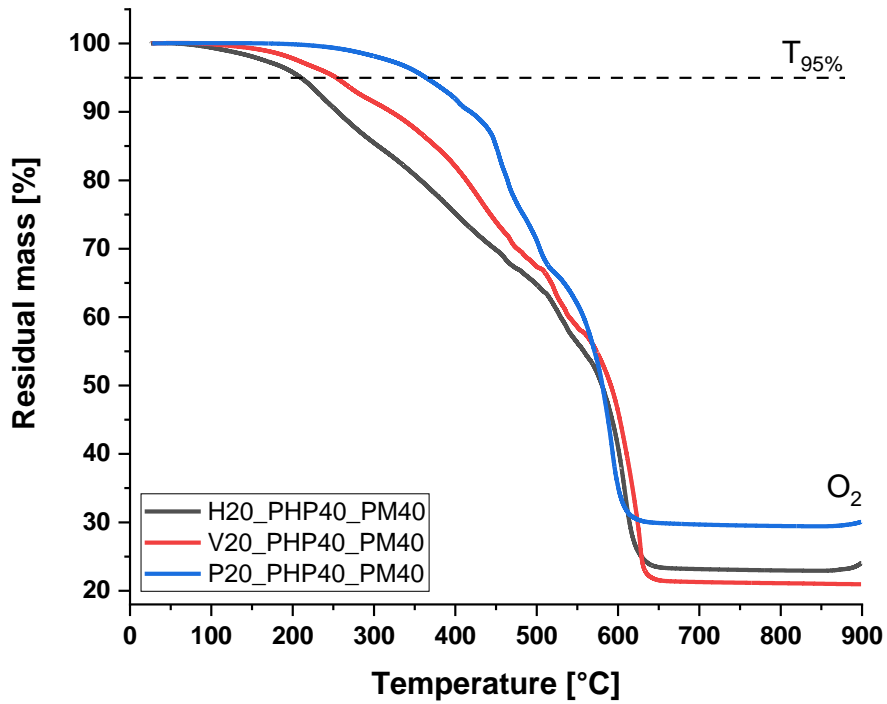
Figure 433: TGA curves under oxygen atmosphere of X20_PHP40_PM40.
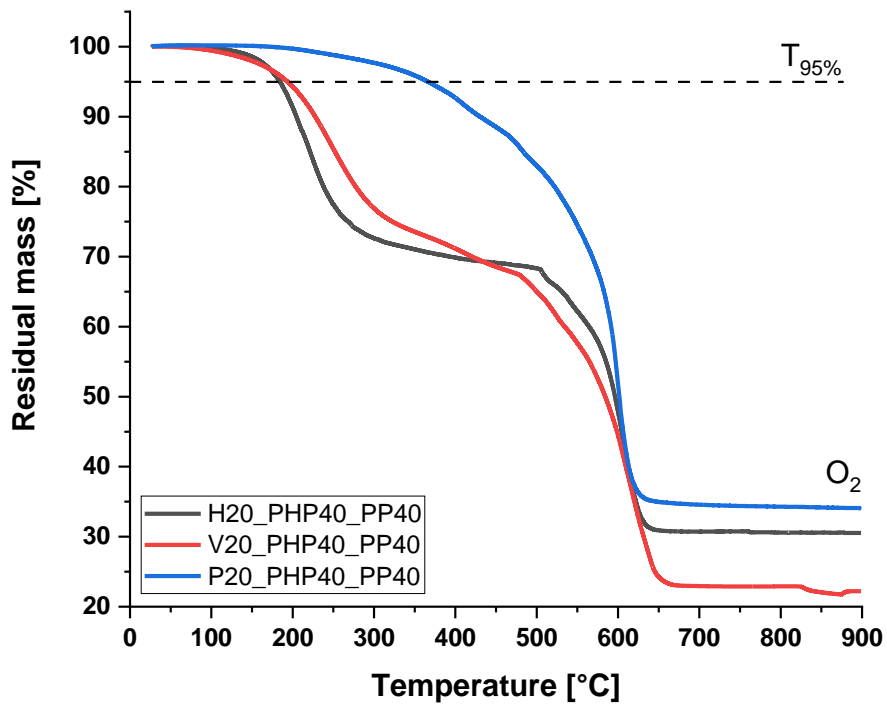
Figure 434: TGA curves under oxygen atmosphere of X20_PHP40_PP40.
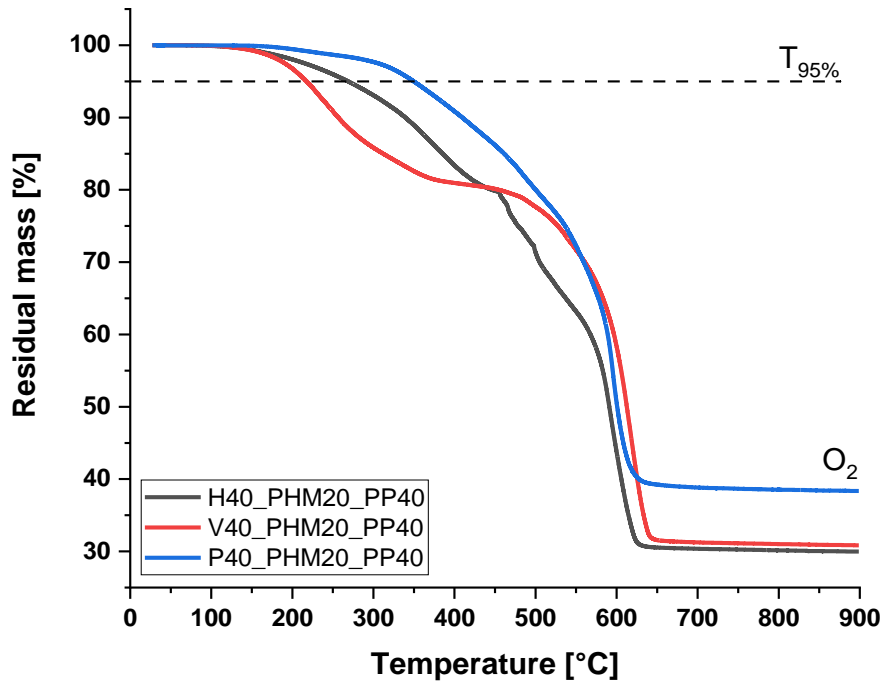
Figure 435: TGA curves under oxygen atmosphere of X40_PHM20_PP40.
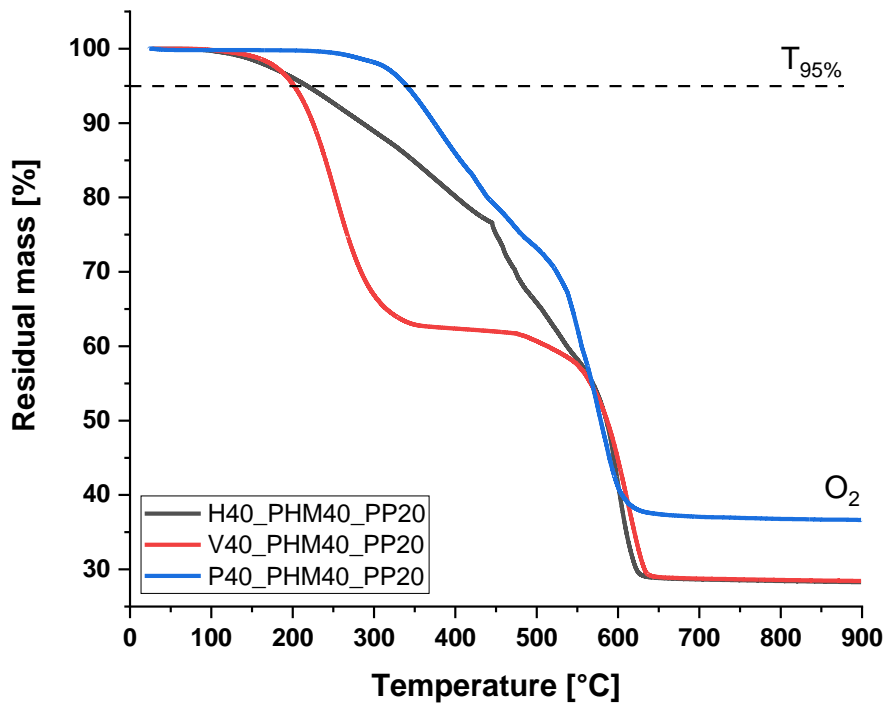
Figure 436: TGA curves under oxygen atmosphere of X40_PHM40_PP20.

6.2.10.4.4 TGA curves under nitrogen atmosphere of the phenanthrenyl-group containing polymers
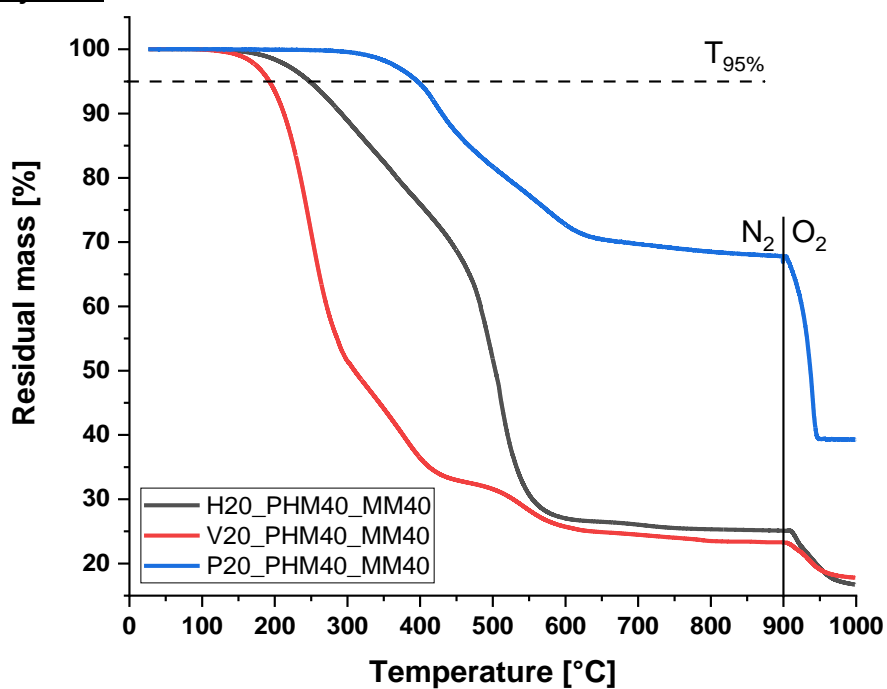
Figure 437: TGA curves under nitrogen atmosphere of X20_PHM40_MM40.
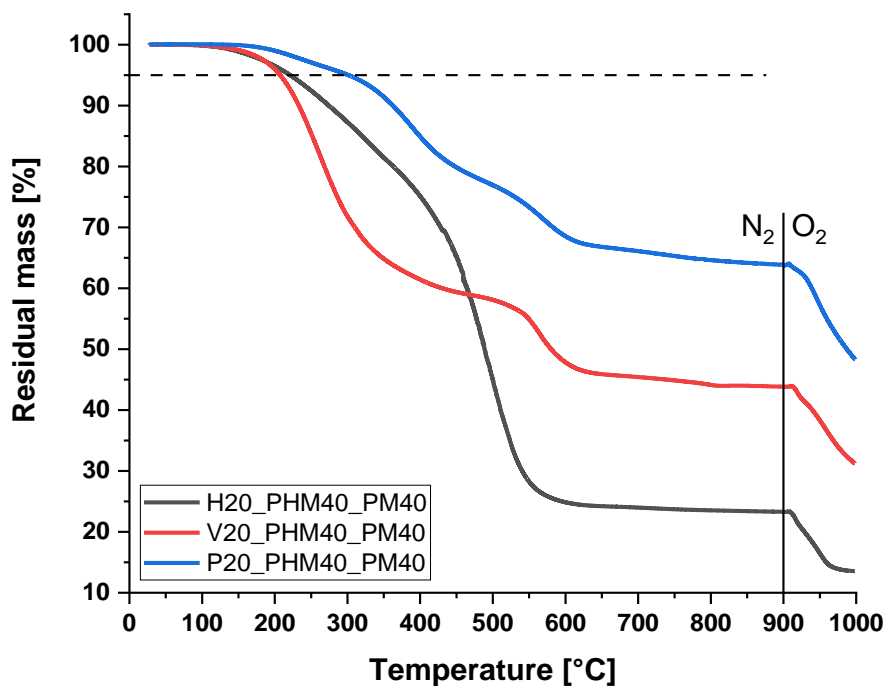
Figure 438: TGA curves under nitrogen atmosphere of X20_PHM40_PM40.
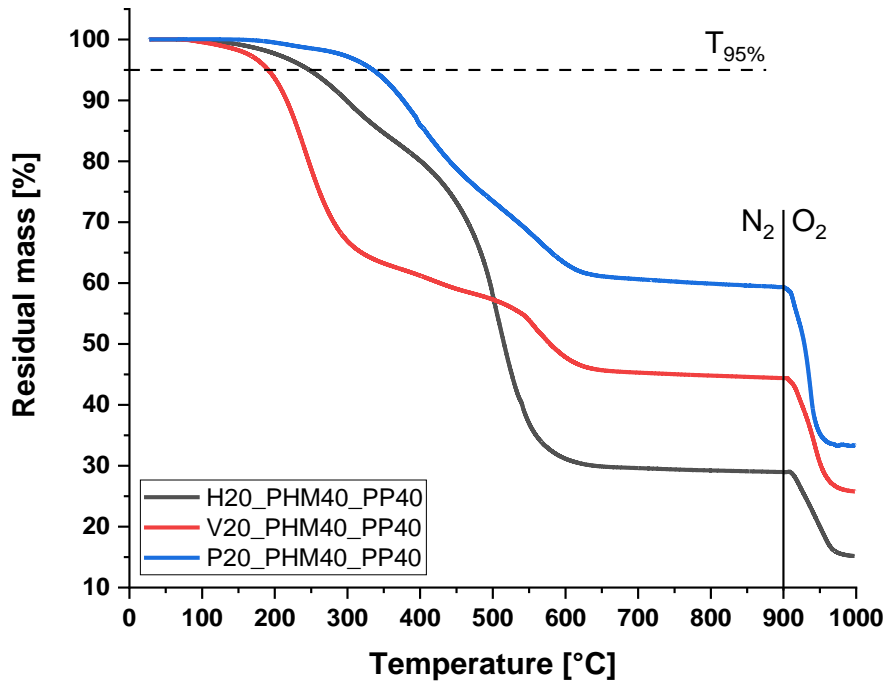
Figure 439: TGA curves under nitrogen atmosphere of X20_PHM40_PP40.
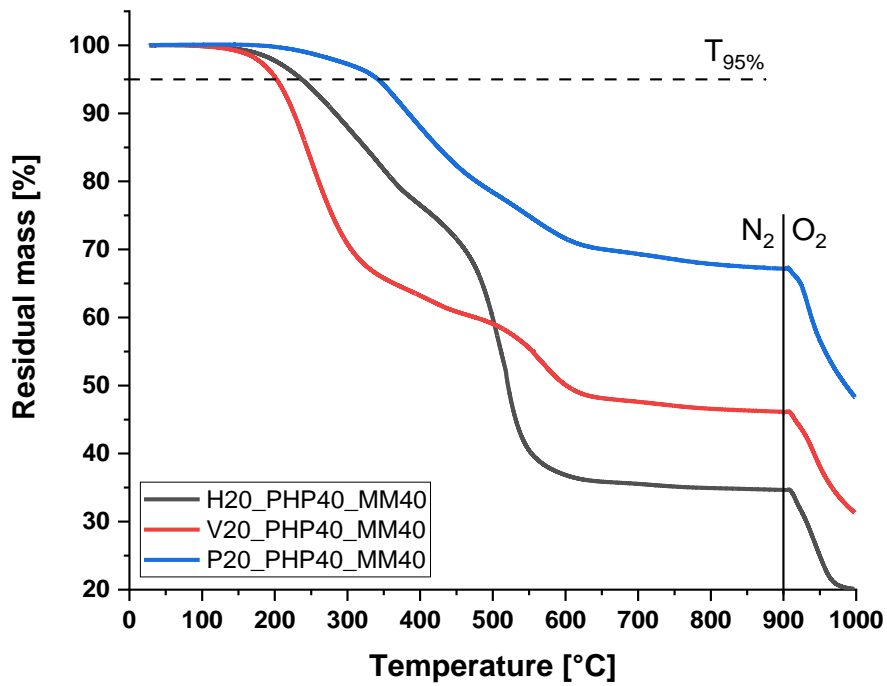
Figure 440: TGA curves under nitrogen atmosphere of X20_PHP40_MM40.
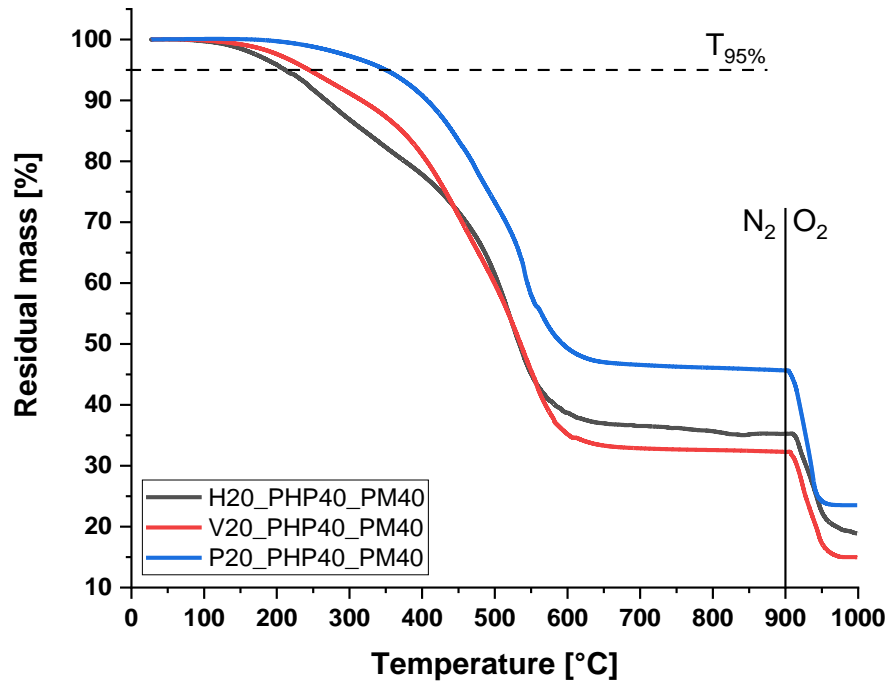
Figure 441: TGA curves under nitrogen atmosphere of X20_PHP40_PM40.
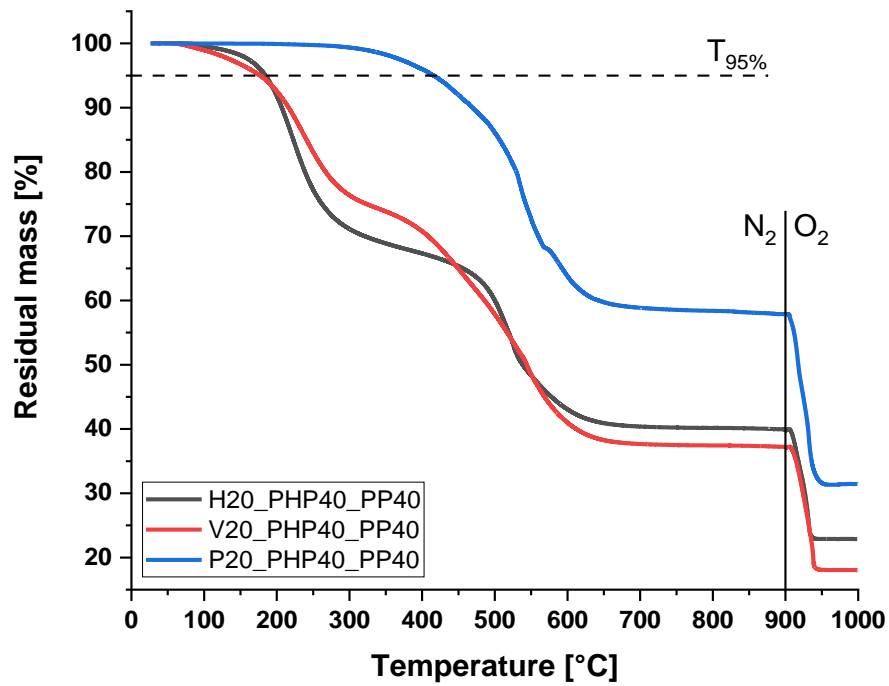
Figure 442: TGA curves under nitrogen atmosphere of X20_PHP40_PP40.
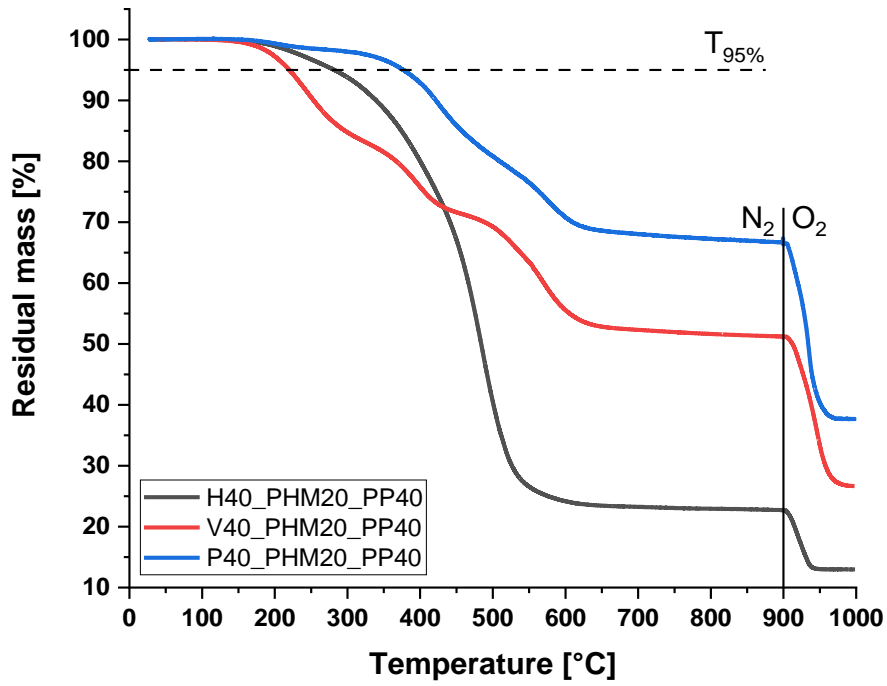
Figure 443: TGA curves under nitrogen atmosphere of X40_PHM20_PP40.
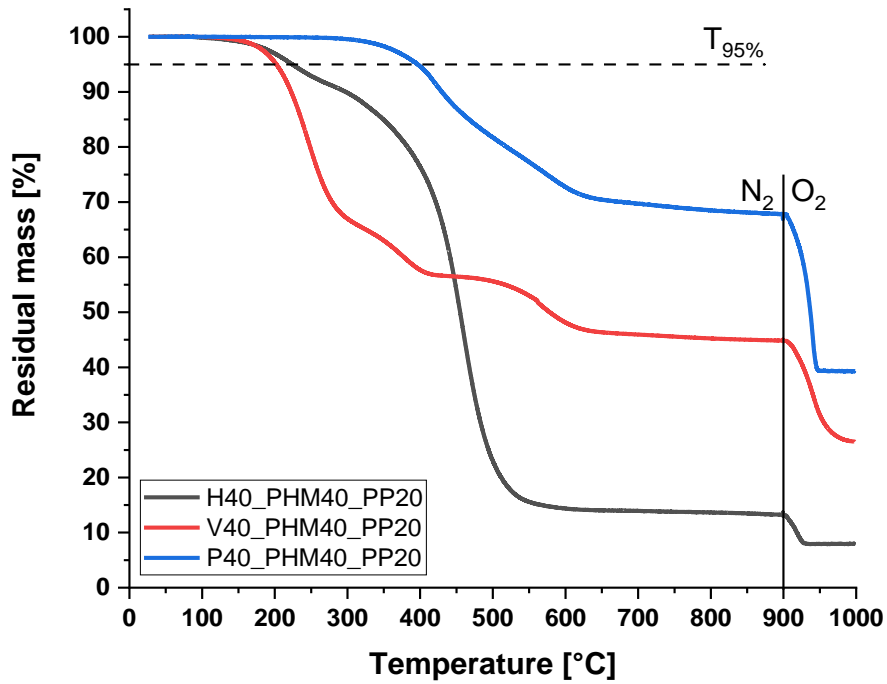
Figure 444: TGA curves under nitrogen atmosphere of X40_PHM40_PP20.

6.2.10.4.5 DSC curves of the hydride- or vinyl- and phenanthrenyl-group containing copolymers
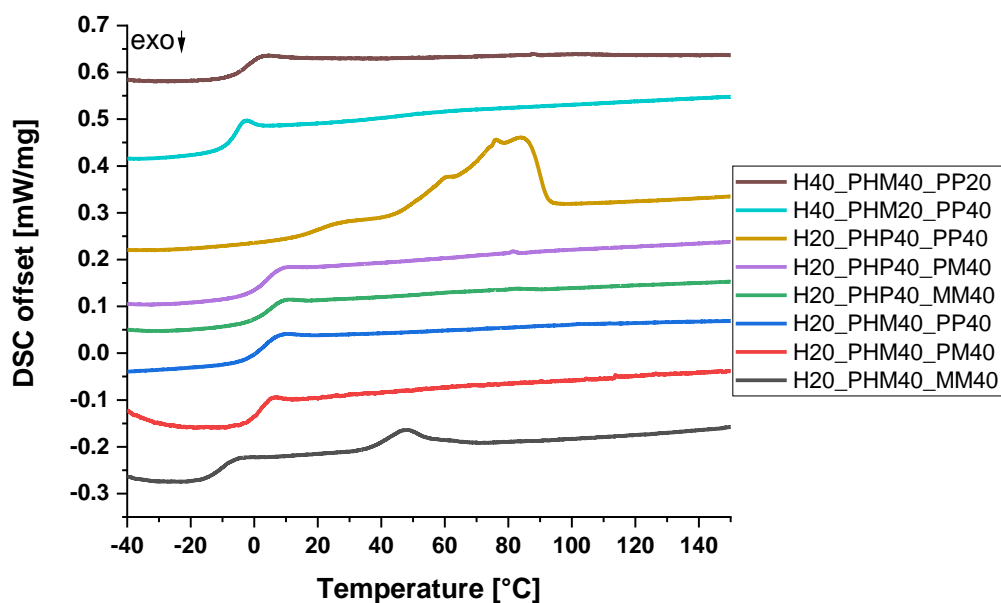
Figure 445: DSC curves of the 1st heating cycle of the hydride- and phenanthrenyl-group containing copolymers.
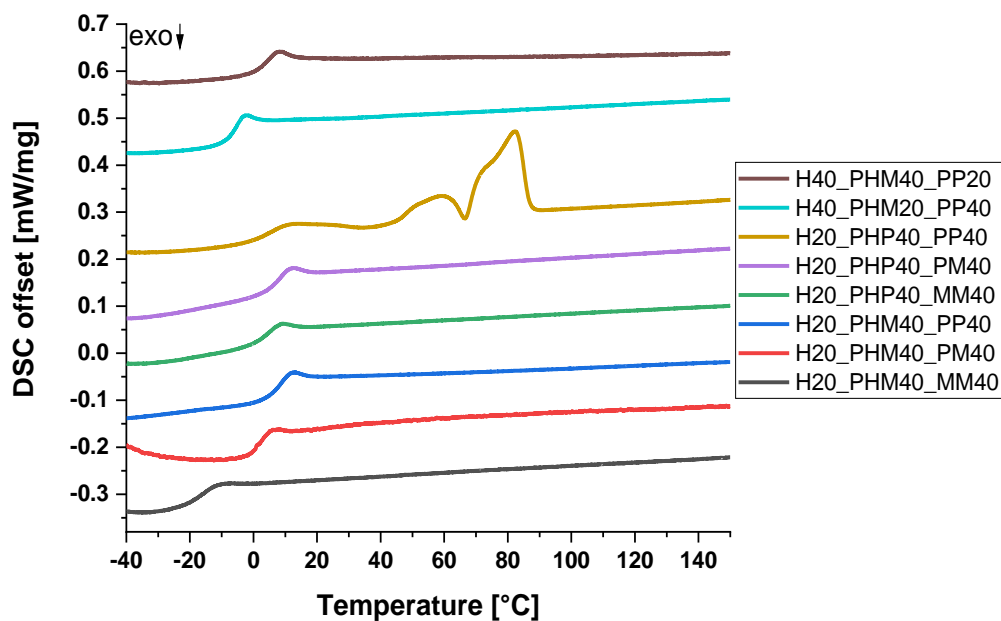
Figure 446: DSC curves of the 2nd heating cycle of the hydride- and phenanthrenyl-group containing copolymers.
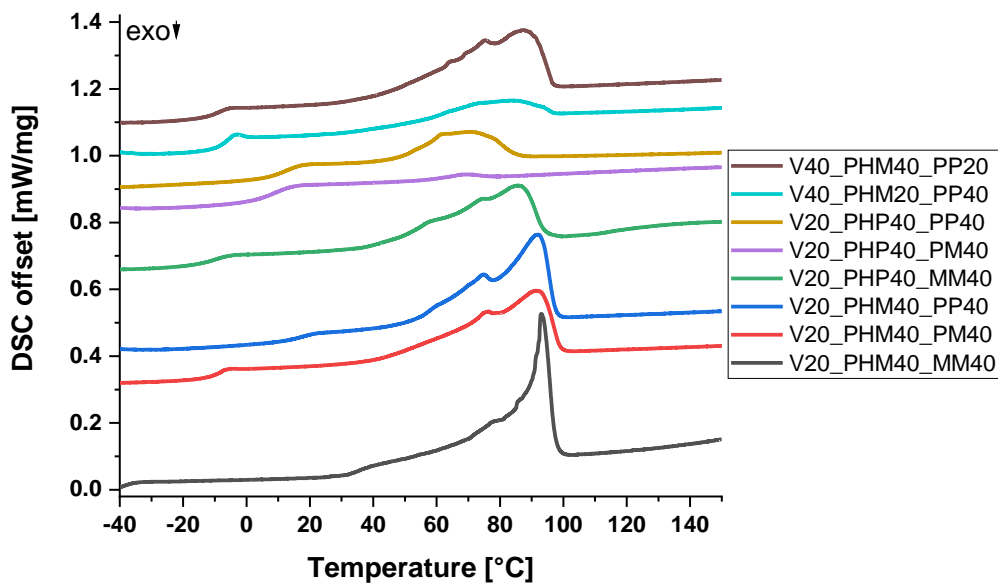
Figure 447: DSC curves of the 1st heating cycle of the vinyl- and phenanthrenyl-group containing copolymers.
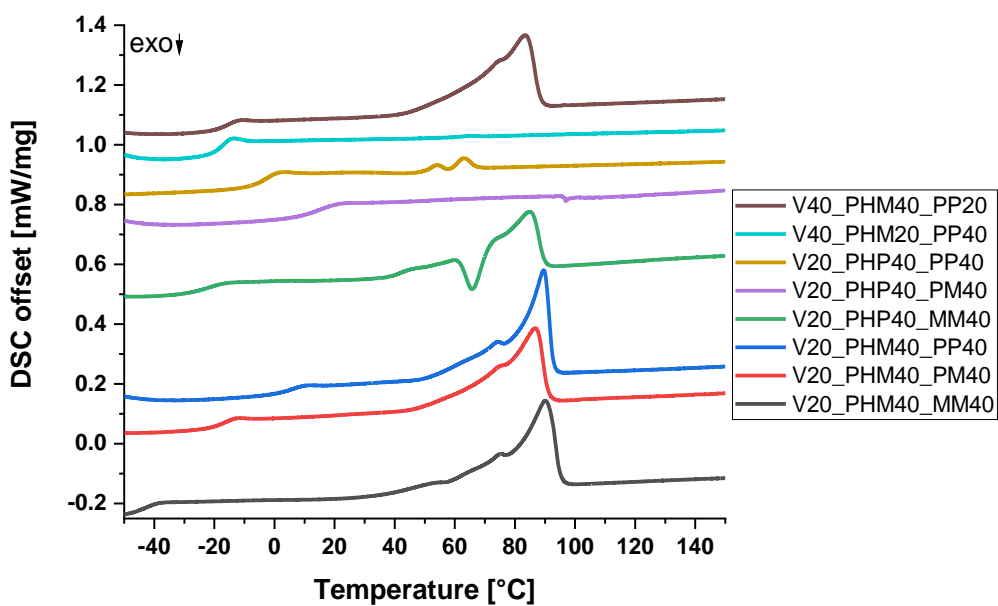
Figure 448: DSC curves of the 2nd heating cycle of the vinyl- and phenanthrenyl-group containing copolymers.

6.2.10.4.6 DSC curves of the cured phenanthrenyl-group containing polysiloxanes
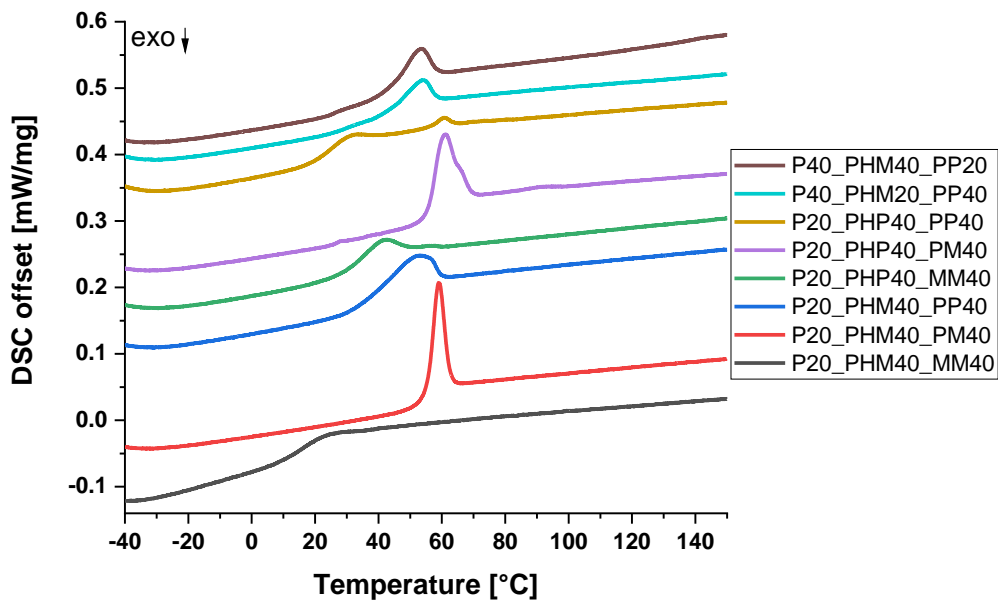
Figure 449: 1st heating cycle of the DSC measurements of the cured phenanthrenyl-group containing polysiloxanes.
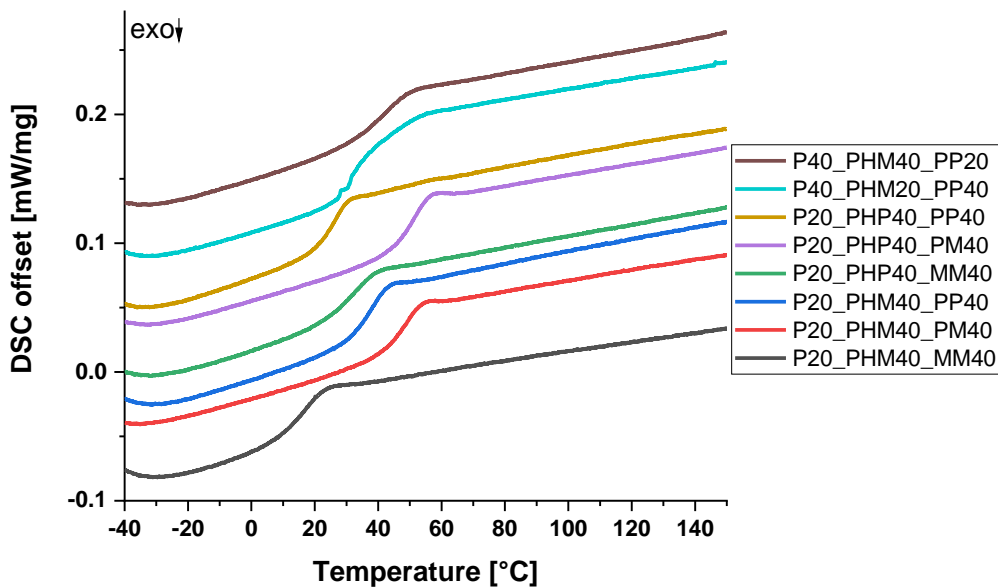
Figure 450: 2nd heating cycle of the DSC measurements of the cured phenanthrenyl-group containing polysiloxanes.

6.2.10.4.7 Haze curve of the cured phenanthrenyl-group containing polysiloxanes
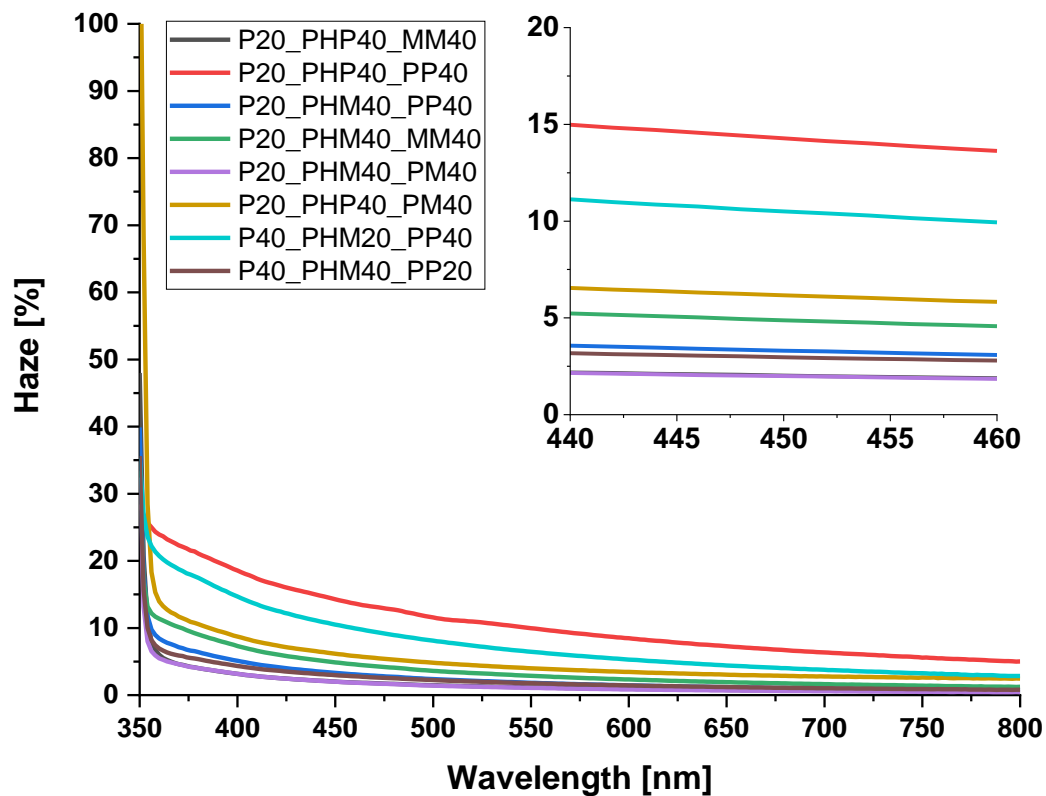
Figure 451: Calculated haze curve of the cured phenanthrenyl-group containing polysiloxanes.

7 References

1. Cho, J.; Park, J. H.; Kim, J. K.; Schubert, E. F., White light-emitting diodes: History, progress, and future. *Laser Photonics Rev.* **2017,** *11* (2), 1600147-1600164.
2. Anon, S., Packaging an organic light emitting diode. *Res. Discl.* **1998,** *416* (Dec.), P1620.
3. Liu, Y.; Luan, X.; Feng, Y.; Tan, X.; Han, Y.; Sun, X., Self-adhesive epoxy modified silicone materials for light emitting diode encapsulation. *Polym. Adv. Technol.* **2017,** *28* (11), 1473-1479.
4. Atif, M.; Bongiovanni, R.; Yang, J., Cationically UV-Cured Epoxy Composites. *Polym. Rev.* **2015,** *55* (1), 90-106.
5. Tao, P.; Li, Y.; Siegel, R. W.; Schadler, L. S., Transparent Dispensible High-Refractive Index ZrO_2 Epoxy Nanocomposites for LED Encapsulation. *J. Appl. Polym. Sci.* **2013,** *130* (5), 3785-3793.
6. Kim, J.; Ma, B.; Lee, K., Comparison of effect of epoxy and silicone adhesive on the lifetime of plastic LED package. *Electron. Mater. Lett.* **2013,** *9* (4), 429-432.
7. Li, T.; Zhang, J.; Wang, H.; Hu, Z.; Yu, Y., High-Performance Light-Emitting Diodes Encapsulated with Silica-Filled Epoxy Materials. *ACS Appl. Mater. Interfaces* **2013,** *5* (18), 8968-8981.
8. Gao, N.; Liu, W. Q.; Ma, S. Q.; Tang, C.; Yan, Z. L., Cycloaliphatic epoxy resin modified by two kinds of oligo-fluorosiloxanes for potential application in light-emitting diode (LED) encapsulation. *J. Polym. Res.* **2012,** *19* (8), 1-10.
9. Gao, N.; Liu, W. Q.; Ma, S. Q.; Yan, Z. L.; Zhao, Y., Modification of epoxy Resin with cycloaliphatic-epoxy oligosiloxane for light-emitting diode (LED) encapsulation application. *J. Macromol. Sci., Part B: Phys.* **2012,** *51* (8), 1509-1524.
10. Chung, P. T.; Yang, C. T.; Wang, S. H.; Chen, C. W.; Chiang, A. S. T.; Liu, C.-Y., ZrO_2/epoxy nanocomposite for LED encapsulation. *Mater. Chem. Phys.* **2012,** *136* (2-3), 868-876.
11. Clapp, T. Silicone Solutions for LED Lighting. https://www.dow.com/en-us/market/mkt-electronics/sub-elec-lighting.html (accessed 06.07.2020).
12. Wu, K.-H.; Cheng, K.-F.; Yang, C.-C.; Wang, C.-P.; Liu, C.-I., Thermal and Optical Properties of Epoxy/Siloxane Hybrimer Based on Sol-Gel-Derived Phenyl-Siloxane. *OJCM* **2015,** *05* (03), 49-59.
13. ShinEtsu Chemical Co.Ltd., KJR Series & SEMICOAT Series. Shin-Etsu Chemical Co., L., Ed. 1998; p 14.
14. Dow Corning, Dow Corning® OE-6630 - Premilinary Data. Corporation, D. C., Ed. 2006.
15. Hsu, C.-Y.; Han, W.-G.; Chiang, S.-J.; Sub, W.-C.; Liu, Y.-L., Multi-functional branched polysiloxanes polymers for high refractive index and flame retardant LED encapsulants. *RSC Adv.* **2016,** *6*, 4377-4381.
16. Liu, C.; Hajagos, T. J.; Chen, D.; Chen, Y.; Kishpaugh, D.; Pei, Q., Efficient One-Pot Synthesis of Colloidal Zirconium Oxide Nanoparticles for High-Refractive-Index Nanocomposites. *ACS Appl. Mater. Interfaces* **2016,** *8* (7), 4795-802.
17. Huang, J.-H.; Li, C.-P.; Chang-Jian, C.-W.; Lee, K.-C.; Huang, J.-H., Preparation and characterization of high refractive index silicone/TiO_2 nanocomposites for LED encapsulants. *J. Taiwan Inst. Chem. Eng.* **2015,** *46*, 168-175.
18. Higashihara, T.; Ueda, M., Recent Progress in High Refractive Index Polymers. *Macromolecules* **2015,** *48* (7), 1915-1929.
19. Lai, Y.; Jin, L.; Hang, J.; Sun, X.; Shi, L., Highly transparent thermal stable silicone/titania hybrids with high refractive index for LED encapsulation. *J. Coat. Technol. Res.* **2015,** *12* (6), 1185-1192.
20. Macdonald, E. K.; Shaver, M. P., Intrinsic high refractive index polymers. *Polym. Int.* **2015,** *64* (1), 6-14.

21. Ren, Z.; Yan, S., Polysiloxanes for optoelectronic applications. *Prog. Mater. Sci.* **2016,** *83*, 383-416.

22. Sun, D.; Ren, Z.; Bryce, M. R.; Yan, S., Arylsilanes and siloxanes as optoelectronic materials for organic light-emitting diodes (OLEDs). *J. Mater. Chem. C.* **2015,** *3* (37), 9496-9508.

23. INSTRUMENT SYSTEMS GmbH, *Handbuch der LED-Messtechnik*. INSTRUMENT SYSTEMS GmbH: Munich, 2008; Vol. 1.0.

24. Schubert, E. F., *Light-Emitting Diodes*. 2 ed.; Cambridge University Press: New York, 2006; p 434.

25. Schubert, E. F.; Gessmann, T.; Kim, J. K. In *Light emitting diodes*, John Wiley & Sons, Inc.: 2005; pp 832-867.

26. Born, M.; Jüstel, T., Elektrische Lichtquellen: Chemie in Lampen. *Chem. unserer Zeit* **2006,** *40* (5), 294-305.

27. Ananda, W., External Quantum Efficiency Measurement of Solar Cell. *IEEE* **2017,** *15th Intl. Conf. QiR: Intl. Symp. Elec. and Com. Eng.*, 450-456.

28. Magazine, L. Terminology: LED efficiency. https://www.ledsmagazine.com/home/article/16701295/terminology-led-efficiency.

29. Chang, M.-H.; Das, D.; Varde, P. V.; Pecht, M., Light emitting diodes reliability review. *Microelectron. Reliab.* **2012,** *52* (5), 762-782.

30. Ferguson, I. T.; Tanabe, S.; Carrano, J. C.; Fujita, S.; Yoshihara, S.; Taguchi, T.; Ashdown, I. E.; Sakamoto, A.; Yamamoto, S., YAG glass-ceramic phosphor for white LED (II): luminescence characteristics. In *Fifth International Conference on Solid State Lighting*, Proc. of SPIE: 2005; Vol. 5941, pp 594112-1-6.

31. Li, S.; Wang, L.; Tang, D.; Cho, Y.; Liu, X.; Zhou, X.; Lu, L.; Zhang, L.; Takeda, T.; Hirosaki, N.; Xie, R.-J., Achieving High Quantum Efficiency Narrow-Band β-Sialon:Eu^{2+} Phosphors for High-Brightness LCD Backlights by Reducing the Eu^{3+} Luminescence Killer. *Chem. Mater.* **2017,** *30* (2), 494-505.

32. Xia, Z.; Liu, Q., Progress in discovery and structural design of color conversion phosphors for LEDs. *Prog. Mater. Sci.* **2016,** *84*, 59-117.

33. Ye, S.; Xiao, F.; Pan, Y. X.; Ma, Y. Y.; Zhang, Q. Y., Phosphors in phosphor-converted white light-emitting diodes: Recent advances in materials, techniques and properties. *Mat. Sci. Eng. R.* **2010,** *71* (1), 1-34.

34. Xie, R.-J.; Hirosaki, N.; Li, H.-L.; Li, Y. Q.; Mitomo, M., Synthesis and Photoluminescence Properties of β-sialon:Eu^{2+} (Si$_{6-z}$Al$_z$O$_z$N$_{8-z}$:Eu^{2+}) - A Promising Green Oxynitride Phosphor for White Light-Emitting Diodes. *J. Electrochem. Soc.* **2007,** *154* (10), J314-J319.

35. Feldmann, C.; Jüstel, T.; Ronda, C. R.; Schmidt, P. J., Inorganic Luminescent Materials: 100 Years of Research and Application. *Adv. Funct. Mater.* **2003,** *13* (7), 511-516.

36. Narukawa, Y.; Niki, I.; Izuno, K.; Yamada, M.; Murazaki, Y.; Mukai, T., Phosphor-Conversion White Light Emitting Diode Using InGaN Near-Ultraviolet Chip. *Jpn. J. Appl. Phys.* **2002,** *41* (Part 2, No. 4A), L371-L373.

37. Jüstel, T.; Nikol, H.; Ronda, C., New Developments in the Field of Luminescent Materials for Lighting and Displays. *Angew. Chem. Int. Ed. Engl.* **1998,** *37*, 3084-3103.

38. Schlotter, P.; Schmidt, R.; Schneider, J., Luminescence conversion of blue light emitting diodes. *Appl. Phys. A* **1997,** *64*, 417-418.

39. Ronda, C. R., Phosphors for lamps and displays: an applicational view. *J. Alloys Compd.* **1995,** *225*, 534-538.

40. Steigerwald, D. A.; Bhat, J. C.; Collins, D.; Fletcher, R. M.; Holcomb, M. O.; Ludowise, M. J.; Martin, P. S.; Rudaz, S. L., Illumination With Solid State Lighting Technology. *IEEE J. Quantum Electron.* **2002,** *8* (2), 310-320.

41. Baretz, B.; Tischler, M. A. Solid state white light emitter and display using same. US 6,600,175 B1, 2003.

42. Stevenson, D. A.; Rhines, W. C.; Maruska, H. P. Gallium nitride metal-semiconductor junction light emitting diode. 3,819,974, 1974.

43. Shimizu, Y.; Sakano, K.; Noguchi, Y.; Moriguchi, T. Light emitting device having a nitride compound semiconductor and a phosphor containing a garnet fluorescent material. US 5,998,925, 1999.

44. Hide, F.; Kozodoy, P.; DenBaars, S. P.; Heeger, A. J., White light from InGaN/conjugated polymer hybrid light-emitting diodes. *Appl. Phys. Lett.* **1997,** *70* (20), 2664-2666.

45. Dai, X.; Deng, Y.; Peng, X.; Jin, Y., Quantum-Dot Light-Emitting Diodes for Large-Area Displays: Towards the Dawn of Commercialization. *Adv. Mater.* **2017,** *29* (14).

46. Boesing, M.; Lindla, F.; Koehnen, A.; Gohri, V.; Ruske, M.; Hartmann, S.; Meulenkamp, E. *Recent Advances in OLED Lighting*; Philips GmbH Business Center OLED Lighting, OLEDWorks GmbH: 2015.

47. Tsutsui, T.; Takada, N., Progress in Emission Efficiency of Organic Light-Emitting Diodes: Basic Understanding and Its Technical Application. *Jpn. J. Appl. Phys.* **2013,** *52* (11R).

48. Chen, J.; Cranton, W.; Fihn, M., *Handbook of Visual Display Technology*. Springer Heidelberg Dordrecht London New York: 2016; Vol. second, p 3454.

49. Tang, C. W.; VanSlyke, S. A., Organic electroluminescent diodes. *Appl. Phys. Lett.* **1987,** *51* (12), 913-915.

50. Burroughes, J. H.; Bradley, D. D. C.; Brown, A. R.; Marks, R. N.; Mackay, K.; Friend, R. H.; Burnst, P. L.; Holmest, A. B., Light-emitting diodes based on conjugated polymers. *Nature* **1990,** *347*, 539-541.

51. Yang, X.; Neher, D.; Hertel, D.; Däubler, T. K., Highly Efficient Single-Layer Polymer Electrophosphorescent Devices. *Adv. Mater.* **2004,** *16* (2), 161-166.

52. Steinbrück, N.; Könemann, M.; Kickelbick, G., Effect of polysiloxane encapsulation material compositions on emission behaviour and stabilities of perylene dyes. *RSC Adv.* **2018,** *8* (32), 18128-18138.

53. Kim, L. A.; Anikeeva, P. O.; Coe-Sullivan, S. A.; Steckel, J. S.; Bawendi, M. G.; Bulovic, V., Contact Printing of Quantum Dot Light-Emitting Devices. *Nano Lett.* **2008,** *8* (12), 4513-4517.

54. Coe, S.; Woo, W.-K.; Bawendi, M.; Bulovic, V., Electroluminescence from single monolayers of nanocrystals in molecular organic devices. *Nature* **2002,** *420* (6917), 800-803.

55. González-Carrero, S.; Pérez-Prieto, J., Colloidal photoemissive nanoparticles. *ChemTexts* **2018,** *4* (3).

56. Oh, S.; Han, C. Y.; Yang, H.; Kim, J., Highly efficient white electroluminescent devices with hybrid double emitting layers of quantum dots and phosphorescent molecules. *Nanoscale* **2019,** *11* (19), 9276-9280.

57. Zibold, A.; Dammann, M.; Schmidt, R.; Konstanzer, H.; Kunzer, M., Influence of air pollutants on the lifetime of LEDs and analysis of degradation effects. *Microelectron. Reliab.* **2017,** *76-77*, 566-570.

58. Singh, P.; Tan, C. M.; Chang, L.-B., Early degradation of high power packaged LEDs under humid conditions and its recovery — Myth of reliability rejuvenation. *Microelectron. Reliab.* **2016,** *61*, 145-153.

59. Tsai, M.-Y.; Tang, C.-Y.; Wang, C. H.; Tsai, Y. Y.; Chen, C.-H., Investigation on Some Parameters Affecting Optical Degradation of LED Packages During High-Temperature Aging. *IEEE T. Device Mat. Re.* **2015,** *15* (3), 335-341.

60. Anderson, J.; Baker, A.; Bartine, D.; Bradley, D.; Bremser, M.; Clark, T.; Dasgupta, A.; Elizondo, P.; Gaines, J.; Harvey, R.; Haugaard, E.; Kostrun, M.; Ledbetter, M.; McAnally,

R.; Pan, J.; Pattison, M.; Robinson, C.; Rowell, D.; Shaddock, D.; Sierra, J.; Taylor, M.; Driel, W. v.; Welsh, F.; Yon, J., *LED luminaire lifetime: recommendations for testing and reporting*. Next Generation Lighting Industry Alliance: 2014.

61. McCluskey, P.; Mensah, K.; O'Connor, C.; Lilie, F., Reliability of commercial plastic encapsulated microelectronics at temperatures from 125 °C to 300 °C. In *IEEE Proc. HITEN 1999*, 1999; pp 155-162.

62. McCluskey, P.; Mensah, K.; O'Connor, C.; Gallo, A., Reliable use of commercial technology in high temperature environments. *Microelectron. Reliab.* **2000,** *40*, 1671-1678.

63. Lumileds, P., Lumileds. Luxeon reliability Reliability Datasheet RD25. 2006; p 18.

64. Kim, H.-H.; Choi, S.-H.; Shin, S.-H.; Lee, Y.-K.; Choi, S.-M.; Yi, S., Thermal transient characteristics of die attach in high power LED PKG. *Microelectron. Reliab.* **2008,** *48* (3), 445-454.

65. Gladkov, A.; Bar-Cohen, A., Parametric Dependence of Fatigue of Electronic Adhesives. *IEEE Trans. Compon., Packag. Technol.* **1999,** *22* (2), 200-208.

66. Xiaobing, L.; Bulong, W.; Sheng, L., Effects of Moist Environments on LED Module Reliability. *IEEE T. Device Mat. Re.* **2010,** *10* (2), 182-186.

67. Narendran, N.; Gu, Y.; Freyssinier, J. P.; Yu, H.; Deng, L., Solid-state lighting: failure analysis of white LEDs. *J. Cryst. Growth* **2004,** *268* (3-4), 449-456.

68. Li, H.-T.; Hsu, C.-W.; Chen, K.-C., The Study of Thermal Properties and Thermal Resistant Behaviors of Siloxane-modified LED Transparent Encapsulant. In *IMPACT 2007*, 2007; pp 246-249.

69. Torikai, A.; Hasegawa, H., Accelerated photodegradation of poly(vinyl chloride). *Polm. Degrad. Stabil.* **1999,** *63*, 441-445.

70. Meneghini, M.; Trevisanello, L.-R.; Meneghesso, G.; Zanoni, E., A Review on the Reliability of GaN-Based LEDs. *IEEE T. Device Mat. Re.* **2008,** *8* (2), 323-331.

71. Zhanga, Q.; Mu, X.; Wang, K.; Gan, Z.; LuoS, X.; Liua, h., Dynamic Mechanical Properties of the Transparent Silicone Resin for High Power LED Packaging. In *ICEPT-HDP 2008*, 2008.

72. Down, J. L., The Yellowing of Epoxy Resin Adhesives: Report on High-Intensity Light Aging. *Stud. Conserv.* **1986,** *31*, 159-170.

73. Hewlett Packard, Reliability of precision optical performance AllnGaP LED lamps in traffic signals and variable message signs *Application Brief I-004* **1997**.

74. Hsu, Y.-C.; Lin, Y.-K.; Chen, M.-H.; Tsai, C.-C.; Kuang, J.-H.; Huang, S.-B.; Hu, H.-L.; Su, Y.-I.; Cheng, W.-H., Failure Mechanisms Associated With Lens Shape of High-Power LED Modules in Aging Test. *IEEE T. Electron. Dev.* **2008,** *55* (2), 689-694.

75. Xie, R.-J.; Hirosaki, N., Silicon-based oxynitride and nitride phosphors for white LEDs - A review. *Sci. Technol. Adv. Mat.* **2016,** *8* (7-8), 588-600.

76. Xie, R.-J.; Hirosaki, N.; Kimura, N.; Sakuma, K.; Mitomo, M., 2-phosphor-converted white light-emitting diodes using oxynitride/nitride phosphors. *Appl. Phys. Lett.* **2007,** *90* (19).

77. Jia, D.; Jia, W.; Jia, Y., Long persistent alkali-earth silicate phosphors doped with Eu^{2+},Nd^{3+}. *J. Appl. Phys.* **2007,** *101* (2).

78. Arik, M.; Setlur, A.; Weaver, S.; Haitko, D.; Petroski, J., Chip to System Levels Thermal Needs and Alternative Thermal Technologies for High Brightness LEDS. *J. Electron. Pack.* **2007,** *129*, 328-338.

79. Misra, S.; Kolbe, J. *Reliability of thermal management substrates for LEDs*; Electronic design online conference series, session, 2010; pp 1-27.

80. Haiyu, Q.; Vichare, N. M.; Azarian, M. H.; Pecht, M., Analysis of Solder Joint Failure Criteria and Measurement Techniques in the Qualification of Electronic Products. *IEEE T. Compon. Pack. T.* **2008,** *31* (2), 469-477.

81. Hong, E.; Ferguson, I. T.; Narendran, N.; Narendran, N.; DenBaars, S. P.; Carrano, J. C., A method for projecting useful life of LED lighting systems. In *Third International Conference on Solid State Lighting*, 2004.

82. IPC-SM-785 In *Guidelines for Accelerated Reliability Testing of Surface Mount Solder Attachments*, IPC Northbrook, Illinois: 1992.

83. Song, B.; Han, B., Reliability guidelines of high power LED. In *2008 CALCE EPS Consortium Report. Project No. C08-26*, 2008; pp 1-11.

84. Meneghesso, G.; Crosato, C.; Garat, F.; Martines, G.; Paccagnella, A.; Zanoni, E., Failure mechanisms of Schottky gate contact degradation and deep traps creation in AIGaAs/InGaAs PM-HEMTs submitted to accelerated life tests. *Microelectron. Reliab.* **1988,** *38*, 1227-1232.

85. Dammann, M.; Leuther, A.; Benkhelifa, F.; Feltgen, T.; Jantz, W., Reliability and degradation mechanism of AlGaAs/InGaAs and InAlAs/InGaAs HEMTs. *physica status solidi (a)* **2003,** *195* (1), 81-86.

86. Lu, G.; Yang, S.; Huang, Y., Analysis on Failure Modes and Mechanisms of LED. In *8th ICRMS*, 2009; pp 1237-1241.

87. Wu, F.; Zhao, W.; Yang, S.; Zhang, C., Failure Modes and Failure Analysis of White LEDs In *9th ICEMI 09*, 2009; pp 4-978-4-981.

88. Yanagisawa, T.; Kojima, T., Long-term accelerated current operation of white light-emitting diodes. *J. Lumin.* **2005,** *114* (1), 39-42.

89. Yin, L.; He, P.; Nan, T.; Zhang, J., The degradation mechanism of GaN HP-LED under accelerated aging was analyzed by illuminance and temperature distribution. *Mol. Cryst. Liq. Cryst.* **2017,** *651* (1), 149-154.

90. Pavesi, M.; Rossi, F.; Zanoni, E., Effects of extreme dc-ageing and electron-beam irradiation in InGaN/AlGaN/GaN light-emitting diodes. *Semicond. Sci. Technol.* **2006,** *21* (2), 138-143.

91. Shun-Lien, C.; Ishibashi, A.; Kijima, S.; Nakayama, N.; Ukita, M.; Taniguchi, S., Kinetic model for degradation of light-emitting diodes. *IEEE J. Quantum Electron.* **1997,** *33* (6), 970-979.

92. Meneghesso, G.; Levada, S.; Zanoni, E.; Podda, S.; Mura, G.; Vanzi, M.; Cavallini, A.; Castaldini, A.; Du, S.; Eliashevich, I., Failure Modes and Mechanisms of DC-Aged GaN LEDs. *Phys. Stat. Sol. (a)* **2002,** *194* (2), 389-392.

93. Meneghesso, G.; Levada, S.; Pierobon, R.; Rampazzo, F.; Zanoni, E.; Cavallini, A.; Castaldini, A.; Scamarcio, G.; Du, S.; Eliashevich, I., Degradation mechanisms of GaN-based LEDs after accelerated DG current aging. *IEEE* **2002,** *IEDM 02 Digest Int*, 103-106.

94. Ott, M., Capabilites and Reliability of LEDs and Laser Diodes. *NASA NEPP* **2001**, 1-7.

95. Arnold, J., When the Lights Go Out: LED Failure Modes and Mechanisms. In *DfR solutions*, 2004; pp 1-4.

96. Hwang, N.; Naidu, P. S. R.; Trigg, A., Failure analysis of plastic packaged optocoupler light emitting diodes. In *5th conference EPTC*, 2003; pp 346-349.

97. Philips Lumileds *Understanding power LED lifetime analysis*; Technology White Paper, 2007; p 11.

98. Hamid, S. H.; Usmani, A. M., Applications of Polymers in Led Devices. *Polym.-Plast. technol. Eng.* **1984,** *22* (2), 155-176.

99. Usmani, A. M.; Salyer, I. O., New flexibilized diallyl phthalate resins for encapsulating electronic display devices *J. Mater. Sci.* **1981,** *16*, 915-926.

100. Grzegorczyk, D.; Feineman, G., Handbook of plastics in electronics. **1974**.

101. Electrolube, UR5634 Polyurethane Resin. 2019.

102. May, C., *Epoxy resins: chemistry and technology*. Routledge: 2018.

103. Hsu, C.-W.; Ma, C.-C. M.; Tan, C.-S.; Li, H.-T.; Huang, S.-C.; Lee, T.-M.; Tai, H., Effect of thermal aging on the optical, dynamic mechanical, and morphological properties of

phenylmethylsiloxane-modified epoxy for use as an LED encapsulant. *Mater. Chem. Phys.* **2012,** *134* (2-3), 789-796.

104. Kumar, R. N.; Keem, L. Y.; Mang, N. C.; Abubakar, A., Ultraviolet radiation curable epoxy resin encapsulant for light emitting diodes. *J. Appl. Polym. Sci.* **2006,** *100* (2), 1048-1056.

105. Pham, H. Q.; Marks, M. J., Epoxy Resins. In *Ullmann's Encyclopedia of Industrial Chemistry*, 2005.

106. Wang, L.; Wong, C. P., Novel Thermally Reworkable Underfill Encapsulants For Flip-Chip Applications. *IEEE Trans. Adv. Packag.* **1999,** *22* (1), 46-53.

107. Wang, L.; Wong, C. P., Syntheses and Characterizations of Thermally Reworkable Epoxy Resins. Part I. *J. Polym. Sci. A Pol. Chem.* **1999,** *37*, 2991-3001.

108. Yang, S.; Kwak, S.-Y.; Jin, J.; Kim, J.-S.; Choi, Y.; Paik, K.-W.; Bae, B.-S., Thermally resistant UV-curable epoxy–siloxane hybrid materials for light emitting diode (LED) encapsulation. *J. Mater. Chem.* **2012,** *22* (18).

109. Barton, D. L.; Osinski, M.; Perlin, P.; Helms, C. J.; Berg, N. H., Life Tests and Failure Mechanisms of GaN/AlGaN/InGaN Light Emitting Diodes. *Proc. SPIE* **1997,** *3279* (17), 276-281.

110. Mark, J. E.; Allcock, H. R.; West, R., *Inorganic Polymers - Second Edition*. Oxford University Press: 2005.

111. Yuan, X.; Yue, Z. F.; Chen, X.; Wen, S. F.; Li, L.; Feng, T., The protective and adhesion properties of silicone-epoxy hybrid coatings on 2024 Al-alloy with a silane film as pretreatment. *Corros. Sci.* **2016,** *104*, 84-97.

112. Fischer, H. R.; Semprimoschnig, C.; Mooney, C.; Rohr, T.; van Eck, E. R. H.; Verkuijlen, M. H. W., Degradation mechanism of silicone glues under UV irradiation and options for designing materials with increased stability. *Polym. Degrad. Stabil.* **2013,** *98* (3), 720-726.

113. Panavaite, D.; Padarauskas, A.; Vickackaite, V., Silicone glue coated stainless steel wire for solid phase microextraction. *Anal. Chim. Acta* **2006,** *571* (1), 45-50.

114. Kofod, G.; Sommer-Larsen, P., Silicone dielectric elastomer actuators: Finite-elasticity model of actuation. *Sensor. Actuat. A-Phys.* **2005,** *122* (2), 273-283.

115. Ordonez, J. S.; Boehler, C.; Schuettler, M.; Stieglitz, T., Silicone rubber and thin-film polyimide for hybrid neural interfaces -a MEMS-based adhesion promotion technique-. In *6th Annual International IEEE EMBS Conference on Neural Engineering*, San Diego, California, 2013; pp 872-875.

116. Zhou, T.; Wang, X.; Cheng, P.; Wang, T.; Xiong, D.; Wang, X., Improving the thermal conductivity of epoxy resin by the addition of a mixture of graphite nanoplatelets and silicon carbide microparticles. *eXPRESS Polym. Lett.* **2013,** *7* (7), 585-594.

117. Su, Y.-K.; Wang, P.-C.; Lin, C.-L.; Huang, G.-S.; Wei, C.-M., Enhanced light extraction using blue LED package consisting of TiO_2-doped silicone layer and silicone lens. *IEEE Electron Device Lett.* **2014,** *35* (5), 575-577.

118. Lee, S.; Hong, J.-Y.; Jang, J., Multifunctional Graphene Sheets Embedded in Silicone Encapsulant for Superior Performance of Light-Emitting Diodes. *ACS Nano* **2013,** *7* (7), 5784-5790.

119. Dvornic, P. R.; Jones, R. G.; Ando, W., Thermal Properties of Polysiloxanes. In *Silicon-Containing Polymers*, Springer: Dordrecht, 2000.

120. Pauling, L., *The Nature of the Chemical Bond*. Cornell university press Ithaca, NY: 1960; Vol. 260.

121. Stark, F. O.; Falender, J. R.; Wright, A. P., 9.3 Silicones. In *Comprehensive Organometallic Chemistry*, Wilkinson, G.; Stone, F. G. A.; Abel, E. W., Eds. Elsevier Science Ltd. : Dow Corning Corporation, Midland, Michigan, 1982; Vol. 2, p 9460.

122. Mohoric, I.; Krajnc, M.; Šebenik, U., Model-free Kinetics Analysis of Thermal Degradation of Polysiloxane Lubricant. *Chem. Biochem. Eng. Q.* **2009,** *23* (4), 493-496.

123. Cottrell, T. L., *The Strengths of Chemical Bonds*. 2nd ed. ed.; Butterworths: London, 1958.

124. He, C.; Li, B.; Ren, Y.; Lu, W.; Zeng, Y.; He, W.; Feng, A., How the Crosslinking Agent Influences the Thermal Stability of RTV Phenyl Silicone Rubber. *Materials* **2018,** *12* (1).
125. Harris, F. W.; Seymour, R. B., Structure-solubility relationships in polymers. *J. Polym. Sci. B Polym. Lett. Ed.* **1977,** *15* (10), 634.
126. Timpe, D. C. *Low Temperature Flexibility of Silicone Fusible Tapes*; Arlon – Silicone Technologies Division: Delaware, USA, 2008.
127. Mark, J. E.; Schaefer, D. W.; Lin, G., *The Polysiloxanes*. Oxford University Press: 2015.
128. CROW Polymer Properties Database. https://polymerdatabase.com/polymer%20chemistry/Polysiloxanes.html (accessed 23.06.2020).
129. Schmerl, N. M.; Khodakov, D. A.; Stapleton, A. J.; Ellis, A. V.; Andersson, G. G., Valence band structure of PDMS surface and a blend with MWCNTs: A UPS and MIES study of an insulating polymer. *Appl. Surf. Sci.* **2015,** *353*, 693-699.
130. Cai, D. K.; Neyer, A.; Kuckuk, R.; Heise, H. M., Optical absorption in transparent PDMS materials applied for multimode waveguides fabrication. *Opt. Mater.* **2008,** *30* (7), 1157-1161.
131. Zhang, H.; Cloud, A. *The Permeability Characteristics of Silicone Rubber*; Arlon Silicone Technologies Division: Delaware, USA, 2007.
132. Le, B. Q.; Nhan, E.; Maurer, R. H.; Jenkins, R. E.; Lew, A. L.; Feldmesser, H. S.; Lander, J. R., Miniaturization of Space Electronics with Chip-on-Board Technology. *J. Hopkins Apl. Tech. D.* **1999,** *20* (1), 50-61.
133. Metz, S. J. Water vapor and gas transport through polymeric membranes. Dissertation, University of Twente, Netherlands, 2003.
134. Rucker, C.; Kümmerer, K., Environmental chemistry of organosiloxanes. *Chem. Rev.* **2015,** *115* (1), 466-524.
135. Brook, M. A., *Silicon in organic, organometallic, and polymer chemistry*. Wiley New York: 2000; Vol. 123.
136. Mosley, D. W.; Khanarian, G.; Conner, D. M.; Thorsen, D. L.; Zhang, T.; Wills, M., High Refractive Index Thermally Stable Phenoxyphenyl and Phenylthiophenyl Silicones for Light-Emitting Diode Applications. *J. Appl. Polym. Sci.* **2014,** *131* (3), 39824-39833.
137. Mosley, D. W.; Auld, K.; Conner, D.; Gregory, J.; Liu, X.-Q.; Pedicini, A.; Thorsen, D.; Wills, M.; Khanarian, G.; Simon, E. S., High performance encapsulants for ultra high-brightness LEDs. *Proc. SPIE* **2008,** *6910* (Light-Emitting Diodes: Research, Manufacturing, and Applications XII), 691017/1-691017/8.
138. Kim, Y. H.; Bae, J. Y.; Jin, J.; Bae, B. S., Sol-gel derived transparent zirconium-phenyl siloxane hybrid for robust high refractive index LED encapsulant. *ACS Appl. Mater. Interfaces* **2014,** *6* (5), 3115-3121.
139. Brinker, C. J.; Scherer, G. W., *Sol-gel science: the physics and chemistry of sol-gel processing*. Academic press: 2013.
140. Hench, L. L.; West, J. K., The Sol-Gel Process. *Chem. Rev.* **1990,** *90* (1), 33-72.
141. Schmidt, H.; Scholze, H.; Kaiser, A., Principles of hydrolysis and condensation reaction of alkoxysilanes. *J. Non-Cryst. Solids* **1984,** *63*, 1-11.
142. Alothman, Z., A Review: Fundamental Aspects of Silicate Mesoporous Materials. *Materials* **2012,** *5* (12), 2874-2902.
143. Chojnowski, J.; Cypryk, M., Synthesis of Linear Polysiloxanes. In *Silicon-Containing Polymers*, Jones, R. G.; Ando, W.; Chojnowski, J., Eds. Springer: Dordrecht, 2000; p 39.
144. Brinker, C. J. *Sol-gel processing of silica*; American Chemical Society, Washington, DC (United States): 1994.
145. Schubert, U., Chemistry and Fundamentals of the Sol–Gel Process. In *The Sol–Gel Handbook: Synthesis, Characterization, and Applications*, 1st ed.; Levy, D.; Zayat, M., Eds. Wiley-VCH Verlag GmbH & Co. KGaA.: 2015; p 28.

146. Fjellvåg, H.; Sjåstad, A. O., Synthesis; sol-gel. Department of Chemistry, University of Oslo: Central University of Tamil Nadu, 2016; p 38.

147. Loy, D. A.; Mather, B.; Straumanis, A. R.; Baugher, C.; Schneider, D. A.; Sanchez, A.; Shea, K. J. In *Effects of pH on the Gelation Time in the Sol-Gel Polymerization of 1,6-Bis(trimethoxysilyl)hexane* 2005; p 18.

148. McNeil, K. J.; DiCaprio, J. A.; Walsh, D. A.; Pratt, R. F., Kinetics and Mechanism of Hydrolysis of a Silicate Triester, Tris(2-methoxyethoxy)phenylsilane. *J. Am. Chem. Soc.* **1980,** *102* (6), 1859-1865.

149. Osterholtz, F. D.; Pohl, E. R., Kinetics of the hydrolysis and condensation of organofunctional alkoxysilanes: a review *J. Adhesion Sci. Technol.* **1992,** *6* (1), 127-149.

150. Delattre, L.; Depuy, C.; Babonneau, F., Characterization of the Hydrolysis and Polymerization Processes of Methacryloxypropyltrimethoxysilane *J. Sol-Gel Sci. Technol.* **1994,** *2*, 185-188.

151. Iwasawa, A.; Ape, R.; Sasakit, H.; Takahashi, o.; Omoto, H., The Effects of Organotin Catalysts on Hydrolytic Condensation of Polymethylsiloxane Oligomer and Moisture Cure of the Coatings. *J. Jpn. Sco. Colour Mater.* **2003,** *76* (10), 373-379.

152. Wang, S. P.; Li, Q.; Qi, Z., Studies on Silicone Rubber / Montmorillonite Hybrid Composites. *Key Eng. Mat.* **1997,** *137*, 87-93.

153. Yokoyama, T.; Kinjo, N.; Mukai, J., Effects of Catalyst on the Electrical Properties of Silicone Rubber. *J. Appl. Polym. Sci.* **1984,** *29*, 1951-1958.

154. Wacker Chemie AG, ELASTOSIL® RT 625 A/B. Munich, Germany, 2019; p 4.

155. Dow Corning, SYLGARD® 182 Silicone Elastomer. 1999; p 5.

156. Choi, K. M.; Rogers, J. A., A Photocurable Poly(dimethylsiloxane) Chemistry Designed for Soft Lithographic Molding and Printing in the Nanometer Regime. *J. Am. Chem. Soc.* **2003,** *125*, 4060-4061.

157. Jothimuthu, P.; Carroll, A.; Bhagat, A. A. S.; Lin, G.; Mark, J. E.; Papautsky, I., Photodefinable PDMS thin films for microfabrication applications. *J. Micromech. Microeng.* **2009,** *19* (4).

158. Begum, F.; Zhao, H.; Simon, S. L., Modeling methyl methacrylate free radical polymerization: Reaction in hydrophobic nanopores. *Polymer* **2012,** *53* (15), 3261-3268.

159. Müller, U., Photocrosslinking of Silicones. Part 11. Radical Photopolymerization Under Oxygen-Silicone Acrylates as Model Systems. *J. Macromol. Sci. A* **1994,** *31* (12), 1905-1926.

160. Wang, J. J.; Liu, F., Photoinduced graft polymerization of 2-methacryloyloxyethyl phosphorylcholine on silicone hydrogels for reducing protein adsorption. *J. Mater. Sci. Mater. Med.* **2011,** *22* (12), 2651-7.

161. Meng, Y.; Tsai, M.; Schmidt, G. R.; Anthamatten, M., Gradient-index materials based on thiol-ene networks. *ACS Appl. Mater. Interfaces* **2015,** *7* (16), 8601-5.

162. Bhagat, S. D.; Chatterjee, J.; Chen, B.; Stiegman, A. E., High Refractive Index Polymers Based on Thiol–Ene Cross-Linking Using Polarizable Inorganic/Organic Monomers. *Macromolecules* **2012,** *45* (3), 1174-1181.

163. Lewis, L. N.; Stein, J.; Smith, K. A.; Messmer, R. P.; Legrand, D. G.; Scott, R. A. In *Recent mechanism studies on hydrosilylation*, Gordon & Breach: 1995; pp 263-285.

164. Cramer, R. D.; Jr., R. V. L.; Prewitt, C. T.; Stolberg, U. G., Five-Coordinate Platinum(II) Complexes. *J. Am. Chem. Soc.* **1964,** *87* (3), 658-658.

165. Hofmann, R. J.; Vlatkovic, M.; Wiesbrock, F., Fifty Years of Hydrosilylation in Polymer Science: A Review of Current Trends of Low-Cost Transition-Metal and Metal-Free Catalysts, Non-Thermally Triggered Hydrosilylation Reactions, and Industrial Applications. *Polymers* **2017,** *9* (10).

166. Maciejewski, H.; Marciniec, B.; Kownacki, I., Catalysis of hydrosilylation. Part XXXIV. High catalytic efficiency of the nickel equivalent of Karstedt catalyst [{Ni(η-

CH$_2$=CHSiMe$_2$)$_2$O}$_2${μ-(η-CH$_2$=CHSiMe$_2$)$_2$O}]. *J. Organomet. Chem.* **2000,** *597* (1-2), 175-181.

167. Gulinski, J.; Marciniec, B.; Maciejewski, H.; Oczkowicz, S., Catalysis of hydrosilylation. Part XXXV. Synthesis of 3-chloropropyltrichlorosilane via the catalytic hydrosilylation of allyl chloride with trichlorosilane catalyzed by platinum catalyst - from laboratory scale to pilot plant. *Pol. J. Chem. Technol.* **1999,** *1* (1), 11-15.

168. Marciniec, B.; Krzyzanowski, P.; Walczuk-Gusciora, E.; Duczmal, W., Catalysis of hydrosilylation. Part XXXIII. Catalytic activity of silyloxy-rhodium(I) complexes in hydrosilylation of alkenes. *J. Mol. Catal. A: Chem.* **1999,** *144* (2), 263-271.

169. Marciniec, B.; Kitynski, D.; Oczkowicz, S.; Tyrka, M.; Lewandowski, M.; Foltynowicz, Z., Process for preparation of propyltrichlorosilane. *Przem. Chem.* **1998,** *77* (9), 336-339.

170. Marciniec, B.; Maciejewski, H.; Kownacki, I., Dehydrogenative coupling of styrene with trisubstituted silanes catalyzed by nickel complexes. *J. Mol. Catal. A: Chem.* **1998,** *135* (3), 223-231.

171. Urbaniak, W.; Marciniec, B., Silane coupling agents. Part VII. Alkyl-trisubstituted silanes. *Polimery* **1998,** *43* (3), 148-154.

172. Sakaki, S.; Mizoe, N.; Sugimoto, M., Theoretical Study of Platinum(0)-Catalyzed Hydrosilylation of Ethylene. Chalk-Harrod Mechanism or Modified Chalk-Harrod Mechanism. *Organometallics* **1998,** *17*, 2510-2523.

173. Marciniec, B.; Gulinski, J.; Kopylova, L.; Maciejewski, H.; Grundwald-Wyspianska, M.; Lewandowski, M., Catalysis of hydrosilylation: Part XXXI. Functionalization of poly(methylhydro)siloxanes via hydrosilylation of allyl derivatives. *Appl. Organomet. Chem.* **1997,** *11* (10 & 11), 843-849.

174. Marciniec, B., Dehydrogenative coupling of olefins with silicon compounds catalyzed by transition-metal complexes. *New J. Chem.* **1997,** *21* (6-7), 815-824.

175. Marciniec, B. In *Hydrosilylation and related reactions of silicon compounds*, VCH: 1996; pp 487-506.

176. Marciniec, B.; Maciejewski, H.; Gulinski, J.; Maciejewska, B.; Duczmal, W., Catalysis of hydrosilylation XXX. Competitive dehydrogenative silylation and hydrogenative dimerization of vinyltriethoxysilane catalyzed by the [Ni(acac)$_2$] + PPh$_3$ system, intermediate and mechanistic implications. *J. Organomet. Chem.* **1996,** *521* (1-2), 245-251.

177. Lewis, L. N.; Sumpter, C. A., Cyclodextrin modification of the hydrosilylation reaction. *J. Mol. Catal. A: Chem.* **1996,** *104*, 293-297.

178. Duczmal, W.; Sliwinska, E.; Maciejewska, B.; Marciniec, B.; Maciejewski, H., Catalysis of hydrosilylation. Part XXVII. Stereoelectronic effects of substituents at silicon on the hydrosilylation of 1-hexene catalyzed by [RhCl(cod)(1-hexene)]. *Transition Met. Chem.* **1995,** *20* (5), 435-9.

179. Gulinski, J.; James, B. R.; Marciniec, B., Catalysis of hydrosilylation. XXVIII. The role of dioxygen in hydrosilylation of alkenes catalyzed by ruthenium phosphine complexes. *J. Organomet. Chem.* **1995,** *499* (1-2), 173-9.

180. Marciniec, B.; Foltynowicz, Z., Silane coupling agents. Part V. Vinyl-trisubstituted silanes. *Polimery* **1995,** *40* (3), 144-50.

181. Marciniec, B.; Maciejewski, H.; Rosenthal, U., Catalysis of hydrosilylation. Part XXV. Effect of nickel(0) and nickel(II) complex catalysts on dehydrogenative silylation, hydrosilylation and dimerization of vinyltriethoxysilane. *J. Organomet. Chem.* **1994,** *484* (1-2), 147-51.

182. Gulinski, J.; Klosin, J.; Marciniec, B., Catalysis of hydrosilylation: Part XXIV. H$_2$PtCl$_6$ in cyclohexanone as hydrosilylation catalyst - what is the active species in this catalytic system? *Appl. Organomet. Chem.* **1994,** *8* (4), 409-14.

183. Marciniec, B.; Maciejewski, H., Catalysis of hydrosilylation. XXIII. Effect of substituents at silicon on unusual hydrosilylation of vinylsilanes catalyzed by nickel acetylacetonate. *J. Organomet. Chem.* **1993,** *454* (1-2), 45-50.

184. Marciniec, B.; Foltynowicz, Z.; Lewandowski, M., Catalysis of hydrosilylation. Part XXII. Polymer-protected immobilized platinum complex catalysts for gas-phase hydrosilylation of acetylene. *Appl. Organomet. Chem.* **1993,** *7* (3), 207-12.

185. Marciniec, B.; Gulinski, J., Recent advances in catalytic hydrosilylation. *J. Organomet. Chem.* **1993,** *446* (1-2), 15-23.

186. Marciniec, B. In *Chemical processes in production of silane coupling agents and silyl olefins*, Norw. Inst. Technol. Inst. Inorg. Chem.: 1992; pp 119-30.

187. Gevorgyan, V.; Borisova, L.; Popelis, J.; Lukevics, E.; Foltynowicz, Z.; Gulinski, J.; Marciniec, B., Synthesis of new vinylsilanes containing an asymmetric silicon via platinum catalyzed hydrosilylation of acetylene and monosubstituted alkynes. *J. Organomet. Chem.* **1992,** *424* (1), 15-22.

188. Marciniec, B.; Maciejewski, H.; Mirecki, J., Catalysis of hydrosilylation. XX. Unusual reaction of vinyltriethoxysilane with triethoxysilane catalyzed by nickel acetylacetonate. *J. Organomet. Chem.* **1991,** *418* (1), 61-7.

189. Marciniec, B.; Gulinski, J.; Urbaniak, W.; Nowicka, T.; Mirecki, J., Catalysis of hydrosilylation. Part XVIII. Pt(PPh$_3$)$_2$(CH$_2$=CH$_2$) - a versatile catalyst for hydrosilylation of olefins. *Appl. Organomet. Chem.* **1990,** *4* (1), 27-34.

190. Marciniec, B.; Duczmal, W.; Urbaniak, W.; Sliwinska, E., Catalysis of hydrosilylation. XIX. Mechanism of hydrosilylation of 1-hexene catalyzed by [RhCl(COD)(phosphine)]. *J. Organomet. Chem.* **1990,** *385* (3), 319-27.

191. Marciniec, B., Hydrosilylation of vinylsilanes. *Ser. Chem.* **1989,** *57* (Osiagniecia Chem. Technol. Org.), 327-36.

192. Marciniec, B.; Mackowska, E., Catalysis of hydrosilylation. Part XVII. Intermediates in hydrosilylation of vinyltrichlorosilane catalyzed by palladium phosphine complexes. *J. Mol. Catal.* **1989,** *51* (1), 41-51.

193. Marciniec, B.; Foltynowicz, Z.; Urbaniak, W., Catalysis of hydrosilylation. XV. A poly(phosphinoorganosiloxanyl)silicate-supported rhodium(I) catalyst for gas-phase hydrosilylation of acetylene. *Appl. Organomet. Chem.* **1987,** *1* (5), 459-63.

194. Marciniec, B.; Foltynowicz, Z.; Urbaniak, W.; Perkowski, J., Catalysis of hydrosilylation. XIII. Gas-phase hydrosilylation of acetylene by trichlorosilane on functionalized silica supported rhodium and ruthenium phosphine complexes. *Appl. Organomet. Chem.* **1987,** *1* (3), 267-73.

195. Marciniec, B.; Foltynowicz, Z.; Urbaniak, W., Catalysis of hydrosilylation. Part XIV. Aminoorganosiloxane-silicate-supported rhodium complexes as catalysts for hydrosilylation of alkenes and vinylsilanes. *J. Mol. Catal.* **1987,** *42* (2), 195-203.

196. Duczmal, W.; Marciniec, B.; Urbaniak, W., Catalysis of hydrosilylation. XII. Spectrophotometric study of the reactivity of the [RhCl(COD)]$_2$-bis(diphenylphosphinoethyl)tetramethyldisiloxane complex with substrates of the hydrosilylation reaction. *J. Organomet. Chem.* **1987,** *327* (3), 295-302.

197. Duczmal, W.; Urbaniak, W.; Marciniec, B., Catalysis of hydrosilylation. XI. Rhodium(I)-siloxyalkylphosphine complexes; synthesis, characteristics, and catalytic activity. *J. Organomet. Chem.* **1986,** *317* (1), 85-92.

198. Marciniec, B.; Mackowska, E.; Gulinski, J.; Urbaniak, W., Addition of tri(chloro, methyl)silanes to vinyltri(chloro, methyl)silanes catalyzed by palladium phosphine complexes. *Z. Anorg. Allg. Chem.* **1985,** *529*, 222-8.

199. Marciniec, B., Present directions of study and application of hydrosilylation processes. *Ser. Chem.* **1985,** *47* (Wybrane Zagadnienia Chem. Krzemu), 93-121.

200. Marciniec, B. In *Catalysis of hydrosilylation and metathesis of vinyl-substituted silanes*, Horwood: 1985; pp 183-94.
201. Marciniec, B.; Gulinski, J., Catalysis of hydrosilylation. VII. Catalysis of hydrosilylation of carbon-carbon double bonds by ruthenium phosphine complexes. *J. Organomet. Chem.* **1983,** *253* (3), 349-62.
202. Marciniec, B.; Urbaniak, W., Organosiloxane-silicate macromolecules as supports for rhodium(I) phosphine catalyst. *J. Mol. Catal.* **1983,** *18* (1), 49-56.
203. Marciniec, B.; Gulinski, J.; Urbaniak, W., Catalysis of hydrosilylation. Part II. Addition of trialkoxysilanes to vinyltrialkoxysilanes catalyzed by transion metal complexes. *Pol. J. Chem.* **1982,** *56* (2), 287-96.
204. Marciniec, B.; Gulinski, J.; Urbaniak, W., Catalysis of hydrosilylation. IV. Synthesis of bis(trichlorosilyl)ethanes via hydrosilylation. *Synth. React. Inorg. Met.-Org. Chem.* **1982,** *12* (2), 139-47.
205. Marciniec, B.; Urbaniak, W.; Pawlak, P., Catalysis of hydrosilylation. V. Rhodium(I) complexes with phosphinoalkyl organosilicon ligands as hydrosilylation catalysts. *J. Mol. Catal.* **1982,** *14* (3), 323-31.
206. Marciniec, B.; Kornetka, Z. W.; Urbaniak, W., Platinum and rhodium complexes supported on aminated silica as hydrosilylation catalysts. *J. Mol. Catal.* **1981,** *12* (2), 221-30.
207. Marciniec, B.; Gulinski, J., Ruthenium phosphine complexes as catalysts for the hydrosilylation of the carbon-carbon double bond. *J. Mol. Catal.* **1980,** *10* (1), 123-6.
208. Lewis, L. N.; Stein, J.; Gao, Y.; Colborn, R. E.; Hutchins, G., Platinum Catalysts Used in the Silicones Industry. *Platinum Metals Rev.* **1997,** *41* (2), 66-75.
209. Gelest *Platinum*; Morrisville, Pennsylvania, 2011; p 2.
210. Polytech, P. *PLATINUM CATALYSTS*; 2016.
211. Franczyk, A.; Stefanowska, K.; Dutkiewicz, M.; Frackowiak, D.; Marciniec, B., A highly selective synthesis of new alkenylsilsesquioxanes by hydrosilylation of alkynes. *Dalton Trans.* **2017,** *46* (1), 158-164.
212. Franczyk, A.; Stefanowska, K.; Dutkiewicz, M.; Frackowiak, D.; Marciniec, B., A highly selective synthesis of new alkenylsilsesquioxanes by hydrosilylation of alkynes. *Dalton Trans.* **2016,** *46* (1), 158-164.
213. Products, J. M. C. *Ashby Katalyst*; 2015.
214. Żak, P.; Bołt, M.; Pietraszuk, C., Selective Hydrosilylation of Dienes, Enynes, and Diynes Catalyzed by a Platinum Complex with a Very Bulky NHC Ligand - The Crucial Role of Precise Tuning of the Reaction Conditions. *Eur. J. Inorg. Chem.* **2019,** *2019* (19), 2455-2461.
215. Komine, N.; Abe, M.; Suda, R.; Hirano, M., Markovnikov-Selective Hydrosilylation of Electron-Deficient Alkenes with Arylsilanes Catalyzed by Mono(phosphine)palladium(0). *Organometallics* **2015,** *34* (2), 432-437.
216. Xie, X.; Zhang, X.; Gao, W.; Meng, C.; Wang, X.; Ding, S., Iridium-catalyzed Markovnikov hydrosilylation of terminal alkynes achieved by using a trimethylsilyl-protected trihydroxysilane. *Commun. Chem.* **2019,** *2* (1).
217. Grassie, N.; Macfarlane, I. G., The thermal degradation of polysiloxanes - I poly(dimethylsiloxane). *Eur. Polym. J.* **1978,** *14*, 874-884.
218. Grassie, N.; Macfarlane, I. G.; Francey, K. F., The thermal degradation of poylsiloxanes - II poly(methylphenylsiloxane). *Eur. Polym. J.* **1979,** *15*, 415-422.
219. Unno, M.; Tanaka, R., Silanols and Silsesquioxanes. In *Efficient Methods for Preparing Silicon Compounds*, 2016; pp 399-440.
220. Dire, S.; Egger, P.; Vona, M. L. D.; Trombetta, M.; Licoccia, S., Siloxane-Based Nanobuilding Blocks by Reaction Between Silanediol and Trifunctional Silicon Alkoxides. *J. Sol-Gel Sci. Technol.* **2004,** *32*, 57-61.

221. Corey, E. J.; Venkateswarlu, A., Protection of hydroxyl groups as tert-butyldimethylsilyl derivatives. *J. Am. Chem. Soc.* **1972,** *94* (17), 6190-6191.
222. Grassie, N.; Francey, K. F.; Macfarlane, I. G., The thermal degradation of polysiloxanes - part 4: poly(dimethyl/diphenylsiloxane). *Polym. Degrad. Stab.* **1980,** *2* (67-83).
223. Wenderoth, P.; Betke, U.; Kickelbick, G. Optoelectronic component and method for producing an optoelectronic component. WO 2018/036883, 2018.
224. Wenderoth, P.; Betke, U.; Kickelbick, G. Method for producing a siloxane, method for producing a polysiloxane, method for casting optoelectronic components. WO 2018/050514, 2018.
225. Kickelbick, G.; Wenderoth, P.; Betke, U. *Improvement of LED Encapsulants*; Saarland University, OSRAM Opto Semiconductors: Saarbrücken, 2015; p 46.
226. Sobolevskii, M. V.; Skorokhodov, I. I.; Ditsent, V. Y.; Sobolevskaya, L. V.; Vovshin, E. I.; Blekh, L. M., Thermally induced changes in oligomethylphenylsiloxanes. *Vysokomol. soyed.* **1974,** *A16* (4), 729-734.
227. Soares, J. A. N. T., Introduction to Optical Characterization of Materials. In *Practical Materials Characterization*, 2014; pp 43-92.
228. Brunchi, C. E.; Filimon, A.; Cazacu, M.; Ioan, S., Properties of Some Poly(siloxane)s for Optical Applications. *High Perform. Polym.* **2008,** *21* (1), 31-47.
229. Liu, J.-g.; Ueda, M., High refractive index polymers: fundamental research and practical applications. *J. Mater. Chem.* **2009,** *19* (47), 8907.
230. Fedors, R. F., A method for estimating both the solubility parameters and molar volumes of liquids. *Polym. Eng. Sci.* **1974,** *14* (2), 147-154.
231. Nakagawa, Y.; Yoshida, T.; Ogawa, S.; Kuramoto, M.; Bando, M. Curable Resin Composition, Method for producing curable resin Composition, and Method for measuring surface Tackiness of viscoelastic Material. US 2017/0369751, 2017.
232. Liu, L.; Deshazer, D.; Grasmann, M.; Liu, N.; Shahinian, K. M. Polyheterosiloxane Composition and Silicone Composition including a Polyheterosiloxane. WO 2014/152824, 2014.
233. Kurtin, J. N.; Stott, N. E. Highly refractive, transparent thermal conductors for better heat dissipation and light extraction in white LEDs. US 20150028365A1, 2015.
234. Bae, J.-y.; Kim, Y.; Kim, H.-Y.; Lim, Y.-w.; Bae, B.-S., Sol–gel synthesized linear oligosiloxane-based hybrid material for a thermally-resistant light emitting diode (LED) encapsulant. *RSC Adv.* **2013,** *3* (23).
235. Kim, J.-S.; Yang, S. C.; Kwak, S.-Y.; Choi, Y.; Paik, K.-W.; Bae, B.-S., High performance encapsulant for light-emitting diodes (LEDs) by a sol–gel derived hydrogen siloxane hybrid. *J. Mater. Chem.* **2012,** *22* (16), 7954-7960.
236. Chung, P. T.; Chiou, S. H.; Tseng, C. Y.; Chiang, A. S., Preparation and Evaluation of a Zirconia/Oligosiloxane Nanocomposite for LED Encapsulation. *ACS Appl. Mater. Interfaces* **2016,** *8* (15), 9986-93.
237. Karpovich, N. F.; Pugachevsky, M. A.; Panfilov, V. I.; Kuzmenko, A. P.; Dobromyslov, M. B., The Hydrothermal Autoclave Synthesis of the Nanopowders of the Refractory ZrO_2 and HfO_2 Oxides. *J. Nano- Electron. Phys.* **2015,** *7* (4), 04076.
238. Stolzenburg, P.; Freytag, A.; Bigall, N. C.; Garnweitner, G., Fractal growth of ZrO_2 nanoparticles induced by synthesis conditions. *CrystEngComm.* **2016,** *18* (43), 8396-8405.
239. Cheng, Y.; Lü, C.; Yang, B., A Review on High Refractive Index Nanocomposites for Optical Applications. *Recent Pat. Mat. Sci.* **2011,** *4*, 15-27.
240. Chen, X.; Mao, S. S., Titanium dioxide nanomaterials: synthesis, properties, modifications, and applications. *Chem. Rev.* **2007,** *107* (7), 2891-959.
241. Niederberger, M.; Garnweitner, G.; Buha, J.; Polleux, J.; Ba, J.; Pinna, N., Nonaqueous synthesis of metal oxide nanoparticles:Review and indium oxide as case study for the

dependence of particle morphology on precursors and solvents. *J. Sol-Gel Sci. Technol.* **2006,** *40* (2-3), 259-266.

242. Li, Y.; Wang, L.; Natarajan, B.; Tao, P.; Benicewicz, B. C.; Ullal, C.; Schadler, L. S., Bimodal matrix-free polymer nanocomposites. *RSC Adv.* **2015,** *5,* 14788-14795.

243. Mont, F. W.; Kim, J. K.; Schubert, M. F.; Schubert, E. F.; Siegel, R. W., High-refractive-index TiO₂-nanoparticle-loaded encapsulants for light-emitting diodes. *J. Appl. Phys.* **2008,** *103* (8).

244. Caseri, W., Inorganic Nanoparticles as Optically Effective Additives for Polymers. *Chem. Eng. Commun.* **2008,** *196* (5), 549-572.

245. Novak, B. M., Hybrid Nanocomposite Materials-Between Inorganic Glasses and Organic Polymers. *Adv. Mater.* **1993,** *5* (6), 422-433.

246. Nussbaumer, R. J. Synthese und Charakterisierung von Rutilnanopartikeln und deren Einbau in transparente Polymer-Nanoverbundwerkstoffe. Dissertation, Eidgenössischen Technischen Hochschule Zürich, Zürich, 2004.

247. Wood, D. L.; Nassau, K., Refractive index of cubic zirconia stabilized with yttria. *Appl. Opt.* **1982,** *21,* 2978-2981.

248. Wood, D. L.; Nassau, K.; Kometani, T. Y.; Nash, D. L., Optical properties of cubic hafnia stabilized with yttria. *Appl. Opt.* **1990,** *29* (4), 604-607.

249. Garnweitner, G.; Goldenberg, L. M.; Sakhno, O. V.; Antonietti, M.; Niederberger, M.; Stumpe, J., Large-scale synthesis of organophilic zirconia nanoparticles and their application in organic-inorganic nanocomposites for efficient volume holography. *Small* **2007,** *3* (9), 1626-1632.

250. Garnweitner, G.; Niederberger, M., Nonaqueous and Surfactant-Free Synthesis Routes to Metal Oxide Nanoparticles. *J. Am. Ceram. Soc.* **2006,** *89* (6), 1801-1808.

251. Liu, C.; Hajagos, T. J.; Kishpaugh, D.; Jin, Y.; Hu, W.; Chen, Q.; Pei, Q., Facile Single-Precursor Synthesis and Surface Modification of Hafnium Oxide Nanoparticles for Nanocomposite γ-Ray Scintillators. *Adv. Funct. Mater.* **2015,** *25* (29), 4607-4616.

252. Holzinger, D. Synthesis and Characterization of Hybrid Inorganic-Organic Core-Shell Nanoparticles by a Grafting-from approach of Polymers from Metal and Metal Oxid Cores. Dissertation, Technische Universität Wien, Wien, 2004.

253. Frantz, R.; Durand, J.-O.; Granier, M.; Lanneau, G. F., Triisopropoxysilyl-functionalized oxide nanoparticles using a di-tert-butyl phosphonate ester as the surface grafting agent. *Tetrahedron Lett.* **2004,** *45* (14), 2935-2937.

254. Lü, C.; Yang, B., High refractive index organic–inorganic nanocomposites: design, synthesis and application. *J. Mater. Chem.* **2009,** *19* (19), 2884.

255. Feichtenschlager, B. Chemical Tailoring of Metal Oxide NP Surfaces to control structure and properties of Polymer Nanocomposites. Dissertation, Technischen Universität Wien, 2011.

256. Li, Y.; Krentz, T. M.; Wang, L.; Benicewicz, B. C.; Schadler, L. S., Ligand engineering of polymer nanocomposites: from the simple to the complex. *ACS Appl. Mater. Interfaces* **2014,** *6* (9), 6005-21.

257. Li, Y.; Tao, P.; Viswanath, A.; Benicewicz, B. C.; Schadler, L. S., Bimodal surface ligand engineering: the key to tunable nanocomposites. *Langmuir* **2013,** *29* (4), 1211-20.

258. Schottner, G., Hybrid Sol-Gel-Derived Polymers: Applications of Multifunctional Materials. *Chem. Mater.* **2001,** *13* (10), 3422-3435.

259. White, M. A.; Johnson, J. A.; Koberstein, J. T.; Turro, N. J., Toward the Syntheses of Universal Ligands for Metal Oxide Surfaces: Controlling Surface Functionality through Click Chemistry. *J. Am. Chem. Soc.* **2006,** *128,* 11356-11357.

260. Pawsey, S.; Yach, K.; Halla, J.; Reven, L., Self-Assembled Monolayers of Alkanoic Acids: A Solid-State NMR Study. *Langmuir* **2000,** *16* (7), 2000.

261. Tao, Y. T.; Huang, C. Y.; Chiou, D. R.; Chen, L. J., Infrared and Atomic Force Microscopy Imaging Study of the Reorganization of Self-Assembled Monolayers of Carboxylic Acids on Silver Surface. *Langmuir* **2002,** *18*, 8400-8406.

262. Aronoff, Y. G.; Chen, B.; Lu, G.; Seto, C.; Schwartz, J.; Bernasek, S. L., Stabilization of Self-Assembled Monolayers of Carboxylic Acids on Native Oxides of Metals. *J. Am. Chem. Soc.* **1997,** *119* (2).

263. Zhang, B.; Kong, T.; Xu, W.; Su, R.; Gao, Y.; Cheng, G., Surface functionalization of zinc oxide by carboxyalkylphosphonic acid self-assembled monolayers. *Langmuir* **2010,** *26* (6), 4514-22.

264. Gawalt, E. S.; Lu, G.; Bernasek, S. L.; Schwartz, J., Enhanced Bonding of Alkanephosphonic Acids to Oxidized Titanium Using Surface-Bound Alkoxyzirconium Complex Interfaces. *Langmuir* **1999,** *15* (26), 8929-8933.

265. Gao, W.; Dickinson, L.; Grozinger, C.; Morin, F. G.; Reven, L., Self-Assembled Monolayers of Alkylphosphonic Acids on Metal Oxides. *Langmuir* **1996,** *12*, 7.

266. Queffelec, C.; Petit, M.; Janvier, P.; Knight, D. A.; Bujoli, B., Surface modification using phosphonic acids and esters. *Chem. Rev.* **2012,** *112* (7), 3777-807.

267. De Roo, J.; De Keukeleere, K.; Feys, J.; Lommens, P.; Hens, Z.; Van Driessche, I., Fast, microwave-assisted synthesis of monodisperse HfO_2 nanoparticles. *J. Nanopart. Res.* **2013,** *15* (7).

268. Buha, J.; Arcon, D.; Niederberger, M.; Djerdj, I., Solvothermal and surfactant-free synthesis of crystalline Nb_2O_5, Ta_2O_5, HfO_2, and Co-doped HfO_2 nanoparticles. *Phys. Chem. Chem. Phys.* **2010,** *12* (47), 15537-43.

269. Sartori, P.; Weidenbruch, M., Reactions of Halides of Group IV Elements with Trifluoroacetic Acid. *Angew. Chem. Internat. Edit.* **1964,** *3* (5), 376-377.

270. Schäfer, S.; Kickelbick, G., Diels–Alder Reactions on Surface-Modified Magnetite/Maghemite Nanoparticles: Application in Self-Healing Nanocomposites. *ACS Appl. Nano Mater.* **2018,** *1* (6), 2640-2652.

271. Davis, K.; Qi, B.; Witmer, M.; Kitchens, C. L.; Powell, B. A.; Mefford, O. T., Quantitative measurement of ligand exchange on iron oxides via radiolabeled oleic acid. *Langmuir* **2014,** *30* (36), 10918-25.

272. Chiang, A. S.-T.; Wang, S.-H.; Pai, C.-T.; Chen, C.-W. Metal Oxide Nanoparticle Material. US 2016/0096738, 2016.

273. Riegler, B.; Thomaier, R. *Index Matching Silicone for High Brightness LED Packaging*; NuSil Lightspan Application Laboratory: IMAPS International Conference on Device Packaging, 2005.

274. Hoebbel, D.; Reinert, T.; Schmidt, H., ^{29}Si NMR Investigation of Condensation Reactions of Diphenylsilanediol in Presence of Ti-, Zr-, Al-, Sn- and Si-Alkoxides. *J. Sol-Gel Sci. Technol.* **1996,** *7* (3), 217-224.

275. Bae, J.-Y.; Yang, S.; Jin, J. H.; Jung, K.; Kim, J.-S.; Bae, B.-S., Fabrication of transparent methacrylate zirconium siloxane hybrid materials using sol–gel synthesized oligosiloxane resin. *J. Sol-Gel Sci. Technol.* **2010,** *58* (1), 114-120.

276. Gopalakrishnan, M.; Palanisami, N., New sterically hindered tin(iv) siloxane precursors to tinsilicate materials: synthesis, spectral, structural and photocatalytic studies. *RSC Adv.* **2016,** *6* (3), 1760-1768.

277. Wang, Y.; Wang, D.; Qing, X.; Kim, H., Synthesis and characterization of hysteresis-free zirconium oligosiloxane hybrid materials for organic thin film transistors. *Synth. Met.* **2017,** *223*, 226-233.

278. McCrea-Hendrick, M. L.; Wang, S.; Gullett, K. L.; Fettinger, J. C.; Power, P. P., The Reactions of Aryl Tin(II) Hydrides {$Ar^{iPr6}Sn(\mu$-H)$}_2$ ($Ar^{iPr6} = C_6H_3$-2,6-(C_6H_2-2,4,6-$^iPr_3$)$_2$) and {$Ar^{iPr4}Sn(\mu$-H)$}_2$ ($Ar^{iPr4} = C_6H_3$-2,6-(C_6H_3-2,6-$^iPr_2$)$_2$) with Aryl Alkynes: Substituent Dependent Structural Isomers. *Organometallics* **2017,** *36* (19), 3799-3805.

279. Wetton, E. A. M.; Higginson, W. C. E., Reducing Reactions of Tin(II) in Aqueous Solution. Part III.The Reduction of Various Common Oxidising Agents. *J. Chem. Soc.* **1965,** *1106*, 5890-5906.

280. Morrison, J. S. Some Reactions of Tin(II)chloride in non-aqueous solution. Dissertation, University of New Hampshire, 1965.

281. Meyer, G.; Melnick, M. A., The exchange reaction between tin(IV)chloride and tin(II)chloride in absolute methanol. *J. Phys. Chem.* **1957,** *61* (3), 367-369.

282. Tomaszewski, A.; Busselberg, D., $SnCl_2$ reduces voltage-activated calcium channel currents of dorsal root ganglion neurons of rats. *Neurotoxicology* **2008,** *29* (6), 958-63.

283. Nava, N.; Del Angel, P.; Salmones, J.; Baggio-Saitovitch, E.; Santiago, P., Tin-Platinum catalysts interactions on titania and silica. *Appl. Surf. Sci.* **2007,** *253* (23), 9215-9220.

284. Burch, R.; Garla, L. C., Platinum-Tin Reforming Catalysts II. Activity and Selectivity in Hydrocarbon Reactions. *J. Catal.* **1981,** *71*, 360-372.

285. Burch, R., Platinum-Tin Reforming Catalysts I. The Oxidation State of Tin and the Interaction between Platinum and Tin. *J. Catal.* **1981,** *71*, 348-359.

286. Muller, A. C.; Engelhard, P. A.; Weisang, J. E., Surface Study of Platinum-Tin Bimetallic Reforming Catalysts. *J. Catal.* **1979,** *56*, 65-72.

287. Verbeek, H.; Sachtler, W. M. H., The Study of the Alloys of Platinum and Tin by Chemisorption. *J. Catal.* **1976,** *42*, 257-267.

288. Janssem, M. M. P.; Moolhysen, J., Platinum-Tin catalysts for methanol fuel cells prepared by a novel immersion technique, by electrocodeposition and by alloying. *Electrochim. Acta* **1976,** *21*, 861-868.

289. Cathro, K. J., The Oxidation of Water-Soluble Organic Fuels Using Platinum-Tin Catalysts. *J. Electrochem. Soc.* **1969,** *116* (11), 1608-1611.

290. Jr., A. S. M.; Ayres, G. H., The Interaction of Platinum(II) and Tin(II) Chlorides. *J. Am. Chem. Soc.* **1955,** *77*, 2671-2675.

291. Ayres, G. H.; Jr., A. S. M., Spectrophotometric Study of the Platinum(lV)-Tin(ll) Chloride System. *Anal. Chem.* **1951,** *23* (2), 299-304.

292. Willem van der Weij, F., The Action of Tin Compounds in Condensation-type RTV Silicone Rubbers. *Makromol. Chem.* **1980,** *181*, 2541-2548.

293. Froese, R. D. J.; Musaev, D. G.; Matsubara, T.; Morokuma, K., Theoretical Studies of Ethylene Polymerization Reactions Catalyzed by Zirconium and Titanium Chelating Alkoxide Complexes. *J. Am. Chem. Soc.* **1997,** *119*, 7190-7196.

294. van der Linden, A.; Schaverien, C. J.; Meijboom, N.; Ganter, C.; Guy Orpen, A., Polymerization of α-Olefins and Butadiene and Catalytic Cyclotrimerization of 1-Alkynes by a New Class of Group IV Catalysts. Control of Molecular Weight and Polymer Microstructure via Ligand Tuning in Sterically Hindered Chelating Phenoxide Titanium and Zirconium Species. *J. Am. Chem. Soc.* **1995,** *117*, 3008-3021.

295. Corey, J. Y.; Zhu, X.-H., Reactions of Hydrosilanes and Olefins in the Presence of Cp_2MCl_2/n BuLi. *Organometallics* **1992,** *11* (2), 672-683.

296. Harrod, J. F.; Yun, S. S., Silyltitanocene Complexes as Catalysts for the Hydrogenation, Isomerization, and Hydrosilation of Olefins. *Organometallics* **1987,** *6* (7), 1381-1387.

297. Lee, M. L.; Kuei, J. C.; Adams, N. W.; Tarbet, B. J.; Nishioka, M.; Jones, B. A.; Bradshaw, J. S., Polarizable Polysiloxane stationary phases for capillary column gas chromatography. *J. Chrom.* **1984,** *302*, 303-318.

298. Mefteh, W. B.; Touzi, H.; Chevalier, Y.; Ouada, H. B.; Othmane, A.; Kalfat, R.; Jaffrezic-Renault, N., Comparison of polysiloxane films substituted by undecenyl-cyclam and by naphthyl-cyclam for the design of ISFET devices sensitive to Fe^{3+} ions. *Sens. Actuator B-Chem.* **2014,** *204*, 723-733.

299. Domingues, R. A.; Yoshida, I. V. r. P.; Atvars, T. D. Z., Fluorescence spectroscopy and thermal relaxation processes of anthracenyl-labeled polysiloxanes. *J. Polym. Sci. Pol. Phys.* **2010,** *48* (1), 74-81.

300. Lu, Z.; Ohshita, J.; Tanaka, D.; Mizumo, T.; Fujita, Y.; Kunugi, Y., Preparation, hybrid formation with single-walled carbon nanotube, and film morphology of pyrene-containing polysiloxanes. *Compos. Interface.* **2013,** *19* (9), 573-581.

301. Meazzini, I.; Willis-Fox, N.; Blayo, C.; Arlt, J.; Clément, S.; Evans, R. C., Targeted design leads to tunable photoluminescence from perylene dicarboxdiimide–poly(oxyalkylene)/siloxane hybrids for luminescent solar concentrators. *J. Mater. Chem. C.* **2016,** *4* (18), 4049-4059.

302. Steinbrück, N. Polysiloxane and Polysilsesquioxane based Materials for Optoelectronic Applications and Organic Dye Integration. Dissertation, Saarland University, Saarbrücken, 2019.

303. Wenderoth, P.; Betke, U.; Kickelbick, G. Optoelectronic component and method for producing an optoelectronic component. WO 2018/036883, 2018.

304. Chang, Y.-Y.; Glorieux, B.; Hsu, C.-H.; Sun, C.-C.; Yu, L.-Z.; Yang, T.-H.; Chung, T.-Y., Influence of ZrO_2 particles on the optical properties of pc-LEDs. *Opt. Mater.* **2016,** *55*, 55-61.

305. Alaei, M.; Rashidi, A. M.; Bakhtiari, I., Preparation of High Surface Area ZrO_2 Nanoparticles. *Iran. J. Chem. Chem. Eng.* **2014,** *33* (2), 47-53.

306. Lomoschitz, C. Synthesis of Phosphorus Coupling Agents and Their Use in the Modification of ZrO_2 and Barium-Glass Surfaces. Dissertation, Technischen Universität Wien, Fakultät für Technische Chemie, 2011.

307. Ramadoss, A.; Kim, S. J., Synthesis and characterization of HfO_2 nanoparticles by sonochemical approach. *J. Alloy. Compd.* **2012,** *544*, 115-119.

308. Kockmann, A.; Porsiel, J. C.; Saadat, R.; Garnweitner, G., Impact of nanoparticle surface modification on the mechanical properties of polystyrene-based nanocomposites. *RSC Adv.* **2018,** *8* (20), 11109-11118.

309. Sperling, R. A.; Parak, W. J., Surface modification, functionalization and bioconjugation of colloidal inorganic nanoparticles. *Phil. Trans. R. Soc. A* **2010,** *368* (1915), 1333-83.

310. Wang, P.-C.; Lin, C.-L.; Su, Y.-K.; Chien, P.-C.; Yeh, Y.-H.; Liou, J.-K.; Wei, C.-M., Reliability testing in GaN-based blue light-emitting diodes by doping TiO_2 nanoparticles into silicone encapsulation. *Jpn. J. Appl. Phys.* **2014,** *53* (6S), 06JE10/1-06JE10/4, 4 pp.

311. Wang, P.-C.; Su, Y.-K.; Lin, C.-L.; Huang, G.-S., Improving performance and reducing amount of phosphor required in packaging of white LEDs with TiO_2-doped silicone. *IEEE Electron. Device L.* **2014,** *35* (6), 657-659.

312. Jayaraman, V.; Bhavesh, G.; Chinnathambi, S.; Ganesan, S.; Aruna, P., Synthesis and characterization of hafnium oxide nanoparticles for bio-safety. *Mater. Express* **2014,** *4* (5), 375-383.

313. Niederberger, M.; Pinna, N., *Metal Oxide Nanoparticles in Organic Solvents*. Springer-Verlag: London, 2009; p 230.

314. Santhoshkumar, T.; Rahuman, A. A.; Jayaseelan, C.; Rajakumar, G.; Marimuthu, S.; Kirthi, A. V.; Velayutham, K.; Thomas, J.; Venkatesan, J.; Kim, S.-K., Green synthesis of titanium dioxide nanoparticles using Psidium guajava extract and its antibacterial and antioxidant properties. *Asian Pac. J. Trop. Med.* **2014,** *7* (12), 968-976.

315. Hu, X.; Lin, Z.; Zheng, Y.; Xu, Y., Preparation and characterization of two component transparent zinc oxide/silicone nanocomposites for power light emitting diodes encapsulant. *Asian J. Chem.* **2015,** *27* (8), 2905-2910.

316. Zhan, X.; Xing, Q.; Liu, H.; Zhang, J.; Cheng, J.; Lin, X., A facile method for fabrication of titanium-doped hybrid materials with high refractive index. *RSC Adv.* **2014,** *4* (27), 13909.

317. Kim, Y. H.; Lim, Y.-W.; Lee, D.; Kim, Y. H.; Bae, B.-S., A highly adhesive siloxane LED encapsulant optimized for high thermal stability and optical efficiency. *J. Mater. Chem. C.* **2016,** *4*, 10791-7.

318. Bae, J.-y.; Kim, Y.-H.; Kim, H.-Y.; Kim, Y.-B.; Jin, J.; Bae, B.-S., Ultraviolet Light Stable and Transparent Sol-Gel Methyl Siloxane Hybrid Material for UV Light-Emitting Diode (UV LED) Encapsulant. *ACS Appl. Mater. Interfaces* **2015,** *7* (2), 1035-1039.

319. Kim, J.-S.; Yang, S.; Bae, B.-S., Thermally Stable Transparent Sol−Gel Based Siloxane Hybrid Material with High Refractive Index for Light Emitting Diode (LED) Encapsulation. *Chem. Mater.* **2010,** *22* (11), 3549-3555.

320. Kherroub, D. E.; Belbachir, M.; Lamouri, S., Synthesis and characterization of polyvinylmethylsiloxanes by cationic polymerization using a solid green catalyst. *e-Polymers* **2017,** *17* (5).

321. Engelhardt, G.; Jancke, H.; Lippmaa, E.; Samoson, A., Structure Investigations of Solid Organosilicon Polymers by High Resolution Solid State ^{29}Si NMR. *J. Organomet. Chem.* **1981,** *210*, 295-301.

322. Engelhardt, G.; Jancke, H.; Mägi, M.; Pehk, T.; Lippmaa, E., Über die ^{1}H-, ^{13}C- und ^{29}Si-NMR chemischen Verschiebungen einiger linearer, verzweigter und cyclischer Methylsiloxan-verbindungen. *J. Organomet. Chem.* **1971,** *28*, 293-300.

323. Gray, G. W.; Hawthorne, W. D.; Lacey, D.; White, M. S.; Semlyen, J. A., ^{29}Si N.M.R. investigations of polysiloxanes. *Liq. Cryst.* **1989,** *6* (5), 503-513.

324. Uhlig, F.; Marsmann, H. C. *^{29}Si NMR - Some Practical Aspects*; Gelest Inc. AZmax: Germany, 2008; p 15.

325. Beshah, K.; Mark, J. E.; Ackerman, J. L., Characterization of PDMS Model Junctions and Networks by Solution and Solid-state Silicon-29NMR Spectroscopy. *J. Polym. Sci. Pol. Phy.* **1986,** *24*, 1207-1225.

326. Ramli, M. R.; Othman, M. B. H.; Arifin, A.; Ahmad, Z., Cross-link network of polydimethylsiloxane via addition and condensation (RTV) mechanisms. Part I: Synthesis and thermal properties. *Polym. Degrad. Stabil.* **2011,** *96* (12), 2064-2070.

327. Belot, V.; Corriu, R. J. P.; Leclercq, D.; Mutin, P. H.; Vioux, A., Thermal Redistribution Reactions in Crosslinked Polysiloxanes. *J. Poly Sci. Pol. Chem.* **1992,** *30*, 613-623.

328. Harris, R. K.; Robins, M. L., ^{29}Si nuclear magnetic resonance studies of oligomeric and polymeric siloxanes: 4. Chemical shift effects of end-groups. *Polymer* **1978,** *19*, 1123-1132.

329. Harris, R. K.; Kimber, B. J., ^{29}Si and ^{13}C Nuclear Magnetic Resonance Studies of Organosilicon Chemistry IV. Spin-lattice Relaxation and Motional Effects in Compounds Containing Phenyl Groups. *Adv. Mol. Relax. Pr.* **1975,** *8*, 23-35.

330. Casserly, T. B.; Gleason, K. K., Density Functional Theory Calculation of ^{29}Si NMR Chemical Shifts of Organosiloxanes. *J. Phys. Chem. B* **2005,** *109* (28), 13605-13610.

331. Wu, Q.; Hetem, M.; Cramers, C. A.; Rijks, J. A., Preparation of Thermally Stable Phenylpolysiloxane Fused Silica Capillary Columns. *J. High. Resolut. Chromatogr.* **1990,** *13*, 811-816.

332. Meng, Y.; Chu, J.; Xue, J.; Liu, C.; Wang, Z.; Zhang, L., Design and synthesis of non-crystallizable, low-T_g polysiloxane elastomers with functional epoxy groups through anionic copolymerization and subsequent epoxidation. *RSC Adv.* **2014,** *4* (59), 31249-31260.

333. Herbert, I. R.; Clague, A. D. H., Detailed Structural Analysis of Polysiloxane Antifoam Agents Using Carbon-13 and Silicon-29 NMR Spectroscopy. *Macromolecules* **1989,** *22* (8), 3267-3275.

334. Faulkner, R. A.; DiVerdi, J. A.; Yang, Y.; Kobayashi, T.; Maciel, G. E., The Surface of Nanoparticle Silicon as Studied by Solid-State NMR. *Materials* **2013,** *6* (1), 18-46.

335. Saalwächter, K.; Spiess, H. W., Solid-State NMR of Polymers. In *Polym. Sci. Ser. A+*, 2012; pp 185-219.

336. Gröger, C. Solid-State NMR Spectroscopic Studies Concerning the Biomineralization Process in Diatoms and on Inorganic Phosphorus Chalcogenide Cage Compounds. Dissertation, Regensburg University, Regensburg, 2008.

337. Unno, M.; Takada, K.; Kawaguchi, Y.; Matsumoto, H., Supramolecular Aggregates of Silanols and Solid-State Synthesis of Siloxanes. *Mol. Cryst. Liq. Cryst.* **2005,** *440* (1), 259-264.

338. Birkefeld, A. B.; Bertermann, R.; Eckert, H.; Pfleiderer, B., Liquid- and solid-state high-resolution NMR methods for the investigation of aging processes of silicone breast implants. *Biomaterials* **2003,** *24* (1), 35-46.

339. Brus, J., Solid-State NMR Study of Phase Separation and Order of Water Molecules and Silanol Groups in Polysiloxane Networks. *J. Sol-Gel Sci. Technol.* **2002,** *25*, 17-28.

340. Brus, J.; Dybal, J., Solid-state NMR study of structure, size and dynamics of domains in hybrid siloxane networks. *Polymer* **2000,** *41*, 5269-5282.

341. Yang, J. J.; El-Nahhal, I. M.; Maciel, G. E., Synthesis and solid-state NMR structural characterization of some functionalized polysiloxanes. *J. Non-Cryst. Solids* **1996,** *204*, 105-117.

342. Lindner, E.; Schreiber, R.; Kemmler, M.; Schneller, T.; Mayer, H. A., Solid-state NMR Characterization of Polysiloxane Matrixes Functionalized with Ether-Phosphines and Their Ruthenium(II) and Palladium(II) Complexes. *Chem. Mater.* **1995,** *7*, 951-960.

343. Deshpande, G.; Rezac, M. E., The effect of phenyl content on the degradation of poly(dimethyl diphenyl) siloxane copolymers. *Polym. Degrad. Stab.* **2001,** *74* (2), 363-370.

344. Gädda, T. M.; Weber, W. P., Pt-catalyzed chemical modification of α,ω-bis(hydrido)polydimethylsiloxanes and copoly(methylhydridosiloxane/dimethylsiloxane) with vinylheptaphenylcyclotetrasiloxane. *J. Polym. Sci. A Pol. Chem.* **2005,** *43* (14), 3007-3017.

345. Steinbrück, N.; Pohl, S.; Kickelbick, G., Platinum free thermally curable siloxanes for optoelectronic application – synthesis and properties. *RSC Adv.* **2019,** *9* (4), 2205-2216.

346. Launer, P. J.; Arkles, B. *Infrared analysis of organosilicon compounds: Spectra-Structure Correlations*; Gelest, Inc.: Morrisville, PA, 2013; p 4.

347. Smith, A. L., Infrared spectra-structure correlations for organosilicon compounds. *Spectrochim. Acta* **1960,** *16*.

348. Sharma, R. K.; Das, S.; Maitra, A., Surface modified ormosil nanoparticles. *J. Colloid Interface Sci.* **2004,** *277* (2), 342-6.

349. Karlsson, A. New Analytical Methods For Silicone Elastomers Used in Drug Delivery Systems. Dissertation, Department of Polymer Technology, Royal Institute of Technology, Stockholm, 2003.

350. Furniss, B. S.; Hannaford, A. J.; Smith, P. W. G.; Tatchell, A. R., *Vogel's - Textbook of Practical Organic Chemistry*. John Wiley & Sons, Inc.: New York, 1989; Vol. 5th.

351. Hamciuc, C.; Lisa, G.; Hamciuc, E.; Tudorachi, N., Thermal decomposition study of some polyimide-polydimethylsiloxane copolymers. *J. Anal. Appl. Pyrol.* **2018,** *129*, 204-214.

352. Wang, F.; Luo, Z.; Qing, S.; Qiu, Q.; Li, R., Sol–gel derived titania hybrid thin films with high refractive index. *J. Alloy. Compd.* **2009,** *486* (1-2), 521-526.

353. Schiavon, M. A.; Redondo, S. U. A.; Pina, S. R. O.; Yoshida, I. V. P., Investigation on kinetics of thermal decomposition in polysiloxane networks used as precursors of silicon oxycarbide glasses. *J. Non-Cryst. Solids* **2002,** *304*, 92-100.

354. Camino, G.; Lomakin, S. M.; Lazzari, M., Polydimethylsiloxane thermal degradation Part 1. Kinetic aspects. *Polymer* **2001,** *42* (6), 2395-2402.

355. Deshpande, G.; Rezac, M. E., Kinetic aspects of the thermal degradation of poly(dimethyl siloxane) and poly(dimethyl diphenyl siloxane). *Polym. Degrad. Stab.* **2002,** *76* (1), 17-24.

356. Rucigaj, A.; Krajnc, M.; Sebenik, U., Kinetic Study of Thermal Degradation of Polydimethylsiloxane: The Effect of Molecular Weight on Thermal Stability in Inert Atmosphere. *Polym. Sci.* **2017,** *3* (2:9), 1-7.

357. Grassie, N.; Beattie, S. R., The thermal degradation of polysiloxanes - part 5: synthesis, characterisation and thermal analysis of poly(tetramethyl-p-silphenylene siloxane) and copolymers with dimethylsiloxane. *Polym. Degrad. Stab.* **1984,** *7*, 109-126.

358. Homma, H.; Mirley, C. L.; Ronzello, J.; Boggs, S. A., Field and Laboratory Aging of RTV Silicone Insulator Coatings. *IEEE T. Power Deliver.* **2000,** *15* (4), 1298-1303.

359. Camino, G.; Lomakin, S. M.; Lageard, M., Thermal polydimethylsiloxane degradation. Part 2. The degradation mechanisms. *Polymer* **2002,** *43* (7), 2011-2015.

360. Psaltis, D.; Whitesides, G. M.; Fainman, Y.; Tang, S. K. Y., Fluidic optics. In *Optofluidics*, 2006.

361. Little, J. R. L. Tunable and high refractive index polydimethylsiloxane polymers for label-free optical sensing. Dissertation, Queen's University, Kingston, Ontario, Canada, 2013.

362. Klein, L. C., *Sol-Gel Technology for thin Films, Fibers, Preforms, Electronics and special Shapes*. Noyes Publications: New Jersey, U.S.A., 1988.

363. Yang, M.-H.; Liu, H.-W.; Lin, H.-T., Synthesis and Characterization of Base-catalyzed Phenyl Modified PDMS/PHMS Copolymers. *J. Chin. Chem. Soc.* **2004,** *51*, 791-799.

364. Watzke, S.; Altieri-Weimar, P., Degradation of silicone in white LEDs during device operation: a finite element approach to product reliability prediction. *Microelectron. Reliab.* **2015,** *55* (5), 733-737.

365. Siltech Silicone MQ Resins. https://www.siltech.com/products/silicone-mq-resins/.

366. Resins, S. S. Selicone Resin Introduction. https://www.sisib.com/silicone_resin/silicone_resin_MQ.html.

367. Chen, D.; Chen, F.; Hu, X.; Zhang, H.; Yin, X.; Zhou, Y., Thermal stability, mechanical and optical properties of novel addition cured PDMS composites with nano-silica sol and MQ silicone resin. *Compos. Sci. Technol.* **2015,** *117*, 307-314.

368. Engelhardt, G.; Mägi, M.; Lippmaa, E., ^{29}Si-NMR-Spektroskopische Untersuchungen an methyl und methyl-phenyl Siloxanen und ihre Anwendung in der Silikonanalytik. *J. Organomet. Chem.* **1973,** *54*, 115-122.

369. Rakita, P. E.; Worsham, L. S., ^{13}C NMR Studies of Organosilanes - III. Silicon-Phenyl Bonding in Phenylsilanes. *J. Organomet. Chem.* **1977,** *137*, 145-155.

370. Delor-Jestin, F.; Tomer, N. S.; Singh, R. P.; Lacoste, J., Characterization of polydimethylsiloxane rubber upon photochemical, thermal, salt-fog ageings and exposure to acid vapours. *e-Polymers* **2006,** *6* (1), 1-13.

371. Tudorachi, N.; Mustata, F., Thermal degradation and evolved gas analysis of some vegetable oils using TG/FT-IR/MS technique. *J. Therm. Anal. Calorim.* **2014,** *119* (3), 1703-1711.

372. Ahn, H. W.; Clarson, S. J., Synthesis And Characterization Of Cis- and Trans-Trimethyltriphnylcyclotrisiloxane. *J. Inorg. Organomet. P.* **2001,** *11* (4), 203-216.

373. Almeida, R. M.; Xu, J., Characterization of Sol–Gel Materials by Optical Spectroscopy Methods. In *The Sol-Gel Handbook*, Levy, D.; Zayat, M., Eds. 2015.

374. Villa, A.; Ferri, D.; Campisi, S.; Chan-Thaw, C. E.; Lu, Y.; Kröcher, O.; Prati, L., Operando Attenuated Total Reflectance FT-IR Spectroscopy: Studies on the Different Selectivity Observed in Benzyl Alcohol Oxidation. *ChemCatChem* **2015,** *7* (16), 2534-2541.

375. Zhang, X.; Ke, X.; Zhu, H., Zeolite-supported gold nanoparticles for selective photooxidation of aromatic alcohols under visible-light irradiation. *Chemistry* **2012,** *18* (26), 8048-56.

376. Li, X.-G.; Huang, M.-R.; Bai, H.; Yang, Y.-L., High-resolution thermogravimetry of polyphenylene sulfide film under four atmospheres. *J. Appl. Polym. Sci.* **2002,** *83* (10), 2053-2059.

377. Spijksma, G. I.; Seisenbaeva, G. A.; Fischer, A.; Bouwmeester, H. J. M.; Blank, D. H. A.; Kessler, V. G., The molecular composition of non-modified and acac-modified propoxide and butoxide precursors of zirconium and hafnium dioxides. *J. Sol-Gel Sci. Technol.* **2009,** *51* (1), 10-22.

378. Spijksma, G. I.; Bouwmeester, H. J. M.; Blank, D. H. A., Chemistry of 2,2,6,6,-Tetramethyl-3,5-heptanedione (Hthd) Modification of Zirconium and Hafnium Propoxide Precursors. *Inorg. Chem.* **2006,** *45* (13), 4938-4950.

379. Leyden, D. E.; Shreedhara Murthy, R. S.; Atwater, J. B.; Blitz, J. P., Studies of alkoxysilane hydrolysis and condensation by fourier-transform infrared spectroscopy with a cylindrical internal-reflection cell. *Anal. Chim. Acta* **1987,** *200*, 459-468.

380. Chaplin, M., Infrared Spectroscopy. 2013; p 85.

381. American Chemical Society SciFinder. https://scifinder.cas.org.

382. Taguchi, M.; Nakane, T.; Matsushita, A.; Sakka, Y.; Uchikoshi, T.; Funazukuri, T.; Naka, T., One-pot synthesis of monoclinic ZrO_2 nanocrystals under subcritical hydrothermal conditions. *J. Supercrit. Fluid.* **2014,** *85*, 57-61.

383. Davar, F.; Loghman-Estarki, M. R., Synthesis and optical properties of pure monoclinic zirconia nanosheets by a new precursor. *Ceram. Int.* **2014,** *40* (6), 8427-8433.

384. Lutterbeck, K.; Winkel, H., Infrarot-Spektroskopie. Werkstoffe, L. f., Ed. Fachhochschule Köln, 2009; p 7.

385. Mishra, R.; Ningthoujam, R. S., High-Temperature Ceramics. In *Materials Under Extreme Conditions*, 2017; pp 377-409.

386. Skov, A. L.; Yu, L., Optimization Techniques for Improving the Performance of Silicone-Based Dielectric Elastomers. *Adv. Eng. Mater.* **2018,** *20* (5).

387. Chiang, A. S.-T.; Wang, S.-H.; Pai, C.-T.; Chen, C.-W. Metal Oxide Nanoparticle Material. 20150329373, 2015.

388. Andrievski, R. A., Review of thermal stability of nanomaterials. *J. Mater. Sci.* **2013,** *49* (4), 1449-1460.

389. Chrissafis, K.; Bikiaris, D., Can nanoparticles really enhance thermal stability of polymers? Part I: An overview on thermal decomposition of addition polymers. *Thermochim. Acta* **2011,** *523* (1-2), 1-24.

390. Zhang, G.-Q.; Wang, L.-S.; Fan, R.-L.; Shao, X.-Z.; Wang, X.-F., Solubilities of Diphenylphosphinic Acid in Selected Solvents. *J. Chem. Eng. Data* **2008,** *53* (5), 1192-1195.

391. Jitianu, A.; Cadars, S.; Zhang, F.; Rodriguez, G.; Picard, Q.; Aparicio, M.; Mosa, J.; Klein, L. C., ^{29}Si NMR and SAXS investigation of the hybrid organic-inorganic glasses obtained by consolidation of the melting gels. *Dalton Trans.* **2017,** *46* (11), 3729-3741.

392. González, M. G.; Cabanelas, J. C.; Baselga, J., Applications of FTIR on Epoxy Resins – Identification, Monitoring the Curing Process, Phase Separation and Water Uptake In *Infrared Spectroscopy – Materials Science, Engineering and Technology* Theophile, T., Ed. InTech Europe: Croatia 2012; Vol. 1, pp 261-284.

393. Al-Ali, A. A. S.; Kassab-Bashi, T. Y., Fourier Transform Infra Red (FT-IR) Spectroscopy of New Copolymers of Acrylic Resin Denture Base Materials. *IJERSTE* **2015,** *4* (4), 172-180.

394. Shang, X. X.; Duan, S.; Zhang, M.; Cao, X. Y.; Zheng, K.; Zhang, J. N.; Ma, Y. M.; Zhang, R. B., UV-curable ladder-like diphenylsiloxane-bridged methacryl-phenyl-siloxane for high power LED encapsulation. *RSC Adv.* **2018,** *8* (17), 9049-9056.

395. Loh, T. C.; Ng, C. M.; Kumar, R. N.; Ismail, H.; Ahmad, Z., Improvement of thermal ageing and transparency of methacrylate based poly(siloxane–silsesquioxane) for optoelectronic application. *J. Appl. Polym. Sci.* **2017**, 45285 - 45295.

396. Wang, J.; Du, M.-L.; Xu, C.-S.; Zhu, H.; Fu, Y.-Q., Synthesis of Transparent Densely Crosslinked Polysiloxane with High Refractive Index. *J. Macromol. Sci. B* **2012,** *51* (12), 2462-2472.

397. Bashkatov, A. N.; Genina, E. A., Water refractive index in dependence on temperature and wavelength: a simple approximation. *Proc. of SPIE* **2003,** *5068*.

398. Murinov, Y. I.; Grabovskiy, S. A.; Islamova, R. M.; Kuramshina, A. b. R.; Kabal'nova, N. N., Mechanism of Methyl Methacrylate Polymerization Initiated by Benzoyl Peroxide and Ferrocene in the Presence of Oxygen. *Mendeleev Commun.* **2013,** *23* (1), 53-55.

399. Yang, M.-H.; Huang, W.-J.; Chien, T.-C.; Chen, C.-M.; Chang, H.-Y.; Chyan, Y.-S.; Chou, C., Synthesis and thermal properties of diphenylsiloxane block copolymers *Polymer* **2001,** *42*, 8841-8846.

400. Fichet, O.; Vidal, F.; Laskar, J.; Teyssie, D., Polydimethylsiloxane–cellulose acetate butyrate interpenetrating polymer networks synthesis and kinetic study. Part I. *Polymer* **2005,** *46* (1), 37-47.

401. Studer, K.; Nesvadba, P.; Jung, T.; Benkhoff, J.; Powell, K.; Lordelot, C., Novel curing agents: Thermal radical initiators as viable alternatives to peroxides. *Prog. Org. Coat.* **2008,** *61* (2-4), 119-125.

402. Chou, C.; Yang, M.-H., Structural Effects on the Thermal Properties of PDPS/PDMS Copolymers. *J. Therm. Anal. Calorim.* **1993,** *40*, 657-667.

403. Babu, G. N.; Christopher, S. S.; Newmark, R. A., Poly(dimethylsiloxane-co-diphenylsiloxanes): Synthesis, Characterization, and Sequence Analysis. *Macromolecules* **1987,** *20*, 2654-2659.

404. Yang, M.-H.; Chou, C., Synthetic Control of Sequence Distribution in PDPS/PDMS Copolymers. *J. Polym. Res.* **1994,** *1* (3), 305-312.

405. Tanasini, P.; Widmer, G.; Raballand, R., Crosslinking and Decomposition of Epoxy Resins Induced by Contamination with Water – Assessment of an Industrial Scale Scenario. *Chem. Eng. Trans.* **2016,** *48*, 703-708.

406. Chiniwalla, P.; Bai, Y.; Elce, E.; Shick, R.; Allen, S. A. B.; Kohl, P., Crosslinking and Decomposition Reactions of Epoxide-Functionalized Polynorbornene. II. Impact of Reactions on Mechanical Properties. *J. Appl. Polym. Sci.* **2004,** *91*, 1020-1029.

407. Chiniwalla, P.; Bai, Y.; Elce, E.; Robert Shick; McDougall, W. C.; Allen, S. A. B.; Kohl, P. A., Crosslinking and Decomposition Reactions of Epoxide Functionalized Polynorbornene. Part I. FT-IR and Thermogravimetric Analysis. *J. Appl. Polym. Sci.* **2003,** *89*, 568-577.

408. Bellenger, V.; Morel, E.; Verdu, J., Structure-properties relationships for densely crosslinked epoxide-amine systems based on epoxide or amine mixtures. *J. Mater. Sci.* **1988,** *23*, 4244-4250.

409. Marsmann, H. C., Silicon-29 NMR. In *Encyclopedia of Magnetic Resonance*, 2011.

410. Rohatgi, A. WebPlotDigitizer. https://automeris.io/WebPlotDigitizer/.

411. Sadow, A. D.; Tilley, T. D., Cationic Hafnium Silyl Complexes and Their Enhanced Reactivity in sigma-Bond Metathesis Processes with Si-H and C-H Bonds. *J. Am. Chem. Soc.* **2003,** *125* (31), 9462-9475.

412. Sadow, A. D.; Tilley, T. D., Activation of Arene C-H Bonds by a Cationic Hafnium Silyl Complex Possessing an alpha-Agostic Si-H Interaction. *J. Am. Chem. Soc.* **2002,** *124* (24), 6814-6815.

413. Zambelli, S.; Kaganovich, B. M.; Keiko, A. V.; Shamansky, V. A.; Zarodnyuk, M. S.; Martinez-Luaces, V.; Løvås, T.; Kustova, E. V.; Nagnibeda, E. A.; Lim, O. T.; Iida, N.; Kawanabe, H.; Barni, R.; Riccardi, C.; Holloway, D. M.; Pothiraja, R.; Bibinov, N.;

Awakowicz, P.; Zeng, Z.; Cui, L.; Xue, W.; Chen, J.; Che, Y.; Akatsuka, H.; Mosienko, B. A.; Peter, P., *Chemical kinetics*. InTech: Croatia, 2012; p 354.

414. Atkins, P.; Paula, J., *Physical Chemistry*. 9th ed.; W. H. Freeman Co.: New York, 2010.

415. Pilling, M. J.; Seakins, P. W., *Reaction Kinetics*. 2nd ed.; Oxford University Press: New York, 1995.

416. Cox, B. G., *Modern Liquid Phase Kinetics*. Oxford University Press: 1994.

417. Janakiraman, B.; Sharma, M. M., Solid-liquid and liquid-liquid slow and fast reactions: enhancements by fine carbon particles. *Chem. Eng. Sci.* **1985,** *40* (2), 235-247.

418. King, C. V., Reaction Rates at Solid-Liquid Interfaces. *J. Am. Chem. Soc.* **1935,** *57* (5), 828-831.

419. American Chemical Society SciFinder. https://scifinder.cas.org.

420. Kulkarni, S.; Shearrow, A. M.; Malik, A., Sol-gel immobilized short-chain poly(ethylene glycol) coating for capillary microextraction of underivatized polar analytes. *J. Chromatogr. A* **2007,** *1174* (1-2), 50-62.

421. Dang, Z.; Anderson, B. G.; Amenomiya, Y.; Morrow, B. A., Silica-Supported Zirconia. 1. Characterization by Infrared Spectroscopy, Temperature-Programmed Desorption, and X-ray Diffraction. *J. Phys. Chem.* **1995,** *99*, 14437-14443.

422. Guermeur, C.; Lambard, J.; Gerard, J.-F.; Sanchez, C., Hybrid polydimethylsiloxane–zirconium oxo nanocomposites. Part 1 Characterization of the matrix and the siloxane–zirconium oxo interface. *J. Mater. Chem.* **1999,** *9*, 769-778.

423. Baltes, M.; Kytökivi, A.; Weckhuysen, B. M.; Schoonheydt, R. A.; Van Der Voort, P.; Vansant, E. F., Supported Tantalum Oxide and Supported Vanadia-tantala Mixed Oxides: Structural Characterization and Surface Properties. *J. Phys. Chem. B* **2001,** *105*, 6211-6220.

424. Lauer, P. J., *Silicone Compounds Register and Review*. Petrarch Systems, Inc: 1987; p 100-103.

425. Beckmann, J.; Jurkschat, K.; Schollmeyer, D.; Schürmann, M., On the reaction of [Ph$_2$(OH)Si]$_2$O with t-Bu$_2$SnCl$_2$: synthesis and characterization of the first well defined polystannasiloxane [(t-Bu$_2$SnO)(Ph$_2$SiO)$_2$]$_n$. *J. Organomet. Chem.* **1997,** *543*, 229-232.

426. Pretsch, E.; Bühlmann, P.; Badertscher, M., *Structure Determination of Organic Compounds*. Springer-Verlag Berlin Heidelberg: 2009.

427. Bruker *NMR Frequency Tables, Tables and Formulas*; 2012; p 38.

428. Fulmer, G. R.; Miller, A. J. M.; Sherden, N. H.; Gottlieb, H. E.; Nudelman, A.; Stoltz, B. M.; Bercaw, J. E.; Goldberg, K. I., NMR Chemical Shifts of Trace Impurities: Common Laboratory Solvents, Organics, and Gases in Deuterated Solvents Relevant to the Organometallic Chemist. *Organometallics* **2010,** *29* (9), 2176-2179.

429. Bauer, J. O.; Strohmann, C., Stereoselective synthesis of silicon-stereogenic aminomethoxysilanes: easy access to highly enantiomerically enriched siloxanes. *Angew. Chem.* **2014,** *53*, 720-724.

430. Lee, A. S.; Choi, S. S.; Lee, H. S.; Baek, K. Y.; Hwang, S. S., A new, higher yielding synthetic route towards dodecaphenyl cage silsesquioxanes: synthesis and mechanistic insights. *Dalton Trans.* **2012,** *41* (35), 10585-8.

431. Tran, N. T.; Wilson, S. O.; Franz, A. K., Cooperative Hydrogen-Bonding Effects in Silanediol Catalysis. *Org. Lett.* **2011,** *14* (1), 186-189.

432. Chen, X.; Zhou, S.; You, B.; Wu, L., Ambient-curable polysiloxane coatings: structure and mechanical properties. *J. Sol-Gel Sci. Technol.* **2011,** *58* (2), 490-500.

433. Sun, X.; Xu, Y.; Jiang, D.; Yang, D.; Wu, D.; Sun, Y.; Yang, Y.; Yuan, H.; Deng, F., Study on the ammonia-catalyzed hydrolysis kinetics of single phenyltriethoxysilane and mixed phenyltriethoxysilane/tetraethoxysilane systems by liquid-state ^{29}Si NMR. *Colloid. Surface. A* **2006,** *289*, 149-157.

434. Nam, K.-H.; Lee, T.-H.; Bae, B.-S.; Popall, M., Condensation reaction of 3-(methacryloxypropyl)-trimethoxysilane and diisobutylsilanediol in non-hydrolytic sol-gel process. *J. Sol-Gel Sci. Technol.* **2006,** *39* (3), 255-260.

435. Kuniyoshi, M.; Takahashi, M.; Tokuda, Y.; Yoko, T., Hydrolysis and polycondensation of acid-catalyzed Phenyltriethoxysilane (PhTES). *J. Sol-Gel Sci. Technol.* **2006,** *39* (2), 175-183.

436. Dong, H.; Zhang, Z.; Lee, M.-H.; Mueller, D. W.; Reidy, R. F., Sol-gel polycondensation of methyltrimethoxysilane in ethanol studied by ^{29}Si NMR spectroscopy using a two-step acid/base procedure. *J. Sol-Gel Sci. Technol.* **2006,** *41* (1), 11-17.

437. Mayer, B. X.; Zöllner, P.; Rauter, W.; Kählig, H., Characterization of stationary phases for gas chromatography by ^{29}Si NMR spectroscopy - II. Silphenylene–siloxane copolymers. *J. Chromatogr. A* **2001,** *917*, 219-226.

438. Semchyschyn, D. J.; Macdonald, P. M., Limits of Detection of Polydimethylsiloxane in ^{29}Si NMR Spectroscopy. *Magnet. Reson. Med.* **2000,** *43*, 607-610.

439. Brunet, F., Polymerization reactions in methyltriethoxysilane studied through ^{29}Si NMR with polarization transfer. *J. Non-Cryst. Solids* **1998,** *231*, 58-77.

440. Alam, T. M.; Assink, R. A.; Loy, D. A., Hydrolysis and Esterification in Organically Modified Alkoxysilanes: A ^{29}Si NMR Investigation of Methyltrimethoxysilane. *Chem. Mater.* **1996,** *8*, 2366-2374.

441. Jermouni, T.; Smaihi, M.; Hovnanian, N., Hydrolysis and initial polycondensation of phenyltrimethoxysilane and diphenyldimethoxysilane. *J. Mater. Chem.* **1995,** *5* (8).

442. Sugahara, Y.; Okada, S.; Sato, S.; Kuroda, K.; Kato, C., ^{29}Si-NMR study of hydrolysis and initial polycondensation processes of organoalkoxysilanes. II. Methyltriethoxysilane. *J. Non-Cryst. Solids* **1994,** *167*, 21-28.

443. Sugahara, Y.; Okada, S.; Kuroda, K.; Kato, C., ^{29}Si-NMR study of hydrolysis and initial polycondensation processes of organoalkoxysilanes. I. Dimethyldiethoxysilane. *J. Non-Cryst. Solids* **1992,** *139*, 25-34.

444. Ramarao, M.; Packirisamy, S.; Ravindran, P. V., ^{29}Si-NMR Studies of Dimethyl and Vinylmethyl Containing Oligodiorganyl Cyclosiloxanes and Linear Copolymers. *J. Polym. Sci. Pol. Chem.* **1990,** *28*, 2153-2168.

445. Hetem, M.; Rutten, G.; Ven, L. v. d.; Haan, J. d.; Cramers, C., Deactivation by Polysiloxane and Phenyl Containing Disilazane: A ^{29}Si CP-MAS NMR Study after the Formation of Polysiloxane Chains at the Surface. *J. High Res. Chromatog.* **1988,** *11*, 510-516.

446. Williams, E. A.; Cargioli, J. D., Silicon-29 NMR Spectroscopy. 1979; pp 221-318.

447. Horn, H.-G.; Marsmann, H. C., Strukturuntersuchungen von oligomeren und polymeren Siloxanen durch hochauflosende [29]Si-Kernresonanz. *Makromolekul. Chem.* **1972,** *162*, 255-267.

448. Brochier Salon, M.-C.; Belgacem, M. N., Hydrolysis-Condensation Kinetics of Different Silane Coupling Agents. *Phosphorus Sulfur* **2011,** *186* (2), 240-254.

449. Altmann, S.; Pfeiffer, J., The Hydrolysis/Condensation Behaviour of Methacryloyloxyalkylfunctional Alkoxysilanes: Structure-Reactivity Relations. *Monatsh. Chem.* **2003,** *134* (8), 1081-1092.

450. Kruse, M. *From Linear to Long-Chain Branched Poly(ethylene terephthalate) – Reactive Extrusion, Rheology and Molecular Characterization*; Polymertechnik / Kunststofftechnikum: Technische Universität Berlin, 2017; p 193.

451. Robinson, J. W.; Zhou, Y.; Erck, R.; Qu, J.; Bays, J. T.; Cosimbescu, L., Effects of star-shaped poly(alkyl methacrylate) arm uniformity on lubricant properties. *J. Appl. Polym. Sci.* **2016,** *133* (26).

452. Zolper, T. J.; Jungk, M.; Marks, T. J.; Chung, Y.-W.; Wang, Q., Modeling Polysiloxane Volume and Viscosity Variations With Molecular Structure and Thermodynamic State. *J. Tribol.-T. ASME* **2013,** *136* (1).

453. Hao, X.; Jeffery, J. L.; Wilkie, J. S.; Meijs, G. F.; Clayton, A. B.; Watling, J. D.; Ho, A.; Fernandez, V.; Acosta, C.; Yamamoto, H.; Aly, M. G.; Parel, J. M.; Hughes, T. C., Functionalised polysiloxanes as injectable, in situ curable accommodating intraocular lenses. *Biomaterials* **2010,** *31* (32), 8153-63.

454. Hepperle, J.; Münstedt, H.; Haug, P. K.; Eisenbach, C. D., Rheological properties of branched polystyrenes: linear viscoelastic behavior. *Rheol. Acta* **2005**, 1-13.

455. O'Driscoll, K.; Sanayei, R. A., Chain-Length Dependence of the Glass Transition Temperature. *Macromolecules* **1991,** *24*, 4479-4480.

456. Lee, M. K.; Meier, D. J., Synthesis and properties of diarylsiloxane and (aryl/methyl)siloxane polymers: 3. New aryl substituents. *Polymer* **1994,** *35* (19), 4197-4202.

457. Ismeier, J.; Schmidt, A. In *Silicone elastomers beyond traditional self-bonding and self-lubricating technology*, Smithers Rapra Technology Ltd.: 2011; pp 3/1-3/6.

458. Stern, S. A.; Shah, V. M.; Hardy, B. J., Structure-permeability relationships in silicone polymers. *J. Polym. Sci., Part B: Polym. Phys.* **1987,** *25* (6), 1263-98.

459. Paszkiewicz, S.; Pilawka, R.; Dudziec, B.; Dutkiewicz, M.; Marciniec, B.; Kochmanska, A.; Jedrzejewski, R.; Roslaniec, Z., Morphology and phase separation in PTT-block-PTMO nanocomposites containing POSS particles. *Eur. Polym. J.* **2015,** *70*, 37-44.

460. Baba, M.; George, S.; Gardette, J. L.; Lacoste, J., Crosslinking of elastomers upon ageing: a kinetic approach based on crystallinity changes followed by DSC. *Polym. Int.* **2003,** *52* (6), 863-868.

461. Miikkulainen, V.; Leskelä, M.; Ritala, M.; Puurunen, R. L., Crystallinity of inorganic films grown by atomic layer deposition: Overview and general trends. *J. Appl. Phys.* **2013,** *113* (2).

462. Fischer, D. J., Crystallinity of Siloxane Polymers. *J. Appl. Polym. Sci.* **1961,** *V* (16), 436-441.

463. Racles, C.; Alexandru, M.; Bele, A.; Musteata, V. E.; Cazacu, M.; Opris, D. M., Chemical modification of polysiloxanes with polar pendant groups by co-hydrosilylation. *RSC Adv.* **2014,** *4* (71), 37620-37628.

464. Korenman, J. M.; Sheyanova, F. R.; Gureva, Z. M., Instability Constants of Complexes of Zirconium with Some Organic Ligands. *Russ. J. of Inorg. Chem* **1966,** *11*, 1485.

465. Ekberg, C.; Källvenius, G.; Albinsson, Y.; Brown, P. L., Studies on the Hydrolytic Behavior of Zirconium(IV). *J. Solution Chem.* **2004,** *33* (1), 47-79.

466. Guerard, F.; Beyler, M.; Lee, Y. S.; Tripier, R.; Gestin, J. F.; Brechbiel, M. W., Investigation of the complexation of nat Zr(IV) and [89]Zr(IV) by hydroxypyridinones for the development of chelators for PET imaging applications. *Dalton Trans.* **2017,** *46* (14), 4749-4758.

467. Mishra, P. K.; Chakravortty, V.; Dash, K. C., Schiff base complexes of zirconium(IV) derived from Zr(acac)4 *Transition Met. Chem.* **1991,** *16*, 73-75.

468. Chananašvili, L. M.; Michajlov, M. B.; Pitščhadse, Š. V., Polytitanosiloxane und ihre rheologischen Eigenschaften. *Acta Polym.* **1984,** *35*, 181-182.

469. Lim, M.; Kim, D.; Seo, J.; Han, H., Preparation and properties of poly(vinyl alcohol)/vinyltrimethoxysilane (PVA/VTMS) hybrid films with enhanced thermal stability and oxygen barrier properties. *Macromol. Res.* **2014,** *22* (10), 1096-1103.

470. Olah, G. A.; Gupta, B. G. B.; Narang, S. C.; Malhotra, R., Synthesis methods and reactions. 71. Chlorotrimethylsilane and tert-butyl dimethylsilyl chloride/lithium sulfide, mild and efficient silylating reagents. *J. Org. Chem.* **1979,** *44* (24), 4272-4275.

471. Rubinsztajn, S.; Cypryk, M.; Chojnowski, J., Condensation of model linear siloxane oligomers possessing silanol and silyl chloride end groups. The mechanism of silanol silylation by a chlorosilane in the presence of neutral nucleophiles. *J. Organomet. Chem.* **1989,** *367* (1-2), 27-37.

472. Issa, A. A.; Luyt, A. S., Kinetics of Alkoxysilanes and Organoalkoxysilanes Polymerization: A Review. *Polymers* **2019,** *11* (3).

473. Grassie, N.; Beattie, S. R., The thermal degradation of polysiloxanes - part 6: products of degradation of poly(tetramethyl-p-silphenylene siloxane) and copolymers with dimethylsiloxane. *Polym. Degrad. Stab.* **1984,** *7*, 231-250.

474. Thompson, D. B. Methods for control in the synthesis of structured siloxane architectures. Dissertation, McMaster University, Hamilton, Ontario 2008.

475. Ganachaud, F.; Boileau, S.; Boury, B., *Silicon Based Polymers: Advances in Synthesis and Supramolecular Organization*. Springer Science & Business Media B.V: Springer Netherlands, 2008.

476. Maciel, G. E., Siloxane-Based Solid Networks, from Silicas to Silicones. In *Solid-State NMR Spectroscopy of Inorganic Materials*, 1999; pp 326-356.

477. Matějka, L.; Dukh, O.; Brus, J.; Simonsick, W. J.; Meissner, B., Cage-like structure formation during sol-gel polymerization of glycidyloxypropyltrimethoxysilane. *J. Non-Cryst. Solids* **2000,** *270*, 34-47.

478. Torry, S. A.; Campbell, A.; Cunliffe, A. V.; Tod, D. A., Kinetic analysis of organosilane hydrolysis and condensation. *Int. J. Adhes. Adhes.* **2006,** *26* (1-2), 40-49.

479. McGrath, J. E., Synthetic importance and industrial applications of ring-opening polymerization. *Makromol. Chem., Macromol. Symp.* **1991,** *42/43* (1), 69-91.

480. Fuchise, K.; Igarashi, M.; Sato, K.; Shimada, S., Organocatalytic controlled/living ring-opening polymerization of cyclotrisiloxanes initiated by water with strong organic base catalysts. *Chem. Sci.* **2018,** *9* (11), 2879-2891.

481. Marsmann, H. C.; Uhlig, F.; Gupta, R. R.; Lechner, M. D.; Mikhova, B. M., *Chemical Shifts and Coupling Constants for Silicon-29*. 1 ed.; Springer-Verlag Berlin Heidelberg: 2008.

482. Levy, D.; Zayat, M., Chemistry and Fundamentals of the Sol–Gel Process. In *The Sol-Gel Handbook*, Schubert, U., Ed. 2015; pp 1-28.

483. Voronkov, M. G.; Mileshkevich, V. P.; Yuzhelevskii, Y. A., The siloxane bond. Consultants Bureau, New York, 1978; Vol. 196.

484. Dow Corning *Polysiloxanes That Contain Silicon Hydride*; USA, 2009; p 5.

485. Simon, P. F. W. *Gelpermeationschromatographie (GPC) in der Polymeranalytik: Eine kurze Einführung*; Analytik News: Hochschule Rhein-Waal, Fakultät Life Sciences, 28.03.2013, 2013; p 5.

486. Hwang, Y.-H.; Yang, M.-H., Determination of Molecular Weight of POPS Modified Copolymers. *J. Chin. Chem. Soc.* **2000,** *47* (1), 183-188.

487. Chruściel, J. J.; Janowska, G.; Fejdyś, M., Thermal properties of polymethylvinylborosiloxanes. *J. Therm. Anal. Calorim.* **2012,** *109* (2), 1049-1058.

488. Silva, C. R.; Airoldi, C., Acid and Base Catalysts in the Hybrid Silica Sol-Gel Process. *J. Colloid Interface Sci.* **1997,** *195*, 391-387.

489. Percec, V.; Pugh, C.; Nuyken, O.; D.Pask, S., 9 - Macromonomers, Oligomers and Telechelic Polymers. In *Comprehensive Polymer Science and Supplements*, Pergamon: Cleveland, OH, USA, 1989; Vol. 6, pp 281-357.

490. Bauer, J. O.; Strohmann, C., Stereoselective synthesis of silicon-stereogenic aminomethoxysilanes: easy access to highly enantiomerically enriched siloxanes. *Angew. Chem.* **2014,** *53* (3), 720-4.

491. Prince, E., *International Tables for Crystallography*. third ed.; Kluwer Academic Publishers: Dordrecht, Boston, London, 2004.

492. Lide, D. R., A survey of carbon-carbon bond lengths. *Tetrahedron* **1962,** *17*, 125-134.

493. Choudhury, A. R.; Islam, K.; Kirchner, M. T.; Mehta, G.; Row, T. N. G., In Situ Cryocrystallization of Diphenyl Ether: C-H---π Mediated Polymorphic Forms. *J. Am. Chem. Soc.* **2004,** *126*, 12274-12275.

494. Sharp, K. A., Water: Structure and Properties. In *Encyclopedia of life sciences*, John Wiley & Sons, Ltd.: 2001; p 7.

495. Owen, N. L.; Sheppard, N., Infra-red Spectra and Structure of Methyl Vinyl Ether. *Trans. Faraday Soc.* **1964,** *60*, 634-645.

496. Ehlers, G. F. L.; Fisch, K. R. *Correlations between polymer structure and glass transition temperature I. polysiloxanes, polyarylenesiloxanes and polyxylylensiloxanes*; Air Force Materials Laboratory: Wright-Patterson Air Force Base, Ohio, 1975; p 32.

497. Brown, M. E., *Introduction to Thermal Analysis - Techniques and Applications*. Second ed.; Kluwer Academic Publishers: New York, Boston, Dorbrecht, London, Moscow, 2004.

498. Paschotta, R., *Encyclopedia of Laser Physics and Technology*. Wiley-VCH: 2008.

499. Sathyanarayanamoorthi, V.; Karunathan, R.; Kannappan, V., Molecular Modeling and Spectroscopic Studies of Benzothiazole. *J. Chem.-NY* **2013,** *Article ID 258519*, 14.

500. HORIBA *Cauchy and related empirical dispersion formulae for transparent materials*; Horiba Jobin Yvon: 2006; p 8.

501. SCHOTT *TIE-29 Refractive Index and Dispersion*; SCHOTT Advanced Optics: 2016; p 12.

502. Adrianov, K. A., Rearrangements and polymerization of cyclic organosilicon compounds. *Vysokomol. soyed.* **1971,** *A13* (2), 253-265.

503. Colborn, R. E.; Davis, G. C.; Di, J.; Donea, C.; Dris, I.; Jackson, K. L.; Mullen, B. D.; Schultz, L. G.; Sinha, M.; Sybert, P. D. Polysiloxane copolymers, thermoplastic composition, and articles formed therefrom. 2010.

504. van den Bogerd, J.; Cheret, E.; Dekkers, J. H. C. M.; Faber, R. M.; Goedmakers, J. W.; Maas, C. J. J. Multilayered articles and method manufacture thereof. US 7,258,923 B2, 2007.

505. Zheng, H.; Zhang, Y.; Peng, Z.; Zhang, Y., A Comparison Between Cure Systems for EPDM/Montmorillonite Nanocomposites. *Polym. Polym. Compos.* **2004,** *12* (3), 197-206.

506. Phelps, P. D.; Boden, E. P.; Davis, G. C.; Joyce, D. R.; Hoover, J. F. Silicone-polycarbonate block copolymers and polycarbonate blends having reduced haze, and method for making. 5,530,083, 1996.

507. Miller, D. C.; Kempe, M. D.; Muller, M. T.; Gray, M. H.; Araki, K.; Kurtz, S. R., Durability of polymeric encapsulation materials in a PMMA/glass concentrator photovoltaic system. *Prog. Photovoltaics* **2016,** *24* (11), 1385-1409.

508. Montgomery, T. P.; Grandner, J. M.; Houk, K. N.; Grubbs, R. H., Synthesis and Evaluation of Sterically Demanding Ruthenium Dithiolate Catalysts for Stereoretentive Olefin Metathesis. *Organometallics* **2017,** *36* (20), 3940-3953.

509. Bähr, G.; Gelius, R., Organozinnverbindungen mit raumfüllenden Arylgruppen Di-phenanthryl-(9)-zinn. *Chem. Ber.* **1958,** *91* (4), 829-833.

510. Kondo, S.-i.; Harada, T.; Tanaka, R.; Unno, M., Anion Recognition by a Silanediol-Based Receptor. *Org. Lett.* **2006,** *8* (20), 4621-4624.

511. Kondo, S.-i.; Bie, Y.; Yamamura, M., Ratiometric Fluorescence Detection of Anions by Silanediol-Based Receptors Bearing Anthryl and Pyrenyl Groups. *Org. Lett.* **2013,** *15* (3), 520-523.

512. ChemicalBook Phenanthrene (85-01-8) ^{1}H NMR. https://www.chemicalbook.com/SpectrumEN_85-01-8_1HNMR.htm.

513. Pineiro, L.; Novo, M.; Al-Soufi, W., Fluorescence emission of pyrene in surfactant solutions. *Adv. Colloid Interface Sci.* **2015,** *215*, 1-12.

514. Brook, M. A., New Control Over Silicone Synthesis using SiH Chemistry: The Piers-Rubinsztajn Reaction. *Chemistry* **2018,** *24* (34), 8458-8469.

515. Loy, D. A.; Baugher, B. M.; Baugher, C. R.; Schneider, D. A.; Rahimian, K., Substituent Effects on the Sol-Gel Chemistry of Organotrialkoxysilanes. *Chem. Mater.* **2000,** *12*, 3624-3632.

516. Plett, K. L. Development and Characterization of Polysiloxane Polymer Films for Use is Optical Sensor Technology. Dissertation, Queen's University, Kingston, Ontario, Canada, 2008.

517. Hamdani, S.; Longuet, C.; Perrin, D.; Lopez-cuesta, J.-M.; Ganachaud, F., Flame retardancy of silicone-based materials. *Polym. Degrad. Stab.* **2009,** *94* (4), 465-495.

518. Kebritchi, A.; Nekoomansh, M.; Mohammadi, F.; Khonakdar, H. A., The role of 1-hexene comonomer content in thermal behavior of medium density polyethylene (MDPE) synthesized using Phillips catalyst. *POJ* **2014,** *1* (2), 117 - 129.

519. Hegazy, D. E., Flexible Polymeric Materials Prepared by Radiation Copolymerization of MMA/ Pyridene in the Presence of Acrylic Acid. *Arab J. Nucl. Sci. Appl.* **2014,** *47* (2), 112 - 122.

520. Sahraeian, R.; Esfandeh, M.; Hashemi, S. A., Rheological, Thermal and Dynamic Mechanical Studies of the LDPE/Perlite Nanocomposites. *Polym. Polym. Compos.* **2013,** *21* (4), 243 - 249.

521. Zhang, H.; Westmoreland, P. R.; Farris, R. J.; Coughlin, E. B.; Plichta, A.; Brzozowski, Z. K., Thermal decomposition and flammability of fire-resistant, UV/visiblesensitive polyarylates, copolymers and blends. *Polymer* **2002,** *43*, 5463 - 5472.

522. Yilgor, I.; Yilgor, E., Thermal stabilities of end groups in hydroxyalkyl terminated polydimethylsiloxane oligomers. *Polym. Bull.* **1998,** *40*, 525-532.

523. Grassie, N.; Francey, K. F., The thermal degradation of polysiloxanes - Part 3: poly(dimethyl/methylphenylsiloxane). *Polym. Degrad. Stab.* **1980,** *2*, 53-66.

524. Yang, M.-H.; Hwang, Y.-H.; Liu, J. C.; Chou, C., Effect of Monomer Sequencing on the Mesophase Behaviour of PDPS/PDMS Copolymer. *J. Chin. Chem. Soc.* **2001,** *48*, 1065-1068.

525. Quan, X., Properties of Post-Cured Siloxane Networks. *Polym. Eng. Sci.* **1989,** *29* (20), 1419 - 1425.

526. Sichina, W. J. *Characterization of Epoxy Resins Using DSC*; PerkinElmer, Inc.: U.S.A., 2000; p 4.

527. Dollase, T.; Spiess, H. W.; Gottlieb, M.; Yerushalmi-Rozen, R., Crystallization of PDMS: The effect of physical and chemical crosslinks. *Europhys. Lett.* **2002,** *60* (3), 390-396.

528. Kerres, J. A.; Strathmann, H., Synthesis and Properties of a New AB-Cross-Linked Copolymer Membrane System. *J. Appl. Polym. Sci.* **1993,** *50*, 1405-1421.

529. Bac, A.; Roizard, D.; Lochon, P.; Ghanbaja, J., Synthesis and characterization of new highly selective polyaryloxyphosphazene-polysiloxane crosslinked copolymer films. Application to the extraction of organic compounds from water by pervaporation. *Macromol. Symp.* **1996,** *102*, 225-232.

530. Czech, Z.; Goracy, K., Characterization of the crosslinking process of silicone pressure-sensitive adhesives. *Polimery-W.* **2005,** *50* (10), 762-764.

531. Karatas, Y.; Kaskhedikar, N.; Burjanadze, M.; Wiemhöfer, H.-D., Synthesis of Cross-Linked Comb Polysiloxane for Polymer Electrolyte Membranes. *Macromol. Chem. Phys.* **2006,** *207* (4), 419-425.

532. Li, H.; Zhang, J.; Xu, R.; Yu, D., Direct synthesis and characterization of crosslinked polysiloxanes via anionic ring-opening copolymerization with octaisobutyl-polyhedral oligomeric silsesquioxane and octamethylcyclotetrasiloxane. *J. Appl. Polym. Sci.* **2006,** *102* (4), 3848-3856.

533. Lee, D.-H.; Koo, S.-Y.; Lee, H.-S.; Kim, W. S.; Min, K. E.; Park, L. S.; Seo, K. H.; Kang, I. K.; Choi, H.-J., Preparation and properties of aromatic polyimides based on 4,4'-(2,2,2-trifluoro-1-phenylethylidene)diphthalic anhydride. *J. Appl. Polym. Sci.* **2002,** *85* (1), 38-44.

534. Mercado, R.; Wang, Y.; Flaim, T.; DiMenna, W.; Senapati, U., Thin-film polyetherimides with controlled refractive indices. *Proc. SPIE* **2004,** *5351*, 276-283.

535. X-Rite Color iQC and Color iMatch, Color Calculations Guide. https://www.xrite.com/-/media/xrite/files/apps_engineering_techdocuments/c/09_color_calculations_en.pdf.

536. Zhang, K.; Yuen, M. M. F.; Wang, N.; Miao, J. Y.; Xiao, D. G. W.; Fan, H. B., Thermal interface material with aligned CNT and its application in HB-LED packaging. *Proc. - Electron. Compon. Technol. Conf.* **2006,** *56th* (Vol. 1), 177-182.

537. International, A. *Standard Practice for Calculating Yellowness and Whiteness Indices from Instrumentally Measured Color Coordinates*; ASTM International: West Conshohocken, PA 19428-2959, United States, 2005.

538. Riegler, B.; Elgin, R.; Thomaier, R., A characterization of UV effects on optical silicones used in opto-electronic devices and new developments in resistant materials. *Proc. SPIE* **2007,** *6478*, 64780F-1-11.

539. Elgin, R.; Riegler, B.; Thomaier, R., How Temperature Effects Transmission of Silicone Encapsulants. *Photon. Spectra* **2007,** *41* (4), 70-72+74+76-78.

540. Riegler, B.; Thomaier, R.; Bruner, S. *Silicone system choices abound for HB LED packaging*; 1043-8092; PennWell Corp.: 2006; pp 115-118.

541. Chang, L.-B.; Pan, K.-W.; Yen, C.-Y.; Jeng, M.-J.; Wu, C.-T.; Hu, S.-C.; Kuo, Y.-K., Comparison of silicone and spin-on glass packaging materials for light-emitting diode encapsulation. *Thin Solid Films* **2014,** *570* (B), 496-499.

542. OSRAM Opto Semiconducters *Duris S5 White (CCT 2700K - 6500K)*; 2014; p 11.

543. OSRAM Opto Semiconducters *Duris S5 Datasheet*; Regensburg, 2013.

544. Barker, A. S.; Ilegems, M., Infrared Lattice Vibrations and Free-Electron Dispersion in GaN. *Phys. Rev. B* **1973,** *7* (2), 743-750.

545. Leung, M. M. Y.; Djuriŝić, A. B.; Li, E. H., Refractive index of InGaN/GaN quantum well. *J. Appl. Phys.* **1998,** *84* (11), 6312-6317.

546. Sanford, N. A.; Munkholm, A.; Krames, M. R.; Shapiro, A.; Levin, I.; Davydov, A. V.; Sayan, S.; Wielunski, L. S.; Madey, T. E., Refractive index and birefringence of $In_xGa_{1-x}N$ films grown by MOCVD. *Phys. Status Solidi C* **2005,** *2* (7), 2783-2786.

547. OSRAM Opto Semiconducters *Osram setzt mit der Oslon Square Hyper Red neuen Standard im Horticulture-Bereich*; Regensburg, Germany, 2017.

548. Schubert, M.; Gottschalch, V.; Herzinger, C. M.; Yao, H.; Snyder, P. G.; Woollam, J. A., Optical constants of $Ga_xIn_{1-x}P$ lattice matched to GaAs. *J. Appl. Phys.* **1995,** *77* (7), 3416-3419.

549. OSRAM Opto Semiconducters, OSRAM Duris S5. https://www.mouser.com/images/marketingid/2018/img/177075100_OSRAM_DURIS-S-5-PSLM-High-Power-LEDs.png, Ed. 2019.

550. Shin-Etsu Chemical Co. Ltd. *Specifications of junction coating resin, named LPS-5547 and C-5547* Shin-Etsu Chemical Co., Ltd.: 2009.

551. Inkron *Inkron - Optical Quality Coatings and Encapsulants*; Espoo, Finland, 2016.

552. Technology, L. R. e. U. I. f. I. New Class of Siloxane Polymers for Advanced LED Packaging. https://www.led-professional.com/resources-1/articles/new-class-of-siloxane-polymers-for-advanced-led-packaging-by-inkron-oy.

553. Hu, R.; Luo, X.; Feng, H.; Liu, S., Effect of phosphor settling on the optical performance of phosphor-converted white light-emitting diode. *J. Lumin.* **2012,** *132* (5), 1252-1256.

554. Kwak, S. K.; Yoo, T. W.; Kim, B.-S.; Lee, S. M.; Lee, Y. S.; Park, L. S., White LED Packaging with Layered Encapsulation of Quantum Dots and Optical Properties. *Mol. Cryst. Liq. Cryst.* **2012,** *564* (1), 33-41.

555. Wu, Y. P.; Zhang, S. Q.; Jin, S.-z.; Shi, C. S.; Li, L.; Yu, R.-Y., Influencing of various phosphor parameters on the LED performance. *Proc. SPIE* **2012,** *8419* (Optoelectronic Materials and Devices for Sensing, Imaging, and Solar Energy), 84193H/1-84193H/6.

556. Schweitzer, S.; Sommer, C.; Hartmann, P.; Nemitz, W.; Pachler, P.; Hoschopf, H.; Langer, G.; Fulmek, P.; Nicolics, J.; Wenzl, F. P., The impact of the silicone encapsulation layers

on the white light quality of phosphor converted LEDs. *Proc. SPIE* **2012,** *8484* (Twelfth International Conference on Solid State Lighting and Fourth International Conference on White LEDs and Solid State Lighting, 2012), 84840N/1-84840N/8.

557. Hou, Q.; Zhang, P.; Zhang, M.; Lu, Z.; Ren, X., Development of the research on high-power WLEDs. *Adv. Mater. Res.* **2011,** *158* (Powder Technology and Application III), 42-51.

558. Meneghesso, G.; Meneghini, M.; Zanoni, E., Recent results on the degradation of white LEDs for lighting. *J. Phys. D: Appl. Phys.* **2010,** *43* (35), 354007/1-354007/11.

559. Meneghini, M.; Tazzoli, A.; Mura, G.; Meneghesso, G.; Zanoni, E., A review on the physical mechanisms that limit the reliability of GaN-based LEDs. *IEEE T. Electr. Dev.* **2010,** *57* (1), 108-118.

560. Lin, Y.-H.; You, J. P.; Lin, Y.-C.; Tran, N. T.; Shi, F. G., Development of high-performance optical silicone for the packaging of high-power LEDs. *IEEE Trans. Compon., Packag. Technol.* **2010,** *33* (4), 761-766.

561. Zhu, Y.; Narendran, N., Investigation of White LED Performance with Multi-Layer Phosphors. *Mater. Res. Soc. Symp. P.* **2009**, 4.

562. Marchand, D. In situ detection of benzene molecules with UV absorption spectroscopy. Dissertation, Lund University, Lund, Sweden, 2011.